Neural circuit mechanisms of memory coding in the *Drosophila* mushroom body



Oliver Barnstedt

University College

University of Oxford

A thesis submitted for the degree of

Doctor of Philosophy

Trinity 2017

for my son Valentin

Acknowledgements

The work I've done over the past four years and which I present in the following chapters would not have been possible without the help, support and guidance from my supervisor, colleagues and family.

First and foremost, I would like to thank my supervisor Scott Waddell for giving me the chance to follow my research interests, to support me all along even when things seemed bleak, and to push me to perform my best in the final stretches.

I would also like to give special thanks to David Owald for his overall guidance and supervision on the Kenyon cell neurotransmitter project. He showed me how to dissect fly brains, and how to do calcium imaging in *Drosophila*. Without his help and guidance, I could not have done the work presented here.

All behavioural experiments accompanying this work in Barnstedt et al. (2016) were performed by Johannes Felsenberg, who not only worked incredibly hard to complement my physiological and histological data, but who was also kind enough to share his rich experience and insights into the world of science and how memory coding is implemented in the mushroom bodies.

In presenting this thesis, I am also deeply indebted to Scott and several of my colleagues who were kind enough to read parts of it, and to discuss improvements with me. These are Johannes Felsenberg, Pedro Jacob, Emmanuel Perisse, Kristijan Jovanoski, and Carlas Smith.

When I first came to the lab as a complete *Drosophila* novice, my colleage Gaurav Das took much of his time to introduce me to flies, how to train them, and how to interpret their behaviour. My colleague Ruth Brain was kind enough to do vital fly crosses for some of the experiments presented here. Her steady and often invisible hand is what keeps the lab running. Clifford Talbot and John-Paul Moszynski greatly helped me set up all the components required for my physiological experiments, and were always there with a helping hand and advice, when I ran into problems with the imaging setup.

I would also like to thank Emmanuel Perisse and Kristijan Jovanoski for the frequent discussions on MB circuitry and improving the quality and analysis of our calcium imaging data; Diogo Pimentel for his advice and help on pharmacology; and Paola Cognigni for frequent discussions on genetics, memory functions and MB circuitry. I consider myself extremely lucky to be working at the Centre for Neural

Circuits and Behaviour (CNCB), where technical or financial limitations are largely unheard of, and expertise and inspiration could be gathered from its many talented people by simply approaching the person sitting a few metres away.

Besides the people at the CNCB, I am also grateful to Greg Jefferis (LMB Cambridge) and Mike Dolan (now HHMI Janelia Research Campus) for kindly inviting me to Cambridge, and providing me with crucial advice and fly lines, without which I might not have achieved the optogenetic testing of functional connectivity. Quentin Geissmann (Imperial College London) kindly helped me with some data visualisation in R. I would also like to thank the anonymous reviewers for Barnstedt et al. (2016) and Felsenberg et al. (2017), and many of the attendees at CSHL Drosophila Neurobiology 2015 and Neurofly 2016 for their important feedback and experimental suggestions that have greatly shaped many of the experiments presented here.

My way into Scott's lab and neuroscience in general was paved by several scientists and academics that greatly influenced the way I think about the brain and behaviour. Gerhard Roth wrote some of the books that first attracted my curiosity about neuroscience, and his vision of a marriage of biology and psychology has influenced my thinking ever since. Arvid Kappas was my first neuroscience / psychology professor, and his thinking about human behaviour and his great support for me paved my academic path. I spent countless nights discussing the great questions of neuroscience with my good friend Jan-Matthis Lückmann. Without the great influence of my former lecturer Timothy Senior, I would have probably never joined the UK/Oxford neuroscience community, into which I was introduced by Debbie Clarke and Andy King. Johannes Dahmen kindly sacrificed many hours to show me how to perform my first *in vivo* two-photon calcium imaging experiments.

The work here would not have been possible without the unwavering support from both my own and my wife's families. In particular, I need to thank my parents-in-law Heike and Lutz Petzold for giving me much-needed shelter, peace, and space in their home that allowed me to concentrate on writing a (hopefully) coherent thesis despite the pitfalls of being a young father. I could not possibly have imagined a better home away from home than the place you offered me. I also have to thank my parents and grandparents for always supporting me throughout the years – wherever my curiosity would lead me – spiritually and financially; be it tarantula breeding, stirring up the local rock music scene, or living with lepers in India – you always gave me the confidence that I was on the right track.

Lastly, I would like to thank my amazing wife Anne for all the patience, energy, and love she exuded in these last four years despite my bouts of stress and absent-mindedness. All this, even though she was in the same doctoral boat, and – along the way – gave birth to the loveliest little boy the sun has seen. My DPhil accomplishments pale in the light of what you have achieved, and the unwavering composure and fierce resilience you have kept throughout. Thank you.

Abstract

Learning allows animals to adapt their behaviour to changes in the environment. In humans and other mammals, memories are stored in the hippocampus and cerebellum, whereas in insects, they are stored inside the mushroom bodies (MB). Here, MB-intrinsic Kenyon cells (KCs) form plastic synapses to MB output neurons (MBONs) that are modulated by the reinforcing action of dopaminergic neurons (DANs).

Despite decades of research on the MB, the main neurotransmitter underlying the plastic KC → MBON synapse has remained a mystery. Here, I show that this synapse is cholinergic in the fruit fly *Drosophila melanogaster*. MBONs show fast excitatory responses to direct acetylcholine (ACh) application. KCs synthesise ACh-related proteins ChAT and VAChT. MBONs express and require nicotinic ACh receptors (nAChRs) to become fully activated by odour presentation. Lastly, artificial activation of KCs leads to MBON calcium responses that are blocked by nicotinic antagonists and genetic reduction of VAChT in KCs. Short neuropeptide F (sNPF) may play a role as a modulatory co-transmitter that can either excite or inhibit specific MBONs and DANs.

The retrieval of memories is state-dependent and known to potentially change the original memory. Fruit flies need to be hungry to express appetitive memories. Hunger state depends on insulin signalling that activates the GABAergic MBON MVP2, while appetitive memory retrieval depends on decreased activity in M4/6 MBONs. Here, I show that optogenetic MVP2 activation acutely inhibits M4/6 odour responses, rendering MVP2 an inhibitory MBON interneuron. I also show that other MBONs are functionally connected to DANs, thus linking memory reinforcement and retrieval pathways in a way that enables the updating of the original memory.

These findings show that associative memories in *Drosophila* are initially formed at cholinergic KC–MBON synapses, and can be retrieved and modified through an intricate KC–MBON–DAN network.

Parts of this thesis have been adapted from the following published articles: Barnstedt et al. (2016), Perisse et al. (2016), and Felsenberg et al. (2017). These can also be found in the Appendix.

Contents

List of Figures **xv**

List of Tables **xix**

List of Abbreviations **xxi**

1 Introduction **1**

1.1 Learning and memory . . . 2
1.1.1 Classical conditioning . . . 3
1.1.2 Olfactory conditioning in *Drosophila* . . . 3
1.1.3 *Drosophila* memory mutants and the MB . . . 6
1.2 Kenyon cells (KCs) represent the conditioned stimulus (CS) . . . 8
1.2.1 Odour pathways to the MB . . . 8
1.2.2 MB anatomy . . . 10
1.2.3 Odour processing in the MB . . . 12
1.2.4 MB compartmentalisation . . . 13
1.3 Dopamine, the unconditioned stimulus (US), and memory formation 15
1.3.1 DAN anatomy . . . 15
1.3.2 PPL1 DANs convey aversive reinforcement . . . 16
1.3.3 PAM DANs convey appetitive reinforcement . . . 18
1.4 MBONs mediate memory retrieval . . . 20
1.4.1 A specific group of MBONs mediates aversive memory retrieval 21
1.4.2 A complementary group of MBONs mediates appetitive memory retrieval . . . 21
1.4.3 Olfactory conditioning depresses KC → MBON synapses . . 22
1.4.4 A model for associative learning and memory in the MB . . 23
1.4.5 Research questions . . . 24
1.5 Background to methods . . . 25
1.5.1 *Drosophila* genetics and the GAL4/UAS system . . . 25
1.5.2 Fluorescent proteins and immunohistochemistry . . . 28
1.5.3 Imaging neurons . . . 33
1.5.4 Manipulating neural activity . . . 37
1.5.5 RNA interference . . . 41

2 Materials and Methods **43**

2.1 Fly husbandry 44
2.1.1 Driver lines 44
2.1.2 Reporter and actuator lines 44
2.2 Pharmacology 46
2.2.1 Saline solutions 46
2.2.2 Agonists and antagonists applied 48
2.3 Explant brain widefield imaging 49
2.3.1 Setup 49
2.3.2 Brain preparation 49
2.3.3 Focal application 51
2.3.4 Bath-application of agonists and antagonists 52
2.3.5 Image acquisition 52
2.3.6 Image analysis 53
2.4 Explant brain two-photon imaging 55
2.4.1 Brain preparation 55
2.4.2 Optogenetic activation 56
2.4.3 Two-photon image acquisition 56
2.4.4 Field of view 56
2.4.5 Washout experiments 57
2.4.6 Image analysis 57
2.5 *In vivo* two-photon calcium imaging 58
2.5.1 Fly preparation 58
2.5.2 Odour delivery protocol 58
2.5.3 Odour delivery with optogenetic stimulation 59
2.5.4 Image acquisition 60
2.5.5 Image analysis 60
2.6 Immunohistochemistry 61
2.6.1 Antibodies 61
2.6.2 Staining protocol 64
2.6.3 Antibody quantification 64
2.6.4 Deconvolution and Dα7::GFP quantification 65
2.6.5 Brain registration 65
2.7 Statistics 65

3 Acetylcholine is the principal neurotransmitter of MB Kenyon cells 67

3.1 Background . . . 68
3.1.1 Neurotransmitters in the *Drosophila* brain . . . 68
3.1.2 Taurine in the MB . . . 75
3.1.3 Aspartate in the MB . . . 76
3.1.4 Glutamate in the MB . . . 78
3.1.5 GABA in the MB . . . 80
3.1.6 Acetylcholine (ACh) in the MB . . . 82
3.1.7 sNPF . . . 90
3.2 Calcium responses in MBONs to ACh application . . . 91
3.2.1 Approach . . . 91
3.2.2 Application of candidates . . . 93
3.2.3 Dose-dependence of ACh-evoked calcium responses . . . 94
3.2.4 ACh acts directly on M4/6 dendrites . . . 95
3.2.5 Individual MBONs respond to ACh . . . 102
3.3 Kenyon cells express ChAT and VAChT . . . 106
3.3.1 α-ChAT staining . . . 106
3.3.2 α-VAChT staining . . . 110
3.3.3 α-acetylcholinesterase staining . . . 115
3.3.4 Cha-GAL4 . . . 115
3.3.5 Cha-LexA . . . 117
3.4 MBONs have nicotinic ACh receptors . . . 119
3.4.1 Nicotine elicits calcium responses . . . 119
3.4.2 Histological evidence for nAChR in MBONs . . . 121
3.4.3 Bath application of nAChR blockers during ACh application 127
3.4.4 RNA interference of nAChRs . . . 130
3.5 Kenyon cells use ACh for neurotransmission to M4/6 MBONs . . . 133
3.5.1 Electrical and pharmacological KC activation . . . 134
3.5.2 Optogenetic KC activation with mecamylamine . . . 136
3.5.3 Optogenetic KC activation with RNAi . . . 141
3.6 Discussion . . . 143
3.6.1 Results summary . . . 143
3.6.2 Recent related studies . . . 145
3.6.3 ChAT/VAChT expression in KCs . . . 148
3.6.4 ACh receptors in MBONs . . . 160
3.6.5 Implications and outlook . . . 167

4 Kenyon cell co-transmitters **173**
4.1 Background . . . 173
4.1.1 Neuropeptides in *Drosophila* . . . 174
4.1.2 sNPF in the *Drosophila* brain . . . 175
4.1.3 sNPFR1 in the *Drosophila* brain . . . 177
4.1.4 sNPF in the *Drosophila* MB . . . 178
4.2 Results . . . 179
4.2.1 sNPFR1 expression . . . 179
4.2.2 Application of sNPF . . . 180
4.2.3 sNPF- and sNPFR1-RNAi . . . 183
4.2.4 Taurine . . . 187
4.3 Discussion . . . 189
4.3.1 Results summary . . . 189
4.3.2 sNPF and sNPFR1 expression . . . 190
4.3.3 sNPF effects on MBONs . . . 192
4.3.4 sNPF effects on DANs . . . 194
4.3.5 Further sNPF targets? . . . 195
4.3.6 Potential molecular mechanisms . . . 197
4.3.7 State-dependent regulation of sNPF modulation . . . 198

5 MVP2 are inhibitory MBON interneurons **199**
5.1 Background . . . 199
5.1.1 Hunger as a motivational state . . . 199
5.1.2 Circuits of state-dependent memory expression . . . 202
5.2 Results . . . 203
5.2.1 Voltage imaging of GABA injections into M4/6 . . . 204
5.2.2 Optogenetic MVP2 stimulation in explant brain . . . 204
5.2.3 Optogenetic MVP2 stimulation, combined with odours . . . 207
5.2.4 Optogenetic MVP2 stimulation with odours in starved flies . 208
5.3 Discussion . . . 211
5.3.1 Results summary . . . 211
5.3.2 Voltage imaging . . . 211
5.3.3 Shunting inhibition in MBONs . . . 214
5.3.4 Why is no effect of MVP2 activation observed in V2? . . . 215
5.3.5 Comparison with MV2 . . . 217
5.3.6 A model of hunger-dependent retrieval . . . 219

6 Neural circuit mechanisms of extinction and reconsolidation 223
6.1 Background . . . 223
6.1.1 Extinction . . . 224
6.1.2 Reconsolidation . . . 229
6.2 Results . . . 232
6.2.1 Driver line access . . . 232
6.2.2 Functional connectivity between V2 and DANs . . . 232
6.2.3 Functional connectivity between M4/6 and PAM neurons . . . 237
6.2.4 MBON-γ2α′1 excites several DANs for reconsolidation . . . 240
6.2.5 MBON-γ2α′1 carries a CS^--specific memory trace . . . 245
6.3 Discussion . . . 249
6.3.1 Results summary . . . 249
6.3.2 Functional connectivity between V2 and PPL1 . . . 251
6.3.3 Functional connectivity between V2 and PAM . . . 255
6.3.4 M4/6 – PAM interplay . . . 256
6.3.5 MBON-γ2α′1 carries a CS^- memory trace . . . 261
6.3.6 Updating memories through MBON–DAN interplay . . . 262

A Appendix 265

References 349

List of Figures

1.1 Aversive and appetitive conditioning and memory phases. 5
1.2 Odour sensing pathways to the MB. 9
1.3 MB compartments and MBON/DAN innervation. 14
1.4 A simplified model of associative learning in the MB. 24
1.5 The GAL4/UAS system and GCaMP. 27

2.1 The imaging setup, based on a customised Scientifica Slicescope. . . 50
2.2 *In vivo* tethered fly preparation. 59
2.3 Sample calculation of normalised area under curve (AUC). 62

3.1 Synaptic acetylcholine synthesis and packaging pathway. 83
3.2 Original ChAT antibody staining showing MBs. 84
3.3 R21D02-GAL4 expression pattern and experimental approach. . . . 92
3.4 Application of 1 mM of six transmitter candidates. 94
3.5 Dose-dependence of ACh injection-evoked calcium responses. 96
3.6 ACh-evoked calcium responses in M4/6 dendritic vicinity. 98
3.7 M4/6 calcium response depends on the spread of ACh solution. . . 99
3.8 High magnesium does not affect ACh-evoked responses in M4/6. . . 101
3.9 KCs are not excited by ACh injected into the lobes. 103
3.10 All main classes of MBONs show ACh-evoked calcium responses. . . 105
3.11 α-ChAT staining (DSHB ChAT4B1) with KC-driven RFP. 108
3.12 ChAT-RNAi reduces ChAT-positive staining. 109
3.13 KC-driven ChAT-RNAi reduces α-ChAT staining across MB lobes. . 110
3.14 Rabbit α-*Drosophila* VAChT antibody staining. 112
3.15 KC-driven VAChT-RNAi reduces α-VAChT immunostaining. 113
3.16 ChAT-/VAChT-RNAi reduce α-ChAT/α-VAChT staining. 114
3.17 Potential AChE immunoreactivity in brain astroglia. 116
3.18 Cha-GAL4 expresses in several α/βs KCs. 118
3.19 Cha-LexA expresses in KCs. 120
3.20 Nicotine injections cause calcium responses in M4/6 neurons. 122
3.21 Conjugated α-bungarotoxin staining shows shows MB labelling. . . 124
3.22 Dα7::GFP expresses in M4/6 dendrites. 126

3.23 Mecamylamine blocks ACh-evoked calcium responses in M4/6 dendrites. 129
3.24 Hexamethonium and MLA block M4/6 ACh responses. 131
3.25 nAChR-RNAi decreases odour-evoked calcium responses in M4β′. . 132
3.26 KC stimulation through $P2X_2$ activates M4/6 neurons through nAChRs. 135
3.27 Optogenetic KC stimulation activates M4/6 neurons through nAChRs. 137
3.28 Mecamylamine block of KC → MBON nicotinic synapse is reversible. 139
3.29 CsChrimson activates KCs despite mecamylamine. 140
3.30 VAChT-RNAi in KCs reduces KC → MBON calcium responses. . . 142
3.31 The cholinergic locus on 3R and locations of RNAi. 149

4.1 sNPFR1 may be expressed in MB extrinsic neurons. 181
4.2 sNPF bath application has no effect on ACh-evoked M4/6 responses. 183
4.3 sNPF co-application with ACh facilitates calcium responses in M4/6. 184
4.4 Differential effects of γ KC sNPF transmission to different γ MBONs. 186
4.5 sNPFR1-RNAi in PPL1 affects odour-evoked calcium responses. . . 188
4.6 Taurine antibody labels SOG and dFB, but no MB neurons. 189

5.1 Voltage imaging of M4/6 MBONs during GABA injections. 205
5.2 Optogenetic activation of MVP2 neurons in explant brain. 206
5.3 Activating MVP2 neurons depresses M4/6 but not V2 odour responses. 209
5.4 Control experiments for MVP2 activation and MBON odour imaging. 210
5.5 Starved flies have smaller odour responses in M4/6 but not V2 neurons. 212
5.6 Circuit model of hunger-dependent appetitive memory retrieval. . . 220

6.1 Anatomy of driver lines used for experiments. 233
6.2 Activating V2 MBONs triggers PPL1 calcium responses. 235
6.3 Activating V2 MBONs triggers heterogeneous PPL1 responses. . . . 236
6.4 Activating V2 MBONs triggers calcium responses in PAM neurons. 238
6.5 Activating M4/6 MBONs triggers calcium responses in PAM-γ5. . . 239
6.6 Effects of optogenetic activation of PAM neurons on M6 MBONs. . 241
6.7 Activating MBON-γ2α′1 triggers calcium responses in MV1. 243
6.8 Activating MBON-γ2α′1 triggers calcium responses in PAM neurons. 244
6.9 MBON-γ2α′1 shows enhanced CS^- odour responses. 247
6.10 Calcium responses to odours after appetitive training in V2 MBONs. 248
6.11 Calcium responses to odours after appetitive training in PPL1 neurons. 250

A.1 Sample traces of different concentrations of ACh injections. 266
A.2 Overview of ACh-evoked calcium transients in 25 explant brains. . . 270
A.3 Calcium responses to ACh are fast and temporally correlated. . . . 271
A.4 M4/6 calcium responses to ACh stimulation around protocerebrum. 272
A.5 M4/6 calcium responses to ACh stimulation in vicinity of dendrite. 273

A.6 KC-driven ChAT-RNAi generally reduces ChAT-positive staining. . 274
A.7 VAChT-RNAi decreases α-VAChT immunostaining in MBs. 275
A.8 Further antibodies against cholinergic neurons. 276
A.9 Cha3.3kb-GAL4 and Cha-GAL80 expression. 277
A.10 MiMIC expression of cholinergic genes. 278
A.11 Comparison of α-AChE staining pattern with ALG expression. . . . 279
A.12 Dα7::GFP reliably forms punctae in M4/6 dendrites. 280
A.13 Dα7::GFP expresses closely to postsynaptic sites in M4/6 neurons. . 281
A.14 nAChR and mAChR promoter fragment expression. 282
A.15 Mecamylamine blocks ACh-induced calcium responses in KC calyx. 283
A.16 sNPFR1-GAL4 (R64F07) expresses specifically in MB-CP1 neurons. 283
A.17 V2 MBONs and PPL1 DANs have overlapping neurites. 284

List of Tables

1.1 MB compartments and corresponding DANs and MBONs. 15

2.1 Driver lines 45
2.2 Reporter/actuator lines 46
2.3 AHLS recipe 47
2.4 Extracellular saline recipe 48
2.5 Receptor agonists and antagonists. 49
2.6 Antibodies 63

3.1 Overview of *Drosophila melanogaster* neurotransmitter expression. . 69
3.2 Overview of *Drosophila melanogaster* neurotransmitter proteins. . . 69
3.3 nAChR-GAL4 lines drive expression in MBONs. 127
3.4 ChAT/VAChT expression summary. 160

A.1 VAChT immunostaining of VAChT-RNAi quantification table. . . . 267
A.2 Absolute quantification of α-ChAT and α-VAChT immunoreactivity. 268
A.3 Relative quantification of α-ChAT and α-VAChT immunoreactivity. 269

List of Abbreviations

2PEM . . . . . 2-photon excitation microscopy.

5-HT . . . . . 5-hydroxytryptamine, serotonin.

AB . . . . . Antibody.

AC . . . . . Adenylyl cyclase.

ACA . . . . . Accessory calyx.

ACh . . . . . Acetylcholine.

AChE . . . . . Acetylcholinesterase.

AHLS . . . . . Adult hemolymph-like saline.

AL . . . . . Antennal lobe.

ALG . . . . . Astrocyte-like glia.

AMPA . . . . α-amino-3-hydroxy-5-methyl-4-isoxazolepropionic acid.

AP . . . . . Action potential.

APD . . . . . Avalanche photodiode.

APL . . . . . Anterior paired lateral.

ARM . . . . . Anaesthesia-resistant memory.

ASM . . . . . Anaesthesia-sensitive memory.

ATP . . . . . Adenosine triphosphate.

ATR . . . . . All-*trans*-retinal.

BDSC . . . . . Bloomington *Drosophila* Stock Center.

BLA . . . . . Basolateral amygdala.

cAMP . . . . . Cyclic adenosine monophosphate.

CC . . . . . Central complex.

CCD . . . . . Charge-coupled device.

ChAT . . . . . Choline acetyltransferase.

ChR2 . . . . . Channelrhodopsin-2.

CHT . . . . . Choline transporter.

CR . . . . . Conditioned response.

CRE . . . . . Crepine.

CS . . . . . Conditioned stimulus.

CS$^+$ . . . . . Conditioned stimulus plus.

CS$^-$ . . . . . Conditioned stimulus minus.

CXM . . . . . Cyclohexamide.

DANs . . . . . Dopaminergic neurons.

DPM . . . . . Dorsal paired medial.

DSHB . . . . . Developmental Studies Hybridoma Bank.

dsRNA . . . . Double-stranded ribonucleic acid.

EB . . . . . Ellipsoid body.

EMCCD . . . Electron multiplying charge-coupled device.

ER . . . . . Endoplasmic reticulum.

FB . . . . . Fan-shaped body.

FOV . . . . . Field of view.

FP . . . . . Fluorescent protein.

FRET . . . . . Förster resonance energy transfer.

GaAsP . . . . Gallium arsenide phosphide.

GABA . . . . . γ-aminobutyric acid.

GECI . . . . . Genetically encoded calcium indicator.

GEVI . . . . . Genetically encoded voltage indicator.

GFP . . . . . Green fluorescent protein.

GR . . . . . Gustatory receptor.

GRN . . . . . Gustatory receptor neuron.

***Gt*ACR** . . . . *Guillardia theta* Anion Channel Rhodopsin.

GPCR . . . . . G-protein coupled receptor.

IL . . . . . Infralimbic cortex.

ITI . . . . . Inter-trial interval.

KCs . . . . . Kenyon cells.

LED . . . . . Light-emitting diode.

LH . . . . . Lateral horn.

LTM . . . . . Long-term memory.

mAChR . . . . Muscarinic acetylcholine receptor.

MB . . . . . Mushroom bodies.

MIP . . . . . Myoinhibitory peptide.

MLA . . . . . Methyllycaconitine.

mPFC . . . . . Medial prefrontal cortex.

mRNA . . . . Messenger ribonucleic acid.

MTM . . . . . Middle-term memory.

nAChR . . . . Nicotinic acetylcholine receptor.

NLS . . . . . Nuclear localisation signal.

NMDAR . . . *N*-methyl-D-aspartate receptor.

OA . . . . . Octopamine.

PAM . . . . . Protocerebral anterior medial.

PBS . . . . . Phosphate buffered saline.

PBT . . . . . Phosphate buffered saline with Triton-X.

PDE . . . . . Phosphodiesterase.

PFA . . . . . Paraformaldehyde.

PMT . . . . . Photon multiplier tube.

PNs . . . . . Projection neurons.

PPL . . . . . Protocerebral posterior lateral.

PSF . . . . . Point spread function.

QE . . . . . Quantum efficiency.

RFP . . . . . Red fluorescent protein.

RNA . . . . . Ribonucleic acid.

RNAi . . . . . Ribonucleic acid (RNA) interference.

ROI . . . . . Region of interest.

sCMOS . . . . Scientific complementary metal oxide semiconductor.

SEM . . . . . Standard error of the mean.

Shi^{ts1} . . . . . Temperature-sensitive shibire.

SIP . . . . . Superior intermediate protocerebrum.

siRNA . . . . . Small interfering ribonucleic acid.

SLP . . . . . Superior lateral protocerebrum.

SMP . . . . . Superior medial protocerebrum.

sNPF . . . . . Short neuropeptide F.

SNR . . . . . Signal-to-noise ratio.

SOG . . . . . Suboesophageal ganglion.

STM . . . . . Short-term memory.

TTX . . . . . Tetrodotoxin.

TXR . . . . . Texas red.

UAS . . . . . Upstream activating sequence.

UR . . . . . Unconditioned response.

US . . . . . Unconditioned stimulus.

VAChT . . . . Vesicular acetylcholine transporter.

VDRC . . . . . Vienna Drosophila Resource Center.

VGCC . . . . . Voltage-gated calcium channel.

VGSC . . . . . Voltage-gated sodium channel.

1 Introduction

Contents

1.1 Learning and memory 2
1.1.1 Classical conditioning 3
1.1.2 Olfactory conditioning in *Drosophila* 3
1.1.3 *Drosophila* memory mutants and the MB 6
1.2 Kenyon cells (KCs) represent the conditioned stimulus (CS) 8
1.2.1 Odour pathways to the MB 8
1.2.2 MB anatomy 10
1.2.3 Odour processing in the MB 12
1.2.4 MB compartmentalisation 13
1.3 Dopamine, the unconditioned stimulus (US), and memory formation 15
1.3.1 DAN anatomy 15
1.3.2 PPL1 DANs convey aversive reinforcement 16
1.3.3 PAM DANs convey appetitive reinforcement 18
1.4 MBONs mediate memory retrieval 20
1.4.1 A specific group of MBONs mediates aversive memory retrieval 21
1.4.2 A complementary group of MBONs mediates appetitive memory retrieval 21
1.4.3 Olfactory conditioning depresses KC → MBON synapses 22
1.4.4 A model for associative learning and memory in the MB 23
1.4.5 Research questions 24
1.5 Background to methods 25
1.5.1 *Drosophila* genetics and the GAL4/UAS system 25
1.5.2 Fluorescent proteins and immunohistochemistry 28
1.5.3 Imaging neurons 33
1.5.4 Manipulating neural activity 37

1.5.5 RNA interference 41

1.1 Learning and memory

Most animals have the ability to learn about changes in their environment and use these memories to guide future behaviour in an adaptive way. On the level of the brain, neural plasticity allows individual animals to rapidly adapt to their environment. Learning can be separated into non-associative learning, including habituation and sensitisation, and into associative learning which includes classical and operant conditioning (Gluck et al., 2016). The maintenance of these memories requires a time-dependent stabilisation process called consolidation (see McGaugh, 2000).

Repeated presentation of stimuli can lead to a successive decrease in strength or occurrence of a behavioural response. This **habituation** learning is found in many species including the sea hare *Aplysia californica* (Castellucci and Kandel, 1974).

Sensitisation, on the other hand, describes an increase of responsiveness to stimuli after the presentation of a salient stimulus such as an electric shock (e.g. Brunelli et al., 1976).

Classical conditioning is a form of associative learning in which a previously neutral stimulus gains behavioural relevance by pairing it with an appetitive or aversive stimulus (Pavlov, 1927; see also 1.1.1).

Operant conditioning shares many similarities to classical conditioning, but instead of a neutral stimulus gaining behavioural relevance, an animal's behavioural action is either reinforced or punished to increase or decrease the future occurrence of such behaviour (see Skinner, 1953).

More complex forms of learning include generalisation and discrimination learning, as well as concept formation, and can be found in many animals including insect species (see Giurfa, 2003).

In the following, I will focus on classical olfactory conditioning in fruit flies as a tool to understand the neural substrates and mechanisms of associative memory formation.

1.1.1 Classical conditioning

Classical conditioning has been widely studied as a simple form of associative learning in which a neutral stimulus (conditioned stimulus, CS) becomes associated with an inherently appetitive or aversive stimulus (unconditioned stimulus, US) (Pavlov, 1927). The appetitive or aversive US elicits an unconditioned response (UR) in naïve animals, but the neutral CS does not. After pairing the CS with the US, the CS alone will elicit a conditioned response (CR), often similar to the UR. If the CS is presented multiple times without US, the CR becomes attenuated and vanishes in a process called extinction (Konorski, 1948; Pavlov, 1927).

In the original study by Pavlov (1927), experimental dogs were trained to associate the ringing of a bell (CS) with the presentation of food (US). The presentation of food (US) would naïvely cause dogs to salivate (UR), whereas the ringing of a bell elicited no response. After a conditioning procedure in which the CS was repeatedly followed closely by the US, salivation (UR) was already observed after only ringing the bell (CS) without food presentation. The CS has thus become predictive of the US, leading the dogs to salivate in anticipation of the predicted US.

In Pavlov's studies, the food served as a positive US for the dogs to induce appetitive conditioning. A negative US, on the other hand, can also serve as aversive reinforcement, as first demonstrated by B. F. Skinner's group in the 1940s. Both appetitive and aversive conditioning have since been found across the animal kingdom, with surprisingly similar rules in many species (Estes and Skinner, 1941; Schneiderman et al., 1962; Thompson, 1990). This suggests that the underlying neural mechanisms may be very similar, and probably assessable in animals as small as fruit flies.

1.1.2 Olfactory conditioning in *Drosophila*

In the 1970s it was discovered that the fruit fly *Drosophila melanogaster* is able to form associative olfactory memories (Quinn et al., 1974). Besides olfactory conditioning, *Drosophila* can also undergo visual conditioning (Quinn et al., 1974;

Spatz et al., 1974), taste conditioning (Keene and Masek, 2012; Kirkhart and Scott, 2015), and other forms of learning (see McGuire, 1984).

Aversive conditioning

In the first behavioural task developed, adult *Drosophila melanogaster* flies were kept in a lower tube and were free to walk upwards toward a fluorescent lamp into one of five vials that were subsequently made available by sliding them into alignment (Quinn et al., 1974). The first vial served as a mere resting vial, while the second vial contained an odour A (CS^+) with electric shocks, and the third vial contained only odour B (CS^-). After this training procedure, the flies that entered the fourth vial (CS^+ only) and the fifth vial (CS^-) were recorded. Importantly, flies preferentially avoided the CS^+ odour, demonstrating a learned CS–US association that would last for 24 hours, and that could be extinguished.

This first behavioural setup had some drawbacks (see McGuire, 1984; Tully, 1984), among them the fact that flies had to "volitionally" enter the training tubes, without which they received no conditioning, or the dependence on positive phototaxis for flies to enter the training tubes. These shortcomings led Tully and Quinn (1985) to introduce a behavioural paradigm that tests classical conditioning in *Drosophila* more stringently. Here, flies are trained and tested in a T-maze apparatus which includes an electrifiable training tube, a central sliding compartment for fly transfer, and two test tubes that can be approached from a choice point (Tully and Quinn, 1985; see Figure 1.1A). This design has the advantage of minimising fly handling (which was shown to be aversive, Dudai, 1977b), and has since been widely used to test aversive olfactory learning (see Aso et al., 2014b; Pascual and Préat, 2001; Tully et al., 1994).

Appetitive conditioning

Flies can not only learn to associate odours with punishment, but also learn positive associations by reward learning. The first study to demonstrate this used a paradigm similar to that of Quinn and Tully (Quinn et al., 1974; Tully and Quinn, 1985), in which flies were first introduced to two tubes, each being wetted with either OCT or

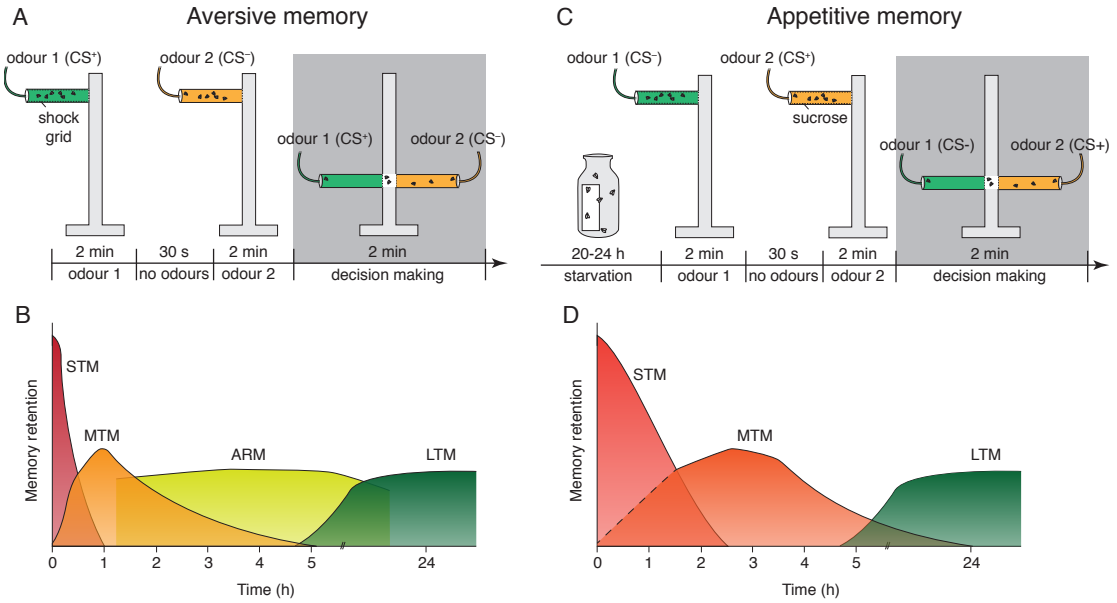


Figure 1.1: Aversive and appetitive conditioning and memory phases. A) Aversive memory is established by exposing ~ 100 flies to electric shocks while presenting a CS^+ odour for two minutes, followed by 30 s no odours, followed by two minutes of unreinforced CS^- odour. Depending on the form of memory tested, flies are either directly or later tested to decide between both odours in a T-maze for two minutes. The performance index (PI) is calculated by subtracting the number of flies in the CS^- arm from those in the CS^+ arm, divided by the total number of flies counted (Tully and Quinn, 1985). B) There are at least four separable aversive memory phases in *Drosophila*, spanning from short-term memory (STM) to middle-term memory (MTM) to consolidated anaesthesia-resistant memory (ARM) and long-term memory (LTM). Adapted from DeZazzo and Tully (1995). C) Appetitive memory is established similarly to aversive training, but flies are starved $\sim 20-24$ hours before training, are first presented with the CS^- odour, and then with the CS^+ odour paired with dried sucrose on filter paper (Krashes and Waddell, 2008; Tempel et al., 1983). D) Appetitive memory phases are similar to those for aversive memory, but no ARM is formed, and it is yet unclear if STM and MTM fundamentally differ from one another (Krashes and Waddell, 2008; Perisse et al., 2013a; Trannoy et al., 2011).

MCH odorants, and one of them being painted with 1 M sucrose, before they were transferred to a T-maze (Tempel et al., 1983; see Figure 1.1C). Immediate learning scores with this method are comparable to those for aversive conditioning (Quinn et al., 1974; Tully and Quinn, 1985), but single trial memory retention is much higher with appetitive conditioning (Tempel et al., 1983). Indeed, it was later shown in a similar appetitive conditioning paradigm that already a single learning trial can produce long-lasting memories of at least 36 h (Krashes and Waddell, 2008).

Memory phases in *Drosophila*

Different aversive and appetitive conditioning protocols can induce different forms of memory that can co-exist in parallel and may be distinguished based on the retrieval time, their sensitivity to anaesthesia, the need for protein synthesis, and the involvement of specific neurons and genes (see also 1.3; DeZazzo and Tully, 1995).

Aversive memory can be operationally divided into at least four memory phases: short-term memory (STM), middle-term memory (MTM) including anaesthesia-sensitive (ASM) and anaesthesia-resistant (ARM) memory, and long-term memory (LTM) (see Figure 1.1B). STM is rapidly formed after just one trial of odour–shock pairing, but decays within 30 min (DeZazzo and Tully, 1995). ASM is also formed after a single learning trial, peaks at about one hour, and decays within 3–4 h (Quinn and Dudai, 1976). ARM is produced by either single trial or massed training with 5× cycles, forms within the first ∼30 min, and persists for about 24 h (Folkers et al., 1993; Lee et al., 2011; Quinn and Dudai, 1976; Tully et al., 1994). LTM requires spaced training and protein synthesis, develops at about 5 h, and lasts for several days (Tully et al., 1994).

Appetitive memory contains at least two to three memory phases: STM, MTM and LTM (see Figure 1.1D). STM forms rapidly, decays within one hour, and depends on *rut* (Trannoy et al., 2011). MTM is typically measured at about 3 h but may be merely a transition period between STM and LTM (see Perisse et al., 2013b). LTM is rapidly consolidated within 2 h, depends on protein synthesis, and *crammer*, *radish* and *tequila* (Krashes and Waddell, 2008; Trannoy et al., 2011).

1.1.3 *Drosophila* memory mutants and the MB

The ability of fruit flies to form various kinds of associative memories allowed the investigation of the genes underlying this cognitive ability (reviewed in Keene and Waddell, 2007; McGuire et al., 2005), using the previously established genetic screens pioneered by Thomas Hunt Morgan and Seymour Benzer (see Benzer, 1971; Morgan, 1910). Based on the premise that not only phenotypic variations arise from genes but also complex behaviours, Benzer had previously used chemical

mutagenesis to uncover genes required for phototaxis (Benzer, 1967) as well as circadian rhythms (Konopka and Benzer, 1971).

Using ethyl methane sulfonate (EMS) to cause small mutations on the X chromosome, Benzer's lab initially screened about 4,000 strains for defects in associative learning, and first uncovered the mutant *dunce* (Byers et al., 1981; Dudai et al., 1976). This was followed by several more mutants discovered in Quinn's lab: *cabbage*, *radish*, *rutabaga*, *turnip*, and *amnesiac* (Aceves-Piña and Quinn, 1979; Aceves-Pina et al., 1983; Quinn et al., 1979), followed later by P-element mutant screens that uncovered *latheo*, *linotte*, and *nalyot* (Boynton and Tully, 1992; DeZazzo et al., 2000; Dura et al., 1993; Tully et al., 1990). Dubnau et al. (2003) reported a further 102 candidate genes involved in memory formation in a large screen using both P-element mutagenesis and DNA microarray data.

Besides behavioural mutant screens, structural mutant screens were also employed and tested for memory defects, with the resulting *mushroom body deranged* (*mbd*) and *mushroom bodies miniature* (*mbm*) both showing mushroom body (MB) structural defects as well as appetitive and aversive olfactory memory deficits (Heisenberg and Böhl, 1979; Heisenberg et al., 1985). A role for the MB in learning and memory was already previously demonstrated in the honeybee, where local cooling of the MB produced amnesia (Erber et al., 1980). Yet, there were more pieces of evidence suggesting a role for the MB in learning and memory: *dunce* was shown to preferentially express in the MB (Nighorn et al., 1991), as well as several *rutabaga* alleles: DC0, *leonardo*, *volado*, and *fasciclin II* (Cheng et al., 2001; Grotewiel et al., 1998; Han et al., 1992; Skoulakis and Davis, 1996; Skoulakis et al., 1993). Further experiments involving chemical ablation of the MB and temporal block of synaptic transmission firmly established the MB as the main centre for learning and memory in *Drosophila* (Belle and Heisenberg, 1994; Dubnau et al., 2001; McGuire et al., 2001).

The MB is a bilateral neuropil region, first described by Félix Dujardin (Dujardin, 1850), that largely consists of axons from the MB-intrinsic Kenyon cells (KCs), named after Frederick C. Kenyon who first used the Golgi method to describe

MB anatomy (Kenyon, 1896a,b). The MB receives mostly third-order olfactory information through antennal lobe (AL) projection neurons (PNs), but also sensory input from non-olfactory PNs conveying visual, gustatory, and thermal information (Eichler et al., 2017; Yagi et al., 2016; Zheng et al., 2017). The MB lobes are heavily innervated by dopaminergic terminals (see 1.3) that modulate synapses to MB output neurons (MBONs; see 1.4).

1.2 Kenyon cells (KCs) represent the conditioned stimulus (CS)

1.2.1 Odour pathways to the MB

Drosophila detects odours via ∼1,400 olfactory receptor neurons (ORNs) of about 50 individual classes that are housed in sensillae of the third antennal segment and the maxillary palp (reviewed in Laissue and Vosshall, 2008; Masse et al., 2009; Wilson, 2013). Most ORNs express the obligatory odourant receptor subunit Or83b which is required for odour responses (Couto et al., 2005; Larsson et al., 2004). ORNs with the same receptor send axons through the antennal nerve bilaterally into the same one of about 50 glomeruli per AL, the invertebrate equivalent to the mammalian olfactory bulb (Vosshall et al., 2000).

In the AL, cholinergic PNs each innervate a single glomerulus and send projections via the inner antennocerebral tract (iACT) to the MB calyx and the lateral horn (LH) (Stocker et al., 1990; see Figure 1.2). Each glomerulus receives on average a bilateral input of 50 ORNs, each forming synapses with about three PNs (Vosshall et al., 2000). In contrast to the mammalian olfactory bulb, the AL seems to receive no feedback projections from MB or LH (Masse et al., 2009), but it has local neurons that interconnect glomeruli and release either GABA or ACh (Malun, 1991; Shang et al., 2007). This circuitry ensures odour information stays well clustered and separated between ORNs, glomeruli, and PNs (see Ng et al., 2002; Seki et al., 2017; Wilson and Laurent, 2005). PN projections to the LH are thought to provide experience-independent olfactory information, while projections to the MB are crucial for olfactory memory tasks (Heimbeck et al., 2001; Seki et al., 2017).

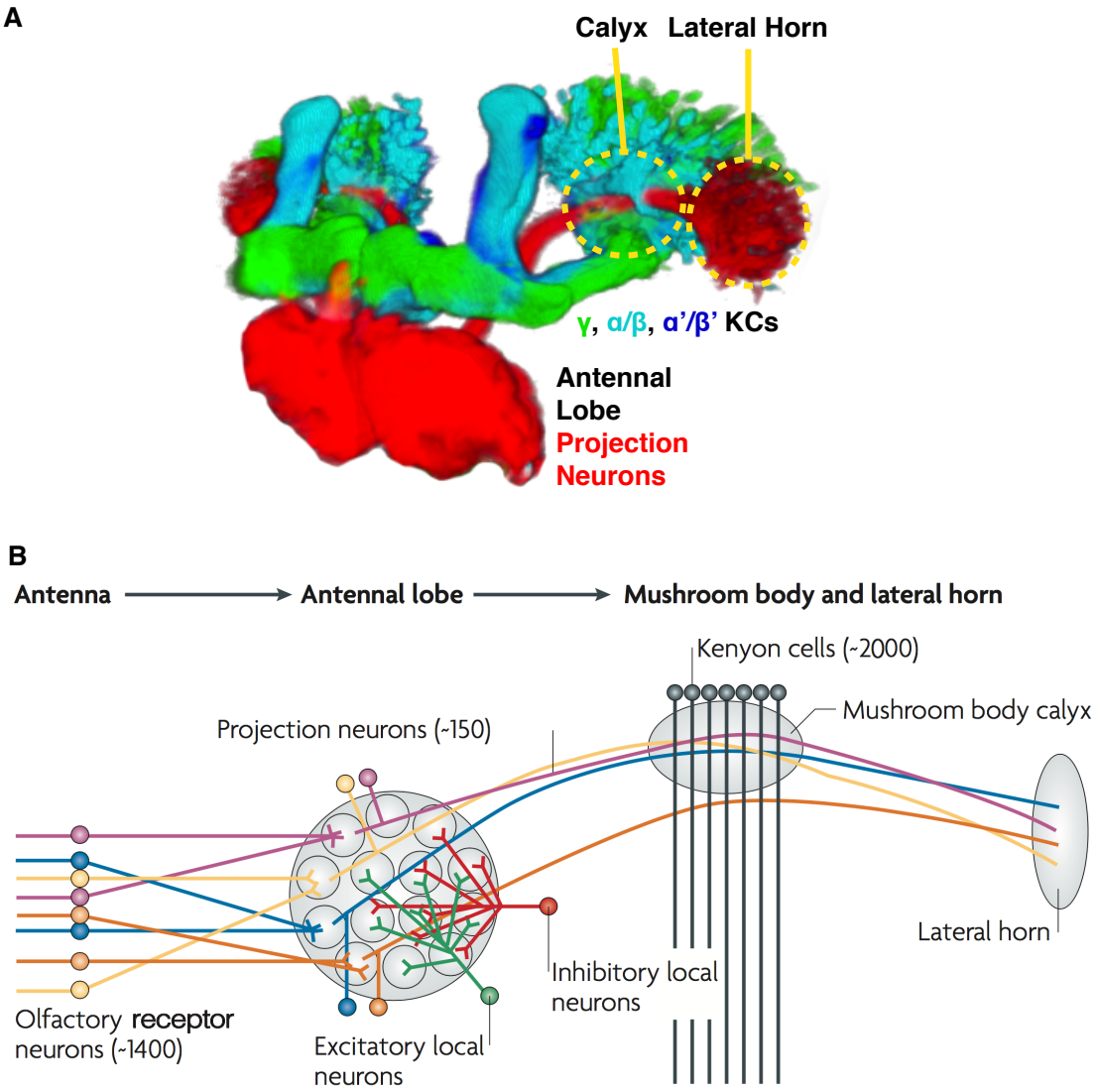


Figure 1.2: Odour sensing pathways to the MB. A) Antennal lobe (AL) projection neurons (PNs; red) project cholinergic axons from AL glomeruli into calyx and lateral horn (LH). KCs form dendritic claws around PN terminals in the calyx, and project through the peduncle into the horizontal γ, β, or β′, or into the vertical α or β lobes. Image was generated in Fiji with 3D Viewer, based on VDRC BrainBase images (`http://brainbase.imp.ac.at`) from GAL4 lines VT33006, VT58938, VT30604, and VT49246 (Kvon et al., 2014). B) ORNs with the same receptor (indicated by colour) project into the same AL glomerulus. Several uniglomerular and multiglomerular AL interneurons modulate odour processing. PNs make *en passant* synapses with KCs in the calyx before terminating in the LH, while some PNs only project to the LH. Adapted from Keene and Waddell (2007).

1.2.2 MB anatomy

Kenyon cell bodies

Each hemisphere of the *Drosophila melanogaster* brain contains about 2,000 to 2,050 Kenyon cell bodies (Aso et al., 2009, 2014a) with a diametre of about 2 µm to 4 µm, all densely populating the posterior end of the superior protocerebrum (see Wang et al., 2004).

Calyx

Each cell body extends a single neurite through one of four fascicles into the MB calyx, the main input region of the MB, where they form around seven synaptic claws around large ACh-releasing PN presynaptic boutons (Caron et al., 2013; Gruntman and Turner, 2013; Ito et al., 1997). Each claw receives input from only one PN. There has been controversy about whether PNs provide structured input from specific glomeruli into specific calycal zones, as was previously suggested based on anatomical data (Lin et al., 2007), or whether PNs converge randomly onto KCs as later physiological data strongly suggested (Caron et al., 2013; Gruntman and Turner, 2013), and as recent electron microscopy studies largely confirmed (Eichler et al., 2017; Zheng et al., 2017).

Interestingly, recent studies suggested that γ and α/β KCs may also contain presynaptic active zones in the calyx, the function of which remains unknown (Butcher et al., 2012; Christiansen et al., 2011; Zheng et al., 2017). Besides plasticity in MB lobes, however, there is also evidence for structural plasticity in the calyx (Kremer et al., 2010).

MB peduncle

From the calyx, KC neurites extend towards the anterior and fasciculate to form the peduncle, a dense bundle of KC neurites (Crittenden and Skoulakis, 1998). The peduncle seems to be mainly important for guiding neurites towards the lobes as there are only few to no pre- or postsynaptic sites, and it is shielded from the surrounding neuropil by a glial sheath (see Kremer et al., 2017; Schürmann, 2016). There is some

structure, however, in that KC subtypes cluster together to form peduncular zones that can be seen in cross-sections (see Perisse et al., 2013b; Tanaka et al., 2008).

In *Drosophila* larvae and locusts, KC–KC axo-axonic *en passant* chemical synapses have been found (Eichler et al., 2017; Leitch et al., 1996), but it is not yet clear if these synapses also exist in adult *Drosophila*.

MB lobes and KC subtypes

Near the anterior front, the peduncle splits into two lobes at a site called the junction: a vertical lobe extending to the dorsal top of the brain, and a horizontal lobe extending all the way to the midline. These distinct lobes form the basis of KC subtypes and align well with the MB's role in appetitive and aversive memory formation and expression. The subdivision between γ, α/β lobes, and the α′ lobe was first described by Heisenberg (1980). The final five lobe structure was described by Crittenden and Skoulakis (1998), with finer subdivisions suggested later (Aso et al., 2014a; Lin et al., 2007; Tanaka et al., 2008). Figure 1.2 shows a simplified image of MB anatomy and PN projections.

All KC axons contain several *en passant* presynaptic terminals from junction to lobe tip (Aso et al., 2014a; Cohn et al., 2015; Eichler et al., 2017; Takemura et al., 2017). KCs synapse mostly onto MBONs, but also onto APL and DPM neurons, as well as DANs and other KCs (Eichler et al., 2017; Takemura et al., 2017). Besides chemical synapses, KCs may also form gap junctions between each other and with MBONs (Liu et al., 2016).

γ lobe. The anterior side of the horizontal lobe (near the brain surface) forms the γ lobe, and consists of the axons of around 675 γ KCs, that can be further divided into 600 γ main (γm), and 75 γ dorsal (γd) neurons (Aso et al., 2014a). γd neurons form a special subgroup that receives visual information from the ventral accessory calyx (vACA), and projects solely to the dorsal region of the γ lobe. γ KCs are the only KCs that only extend into the horizontal lobe. Early branching off laterally from the peduncle results in the γ1 region, also called the heel (Aso et al., 2014a; Crittenden and Skoulakis, 1998).

α/β lobes. α/β KCs each have a bifurcated axon in the horizontal lobe and in the vertical lobe. The horizontal part, the β lobe, lies posterior and ventrally adjacent to the γ lobe, with its tip in close vicinity to the ellipsoid body (EB). The vertical part, the α lobe, extends straight from the junction to the dorsal end of the brain, with its tip at the surface of the brain. Based on anatomical differences, these neurons can be further subdivided into α/β core (α/βc), α/β surface (α/βs), and α/β posterior (α/βp) neurons. Axons from the ∼ 400 α/βc neurons form the innermost layer of the α/β lobes, surrounded by the axons of the ∼ 500 α/βs neurons, which may be functionally segregated (Perisse et al., 2013b). There may be further anatomical/functional subdivisions into inner and outer core neurons (Takemura et al., 2017; Tanaka et al., 2008), although such subdivision is not universally accepted (Aso et al., 2014a). The ∼ 75–90 α/βp neurons receive visual input from the dorsal accessory calyx (dACA) and project into specific regions of the α and β lobes (Aso et al., 2014a; Takemura et al., 2017).

α′/β′ lobes. α′/β′ KCs also have bifurcated axons in the horizontal and the vertical lobes. The horizontal part, the β′ lobe, also lies posterior to the γ lobe, and dorsal of the β lobe, with the tip of the β′ lobe in close vicinity to the EB. The vertical part, the α′ lobe, wraps around the α lobe such that it traverses from dorsal–medial near the heel to medial–posterior midway to lateral at its tip. α′/β′ KCs have been recently further subdivided into ∼ 210 α′/β′ap neurons and ∼ 140 α′/β′m neurons based on the specific innervation in the β′2 compartment (Aso et al., 2014a).

1.2.3 Odour processing in the MB

Odour information is thus passed on from specific ORNs to odour-specific glomeruli with single-glomeruli innervating PNs in a labelled-line manner. This labelled line is then broken up by the random convergence of PN boutons with KC postsynaptic claws in the calyx (Caron et al., 2013; Gruntman and Turner, 2013).

KCs need to receive signals from multiple claws in order to start spiking (Gruntman and Turner, 2013), which may explain why any given odour elicits

responses in only ∼ 5–10 % of KCs (Honegger et al., 2011; Ito et al., 2008; Perez-Orive et al., 2002; Turner et al., 2008; Wang et al., 2001).

Further mechanisms for such a sparse KC odour activity include GABAergic feedback from APL (Lin et al., 2014a), oscillatory activity of PNs (Cassenaer and Laurent, 2007; Tanaka et al., 2009), and unusual channel conductances that support sparseness (Demmer and Kloppenburg, 2009).

At the same time, odour intensity coding in the MB is largely lost (Gruntman and Turner, 2013; Turner et al., 2008; Wang et al., 2001), presumably by GABAergic feedback from APL that serves as gain control (Lin et al., 2014a; Stopfer, 2014). Furthermore, APL activity serves to decorrelate KC odour activity to maintain specificity of olfactory memories (Lin et al., 2014a).

This arrangement of random sparse activity with gain control, tonic inhibition, oscillatory activation, and intrinsic KC properties has been suggested as ideal for the efficient representation of high dimensional stimuli like odours, and to offer computational benefits for synaptic plasticity (Jortner et al., 2007; Laurent, 2002; Stopfer, 2014).

Indeed, it was recently causally shown that sparse KC activity can serve as a CS by Vasmer et al. (2014). The authors thermogenetically activated a sparse KC subset during aversive reinforcement, and observed flies subsequently avoiding thermogenetic reactivation.

1.2.4 MB compartmentalisation

Based on the discrete MB innervation patterns of DANs (chapter 1.3) and MBONs (chapter 1.4), each MB lobe forms several compartments. The γ lobe has five compartments (γ1–5), α and α′ lobes each have three compartments (α1–3, α′1–3), while β and β′ lobes each have two compartments (β1–2, β′1–2), which are numbered upwards from the MB heel towards midline/dorsal end (Aso et al., 2014a; see also Figure 1.3A and Table 1.1).

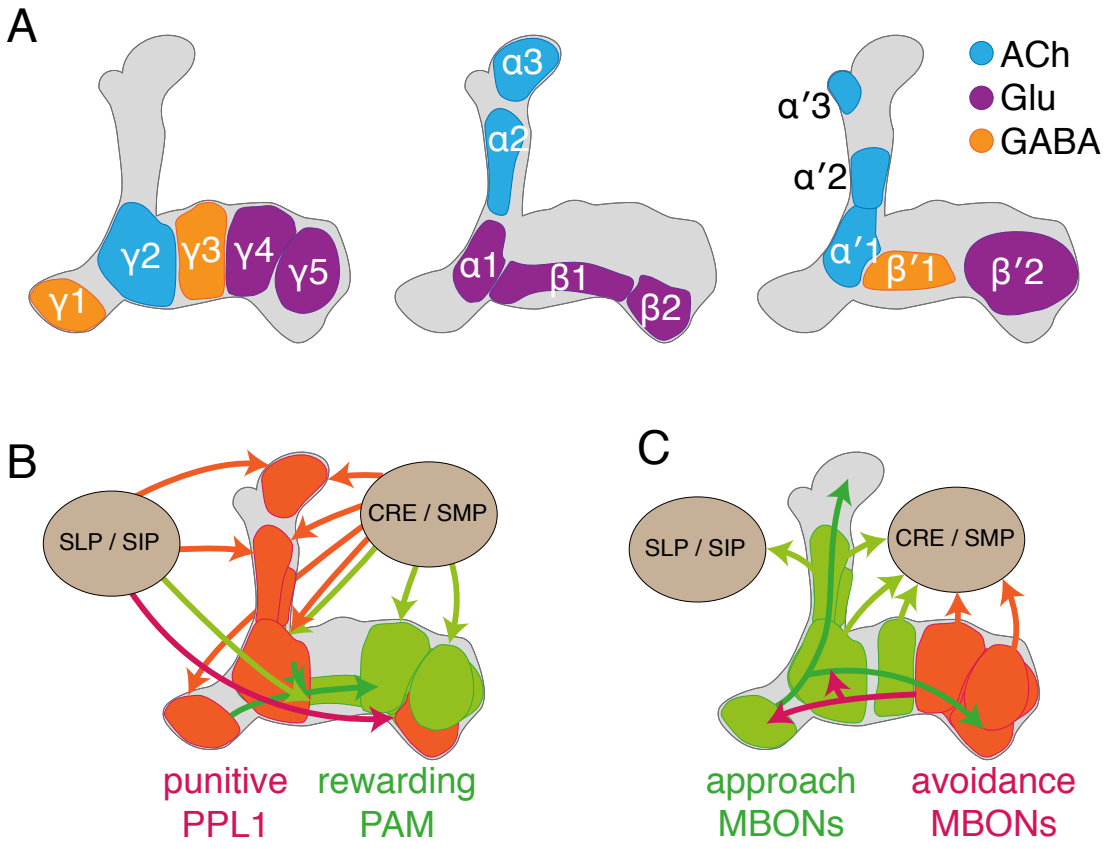


Figure 1.3: MB compartments and MBON/DAN innervation. A) The MB contains 15 discrete compartments, that are each innervated by specific MBONs and DANs. There are three classes of MBONs using either ACh (blue), Glu (purple), or GABA (orange) as neurotransmitters. The γ lobe contains five compartments (γ1-5), the α lobe three (α1-3), the β lobe two (β1-2), the α′ lobe three (α′1-3), and the β′ lobe two (β′1-2). B) Punishment-coding PPL1 DANs largely occupy the vertical lobe, and receive inputs from superior lateral protocerebrum (SLP), superior intermediate protocerebrum (SIP), the crepine (CRE), and the superior medial protocerebrum (SMP). Reward-coding PAM DANs largely occupy the horizontal lobe, and receive most input from SMP and CRE. C) Approach-coding MBONs are largely cholinergic and occupy the vertical lobe and γ1-3. They project into SLP, SIP, CRE, and SMP. Avoidance-coding MBONs are glutamatergic and occupy the tip of the horizontal lobe. They mostly project into SMP and CRE. Adapted from Aso et al. (2014a) and Felsenberg and Waddell (2017).

Table 1.1: MB compartments and corresponding DANs and MBONs. Nomenclature by Tanaka et al. (2008) is used where available, with nomenclature by Aso et al. (2014a) included in brackets. Note that α/β lobes include surface (s), core (c), and posterior (p). The β′2 compartment has three subcompartments: anterior (a), medial (m), and posterior (p). 'MBON TM' refers to MBON transmitter.

Compartment	DAN(s)	MBON(s)	MBON TM
gamma 1	MB-MP1 (PPL1-γ1pedc); PPL1-γ1	MB-MVP2 (MBON-γ1pedc>α/β)	GABA
gamma 2	MB-MV1 (PPL1-γ2α′1)	MBON-γ2α′1	ACh
gamma 3	PAM-γ3	MBON-γ3β′1; MBON-γ3	GABA
gamma 4	PAM-γ4<γ1γ2; PAM-γ4	MBON-γ4>γ1γ2	Glu
gamma 5	PAM-γ5	MB-M6 (MBON-γ5β′2a)	Glu
alpha 1	PAM-α1	MBON-α1	Glu
alpha 2	MB-V1 (PPL1-α′2α2)	MBON-α2p3p; MB-V2α (MBON-α2sc)	ACh
alpha 3	PPL1-α3	MB-V3 (MBON-α3)	ACh
beta 1	PAM-β1ped; PAM-β1	MB-MV2 (MBON-β1>α)	Glu
beta 2	PAM-β2β′2a; PAM-β2	MB-M4β (MBON-β2β′2mp)	Glu
alpha' 1	MB-MV1 (PPL1-γ2α′1)	MBON-γ2α′1; MBON-α′1	ACh
alpha' 2	MB-V1 (PPL1-α′2α2)	MB-V4 (MBON-α′2)	ACh
alpha' 3	PPL1-α′3	MB-V2α′ (MBON-α′3ap; MBON-α′3m)	ACh
beta' 1	PAM-β′1 ap; PAM-β′1 m	MBON-β′1; MBON-γ3β′1	GABA
beta' 2	PAM-β′2a; PAM-β2β′2a	MB-M6 (MBON-γ5β′2a)	Glu
	PAM-β′2m; PAM-β′2p	MB-M4β′ (MBON-β′2mp);	Glu
		MB-M4β (MBON-β2β′2mp);	Glu
		MBON-β′2mp_bilateral	Glu

1.3 Dopamine, the unconditioned stimulus (US), and memory formation

Valence can be attached to environmental representations of sparse KC activity by dopaminergic neurons (DANs) that target specific MB compartments and modulate the KC → MBON synapse (Aso et al., 2014a, 2012; Burke et al., 2012; Huetteroth et al., 2015; Owald and Waddell, 2015).

Dopamine has long been known to be involved in mammalian reinforcement learning and reward prediction (Maia, 2009; Schultz et al., 1997). It is synthesised by tyrosine hydroxylase (TH) which converts tyrosine to L-3,4-dihydroxyphenylalanine (L-DOPA), which is then converted to dopamine by dopamine decarboxylase (DDC).

1.3.1 DAN anatomy

The MB is innervated by 20 types of DANs, each innervating one of the 15 MB compartments (Aso et al., 2014a; see Table 1.1 and Figure 1.3B). They fall into

two clusters: paired posterior lateral 1 (PPL1) DANs that have 1–2 cell bodies per type and mostly target the vertical MB lobe, and paired anterior medial (PAM) DANs with up to 23 cell bodies per type targeting mostly the horizontal MB lobe (Aso et al., 2014a; Burke et al., 2012; Huetteroth et al., 2015; Mao and Davis, 2009; Riemensperger et al., 2005). Their dendrites mostly occupy SLP, SIP, SMP, and CRE (Aso et al., 2014a).

In the following, I will follow the DAN and MBON nomenclature suggested by Tanaka et al. (2008) for ease of reading, except in cases that were not described by Tanaka et al. (2008) or for those that were described ambiguously (as is the case for most PAM neurons), for which I will follow the nomenclature used by Aso et al. (2014a).

1.3.2 PPL1 DANs convey aversive reinforcement

A requirement for DANs in *Drosophila* olfactory conditioning was first demonstrated by Schwaerzel et al. (2003) who showed that blocking (mostly PPL1) DANs contained in TH-GAL4 (Friggi-Grelin et al., 2003) impaired aversive learning. Such a role was later confirmed by finding DAN calcium responses to electric shocks (Mao and Davis, 2009; Riemensperger et al., 2005), and by substituting the US with optogenetic stimulation of TH-GAL4 DANs (Claridge-Chang et al., 2009; Schroll et al., 2006). Later studies using more specific driver lines demonstrated a role in aversive reinforcement specifically for PPL1 DANs MB-MP1, MB-MV1, MB-V1, and PPL1-α3, but with differential temporal involvement (Aso et al., 2012; Aso and Rubin, 2016; Aso et al., 2010). Besides PPL1, some PAM DANs may also play a role in aversive reinforcement, namely MB-M3 (contained in TH-GAL4) and PAM-γ3 (Aso et al., 2010; Yamagata et al., 2016).

Electric shock stimulation reaches PPL1 DANs through yet unknown pathways but is thought to involve nociceptive streams that terminate in the PPL1 dendritic neuropils CRE, SMP, SIP, SLP (Aso et al., 2014a). *pyrexia* mutants were shown to be mildly impaired in shock reinforcement, suggesting a potential role for this gene in the aversive pathway (Galili et al., 2014).

Aversive STM formation

Aversive memory formation relies on coincident activity of KCs and PPL1 DANs that results in subsequent decreased presynaptic strength between KCs and MBONs (Aso et al., 2010; Hige et al., 2015a; Owald and Waddell, 2015; Schwaerzel et al., 2003; Séjourné et al., 2011).

Memory acquisition depends on DopR1 receptors in γ (and α/β) KCs (Kim et al., 2007; Qin et al., 2012), even though KC synaptic output does not seem to be required at this time (Dubnau et al., 2001; McGuire et al., 2001; but see Ichinose et al., 2015). This suggests presynaptic plasticity mechanisms that are largely independent from downstream activation (see Hige et al., 2015a). These mechanisms are not yet fully understood, but seem to largely rely on the cAMP pathway in KCs, involving several memory genes (see also 1.1.3, and McGuire et al., 2005 for review).

Coincident Ca^{2+} influx by KC odour activation and DopR1-mediated G(o) signalling may activate the adenylyl cyclase (AC) *rutabaga* that converts ATP into cAMP (Boto et al., 2014; Ferris et al., 2006; Levin et al., 1992; McGuire et al., 2003; Tomchik and Davis, 2009). cAMP activates a protein kinase (PKA, with its catalytic subunit DC0) that phosphorylates further targets and ultimately induces synaptic plasticity through pathways not yet fully understood (Boto et al., 2014; Skoulakis et al., 1993). A phosphodiesterase (*dunce*) terminates this process by converting cAMP to AMP (Byers et al., 1981; Gervasi et al., 2010).

It is not entirely clear how DAN activity modulates KC synapses, but MBON activity is decreased after a paired coupling (Cohn et al., 2015; Hige et al., 2015a), in line with G(o) signalling depressing KC presynaptic activity (Zhang and Roman, 2013). Interestingly, unpaired KC and DAN activation may lead to synaptic facilitation (Cohn et al., 2015; Hige et al., 2015a).

Aversive MTM and LTM

Memory consolidation into longer-lasting forms of memory requires further MB neural circuitry and molecular mechanisms.

MTM formation requires α′/β′ KCs (Cervantes-Sandoval et al., 2013; Krashes et al., 2007) that take part in a consolidation feedback loop with DPM/APL (Keene et al., 2006; Lee et al., 2011; Pitman et al., 2011; Wu et al., 2011). Serotonergic DPM and GABAergic APL neurons consist of only one cell body per hemisphere but densely innervate all MB lobes (Lee et al., 2011; Liu and Davis, 2009; Pitman et al., 2011; Tanaka et al., 2008; Waddell et al., 2000; Wu et al., 2011; Yu et al., 2005). They are likely coupled with each other via gap junctions (Wu et al., 2011).

LTM formation requires neuronal remodelling in α/β KCs, MBONs and DAL neurons, partly based on CREB-mediated signalling (from PKA), that involves widespread transcriptional and translational regulation, and posttranslational modifications (Akalal et al., 2010; Chen et al., 2012; Crocker et al., 2016; Dubnau et al., 2003; Hirano et al., 2013; Perazzona et al., 2004; Yin et al., 1994; Yu et al., 2006). This effort seems heavily gated so that it is only elicited by specific training protocols (Plaçais et al., 2013a, 2012, 2017).

1.3.3 PAM DANs convey appetitive reinforcement

Insect appetitive reinforcement has classically been attributed to octopaminergic neurons (OANs), based on work in honey bees and *Drosophila* (Hammer, 1993; Schroll et al., 2006; Schwaerzel et al., 2003). Octopamine (OA) is synthesised from tyrosine by tyrosine decarboxylase (encoded by Tdc2), resulting in the functional neurotransmitter tyramine (Bayliss et al., 2013; see 3.1.1). Tyramine is then converted to OA by the action of tyramine β-hydroxylase (TβH) (Monastirioti et al., 1996). It was only recently shown that sugar reward relies on OANs that, in turn, act on PAM DANs to positively reinforce odours in the MB (Burke et al., 2012; Liu et al., 2012), suggesting that presynaptic plasticity at KCs is mediated by dopamine for both appetitive and aversive memory formation (Waddell, 2013).

Depending on the state of the fly, other stimuli can also serve as positive reinforcers, among them water (Lin et al., 2014b; Shyu et al., 2017), ethanol (Kaun et al., 2011), amino acids (Schleyer et al., 2015; Toshima and Tanimura, 2012), salt

(Niewalda et al., 2008), and pain relief (Perisse et al., 2013b; Tanimoto et al., 2004; Yarali et al., 2008), many of which rely on different PAM subsets.

Appetitive STM formation

The acquisition of appetitive STM relies on the activity of sweetness-coding octopaminergic neurons (Schwaerzel et al., 2003) that act on dopaminergic neurons of the PAM cluster (Burke et al., 2012; Liu et al., 2012) via octopamine receptors Octβ2R and Oamb (Burke et al., 2012). Specifically, activity of PAM-β′2am and PAM-γ4 seems required to form appetitive STM (Huetteroth et al., 2015).

Similar to aversive STM acquisition, PAM DANs also act on (γ) KC-expressed DopR1, and G(o) signalling likely activates a *rutabaga* AC that, in turn, elicits a cAMP signalling cascade (Burke et al., 2012; Cervantes-Sandoval et al., 2013; Cohn et al., 2015; Kim et al., 2007; Liu et al., 2012; Madalan et al., 2011; Tomchik and Davis, 2009; Trannoy et al., 2011).

Appetitive MTM and LTM

Longer-lasting forms of appetitive memory require the intake of calories from sugars, in contrast to mere sugar sweetness (Burke and Waddell, 2011). Sugar nutrient information may be mediated by the fructose-sensing Gr43a onto PAM-α1 neurons (Freeman et al., 2014; Fujii et al., 2015; Miyamoto et al., 2012; Yamagata et al., 2015). Other PAM neurons such as PAM-γ5b, PAM-β2, and PAM-β1 also likely play a role in nutrient reinforcement (Huetteroth et al., 2015; Ichinose et al., 2015; Shyu et al., 2017; Yamagata et al., 2015).

The consolidation of appetitive memories has been suggested to depend on three processes whose interactions are currently unclear: (1) The activity of α′/β′ KCs along with DPM and APL neurons is required during the first hour after training (Keene et al., 2006; Krashes et al., 2007; Krashes and Waddell, 2008; Pitman et al., 2011; Trannoy et al., 2011). This involves dCreb2-b, *rutabaga*, as well as *crammer*, *tequila*, and *radish* in α/β KCs (Krashes and Waddell, 2008; Trannoy et al., 2011). (2) Gr43a-mediated sensing of hemolymph fructose levels may activate a PAM-α1 $\leftrightarrows$ MBON-α1 feedback loop (Ichinose et al., 2015). (3) The

consolidation process is possibly gated by PPL1 MP1 oscillatory activity acting on DAMB receptors in KCs (Musso et al., 2015).

1.4 MBONs mediate memory retrieval

As KCs convey the odour information (CS) to the MB lobes, and DANs reinforce these with reward or punishment (US), another class of neurons needs to read out these changes in synaptic strength to bias behaviour away from or towards the CS (see Heisenberg, 2003). These neurons are called MB output neurons (MBONs), and their roles in guiding learned behaviours have only recently been explored (Aso et al., 2014b; Hige et al., 2015a; Owald and Waddell, 2015; Séjourné et al., 2011), partly because of previously poor driver line access (until Aso et al., 2014a; Jenett et al., 2012). The chemical identity of this KC → MBON synapse has remained unknown until recently (Barnstedt et al., 2016; see chapter 3).

MBON anatomy and odour responses

There are 21 types of MBONs (found in Table 1.1, and in Figure 1.3C), most of which innervate only one of the 15 MB compartments with a dense dendritic mesh (Aso et al., 2014a; Ito et al., 1998; Tanaka et al., 2008). From there they project mostly into neighbouring neuropils CRE, SMP, SLP, SIP, but some also make projections into other MB compartments, or further lateral in the protocerebrum, using either acetylcholine (ACh), glutamate (Glu), or GABA as neurotransmitters (Aso et al., 2014a; Tanaka et al., 2008). This compartmentalisation and innervation of neighbouring neuropils is similar to that seen by DANs (see 1.3), but with reversed polarity (Aso et al., 2014a; Felsenberg et al., 2017).

Besides these three main classes of MBONs, some have yet unknown neurotransmitters, namely MBON-γ1γ2, MBON-γ4γ5, as well as the atypical MB-CP1 (MBON-calyx) and MB-CP2 that innervate calyx and peduncle(Aso et al., 2014a; Tanaka et al., 2008; Zheng et al., 2017).

Most MBONs broadly respond to a wide range of odours as can be expected from fourth-order olfactory neurons (Hige et al., 2015b). In contrast to sparse and

decorrelated KC odour coding (Campbell et al., 2013; Lin et al., 2014a), MBON odour tuning was found to be widely correlated across odours (Hige et al., 2015b), demonstrating that MBONs do not code naïve odour identity, but rather the learned valence of an odour (see Aso et al., 2014b; Owald and Waddell, 2015).

1.4.1 A specific group of MBONs mediates aversive memory retrieval

Vertical lobe MBONs were found to play a role in aversive memory retrieval, in line with their innervation of MB compartments that are also occupied by aversively reinforcing PPL1 DANs (see 1.3.2). Specifically, cholinergic V2 and V4 neurons are broadly required for the retrieval of STM, ASM, ARM, and LTM (Aso et al., 2014b; Bouzaiane et al., 2015; Séjourné et al., 2011). In line with the STM requirements for MP1 (Aso et al., 2012; Hige et al., 2015a), its respective MBON MVP2 is required for aversive STM retrieval (Aso et al., 2014b; Perisse et al., 2016). Aversive (f)LTM, on the other hand, relies on V3 neurons (Pai et al., 2013; Plaçais et al., 2013b). Perhaps surprisingly, M4/6 MBONs of the horizontal lobe are also required for aversive STM retrieval, and M6 neurons also for ARM and LTM retrieval (Bouzaiane et al., 2015; Owald et al., 2015a).

As memory retrieval depends on the KC → MBON synapse, γ, α/β, and α′/β′ KC output is required for aversive STM retrieval (Bouzaiane et al., 2015; Cervantes-Sandoval et al., 2013; Dubnau et al., 2001; Isabel et al., 2004; McGuire et al., 2001). MTM and LTM retrieval, on the other hand, largely depend on α/β(s) KC output (Bouzaiane et al., 2015; Cervantes-Sandoval et al., 2013; Isabel et al., 2004; Krashes et al., 2007; McGuire et al., 2001; Perisse et al., 2013b; Xie et al., 2013; Yang et al., 2016a), and maybe that of γ KCs (Bouzaiane et al., 2015; Xie et al., 2013) and that of α′/β′ KCs (Yang et al., 2016a).

1.4.2 A complementary group of MBONs mediates appetitive memory retrieval

Conversely to the vertical lobe, the horizontal lobe contains the terminals of rewarding DANs (Burke et al., 2012; Huetteroth et al., 2015), and its MBONs

are largely required for the retrieval of appetitive memories (Aso et al., 2014b; Felsenberg et al., 2017; Owald et al., 2015a). Specifically, glutamatergic M4/6 neurons are required for appetitive STM, MTM and LTM retrieval (Aso et al., 2014b; Owald et al., 2015a). Appetitive MTM and LTM retrieval also depends on the glutamatergic MBON-α1 (Aso et al., 2014b; Ichinose et al., 2015).

However, besides these PAM-innervated MBONs, MBONs of the vertical lobe also play a necessary role in appetitive memory retrieval: MVP2 is required for STM, MTM, and LTM, and MBON-γ2α′1 is required at least for MTM (Felsenberg et al., 2017; Perisse et al., 2016). Furthermore, cholinergic MBONs V2, V3, and V4 may also be involved (Aso et al., 2014b; Plaçais et al., 2013b). This suggests that large parts of the MBON ensemble need to act together for correct memory retrieval (see Owald and Waddell, 2015).

Appetitive memory retrieval also requires flies to be hungry (Tempel et al., 1983) – a state that is mediated by dNPF signalling onto MP1 (Krashes et al., 2009; Wu et al., 2005b). How the associated MVP2 MBON can mediate hunger-dependent memory retrieval has remained unknown (until Perisse et al., 2016), but will be further discussed in chapter 5.

1.4.3 Olfactory conditioning depresses KC → MBON synapses

How does olfactory conditioning change MBON responses? Odour-evoked calcium responses in V2 and MVP2 MBONs are reduced after aversive conditioning or artificial PPL1 DAN–odour pairing (Hige et al., 2015a; Séjourné et al., 2011). Similarly, odour-evoked calcium responses in M4/6 neurons and MBON-γ4>γ1γ2 are significantly depressed after appetitive training or artificial PAM–odour pairing (Cohn et al., 2015; Owald et al., 2015a). This suggests that instead of presynaptic facilitation (such as in *Aplysia*, see Byrne and Kandel, 1996), coincident CS–US activity actually results in presynaptic depression of KCs (see Owald and Waddell, 2015).

In line with these findings, PPL1-innervated MBONs actually induce naïve approach when artificially activated, whereas PAM-innervated MBONs induce naïve

avoidance (Aso et al., 2014b; Lewis et al., 2015). Similarly, blocking PAM-innervated M4/6 neurons during naïve avoidance tasks actually results in relative approach behaviours (Lewis et al., 2015; Owald et al., 2015a).

This means that punishment-coding PPL1 DANs can induce presynaptic depression at the KC → MBON synapse that subsequently leads to weakened approach, resulting in odour avoidance. Similarly, rewarding PAM DANs also induce presynaptic depression that leads to weakened avoidance, thus enhanced odour approach after training (see Owald and Waddell, 2015).

Yet, if DANs generally induce presynaptic depression, how can training-induced facilitation, observed in M4/6 and V3 neurons (Bouzaiane et al., 2015; Owald et al., 2015a; Plaçais et al., 2013b), be explained? The answer to this may be found in the GABAergic MVP2 neuron that projects into other MB compartments (see chapter 5; Aso et al., 2014a; Perisse et al., 2016; Tanaka et al., 2008).

1.4.4 A model for associative learning and memory in the MB

These findings lead to a model of MB-mediated associative learning in which the sparse and decorrelated activity of a subset of the thousands of KCs represents environmental stimuli (in *Drosophila* dominated by odours; the CS), to which positive or negative valence (US) can be attached by coincident activity of compartment-specific DANs (Owald and Waddell, 2015). This CS–US coincidence results in DopR1-mediated presynaptic depression of the compartment-specific KC → MBON synapse (Hige et al., 2015a; Owald and Waddell, 2015; Qin et al., 2012). The chemical nature of this synapse has remained unknown until recently (see chapters 3 and 4; Barnstedt et al., 2016). Subsequent encounters of the CS result in an imbalanced activation of the MBON network, with a skew towards the arm that did not undergo synaptic plasticity, thus biasing the fly's behaviour towards approach or avoidance (Owald and Waddell, 2015; see also Figure 1.4). For the retrieval of appetitive memories, flies need to be hungry, but it has been unclear how hunger state can affect MBON-mediated memory retrieval (see chapter 5; Perisse et al.,

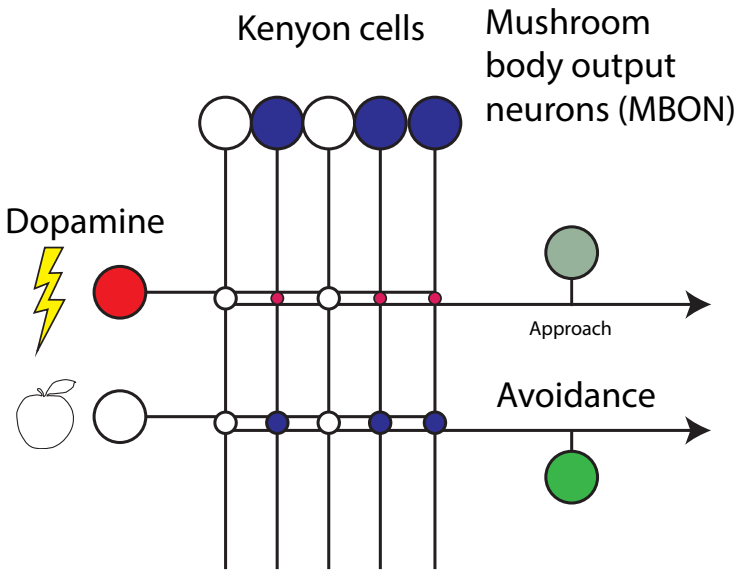


Figure 1.4: A simplified model of associative learning in the MB. Environmental stimuli such as odours (CS) are represented in the MB as activity in sparse subpopulations of KCs. Naïvely, these drive approach- and avoidance-coding MBONs equally. Coincident reinforcement of a CS through either punishment- or reward-coding DANs results in synaptic depression at the respective synapses. During retrieval, this depressed drive to the respective MBONs leads flies to approach or avoid a certain CS. Model based on Gerber et al., 2004; Owald and Waddell, 2015.

2016). The downstream targets of MBONs currently remain largely unknown, but the anatomy suggests an overlap with DAN dendrites (Aso et al., 2014a). Such potential feedback loops could play an important role in updating once established memories (see chapter 6; Felsenberg et al., 2017).

1.4.5 Research questions

In the context of my thesis research, I thus wanted to answer four questions that have remained open:

1. What is the fast-acting neurotransmitter of KCs? (chapter 3)
2. What is the role of KC-released neuropeptide sNPF and other potential co-transmitters? (chapter 4)
3. How does MVP2 exert influence over MB output pathways involved in appetitive memory retrieval? (chapter 5)

4. What are the neural circuit mechanisms that underlie memory extinction and reconsolidation? (chapter 6)

In the following, I will first present some background to the methods that I have used to tackle these questions.

1.5 Background to methods

1.5.1 *Drosophila* genetics and the GAL4/UAS system

Drosophila melanogaster

Drosophila melanogaster, or common fruit fly, is the name of a species of the order Diptera in the family Drosophilidae. It has been widely used as a model organism for biological research since at least the beginning of the last century, largely driven by the seminal work on genetics by Thomas Hunt Morgan (Morgan, 1915). *Drosophila melanogaster* offers several advantages compared to other experimental model organisms, mainly based on the ease of husbandry and genetic manipulations (Greenspan, 1997).

Drosophila melanogaster are relatively self-sufficient and require only small vials with a simple cornmeal-agar food mixture at the bottom from which they feed and lay eggs on and in which they can be kept over many generations. At 25 °C, the generation time from freshly laid egg via pupal stage to the emergence of an adult is about 9 days, although this may be prolonged with certain genetic manipulations (Greenspan, 1997).

Drosophila melanogaster only has four chromosomes, out of which one (X) is the sex chromosome and one (IV) is so small that it is often neglected. In order to avoid recombinations that could take out inserted transgenes, a wide variety of balancer chromosomes exists. Balancer chromosomes contain large areas of a given chromosome that are inverted and scrambled in a way that prevents recombination from occurring within these areas. Furthermore, male flies show no recombination even without the use of balancers. Balancer chromosomes as well as healthy chromosomes come with a wide variety of markers that affect appearance of

the eyes, wings, bristles, or other body parts. This makes it possible to keep track of transgenic insertions throughout many generations, as well as to maintain stable stocks that do not lose their transgenes over many years (Greenspan, 1997).

The GAL4/UAS system

Drosophila melanogaster has gained wider popularity in neurobiological research with the emergence of the GAL4/UAS system which allows the manipulation of targeted subsets of neurons by the simple crossing of a GAL4 driver fly with an upstream activating sequence (UAS) reporter fly (Brand and Perrimon, 1993; Fischer et al., 1988). GAL4 is a yeast regulatory protein that can be artificially expressed in a variety of tissues by inserting the *GAL4* region into a native promoter region or by attaching specific promoter regions upstream of the *GAL4* region (Brand and Perrimon, 1993; Fischer et al., 1988; Jenett et al., 2012; Kvon et al., 2014; Pfeiffer et al., 2008). Tdc2-GAL4 flies, for example, express GAL4 mostly in octopaminergic/tyraminergic neurons that inherently activate the *Tdc2* promoter to express tyrosine decarboxylase 2 (Busch et al., 2009). Yet, GAL4 expression does not always fully recapitulate the expression of the desired gene, as the case of TH-GAL4 demonstrates (see 1.3; Burke et al., 2012; Liu et al., 2012; Owald et al., 2015b). Flies with tissue-restricted GAL4 expression can subsequently be crossed to flies carrying a UAS-driven transgene. UAS-driven transgenes remain largely silent unless activated by the presence of GAL4 in any given cell, so that the progeny from a GAL4×UAS cross will show UAS-driven transgene expression only in cells also expressing GAL4 (Brand and Perrimon, 1993; see Figure 1.5A).

The GAL4/UAS system has proven extremely successful over the past years in allowing wide-ranging manipulations in very well-defined populations of cells (see review by Owald et al., 2015b). At this point, there exist $> 15,000$ GAL4 driver lines (Jenett et al., 2012; Kvon et al., 2014) that can be used to target specific groups of cells. At the same time, there are $> 50,000$ UAS reporter lines available at Bloomington Drosophila Stock Center (BDSC) and at Vienna Drosophila Resource Center (VDRC) together. Common tools for UAS reporter

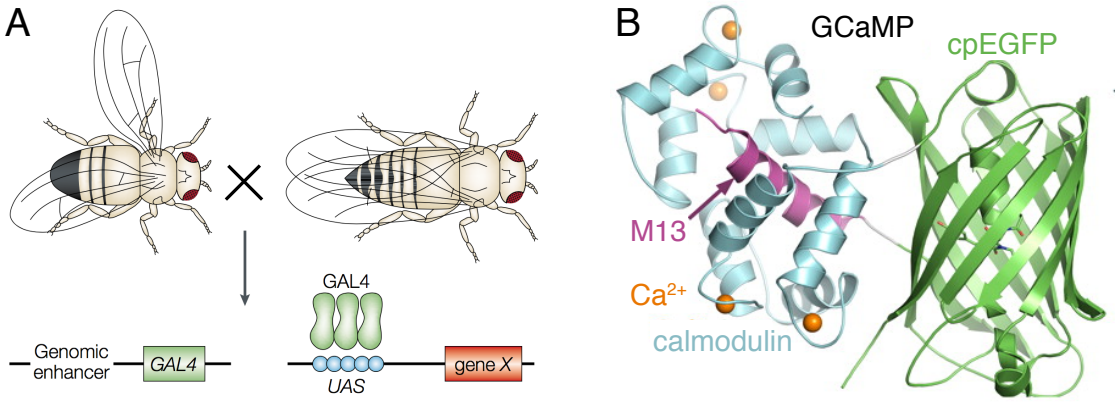


Figure 1.5: The GAL4/UAS system and GCaMP. A) The GAL4/UAS system allows tissue-specific transcription of various transgenes (Brand and Perrimon, 1993). A *GAL4* sequence is placed after a specific genomic enhancer, so that *GAL4* expression is limited to neurons where that enhancer is active. GAL4 is a transcription factor that enables transcription at upstream activating sequences (UAS) that are linked to transgenes. Adapted from Johnston, 2002. B) The calcium indicator GCaMP consists of a circularly permutated EGFP (cpEGFP) linked to calmodulin (CaM) and CaM-interacting M13 peptide. The CaM-M13 complex undergoes calcium-dependent conformational changes that, due to its proximity to the cpEGFP β-barrel, induce fluorescent increases of the cpEGFP upon increased [Ca^{2+}]. Adapted from Akerboom et al., 2009.

lines include various fluorescent proteins for anatomical visualisation (see 1.5.2; Shaner et al., 2005 and Rodriguez et al., 2017 for review), shi^{ts1} and *dTrpA1* for thermogenetic in/activation (Hamada et al., 2008; Kitamoto, 2001), calcium indicators (see 1.5.3; Chen et al., 2013a; Dana et al., 2016; Nakai et al., 2001), voltage indicators (see 1.5.3; Cao et al., 2013; Gong et al., 2015; Yang et al., 2016b), optogenetic in/activators (see 1.5.4; Klapoetke et al., 2014; Lima and Miesenböck, 2005; Mohammad et al., 2017), and RNA interference (see 1.5.5; Boutros and Ahringer, 2008; Dietzl et al., 2007; Ni et al., 2009).

Beyond GAL4/UAS

In addition, the GAL4/UAS system has also been refined and expanded by various tools. Gal80, for example, antagonises the action of GAL4 and can thus be used in combination with the GAL4/UAS system to restrict the original GAL4 expression (Lee and Luo, 1999). A temperature-sensitive variant also allows temporally precise induction of GAL4 (McGuire et al., 2003). To enable simultaneous use of two different driver lines in the same fly, the LexA/lexAop system has been developed

(Lai and Lee, 2006) which works similarly to but often independently from the GAL4/UAS system. There are currently $> 1,500$ LexA lines and > 150 lexAop lines at BDSC. This allows, for example, stimulation in one set of neurons while recording from another (Barnstedt et al., 2016; Kim et al., 2017). Using these two systems in combination with the FLP-FRT system can restrict expression to only the overlap between GAL4 and lexA driver lines (Golic and Lindquist, 1989; Perrat et al., 2013). Recently, the Q system has been introduced as a third independent driver/reporter system to add further combinatorial possibilities (Potter et al., 2010). As most driver lines normally express GAL4 in a variety of cells including undesired "ectopic" expression, a recent effort has sought to restrict GAL4 expression by generating splitGAL4 (Luan et al., 2006; Pfeiffer et al., 2010) variants from previously generated GAL4 enhancer fragments (Jenett et al., 2012), and combining two of these to induce functional GAL4 expression only at the intersection of the original two GAL4 lines (Aso et al., 2014a,b). This approach has allowed driver line access to be limited to individual neurons, ruling out possible effects from ectopic expression.

1.5.2 Fluorescent proteins and immunohistochemistry

GFP and fluorescent proteins

In order to visualise driver line expression, one can genetically express fluorescent proteins that are then transported throughout the cell or to specific compartments such as nucleus, cell membrane, or pre- and postsynaptic sites.

The first fluorescent protein (FP) to be described (Shimomura et al., 1962), cloned (Prasher et al., 1992), and artifically expressed in another organism (Chalfie et al., 1994) was green fluorescent protein (GFP; reviewed in Tsien, 1998). GFP was originally purified from the jellyfish *Aequorea victoria* where it was found to be most excited by light of wavelengths around 470 nm, while emitting light at about 510 nm (Shimomura et al., 1962; see Figure 1.5B). Fluorescence works by the photon-induced excitation of orbital electrons, and the subsequent fluorescent emission of photons of a longer wavelength as the electron relaxes to its ground

state (Lakowicz, 2006). This shift to longer wavelength light being emitted from fluorophores is called Stokes' shift.

As the original GFP suffered from various drawbacks such as two excitation peaks, pH sensitivity, and poor quantum yield, several variants with improved properties have soon been synthesised (Tsien, 1998). Most widely used today is probably Enhanced GFP (EGFP; Cormack et al., 1996), although brighter variants and new fluorescent proteins with enhanced characteristics appear in a fast cycle (e.g. Shaner et al., 2013; Shearin et al., 2014). At this point, countless fluorescent proteins cover the entire range of light from 350 nm to 700 nm with their excitation spectra (Rodriguez et al., 2017).

As GFP and other FPs are genetically expressed by the respective cells, these can also be fused to specific proteins that allows intracellular localisation of these proteins (reviewed in Sivanantharajah and Zhang, 2015). Frequently, GFP is fused to cell membrane markers such as mouse lymphocyte marker mCD8 (Lee and Luo, 1999) or targeted to the membrane by myristoylation (Pfeiffer et al., 2010; Resh, 1999). In order to resolve neuronal polarity, DenMark, an ICAM5-mCherry fusion, can be used to resolve dendritic compartments (Nicolaï et al., 2010), and presynaptic protein fusions Syt I-GFP or GFP-Syd-1 for presynaptic terminals (Li et al., 2014; Robinson et al., 2002). Similarly, specific receptors or receptor subunits can be tagged with GFP and subsequently visualised to infer endogenous protein expression, for example with the nicotinic acetylcholine receptor (nAChR) subunit Dα7 (Leiss et al., 2009). To label the cell nucleus, RedStinger can be used – a red fluorescent protein (RFP) with a nuclear localisation signal (NLS) that causes it to stay and accumulate inside the cell nucleus (Barolo et al., 2004).

Genetic fluorescent labelling is often combined with immunohistochemistry (IHC) to increase the fluorescent signal or to validate genetic expression of FPs (see 1.5.2).

Calcium indicators

Fluorescent proteins can also be used to detect changes of neural activity in live brains. Calcium indicators are a useful tool for this because of the close

correlation of [Ca^{2+}] with neural activity and the power of current indicators to report [Ca^{2+}] changes.

At rest, most neurons have a [Ca^{2+}] of about 50 to 100 nM that can briefly rise to levels 10–100 times higher upon electrical activity. There are many sources of this Ca^{2+} influx into the cytosol: voltage-gated calcium channels (VGCCs), calcium-permeable AMPA receptors, NMDA receptors, nAChRs, TRPC, and internal Ca^{2+} stores in the endoplasmic reticulum (ER) and mitochondria (reviewed in Grienberger and Konnerth, 2012).

In parallel to the optical developments described earlier, calcium indicators have also steadily improved over the last decades. The earliest Ca^{2+} indicators were the protein aequorin and the chemical dye arsenazo III (Brown et al., 1975; Shimomura et al., 1962), followed by the development of further fluorescent dyes such as fura-2 and Oregon Green BAPTA (Grynkiewicz et al., 1985; Lin et al., 1999). A breakthrough was the development of genetically-encoded calcium indicators (GECIs) based on GFP, the first of which included the FRET reporter cameleon (Miyawaki et al., 1997) and the single-GFP GECI G-CaMP (Nakai et al., 2001). GECIs have the advantage that they allow the chronic, noninvasive imaging of genetically defined cells and compartments (Mao et al., 2008), and can be fused to pre- or postsynaptic proteins (see Cohn et al., 2015; Pech et al., 2015). G-CaMP, in particular, has since then undergone several iterations of improvements to its properties, achieved by screening random or guided mutations to the original G-CaMP or later versions: GCaMP2 saw drastic increases in brightness, SNR and thermal stability (Tallini et al., 2006). GCaMP3 saw again increases in brightness as well as in its dynamic range (Tian et al., 2009), while G-CaMP4.1 remained largely uncharacterised (Shindo et al., 2010). GCaMP5 improved the SNR at least 2- to 3-fold (Akerboom et al., 2012). GCaMP6 comes in three "flavours", all of which have improved brightness compared to GCaMP5, but differ in their kinetics from slow(s) to medium(m) to fast(f): GCaMP6s has improved Ca^{2+} affinity and is even brighter than EGFP, while GCaMP6f has rapid kinetics that allow it to track single sensory events (Chen et al., 2013a).

The original G-CaMP uses a circularly permutated EGFP (cpEGFP) linked to calmodulin (CaM) and CaM-interacting M13 peptide (Nakai et al., 2001; see Figure 1.5B). The CaM-M13 complex undergoes calcium-dependent conformational changes that, due to its proximity to the cpEGFP β-barrel, induce fluorescent increases of the cpEGFP upon increased [Ca^{2+}] (Chen et al., 2013a). The Ca^{2+} concentration measured through indicators is only the "tip of the iceberg" because most of the Ca^{2+} entering the cytoplasm is bound by cytosolic buffers like parvalbumin, calbindin, or calretinin (Berridge et al., 2000).

As shorter wavelengths in the green spectrum are more prone to scatter around brain tissue, probes with longer wavelengths should be able to yield more signal from deeper brain regions. Furthermore, to correlate activity of two different (spatially overlapping) neural populations in real time, dual-colour calcium imaging would be required with an additional wavelength spectrum other than GFP. To achieve this, progress has been made recently to create red GECIs with similar properties to GCaMP6, allowing comparable sampling of green and red channels required for dual colour calcium imaging (Akerboom et al., 2013; Dana et al., 2016; Green et al., 2017; Inoue et al., 2015).

Other indicators of neural activity

Because [Ca^{2+}] is only a coarse indicator of neural activity compared with voltage changes observed through patch-clamp electrophyiosology, efforts have been undertaken to generate genetically encoded voltage indicators (GEVIs) (Akemann et al., 2010; Perron et al., 2009). So far, most of these, however, suffer from very low SNR and require elaborate camera systems with high sensitivity at high acquisition rates. Nonetheless, the latest generation of GEVIs shows promise in becoming an equal or in some regards even superior partner to GECIs (Gong et al., 2015; Yang et al., 2016b).

Besides calcium and voltage, other fluorescent sensors are also able to report [Cl^{-}] (Grimley et al., 2013), [Mg^{2+}] (Lindenburg et al., 2013), [cAMP] (Shafer et al., 2008), or synaptic vesicle release (Miesenböck et al., 1998), among others. Many

of these, however, are FRET sensors that require simultaneous recording of two fluorescent emission channels (mostly CFP and YFP).

Immunohistochemistry

Immunohistochemistry (IHC) allows the fluorescent labelling of proteins in a fixed tissue with the use of specific antibodies. This process mostly involves the sequential incubation of the tissue with first a primary antibody (AB) that attaches to the antigen, followed by a secondary AB carrying a fluorophore that attaches to the primary AB (Alberts et al., 2014; Coons et al., 1941; Nelson and Cox, 2013).

Primary AB sera can contain either polyclonal antibodies or monoclonal ABs, mostly of the immunoglobulin G (IgG) type. Polyclonal ABs are produced by various B lymphocytes and bind various epitopes of a given antigen. Monoclonal ABs, in contrast, are produced by identical B lymphocytes and only bind to one specific epitope (Alberts et al., 2014; Nelson and Cox, 2013). While monoclonal ABs are thus more specific and give a smaller likelihood of a false positive, their usefulness depends strongly on the accessibility of the specific epitope in the specimen, and may thus increase the chance of a false negative (Alberts et al., 2014).

Primary ABs are raised by injecting a purified antigen into a host species such as rabbit, mouse, rat, chicken, hamster, guinea pig, goat, or donkey. B lymphocytes of the animal's immune system then produce ABs which are contained in an antiserum extracted from the animal's blood. These antisera can then be further purified (Alberts et al., 2014; Nelson and Cox, 2013). Primary ABs can be combined to label different epitopes in a tissue with different colours, so long as the host species are different. This can be useful in *Drosophila* brains to introduce a background staining like α-Brp or α-N-Cadherin which labels the whole brain neuropil (Iwai et al., 1997; Wagh et al., 2006), and thus allows orientation of the main staining results along major landmarks as well as for registration purposes (see Aso et al., 2014a; Manton et al., 2014b; Milyaev et al., 2012).

As most primary ABs are unconjugated, fluorophore-conjugated secondary ABs that bind to IgG binding sites are mostly added in a second step. This step

not only allows visualisation of an unconjugated primary AB but also amplifies the original tagging as multiple secondary ABs will bind to a single primary AB. Importantly, the secondary AB needs to specifically match the IgG of the host species in which the primary AB was raised in. For fluorescent visualisation of the antigen, secondary ABs are often conjugated to a chemical fluorophore, such as Alexa Fluor™ dyes that range in their spectra from 350 nm to 790 nm (Alberts et al., 2014; Wu and Luo, 2006).

With the advent of confocal microscopy (see chapter 1.5.3), *Drosophila* brains no longer need to be sectioned for imaging, and can be directly fixed in paraformaldehyde (PFA) after dissection to stabilise the tissue. Due to their small volume, whole brains are penetrated even by large antibodies within one to two days at 4 °C. After incubation, they can be wholly cleared using clearing agents such as VectaShield (Wu and Luo, 2006). In order to reduce the time required for classical antibody stainings in *Drosophila* brains, chemical staining procedures have recently been introduced that, in many cases, can yield similar results in just 1 % of the time (Kohl et al., 2014).

1.5.3 Imaging neurons

Epi-fluorescence microscopy

Fluorescence can be captured in various ways, based on the general principle that fluorophores are excited only by a certain spectrum of light while emitting light of a longer wavelength (see chapter 1.5.2). One simple setup of a fluorescent microscope would take a white light source with a broad spectrum that is narrowed down by an excitation filter (e.g., to blue light) before being reflected by a dichroic mirror which reflects the excitation wavelength. The excitation light is then targeted through an objective onto the specimen where fluorophores emit longer wavelength light (e.g., green), which is again funneled through the objective, passes through the dichroic mirror and through an emission filter before entering a tube lens and eyepiece, a camera, and/or another detector (Kubitscheck, 2017; Spring and Davidson, 2016).

Light sources

There are different ways to create high-power excitation illumination, most notably arc lamps, LEDs, or laser light. Arc-discharge lamps burn either xenon or mercury, and provide light at a broad spectrum between about 300 nm to 600 nm, but lose light power after their limited lifetime. When imaging at faster rates, arc lamps may also introduce flicker (Aswani et al., 2012). Light-emitting diodes (LEDs) can provide a flicker-less alternative, but each LED is generally only limited to a small bandwidth of the spectrum, compared to arc lamps (Aswani et al., 2012). Laser light sources using either argon-ion or argon-krypton have become more widely used in the past, enabling line scanning confocal microscopy that allows very sharp fluorescence images (see chapter 1.5.3; Kubitscheck, 2017; Spring and Davidson, 2016).

Excitation/emission

Excitation and emission filters need to correspond to the excitation/emission spectra of the fluorophores to be imaged. The bandwidth of the filter determines how much light can be used for excitation and how much light is captured from the fluorophore, with narrower filter bandwidths providing less signal but also less nonspecific fluorescence (Kubitscheck, 2017; Spring and Davidson, 2016). Combining different excitation/emission filters also allows dual-colour imaging (e.g., Dana et al., 2016; Gervasi et al., 2010; Miyawaki et al., 1997).

Photodetectors

To record the incoming emitted light, various kinds of photodetectors are available, among them CCD, EMCCD, sCMOS, (GaAsP) PMT, APD, and HyD (mostly reviewed in Göhler, 2015; Kubitscheck, 2017). Charge-coupled devices (CCD) consist of an array of semiconductive light-sensitive elements that generate an electric charge in proportion to the intensity of the incident light (Kubitscheck, 2017, pp. 104-107). While CCDs provide a cheap option with high quantum efficiency (QE), they suffer from high noise ratios that render them unuseful for low light levels, as well as slow readout speeds (Andor, 2017; Kubitscheck, 2017). Electron-multiplying CCDs

(EMCCDs) add a high voltage 'gain register' to increase the signal relative to the fixed camera noise, and have faster readout speeds than conventional CCDs (Göhler, 2015). EMCCD cameras, however, are also very expensive, need cooling down to up to −100 °C, have relatively small fields of view and have slower readout speeds than other systems (Andor, 2017; Kubitscheck, 2017). Scientific complementary-metal-oxide semiconductor (sCMOS) cameras, on the other hand, can achieve similar QEs with 5 megapixel fields of view and frame rates up to 1.000 Hz (Andor, 2017; Kubitscheck, 2017). CMOS sensors use arrays in which each pixel point is immediately digitised and amplified (Göhler, 2015; Kubitscheck, 2017).

Photomultiplier tubes (PMTs) are different from the previously described sensors in that PMTs do not capture a complete two-dimensional image, and can thus only be used as point detectors in line-scanning systems (Kubitscheck, 2017). PMTs detect photons through a photocathode whose electrons are then amplified by several dynodes to reach a QE of about 30 % at nanosecond response time (Göhler, 2015; Kubitscheck, 2017). The sensitivity of conventional PMTs can be increased by the use of gallium arsenide phosphide (GaAsP) as photosensitive substrate for the photocathode in a PMT (Scientifica, 2015). Avalanche photodiodes (APDs) are also signal-amplifying devices that use semiconductor p–n junctions to create a flow of electrons from a single photon, resulting in QEs of up to 90 %, but lower gain than PMTs (Kubitscheck, 2017). In order to maximise the benefits of some systems but to avoid the pitfalls, systems can also be combined, such as the APD and PMT in Leica's HyD detectors (Kappel, 2011).

Confocal microscopy

Because widefield fluorescence microscopy also captures a lot of out-of-focus fluorescence, resulting in images with low signal to background ratio, it is best suited for comparatively flat samples or thin sections, while larger specimens such as whole brains have been difficult to clearly image until the invention of the confocal microscope, pioneered by Marvin Misky in the late 1950s. The idea behind the confocal microscope is the use of two pinholes to restrict excitation

and detection beams, thus suppressing out-of-focus light. While this means that less light reaches the detector, SNR is nonetheless improved as the respective light only comes from a single imaging plane that passes through the pinhole (Kubitscheck, 2017, pp. 166-169).

As the detection in confocal microscopy is diffraction-limited, the samples must be scanned point by point and plane by plane, thus increasing the recording time dramatically. Today, the most commonly used scanning mode is laser scanning, whereby a pair of galvanometric mirrors guides a laser beam in x- and y-dimensions to reconstruct a 2D image. This method is employed in laser scanning confocal microscopes. Most commonly used detectors are APDs and PMTs (Kubitscheck, 2017, pp. 179-180).

In order to further improve image contrast beyond the diffraction limit, deconvolution algorithms can be applied to sharpen confocal images. Confocal images are generally convoluted with the point spread function (PSF) of the microscope. If the PSF is known, the image can be sharpened by mathematically subtracting PSF-related noise. Without knowing the PSF, however, blind deconvolution can estimate the PSF by using iterative processes (Kubitscheck, 2017, pp. 180-185). Common software for this are AutoQuant (Bitplane) and Huygens (Scientific Volume Imaging B.V.).

Despite these improvements, light microscopy is still largely restricted by a diffraction limit of half the wavelength used, which is ∼200 nm for visible light. Super-resolution microscopy techniques such as STED or STORM attempt to overcome these limits by making use of the nonlinear response characteristics of fluorophores (Kubitscheck, 2017).

Two-photon microscopy

While confocal microscopy allows imaging of whole tissues with only small amounts of out-of-focus light blurring the image, it is often problematic when trying to image in deeper living tissues. This is because shorter-wavelength light gets scattered more strongly when penetrating (especially uncleared) tissues, and because the

confocal pinhole requires a high intensity of light excitation to capture enough in-plane emission light. This makes it unsuitable for tissues deeper than a couple of micrometres, and for live tissues where phototoxicity becomes problematic at high excitation intensities (Kubitscheck, 2017, pp. 203-204).

These two issues with deep imaging of live tissue are overcome by the use of two-photon excitation microscopy (2PEM) (Denk et al., 1990; reviewed in Svoboda and Yasuda, 2006). The principle behind 2PEM relies on the fact that fluorophores can not only be excited by one photon of a given wavelength (e.g. 450 nm), but also by two photons with each half that energy (e.g. 900 nm). This can be achieved by using focused and pulsed laser light that converges only in a tiny volume that can be as small as $\sim 0.1\,\mu m^3$ (Zipfel et al., 2003). The advantages of this method are that higher wavelengths can penetrate deep tissue more easily without scattering, and single photons are less likely excite fluorophores, effectively reducing out-of-focus emissions. Problems with 2PEM include the limitations in spatial resolution, sample heating by the use of high laser powers, and the nonlinear dynamics of 2P excitation spectra (Kubitscheck, 2017, pp. 205-229).

1.5.4 Manipulating neural activity

In order to understand a (neural) system, it is often not sufficient to only observe patterns of activity, but to specifically interfere with the activity to uncover causal relationships.

Thermogenetics

One way to manipulate neural activity is by using changes in temperature to change specific temperature-sensitive proteins that, in turn, activate or inactivate specific neurons. The two most commonly used tools for this in flies are *shibire* for inactivation and dTrpA1 for activation of neural activity.

Drosophila shibire encodes the protein dynamin which is involved in endocytosis and essential for synaptic vesicle recycling (Bliek and Meyerowitz, 1991; Kosaka and Ikeda, 1983). The temperature-sensitive allele Shi^{ts1} is defective at vesicle recycling

at restricted temperatures > 29 °C, effectively blocking synaptic transmission (Chen et al., 1991; Koenig et al., 1983). Using the GAL4/UAS system it was shown in 2000/1 to rapidly block neural activity and behavioural responses, thus demonstrating the non-invasive block of specific neurons in behaving flies (Kitamoto, 2001; Waddell et al., 2000), and has been widely used since then.

The *Drosophila melanogaster* transient receptor potential (TRP) channel dTrpA1 is a cation channel with highly temperature-dependent conductances that plays an important role in thermosensation. When ectopically expressed using the GAL4/UAS system, it was shown to persistently depolarise neurons within seconds of shifting to restricted temperatures (> 29 °C) (Hamada et al., 2008). It has since been widely used to activate neuronal populations during specific time points in behavioural tasks (see Albin et al., 2015; Aso et al., 2010; Burke et al., 2012; Krashes et al., 2009; Plaçais et al., 2012).

One of the downsides of thermogenetics is the fact that manipulating the environmental temperature can lead to considerable effects on cell dynamics and an animal's behaviour, particularly when the animal is ectothermic. This downside can be avoided by the use of stimulating neurons with light.

Optogenetic activation

Optogenetics uses genetic targeting of optically sensitive proteins into neurons to manipulate specific neural subsets by the use of light pulses (reviewed in Allen et al., 2015; Bernstein et al., 2012; Boyden, 2015; Deisseroth, 2011; Tye and Deisseroth, 2012).

The first optogenetic experiment in which neurons were transfected to express optogenetic transgenes by which they could be activated with light was published in 2002. Here, Zemelman et al. (2002) developed a method relying on three individual components to render vertebrate neurons light-sensitive: arrestin-2, rhodopsin, and the α subunit of the cognate heterotrimeric G protein. The same group demonstrated in 2005 that optogenetics could be used to manipulate the behaviour of an animal; this time light was used to uncage adenosine triphosphate (ATP) in flies

expressing the ATP receptor $P2X_2$ in giant fibre neurons to elicit an escape response in decapitated flies (Lima and Miesenböck, 2005). Using this same method of activation, dopaminergic neurons of the PPL1 cluster were shown to induce aversive reinforcement in olfactory conditioning of *Drosophila* (Claridge-Chang et al., 2009).

Channelrhodopsin-2. The field of optogenetics, however, did not take off until late 2005, when the lab of Karl Deisseroth introduced the algal protein Channelrhodopsin-2 (ChR2) to photostimulate mammalian neurons (Boyden et al., 2005). In contrast to previous optogenetic tools, ChR2 required only delivery of a single gene into neurons, without the need for additional molecules to be fed or injected. ChR2 is a light-gated cation channel, taken from the unicellular green alga *Chlamydomonas reinhardtii*, that is composed of a seven-transmembrane channel containing the light-isomerisable chromophore all-*trans*-retinal (ATR). When blue light (at about 480 nm) is absorbed, the ATR complex undergoes a conformational change to 13-*cis*-retinal that induces an opening of the ion pore of at least 6 Å, making it permeable to various cations such as Na^+, before closing again within milliseconds (Harz and Hegemann, 1991; Nagel et al., 2003).

ChR2 has since been widely used in mammalian systems neuroscience to probe causal roles of genetically defined groups of neurons. The first such study could show that optogenetic activation of hypocretin-producing neurons in the hypothalamus could drive awakening of previously asleep mice (Adamantidis et al., 2007). Further studies using ChR2 could show a causal role for dopaminergic neurons in behavioural conditioning (Tsai et al., 2009), the regulation of parkinsonian motor behaviours through the basal ganglia (Kravitz et al., 2010), or a causal role for parvalbumin neurons in generating gamma-frequency rhythmicity (Sohal et al., 2009).

ChR2 can also be used in *Drosophila*, when complementing the food with ATR, but has been rarely used in adult *Drosophila*, due to low levels of membrane integration and limited stability that prevents ChR2 to efficiently depolarise central brain neurons (Riemensperger et al., 2016). In larvae and peripheral sensory neurons of adult *Drosophila*, however, ChR2 has been successfully used (Bellmann et al.,

2010; Hwang et al., 2007; Ljaschenko et al., 2013; Pulver et al., 2009; Schroll et al., 2006; Suh et al., 2007; Zimmermann et al., 2009). A recently developed ChR2 mutation, termed ChR2-XXL, shows highly elevated expression and strongly increased photocurrent amplitudes, allowing for efficient optogenetic stimulation with blue light in adult *Drosophila* (Dawydow et al., 2014). Blue light, however, is still strongly sensed by flies (see Salcedo et al., 1999), thus potentially biasing behaviour, is largely incompatible with imaging (of fluorophores in the green spectrum), and penetrates tissue relatively ineffectively.

Red-shifted channelrhodopsins. One strategy to circumvent these confounds was the recent development of red-light-activated channelrhodopsins such as ReaChR (Lin et al., 2013) or Chrimson (Klapoetke et al., 2014). Since *Drosophila melanogaster* has poor vision in the far red spectrum (Salcedo et al., 1999), red light > 600 nm should introduce minimal bias to experiments. Indeed, both ReaChR and Chrimson have since been frequently used in *Drosophila melanogaster* (see Aso and Rubin, 2016; Cervantes-Sandoval et al., 2017; Hige et al., 2015a; Hoopfer et al., 2015; Inagaki et al., 2014; Klapoetke et al., 2014; Shimizu and Stopfer, 2017; Takemura et al., 2017). Another advantage of red-shifted channelrhodopsins is the fact that they can be combined with calcium imaging at minimal interference with the blue-green excitation/emission spectrum of GCaMP (cf. Hoopfer et al., 2015; Inagaki et al., 2014), and that red light has higher penetrance into tissue with less light scattering. Chrimson has several variants, out of which CsChrimson with its enhanced membrane trafficking and high sensitivity is the most widely used one (see Kim et al., 2015; Klapoetke et al., 2014).

Beyond mere activation

To this date, most optogenetic experiments have used the light-gated opening of a broad cation channel to investigate the effects of activating specific neural subsets. Since the introductin of ChR2, however, many optogenetic tools have come to light that can also manipulate neurons in different ways.

One such way is the optogenetic activation of G-protein coupled receptors (GPCRs). GPCRs are involved in a wide range of intracellular functions involving second messenger cascades, such as CREB-mediated transcription (see for example Leurs et al., 2005). The development of optoXRs now allows optogenetic stimulation of α_1 and β_2 adrenergic receptors that were shown to significantly raise IP_1 and cAMP levels, respectively, *in vivo* (Airan et al., 2009; Siuda et al., 2015). Step-function opsins, on the other hand, allow prolonged bi-stable subthreshold depolarisation for up to 30 minutes, once stimulated (Berndt et al., 2009; Yizhar et al., 2011).

Optogenetic silencing of neurons has historically proven difficult as most tools until very recently have relied on anion pumps that can only transport one charge per photon, and have thus proven rather uneffective. Very recently, however, the first light-gated anion channels have been described: *Guillardia theta* Anion Channel Rhodopsins (*Gt*ACR) 1 and 2 (Govorunova et al., 2015). *Gt*ACRs were shown to be highly sensitive to light stimulation and highly selective to anions, effectively hyperpolarising mammalian cells (Govorunova et al., 2015), and inhibiting a wide range of specific behaviours in *Drosophila melanogaster* (Mohammad et al., 2017). Future studies will determine the further usefulness of these tools, and how tonic neural activity may be a staple of information processing in neural systems.

1.5.5 RNA interference

Another way of manipulating cells is to interfere with gene translation, effectively blocking the synthesis of specific proteins. Ribonucleic acid interference (RNAi) is an endogenous process by which messenger RNA (mRNA) is targeted for degradation by double-stranded RNA (dsRNA) with the same sequence, thereby silencing the gene of interest (Fire et al., 1998; reviewed in Boutros and Ahringer, 2008).

RNAi relies on an evolutionarily ancient cell defense mechanism to protect them from viruses and transposable elements that can produce dsRNA, which attracts a protein complex containing *Dicer*. This protein complex cleaves the dsRNA into small fragments called small interfering RNAs (siRNA). The RNA-induced silencing complex (RISC) then binds to double-stranded siRNAs, and the RISC protein

Argonaute cleaves and discards one strand. With the help of the bound single-stranded siRNA, RISC can then bind to further complementary RNA molecules to amplify RNA degradation (Alberts et al., 2008, p. 495).

In *Drosophila melanogaster*, GAL4-directed RNAi can be used to knock down specific genes in specific neuronal subsets. There are three main libraries with UAS-RNAi lines: VDRC GD and KK lines, as well as Harvard/BDSC TRiP lines. The GD library consists of >16,000 lines, each with 300-400bp gene fragments from predicted protein-coding genes. These were cloned as inverted repeats (IR) with 10× UAS, and inserted into the genome randomly by P-element mobilisation. When crossed with a GAL4 line, these UAS-RNAi lines should form double-stranded long hairpin RNA structures due to the inverted repeats (Dietzl et al., 2007). The more recent KK library was constructed similarly but used a targeted insertion (at 30B3) instead of a random P-element insertion to ensure consistency and viability, and used an improved IR design (VDRC, 2017). However, recent studies unveiled that in 25 % of KK lines, an additional RNAi construct insertion (at 40D3) can lead to false positives (Green et al., 2014; Manning et al., 2016). A similar effort by the Transgenic RNAi Project (TRiP) at Harvard Medical School led to the generation of close to 13,000 lines that are site-targeted to either attP2 or attP40 landing sites (Ni et al., 2009). TRiP lines use a Vermilion-AttB-Loxp-Intron-UAS-MCS (VALIUM) vector that contains two 5× UAS sites and a *vermilion* marker (Ni et al., 2008). As TRiP lines contain both *yellow* and *vermilion* on the X chromosome, the selection of sexes for setting up crosses and experimental flies is of importance. Ni et al. (2008) also note a stronger RNAi effect in males compared to females.

Dicer-2 (Dcr-2) is a dsRNA endonuclease and part of the endogenous RNAi machinery (Alberts et al., 2008, p. 496). Overexpression of *Dcr-2* was shown to enhance the effects of *UAS-RNAi* in many cases, although off-target effects could also be enhanced (Dietzl et al., 2007). This holds true for both GD/KK libraries. For TRiP lines, flies using the VALIUM1 vector are reported to benefit from Dcr-2 inclusion, while other VALIUM vectors do not require Dcr-2 (DRSC/TRiP Functional Genomics Resources, 2017).

2

Materials and Methods

Contents

2.1 Fly husbandry 44
2.1.1 Driver lines 44
2.1.2 Reporter and actuator lines 44
2.2 Pharmacology 46
2.2.1 Saline solutions 46
2.2.2 Agonists and antagonists applied 48
2.3 Explant brain widefield imaging 49
2.3.1 Setup 49
2.3.2 Brain preparation 49
2.3.3 Focal application 51
2.3.4 Bath-application of agonists and antagonists 52
2.3.5 Image acquisition 52
2.3.6 Image analysis 53
2.4 Explant brain two-photon imaging 55
2.4.1 Brain preparation 55
2.4.2 Optogenetic activation 56
2.4.3 Two-photon image acquisition 56
2.4.4 Field of view 56
2.4.5 Washout experiments 57
2.4.6 Image analysis 57
2.5 *In vivo* two-photon calcium imaging 58
2.5.1 Fly preparation 58
2.5.2 Odour delivery protocol 58
2.5.3 Odour delivery with optogenetic stimulation 59
2.5.4 Image acquisition 60
2.5.5 Image analysis 60
2.6 Immunohistochemistry 61
2.6.1 Antibodies 61

2.6.2 Staining protocol 64
2.6.3 Antibody quantification 64
2.6.4 Deconvolution and Dα7::GFP quantification 65
2.6.5 Brain registration 65
2.7 Statistics 65

2.1 Fly husbandry

All flies used herein are *Drosophila melanogaster*, raised at 25 °C and at 50 % relative humidity. Flies for behavioural experiments were raised in plastic bottles on standard cornmeal food. Flies used for physiological experiments were raised in vials on standard cornmeal food with additional molasses, complemented with active dried yeast.

Flies used for optogenetic experiments were transferred to vials containing standard cornmeal food with additional 1 mM ATR (previously dissolved in ethanol) within one day of eclosing from their pupae, and kept in these for 2 to 7 days before the start of experiments, wrapped in aluminium foil.

Great care was taken that all flies to be experimentally compared were handled the same way, including simultaneous raising, the same level of CO_2 exposure, the same housing conditions, and near-simultaneous testing with interleaving trials. If not stated otherwise, wildtype flies used were Canton-S (CS).

2.1.1 Driver lines

For a complete list of fly driver lines used, please refer to Table 2.1.

2.1.2 Reporter and actuator lines

For a complete list of fly reporter and actuator lines used, please refer to Table 2.2.

Table 2.1: All driver lines used for the experiments in this work. Stock numbers refer to BDSC, unless preceded by k (Kyoto Stock Center) or by v (VDRC). All MB split-GAL4 lines can be obtained directly from Janelia (`http://splitgal4.janelia.org`). All other fly lines with no stock number were kind gifts from the respective authors.

Line	Stock no.	Expression	Generated by	Described in
c739-GAL4	7362	α/β KCs	Yang et al., 1995	
Cha-GAL4		cholinergic neurons	Salvaterra and Kitamoto, 2001	Mehren and Griffith, 2006
Cha3.3kb-GAL4		cholinergic neurons	Diegelmann et al., 2008	
GH146-GAL4	30026	AL PNs	Heimbeck et al., 2001	
OK107-GAL4	k106098	most KCs	Connolly et al., 1996	
R13F02-GAL4	48571	most KCs	Jenett et al., 2012	
R16A06-GAL4	48709	γ KCs	Jenett et al., 2012	
R21D02-GAL4	48939	M4/6 MBONs	Jenett et al., 2012	Owald et al., 2015a
R24H08-GAL4	49100	V2α' MBON	Jenett et al., 2012	
R39A05-GAL4	50033	M4β' MBON	Jenett et al., 2012	
R48B04-GAL4	50347	PAM DANs	Jenett et al., 2012	
R56F01-GAL4	39156	M4β MBON	Jenett et al., 2012	
R58E02-GAL4	41347	PAM DANs	Jenett et al., 2012	
R64H09-GAL4	46547	sNPFR-expressing	Jenett et al., 2012	
R66C08-GAL4	49412	M6 MBON	Jenett et al., 2012	Owald et al., 2015a
R71D08-GAL4	61645	V2 MBONs	Jenett et al., 2012	Perisse et al., 2016
R93F01-GAL4	47230	M4 MBONs	Jenett et al., 2012	
VT1211-GAL4	v202324	M4β' + M6 MBONs	Kvon et al., 2014	Owald et al., 2015a
Cha-GAL80	60321	cholinergic neurons	Kitamoto, 2002	
MB-GAL80	64306	Kenyon cells	H. Tanimoto	Krashes et al., 2007
MB002B		M4β' + M6 MBONs	Aso et al., 2014a	
MB011B		M4β' + M6 MBONs	Aso et al., 2014a	
MB027B		V2α' MBON	Aso et al., 2014a	
MB052B		V2 MBONs	Aso et al., 2014a	
MB058B		V1 DANs	Aso et al., 2014a	
MB077C		γ2α'1 MBON	Aso et al., 2014a	
MB210B		M4β' + M6 MBONs	Aso et al., 2014a	
MB296B		MV1 DAN	Aso et al., 2014a	
MB308B		PPL1-α'3	Aso et al., 2014a	
MB438B		MP1	Aso et al., 2014a	
MB504B		PPL1 DANs	Aso et al., 2014a	
MB549C		V2 MBONs	Aso et al., 2014a	
247-LexA::VP16		most KCs	Pitman et al., 2011	
Cha3.3kb-LexA		cholinergic neurons	Diegelmann et al., 2008	
R11D09-LexA	54456	γ KCs	Jenett et al., 2012	
R12G04-LexA	52448	MVP2 MBON	Jenett et al., 2012	Perisse et al., 2016
R15B01-LexA	52485	M4β' + V2 MBONs	Jenett et al., 2012	Lewis et al., 2015
R24H08-LexA	52732	V2α' MBON	Jenett et al., 2012	
R25D01-LexA	53519	γ2α'1 MBON	Jenett et al., 2012	Cohn et al., 2015
R52G04-LexA	52738	γ3 and α1 MBONs	Jenett et al., 2012	
R58E02-LexA	52740	PAM DANs	Jenett et al., 2012	
R65B09-LexA	52687	V2 MBONs	Jenett et al., 2012	
R71D08-LexA	52841	V2 MBONs	Jenett et al., 2012	
VT1211-LexA		M4β' + M6 MBONs	Y. Huang and D. Owald	

Table 2.2: All reporter/actuator lines used for the experiments in this work. Stock numbers refer to BDSC, unless preceded by k (Kyoto Stock Center) or by v (VDRC). All fly lines with no stock number were kind gifts from the respective authors.

Line	Stock no.	Generated by
lexAop-mCD8::GFP		
lexAop-rCD2::mRFP		
UAS-Dα7::GFP	39692	Leiss et al., 2009
UAS-DenMark	33061	Nicolaï et al., 2010
UAS-mCD8::GFP		Lee and Luo, 1999
UAS-mCherry		
247::GCaMP5		Chen et al., 2013a
lexAop-GCaMP6f (su(Hw)attP5)	44277	Chen et al., 2013a
lexAop-GCaMP6m (su(Hw)attp5)		Chen et al., 2013a; Andrew Lin
UAS-Ace2::mNeonGreen (attP40)	64317	Gong et al., 2015
UAS-GCaMP5 (attP40)	42037	Akerboom et al., 2012
UAS-GCaMP6f (attP40)	42747	Chen et al., 2013a
lexAop-CsChrimson-tdtomato::uas-GCaMP6f		Hoopfer et al., 2015; Wong; Anderson; Pfeiffer
lexAop-CsChrimson::mVenus	55138	Klapoetke et al., 2014
lexAop-CsChrimson::tdtomato		Klapoetke et al., 2014; gift from V. Jayaraman
lexAop-$P2X_2$		Lima and Miesenböck, 2005; Andrew Lin
UAS-CsChrimson::mCherry		Klapoetke et al., 2014; gift from V. Jayaraman
UAS-CsChrimson::mVenus	55135	Klapoetke et al., 2014
UAS-ChAT-RNAi	25856	Ni et al., 2009
UAS-Dα1-RNAi	28688	Ni et al., 2009
UAS-Dα3-RNAi	27671	Ni et al., 2009
UAS-Dα4-RNAi	31985	Ni et al., 2009
UAS-Dα5-RNAi	25943	Ni et al., 2009
UAS-Dα6-RNAi	25835	Ni et al., 2009
UAS-sNPF-RNAi	25867	Ni et al., 2009
UAS-sNPFR1-RNAi	27507	Ni et al., 2009
UAS-VAChT-RNAi	v40918	Dietzl et al., 2007
taurine (CG5618) mutant	k141210	Schuldiner et al., 2008

2.2 Pharmacology

2.2.1 Saline solutions

Two different saline solutions were used for explant brain injection experiments, and for explant brain optogenetic and *in vivo* experiments, respectively. The difference in the use of solutions stems from the observation that AHLS seemed not well suited to investigate circuit function, while carbogenated solution seemed to interfere with brain viability in conjunction with microinjections.

AHLS

All *Drosophila* explant brain experiments with microinjections were performed with *Drosophila* adult hemolymph like saline (AHLS) from Wang et al. (2003) (see also Harris et al., 2015; Haynes et al., 2015; Li et al., 2014; Root et al., 2008, 2013). The recipe can be found in Table 2.3.

Table 2.3: AHLS recipe from Wang et al., 2003, used for all explant brain experiments with microinjections.

Compound	Concentration in mM
$CaCl_2$	2
HEPES	5
KCl	5
$MgCl_2$	8.2
NaCl	108
$NaHCO_3$	4
NaH_2PO_4	1
Sucrose	10
Trehalose	5

The pH was adjusted to 7.5, and the osmolarity was adjusted to 265 mOsm. A 500 ml bottle was prepared freshly every two weeks, with $MgCl_2$ and $CaCl_2$ solutions added freshly for every day's aliquot, while a small aliquot was additionally prepared without $CaCl_2$ for dissection. AHLS was kept at 4 °C until the start of the experiment. AHLS was not perfused as all experiments were completed within a few minutes. For high magnesium experiments (Figure 3.8), an additional solution with 18.2 mM of $MgCl_2$ was prepared.

Extracellular saline

All *Drosophila* explant brain experiments with optogenetic stimulation, and *in vivo* experiments were performed with carbogenated external saline (Wilson et al., 2004; see also Akerboom et al., 2012; Gruntman and Turner, 2013; Hige et al., 2015a; Liu et al., 2015; Tian et al., 2009). The recipe can be found in Table 2.4.

10× concentrated stocks were prepared without $MgCl_2$ and $CaCl_2$, aliquotted and frozen at −20 °C. Individual frozen aliquots were then diluted to 1×, the pH

Table 2.4: Extracellular saline recipe from Wilson et al. (2004), used for all explant brain experiments with optogenetics and *in vivo* experiments. N-tris refers to N-tris(hydroxymethyl) methyl-2-aminoethane-sulfonic acid. The solution was bubbled with carbogen (95 % O_2 / 5 % CO_2) at room temperature for $\sim$ 30 min before the start of experiments.

Compound	Concentration in mM
$CaCl_2$	1.5
Glucose	10
KCl	3
$MgCl_2$	4
N-tris	5
NaCl	103
NaH_2PO_4	1
$NaHCO_3$	26
Sucrose	7
Trehalose	10

was adjusted to 7.3, and the osmolarity was adjusted to 275 mOsm. Bottles of this solution were kept at 4 °C. From this, daily aliquots were prepared by adding solutions of $MgCl_2$ and $CaCl_2$. For explant brains, a smaller aliquot without $CaCl_2$ was prepared for dissection. The solution was bubbled with carbogen (95 % O_2 / 5 % CO_2) at room temperature for $\sim$ 30 min before the start of experiments. Extracellular saline was not perfused except for washout experiments. For these, explant brains were continuously perfused at about 2 ml/min using a Watson-Marlow 120S/DV WM Sci Q400-1H1D perfusion system.

2.2.2 Agonists and antagonists applied

All (potential) receptor agonists and antagonists were prepared in AHLS to a concentration of 100 mM before they were aliquotted in 1.5 ml Eppendorf tubes, frozen at −20 °C, and individually thawn each day for experiments, and diluted to the final concentration with each day's AHLS. These compounds can be found in Table 2.5.

Short neuropeptide F (sNPF; Ala-Gln-Arg-Ser-Pro-Ser-Leu-Arg-Leu-Arg-Phe-NH_2) was synthesised by PolyPeptide (Strasbourg, France) to a purity of > 95% and was dissolved in DMSO (see also Shang et al., 2013). Vehicle control for sNPF experiments was hence DMSO, diluted to the same degree as sNPF.

Table 2.5: Receptor agonists and antagonists used in this study.

Compound	Manufacturer	Product number
Acetylcholine	Sigma Aldrich	A6625
Adenosine triphosphate (ATP)	Sigma Aldrich	A9187
Alpha-bungarotoxin	Life Technologies	B-1601
Aspartate	Sigma Aldrich	A9256
D-tubocurarine	Sigma Aldrich	T2379
GABA	Sigma Aldrich	A2129
Glutamate	Sigma Aldrich	G8415
Hexamethonium	Sigma Aldrich	H2138
Mecamylamine	Sigma Aldrich	M9020
Methyllycaconitine (MLA)	Sigma Aldrich	M168
Muscarine	Sigma Aldrich	M104
Nicotine	Sigma Aldrich	N3876
Taurine	Sigma Aldrich	T0625

5 µM of Texas Red Dextran (TXR; Life Technologies D-1863) were applied to each solution to monitor the spread of solution within the tissue through red fluorescence.

2.3 Explant brain widefield imaging

2.3.1 Setup

For both widefield imaging as well as two-photon imaging of explant brains and flies *in vivo*, a customised Scientifica Slicescope was used with a 40× objective (Olympus LUMPLan FLN) (see Figure 2.1 for an annotated image).

2.3.2 Brain preparation

Young flies (1-7 d) were briefly (∼ 20 s) anaesthetised on ice, and brains were dissected in a 200 µl drop of 4 °C cold calcium-free AHLS (see 2.2.1). All explant brain dissections were performed with great care to maintain the brain's integrity as best as possible. Retina and laminae were completely removed, while trachea were only removed as far as visibility of the respective areas of the brain required it. For experiments requiring access with an injection pipette, a small (∼20 µm) hole into the perineural sheath was made with fine forceps (Dumont # 5SF Forceps - Inox Super Fine Tip, Fine Science Tools) at a site allowing both for pipette access to the

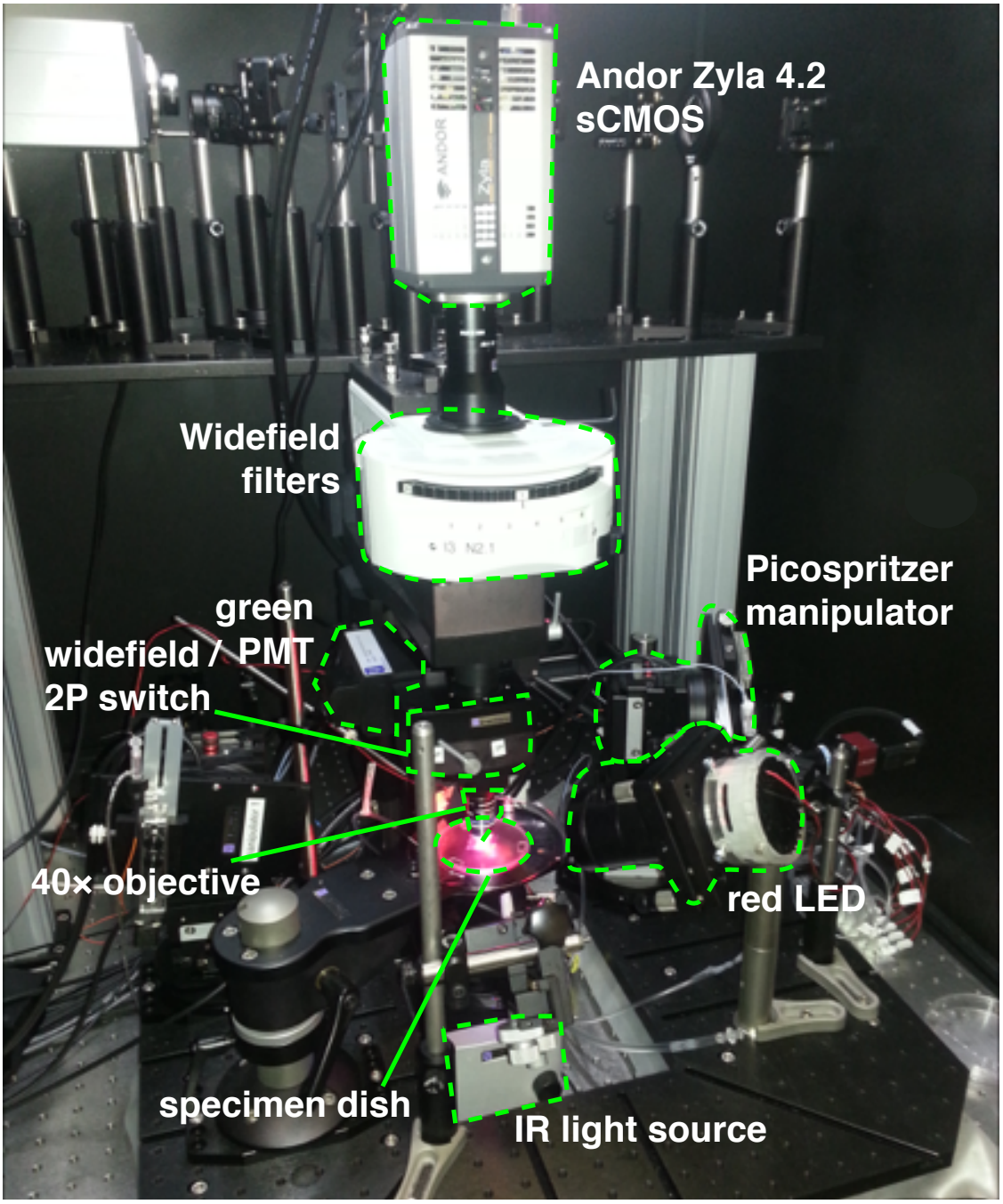


Figure 2.1: The imaging setup, based on a customised Scientifica Slicescope. Widefield images were acquired using an Andor Zyla 4.2 sCMOS camera (top), through a fluorescent filter set. Two-photon images were acquired using a GaAsP PMT through a green filter. A switch allows rapid change between widefield and two-photon imaging. Specimens placed on a custom-made dish were imaged through a 40× objective. Specimens were stimulated by Picospritzer injections, a red LED, or odourants (system not visible here). Illumination came from either a Scientifica IR light source (bottom), arc lamp light (not visible here), or a Ti-Sapphire laser (behind setup). In the background on the top, a novel optical setup for volumetric imaging can be found (see Žurauskas et al., 2017) which was not used in this study.

target site as well as some distance to the target neurons to minimise damage to the neurons of interest. In the case of γ5 injections, this was lateral of the γ2 region. With practice, the whole procedure takes less than 3 minutes. For imaging, explant brains were carefully taken up from the dissection solution with a custom-made copper wire sling, and placed anterior side up (posterior side up for calyx injections, Figure 3.26) on a polylysine-coated (Sigma Aldrich, P8920) circular glass cover slip (Fisherbrand, 1232-3148, ⌀ 16 mm) on a custom 3D printed imaging dish. 1.2 ml of cold AHLS (with $CaCl_2$) were added, and the imaging dish placed under a customised Scientifica Slicescope setup (see Figure 2.1) for widefield imaging.

2.3.3 Focal application

For focal application experiments, the ROI and the hole in the perineural sheath were located using IR and green fluorescence. If needed, the imaging dish was rotated so that the hole in the perineural sheath was in line with the ROI. A previously pulled pipette (glass capillaries, Harvard Apparatus, 300092; pulled by a Narishige pipette puller, PP-830) with an opening diameter of approximately 3 µm was filled with the solution to be injected, mounted on a picospritzer III (Intracel) holder mounted on a Scientifica PatchStar micromanipulator.

The tip of the pipette was then carefully positioned at the ROI (γ5 in most experiments, or the respective dendritic arbour in Figure 3.10) after passing the tissue through the hole in the perineural sheath. For experiments in Figure 3.6, Figure A.4, and Figure A.5, I carefully repositioned the microinjection pipette several times. For ATP injections (Figure 3.26), I targeted the calyx (posterior side up) using IR guidance.

The air pressure to the PicoSpritzer was set to the minimum level that still resulted in the ejection of solution from the pipette, around 5 psi. At the beginning of each experiment, small test pulses were given while observing the red fluorescent channel for release of solution. Pulse duration was successively increased to find the shortest pulse that still resulted in the release of solution. This ensured that the spread of solution was kept focal. Pulse duration was normally around 10 ms.

Depending on the concentration of the agonist to be applied and the resulting rise and decay times of the calcium responses, intertrial intervals (ITI) were set to either 10 or 20 seconds. In each experiment, between 10 to 60 pulses were delivered.

Using AHLS without perfusion, most brains stayed healthy and responsive for about 10-15 minutes, before irreversible calcium influx throughout the somata and neurites would mark the loss of tissue viability. At the end of each experiment, the addition of KCl to a final concentration of 1 M was used to judge the final state of the tissue. If no major calcium influx was visible anymore with KCl, the experiment was dismissed from further analysis.

2.3.4 Bath-application of agonists and antagonists

In some cases, I have added receptor agonists and antagonists to the bath solution to monitor modulation of responses evoked by focal stimulation. For mecamylamine (see Figures 3.23, A.15, 3.26), hexamethonium, and MLA (Figure 3.24), 200 µl of these or vehicle were manually added to the bath with a Gibson pipette after the recording of initial ACh-evoked responses. Vehicle was AHLS.

12 µl of 2 mM sNPF were bath-applied in Figure 4.2.2 to achieve a final concentration of 20 µM.

Despite relatively long recordings, ACh-evoked calcium responses stayed robust. Minor shifts in baseline were accounted for by taking the F_0 for each stimulation from F one second before stimulation.

2.3.5 Image acquisition

Widefield fluorescence was excited using an X-Cite 120PC Q (Lumen Dynamics) arc lamp and a Scientifica infrared (IR) light source, with either a green, red, or IR filter set in place (EGFP 49002, Dsred 49005; Chroma Technology Corp.). GCaMP fluorescence was measured from the green channel, while the red channel served as injection control, and the IR channel was used for micropipette targeting.

Widefield images were mostly acquired using an Andor Zyla 4.2 sCMOS camera with Andor Solis software (v4.27). Time series were mostly acquired at 33.3 Hz with 512×512 pixels and 16 bit for up to 15 minutes.

For fast imaging, time series were acquired at 100 Hz (Figure A.3, Figure 3.6).

In the case of voltage imaging (Figure 5.1), time series were acquired at 200 Hz with a resolution of 64×64 pixels and 8 bit.

Experiments in Figures 3.8 and 3.9 were acquired with a Guppy Pro CCD camera (Allied) with AVT SmartView software (v1.14). These time series were acquired at 12 Hz with 640×480 pixels and 8 bit.

A custom-made white-light LED served as stimulus trigger signal that briefly (50–130 ms) lit up precisely one second before stimulation (except for Figures 3.10J, 3.4, and A.1 where it occurred simultaneously). This served as a trigger signal for later $\Delta F/F_0$ response analysis.

2.3.6 Image analysis

Image stacks were mostly analysed in Matlab (Mathworks Inc.) using custom-written scripts. In brief, elliptic ROIs were manually drawn around (mostly at M4/6 dendrites), and the mean fluorescence (F) of this ROI was calculated for each time point.

The resulting trace was scanned for LED trigger signals, and individual $\Delta F/F_0$ response traces 1 s before and 3–10 s after the stimulation trigger were extracted. F_0 was defined for each trial as the mean F from one second before stimulation up to the point of stimulation before the LED trigger signal. This also accounted for potential minor shifts in baseline.

For further analysis, peak $\Delta F/F_0$ was extracted by taking the maximum $\Delta F/F_0$ value from the time after the trigger signal to 3 seconds after, applying a threshold of 4 standard deviations above F_0. The sigmoid dose-response curve fit for ACh application (Figure 3.5A) was performed in GraphPad Prism, based on the average of three trials per brain, with five brains per condition.

Time to peak (Figure 3.5B and Figure 3.20D) was measured from stimulus onset up to the peak $\Delta F/F_0$.

Response onset in Figure 3.5D was defined as the time between stimulus onset up to the first time point with a $\Delta F/F_0$ that is 2 SD above F_0.

Rise time in Figure 3.5C was measured as the number of frames between 10 % and 90 % of response peak $\Delta F/F_0$.

Peak to decay time in Figure 3.20E and Figure 4.3E was measured from the peak time to the first time point where $\Delta F/F_0$ falls below 50 % of peak $\Delta F/F_0$.

Rise–decay time in Figure 4.3E was measured from the first time point where $\Delta F/F_0$ is above 50 % of peak $\Delta F/F_0$ up to the first time point where $\Delta F/F_0$ falls below 50 % peak $\Delta F/F_0$ again. This measure and decay time were normalised by the mean peak $\Delta F/F_0$ of each brain to account for response magnitude-related response dynamics.

Calcium responses are mostly displayed as arithmetic mean of transients, with the standard error of the mean (SEM = $\frac{SD}{\sqrt{N}}$) displayed as a shade behind the transient. These were mostly calculated and visualised in Matlab, except for Figures 3.4, 3.9, and 3.25 which were produced in R using ggplot2.

Injection trials are normally pooled within one brain before further analysis to account for small trial-to-trial differences.

In the case of voltage imaging (Figure 5.1), F_0 was taken as the average F from 5 s before stimulation up to stimulation. Mean $\Delta F/F_0$ before GABA is taken from 500 ms before stimulation up to stimulation, and mean $\Delta F/F_0$ after GABA is taken from 200 ms after stimulation up to 700 ms after stimulation.

Two-channel imaging

The temporal correlation map in Figure A.3B was produced by first calculating the pixel-wise $\Delta F/F_0$ for each of the green and red channels individually, for all frames between stimulus onset up to 3 s after. Each pixel's $\Delta F/F_0$ over time was then correlated across channels, resulting in a single correlation value for each

pixel. The resulting correlation matrix was then colour-coded and laid over the greyscale fluorescent images from each channel.

The spread of solution / calcium response analysis in Figure 3.7A was performed as follows: The TXR spread of solution is displayed as a maximum projection over time from one stimulation trial onset until 1 s after. The max $\Delta F/F_0$ displayed in the green channel represents each pixel's highest $\Delta F/F_0$ between stimulation onset until 1 s after.

Spread of ACh in Figure 3.7B was monitored by TXR and the red channel. Picospritzer pressure times were gradually increased from 5 ms to 50 ms, and at each step first the red channel, and then the green channel were recorded. GCaMP6f ΔF was calculated as the difference between F before stimulus onset with the F 200 ms after stimulation.

Because widefield imaging only allowed for the simultaneous recording of one channel, both channels were recorded subsequently, shortly after one another, using the same stimulation parameters.

2.4 Explant brain two-photon imaging

For optogenetic stimulation and *in vivo* experiments, two-photon imaging was used instead of widefield imaging. In the case of optogenetic stimulation, widefield light exposure was found to interfere with CsChrimson, presumably due to inadvertent stimulation (personal observations).

2.4.1 Brain preparation

For optogenetic stimulation of explant brain experiments, flies were briefly (< 1 min) anaesthetised, and then quickly and carefully dissected in Ca^{2+}-free carbogenated extracellular solution at room temperature (see Table 2.4). Dissection was performed as described in 2.3.2, but generally in less than one minute. Great care was taken to keep light exposure at an absolute minimum, from the housing in aluminium-clad vials to minimal lighting in the experimental room, to minimal light exposure

during dissection, and the rapid focusing of laser light away from CsChrimson-expressing neurons.

2.4.2 Optogenetic activation

For stimulation, a high-power LED (Multicomp OSW-6338, 630 nm) was used at a distance to the brain of approx. 10–15 cm through a 50 mm diameter lens with focal length 60 mm. The LED was filtered through an additional 632/10 bandpass filter (Edmund Optics, 65227) to shield the PMTs from any off-target light (unpublished observations). The power at the specimen was measured to be 0.85 mW/mm^2. The LED was triggered using a microcontroller (Arduino MEGA). Light pulses were delivered at 40 Hz, with a duration of 10 ms, for a total of 200 ms / 500 ms per stimulation.

2.4.3 Two-photon image acquisition

Two-photon experiments were performed on the same Scientifica Slicescope setup as widefield experiments (see 2.3); two switches on the setup allowed the quick shift between widefield and two-photon imaging.

After rapid identification of focus on the respective field of view, brains were left to settle for 5 min before being imaged. Following 10 s of baseline recording, light pulses were delivered. Generally, five light pulses with an ITI of 6 s were delivered to confirm reliability of calcium responses.

Two-photon fluorescence was excited using 140 fs pulses at 80 MHz repetition rate, centred on 910 nm generated by a Ti-Sapphire laser (Chameleon Ultra II, Coherent). Images of 256×256 pixels were acquired at 5.92 Hz (pixel dwell time 0.5 µs), controlled by ScanImage 3.8 software (Pologruto et al., 2003).

2.4.4 Field of view

In order to avoid inadvertent CsChrimson stimulation from the two-photon imaging laser, imaging fields of view (FOV) were placed over GCaMP6f-expressing neural

compartments that were ideally spatially well separated from CsChrimson-expressing neural compartments.

In the case of MBONs (Figures 3.27, 3.28, 3.30, 4.4), this meant that the FOV was rapidly focused on axon terminals as MBON dendrites overlapped with CsChrimson-expressing KCs in the MB lobes (Aso et al., 2014a). Indeed, even brief shifts of FOV to the lobes resulted in irreversible calcium increases (personal observations).

In the case of PPL1 DANs (Figures 6.2, 6.3, 6.7), cell bodies were imaged because PPL1 axons and dendrites are closely intermingled with MBON processes (see Aso et al., 2014a).

In some cases, it was unavoidable to place the FOV over CsChrimson-positive processes. For simultaneous optogenetic stimulation of KCs with GCaMP6f read-out (Figure 3.29), laser intensity was greatly reduced; nonetheless an upward shift of baseline with onset of imaging is visible. In the case of PAM neurons expressing CsChrimson and an FOV above γ5, a downward shift of baseline is visible (Figure 6.6).

In other cases, with smaller CsChrimson-expressing populations, no effects of the imaging FOV over CsChrimson were observed (see Figure 6.5).

2.4.5 Washout experiments

For mecamylamine washout experiments (Figure 3.28), 200 µl of mecamylamine pre-diluted in extracellular saline were added to the bath to a final concentration of 100 / 250 µM with a Gibson pipette, after the recording of initial responses. After 5 min, effects of mecamylamine were tested, and mecamylamine was started to be washed out. For this, explant brains were continuously perfused at about 2 ml/min using a Watson-Marlow 120S/DV WM Sci Q400-1H1D perfusion system for at least 30 minutes.

2.4.6 Image analysis

Two-photon fluorescence images were manually segmented using ImageJ. Mostly, this meant drawing an ROI around axon terminals, dendritic arbours, or cell bodies

of interest. In the case of PAM neurons, several compartments were segmented from the same image stack (Figures 6.4,6.5, and 6.8).

These were then further analysed using custom-written MATLAB scripts. For quantification, F_0 was defined as the mean F from the 9 s prior until 1 s before stimulation. $\Delta F/F_0$ was generally compared between before (1 s before) and after (1 s after) the first LED stimulation onset. Subsequent stimulation trials were recorded but not further used for analysis, as trial-to-trial differences were generally very low (see Figure 6.7, for example).

In one case of a pronounced baseline shift (Figure 6.6), $\Delta F/F_0$ from the first frame was compared with the $\Delta F/F_0$ of the last frame.

2.5 *In vivo* two-photon calcium imaging

2.5.1 Fly preparation

Two-photon imaging of odour-evoked calcium responses was performed according to Owald et al. (2015a). Three- to eight-day-old flies were briefly (5-10 s) immobilised on ice and mounted in a custom chamber. The head capsule was opened under room temperature carbogenated buffer (see Table 2.4). The legs and proboscis were carefully immobilised with wax. See also Figure 2.2 for images of a sample preparation.

In the case of reconsolidation experiments (Figures 6.9, 6.10, 6.11), flies were prepared 2.5–3.5 h after appetitive training using MCH or OCT or mock treatment (odour presentation without sugar) (see Felsenberg et al., 2017).

In the case of imaging starved flies with optogenetic stimulation (see Figure 5.5), flies were put onto retinal food for three days before putting them into starvation vials containing only agar for 20–24 hours before imaging experiments.

2.5.2 Odour delivery protocol

Odours were delivered on a clean air carrier stream using a custom-designed system (Shang et al., 2007), which also synchronises the timing of odour delivery and the two-photon image acquisition. Air stream was passed over one of three odours

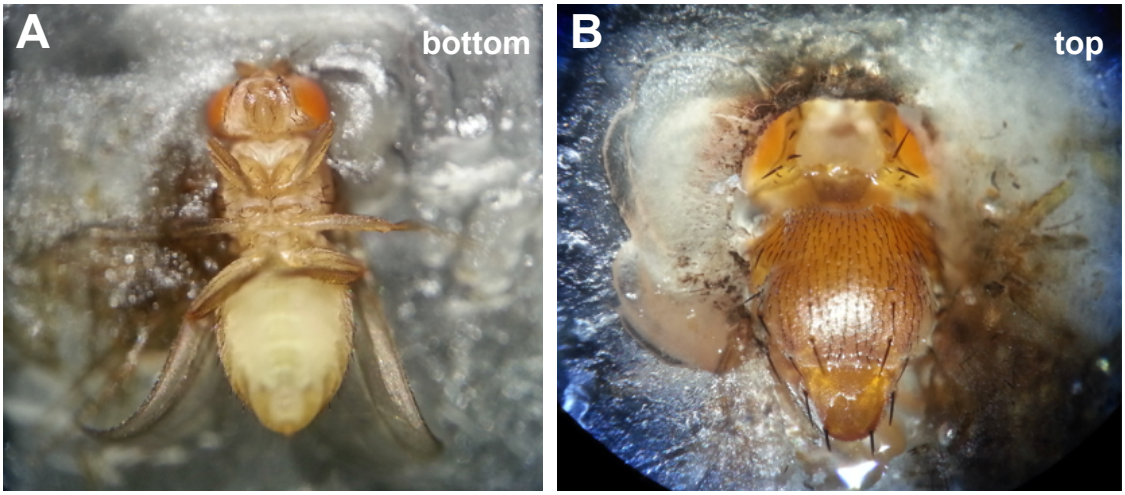


Figure 2.2: *In vivo* tethered fly preparation. Images from bottom (A) and top (B) of a sample tethered fly preparation for *in vivo* calcium imaging. A) Fly is mounted in a custom chamber using wax fixation on the thorax and eyes, while leaving antennae free to move. B) The top of the head capsule between both eyes is removed, trachea and fatty tissue removed, while being immersed in saline solution. This allows optical imaging of large parts of the central brain.

(MCH, OCT, or IAA) at 100× dilution in mineral oil, before being further blended 1:9 with a clean air stream.

For the testing of nAChR-RNAi (Figure 3.25), test pulses were first applied, before flies were exposed to 5 s MCH, then 15 s clean air, followed by a 5 s OCT pulse.

Similarly, effects of sNPFR1-RNAi (Figure 4.4) were tested by exposing flies to 25 s of clean air, then 5 s MCH, then 15 s clean air, followed by a 5 OCT pulse, then 15 s clean air, and finally 5 s of IAA.

For reconsolidation experiments (Figures 6.9, 6.10, 6.11), after 40 s of clean air, flies were exposed to 5 s of either trained odour (MCH or OCT), then 15 s clean air, followed by 5 s of the other odour (MCH or OCT) pulse, then 15 s clean air, followed by 5 s of a novel odour (IAA). The protocol was repeated three times.

2.5.3 Odour delivery with optogenetic stimulation

For *in vivo* optogenetic experiments with odour delivery (Figures 5.3, 5.4, 5.5), female flies were essentially treated as described above (2.5), but also fed ATR for 1–3 days, and kept in aluminium-clad vials.

MCH and OCT were presented twice for 2 s, with 20 s ITI. Red light pulses (described before in 2.4) of one second duration were turned on 1 s after odour onset, during the second round of MCH and OCT presentation.

A 500/10 filter was used to minimise LED artifacts during imaging.

2.5.4 Image acquisition

Two-photon fluorescence images were acquired as for explant brains (see 2.4).

FOVs were set to the initial axon segments of M4/6 and V2 neurons in Figures 3.25, 5.3, 5.4, 5.5, 6.10. MBON-$\gamma 2\alpha' 1$ (Figure 6.9) was also imaged from the initial axon segment, as in (Hige et al., 2015b). PPL1 neurons (Figures 6.11 and 4.5) were imaged from their respective planes within the vertical MB lobe and heel.

2.5.5 Image analysis

Two-photon fluorescence images were manually segmented using ImageJ, and further analysed using custom-written Matlab routines. Movement of the animal was small enough such that images did not require registration.

For imaging with nAChR-RNAi (Figure 3.25), each hemisphere, where possible, was separately evaluated and treated as an independent N. Peaks were taken as maximum $\Delta F/F_0$ between 1 and 2 s after the beginning of odour stimulation. F_0 was defined as the mean F from 2 s before odour stimulation to the beginning of stimulation. Area under curve (AUC) was measured as the integral $\Delta F/F_0$ between odour onset to either the first one or two seconds after. Time to peak was calculated as the time between odour onset up to peak $\Delta F/F_0$. Flies were excluded from further analysis if they did not show any visible odour responses.

For sNPFR1-RNAi odour responses (Figure 4.4), F_0 was defined as the mean F from 5 s before each odour stimulation to the beginning of the repective odour stimulation. Total AUC was measured as the integral of 5 s $\Delta F/F_0$ during odour presentation, while last AUC is the integral of the last 2 s $\Delta F/F_0$ of odour presentation.

For imaging MBONs with optogenetic stimulation of MVP2 neurons (Figures 5.3, 5.4, and 5.5), F_0 was defined as the mean F of two seconds before the first odour onset. Time points chosen for comparison were (1) onset of LED, (2) end of LED stimulation, and (3) 1 s after end of LED stimulation. F_0 was not changed throughout an experiment, as comparisons were made within each 2 s trial.

For imaging of previously trained flies (Figures 6.9, 6.10, and 6.11), F_0 was defined for each stimulus response as the mean F from 1 s before up to the point of stimulation. F/F_0 accordingly describes the fluorescence relative to this baseline. The area under the curve (AUC) was measured as the integral of F/F_0 during the 5 s between odour stimulation onset and offset. In order to reduce the level of variance between flies, CS^+ and CS^- were further normalized by dividing each AUC by the novel odour AUC from the respective trial and the same fly, thus obtaining a normalised AUC (see also Figure 2.3 for a sample calculation). We excluded flies from further analysis if they did not show any visible odour responses. Trained and mock-trained flies were constantly alternated during training and testing. In Figure 6.9, 15 out of 73 flies were excluded (mock group: 9, trained group: 6). In Figure 6.10, 9 out of 56 flies were excluded (mock: 5, trained: 4). In 6.11, 3 out of 34 flies were excluded (mock MP1: 1, trained MP1: 3).

Differences in F_0 calculation were chosen as a result of different signal stability. Generally, longer time spans for F_0 were preferred when fluorescence signals were weak or showed large variance.

2.6 Immunohistochemistry

2.6.1 Antibodies

All antibody information can be found in Table 2.6. All secondary antibodies used were mixed with glycerol (1:1) before being aliquotted and stored at $-20\,°C$ immediately upon reception.

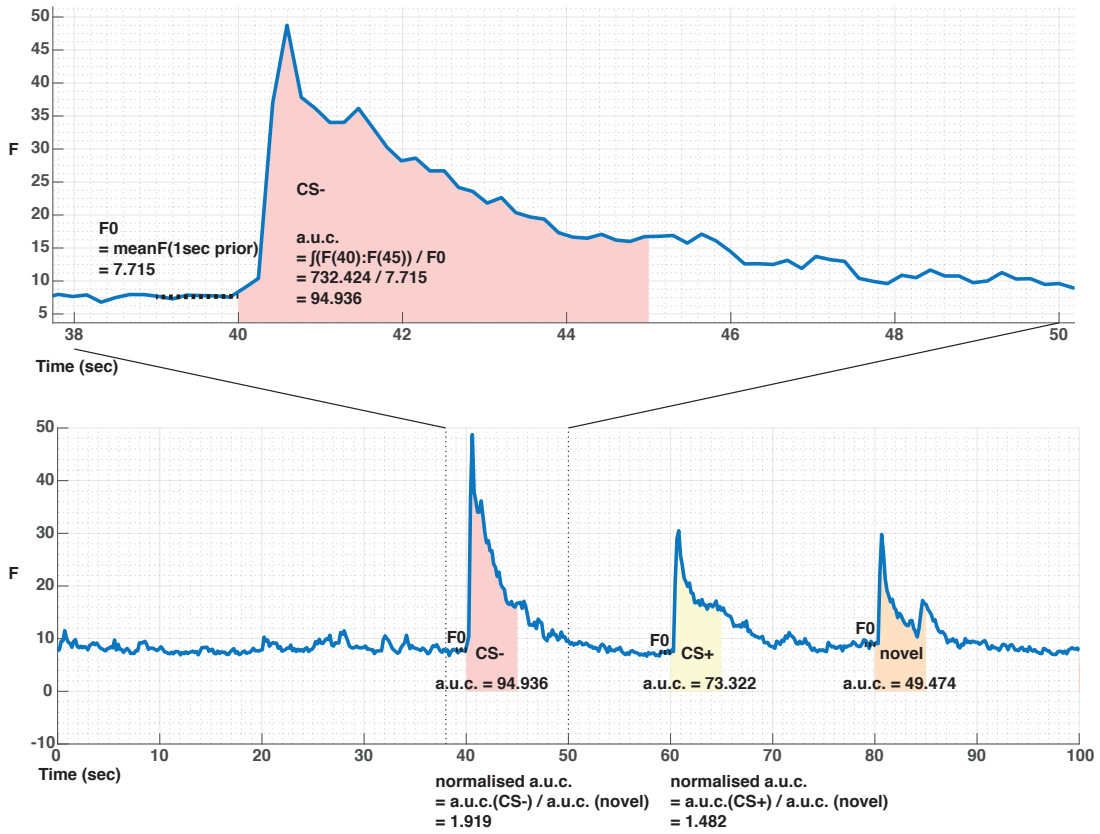


Figure 2.3: Sample calculation of normalised area under curve (AUC) for the first odour response trial. F represents fluorescent signal collected from MB077C ; GCaMP6f ROI. Odours were presented for five minutes; the CS^- odour was always presented first after 40 s, followed by the CS^+ odour at 60 s, followed at last by the novel odour IAA. F_0 was defined for each stimulation as the mean F from the first second prior to stimulus onset. AUC was then calculated as the integral of F during the 5 s of odour stimulation, divided by the respective F_0. The normalised AUC for CS^+ and CS^- was obtained by dividing the respective AUC by the AUC of the novel odour.

Table 2.6: All primary and secondary antibodies used in this work, with their respective antigens, dilutions used, and sources.

Antibody	Antigen	Dilution	Source / References
Anti-ACh HYChol001 mouse monoclonal	conjugated choline-glutaric acid	1:1000	Abcam ab37010 (discontinued)
Anti-AChE rabbit polyclonal	Synthetic peptide of human AChE (aa 551-614)	1:200	Abcam ab97298
Anti-Brp nc82 mouse monoclonal	*Drosophila* Bruchpilot C-terminal (aa 1227-1740)	1:50	DSHB; Wagh et al., 2006
Anti-ChAT 4B1 mouse monoclonal	Choline acetyltransferase (recombinant protein)	1:100	DSHB; Takagawa and Salvaterra, 1996
Anti-ChAT sheep polyclonal	Synthetic peptide of pig ChAT (aa 167-188)	1:1000	Abcam ab18736
Anti-GFP chicken polyclonal	Recombinant full length protein corresponding to GFP	1:2000	Abcam ab13970
Anti-sNPFR1 rat	ASDEDRSGGIIHN - sNPFR1 N-terminal extrac. domain	1:200	Gift from K. Yu; Lee et al., 2008
Anti-taurine rabbit polyclonal	taurine conjugated to a glutaraldehyde linker	1:100	Abcam ab9448
Anti-VAChT rabbit polyclonal	*Drosophila* VAChT C-terminal (aa 441-546)	1:1000	Gift from T. Kitamoto; Kitamoto et al., 1998
Anti-VAChT guinea pig polyclonal	Synth. peptide corr. to the C-terminal of rat VAChT	1:1000	MerckMillipore AB1588; Gras et al., 2002
Goat anti-chicken Alexa Fluor 488	anti-chicken IgY (H+L)	1:2000	Abcam ab150169
Goat anti-mouse Alexa Fluor 488	anti-mouse IgG (H+L)	1:200	Life Technologies A11029
Goat anti-rabbit Alexa Fluor 488	anti-rabbit IgG (H+L)	1:200	Life Technologies A11034
Goat anti-rabbit Alexa Fluor 546	anti-rabbit IgG (H+L)	1:200	Life Technologies A11035
Goat anti-rabbit Alexa Fluor 568	anti-rabbit IgG (H+L)	1:200	Abcam ab175471
Goat anti-mouse Alexa Fluor 633	anti-mouse IgG (H+L)	1:200	Life Technologies A21052
Goat anti-rat Alexa Fluor 633	anti-rat IgG (H+L)	1:200	Life Technologies A21094

2.6.2 Staining protocol

Antibody stainings were basically performed according to Wu and Luo, 2006. In brief, brains of young flies were dissected in ice-cold phosphate-buffered saline (PBS), then fixed for 20 minutes in 4 % paraformaldehyde (PFA), then washed 5× in PBS with 0.3 % Triton-X 100 (PBT), and then blocked in 5 % normal goat serum (NGS) for at least 30 minutes. Primary antibodies were added to a final concentration described before (Table 2.6), and were incubated on a rotator for two nights. Brains were then washed 5× in PBT before secondary antibodies were added to a final concentration described above, and incubated for two nights on a rotator. Brains were then washed 5× in PBT before VectaShield (H-1000, Vector Laboratories) was added and brains were mounted on a glass slide. Stacks were acquired (mostly on the next day) on a Leica SP5 laser-scanning confocal microscope with a white-light laser (WLL), using manually adjusted laser intensity, and either a 25× objective (Leica HCX IRAPO water, 0.95 NA) for whole-brain images or a 40× objective (HCX PL APO oil, 1.3 NA) for more detailed images.

Great care was taken that groups to be compared with one another were treated as simultaneous as possible, undergoing the same protocol steps, and were imaged with the same settings.

For labelling of nicotinic acetylcholine receptors, α-bungarotoxin-tetramethylrhodamine (α-BTX-TMR, Sigma Aldrich, T0195) at a concentration of 500 nM was used. For this, brains were dissected, and without fixing, α-BTX-TMR was added. Brains were left on a rotator to incubate for 1.5 hours. Then brains were fixed, and washed 2× in PBT before VectaShield (H-1000, Vector Laboratories) was added and brains were mounted.

2.6.3 Antibody quantification

For antibody quantification, pre-defined rectangular ROIs were placed over a single frame of the medial γ lobe, β2, β′2, α3, α′3, as well as the superior medial protocerebrum (SMP) as control region. The γ ROI was 40×25 µm, the ROIs over β2, β′2, and α3 circles with 20 µm diametre, and α′3 was a manually drawn

region of about 10×5 µm. The mean fluorescence from these ROIs was assessed using ImageJ, and each brain's experimental ROI intensity was normalised to the respective SMP intensity, individually for each channel (ChAT and VAChT).

2.6.4 Deconvolution and Dα7::GFP quantification

A blind deconvolution algorithm (Autoquant software, Bitplane) was used to deconvolve and clarify Dα7::GFP punctae that were detected in Figure 3.22.

Punctae were counted using Huygens Object Analyzer that were first 3D-segmented.

2.6.5 Brain registration

To illustrate overlap between axons and dendrites of MBON-γ2α′1 and MV1 in Figure 6.7 and Figure A.17, I co-registered previously imaged confocal stacks (from Figure 6.1). For this, I used the Computational Morphometry Toolkit (CMTK; developed by NITRC) with an ImageJ GUI developed by Greg Jefferis (LMB, Cambridge). This software allowed me to register both confocal stacks with the Janelia Farm 2010 template. I subsequently produced an overlay of both registered brains in ImageJ (Schindelin et al., 2012).

2.7 Statistics

Statistical analyses were performed in GraphPad Prism 6.0f, using the statistical tests recommended by the software for the respective type of data. All relevant statistical information can be found in the Figure legends of each Figure containing statistical information.

The sigmoid dose-response curve fit for ACh application (Figure 3.5A) was performed in GraphPad Prism, based on the average of three trials per brain, with five brains per condition.

Paired *t*-tests were used to compare the average response peak before and after application of pharmacological antagonists and agonists (see Figures 3.23, 3.24, 3.26, and 5.1). Also, the effects of optogenetic stimulation were generally

compared before and after the first LED stimulation with paired t-tests (see section 3.5.2 and chapter 6).

Unpaired t-tests were used to compare calcium response peaks for ACh stimulation under high magnesium conditions (Figure 3.8), and the effects of sNPF-RNAi on KC-triggered MBON responses (Figure 4.4). Welch's correction was additionally applied for comparisons of calcium responses to sNPF-coapplication in Figure 4.2.2.

The **Mann-Whitney U-test** for nonparametric data was used to compare the effects of VAChT-RNAi on calcium response peaks (Figure 3.30), as normality tests did not suggest a normal distribution. In this example, however, an unpaired t-test yielded a similarly significant result.

Multiple t-tests with Holm-Sidak correction were used to compare odour response normalised AUC (section 6.2.5), sNPF bath effects on ACh-evoked responses (Figure 4.2.2), and effects of sNPFR1-RNAi on PPL1 odour responses (Figure 4.5) between experimental groups.

One-way ANOVAs with Tukey's multiple comparisons test were used to compare groups in antibody quantification and behavioural experiments. Dunnett's multiple comparisons test was used for nAChR-RNAi odour-evoked calcium responses (Figure 3.25).

A **two-way repeated-measures ANOVA** with Sidak's multiple comparisons test was used for MBON odour imaging data with optogenetic activation of MVP2 neurons.

3

Acetylcholine is the principal neurotransmitter of MB Kenyon cells

Contents

3.1 Background 68
3.1.1 Neurotransmitters in the *Drosophila* brain 68
3.1.2 Taurine in the MB 75
3.1.3 Aspartate in the MB 76
3.1.4 Glutamate in the MB 78
3.1.5 GABA in the MB 80
3.1.6 Acetylcholine (ACh) in the MB 82
3.1.7 sNPF 90
3.2 Calcium responses in MBONs to ACh application . . 91
3.2.1 Approach 91
3.2.2 Application of candidates 93
3.2.3 Dose-dependence of ACh-evoked calcium responses . . . 94
3.2.4 ACh acts directly on M4/6 dendrites 95
3.2.5 Individual MBONs respond to ACh 102
3.3 Kenyon cells express ChAT and VAChT 106
3.3.1 α-ChAT staining 106
3.3.2 α-VAChT staining 110
3.3.3 α-acetylcholinesterase staining 115
3.3.4 Cha-GAL4 115
3.3.5 Cha-LexA 117
3.4 MBONs have nicotinic ACh receptors 119
3.4.1 Nicotine elicits calcium responses 119
3.4.2 Histological evidence for nAChR in MBONs 121
3.4.3 Bath application of nAChR blockers during ACh application 127
3.4.4 RNA interference of nAChRs 130

3.5 Kenyon cells use ACh for neurotransmission to M4/6 MBONs 133
3.5.1 Electrical and pharmacological KC activation 134
3.5.2 Optogenetic KC activation with mecamylamine 136
3.5.3 Optogenetic KC activation with RNAi 141
3.6 Discussion 143
3.6.1 Results summary 143
3.6.2 Recent related studies 145
3.6.3 ChAT/VAChT expression in KCs 148
3.6.4 ACh receptors in MBONs 160
3.6.5 Implications and outlook 167

3.1 Background

Despite decades of research on the MB, the principal neurotransmitter of the MB-intrinsic Kenyon cells has remained elusive so far. Without knowing the neurotransmitter identity of KCs, however, the precise mechanisms behind synaptic plasticity at the memory-relevant KC–MBON synapse will remain a mystery.

3.1.1 Neurotransmitters in the *Drosophila* brain

At least 11 neurotransmitters have so far been described or suggested in *Drosophila melanogaster* (from abundant to sparse/uncharacterised): Acetylcholine (ACh), glutamate (Glu), GABA, dopamine (DA), octopamine (OA), serotonin (5-hydrotryptamine, 5-HT), histamine (HA), tyramine (TA), glycine, taurine, and aspartate (see also Klemm, 1976). An overview of these and their respective molecular machinery can be found in Tables 3.1 and 3.2.

Acetylcholine (ACh)

ACh is the most abundant neurotransmitter in the *Drosophila* brain (Breer, 1987; Buchner et al., 1986; Klemm, 1976). In particular, visual and olfactory pathways are largely cholinergic (Buchner et al., 1986). It has fast excitatory action through nicotinic ACh receptors (nAChRs), forming heteropentamers out of 7 different α-subunits and 3 β-subunits, and modulatory action through muscarinic ACh

Table 3.1: Overview of *Drosophila melanogaster* neurotransmitter expression. Abundance refers to number of neurons in the central *Drosophila melanogaster* brain. Question marks indicate cases with only weak evidence to date. References can be found in the text.

Neurotransmitter	Abundance	MB expression	Main action
Acetylcholine (ACh)	most abundant	mostly calyx	excitatory
Glutamate (Glu)	very abundant	some α/γ	exc (inh)
GABA	several hundred	mostly calyx	inhibitory
Dopamine (DA)	∼ 300	lobes and calyx	modulatory
Octopamine (OA)	60–70	weak γ (esp. γ1) and calyx	modulatory
Serotonin (5HT)	35–40	throughout (DPM)	modulatory
Histamine (HA)	18	-	inhibitory
Tyramine (TA)	several	-	modulatory?
Glycine (Gly)?	?	?	inhibitory
Taurine?	?	?	inhibitory
Aspartate (Asp)?	?	?	excitatory

Table 3.2: Overview of *Drosophila melanogaster* neurotransmitters proteins. Question marks indicate cases with only weak evidence to date. References can be found in the text.

Neurotransmitter	Synthesis	Transporter	Ves. transp.	Ionotropic receptors	Metabotropic receptors
Acetylcholine (ACh)	ChAT	Ctl1/2?	VAChT	nicotinic Dα1-7; Dβ1-3	muscarinic AChR-A/B
Glutamate (Glu)	Gs1/2	EAAT1	VGluT1-3	DGluR-IA/B / IIA-D; DNMDAR-I/II	DmGluRA
GABA	GAD1	Gat	VGAT	$GABA_A$ Rdl / Lcch3	$GABA_B$R1-3
Dopamine (DA)	Ddc	TH/DAT	Vmat	-	DopR1/2; D2R; DopEcR
Octopamine (OA)	Tdc2	TβH/OAT	Vmat	-	Oamb; Octβ1-3; Oct-TyrR
Serotonin (5HT)	Ddc	SerT	Vmat	-	5-HT1A/B; 5-HT2A/B; 5-HT7
Histamine (HA)	Hdc	CarT?	Vmat	HisCl1	-
Tyramine (TA)	Tdc2	DAT?	?	-	Oct-TyrR; TyrR; TyRII
Glycine (Gly)?	CG3011?	GlyT	VGAT	Grd; CG12344; CG7589?	-
Taurine?	CG5618?	EAAT2	?	$GABA_A$ Rdl / Lcch3	$GABA_B$R1-3
Aspartate (Asp)?	AST	EAAT1/2	Sialin?	NMDAR?	-

receptors (mAChRs) (Dale et al., 2008; Lee and O'Dowd, 1999; Sattelle, 1980). See 3.1.6 for a more detailed description.

Glutamate

Glutamatergic neurons are widespread in the *Drosophila* CNS (Daniels et al., 2008; Raghu and Borst, 2011), such as the OL (Raghu and Borst, 2011), the AL (Liu and Wilson, 2013), and several MBONs (Aso et al., 2014a; Owald et al., 2015a). In many cases, Glu may act as an excitatory neurotransmitter through a range of ionotropic Glu receptors (GluR) (Littleton and Ganetzky, 2000), but there are also metabotropic GluRs (Parmentier et al., 1996), and an inhibitory

Glu-gated chloride channel (Cully et al., 1996; Liu and Wilson, 2013). See 3.1.4 for a more detailed description.

GABA

There are several hundred GABAergic neurons in the *Drosophila* brain that form distinct cell clusters (Okada et al., 2009), including one MB-innervating APL neuron (Liu and Davis, 2009), several MBONs (Aso et al., 2014b; Perisse et al., 2016), and AL interneurons (Malun, 1991; Okada et al., 2009; Wilson and Laurent, 2005). There are two ionotropic $GABA_A$ receptors that are directly coupled to chloride channels: Rdl and Lcch3 (Aronstein et al., 1996; Ffrench-Constant et al., 1993); and there are three metabotropic $GABA_B$ GPCRs that are responsible for slower and longer lasting inhibition: GABA-B-R1/2/3 (Mezler et al., 2001; Wilson and Laurent, 2005). See 3.1.5 for a more detailed description.

Dopamine

There are ∼300 dopaminergic neurons in the *Drosophila* brain that can be subdivided into 13 clusters that innervate several brain neuropils including the central complex (Mao and Davis, 2009; Nässel and Elekes, 1992). Two clusters innervate the MB lobes (Mao and Davis, 2009; Tanaka et al., 2008). They are thought to modulate neural activity through the action of GPCRs DopR1 (dumb), DopR2 (DAMB), D2R, and DopEcR, by increasing cAMP levels (Brody and Cravchik, 2000; Gotzes et al., 1993; Han et al., 1996; Kim et al., 2007). MB-innervating DANs are crucial to signal reinforcement signals in associative learning by inducing synaptic plasticity through cAMP (see 1.3; Aso et al., 2014b; Burke et al., 2012; Owald et al., 2015a; Schwaerzel et al., 2003). They also play a role for behavioural state (Cohn et al., 2015), sleep (Sitaraman et al., 2015), and visual attention (Koenig et al., 2016).

Octopamine

There are about 60–70 octopaminergic neurons in the *Drosophila* brain that can be subdivided into 15 clusters whose processes finely arborise throughout the brain (Busch et al., 2009; Sinakevitch and Strausfeld, 2006). OANs have postsynaptic

sites around the esophagus foramen, and presynaptic terminals throughout the brain; four OANs have processes inside the MB (Busch et al., 2009). There are five OA GPCRs: Oamb, Octβ1/2/3R, and Oct-TyrR (Brody and Cravchik, 2000; Han et al., 1998; Saudou et al., 1990), that are related to α/β-adrenergic receptors (Roeder, 2005). Oamb expresses specifically in the MB, increases [Ca^{2+}] and [cAMP] upon OA binding (Han et al., 1998), and has thus been implicated in mediating the sweet-reinforcing signal to the MB (Burke et al., 2012; Huetteroth et al., 2015; Schroll et al., 2006; Schwaerzel et al., 2003). Octβ1/2/3R may also express in the MB (El-Kholy et al., 2015). In the honey bee, activation of a single OAN, VUMmx1 can substitute sugar reward in olfactory learning (Hammer, 1993). Yet, OA has been implicated in a wider range of behaviours such as aggression (Hoyer et al., 2008; Zhou et al., 2008), egg laying (Monastirioti, 2003), ethanol tolerance (Scholz et al., 2000), sensory modulation (Haan et al., 2012), flight initiation and maintenance (Brembs et al., 2007), as well as sleep (Crocker and Sehgal, 2008).

Serotonin

There are about 35–45 serotonergic neurons in each *Drosophila* brain hemisphere that innervate most regions with sparse arborisations (Alekseyenko et al., 2010; Coates et al., 2017; Pech et al., 2013; Pooryasin and Fiala, 2015; Sitaraman et al., 2008). Identified serotonergic neurons include the DPM neuron that targets KCs via 5-HT1A (Lee et al., 2011). 5-HT acts on GPCRs 5-HT1A, 5-HT1B, 5-HT2A, 5-HT2B, and 5-HT7 to modulate neuronal function by activating or inhibiting adenylyl cyclase (AC) (Blenau et al., 2017; Brody and Cravchik, 2000; Saudou et al., 1992; Witz et al., 1990). 5-HT signalling has been implicated in a wide range of behaviours such as aggression (Alekseyenko et al., 2014, 2010), place memory (Sitaraman et al., 2008), hunger (Albin et al., 2015), circadian rhythms (Yuan et al., 2005), sleep (Pooryasin and Fiala, 2015; Yuan et al., 2006), and mating (Pooryasin and Fiala, 2015).

Histamine

Histamine is a major neurotransmitter in insect photoreceptors (Hardie, 1987; Nässel et al., 1988; Pollack and Hofbauer, 1991). In the *Drosophila* brain, there are only 18 described histaminergic neurons that fall into five groups (HP1–4 and HS1), and which sparsely innervate the ventral and lateral protocerebrum (Nässel and Elekes, 1992; Pollack and Hofbauer, 1991; reviewed in Nässel, 1999). The central complex, the MB, the AL, and certain regions of dorsolateral protocerebrum are devoid of HA projections (Nässel, 1999). Interestingly, mechanosensory axons in the antennal nerve show some HA immunoreactivity (Buchner et al., 1993), and HA is required for some visual and mechanosensory behaviours (Melzig et al., 1996). There are probably two histamine receptors: one is a chloride channel (Hardie, 1987), and the other possibly a GPCR (Roeder, 2003).

Tyramine

Tyramine (TA) is a pharmacological precursor to OA (Monastirioti et al., 1996), so a specific role for TA as a neurotransmitter, first suggested in 1978 (Walker and Kerkut, 1978), is only slowly emerging (reviewed in Lange, 2009; Roeder, 2005). While most TA neurons probably also release OA, neurons that only stain for TA but not OA have been identified (Nagaya et al., 2002). Several TA-positive neurons have been described in the locust, including innervations of the CC, but little to no staining in the MB (Homberg et al., 2013; Kononenko et al., 2009). There are three TA-gated GPCRs that have been described thus far. Oct-TyrR decreases [cAMP], inhibits AC, and might be expressed in MBs (Arakawa et al., 1990; El-Kholy et al., 2015; Reale et al., 1997; Robb et al., 1994; Saudou et al., 1990; Thamm et al., 2017). TyrR activates G_q and opens Ca^{2+}-dependent Cl^- channels (Cazzamali et al., 2005), and TyrRII mediates calcium increases (Bayliss et al., 2013). The effects of TA signalling remain poorly understood, but TA was shown to interact with DA vesicles in rats before (Vaccari, 1993). Furthermore, locomotion is altered depending on TA levels in *Drosophila* larvae in a way that suggests opposing effects of OA/TA (Saraswati et al., 2004).

Glycine?

Glycine has been suggested as a functional inhibitory neurotransmitter in the mammalian CNS and PNS (Balu and Coyle, 2015; Curtis and Watkins, 1965; Harvey, 2008; Zeilhofer et al., 2012), but only very recently has a functional role for glycine as a neurotransmitter been described in *Drosophila melanogaster* PDF neurons (Frenkel et al., 2017). The putative glycine transporter (dGlyT) CG5549 (Yamashita et al., 2005), expressed in photoreceptors and a broad array of cells bodies in the CNS (Thimgan et al., 2006), has been shown to mediate glycine transport and plays a role in circadian rhythms (Frenkel et al., 2017).

Taurine?

Taurine has not yet been confirmed as a functional neurotransmitter in *Drosophila*, but a lot of evidence supports its role as a neurotransmitter in the vertebrate CNS (reviewed in Albrecht and Schousboe, 2005; Wu and Prentice, 2010). In insects, thus far, there have been some studies that suggest immunoreactivity in the MBs of several species (Schäfer et al., 1988; Sinakevitch et al., 2001, 2008; Sjöholm et al., 2006) including *Drosophila melanogaster* (Strausfeld et al., 2003). For more details, see 3.1.2.

Aspartate?

The amino acid aspartate has thus far only been hypothesised to serve a role as a neurotransmitter. There seems to be immunoreactivity in the MBs of *Drosophila melanogaster* and other insect species (Sinakevitch et al., 2001; Strausfeld et al., 2003), and a vesicular aspartate transporter has recently been suggested (Miyaji et al., 2008). For more details, see 3.1.3.

KC transmitter candidates

While the transmitter identities of much of the CS and US pathways have been extensively explored (see 1.2), the neurotransmitter identity of KCs has remained unknown so far, in any species, including *Drosophila*.

Many neurotransmitters have been dismissed, such as

- ACh (Buchner et al., 1986; Gorczyca and Hall, 1987; Johard et al., 2008; Yasuyama et al., 1995; Yasuyama and Salvaterra, 1999),
- Glu (Daniels et al., 2008; Johard et al., 2008),
- GABA (Johard et al., 2008),
- DA (Konrad and Marsh, 1987; Neckameyer and White, 1993),
- OA/TA (Cole et al., 2005; Monastirioti et al., 1996),
- 5-HT (Bao et al., 2010; Blenau and Thamm, 2011), and
- histamine (Burg et al., 1993).

Several KC neurotransmitters have previously been postulated in *Drosophila melanogaster* and other insect species, including

- taurine (Schäfer et al., 1988; Sinakevitch et al., 2001; Sjöholm et al., 2006; Strausfeld et al., 2003),
- Asp (Sinakevitch et al., 2001; Sjöholm et al., 2006; Strausfeld et al., 2003),
- Glu (Sinakevitch et al., 2001, 2008; Strausfeld et al., 2003),
- GABA (Brotz et al., 1997; Ganeshina and Menzel, 2001; Sinakevitch et al., 2008; Yamazaki et al., 1998), and
- ACh (Yi et al., 2013),

mostly based on MB immunostainings as well as promoter-driven expression in MBs.

A further KC neurotransmitter was suggested based on the identification of a novel gene, *portabella* (*prt*), which has structural similarities with known vesicular transporters (Brooks et al., 2011). Prt immunostainings suggest labelling in all MB lobes and KC cell bodies, and prt^1 mutants show aversive olfactory learning deficits and copulation defects (Brooks et al., 2011). The substrate, however,

remains elusive and was suggested to be a novel unknown neurotransmitter as Prt's structure differs at multiple sites from known vesicular monoamine transporters (VMAT), despite its similarities (Brooks et al., 2011).

In the following, I will discuss in more detail what is currently known about the aforementioned suggested KC neurotransmitters.

3.1.2 Taurine in the MB

Taurine, or 2-amino-ethanesulfonic acid, was proposed as a neurotransmitter as early as 1971 (Davison and Kaczmarek, 1971). Since then, several lines of evidence have emerged of it being a functional neurotransmitter in the mammalian CNS (reviewed in Albrecht and Schousboe, 2005; Wu and Prentice, 2010), but the evidence for a role in insects remains sparse (see also review by Martin and Krantz, 2014).

Taurine staining in the insect CNS

Taurine accounts for 16 % of the total free amino acids in the honeybee brain, only Glu being higher in concentration (20 %) (Frontali, 1964).

In insects, taurine immunoreactivity has been found by in the KCs of five species: honey bee, locust, cockroach, moth, and *Drosophila melanogaster*, based on three different antibodies (Bicker, 1991; Farris and Strausfeld, 2001; Schäfer et al., 1988; Sinakevitch et al., 2001; Sjöholm et al., 2006; Strausfeld et al., 2003).

In *Drosophila melanogaster*, a taurine antibody showed strong KC labelling in a subset of α/β KCs (possibly α/βp), and visible staining in γ and α/βc KCs (Strausfeld et al., 2003). Another taurine staining detected high levels of immunoreactivity in KCs, possibly γ and α/β (Bicker, 1991).

Unpublished data from our lab furthermore suggests that CG5618 might be expressed specifically in α/βc KCs. The sequence of CG5618 suggests sulfinoalanine decarboxylase activity (FlyBase, 1992) which synthesises hypotaurine, a precursor of taurine.

Effects of taurine

The physiological effects of taurine in insects remain barely explored, but taurine was previously suggested to inhibit spontaneous neural activity in the locust (Frontali, 1964). Taurine also reduced the accumulation of calcium into locust synaptosomes, which affected subsequent neurotransmitter release (Whitton et al., 1988a,b). In the visual system of the fly *Musca*, however, no physiological effects were detected (Hardie, 1987).

A taurine transporter in insects?

While the taurine transporter SLC6A6 has been described in mammals (Pramod et al., 2013), this transporter seems absent in insects, and no further insect taurine transporter has yet emerged (Besson et al., 2011; reviewed in Martin and Krantz, 2014). However, the excitatory amino acid transporter 2 (dEAAT2) was surprisingly found to transport taurine (Besson et al., 2005), and *dEAAT2* mutants contain decreased amounts of taurine (Besson et al., 2011).

While *dEAAT2* mRNA was mainly detected in sensory organs of the PNS and midline glia (Freeman et al., 2003; Soustelle et al., 2002), a dEAAT2-GAL4 drives expression in several neurons, including AL PNs, neurons innervating some α/β MB compartments, and some neurons in the SOG (Besson et al., 2011). *dEAAT2* mutants showed decreased olfactory avoidance of propionic acid, and higher salt sensitivity (Besson et al., 2011). Interestingly, a recent RNA-seq study suggested strong expression of dEAAT2 in the V2 MBON, known to mediate learned avoidance (Aso et al., 2014b; Séjourné et al., 2011), as well as DAL and the M4 MBON (Crocker et al., 2016).

These data suggest that taurine could potentially serve as a neurotransmitter of *Drosophila* KCs.

3.1.3 Aspartate in the MB

The amino acid Asp has long been known as a signalling molecule, but its role as a neurotransmitter is still a matter of debate (reviewed in Nadler, 2011), with

little evidence so far for a role in insects.

Role of aspartate in the mammalian system

L-aspartate was first found to have excitatory action in brain slices in 1960 (Curtis and Watkins, 1960). Indeed, Asp was found to be a potent agonist of NMDARs in the hippocampus (Fleck et al., 1993; Patneau and Mayer, 1990), where it is co-localised and co-released with glutamatergic synaptic vesicles (Bradford and Nadler, 2004; Gundersen et al., 1998). Yet, cerebellar Purkinje cells may also be activated by Asp independently of NMDAR1 through yet unidentified receptors (Yuzaki et al., 1996). Ca^{2+} stimulation causes an aspartate efflux from hippocampal slices (Moss et al., 1976), and may be taken up again into synaptosomes (Logan and Snyder, 1972).

While Asp synthesis, storage, release and receptor activation is characterised, a specific vesicular aspartate transporter, sialin, was only recently described (Miyaji et al., 2008). Follow-up studies, however, contradicted this finding: VGlut knock-out mice show little to no excitatory postsynaptic currents in the hippocampus, as would be expected if Asp might still excite this pathway (Herring et al., 2015). Another study found that Asp can still be taken up and released in the absence of sialin (Morland et al., 2013).

Aspartate stains the MB in insects

Antagonistically to taurine, layered immunoreactivity against Asp was found across the cockroach MB (Sinakevitch et al., 2001). In the *Drosophila melanogaster* MB, the strongest staining was observed in α/β KCs, followed by α'/β', with only little staining in the γ lobe (Strausfeld et al., 2003). Importantly, KC cell bodies were stained as well, and antibody specificity was previously confirmed (Campistron et al., 1986).

Asp was shown to have a hyperpolarising effect at low concentrations, and a depolarising effect at high concentrations in isolated locust neurons (Giles and Usherwood, 1985).

Drosophila aspartate transporters

How could Asp be transported across the membrane in *Drosophila*? There are two excitatory amino acid transporters that could play a role (reviewed in Martin and Krantz, 2014): dEAAT1 is a Na^+-dependent Glu transporter, but also shows high affinity for aspartate, and seems to activate a Cl^- channel (Besson et al., 2000; Seal et al., 1998). dEAAT2 has high affinity for aspartate and taurine, but not for Glu, and possibly acts as an aspartate/taurine transporter (Besson et al., 2005, 2000). dEAAT2 was found to express in *Drosophila* neurons involved in sensory pathways, and *dEAAT2* mutants showed defects in olfaction and salt sensitivity (Besson et al., 2011; see also 3.1.2).

It is thus conceivable that L-aspartate acts as a functional neurotransmitter of KCs.

3.1.4 Glutamate in the MB

> The hypothesis of a glutamatergic nature of Kenyon cells can be tested experimentally because in several species extrinsic neurons [...] of the mushroom bodies can be recorded (Schürmann et al., 2000, p. 237).

Glu is the most abundant amino acid in the bee brain (Frontali, 1964). It is the most abundant excitatory neurotransmitter in the mammalian CNS (Bennett and Balcar, 1999), the main excitatory neurotransmitter at the insect neuromuscular junction (Jan and Jan, 1976), and a described neurotransmitter in the *Drosophila* CNS (Daniels et al., 2008; Raghu and Borst, 2011).

Glu is a precursor to GABA. In *Drosophila*, it is trafficked across the membrane by dEAAT1, and packaged into synaptic vesicles by DVGLUT. There are several receptors.

Glu staining in the insect MB

Glu immunoreactivity was first detected in the MB of honey bees, albeit at low levels, in some KC clusters, sparing the peduncle (Bicker et al., 1988). In crickets, the MB stains stains strongly overall, except the equivalent of α/βc KCs (Schürmann et al., 2000). In the cockroach, only the most recently generated KCs innervating

the ingrowth lamina show positive immunoreactivity (Sinakevitch et al., 2001). Besides this, some innervation likely from glutamatergic MB-extrinsic neurons is visible in the cockroach MB (Sinakevitch et al., 2001). These findings suggest that glutamate might play a role in developing KCs.

In *Drosophila melanogaster*, α/βc KCs were found to moderately stain for α-Glu (Sinakevitch et al., 2010; Sinakevitch-Pean et al., 2001; Strausfeld et al., 2003). This staining was strongest in the first few hours after eclosion, but then quickly fades, again suggesting a role for Glu in α/βc KCs during development (Sinakevitch et al., 2010).

dEAAT1 transports Glu in insects

Because glutamate itself may serve as a mere metabolite (Frontali, 1964), the presence of proteins involved in Glu membrane trafficking may be a better indicator for Glu as a neurotransmitter.

The *Drosophila* excitatory amino acid transporter (dEAAT1) is a sodium-dependent Glu transporter (Seal et al., 1998), that also trafficks aspartate (Besson et al., 2000; see also 3.1.3). EAATs remove Glu from the synaptic cleft and extrasynaptic sites via reuptake into glia or neurons, thus regulating Glu concentration in the extracellular space (Zerangue and Kavanaugh, 1996).

In honey bees, AmEAAT is expressed especially during development in inner compact Kenyon cells (Kucharski et al., 2000) that are possibly equivalent to *Drosophila* α/βc. In *Drosophila*, dEAAT1 and glutamine synthetase were found to be expressed in glia that surround Glu-positive KCs in very young adults (Sinakevitch et al., 2010). A potential role for Glu transport in olfactory memory has been proposed, as pharmacological interference with this transporter in the honey bee MB leads to impaired LTM (Maleszka et al., 2000).

DVGLUT staining in *Drosophila*

Another glutamate transporter, VGLUT is required for trafficking glutamate into synaptic vesicles where it is stored in preparation for presynaptic release upon stimulation (Takamori, 2006). While there are three transporters in the mammalian

system (Takamori, 2006), there seems to be only one in *Drosophila* that is sufficient to fill synaptic vesicles with glutamate: DVGLUT (Daniels et al., 2006, 2004).

There is only little DVGLUT staining in the MB, apparently none in KCs, mainly restricted to the γ1/2 region and to the α lobe, none in the peduncle, but some in the calyx (Daniels et al., 2008; Johard et al., 2008; Mahr and Aberle, 2006; Sinakevitch et al., 2010, and personal observations). Furthermore, the *dvglut* promoter-derived driver line OK371-GAL4 does not seem to label any KCs (Johard et al., 2008; Mahr and Aberle, 2006).

Recently, glutamatergic MBONs have been described that innervate the aforementioned immunopositive MB regions (Aso et al., 2014a). Namely, MBON-γ4>γ1γ2 has glutamatergic terminals in the γ1/2 region, and MB-MV2 has glutamatergic terminals in α1/2/3 (Aso et al., 2014a; Ito et al., 1998; Tanaka et al., 2008). These MBONs might possibly account for the DVGLUT staining detected in MB lobes.

These results suggest that there may be some glutamatergic signalling inside the MB, possibly from KCs.

3.1.5 GABA in the MB

γ-aminobutyric acid (GABA) is the main inhibitory neurotransmitter in mammals and insects (Bennett and Balcar, 1999).

GABA stainings

Immunostainings against conjugated GABA in several insect species including *Drosophila melanogaster* reveals some MB labelling. This staining, however, is largely confined to the calyx and lobes, generally attributed to MB-extrinsic neurons such as APL, while KCs themselves are immunonegative to GABA (Bicker, 1999; Ganeshina and Menzel, 2001; Schürmann et al., 2000; Strausfeld et al., 2003; Yamazaki et al., 1998; Yasuyama et al., 2002; and personal observations).

GAD1 expression

GABA is synthesised by the enzyme glutamic acid decarboxylase (GAD), and the enzyme GAD1 was described in *Drosophila melanogaster*, where it expresses in the adult CNS (Jackson et al., 1990). *gad1*-GAL4 (Ng et al., 2002) was found to express in KCs of the larval brain, but not in the adult (Johard et al., 2008; Nässel et al., 2008). The more recently developed *gad1* driver line R58F02-GAL4 expresses specifically in α/βc KCs (Jenett et al., 2012). An antibody against GAD1 was developed and successfully tested (Aso et al., 2014a; Jackson et al., 1990), but appears to label no KCs (personal observations).

vesicular GABA transporter (VGAT) expression

The vesicular GABA transporter (VGAT) is required for trafficking of GABA into synaptic vesicles. A recently raised antibody against VGAT stains large areas of the fly brain including the calyx, but no expression was detected in the MB peduncle or lobes (Enell et al., 2007).

GABA receptor expression

The ionotropic $GABA_A$ receptor subunit Rdl is expressed throughout the MB: KC cell bodies, calyx, peduncle, and all five lobes show immunopositive staining in *Drosophila* (Aronstein and Ffrench-Constant, 1995; Enell et al., 2007; Harrison et al., 1996; Liu et al., 2007). The $GABA_A$ receptor subunit Lcch3 is broadly expressed throughout the *Drosophila* brain, but the precise distribution of immunoreactivity in the MB is not yet clear (Aronstein et al., 1996). The metabotropic $GABA_B$R2 subunit is expressed in the calyx, but not in other parts of the MB (Enell et al., 2007). The expression of the other metabotropic subunits has not yet been mapped. Overall, these findings suggest that GABA acts on MB calyx and lobes through multiple GABA receptors, but KC expression of GABA seems confined to development and may merely serve as a metabolite.

3.1.6 Acetylcholine (ACh) in the MB

Acetylcholine (ACh) is the major excitatory transmitter in insect brains (Breer, 1987; Buchner et al., 1986; Gorczyca and Hall, 1987; Klemm, 1976; Lee and O'Dowd, 1999; Sattelle and Breert, 1990). The main excitatory input to the MB calyx, coming from AL PNs, relies on excitatory cholinergic neurotransmission (see 1.2.1; Gu and O'Dowd, 2006; Su and O'Dowd, 2003; Yasuyama et al., 2002).

ACh is synthesised from choline by the action of the enzyme choline acetyltransferase (ChAT) (Kitamoto et al., 1998), and transported into synaptic vesicles by the vesicular acetylcholine transporter (VAChT) (Kitamoto et al., 1998; Usdin et al., 1995). Upon release into the synaptic cleft, ACh can bind to either fast-acting ionotropic nicotinic ACh receptors, or act through specific GPCRs: muscarinic ACh receptors. Its mode of action is very rapid and brief, because large quantities of ACh are generally released, and ACh is quickly hydrolysed again at the synaptic cleft through the action of acetylcholinesterase (AChE) (Dale et al., 2008). Choline is then taken up again into the presynapse by the choline transporter (CHT), which is the rate-limiting step (see Kuhar and Murrin, 1978, review by Ferguson and Blakely, 2004, and Figure 3.1).

Cholinergic neurons thus contain at least VAChT and ChAT, and potentially AChE and CHT.

Cha and *VAChT* genes share a phylogenetically conserved "cholinergic locus" in all species examined so far, in which VAChT is nested within the first intron of ChAT (see Kitamoto et al., 1998; Usdin et al., 1995). While there may be common transcriptional control for both genes in *Drosophila*, *Cha* and *VAChT* transcripts may be independently regulated post-transcriptionally (Kitamoto et al., 1998).

Drosophila ChAT comes in two forms: a soluble hydrophilic form, and a plasma membrane-bound amphiphilic form that likely attaches to a membrane component, both of which have the same apparent molecular weight (Pahud et al., 1998).

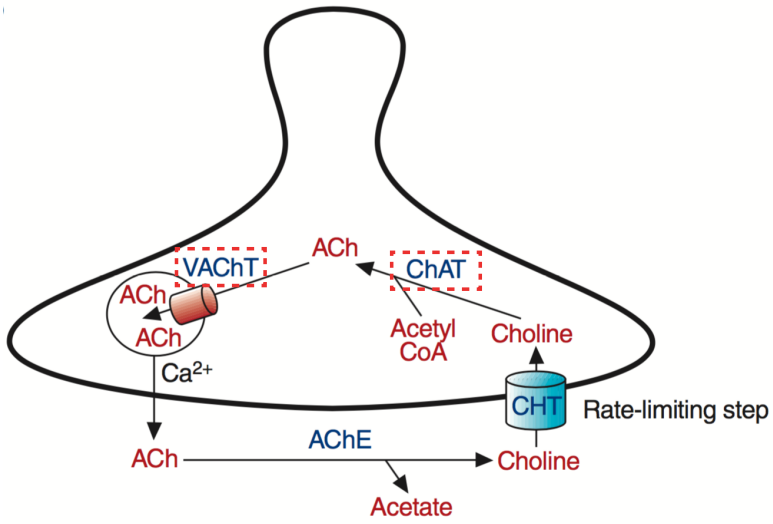


Figure 3.1: Synaptic acetylcholine synthesis and packaging pathway. The enzyme choline acetyltransferase (ChAT) acetylates choline to produce acetylcholine (ACh). ACh is packaged into synaptic vesicles by the vesicular acetylcholine transporter (VAChT). When the neuron is stimulated and the presynaptic calcium concentration increased, ACh-containing vesicles fuse with the cell membrane to release ACh into the synaptic cleft. Here, ACh is quickly hydrolysed by the enzyme acetylcholinesterase (AChE). Choline is then taken up again by the choline transporter (CHT). Adapted from Ferguson and Blakely, 2004.

ChAT expression

ChAT antibodies. Traditionally, ChAT antibodies have mostly been used to define cholinergic neurons in mammals and insects.

The first reported monoclonal antibody (Crawford et al., 1982) staining in the brain of *Drosophila melanogaster* showed widespread immunoreactivity, but "the three lobes and the peduncle of the mushroom bodies [...] are distinctive for their low levels of staining" (Buchner et al., 1986). It should be noted that the immunoreactivity presented (Buchner et al., 1986) seems lowest in the peduncle, slightly higher in the β/γ lobes, clearly visible in what is likely the α' lobe, and very faint in what is likely the α lobe. Also, there seems to be no immunoreactivity in cell bodies. Gorczyca and Hall (1987) later confirmed this staining pattern using the same antibody: they reported no visible staining in the MB peduncle of adults, but detected MB staining in the larval MB.

Another ChAT monoclonal antibody (4B1, Takagawa and Salvaterra, 1996)

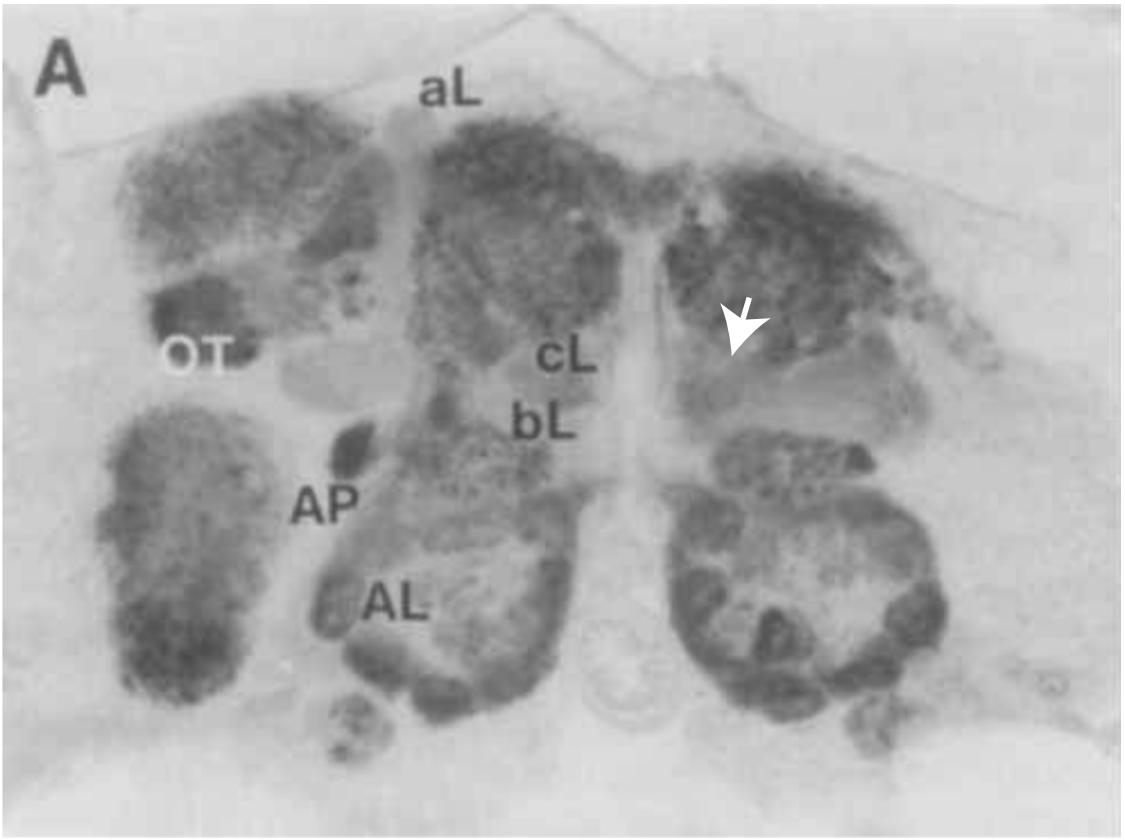


Figure 3.2: Original ChAT antibody staining showing MBs. Original caption states "Notable unstained regions include the three lobes (alpha lobe, aL; beta lobe, bL; gamma lobe, cL; A) [...] of the mushroom bodies". Arrow was added to point to the γ lobe tip that shows relatively strong immunoreactivity. Adapted from Yasuyama et al., 1995.

shows a similar staining pattern to previous results in that the MB lobes are weakly stained and there is absence of staining in the MB peduncle (Yasuyama et al., 1995, 1996). The authors write that "notable unstained regions include the three lobes [...] and the peduncle (P) of the mushroom bodies" (Yasuyama et al., 1995, p. 28; see also Figure 3.2).

The ChAT4B1 antibody was raised against an 83-kDa fusion protein of dChAT, shows a single band at about 80 kDa in Western blots of fly head extracts, and its affinity was confirmed by Scatchard analysis (Takagawa and Salvaterra, 1996). Widely considered to be one of the most reliable markers for cholinergic neurons, this antibody has since been widely used in the adult *Drosophila* CNS, such as the OL (Kolodziejczyk et al., 2008; Raghu et al., 2013; Takemura et al., 2008), AL (Shang et al., 2007; Tanaka et al., 2012), the calyx (Butcher et al., 2012; Leiss

et al., 2009; Yasuyama et al., 2002), MBONs (Aso et al., 2014a; Séjourné et al., 2011), and cultured cells (Lee and O'Dowd, 1999).

Unfortunately, cell bodies are generally found to show no immunoreactivity towards ChAT, presumably because the protein only becomes fully translated at the presynapse where it is required (Buchner et al., 1986; Gorczyca and Hall, 1987; Kahsai and Winther, 2011; Yasuyama et al., 1995), making it harder to identify specific neuronal identities.

***Cha* mRNA.** Besides raising antibodies against ChAT peptide sequences, *Cha* mRNA levels can also be detected by *in situ* hybridisation in which labelled complementary RNA (cRNA) probes bind to RNA sequences of interest. Using radioactive cRNA probes, Barber et al. (1989) detected *Cha* mRNA levels across the brain, but the level of resolution was insufficient to determine *Cha* mRNA in specific neuropils like the MB. Similarly, Yasuyama et al. (1996) saw widespread positive labelling with a non-radioactive cRNA probe, but the resolution was insufficient to detect MB-specific labelling.

***Cha* fragment-driven reporter expression.** Another method for localising gene expression is the use of gene fragments to drive expression of a reporter gene. These methods include *lacZ* reporters with X-gal staining, as well as the GAL4/UAS system and its derivatives (see 1.5.1).

The first such studies used various *Cha* fragments to drive a lacZ reporter, and detected high levels in the OL and AL, but MB labelling could not be clearly discerned (Kitamoto et al., 1995, 1992; Yasuyama et al., 1996). A later study shows clearly the AL and ACT, while the peduncle seems to be negative (Yasuyama et al., 2002).

To use the GAL4/UAS system, Salvaterra and Kitamoto (2001) generated a Cha-GAL4 line with 7.4 kb of 5' flanking DNA from the *Drosophila melanogaster* cholinergic locus. This line drives expression in many thousand cells, including in the OL, the AL and calyx, and the CC (Salvaterra and Kitamoto, 2001). In the

MB, the γ and β lobes show some positive fibres, but the peduncle seems largely clear (Johard et al., 2008; Salvaterra and Kitamoto, 2001).

Kitamoto (2002) also generated a Cha3.3kb-GAL80 line that supresses GAL4 expression in presumably cholinergic neurons. They showed that the introduction of Cha3.3kb-GAL80 greatly sparsened expression in c309-GAL4 driven γ and α/β KCs (Kitamoto, 2002). Further studies found KC expression from GAL4 lines suppressed with Cha3.3kb-GAL80 (Mehren and Griffith, 2006; Yi et al., 2013), leading some authors to suggest that some KCs may be cholinergic (Yi et al., 2013). Cha3.3kb-GAL80 previously also led to a loss of expression in presumably cholinergic EB neurons (Martín-Peña et al., 2014; Wu et al., 2007; Zhang and Roman, 2013), AL PNs (Liu and Davis, 2009), and DPM neurons (Keene et al., 2004). Cha3.3kb-GAL80 expression, however, may not necessarily be restricted to cholinergic neurons (Liu and Davis, 2009).

A recently developed Cha3.3kb-LexA::GAD driver (Diegelmann et al., 2008) has thus far not been described in the adult brain.

VAChT/AChE/CHT expression

VAChT expression. There has been considerably less attention on the expression of VAChT in the *Drosophila* brain. Kitamoto et al. (1998) raised a polyclonal antibody against the hydrophilic C-terminal domain (Arg-441 to Asn-546), which was later confirmed in mutants (Kitamoto et al., 2000). The staining pattern of this antibody was recently shown in the OL where it is largely in line with α-ChAT staining patterns (Kolodziejczyk et al., 2008), but the staining pattern of the central brain has not yet been published.

AChE expression. AChE activity was previously inferred by hydrolysis of acetylthiocholine (Buchner et al., 1986; Hall et al., 1980). Similar to ChAT, the AL, OL, CC, and calyx showed high AChE levels, while the "entire mushroom body" showed "rather low levels of staining" (Buchner et al., 1986, p. 61). Yet, it is not always clear if the MB truly stains less strongly than the rest of the brain (compare staining patterns observed by Hall et al., 1980).

Wolfgang and Forte (1989) generated a monoclonal AChE antibody that stains large parts of the *Drosophila* brain, but due to the focus on the visual system, MB staining can not be clearly discerned (Wolfgang and Forte, 1989).

Choline transporter (CHT). While the mammalian choline transporter (CHT) is well described (Ferguson and Blakely, 2004), the gene in *Drosophila* has not yet been clearly identified. Choline transporter-like 1/2 (CG1311 / CG11880) have been predicted to fulfill this role (see Martin and Krantz, 2014), and CG7708 is also predicted to show choline transmembrane transporter activity (FlyBase, 1992), but further evidence is still needed to establish these functions.

ACh receptors in mammals

Relatively little remains known about nicotinic receptor composition in *Drosophila melanogaster*, but there are many parallels to the well-studied mammalian system.

Nicotinic ACh receptors (nAChRs) are pentameric structures forming ligand-gated ion channels. There are 17 receptor subunits (α1-10, β1-4, δ, ε, and γ) in mammals that mostly form heteropentamers except for the $\alpha7_5$ homomer (Dale et al., 2008). The most broadly expressed subtypes are $(\alpha1)_2\beta1\delta\varepsilon$ (muscle), $(\alpha3)_2(\beta4)_3$ (ganglion), and $(\alpha4)_2(\beta2)_3$ (CNS), but there are many other heteropentameric combinations (Dale et al., 2008). Each of these has distinct kinetic properties and different sensitivities to ant/agonists. Agonists include ACh, carbachol, nicotine, epibatidine, cytisine, and varenicline. Antagonists include α-bungarotoxin, α-conotoxin, tubocurarine, pancuronium, hexamethonium, mecamylamine, MLA, and bupropion (Daly, 2005).

Muscarinic ACh receptors (mAChRs) are GPCRs, and come in five types: M_{1-5}. Agonists include ACh, muscarine, carbachol, and oxotremorine. Antagonists include atropine, scopolamine, hyoscyamine, and thorazine (Dale et al., 2008).

Nicotinic ACh receptors in insects

Less is known about insect nAChRs, but there are 10 different subunits (Dα1-7 and Dβ1-3) that also form heteropentamers with the exception of $(D\alpha5)_5$ and $(D\alpha7)_5$ (reviewed in Jones and Sattelle, 2010; Lansdell et al., 2012; Thany, 2010; Thany et al., 2007).

nAChR subunit composition and pharmacology. Insect nAChRs can be generally divided according to their sensitivity to the antagonist α-bungarotoxin (α-BTX) (Rudloff, 1978; Schloss et al., 1991; Schmidt-Nielsen et al., 1977). α-BTX-sensitive nAChRs include pentamers consisting of (Dα1, Dβ2, Dα2, Dxx, Dxx), as well as $(D\alpha7)_5$, where 'Dxx' refers to yet unknown subunits. α-BTX-insensitive nAChRs consist of (Dα4, Dβ3, Dxx, Dxx, Dxx), as well as (Dβ3, Dβ2, Dxx, Dxx, Dxx) (Thany et al., 2007). Although precise subunit compositions are still largely unknown, antagonist sensitivities have been well-studied as a potential target for novel insecticides (see Millar and Denholm, 2007). Subunit compositions have mostly been investigated by co-expressing 1–2 *Drosophila* subunits in *Xenopus* oocytes along with the chick β2 subunit, and recording from the resulting receptors electrophysiologically (Bertrand et al., 1994). These studies led to several conclusions regarding the subunit composition of *Drosophila* nAChRs:

- Dα1 and Dα2 each form a functional ACh receptor together with β2 (Bertrand et al., 1994).
- Dα3 and β2 form a functional α-BTX-sensitive ACh receptor (Schulz et al., 1998).
- Dα3 and Dβ1 form a functional α-BTX-sensitive ACh receptor (Chamaon et al., 2000).
- Dα1 and 2 form a functional receptor with β2 that is α-BTX-insensitive (Schulz et al., 2002).
- Dα1, Dα2, and Dβ2 form a functional receptor (Chamaon et al., 2002).

- Dα5 and Dα7 can each form homomeric receptors (Lansdell et al., 2012).
- Dα5-7 can together form a functional receptor with high ACh affinity (Lansdell et al., 2012).
- Dα6 confers spinosad-sensitivity to nAChRs (Perry et al., 2007, 2015; Somers et al., 2015).

Expression in the insect brain. Labelled α-BTX can also be used to visualise α-BTX-sensitive nAChR expression in the *Drosophila* brain. Early studies showed the general presence of nAChRs in the fly brain, but it was difficult to identify specific neuropils (Rudloff, 1978; Schmidt-Nielsen et al., 1977). A more recent study, however, shows strong α-BTX labelling in the MB in what is likely β′, γ, β, with relatively weak labelling of α (Schuster et al., 1993).

Antibodies for specific subunits also revealed that Dα2 expresses strongly in α, β, and γ lobes of the MB (Jonas et al., 1994). Dβ2, on the other hand, seems to be mostly confined to the OL (Chamaon et al., 2002). An antibody against Dα7 shows strong staining in the OL, but only little in the MB (Fayyazuddin et al., 2006; Leiss et al., 2009). A Dα7-GAL4, however, expresses strongly in α/β KCs (Fayyazuddin et al., 2006).

A recent study using RNA-seq found high levels of Dα2 in the M4β MBON, Dα4 in M6, Dα4 and Dα7 in MB-V3, and Dα1/3/6/7 and Dβ1/2 in V2 MBONs (Crocker et al., 2016).

Functional roles of nAChRs. While there are many functional roles for nAChRs in insect behaviour (partly reviewed by Thany, 2010), one of the most striking examples of a nicotinic connection in the MB was found in bees (Lozano et al., 2001). When honey bees were trained to associate an odour with sugar, their memory retrieval could be blocked by injecting the nAChR antagonist mecamylamine into the MB α lobe (Lozano et al., 2001). This would suggest that cholinergic transmission is required in the MB lobes for retrieval of olfactory memories.

A behaviour associated with a specific nAChR subunit is the visually mediated jump response that seems to rely on cholinergic transmission via the Dα7 nAChR in the giant fibre circuit (Fayyazuddin et al., 2006).

Recently, the protein Sleepless (SSS) was found to antagonise nAChR function to regulate sleep. Specifically, SSS seemed to interact with Dα3 in the MB, where both showed some level of immunoreactivity (Wu et al., 2014). Furthermore, the gene for the Dα4 subunit, *redeye* (*rye*), was shown to be involved in homeostatic sleep regulation, although the presented expression pattern suggests expression in glia (Shi et al., 2014).

These findings suggest there may be nAChRs in the MB lobes that may receive cholinergic input to fulfill functional roles.

Muscarinic ACh receptors in insects

There are two muscarinic AChRs expressed in the *Drosophila* brain: mAChR-A and mAChR-B (Collin et al., 2013; Shapiro et al., 1989). In line with its role as a GPCR, carbachol stimulation of mAChR-A was found to stimulate inositolphospholipid metabolism (Blake et al., 1993; Shapiro et al., 1989). While mAChR-A shows relatively fast responses to ACh and muscarine, mAChR-B shows slower respones to ACh (also in the presence of atropine, scopolamine, and QNB) but none to muscarine (Collin et al., 2013).

mAChR-A seems to be expressed in some KCs (Blake et al., 1993; Hannan and Hall, 1996; Silva et al., 2015), where it is required for larval aversive olfactory learning (Silva et al., 2015). According to a recent RNA-seq study, mAChR-A does not seem to be expressed in MBONs but in γ and α/β KCs (Crocker et al., 2016, Figure 4).

3.1.7 sNPF

Short neuropeptide F (sNPF) is a neuropeptide expressed by some KCs involved in olfactory memory, growth, and sleep (Johard et al., 2008; Knapek et al., 2013; Lee et al., 2008; Shang et al., 2013). Its background and role is further described in chapter 4.

3.2 Calcium responses in MBONs to ACh application

3.2.1 Approach

MBONs receive olfactory information directly from excitatory KC → MBON synapses (Hige et al., 2015b; Takemura et al., 2017). The principal KC neurotransmitter should thus excite MBON dendrites in the MB lobes. I hence tested the effects of different KC transmitter candidates by applying them directly to M4/6 MBON dendrites while monitoring calcium transients in an explant brain.

Description and advantage of wide-field imaging of explant brains

I used an explant brain preparation for this to facilitate locating the injection pipette directly the the MBON dendritic zone without any potential obstructions from cuticle, as well as to minimise movement that could have misdirected injections.

Widefield imaging was preferred as it facilitated switching between infrared and fluorescent channels for positioning the pipette. Furthermore, the use of an explant brain with neurons located at the anterior side of the brain allowed clear visualisation of MBON calcium signals without the need for two-photon illumination. This was also enabled by the use of a specific GAL4 driver line with minimal expression outside of M4/6 MBONs (see Figure 3.3A).

As can be seen in Figure 3.3A-B, R21D02-GAL4 strongly drives expression in MBON-γ5β′2a, MBON-β′2mp, and MBON-β2β′2a (Aso et al., 2014a) (collectively referred to as M4/6 neurons in the following; see also Owald et al., 2015a; Tanaka et al., 2008), with some weak expression in some optic lobe and antennal lobe neurons.

M4/6 neurons are expressed in R21D02-GAL4

M4/6 neurons are comprised of three cell bodies per hemisphere, located dorsally along the midline. Each cell body extends one neurite to its respective horizontal lobe compartment, where each forms dense postsynaptic sites that join together to form one axon each with extensive presynaptic sites within the SMP (Aso

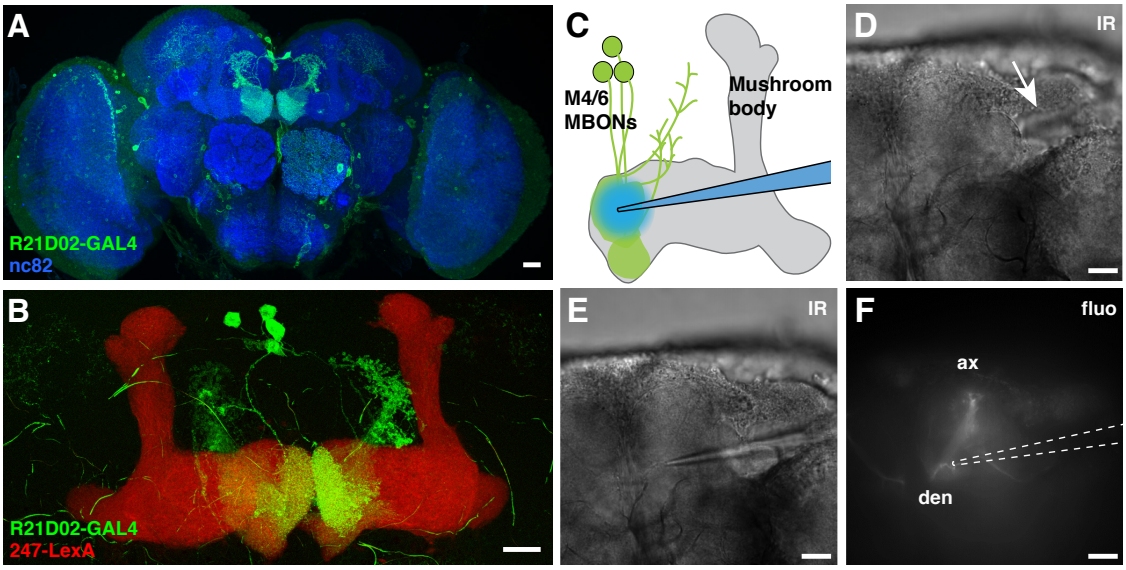


Figure 3.3: R21D02-GAL4 expression pattern and experimental approach of explant brain microinjections. A) R21D02-GAL4 expression (green) is largely confined to MBON-γ5β′2a, MBON-β′2mp, and MBON-β2β′2a (M4/6 neurons), with only some weak expression in optic lobe and antennal lobe neurons. GAL4 drove expression of UAS-GCaMP5, which was stained with α-GFP antibody (green). Brain was counter-stained with α-nc82 (blue). Shown is a maximum projection of a confocal stack. B) R21D02-GAL4 (green) reveals M4/6 neuron anatomy. Three M4/6 cell bodies per hemisphere are located dorsally at the midline, while the dendrites densely innervate the respective MB compartment. Axons leave each dendritic compartment and innervate parts of SMP, SIP, SLP, and CRE neuropils. The MB is visualised through the use of 247-LexA ; lexAop-rCD2::mRFP (red). C) Schematic of experimental approach. M4/6 MBONs, postsynaptic to KCs, genetically express GCaMP5 through R21D02-GAL4. Transmitter candidates are then applied at 1 mM concentration through a microinjection pipette targeted specifically to the M4/6 dendritic arbour. This is done in explant brains to guarantee stability of injection and minimise spontaneous activity. D-F) Sample images of explant brain microinjections approach. D) During dissection, a small hole was carefully opened in the perineural sheath (arrow), laterally to the horizontal lobe to minimise any damage to KCs or M4/6 MBONs. E) A microinjection pipette with a ∼3 µm opening and filled with 1 mM of a candidate transmitter was then lowered into the bath and entered the brain through the respective hole, under infrared light illumination. The pipette then carefully penetrated the tissue, mostly at an angle perpendicular to its axis to minimise tissue damage until it reached the γ5 compartment of M4/6 dendrites (den), under visual guidance of the green fluorescence channel (F). Once in position, test pulses were applied with progressively longer duration, until minimal release was achieved, and the recording started. Scale bars represent 20 µm. Partly adapted from Barnstedt et al. (2016).

et al., 2014a; Owald et al., 2015a; Tanaka et al., 2008), between the horizontal and vertical lobes of the MB (see Figure 3.3B).

I specifically used M4/6 neurons to screen for KC transmitters because these neurons were shown to play an important role for aversive and appetitive memory (Owald et al., 2015a), and because they represent a relatively homogeneous population that nevertheless innervates all three main KC cell types in close proximity. Injecting a candidate into the M4/6 dendritic area should thus allow signals from any of these three neurons to be detected with widefield imaging.

In order to screen for KC transmitters that would excite M4/6 output neurons, I used the GECI GCaMP5 (Akerboom et al., 2013) to monitor neural calcium levels as a proxy for neural activity. While this method may be insensitive to detect the action of inhibitory or modulatory neurotransmitters, it should provide a reliable readout of neural excitation. In later experiments, I used the more recently developed GECI GCaMP6f (Chen et al., 2013a) that allows more precise temporal calcium detection.

Figure 3.3C-F illustrates how the microinjection pipette was placed into position at the right location in the explant brain, while minimising any tissue damage. In brief, a microinjection pipette filled with 1 mM of transmitter candidate entered the explant brain through a small hole torn into the perineural sheath laterally to the MB horizontal lobe. Once in place, small test pulses first ensured proper release before recordings started.

3.2.2 Application of candidates

I applied six different KC transmitter candidates to M4/6 dendrites that have previously been suggested as potential KC transmitters (see 3.1).

For this initial screen, I chose to inject a concentration of 1 mM to minimise the chance of false negatives due to insufficient concentration, assuming that most receptors still become active also at higher concentrations but not at lower concentrations from their optimum.

Testing five individual brains for each candidate transmitter, only ACh application resulted in detectable calcium responses (see Figure 3.4).

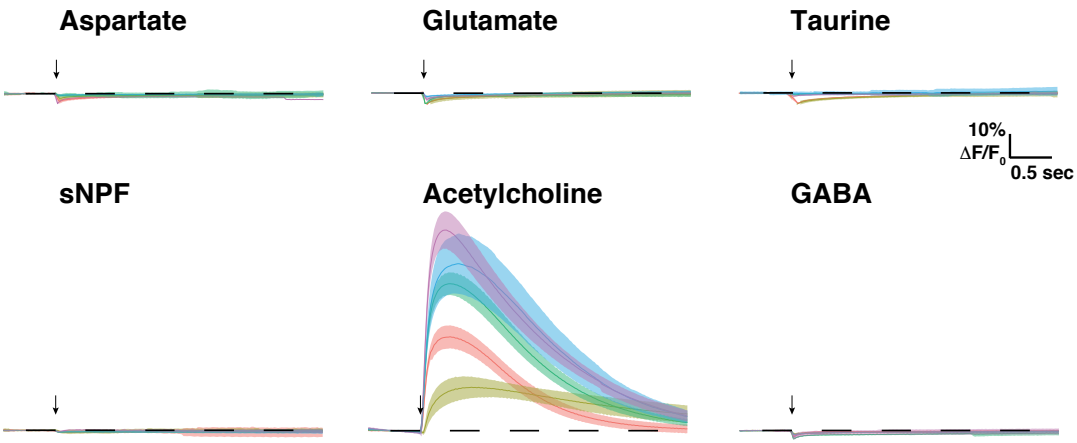


Figure 3.4: Precise application of 1 mM of six transmitter candidates to the M4/6 dendritic arbour yields detectable calcium responses only in the case of ACh (bottom centre). $N = 5$ brains per transmitter candidate; displayed are the mean and SEM of 10 stimulations, each colour representing an individual brain per transmitter candidate. Modified from Barnstedt et al. (2016).

Focal application of 1 mM acetylcholine (ACh) into the MB horizontal lobe tips (the site of M4/6 dendrites) in R21D02-GAL4 ; GCaMP5 flies resulted in an immediate increase in fluorescence at the site of injection, indicative of fast dendritic calcium influx.

3.2.3 Dose-dependence of ACh-evoked calcium responses

In order to reproduce these ACh-induced calcium responses and to determine the dependence of these to varying concentrations, I applied ACh at five different concentrations (logarithmically from 10 µM to 100 mM) on five different brains for each concentration.

Analysis of peaks demonstrates a clear dose-dependence of calcium responses, with 10 µM ACh application $\Delta F/F_0$ peaks only rarely reaching threshold (4 SD above baseline), while already 100 µM ACh reliably elicit considerable calcium responses, with mean peak values of ~ 0.05 $\Delta F/F_0$ (see Figure 3.5A). At concentrations ≥ 1 mM, strong responses with mean peaks of ~ 0.3 $\Delta F/F_0$ are elicited.

Other parameters analysed were time to peak, rise time, and time to response onset (see Figure 3.5B-D). Time to peak was seemingly high at 10 µM, presumably

due to non-specific late responses (Figure 3.5B). From 100 µM to 100 mM, time to peak progressively increases from about 0.5 s to 2 s. Similar kinetics were observed for the rise time (Figure 3.5C).

Interestingly, the time to response onset, calculated from the start of stimulation to the first sign of a fluorescence increase was very low, with an average of only 3-4 frames ($\sim 100 - 130$ ms) with an ACh stimulation of 1 mM. Taking into account the onset times of calcium influx and the kinetics of GCaMP5, this may serve as an indicator for a rather direct receptor response to the ACh injected, and not a secondary response through the network.

Sample images of individual Ca^{2+} traces can be found in Figure A.1, and pooled transients from all brains at 5 different concentrations can be found in Figure A.2.

3.2.4 ACh acts directly on M4/6 dendrites

Timing of ACh-evoked calcium responses

While the inherently slow dynamics of calcium indicators make it difficult to interpret the speed of response onset, we could find relatively fast response onsets of $\sim 30 - 40$ ms, when using a fast imaging protocol with GCaMP6f (see Figure A.3A). Furthermore, the temporal dynamics of ACh spread were highly correlated with calcium signal dynamics at the site of injection (see Figure A.3B), indicative of direct dendritic calcium responses of M4/6 neurons.

Response dependence on injection distance

As ACh is the most abundant neurotransmitter in the *Drosophila* brain (see 3.1.6), it is conceivable that ACh injections, despite being focal to γ5, could spread out to activate nearby neurons with ACh receptors that, in turn, activate M4/6 neurons. Another way to rule out this hypothesis is the application of ACh into different surrounding areas of the superior protocerebrum, while observing calcium transients in M4/6 neurons.

To do this, I used R21D02-GAL4 ; GCaMP6f explant brains, and injected 100 µM ACh into various surrounding brain regions while monitoring calcium transients

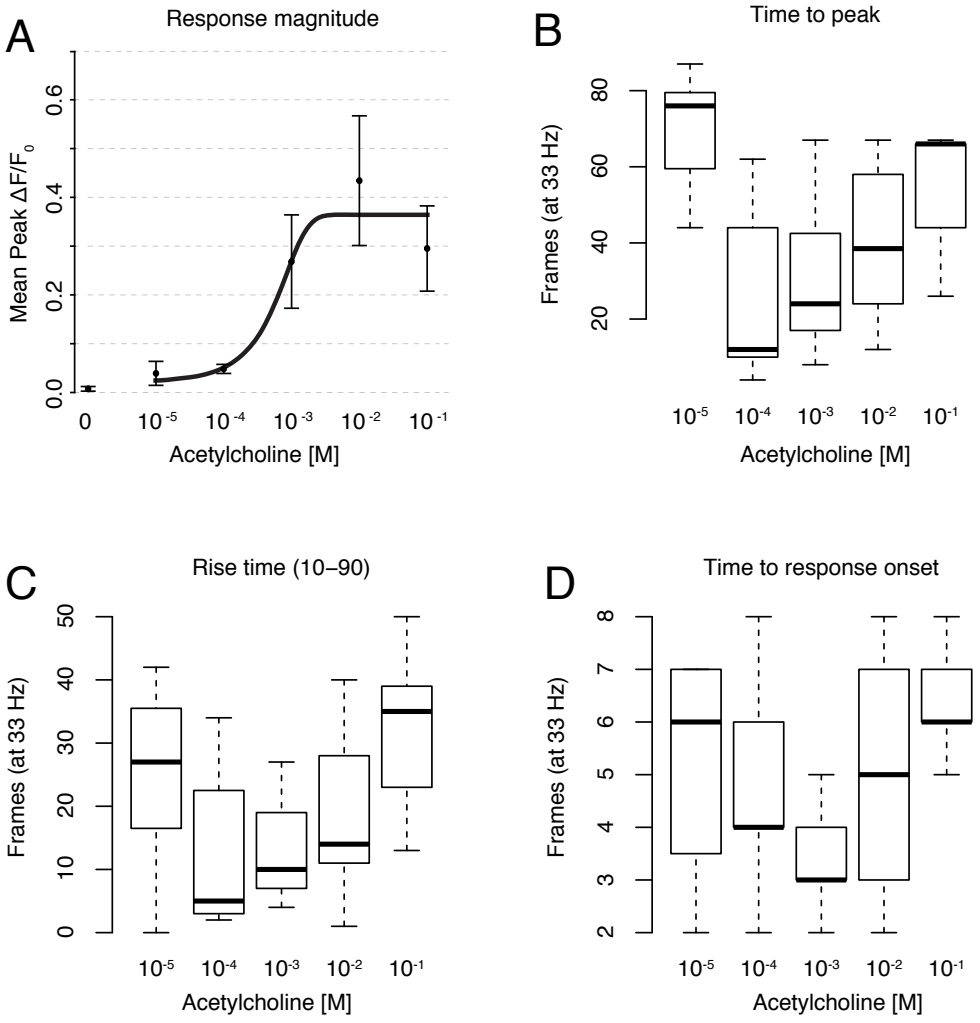


Figure 3.5: Dose-dependent characteristics of ACh injection-evoked calcium responses. Calcium transients were recorded from M4/6 dendrites in R21D02-GAL4 ; GCaMP5 explant brains while different concentrations of ACh were injected into five brains per concentration. A) Dose-response curve of peak calcium responses to ACh stimulation. Doses below 10^{-3} M elicit none or only minor calcium responses, while concentrations at 10^{-3} M or above elicit robust calcium responses. Individual values are derived as the mean of the calcium peak of the first three ACh stimulations in five brains per concentration. Error bars represent SEM. B) Time to peak increases with increasing ACh concentrations injected, starting with 100 µM. Time was measured in frames from recorded stimulus onset up to the maximum $\Delta F/F_0$. C) Rise time of calcium responses increases with higher ACh concentrations injected, starting with 100 µM. Rise time was measured as the number of frames between 10 % and 90 % of response peak $\Delta F/F_0$. D) Time to response onset averages between 3 and 6 frames, i.e. between 100 and 200 ms. Response onset was defined as the time between stimulus onset and a $\Delta F/F_0$ 2 SD above F_0. A brief response onset may be indicative of direct receptor activation. Partly adapted from Barnstedt et al. (2016).

in M4/6 dendrites and monitoring the spread of ACh through TXR. I used 100 µM to minimise the possibility of off-target effects. As before, fast and robust calcium responses were visible when ACh was injected into γ5 or close by, but no calcium responses were visible when ACh was injected into other nearby brain regions, or M4/6 axons (see Figure 3.6).

See also Figures A.4 and A.5 for similar experiments demonstrating response-dependence on distance to M4/6 dendrite.

These findings suggest that M4/6 calcium responses to ACh are not the result of indirect activation through neurons with ACh receptors in surrounding neuropils.

Response dependence on solution spread

If M4/6 calcium responses to ACh are mediated by a secondary ACh-responsive neuron, one would expect calcium responses to cover large parts of the dendrite, irrespective of the precise spread of ACh injected into the dendrite.

To test this, I first used a R21D02-GAL4 ; GCaMP5 explant brain, and injected a small volume of ACh labelled with TXR, while monitoring the spread of ACh in the red fluorescent channel. I then monitored calcium responses to this ACh spread in the green fluorescent channel, and calculated a peak $\Delta F/F_0$ map by calculating the peak $\Delta F/F_0$ for each pixel individually. The resulting map shows a small area with high $\Delta F/F_0$ peaks; this area precisely corresponds to the immediate area at the pipette tip (Figure 3.7A).

Similarly, in a R21D02-GAL4 ; GCaMP6f explant brain, I closely monitored ACh injection spread via TXR and the red fluorescent channel, and recorded calcium transients from the green channel, while progressively injecting larger volumes with wider spread into the M4/6 dendrite. Calculating the pixel-wise ΔF again demonstrates that calcium responses appear only in the area of ACh spread, and increase their area in correspondence with a wider spreach of ACh (Figure 3.7B).

These findings demonstrate that M4/6 calcium responses critically depend on the spread of ACh within the M4/6 dendrite, and are suggestive of a direct action of ACh on the M4/6 dendrite.

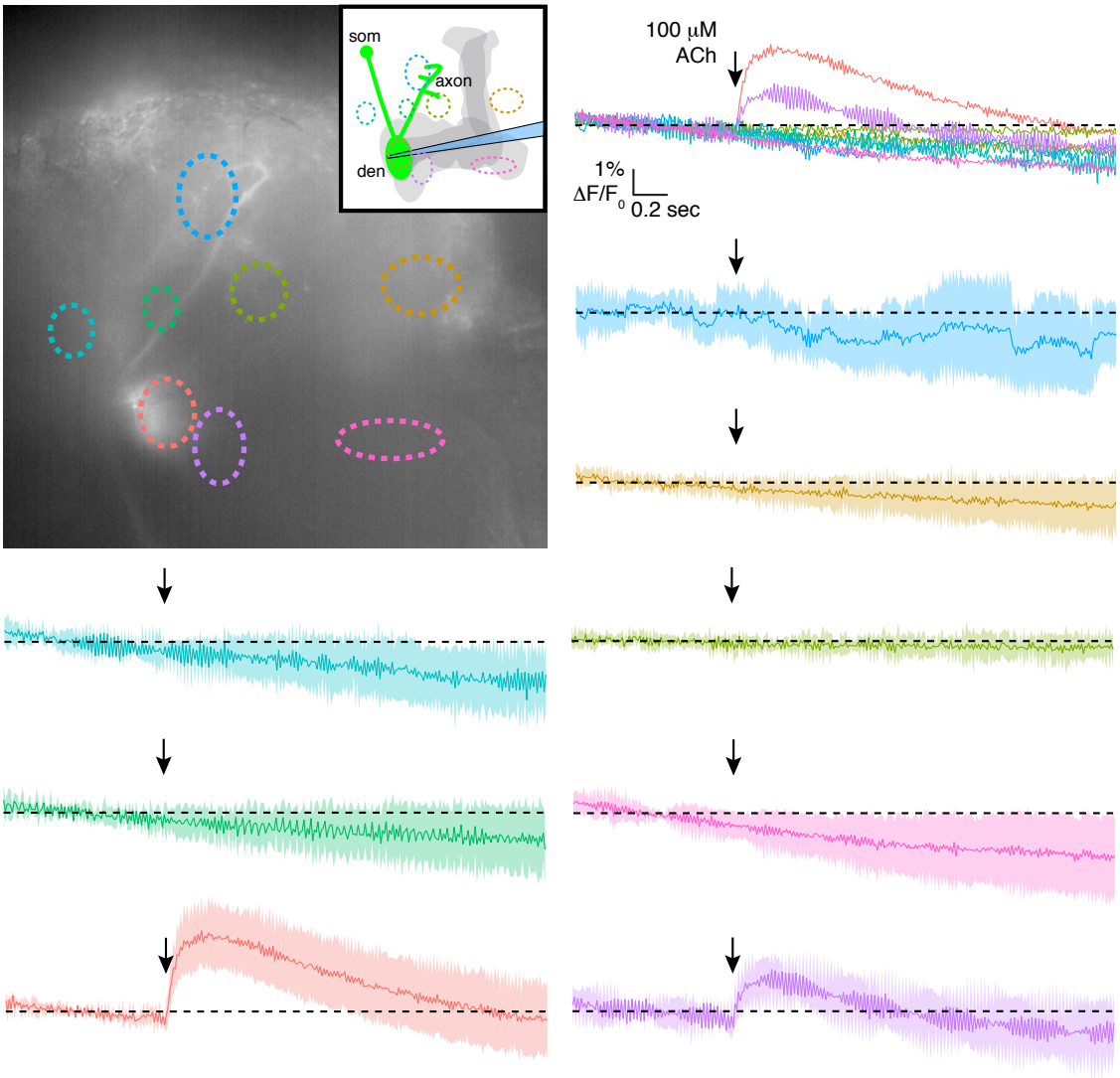


Figure 3.6: Calcium responses in M4/6 dendrites are only elicited when ACh is applied within or near the dendritic field. In one sample brain expressing R21D02-GAL4 driven GCaMP6f the microinjection pipette was positioned at various locations in the right protocerebrum, and 100 µM ACh released. The top left image shows a widefield overview of the area imaged, superimposed with the various locations indicating the spread of solution; the inlay shows a schematic (som–somata; den–dendrites). Calcium transients from the dendrite upon injection at these locations are displayed on the right and bottom, trace colours matching location ellipses to the left. Top right traces show the mean trace from three injection trials per site; all other traces show mean and SEM in shade. Only the two injection sites (displayed in red and purple) closest to the dendritic arbour elicited calcium responses. 1 µM TTX was included to block secondary responses. Modified from Barnstedt et al. (2016).

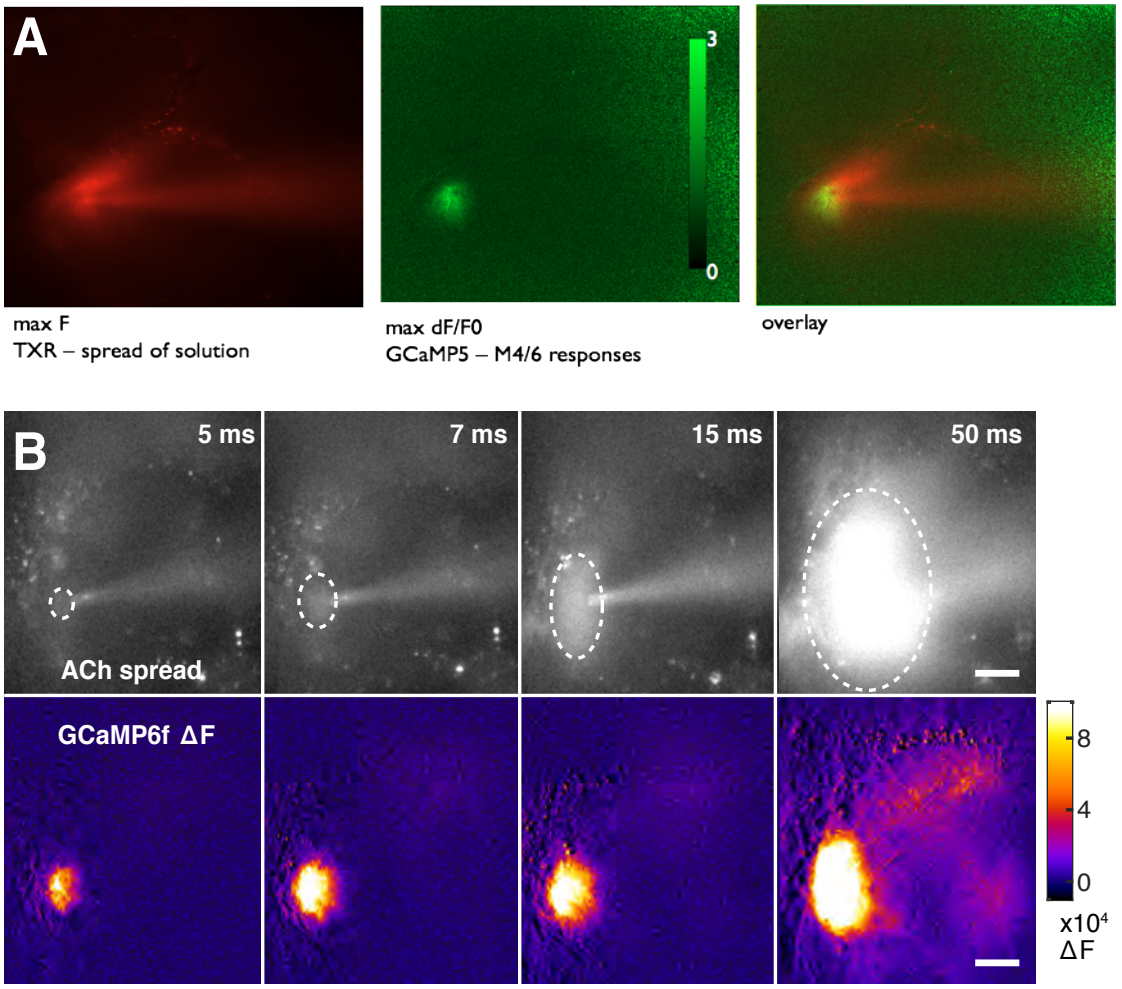


Figure 3.7: M4/6 calcium response depends on the spread of ACh solution. A) Spread of injected ACh is kept to the γ5 region, and M4/6 calcium responses appear only at site of injection. Red fluorescent image shows maximum projection of TXR-marked solution with 100 µM ACh. Green fluorescent image shows maximum $\Delta F/F_0$ from R21D02-GAL4 driven GCaMP5 signal upon ACh stimulation, calculated for each pixel individually. As can be seen from the overlay on the right, calcium responses are only obtained within the spread of solution. B) M4/6 calcium response is proportional to spread of ACh solution. 100 µM ACh with TXR were injected into the M4/6 dendritic arbour of R21D02-GAL4 driven GCaMP6f brains. Upper row shows red fluorescent channel with spread of solution indicated by white dashed ellipsoid, with different release durations indicated above. Lower row shows GCaMP6f fluorescence changes upon stimulation using colour coding. As can be seen, fluorescence responses appear not further than the solution spreads. 1 µM TTX was included to block secondary responses.

Pharmacological block of secondary responses

Another way of ruling out that M4/6 calcium responses to ACh are the result of neural intermediates responsive to ACh is to block the propagation of action potentials (APs). Without AP propagation, other potential ACh-responsive neurons would not be able to propagate their activity on to M4/6 neurons. This can be achieved by including tetrodotoxin (TTX).

TTX blocks voltage-gated sodium channels (VGSCs), thus blocking a neuron's potential to generate action potentials (APs) (Narahashi et al., 1964). It is thus frequently used in neurobiology to study or rule out secondary effects of the activation of other neurons than the one being stimulated.

I have included 1 µM TTX (see Gruntman and Turner, 2013; Sattelle and Breert, 1990; Takemura et al., 2017) in the saline bath to block potential secondary responses in experiments presented in Figure 3.6 and Figure 3.7B. In both cases, robust calcium responses were still found, suggesting ACh activation of the M4/6 dendrites in the absence of AP propagation.

Another possibility to rule out the action of an indirect synaptic connection is to elevate the concentration of Mg^{2+} in the bath. Elevated Mg^{2+} levels have previously been shown to interfere with chemical synaptic transmission (e.g. Evans et al., 1992), and should thus interfere with any secondary neural responses to ACh.

To test this, I imaged dendritic calcium responses from R21D02-GAL ; GCaMP6f upon stimulation with 100 µM ACh. As before, M4/6 dendrites showed reliable calcium responses to ACh stimulation at normal Mg^{2+}, but also at Mg^{2+} levels that were elevated by an additional 10 mM (see Figure 3.8A). These response peaks were not statistically different from one another, and the shape of responses were also similar (see Figure 3.8B).

In contrast to this, stimulating KCs with 10 mM ACh in the calyx (see Cohn et al., 2015; Inada et al., 2017; Tomchik and Davis, 2009) while monitoring calcium responses in M4/6 dendrites shows robust responses under normal Mg^{2+} conditions, but a significant decrease under high Mg^{2+} conditions (Figure 3.8C). This shows that the known synaptic connection from KC to M4/6 requires normal Mg^{2+} levels.

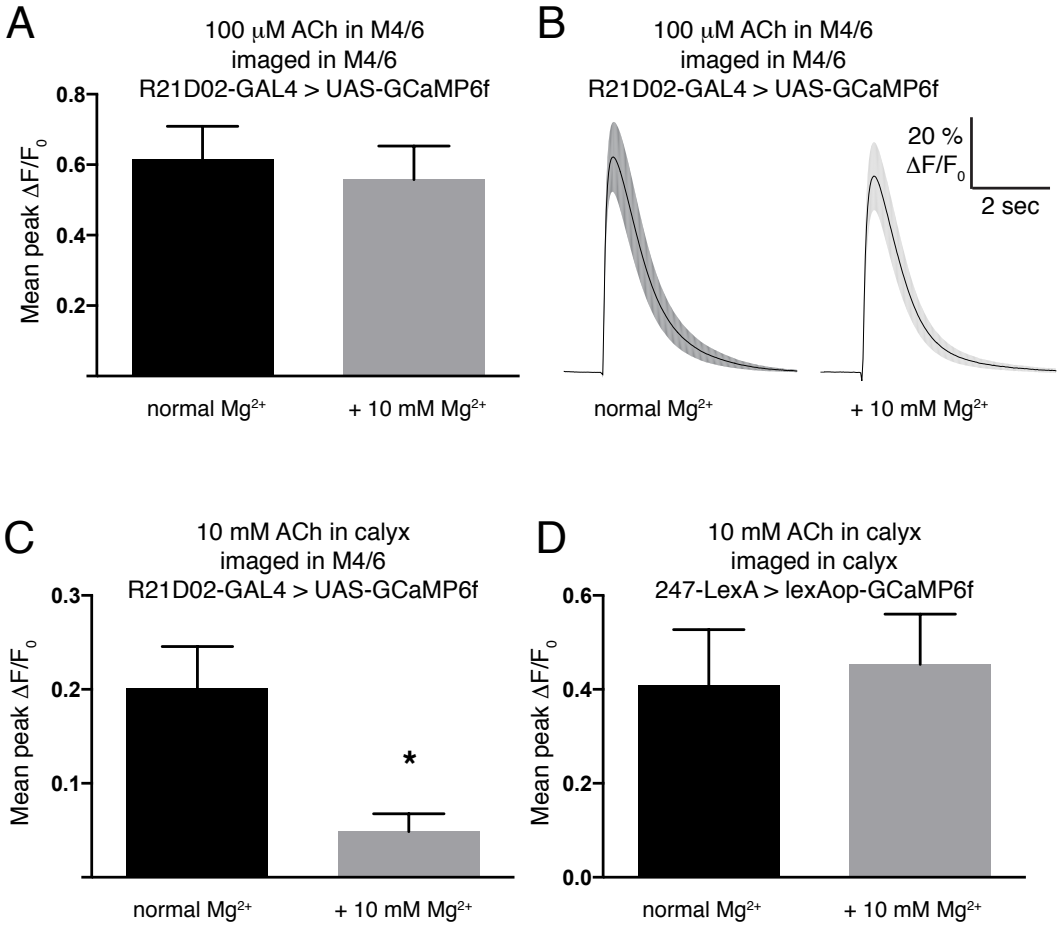


Figure 3.8: High magnesium concentration in bath has no effect on ACh-induced calcium responses in M4/6 dendrites, but reduces known secondary responses that bridge one synapse. A) 100 µM ACh were injected into M4/6 dendrites of R21D02-GAL4 driven GCaMP6f brains bathed in either normal Mg^{2+} concentration (black bars) or by 10 mM elevated Mg^{2+} concentration (grey bars). Neither peak calcium responses (A; unpaired t-test, $p > 0.05$, $N = 6$) nor response shape (B) differ between conditions. B) Mean calcium traces are shown in black, with the SEM as shade. C) 10 mM ACh injected into the MB calyx elicits reliable calcium responses in M4/6 axons. These known secondary responses are significantly reduced under high magnesium conditions (unpaired t-test, $p < 0.05$, $N = 3 - 4$). D) 10 mM ACh elicit strong calcium responses in the calyx when imaged from KCs by 247-LexA driven GCaMP6f that are unaffected by higher magnesium bath conditions (unpaired t-test, $p > 0.05$, $N = 2$). All error bars represent SEM. Adapted from Barnstedt et al. (2016).

To rule out that KCs themselves were negatively affected by high Mg^{2+} levels, I monitored calcium responses in the calyx of 247-LexA ; GCaMP6f flies while injecting 10 mM ACh into the calyx. The resulting calcium responses were not altered by different Mg^{2+} levels (Figure 3.8D).

These findings show that a known synaptic connection (KC → M4/6) relies on normal Mg^{2+} levels, but ACh-evoked calcium responses in the MB calyx and in M4/6 dendrites are independent of Mg^{2+} levels. Furthermore, TTX does not seem to interfere with ACh-evoked calcium responses in M4/6 dendrites, strongly suggesting a direct agonist action.

KC lobes are not excited by ACh

A further possibility of an indirect response could be that KCs themselves respond to ACh, which in turn may lead to the release of another neurotransmitter that activates M4/6 neurons. Such a microcircuit model could explain the previous results reasonably well, provided it is independent of APs and unaffected by high Mg^{2+}.

To rule out secondary excitation of KCs by ACh application into MB lobes, I injected 1 mM ACh into the γ5 region while monitoring calcium responses in KCs from 247::GCaMP5 explant brains. No calcium responses were observed, neither with 1 mM ACh nor with 100 µM nicotine, while robust responses were observed with both agonists in M4/6 dendrites (see Figure 3.9). This finding suggests that KCs themselves are not excited by ACh injections into γ5, and are therefore unlikely to be responsible for the ACh-evoked calcium responses in M4/6.

3.2.5 Individual MBONs respond to ACh

M4/6 neurons consist of three individual MBONs, each innervating different zones in the tips of the three horizontal lobes (γ, β, and β′; Aso et al., 2014a; Tanaka et al., 2008). The injections performed so far mostly focused on the γ5 region of the MB, suggesting a main contribution of calcium signals from the M6 neuron, although widefield imaging would also capture calcium signals from nearby planes. To determine the precise contribution from each of these M4/6 neurons, and to determine if other MBONs also respond to ACh injections, we made use of more precise MBON driver lines expressing GCaMP6f.

I first injected 1 mM ACh into the β′2 compartment of M4β′ neurons, the β2 compartment of M4β neurons, and into the γ5 compartment of M6 neurons, using

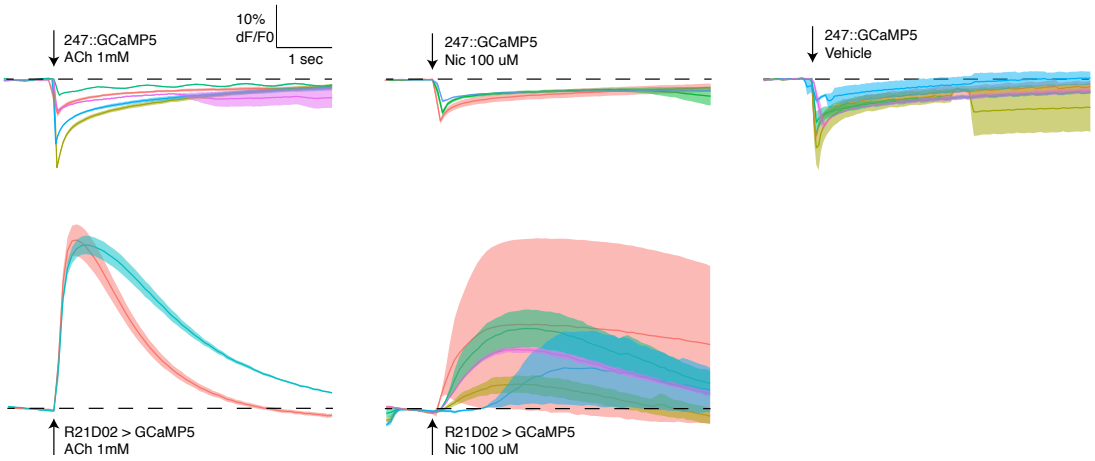


Figure 3.9: KCs are not excited by ACh injected into the lobes. 1 mM ACh or 100 µM nicotine or vehicle were injected into the MB horizontal lobe tips while calcium transients were monitored using GCaMP5 (upper row). KCs show no detectable calcium responses to injection as seen using 247::GCaMP5, whereas M4/6 neurons show strong calcium responses both to 1 mM ACh or 100 µM nicotine (lower row). Initial dips in traces upon application visible in upper row are injection artefacts, as vehicle injection yields similar effects (upper right). Shown are mean traces from 10 trials per brain (strong line) with SEM as shade; each colour represents an individual brain per graph. Adapted from Barnstedt et al. (2016).

specific driver lines for each. Interestingly, all three individual M4/6 neurons showed reliable calcium responses to focal ACh stimulation (see Figure 3.10A-C,G-J). This suggests that indeed all three M4/6 neurons respond to ACh.

While the three M4/6 neurons cover the three main KC subtypes (γ, α/β, and α′/β′), they are nonetheless homogenous in their innervation of only the horizontal MB tip, and their shared neurotransmitter glutamate (Aso et al., 2014a; Owald et al., 2015a; Tanaka et al., 2008). To determine if also other classes of MBONs innervating different MB zones respond to ACh, I next injected 1 mM ACh into cholinergic V2 neurons of the vertical lobe. Both in V2α and V2α′, strong and robust calcium responses to ACh were visible (Figure 3.10D-E,K). Lastly, the GABAergic MVP2 neuron innervating the MB heel/peduncle region was stimulated by ACh, and also showed strong and reliable ACh-evoked calcium responses (Figure 3.10F).

While response magnitude and dynamics seem to differ between MBONs (see Figure 3.10), this can not be fully attributed to the respective MBON receptor

properties, as brain-to-brain differences in precise injection locations, and different strengths of GAL4 expression between genotypes confound such an interpretation.

These findings demonstrate that, while previous calcium signals may have been largely collected from M6, all major classes of MBONs, covering all major KC subtypes and lobes, and neurotransmitter systems, respond to ACh stimulation. This would suggest that all major KC subtypes might release ACh to communicate with their respective MBONs.

In summary, M4/6 MBONs show calcium responses only to injections of ACh (Figure 3.4). These responses are dose-dependent (Figure 3.5A), and likely the result of direct action of ACh on receptors in M4/6 dendrites. The interpretation of a direct action of ACh on M4/6 dendrites is supported by several findings:

1. Pharmacological block of indirect responses has no effect on responses (Figure 3.6, 3.7, 3.8).

2. Responses are only elicited in the M4/6 dendritic area, but not when ACh was released elsewhere in the superior protocerebrum (Figure 3.6 and A.5).

3. Calcium responses in M4/6 dendrites are restricted in space to the spread of ACh (Figure 3.7).

4. Response onset is relatively rapid, and temporal response dynamics are correlated with the dynamics of ACh spread (Figure A.3).

5. KCs themselves do not show calcium responses to stimulation in the $\gamma 5$ region (Figure 3.9).

Furthermore, all classes of MBONs respond to ACh injections (Figure 3.10), suggesting cholinergic input to all/most MBONs.

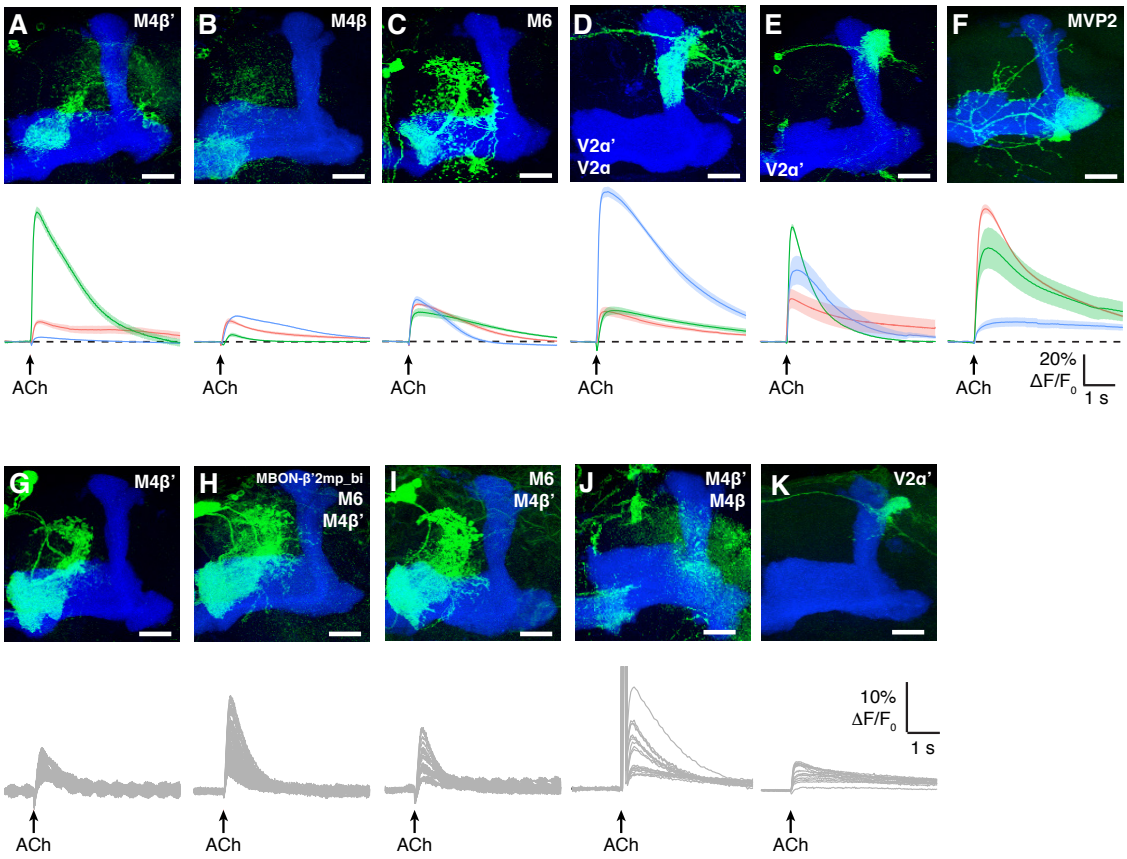


Figure 3.10: All main classes of MBONs show calcium responses to dendritic injections of 1 mM ACh. A-F) Three brains of MBON-specific GAL4 lines expressing GCaMP6f were tested each, with calcium transients underneath anatomy images depicting the mean trace (bold line) and SEM (shade) of 10 injection trials. Each colour represents a separate brain for each panel. A) Glutamatergic M4β′ from R39A05-GAL4. B) Glutamatergic M4βfrom R56F01-GAL4. C) Glutamatergic M6 from R66C08-GAL4. D) Cholinergic V2α with some V2α′ from MB549C. E) Cholinergic V2α′ from R24H08-GAL4. F) GABAergic MVP2 from MB112C. G-K) Further MBON drivers show calcium responses to dendritic injections of 1 mM ACh. One brain of MBON-specific GAL4 lines expressing GCaMP6f was tested, with calcium transients underneath anatomy images depicting single traces of 10 injection trials. G) M4β' from MB002B. H) M4β′, M6, and MBON-β2mp_bi from MB011B. I) M4β′ and M6 from MB210B. J) M4β' and M6 from R93F01-GAL4. K) V2α′ from MB027B. Initial increase in traces of D is an artefact of the LED trigger. Scale bars represent 20 µm. Adapted from Barnstedt et al. (2016).

3.3 Kenyon cells express ChAT and VAChT

Given that MBONs receive their main excitatory input from KCs, it seems likely that KCs release ACh to excite MBONs. If KCs are indeed cholinergic, several proteins would need to be expressed by KCs, particularly ChAT for ACh synthesis, and VAChT for synaptic vesicle trafficking (see 3.1.6 and Figure 3.1). The presence of these proteins in specific tissues can be probed by the use of immunohistochemistry (see also 1.5.2), or by the use of enhancer fragments from gene loci of interest that drive the expression of fluorescent proteins (see also 1.5.1).

3.3.1 α-ChAT staining

Proteins of interest can be visualised in organic tissues by raising specific antibodies that bind to peptide sequences of this protein, and to which secondary fluorescent antibodies can be attached (see 1.5.2). This method can be very reliable, but is often limited by the availability of specific antibodies, and confounded by unspecific labelling that can occur.

α-ChAT (4B1) antibody

The most commonly used antibody for cholinergic neurons is α-ChAT, and in *Drosophila melanogaster*, the most commonly used antibody is the monoclonal antibody ChAT4B1 raised by Takagawa et al. (1996; see also 3.1.6). The first study to use this antibody concluded that MBs were α-ChAT immunonegative (Yasuyama et al., 1995; see also Figure 3.2). Upon closer inspection of the image they provided, however, it seems that a faint staining is visible.

In order to replicate Yasuyama et al.'s (1995) findings, and determine if the observed faint staining is real and what the source of this is, I immunostained brains carrying KC-expressed RFP with this α-ChAT antibody according to a standard staining protocol (Wu and Luo, 2006) at the recommended concentration of 1:100 (DSHB). After dissection, staining, and mounting, I imaged several brains at high resolution using a Leica SP5 confocal laser-scanning microscope (see 2.6 for full details on staining procedure).

Positive α-ChAT immunoreactivity was observed throughout large regions of the brain, particularly in the superior protocerebrum, similar to what was observed by Yasuyama et al. (1995) (Figure 3.11A). Upon closer inspection and with the aid of the co-expressed KC-driven RFP, weak α-ChAT immunoreactivity was found in horizontal and vertical MB lobes, and, to some degree, in the peduncle (Figure 3.11B-E). This staining, however, was markedly weaker and more diffused than what was observed in the calyx, where individual axonal boutons, presumably from AL PN terminals were clearly visible (Figure 3.11F). At the level of the cell bodies, no KCs seemed to be labelled (Figure 3.11G), but no other cell bodies were labelled by this antibody either (Figure 3.11A), in line with previous observations that only cholinergic processes are stained for ChAT (see e.g. Barber et al., 1989).

To both validate the antibody staining observed in the MB lobes as well as to determine the source of α-ChAT immunoreactivity in the MB lobes, I next used genetic RNA interference (see 1.5.5).

α-ChAT staining with RNAi

If the previously tested antibody ChAT4B1 binds specifically to ChAT as has been previously shown (Takagawa and Salvaterra, 1996), then the cell-specific knockdown of ChAT translation with RNAi should decrease the relative staining intensity in those ChAT-positive neurons.

To test this, I expressed ChAT-RNAi (BUN 25856) either in known cholinergic AL projection neurons (GH146-GAL4) or in KCs (OK107-GAL4) (Aso et al., 2009; Connolly et al., 1996; Ni et al., 2009), and stained these brains with α-ChAT4B1. The results clearly show that the observed ChAT-positive staining in LH and calyx from AL PNs is strong when RNAi was driven in KCs, but very weak when RNAi was driven in PNs (see Figure 3.12). On the other hand, ChAT staining in the MB was clearly visible when RNAi was driven in AL PNs, but was almost absent when RNAi was driven in KCs (Figure 3.12). These findings strongly suggest that ChAT-RNAi and α-ChAT4B1 target the same protein, which is expressed in AL PN terminals in calyx and LH, as well as in the MB lobes.

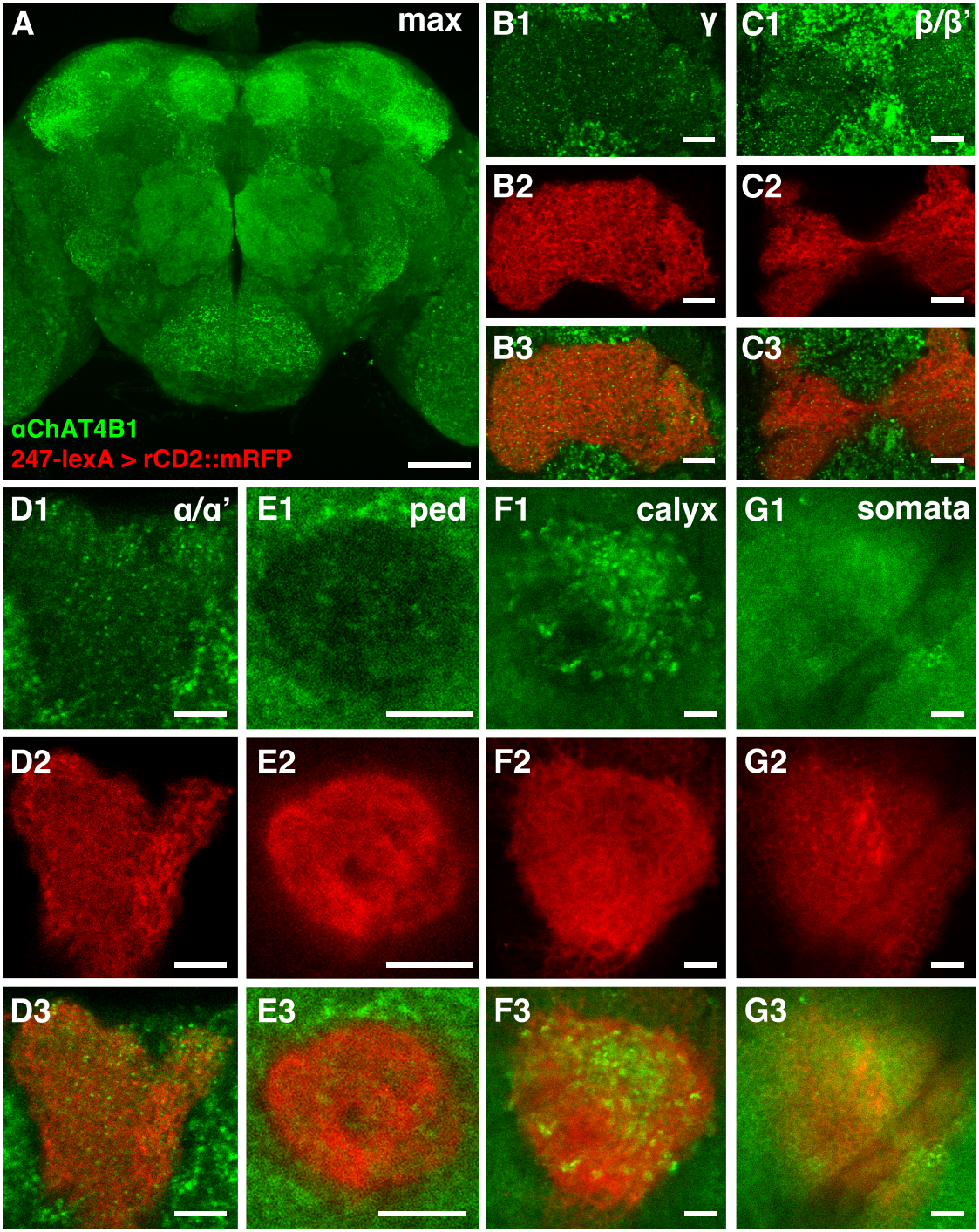


Figure 3.11: Mouse α-ChAT (DSHB ChAT4B1) staining shows weak staining in MB lobes, peduncle and KC somata, as well as strong staining in calyx (green), showing only weak overlap with 247-LexA driven rCD2::mRFP (red). A) Overview of staining pattern in complete central brain, illustrated by a maximum projection. Much of the brain is immunopositive, particularly the superior protocerebrum. B-G) Close-ups of various brain regions. B-D) MB lobes show weak staining, with individual antibody punctae visible throughout . E) The peduncle shows weak and more diffuse staining. F) Large immunopositive boutons are visible in the calyx, presumably from presynaptic terminals of AL PNs. G) KC somata were immunonegative. Scale bar in A represents 50 µm, and in B-G 10 µm. Brains were stained according to Wu and Luo (2006) at a concentration of 1:100.

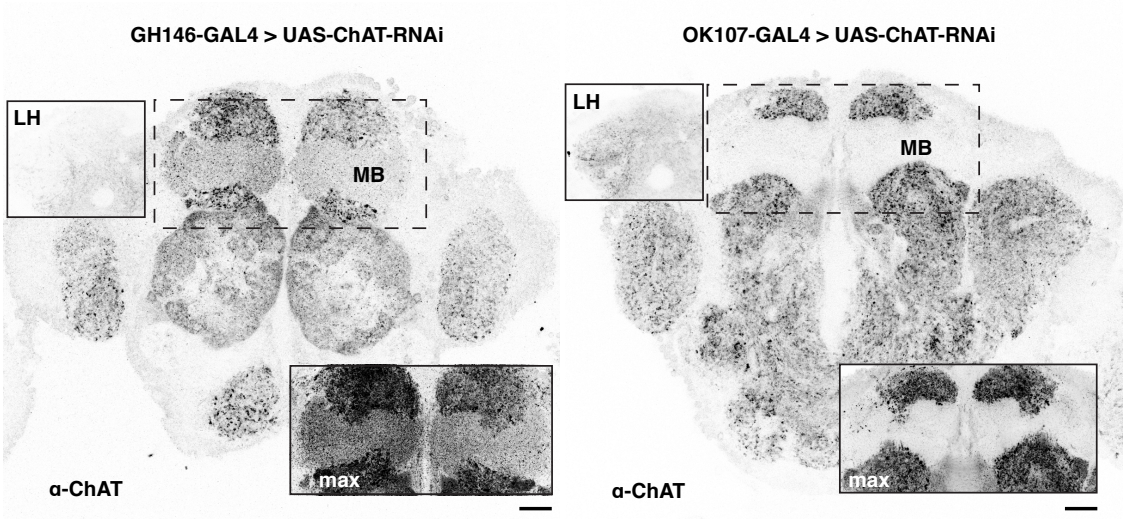


Figure 3.12: ChAT-RNAi reduces ChAT-positive staining in AL projection neurons (PNs) and KCs. ChAT-RNAi (BUN 25856) was either driven in AL PNs using GH146-GAL (left), or KCs using OK107-GAL4 (right). Driving RNAi in PNs greatly reduced immunopositive staining in the LH where its presynaptic terminals are located, while leaving MB lobe staining intact. Driving RNAi in KCs, on the other hand, greatly reduced immunopositive staining in MB lobes, while leaving LH staining intact. Scale bars represent 20 µm.

To reproduce and quantify these findings, I again expressed ChAT-RNAi in OK107-GAL4, and stained several of these brains ($N = 6 - 11$) along with their genetic controls simultaneously. Again, a strong decrease of α-ChAT immunoreactivity was observed when ChAT-RNAi was expressed in KCs, compared to controls (see Figure 3.13A).

To quantify these changes, I measured fluorescence in a defined ROI in different lobes, and normalised this fluorescence by a control ROI in the SMP for each brain. The results of this show that α-ChAT fluorescence in MB lobes is highest in γ where it is about 60 % of that observed in the SMP, followed by β′ with about 50 % of SMP levels, and lowest in β with about 40 % of SMP fluorescence (Figure 3.13B). Importantly, α-ChAT immunoreactivity is significantly reduced in OK107-GAL4 ; ChAT-RNAi flies compared to both genetic controls in γ and β′, while in β, experimental flies were significantly reduced to only one control group. This may be due to the fact that the β lobe shows the weakest staining observed in control flies.

Sample images of six brains per genotype used for analysis, with ROIs in the γ lobe, can be found in Figure A.6.

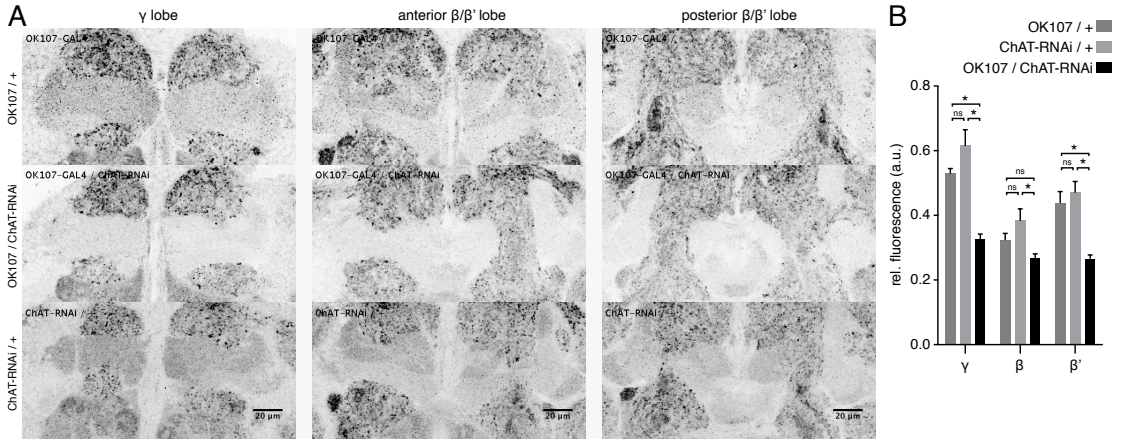


Figure 3.13: KC-driven ChAT-RNAi reduces ChAT-positive staining in all horizontal MB lobes. A) Single-plane images of α-ChAT immunoreactivity in KC-driven ChAT-RNAi flies (middle row), compared to genetic parent controls (upper and lower row). Three brains (one for each genotype) are displayed at the level of the gamma lobes (left column), anterior beta/beta' (centre column), and posterior beta/beta' (right column). On all levels, ChAT-immunopositive staining is visibly reduced in OK107-GAL4 driven ChAT-RNAi flies compared to their genetic controls. B) ChAT antibody fluorescence quantification of ChAT-RNAi reveals significant fluorescence decrease in brains of OK107/ChAT-RNAi flies compared to both their genetic controls in γ and β′ lobe, while β was only significantly different to one genetic control. Asterisks denote significant differences (two-way ANOVA, Tukey's multiple comparisons test, $p < 0.05$, $N = 6 - 11$). Relative fluorescence was calculated for each brain as mean fluorescence of an ROI (γ, β, β′) divided by the mean fluorescence of an ROI in the SMP area.

Overall, these findings cross-validate both ChAT-RNAi and the α-ChAT4B1 antibody, as both seem to target the same protein. Importantly, the ChAT-positive staining in the MB can be reduced by expressing KC-driven ChAT-RNAi. This strongly suggests that the weak α-ChAT immunoreactivity previously observed in MB lobes is indeed ChAT-specific staining that most likely comes mainly from KCs, as the use of the KC-specific driver line OK107-GAL4 suggests.

3.3.2 α-VAChT staining

α-VAChT antibody

If KCs truly release ACh as a neurotransmitter, ACh must not only be synthesised in KCs by ChAT as the findings above suggest, but ACh must also be transported into synaptic vesicles by VAChT (see 3.1.6). Although VAChT antibodies in *Drosophila melanogaster* exist, they are used much more rarely than the ChAT antibody.

Probably the most often used α-VAChT antibody is a rabbit polyclonal AB developed by Kitamoto et al. (1998). This AB has been previously used and its specificity confirmed (Boppana et al., 2017; Kitamoto et al., 1998, 2000; Kolodziejczyk et al., 2008; Yasuyama et al., 2002).

To determine the presence of VAChT in KCs, I used this antibody on wild-type brains that I dissected and stained according to a standard protocol (Wu and Luo, 2006) at the previously employed concentration of 1:1,000. Despite two days of primary AB and two days of secondary AB incubation, penetration of the AB was low, but revealed widespread immunoreactivity throughout the adult *Drosophila* brain (see Figure 3.14A). Importantly, relatively strong and fine VAChT-immunoreactivity was observed in all five main lobes of the MB (Figure 3.14B-C), whereas the peduncle was immunonegative (Figure 3.14D), and the calyx showed distinctive large immunopositive boutons likely from AL PN terminals (Figure 3.14E). This suggests that VAChT is expressed in MB neurons, potentially KCs.

α-VAChT staining with RNAi

In order to cross-validate and determine the source for the α-VAChT immunoreactivity observed in MB lobes, I again used RNAi to specifically knock down VAChT translation in KCs. Staining 4–6 brains with OK107-GAL4 ; VAChT-RNAi and three genetic controls with α-VAChT antibody as before confirmed my previous finding of high levels of VAChT immunoreactivity in MB lobes (see Figure 3.15A). Importantly, relative quantification based on a control ROI in the SMP revealed a very strong and significant reduction of α-VAChT immunoreactivity in experimental flies compared to control flies (Figure 3.15B). While genetic controls showed fluorescence levels of, on average, 74 % to 80 % in γ compared to the SMP, flies with KC-driven VAChT-RNAi showed only 27 % of average relative fluorescence (Figure 3.15B). This finding strongly suggests that the observed α-VAChT immunoreactivity in MB lobes is based on specific binding, and that the source of this VAChT presence are the KCs.

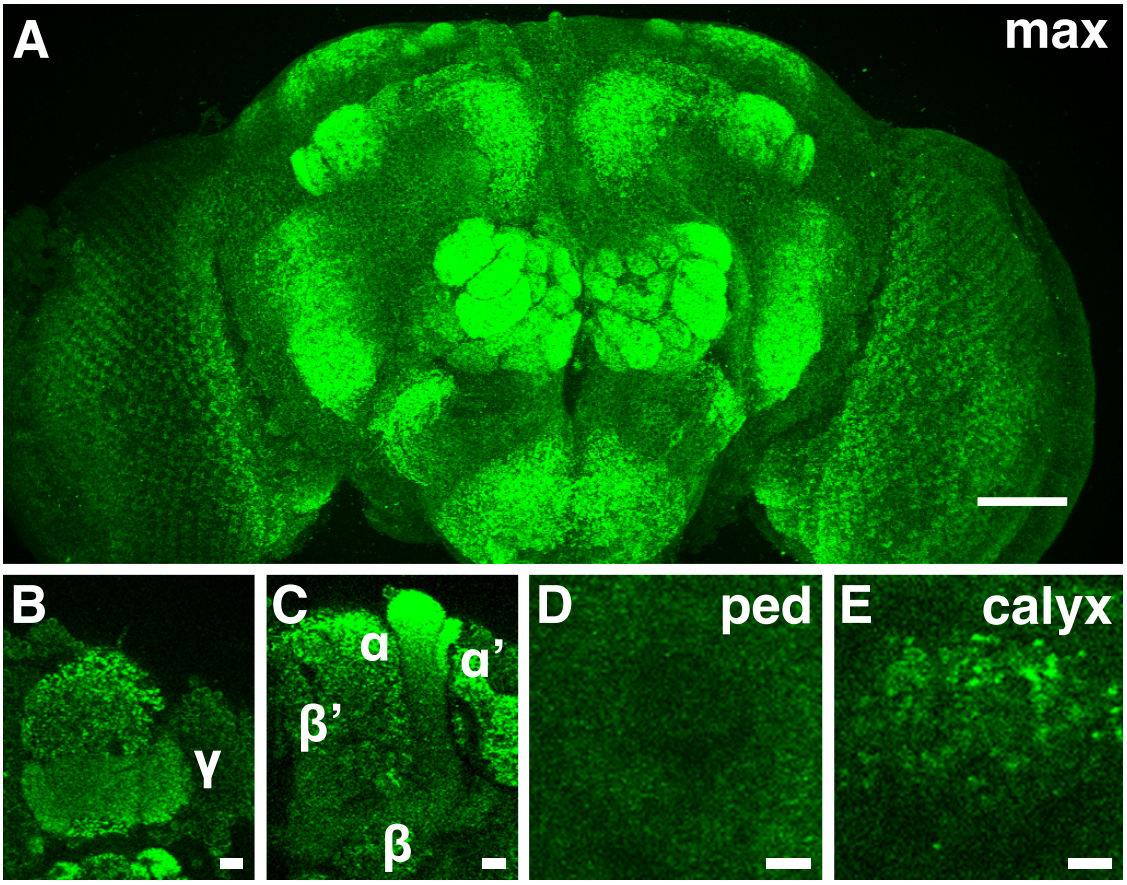


Figure 3.14: Rabbit α-*Drosophila* VAChT antibody stains large parts of the fly brain, including the MB. A) Overview of staining, showing a maximum projection of a confocal stack. B-E) Individual sections of confocal stack show staining in different parts of the MB. B) The γ lobe shows immunopositive staining. C) β/β′ and α/α′ lobes show immunopositive staining. Weak staining in β/β′ is likely due to weak penetration as suggested by the surrounding immunoreactivity. D) The peduncle (ped) is notably immunonegative. E) Large bouton-like immunopositive elements are visible on the level of the calyx. Scale bars represent 50 µm in A, and 10 µm in B-E.

Images of all 4–6 brains per genotype used for quantification are shown in Figure A.7, and the raw values for quantification can be found in Table A.1.

Combined α-ChAT and α-VAChT staining with RNAi

To test for the specificity of RNAi, and to include a direct antibody control, I next used five different genotypes, including OK107-GAL4 ; ChAT-RNAi, OK107-GAL4 ; VAChT-RNAi, and their respective controls, and double-stained these brains with both the mouse α-ChAT as well as the rabbit α-VAChT antibody, as before.

As seen before, the MB lobes were weakly stained against ChAT and moderately

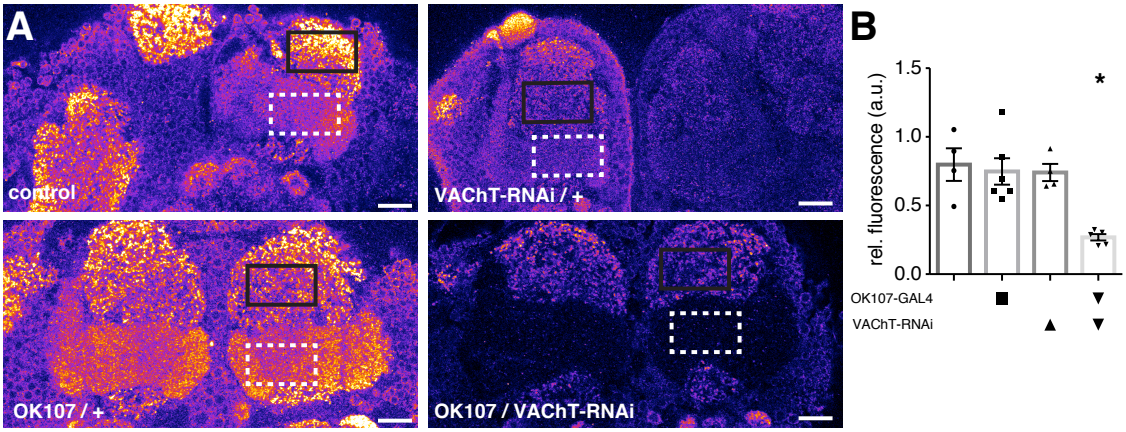


Figure 3.15: VAChT immunostaining is significantly decreased in MBs of KC-driven VAChT-RNAi flies. A) One sample brain per genotype is shown at the level of the MB γ lobe. Lower right brain is taken from the experimental group. Note the strong staining inside the MB γ lobe, which is comparable in intensity to that of the SMP, while the brain in the experimental group has greatly reduced intensity in the MB, compared to the SMP. MB ROIs are marked with white dashed boxes, while control ROIs in SMP are marked by black boxes; both of which are 40×25 µm in size. Scale bar represents 20 µm. B) Quantification of relative fluorescence from MB normalised to SMP reveals significantly lower levels in flies carrying both OK107-GAL4 and VAChT-RNAi, compared to wild-type (one-way ANOVA, Dunnett's multiple comparisons test, $p < 0.01$, $N = 4 - 6$). While control flies showed a relative fluorescence of about 80 %, experimental flies only had about 30 % relative fluorescence in gamma lobes. See also Table A.1 for exact numbers.

stained against VAChT in wild-type flies (see Figure 3.16A). OK107-GAL4 ; ChAT-RNAi flies, on the other hand, showed less α-ChAT immunoreactivity, but normal levels of α-VAChT immunoreactivity. OK107-GAL4 ; VAChT-RNAi showed greatly reduced levels of α-VAChT immunoreactivity, but also showed considerably less α-ChAT immunoreactivity (see Figure 3.16).

Quantification of relative fluorescence (normalised to a defined SMP region) in all five MB lobes reveals a similar picture: α-ChAT immunoreactivity was significantly decreased in OK107-GAL4 ; ChAT-RNAi flies in all lobes except α, but OK107-GAL4 ; VAChT-RNAi reduced α-ChAT staining in all lobes (Figure 3.16B). α-VAChT immunoreactivity was significantly reduced only in OK107-GAL4 ; VAChT-RNAi flies, across all five lobes (Figure 3.16C). These results again strongly suggest the presence of ChAT and VAChT across the MB.

A complete list of absolute fluorescence values extracted from all brains can be found in Table A.2, and the resulting relative fluorescence values can be

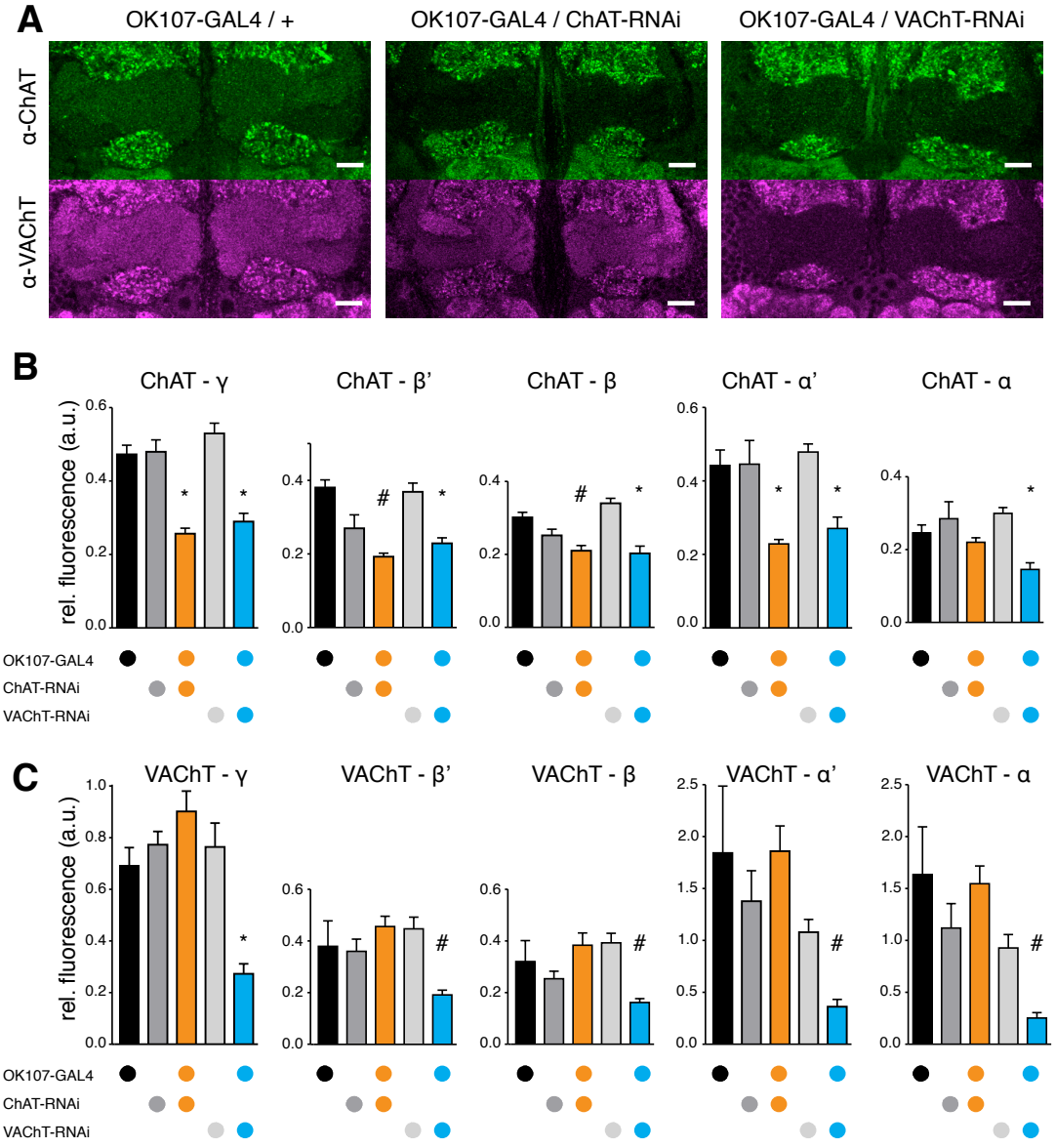


Figure 3.16: ChAT- and VAChT-RNAi reduce α-ChAT and α-VAChT immunostaining, respectively. A) Three sample brains of three genotypes co-stained with α-ChAT (green, top row) and α-VAChT antibody (magenta, bottom row) illustrate specific reductions in immunostaining intensity at the level of the MB γ lobe for the respective RNAi. B-C) Quantification of fluorescence across five MB lobes. Each defined ROI's fluorescence was normalised to each brain's fluorescence in SMP. B) α-ChAT immunoreactivity is significantly reduced in experimental OK107-GAL4 ; ChAT-RNAi flies in γ and α′ against both parental controls, and in β′ and β against OK107-GAL4 / +, while no significant difference was observed in α. OK107-GAL4 ; VAChT-RNAi flies showed a significant reduction against parental controls across all lobes. C) α-VAChT immunoreactivity is significantly reduced in OK107-GAL4 ; VAChT-RNAi flies against both parental controls in γ, and against VAChT-RNAi / + in all other lobes. Asterisks denote significant differences to both parental controls, while hashes denote significant differences to only one parental control (one-way ANOVA, Tukey's multiple comparisons test, $p < 0.05$, $N = 3 - 9$). Partly adapted from Barnstedt et al. (2016).

found in Table A.3.

3.3.3 α-acetylcholinesterase staining

Acetylcholinesterase (AChE) is required to cleave ACh in the synaptic cleft, and thus terminate the agonist action of ACh (see 3.1.6). As AChE thus represents a crucial part of cholinergic synapses, but its expression in the adult *Drosophila* brain currently remains poorly understood (but see Buchner et al., 1986), we set out to investigate AChE expression using a commercially available α-AChE antibody.

I performed immunostaining with this antibody as before (see 2.6), using 247-LexA driven RFP to identify KCs. To our surprise, the resulting staining pattern mainly showed strong labelling of cell bodies that likely belong to astrocyte-like glia (see Figure 3.17A; cp. Kremer et al., 2017, Figure 1B.4). In the MB, however, only weak punctate staining was visible (Figure 3.17B-E), while the calyx also showed only weak diffuse staining, similar to background levels (Figure 3.17F). These findings raise the possibility that astrocyte-like glia express AChE, although glia are also a common target for unspecific antibody binding.

Further commercially available antibodies against VAChT, ChAT, and conjugated ACh were also tested, but produced no convincing staining pattern in the adult *Drosophila* brain, and were thus not further pursued (see Figure A.8).

3.3.4 Cha-GAL4

Another complementary approach of visualising cholinergic neurons is the use of a gene enhancer region to drive GAL4 expression in those neurons transcribing from this locus (see 1.5.1).

The most widely used genetic method of gaining access to cholinergic neurons is the use of a Cha-GAL4 driver line generated by Salvaterra and Kitamoto (2001). This GAL4 line uses 7.4 kb of 5' flanking DNA from the *Drosophila* cholinergic locus, and was shown to express in a wide range of cholinergic neurons that are mostly also co-labelled by α-ChAT and α-VAChT (see Kahsai and Winther, 2011; Mehren and Griffith, 2006; Nässel et al., 2008; Raghu et al., 2013; Salvaterra and

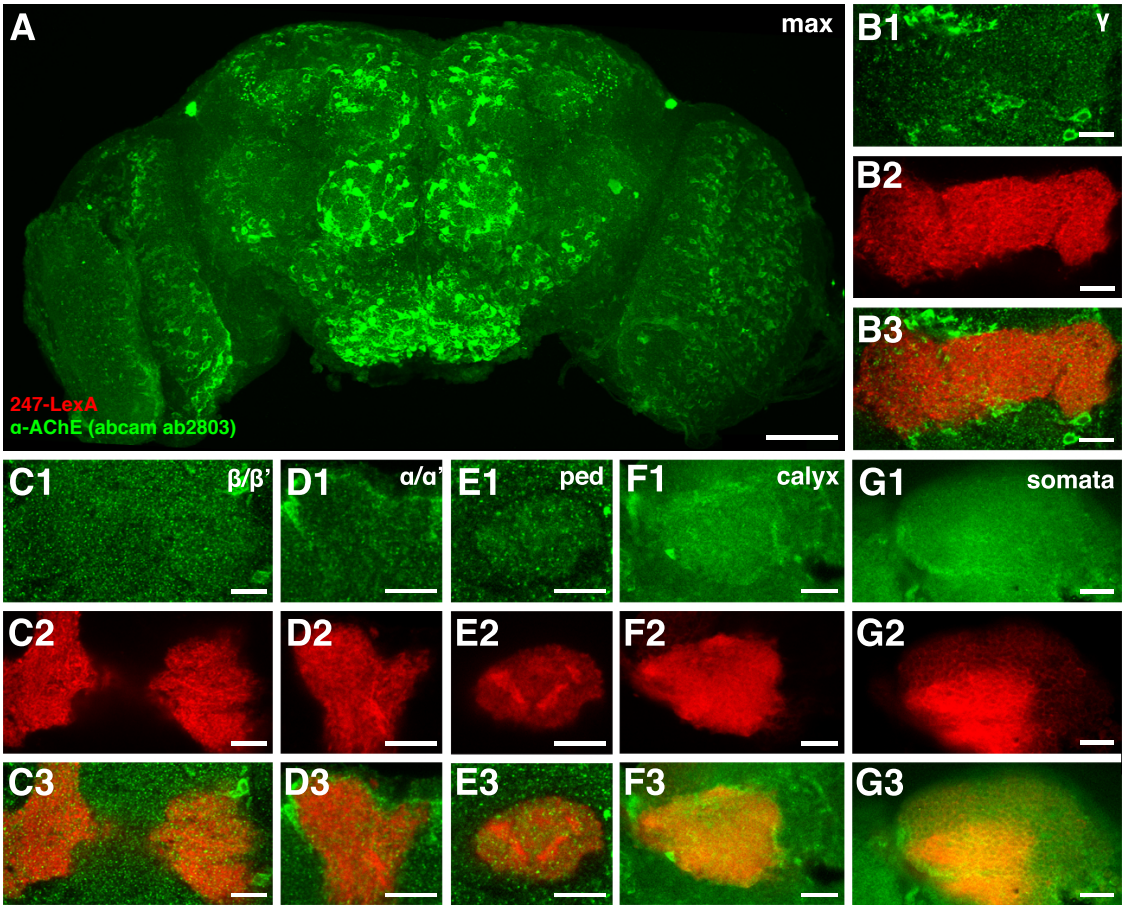


Figure 3.17: Potential AChE immunoreactivity in brain astroglia. Mouse α-AChE (ab2803) antibody (green) was stained against in flies carrying 247-LexA driven rCD2::mRFP (red) to reveal KCs. A) A maximum projection overview clearly shows several hundreds of immunopositive cell bodies with high similarity to astrocyte-like glia. B-E) Staining throughout MB zones is weak and punctate. F) The calyx shows diffuse and weak staining. G) KC somata show immunoreactivity similar to background levels. Scale bar in A represents 50 µm, while those in B-G represent 10 µm.

Kitamoto, 2001). It has since been used in a wide range of studies to characterise and manipulate cholinergic neurons (e.g. Kitamoto, 2001; Lima and Miesenböck, 2005; Mehren and Griffith, 2006; Mohammad et al., 2017). Interestingly, previous characterisation of this Cha-GAL4 line identified several α/β surface KCs contained therein (Mehren and Griffith, 2006).

In order to confirm Cha-GAL4 expression, and identify potential expression in KCs, I combined Cha-GAL4 with a KC LexA driver (247-LexA) to express GFP and RFP, respectively, and imaged the resulting expression pattern. As previously reported, I found Cha-GAL4 to express in a wide range of neurons covering most

parts of the adult *Drosophila* brain, including OL and AL neurons (see Figure 3.18A). At the level of the MB, some expression could be detected, especially in the α/βs but also in the γ area (Figure 3.18B,D-E). This was also reflected by expression in regions of the peduncle, suggesting that expression in γ and α/βs stems from KCs (Figure 3.18C; cp. Tanaka et al., 2008). Importantly, on the level of calyx and KC soma region, several dozens of KC cell bodies were visible (Figure 3.18F-G). A counting estimate in ImageJ resulted in about 80 KC cell bodies contained in Cha-GAL4, that are likely from γ and α/βs KCs.

In line with these findings, Cha3.3kb-GAL80 (Kitamoto, 2002) co-expression with the broad α/β KC driver line c739-GAL4 resulted in the suppresion of GAL4 expression in α/βs KCs, while α/βc KCs were spared (Figure A.9B; see also Mehren and Griffith, 2006; Yi et al., 2013). Similarly, Cha3.3kb-GAL80 also suppressed GAL4 expression in most γ and α′/β′ KCs, leaving mostly only a subset of α/β(c) KCs expressing (see Figure A.9C), when combined with the most comprehensive KC driver line OK107-GAL4 (Connolly et al., 1996).

Other Cha-GAL4 constructs tested failed to label cholinergic neurons (Figure A.9). I have also investigated FP expression in *Cha/VAChT*-driven MiMIC lines (Venken et al., 2011), but failed to observe expression in known cholinergic neurons or KCs (Figure A.10).

3.3.5 Cha-LexA

The more recently introduced transcription factor-based driver system LexA/lexAop can also be used to drive genetic expression from gene enhancer regions of interest (see 1.5.1).

Based on this, a Cha3.3kb-LexA::GAD (Cha-LexA in the following) driver was recently developed (Diegelmann et al., 2008) to drive expression in cholinergic neurons of *Drosophila* larvae, but this line has not yet been characterised in the adult *Drosophila* brain.

To characterise Cha-LexA expression and determine potential overlap with KCs, I combined Cha-LexA with the broad KC driver line R13F02-GAL4 (Jenett et al.,

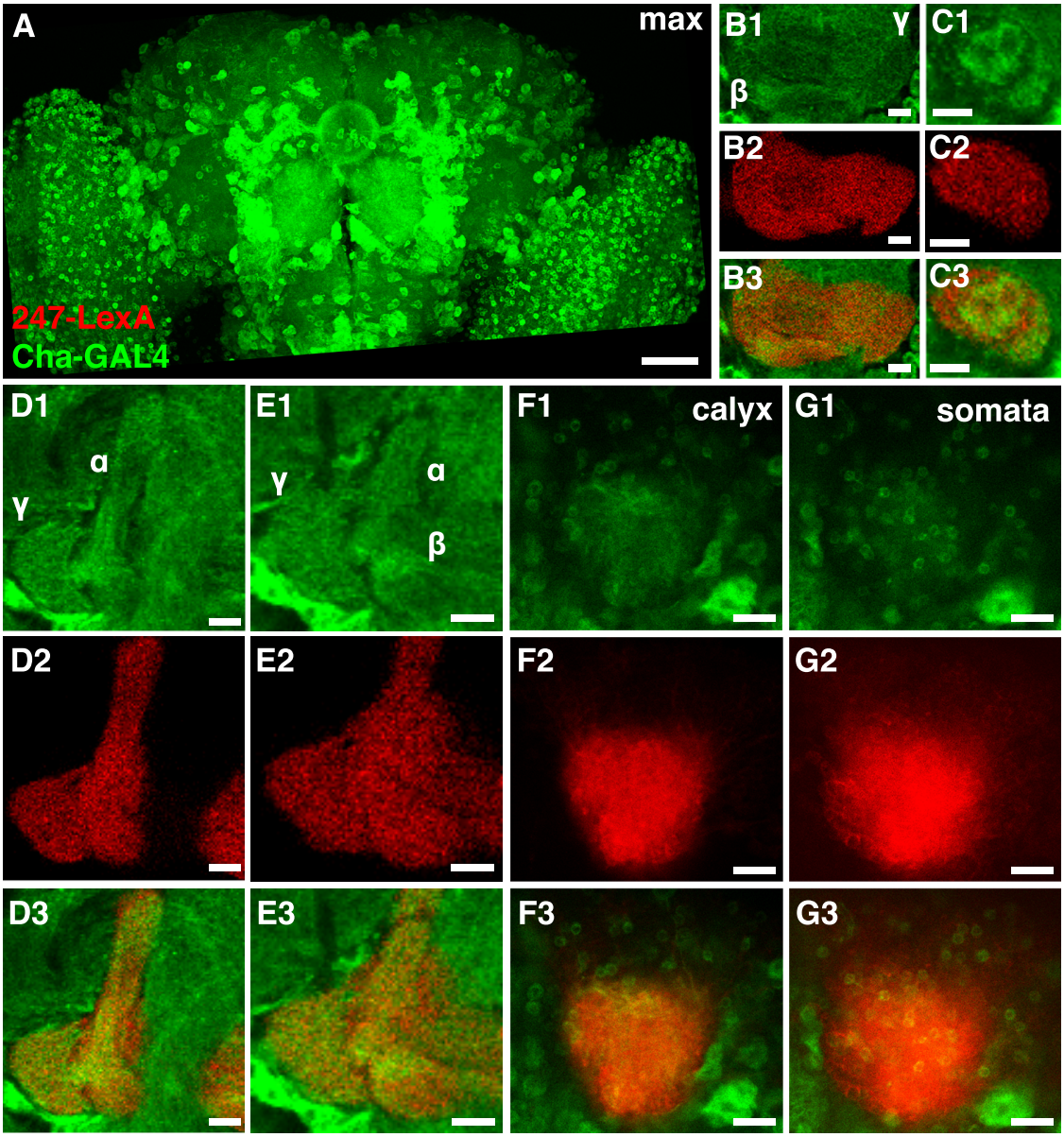


Figure 3.18: Cha-GAL4 expresses in several α/βs KCs. Cha-GAL4 (19B; Salvaterra and Kitamoto, 2001) was used to drive mCD8::GFP (green), and 247-LexA was used to drive rCD2::mRFP (red) to label KCs. A) Maximum projection overview of Cha-GAL4 expression. Many neurons can be found expressed throughout the adult brain, e.g. in OL, AL or the CC. B) The MB γ lobe show some weak expression. C) GAL4 expression can be found in parts of the peduncle, likely corresponding to the γ and α/βs region. D-E) Expression in the lobes is clearly visible in αs, βs, and γ. F-G) Calyx and soma region of the MB show around 80 GAL4-positive KCs. Images in B-G show single planes. Scale bar in A represents 50 µm, and those in B-G represent 10 µm.

2012; see also Cervantes-Sandoval et al., 2017; Hige et al., 2015a; Shyu et al., 2017), to drive expression of rCD2::mRFP and mCD8::GFP, respectively.

The resulting expression pattern revealed that Cha-LexA drives strong expression in much of the adult *Drosophila* brain, particularly in OL and AL neurons (see Figure 3.19A). Interestingly, the MB was labelled, most strongly in inner α/βc and α/βs, but also in α′/β′, while γ was very faintly labelled (see Figure 3.19B,D). This pattern was confirmed by expression in the respective zones in the peduncle (Figure 3.19C). Furthermore, LexA expression was visible in large parts of the calyx and in many cell bodies (Figure 3.19E-G). A rough estimate of cell numbers would suggest that more than half of KCs are contained in Cha-LexA.

These findings suggest that many KCs show gene expression from the Cha locus, although different driver lines indicate different subsets of KCs.

3.4 MBONs have nicotinic ACh receptors

My previous data showed that KCs express ChAT and VAChT required for ACh synthesis and synaptic release (3.3), and that MBONs show calcium responses to focal ACh injections (3.2). If KC-released ACh acts upon MBONs, we would expect MBONs to have ACh receptors that mediate such a response. As discussed previously, there are several metabotropic as well as ionotropic ACh receptors (see 3.1.6). In order to corroborate and extend my previous findings of ACh-evoked calcium responses in MBONs, I next wanted to identify the receptors that mediate these responses.

3.4.1 Nicotine elicits calcium responses

Acetylcholine can act through either ionotropic nicotinic receptors (nAChRs) or metabotropic muscarinic receptors (mAChRs; see also 3.1.6). To investigate the contribution of these receptors to the observed ACh-evoked calcium responses in M4/6 dendrites, I injected different concentrations of the respective agonists nicotine and muscarine into the γ5 region in R21D02-GAL4 ; GCaMP6f explant brains (see Figure 3.20).

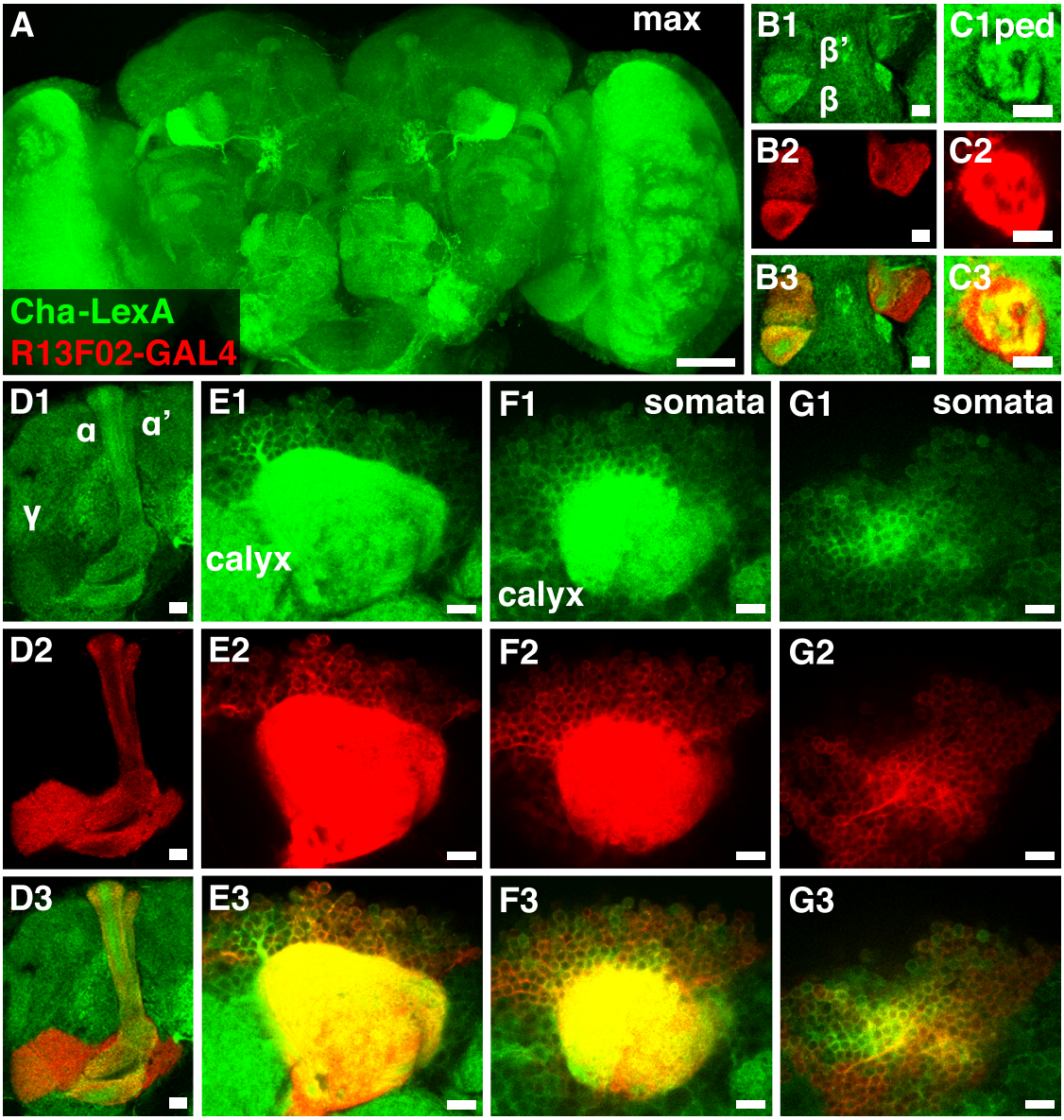


Figure 3.19: Cha3.3kb-LexA::GAD (Diegelmann et al., 2008) expresses in KCs. Cha-LexA drove lexAop-rCD2::mRFP (red), and R13F02-GAL4 drove UAS-mCD8::GFP in KCs. A) Cha-LexA whole brain expression pattern encompasses much of the adult fly brain, including KCs. B) A close-up view of the β/β′ region shows strong Cha-LexA labelling of β regions, while β′ is more faint. C) The peduncle shows wide-ranging LexA expression, with notable lack of zones corresponding to γ and parts of α/βc. D) The vertical lobe and γ lobe show LexA expression in parts of α, and some α′, while γ remains largely unlabelled. E-G) A close-up of the calyx and KC somata shows co-labelling of the majority of KC somata by R13F02-GAL4 and Cha-LexA. Images in B-G show single planes. Scale bar in A represents 50 µm, and those in B-G represent 10 µm.

Nicotine injections elicited no detectable calcium responses at 1 µM, but robust responses at 10 µM (Figure 3.20A-B). 100 µM nicotine elicited calcium responses that showed about double the magnitude to those at 10 µM (Figure 3.20B). Interestingly, muscarine elicited no calcium responses at concentrations between 1 and 100 µM (Figure 3.20B). While this finding does not rule out any contributions of muscarine to the observed ACh-evoked calcium signal, it suggests that the rapid and large calcium influx observed in M4/6 dendrites with ACh stimulation is largely mediated by nAChRs.

Nicotine-evoked calcium responses showed different kinetics to those observed by ACh injections (compare with Figure 3.20C). While the time to peak with 100 µM ACh injections was at about 300 ms, responses evoked by 10 µM nicotine took about 1.5 s to reach peak (Figure 3.20D). Furthermore, decay times were much longer in nicotine-evoked responses: While ACh decay times were at about 500 ms, those for nicotine were at about 2.5 s (Figure 3.20E). These findings demonstrate that nicotinic response decay dynamics are much slower than those of ACh, most likely because ACh is quickly hydrolysed by AChE in the synaptic cleft (see 3.1.6), while no similar mechanism exists for the non-endogenous agonist nicotine (see De Biasi and Dani, 2011).

3.4.2 Histological evidence for nAChR in MBONs

To corroborate these physiological findings suggesting nicotinic ACh receptors in MBONs, I next turned to histology to determine the presence and identity of nAChRs in MBONs.

Conjugated α-bungarotoxin

α-bungarotoxin (α-BTX) is a neurotoxin derived from the krait *Bungarus multicinctus* which acts as a potent antagonist for some nAChRs in mammals (Schoepfer et al., 1990) as well as in flies (Dudai, 1977a).

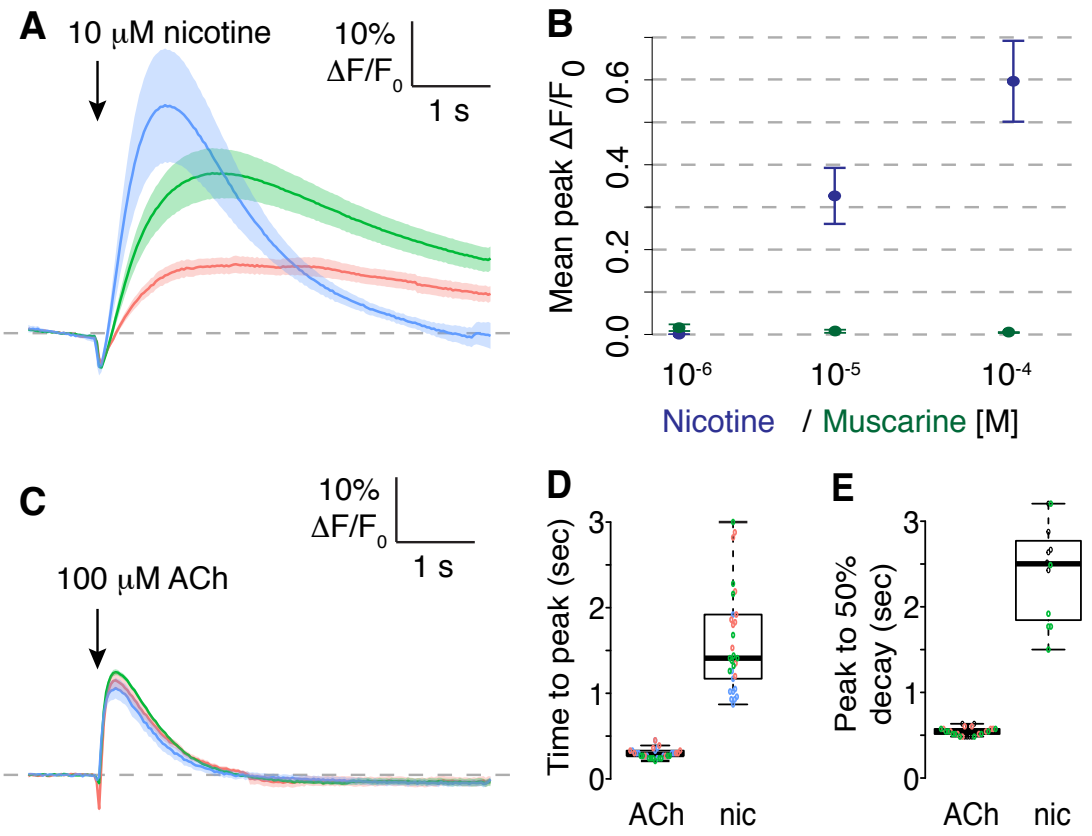


Figure 3.20: A-B) Nicotine elicits calcium responses in M4/6 dendrites, but not muscarine. A) Three trials of injecting 10 µM nicotine into M4/6 dendrites shows rapid strong calcium responses. B) A dose-response analysis with three different concentrations shows increasing calcium peak responses for nicotine (blue) starting at 10 µM, but no responses for muscarine (green) at any of the concentrations tested. Shade and error bars represent SEM. Injections were performed into M4/6 dendrites of R21D02-GAL4 ; GCaMP6f explant brains. C-E) Nicotine responses show different dynamics compared to ACh. C) 100 µM ACh responses for comparison purposes. D) Nicotine injections (10 µM) resulted in peak responses after about 1.5 s, while ACh responses (100 µM) peaked at about 300 ms (left). E) Decay time measured from peak to 50% decay was also prolonged for nicotine responses (about 2.5 s) compared to ACh (0.5 s). Partly adapted from Barnstedt et al. (2016).

While precise nAChR types and subunit compositions remain largely unknown in invertebrates, *Drosophila melanogaster* nAChRs are frequently classified into α-BTX-sensitive and α-BTX-insensitive receptor types. KC-expressed nAChRs, for example, have recently been implicated to be α-BTX-sensitive (Su and O'Dowd, 2003).

To visualise α-BTX-sensitive nAChRs in the fly brain, I used a commercially available α-BTX conjugate with red fluorescent tetramethylrhodamine (TMR) that has previously been used in mammalian nervous tissue (Kim et al., 2008; Rakhilin

et al., 1999; Vilmont et al., 2016), but apparently not yet in flies. I have thus established a method to visualise α-BTX binding in the adult *Drosophila* brain, which consists of a 90 min incubation of unfixed brains with 500 nM α-BTX-TMR before fixation and mounting.

I performed this staining on R21D02-GAL4 ; GCaMP5 flies to co-label M4/6 dendrites. The resulting staining shows strong staining of the AL, and the calyx (Figure 3.21A-B). The calyx staining shows a typical "claw"-like pattern that has been previously described (e.g. Butcher et al., 2012; Caron et al., 2013; Christiansen et al., 2011; Kremer et al., 2010). Interestingly, on the level of the MB, the α′/β′ lobes were clearly stained (Figure 3.21C). Upon closer inspection, the α′ tip was strongly stained, as well as the β′2 region that overlaps with the M4β′ dendrite (see Figure 3.21D). On the other hand, the γ lobe showed no detectable staining, so that overlap with M6 was only visible in the β′2a region (Figure 3.21E). These findings suggest that α-BTX-sensitive nAChRs are located in α′/β′ lobes, so that, potentially, α′/β′ MBONs use α-BTX-sensitive nAChRs.

Dα7::GFP

Dα7 is one of the more commonly described nAChR subunits in *Drosophila*, and is one of only two subunits known to form homopentamers (Lansdell et al., 2012). Together with Dα5 and Dα6 it shows higher homology to the vertebrate α7 receptor than to other insect nicotinic receptors (Grauso et al., 2002)

Recently, a fusion of Dα7 with EGFP was generated, and confirmed to label Dα7-positive dendritic spines with an α-Dα7 antibody (Leiss et al., 2009). This construct has since been used to identify known nAChR sites of KCs in the MB calyx (Christiansen et al., 2011; Kremer et al., 2010; Spühler et al., 2016). Here, I sought to use this tool to identify potential nAChR sites in M4/6 MBONs. To test this, I expressed Dα7::GFP in M4/6 using R21D02-GAL4, and took high-resolution images of these brains.

Expression of Dα7::GFP in M4/6 neurons resulted in clearly visible fluorescent punctae at the previously described dendritic sites in the MB lobe tips (see Figure

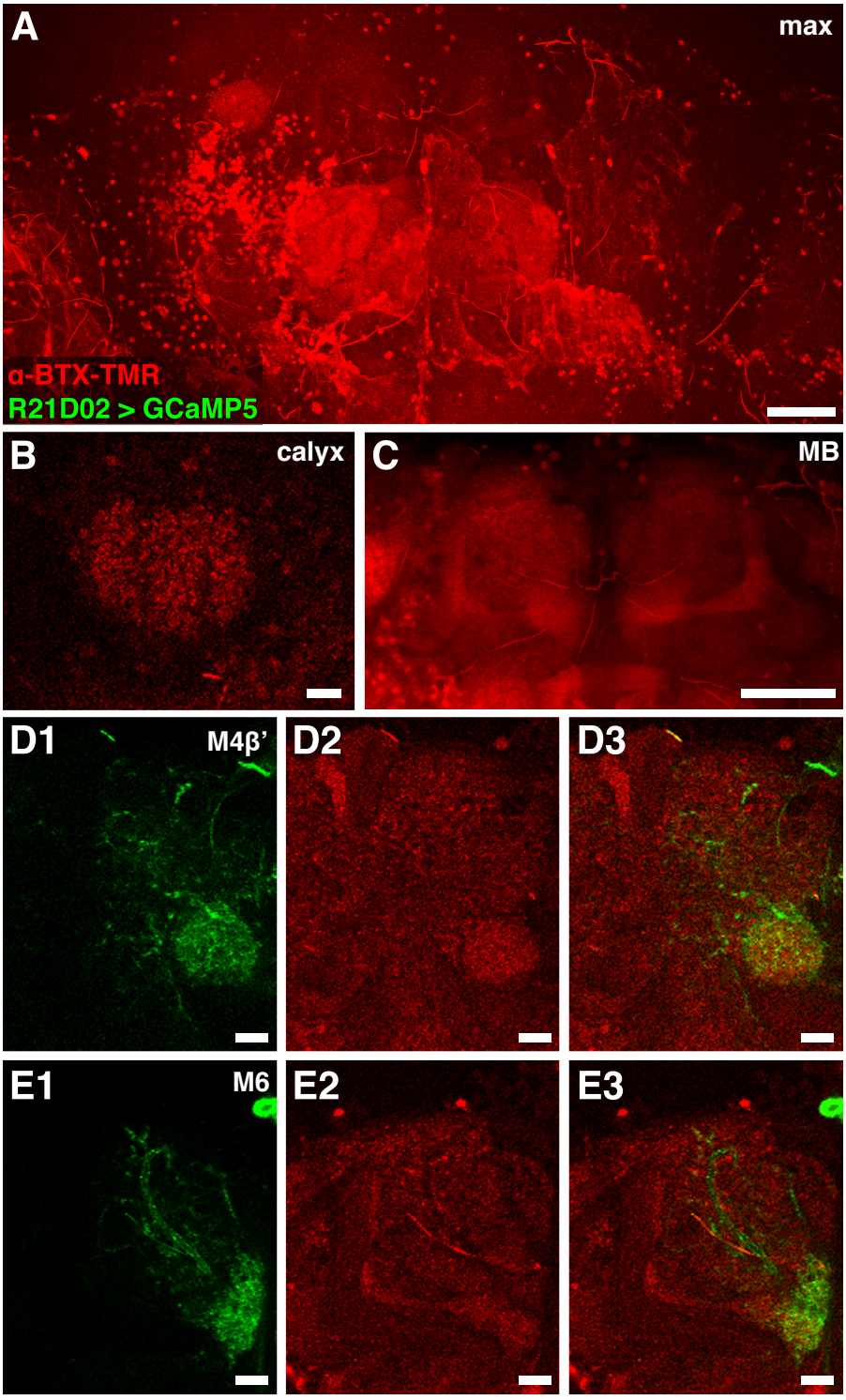


Figure 3.21: Conjugated α-bungarotoxin (α-BTX; red)) staining shows shows labelling in calyx and α′/β′ MB lobes. Unfixed brains expressing R21D02-GAL4 ; GCaMP5 (green) were stained for 90 min with 500 nM of α-BTX-TMR before fixation, mounting and confocal image acquisition. A) A maximum projection of the entire brain shows some unspecific staining artefacts, and the AL prominently stained. B) The calyx shows clear and strong postsynaptic "claws" labelled by α-BTX-TMR. C) A maximum projection of levels covering the MB shows stronger staining in α′/β′ MB lobes compared to the surrounding brain. D) α-BTX-TMR staining is strong on the level of M4β′ dendrites. E) M6 neurons show no overlap with α-BTX-TMR staining except for the β′2a region. Scale bars in A-B represent 50 µm, while those in C-E represent 10 µm.

3.22A), but not in axons, neurites or cell body (data not shown). These Dα7::GFP punctae were previously observed in lobula plate tangential cells (Leiss et al., 2009), but have not been observed in the calyx where KC-expressed Dα7::GFP forms "claws" (Christiansen et al., 2011; Kremer et al., 2010; Spühler et al., 2016).

To improve the resolution on these punctae, I used a blind deconvolution algorithm that clarified these punctae greatly (Figure 3.22A'), and which allowed me to quantify them. I measured a total of 8 hemispheres of unstained R21D02-GAL4 ; Dα7::GFP brains, and used Huygens Object Analyzer to count punctae in deconvolved images. The estimates from this analysis give an average of 3,601 punctae per hemisphere (± 1,657 SD). The respective images and a bar plot of punctae can be found in Figure A.12.

Next, we wondered how these M4/6 Dα7::GFP punctae co-localise with the frequently used dendritic marker DenMark (Nicolaï et al., 2010). Therefore, I co-expressed both Dα7::GFP and DenMark in R21D02-GAL4 M4/6 neurons, and imaged unstained brains. The results show close alignment of both markers in the M4/6 dendritic compartment (see Figure 3.22). Importantly, after deconvolution, close proximity of Dα7::GFP with the more tangle-like structures of DenMark becomes visible (Figure 3.22). In some cases, overlap is visible between both markers, but mostly they are rather interleaved and in close proximity. See also Figure A.13 for a comparison of different deconvolution methods.

While it is not quite clear if this expression reflects the co-localisation of Dα7::GFP with native Dα7 or other nAChRs (see Riemensperger et al., 2017), these findings at least suggest that M4/6 MBONs can traffick Dα7 to its dendritic compartment, where it is aligned with the dendritic protein ICAM5 of DenMark.

nAChR promoter fragments drive in MBONs

As with Cha driver lines (see 3.3.4), nAChR expression patterns can be approximated by the use of promoter fragments from the 10 different nAChR subunit genes. Thanks to recent efforts in generating and publicly cataloguing large libraries of

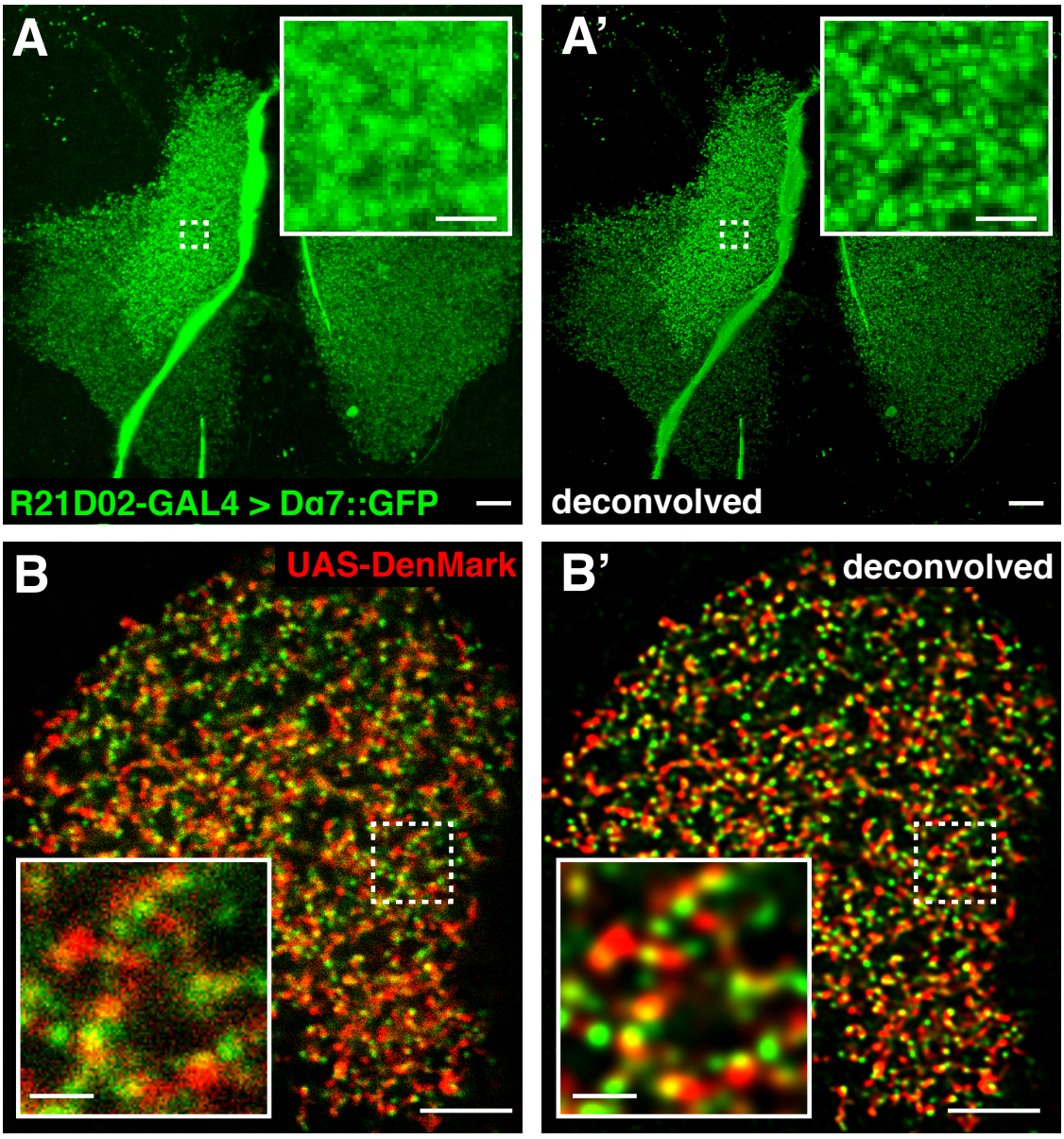


Figure 3.22: Dα7::GFP expresses in M4/6 dendrites, in close proximity to a dendritic marker. A) Unstained R21D02-GAL4 ; Dα7::GFP brains show GFP signal only in M4/6 dendrites. Thousands of individual punctae of about 200 nm size can be resolved after deconvolution (A'). B) Unstained R21D02-GAL4 ; Dα7::GFP ; DenMark brains show that Dα7::GFP punctae are nestled along postsynaptic sites, clearly visualised by deconvolution (B'). Scale bars in main images represent 10 µm, while those in inlays represent 1 µm.

Table 3.3: nAChR-GAL4 lines drive expression in MBONs. 11 GAL4 driver lines with nAChR subunit promoters from the FlyLight collection (Jenett et al., 2012) were identified that express in specific MBONs. Expression pattern was identified based on publicly available images from FlyLight (`flweb.janelia.org`). See also Figure A.14 for the respective images.

nAChR subunit	FlyLight GAL4	Neurons labelled
Dα1	R22G02	M6
	R22F04	MVP2
Dα2	R23A10	V2α'
	R23C06	V3
Dα3	R20G04	V3 and MVP2
	R21E01	V2α'
	R21C11	V2α'
	R21A09	MVP2
	R21C07	M4/6
Dα5	R20D11	M4/6
Dα6	R21D02	M4/6

specific promoter GAL4 drivers (Jenett et al., 2012), it is now possible to rapidly identify expression patterns of specific driver lines.

Making use of this library on FlyLight (`flweb.janelia.org`), I identified 11 different GAL4 lines with nAChR promoter elements that drive expression in some MBONs. These can be found in Table 3.3, while Figure A.14 shows the respective FlyLight images illustrating MBON expression.

These findings would suggest that the various MBONs might express different nAChR subunits, although GAL4 expression does not necessarily fully recapitulate the true gene expression pattern.

3.4.3 Bath application of nAChR blockers during ACh application

If ACh-evoked calcium responses in MBONs are mediated by nAChRs, as the previous data suggests, then pharmacological blockade of these receptors should decrease or even abolish the observed calcium responses. Moreover, as some

pharmacological blockers are known to block only specific subtypes of nAChRs, this method should allow us to characterise MBON nAChRs more fully.

To do this, I injected ACh at regular intervals into M4/6 dendrites while observing calcium responses with GCaMP, before and after bath-application of nAChR antagonists.

Mecamylamine

Mecamylamine is a widely used non-competitive and non-selective nAChR antagonist (see Nickell et al., 2013). In *Drosophila* brains, various concentrations have been used in the past, ranging from 50 µM (Liu and Wilson, 2013) to 100 µM (Gruntman and Turner, 2013; Hige et al., 2015b; Huang et al., 2010) or 200 µM (Gaudry et al., 2013). In order to rule out false negatives and to speed up antagonist diffusion in light of a time-sensitive explant brain preparation, I first used 250 µM mecamylamine.

Expressing GCaMP5 in R21D02-GAL4 M4/6 neurons and injecting 100 µM ACh at 20 s intervals into γ5 of explant brains, I added 250 µM after the first four ACh-evoked responses, and continued to monitor calcium responses. Interestingly, within 30 s of mecamylamine addition, ACh-evoked calcium responses decreased, and vanished within one minute (see Figure 3.23A). Repeating this procedure over five brains showed a significant decrease of ACh-evoked calcium responses before and after the addition of 250 µM mecamylamine (Figure 3.23A). Similar results were obtained at the known nicotinic synapse in the KC calyx (see Figure A.15).

As 250 µM mecamylamine is a very high concentration that could possibly also affect other receptors (see 3.6.4), I repeated these experiments with 100 µM mecamylamine. Effect times were slightly longer, but after 100 s, ACh-evoked calcium responses were again significantly reduced after the application of 100 µM mecamylamine (Figure 3.23B).

Could these decreases in ACh-evoked calcium responses be the result of the explant brain's decreased viability after several minutes of ACh injections? To test this, I performed the same procedure as before, but with vehicle instead of

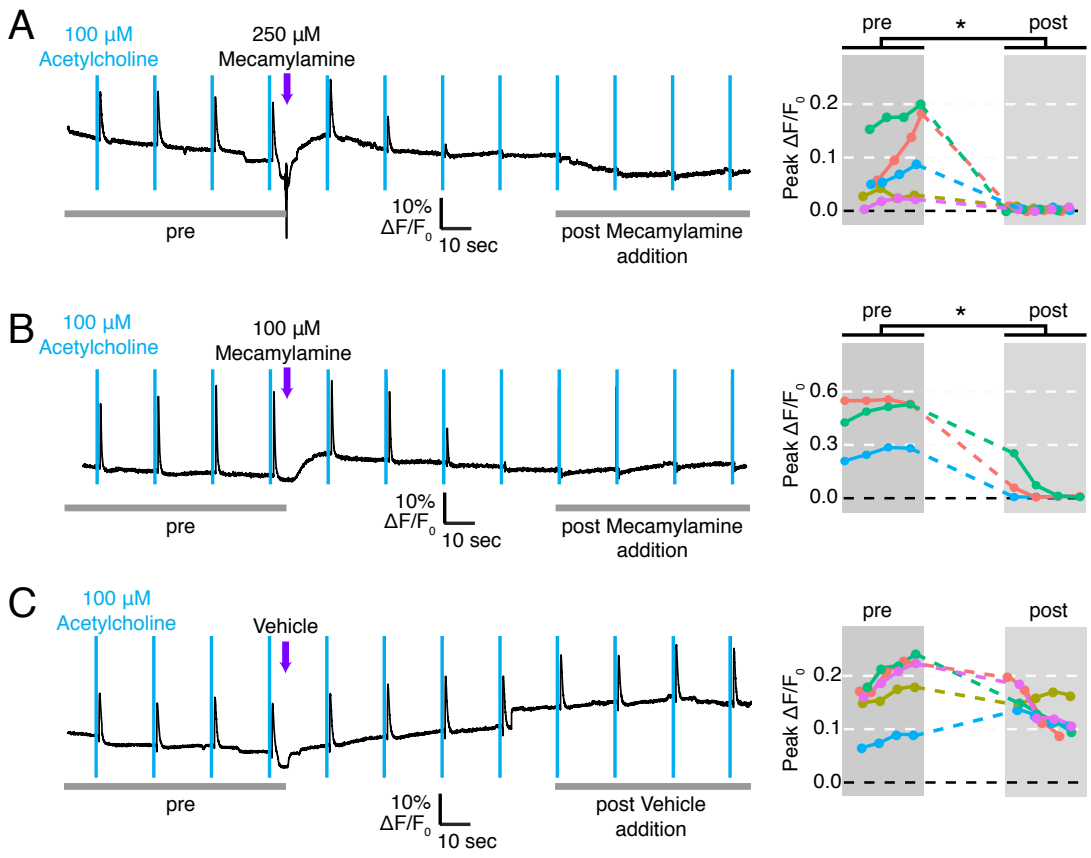


Figure 3.23: Mecamylamine blocks ACh-evoked calcium responses in M4/6 dendrites. 100 µM ACh were injected every 20 seconds into the M4/6 dendrites of R21D02-GAL4 ; GCaMP6f explant brains during widefield calcium imaging (bright blue vertical lines). Black line represents sample calcium transients from M4/6 dendrites. ACh injections reliably induce rapid calcium responses. A) Addition of 250 µM of nicotinic receptor blocker mecamylamine reduces and then abolishes these ACh-evoked calcium responses within one minute. B) Addition of 100 µM mecamylamine also significantly reduces ACh-evoked calcium responses. C) Addition of vehicle has no effect on ACh-evoked calcium responses. Average response peaks from four trials before addition of mecamylamine or vehicle were compared to average response peaks from four trials 100 s after addition. Asterisks denote significant differences pre–post (paired samples t-test, $p < 0.05$, $N = 3 - 5$). Adapted from Barnstedt et al. (2016).

mecamylamine. After vehicle addition, ACh-evoked calcium responses were not significantly changed compared to before addition (Figure 3.23C).

These results suggest that ACh-evoked calcium responses in M4/6 neurons are mediated by mecamylamine-sensitive nAChRs.

Hexamethonium and MLA

In order to make sure that the effects of mecamylamine are not due to non-specific antagonist action, I also used two more non-selective but competitive nAChR antagonists that have been previously used to broadly block nAChRs: hexamethonium (Bennett et al., 1957; Rudloff, 1978; Schmidt-Nielsen et al., 1977; Shomrat et al., 2011; Wut et al., 2005) and methyllycaconitine (MLA; Bertrand et al., 1994; Drasdo et al., 1992; Lansdell and Millar, 2004).

Employing the same protocol as before, with regular injections of 100 µM ACh into M4/6 dendrites while monitoring M4/6 calcium transients before and after bath-application of the respective antagonist, I found a significant decrease with 100 µM hexamethonium (Figure 3.24A), as well as with 10 µM MLA (Figure 3.24B). This suggests that M4/6 nAChRs are not only sensitive to mecamylamine, but also to other broad nAChR antagonists.

3.4.4 RNA interference of nAChRs

As *Drosophila melanogaster* possesses 7 different α and 3 different β subunits that form a wide and largely unknown variety of homo-/heteropentameric nicotinic ACh receptors, I sought to determine the subunit composition of M4/6 nAChRs using gene-specific RNAi knockdown (see 1.5.5).

Odour imaging of M4/6 with nAChR RNAi

As nAChR-RNAi effects might be too subtle to be detected by direct ACh injections, we next sought to test if a more natural stimulation of MBONs might reveal effects for nAChR-RNAi. MBONs have previously been shown to respond to odour stimulation with calcium influx (e.g. Hige et al., 2015b; Owald et al., 2015a; Séjourné et al., 2011), presumably through KCs. We thus wondered if MBON-expressed nAChR-RNAi has negative effects on odour-evoked calcium responses.

To test this hypothesis, I used an *in vivo* tethered fly preparation to record odour-evoked calcium responses with two-photon imaging in R21D02-GAL4 ; GCaMP6f flies carrying additional nAChR-RNAi or control transgenes. I recorded strong and

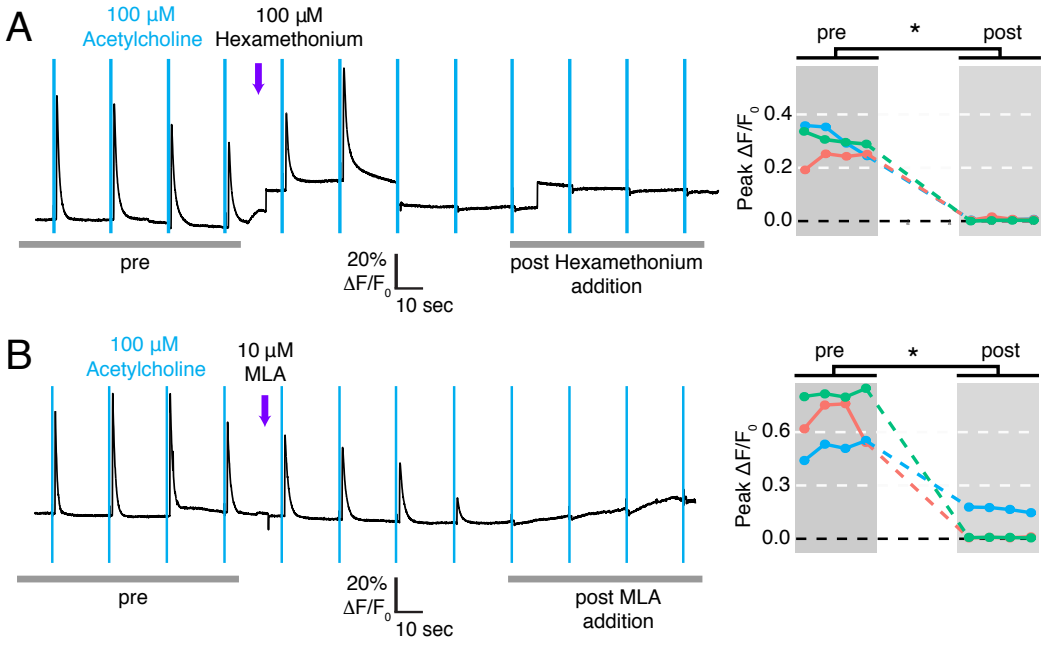


Figure 3.24: Hexamethonium and MLA block ACh-evoked calcium responses in M4/6 dendrites. 100 µM ACh were injected every 20 seconds into the M4/6 dendrites of R21D02-GAL4 ; GCaMP5 explant brains during widefield calcium imaging (bright blue vertical lines). Black line represents sample calcium transients from M4/6 dendrites. ACh injections reliably induce rapid calcium responses. A) Addition of 100 µM of nicotinic receptor blocker hexamethonium reduces and then abolishes these ACh-evoked calcium responses within one minute. B) Addition of 10 µM MLA also significantly reduces ACh-evoked calcium responses. Average response peaks from before addition of mecamylamine or vehicle were compared to average response peaks 100 s after addition. Asterisks denote significant differences pre–post (paired samples t-test, $p < 0.05$, $N = 3$). Adapted from Barnstedt et al. (2016).

robust odour-evoked calcium responses in M4β′ axons to both odours MCH and OCT, and extracted various parameters from these responses in flies additionally carrying RNAi against ChAT, Dα1, Dα3, Dα4, Dα5, or Dα6 (see Figure 3.25). The choice for these subunits was mostly based upon nAChR-GAL4 lines with identified MBON expression (see Table 3.3). The inclusion of ChAT-RNAi served as a negative control as M4/6 neurons are most likely not cholinergic (see Aso et al., 2014a; Owald et al., 2015a). The main control group consisted of an additional CS wild-type allele.

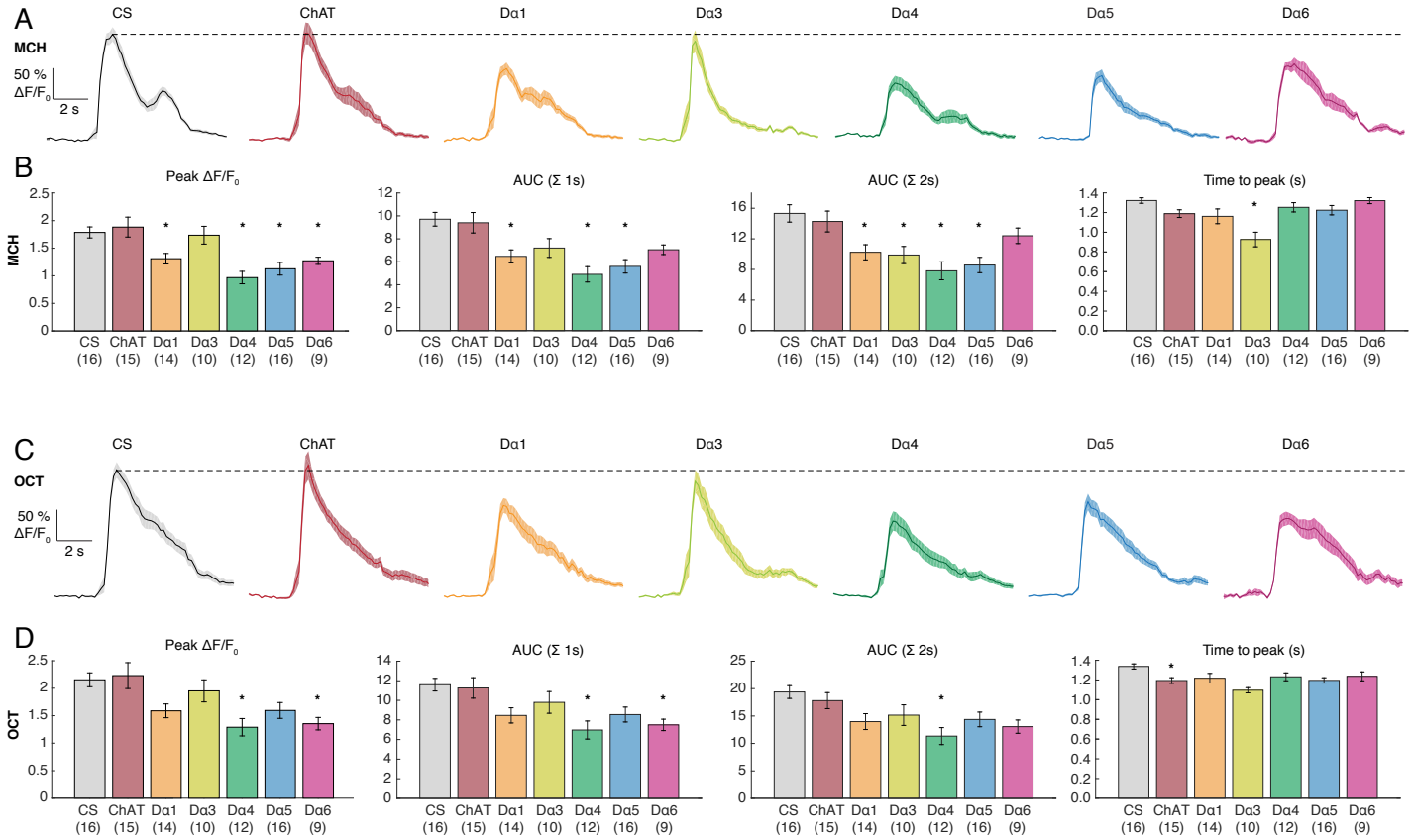


Figure 3.25: RNAi against nAChR subunits decreases odour-evoked calcium responses in M4β′. Head-fixed R21D02-GAL4 ; GCaMP6f flies with RNAi against different nAChR subunits and ChAT were presented with odours OCT and MCH while M4β′ axon calcium responses were recorded with two-photon imaging. A) Mean traces of activity evoked by 5 s of MCH presentation. Odours evoke strong and robust calcium responses. B) Quantification of calcium responses in A. Peak responses were defined as each sample's highest $\Delta F/F_0$ following odour onset. Area under curve (AUC) was measured as the sum of $\Delta F/F_0$ during the first one or two seconds of odour presentation. Time to peak is the time from odour onset until peak response. Peak response and AUC are significantly reduced in animals carrying RNAi against Dα1, Dα4, Dα5, and against Dα6 only for peak responses. C) Same as A, but with OCT as odour. D) Quantification of calcium responses in C. RNAi against Dα4 and Dα6 showed significant reductions in peak responses and AUC. Asterisk denotes significant differences compared to CS control allele (one-way ANOVA, Dunnett's multiple comparisons test, $p < 0.05$, $N = 9 - 15$). Shade in A and C, and error bars in B and D represent SEM. Partly adapted from Barnstedt et al. (2016).

Peak calcium responses were significantly reduced with RNAi against Dα4 and Dα6 for both odours, and additionally RNAi against Dα1 and Dα5 for MCH only (Figure 3.25). The area under curve (AUC) during the first second of odour presentation was significantly reduced with RNAi against Dα1, Dα4, and Dα5 for MCH, and against Dα4 and Dα6 for OCT. AUC during the first two seconds of odour response was significantly reduced with RNAi against Dα1, Dα4, Dα5, and Dα6 for MCH, but only with RNAi against Dα4 for OCT. The time to peak, however, was largely unaffected by these manipulations; only Dα3-RNAi showed a significantly faster rise time with MCH, while ChAT-RNAi showed a significantly shorter time to peak with OCT stimulation.

These findings suggest that some of these nAChR subunits, like Dα1, Dα4, Dα5, and Dα6 may play a role in M4β′ MBONs to mediate odour responses through KC-released ACh.

3.5 Kenyon cells use ACh for neurotransmission to M4/6 MBONs

The previous data showed that KCs express ChAT and VAChT, which enables them to synthesise and synaptically release ACh (see 3.3). I also showed that MBONs specifically respond with rapid calcium increase to focal dendritic stimulation with ACh (see 3.2), and that these responses are mediated by nAChRs likely composed of at least Dα1, Dα4, Dα5, Dα6 (see 3.4). These findings show that the presynapse might release ACh, and that the postsynapse is sensitive to ACh. However, no direct evidence for a cholinergic connection between KCs and MBONs has been presented yet.

In order to ensure that ACh-evoked calcium responses in MBONs are truly from KC-released ACh, we sought to stimulate KCs while monitoring M4/6 calcium responses, and to add pharmacological blockers or RNAi to observe the impact on transmission.

3.5.1 Electrical and pharmacological KC activation

To activate KCs, previous studies have largely relied on focal ACh stimulation in the calyx (see Boto et al., 2014; Cohn et al., 2015; Tomchik and Davis, 2009). Such a method was deemed unsuitable for our experimental aims as the addition of nicotinic antagonists such as mecamylamine would not only block any nicotinic synapses between KCs and MBONs, but also act on nAChRs in the calyx (see Gu and O'Dowd, 2006; Su and O'Dowd, 2003), thus making it hard to interpret any effects of the antagonist.

Instead, I tested three different strategies to repeatedly stimulate KCs and observe neural responses in M4/6 neurons. These are electrical stimulation, ATP/$P2X_2$ pharmacological stimulation, and optogenetic stimulation.

First, I tried electrical stimulation of the calyx while observing calcium responses in R21D02-GAL4 ; GCaMP6f explant brains with widefield imaging. The advantages of this method are that only two transgenes need to be expressed, and no further use of pharmacology is necessary. On the other hand, it is difficult to find stimulation strength that is sufficient to reliably induce trans-synaptic activity in M4/6 neurons while avoiding stimulating tissue outside the calyx. Most problematically, I encountered problems with the explant brain's viability under these conditions so that once trans-synaptic responses could be established, these tended to not be reliably reproduced in the minutes following (data not shown). This, of course, makes the interpretation of pharmacological interventions difficult.

A second and more targeted approach to stimulate KCs is the use of the ATP-gated cation channel $P2X_2$ (Brake et al., 1994; Lima and Miesenböck, 2005; Valera et al., 1994). $P2X_2$ can be specifically activated in neurons of interest by applying ATP to these neurons (e.g. Cohn et al., 2015; Liu and Wilson, 2013; Machado et al., 2017; Sitaraman et al., 2015). Importantly, there are no known endogenous purinoceptors in *Drosophila* that could otherwise be activated by ATP (see Littleton and Ganetzky, 2000).

To stimulate KCs via ATP/$P2X_2$ and observe calcium transients in M4/6 neurons, I expressed $P2X_2$ with the LexA/lexAop driver system in 247-LexA::VP16

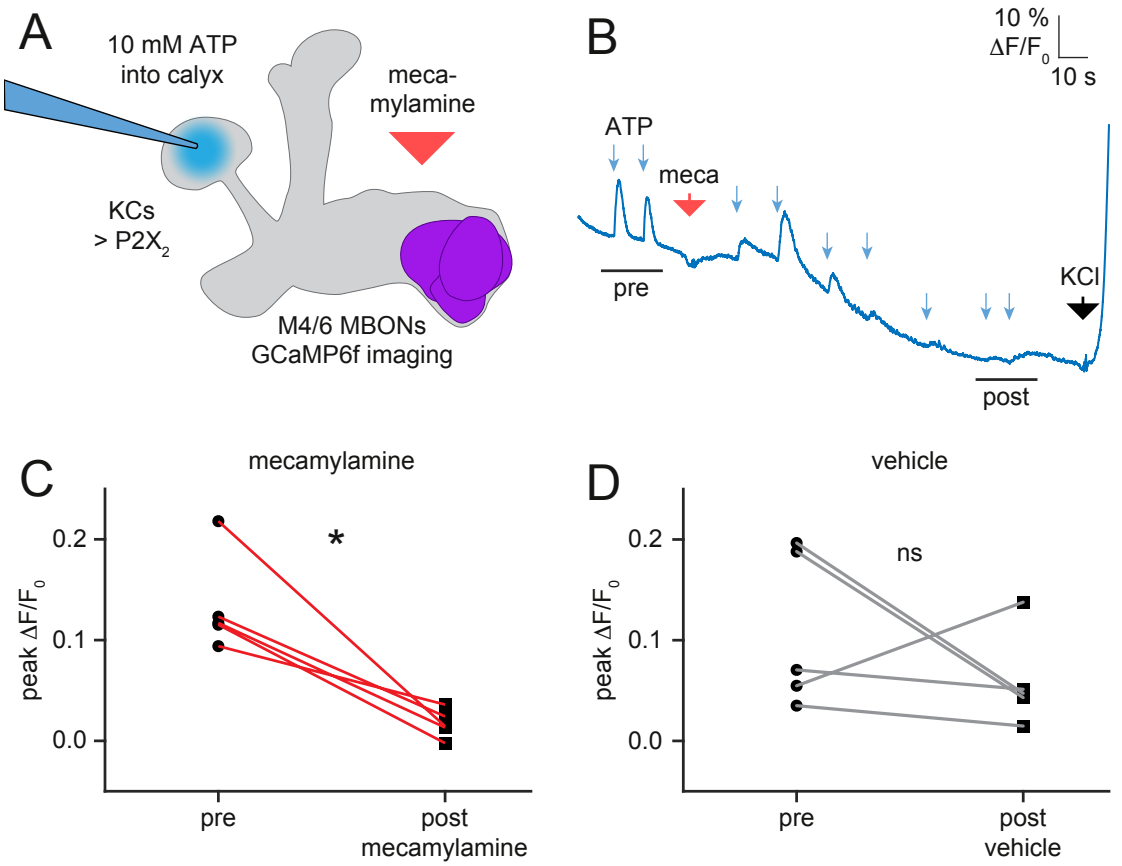


Figure 3.26: KC stimulation through $P2X_2$ activates M4/6 neurons through nAChRs. A) 247-LexA::VP16 expressed lexAop-$P2X_2$ to allow stimulation with 10 mM ATP microinjected into the calyx, while calcium transients were observed in M4/6 axons with R21D02-GAL4 ; GCaMP6f under widefield illumination. After successful stimulation, 250 µM mecamylamine were added to the bath to block nAChRs. B) Repeated ATP stimulation of KCs elicits reliable responses in M4/6 axons. These responses vanish within 100 s of mecamylamine application. At the end of the experiment, KCl was added to assert viability of brain. C-D) 250 µM mecamylamine significantly reduced peak calcium responses (C), while vehicle application did not significantly changes responses (D). Paired t-test, asterisk denotes $p < 0.01$, $N = 5$. Average of two response peaks before bath-application were compared to average of two responses 100 s after bath-application.

KCs, and imaged from M4/6 neurons with R21D02-GAL4 ; GCaMP6f (see Figure 3.26A). Pressure microinjection of 10 mM ATP into the MB calyx resulted in relatively reliable calcium responses in M4/6 axons (see Figure 3.26B). 100 s after bath-application of 250 µM of the non-selective nAChR antagonist mecamylamine these calcium responses were significantly decreased (Figure 3.26C), while responses remained relatively stable after addition of vehicle (Figure 3.26D). This suggests that KCs act on M4/6 neurons via nicotinic ACh receptors.

3.5.2 Optogenetic KC activation with mecamylamine

While $P2X_2$-guided KC stimulation resulted in reliable M4/6 calcium responses, the viability of explant brains under these conditions was not ideal, so that the duration of viability was often not sufficient to test the effects of bath application, let alone washout experiments. To overcome these limitations and corroborate previous findings, I next used optogenetic stimulation (see 1.5.4 for background) of KCs while monitoring calcium transients in M4/6 neurons.

To this end, I expressed the red-shifted channelrhodopsin CsChrimson (Klapoetke et al., 2014) broadly in KCs with 247-LexA::VP16 (see Figure 3.27A). I used a red-shifted channelrhodopsin for this because blue/green light would interfere with simultaneous collection of GCaMP signals. Imaging with widefield microscopy or two-photon imaging of M4/6 dendrites was unsuccessful, presumably due to inadvertent activation of CsChrimson by the imaging light (unpublished observations and personal communication with A. Wong, HHMI Janelia Research Campus).

I observed rapid and strong calcium responses in M6 axons of explant brains additionally expressing R21D02-GAL4 ; GCaMP6f (see Figure 3.27B-C). These calcium responses decreased significantly and in most cases vanished completely 100 s after bath-application of mecamylamine, while the addition of vehicle had no effect on calcium responses (Figure 3.23D). These findings again support the idea that KCs activate M4/6 neurons through mecamylamine-sensitive nAChRs.

Is the observed block of KC-triggered calcium responses in M4/6 neurons terminal, or do explant brains recover from the mecamylamine block? To investigate this, I again bath-applied either 100 µM or 250 µM mecamylamine after recording initial responses, recorded the action of mecamylamine 5 min after application, and then aimed to wash out the antagonist (see Figure 3.28). I included 100 µM mecamylamine as a recent study found KC $\rightarrow$ MBON connectivity in the presence of 100 µM mecamylamine (Hige et al., 2015b).

As before, I observed rapid and strong calcium responses to LED stimulation (see Figure 3.28). These responses were significantly decreased 5 min after the addition of 100 µM mecamylamine, and almost completely vanished after addition

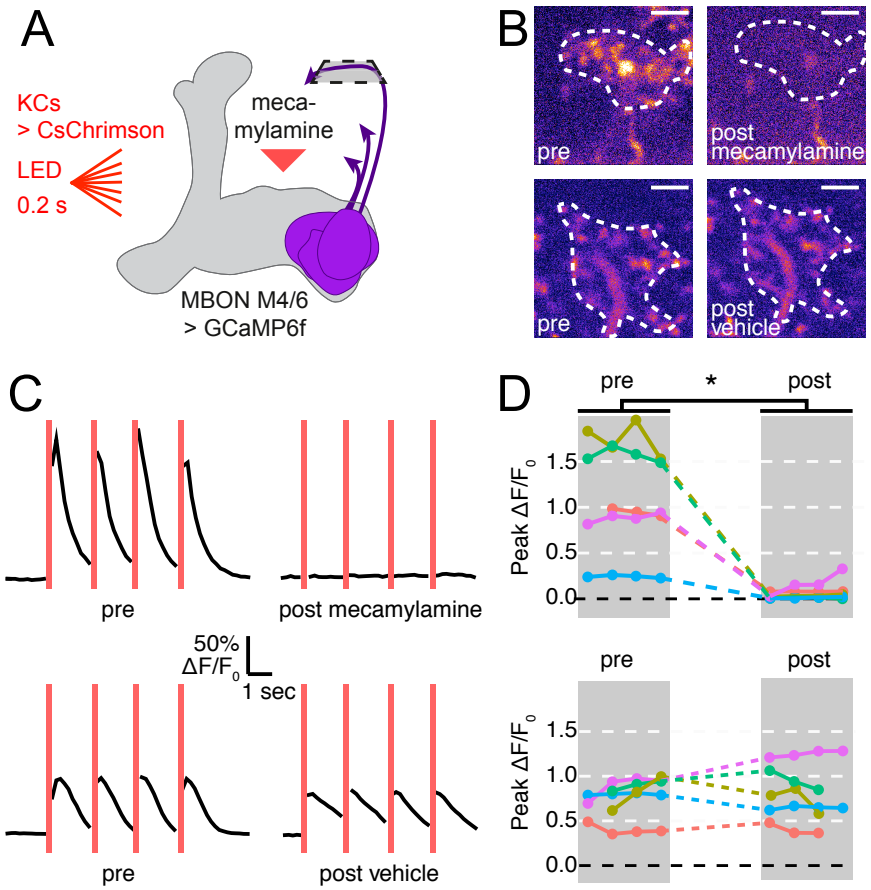


Figure 3.27: Optogenetic KC stimulation activates M4/6 neurons through nAChRs. A) The red-shifted channelrhodopsin CsChrimson was driven in KCs by 247-LexA::VP16, while M6 axon calcium transients were monitored with R21D02-GAL4 ; GCaMP6f. CsChrimson was activated by 200 ms of pulsed (40 Hz, 10 ms) red light from an LED. After initial collection of calcium responses, 250 µM of the non-selective nAChR antagonist mecamylamine were added to the bath, and responses monitored again after 5 min. B) Sample two-photon images from M6 axons after stimulation before and after addition of mecamylamine (top) or vehicle (bottom). Scale bars represent 5 µm. ROI outline is shown as white dashed line. C) Sample calcium transients during LED stimulation (red vertical lines) before (left) and after (right) addition of mecamylamine (top) or vehicle (bottom). Calcium responses appear and decay rapidly with LED stimulation, and vanish after addition of mecamylamine but not vehicle. D) Quantification of peak calcium responses shows a significant decrease of calcium responses after addition of mecamylamine but not after vehicle. Asterisk denotes significant difference, paired t-test, $p < 0.05$, $N = 5$. Average peak response from 3-4 trials were compared before bath application and 5 min after bath application. Adapted from Barnstedt et al. (2016).

of 250 µM mecamylamine. Interestingly, repeated stimulation showed a gradual increase of calcium responses from no detectable response to almost half the earlier response in one example (Figure 3.28A). Importantly, 30 min after washout had started, responses partly recovered considerably for both concentrations. Thus, both concentrations of mecamylamine significantly decreased calcium resonses in M4/6 neurons, and after 30 minutes of wash-out no significant difference to initial responses was observed anymore. This shows that brains are still viable after mecamylamine treatment, and can partly recover from nAChR block.

The previous findings suggest that optogenetic activation of KCs leads to M4/6 calcium responses through a nicotinic synapse that can be reversibly blocked by the addition of mecamylamine. KCs, however, are known to have nicotinic receptors themselves, so it is plausible that a broad bath application of a powerful nicotinic antagonist such as mecamylamine affects KC firing. If it does, this would pose a challenge to the interpretation that M4/6 calcium responses are reduced due to a block of the KC $\rightarrow$ MBON synapse. Instead, it could mean that mecamylamine induces KCs to fail to become activated by optogenetic stimulation.

To rule out such a hypothesis, I directly imaged calcium responses in the γ5 region of KCs that expressed both CsChrimson as well as GCaMP6f. I first imaged calcium responses to red light stimulation in flies expressing CsChrimson::mVenus in KCs. This required extremely low laser intensity levels to avoid inadvertent stimulation of CsChrimson with the imaging laser. Nonetheless, robust calcium responses to red light stimulation could be observed (see Figure 3.29A). Bath-application of 250 µM mecamylamine had no significant effect on these, when tested 5 min after application (Figure 3.29B).

As the CsChrimson fused to the YFP variant mVenus had considerable bleed-through into the green PMT channel used for GCaMP recording, and might thus affect calcium responses imaged, I turned to a more recently developed variant of CsChrimson fused to the RFP tdtomato. I imaged flies carrying CsChrimson::tdtomato at a slightly higher laser power, and observed an increase of fluorescence during the first 5 min of imaging (see Figure 3.29C), presumably due to

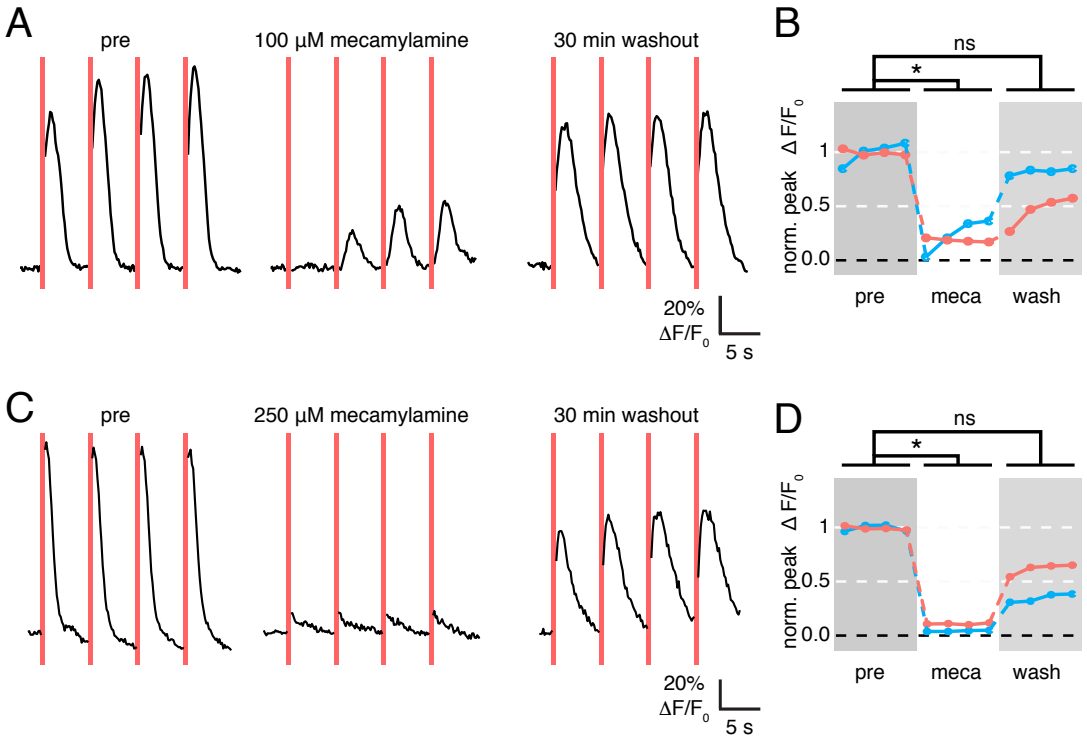


Figure 3.28: Mecamylamine block of nicotinic KC → MBON synapse is reversible. 247-LexA::VP16 was used to drive CsChrimson in KCs, and R21D02-GAL4 ; GCaMP6f to read out calcium transients in M6 axons. 200 ms of pulsed (40 Hz, 10 ms) red LED light were used to stimulate KCs optogenetically. A) Sample calcium transients of one brain. LED stimulation induces rapid and strong calcium responses in M4/6 neurons. 5 min after the addition of 100 µM mecamylamine, these responses are greatly reduced, but show a slight recovery with repeated stimulation. 30 minutes after washout, responses have recovered almost fully. B) Quantification to A of two brains. Asterisk denotes significant difference of normalised average response peaks of four trials before and after addition of 100 µM mecamylamine (paired t-test, $p < 0.05$, $N = 2$. C) Sample calcium transients with addition of 250 µM mecamylamine. 5 min after bath application, responses are almost completely vanished, but recover greatly after washout. D) Quantification to C of two brains. Asterisk denotes significant difference of normalised average response peaks of four trials before and after addition of 250 µM mecamylamine (paired t-test, $p < 0.05$, $N = 2$). Peak $\Delta F/F_0$ responses were normalised to each experiment's average initial four responses. Adapted from Barnstedt et al. (2016).

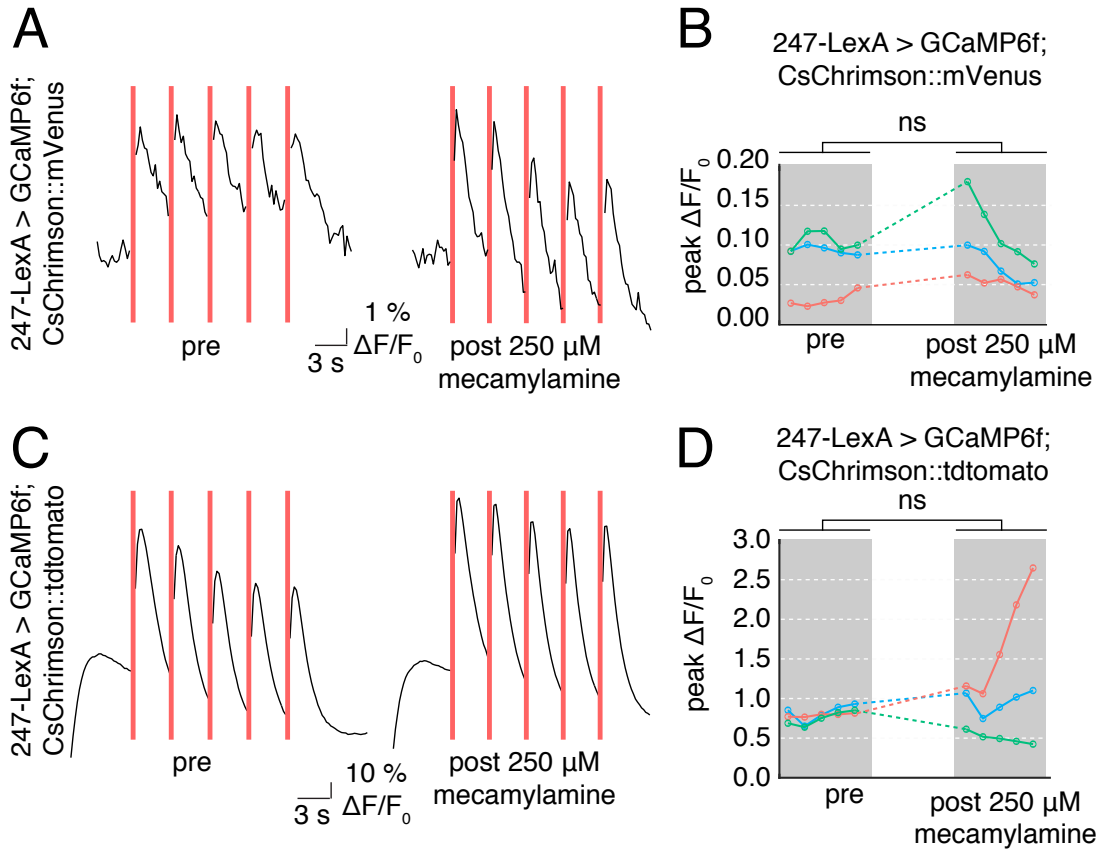


Figure 3.29: CsChrimson stimulation of KCs yields KC calcium responses despite mecamylamine. 247-LexA::VP16 was used to express both GCaMP6f as well as CsChrimson in KCs, to monitor KC responsiveness in the presence of 250 µM of the nicotinic antagonist mecamylamine. A) Sample calcium transients from flies expressing CsChrimson::mVenus. 200 ms of red light induces robust calcium responses, independent of mecamylamine. B) Average response peaks to CsChrimson::mVenus stimulation before and after 5 min of mecamylamine are not significantly different (paired t-test, $p > 0.05$, $N = 3$). C) Sample calcium transients from flies expressing CsChrimson::tdtomato. Imaging onset causes a slight increase in baseline. Red light stimulation results in robust calcium responses, independent of mecamylamine addition. D) Average response peaks to CsChrimson::tdtomato stimulation before and after 5 min of mecamylamine are not significantly different (paired t-test, $p > 0.05$, $N = 3$.

imaging laser activation of CsChrimson. Nonetheless, 200 ms of red light stimulation resulted in strong and robust calcium responses that were unaffected by the addition of 250 µM mecamylamine (Figure 3.29D). This suggests that KCs are still sensitive to CsChrimson stimulation despite the presence of mecamylamine in the bath.

3.5.3 Optogenetic KC activation with RNAi

Previous optogenetic experiments suggest that KC activation leads to M4/6 calcium responses that are blocked in the presence of the nicotinic antagonist mecamylamine. Bath application of this blocker, however, could plausibly also affect other synapses in the system. This means that KCs could theoretically act on other neurons that, in turn, release ACh onto MBONs. While such a circuit model seems unlikely given the clearly identified molecular nature of possible MBON inputs (see Aso et al., 2014a), along with my data on ChAT and VAChT expression in KCs (see 3.3), we wanted to rule out such a model with more experimental evidence.

For this, we generated recombinant lines carrying the M4β′ driver R15B01-LexA, recombined with lexAop-GCaMP6f on II, and combined this with a broad KC GAL4 driver (R13F02-GAL4). We crossed these flies to flies carrying UAS-CsChrimson::mVenus (II) with either VAChT-RNAi or a genetic background allele as control. I subsequently recorded from the M4β′ axons of these neurons in explant brains with red light stimulation. As before, 200 ms of red light induced strong calcium responses in M4β′ axons (see Figure 3.30A). Importantly, the resulting calcium response peaks were significantly smaller in flies carrying KC-driven VAChT-RNAi compared to control flies (Figure 3.30B-C). This suggests that knockdown of ACh vesicle trafficking in KCs reduces responses in M4/6 neurons, and is further evidence of a direct release of ACh from KCs to MBONs.

Interestingly, a rapid stimulation protocol of 20 stimulation trials at 200 ms with 3 s ITI resulted in a rundown of light-evoked responses (see Figure 3.30D). This held true for both control as well as VAChT-RNAi flies, but affected control flies more strongly, so that after 20 trials light-evoked responses in RNAi and control flies were of the same peak magnitude.

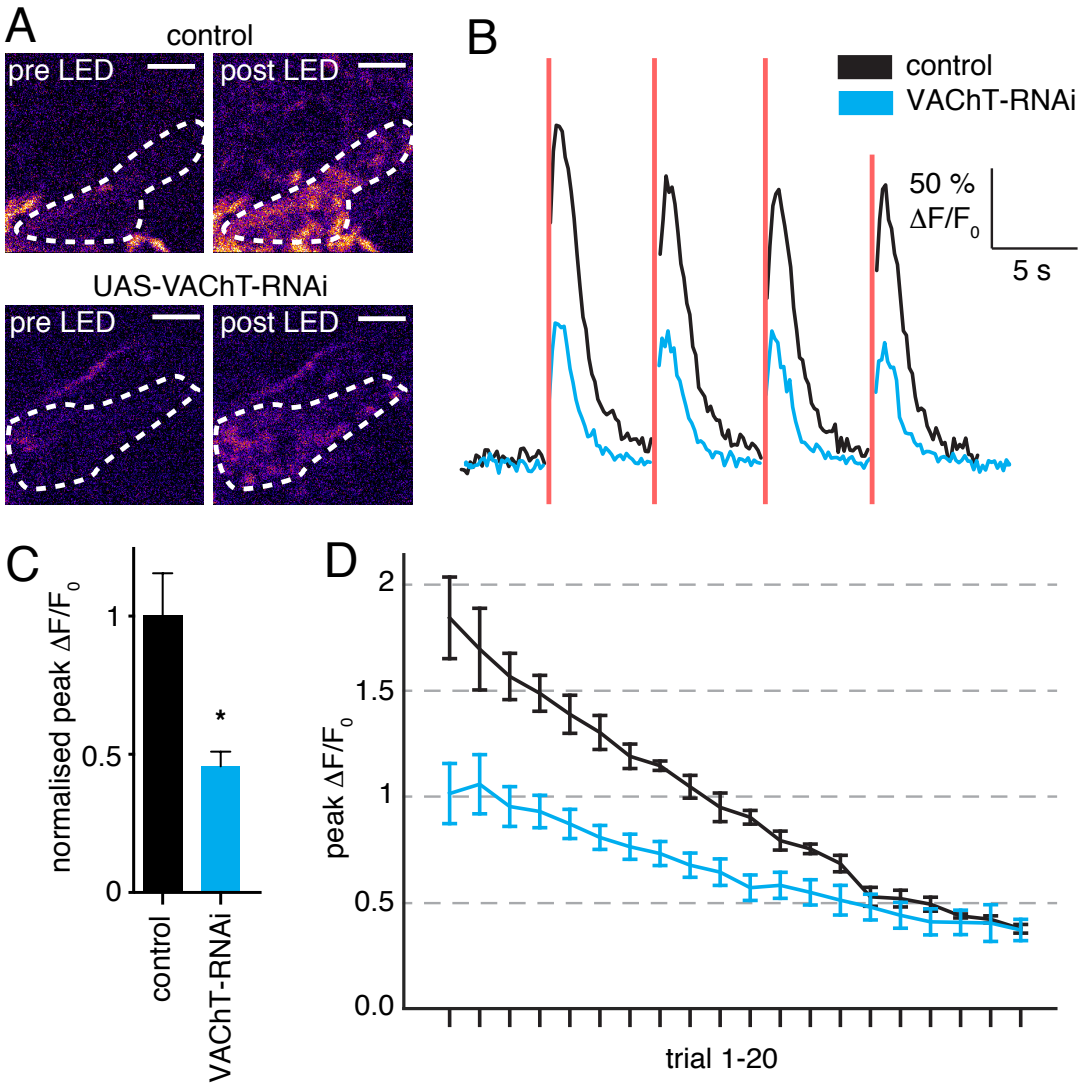


Figure 3.30: VAChT-RNAi in KCs reduces KC → MBON calcium responses. M4β′ axon calcium transients were measured by R15B01-LexA driving GCaMP6f, while KCs were activated by R13F02-GAL4 driven CsChrimson::mVenus. KCs additionally expressed either VAChT-RNAi or a genetic background allele. KCs were stimulated with 200 ms of red pulsed (40 Hz, 10 ms) LED light. A) Sample two-photon images of control (top) and VAChT-RNAi (bottom) brains before (left) and after (right) LED stimulation. ROI is marked as white dashed line, and scale bar represents 5 µm. B) Sample calcium responses to light stimulation in control (black) or VAChT-RNAi (light blue) flies. Note that VAChT-RNAi responses are comparably smaller, but show similar kinetics to control responses. C) Normalised peak $\Delta F/F_0$ is significantly reduced in flies carrying KC-driven VAChT-RNAi compared to controls (Mann-Whitney U-test, $p < 0.05$, $N = 4 - 6$). D) A fast light stimulation protocol of 200 ms with 3 s ITI induces a fast rundown of calcium responses, particularly in control flies, so that calcium response peaks reach the same level after 15-20 stimulation trials. Error bars in C-D represent SEM. Partly adapted from Barnstedt et al. (2016).

3.6 Discussion

3.6.1 Results summary

The neurotransmitter of KCs has remained obscure for decades, despite its importance in understanding the neural mechanisms of associative learning in invertebrates, and despite many decades of intense research on the MB.

There are four established criteria that should be satisfied before a transmitter role is accepted for a substance (Aidley and Ashley, 1998, p. 187):

1. The presynaptic neuron should contain the substance and be able to synthesise it.

2. The substance should be released on stimulation of the presynaptic axons.

3. Application of the substance to the postsynaptic cells should reproduce the effect of the normal transmission.

4. The action of the substance on the postsynaptic cell should be affected by competitive blocking agents in the same way that synaptic transmission is.

In the work presented, I found evidence for all four of these points that strongly suggest that ACh is a neurotransmitter of KCs.

1. Presynapse

As direct measurement of ACh within *Drosophila* brains is currently outside of current technical possibilities (see also 3.6.3), only the presence of proteins required for ACh synthesis and processing could be investigated. I have shown that relatively weak α-ChAT and prominent α-VAChT staining in MB lobes can be significantly reduced by KC-directed RNAi knockdown of these proteins. This strongly suggests that the observed immunoreactivity is protein-specific, and that the observed immunoreactivity comes mainly, if not only, from KCs. These stainings will be further discussed in 3.6.3. Furthermore, experiments performed by my colleague J. Felsenberg show that this KC-driven knockdown results in a functional defect in memory performance (Barnstedt et al., 2016). Additionally, I showed that

Cha-GAL4 and Cha-GAL80 driver lines express in some KCs, while Cha-LexA labels most KCs.

Taken together, these findings strongly support the idea that ChAT and VAChT are expressed in KC axons of the MB lobes, thus enabling presynaptic release of ACh from KCs to downstream neurons in the MB lobes.

2. ACh release

As mentioned before and discussed further in 3.6.3, ACh levels cannot currently be measured inside of *Drosophila* brains. However, I found indirect evidence for ACh release by KC terminals. Knocking down the vesicular ACh transporter VAChT specifically in KCs resulted in a significant reduction of calcium responses in MBONs (Figure 3.30). This strongly suggests that ACh vesicle trafficking in KCs is required for downstream MBON activation. Knocking down VAChT probably results in less ACh released, so that decreased levels of ACh release are probably responsible for a decrease of MBON responsivity to KC stimulation. This suggests that KCs release ACh.

3. Application to postsynapse

Focal injections of ACh to MBON dendrites in the lobes result in strong and robust MBON calcium responses. These responses are likely the result of direct receptor activation on MBON dendrites, as blocking VGSCs with TTX or synaptic transmission through elevated Mg^{2+} had no effects, and response dynamics were tightly linked to ACh release and spread.

These ACh-evoked calcium responses in MBONs are likely mediated through nAChRs, as nicotine elicits similar responses. Histologically, α-bungarotoxin labelling, expression of Dα7::GFP in MBONs, and nAChR-GAL4 expression in MBONs further support the expression of nAChRs on MBON postsynaptic sites. Furthermore, I showed that nAChR-RNAi in MBONs reduces odour-evoked calcium responses.

4. Block of postsynaptic responses

Besides nicotine-evoked calcium responses and histological and genetic evidence for the presence of nAChRs on MBONs, I could also show that blocking nAChRs with broad nicotinic receptor antagonists such as mecamylamine drastically reduces ACh-evoked calcium responses as well as KC-mediated calcium responses in MBONs. This block was reversible, and left KC activity intact. This shows that nicotinic blockers affect the KC → MBON synapse the same way that direct ACh application onto MBON dendrites does.

3.6.2 Recent related studies

Even though the idea that ACh could be the main KC neurotransmitter had been dismissed for a long time (see Brooks et al., 2011; Hige et al., 2015b; Yasuyama et al., 1995), some previous evidence already pointed towards a cholinergic nature of KCs, and since the publication of the key work presented here (Barnstedt et al., 2016), several studies have confirmed our main conclusions.

Earlier studies suggesting cholinergic KCs

As described before (3.1.6), Lozano et al. (2001) found an impairment in associative memory retrieval with mecamylamine injections into the MB α lobe. As the lobes are spatially well separated from nicotinic synapses in the MB calyx, the observed defect could be due to an impairment of a cholinergic KC → MBON synapse in bees. However, in *Drosophila melanogaster*, many MBONs are themselves cholinergic, so that mecamylamine injections might have plausibly affected their output as well, depending on the specificity of the injection. While falling short of claiming KCs are cholinergic, the authors "propose that some of the connections between the α-lobes and the lateral protocerebrum are cholinergic" (Lozano et al., 2001, p. 252). It will be interesting to revisit the KC → MBON synapse in honey bees and other arthropods to confirm the cholinergic nature of KCs found in *Drosophila melanogaster*.

Another more recent study suggested KCs could be cholinergic, based on the effects of Cha3.3kb-GAL80 on the KC expression patterns of c309-GAL4 and

D52h-GAL4 (Yi et al., 2013). Furthermore, ChAT-RNAi and VAChT-RNAi in c309-GAL4 were found to impair sleep, but opposite effects were found when KCs were taken out from c309-GAL4 by addition of MB-GAL80. This suggests that the sleep defects found may at least be partially contributed by non-KC expression in c309-GAL4. Nonetheless, the authors claim that "[t]hese results provide the first functional evidence that at least a portion of MB neurons are cholinergic" (Yi et al., 2013, p. 1819).

Transcriptomic studies support cholinergic KCs

Microarray data from our lab (see Perrat et al., 2013), show that both *ChAT* and *VAChT* mRNA are not significantly different in KCs compared to the rest of the (mostly cholinergic) brain: *ChAT*: $\gamma = 8.83$, $\alpha'/\beta' = 8.43$, $\alpha/\beta = 6.74$, rest = 8.86, all p [neurons to rest of brain] > 0.05; *VAChT*: $\gamma = 7.27$, $\alpha'/\beta' = 5.94$, $\alpha/\beta = 5.89$, rest = 7.00, all p [neurons to rest of brain] > 0.05; t test. These findings are in line with our findings of ChAT and VAChT immunoreactivity in different parts of the lobes (see Figure 3.16). Interestingly, there are striking similarities in that α/β neurons show low ChAT levels both in the microarray as well as for immunoreactivity, while VAChT levels are very high in γ in the microarray data as well as for immunoreactivity. These differences and their implications will be discussed further in 3.6.3.

Another recent transcriptome profiling study (Crocker et al., 2016) came to similar conclusions: The authors used RNA sequencing of specific MB neurons, and found elevated levels of *ChAT* in α/β KCs, and of *VAChT* in α/β and γ KCs. Interestingly, *ChAT* levels for γ KCs were not significantly elevated ($p > 0.2$). This could be the result of high *ChAT* background levels, or the result of KC-intrinsic expression differences (see also 3.6.3). Furthermore, another yet unpublished transcription analysis also supports our findings of the cholinergic nature of KCs (personal communication with T. Hige, 21.05.2017).

Novel methods for VAChT detection

Three further methods for detecting VAChT levels in neurons have recently been developed: a novel transgenic line allowing for the visualisation of endogenous VAChT expression (Pankova and Borst, 2017), a novel VAChT-LexA line (Simpson, 2016), and an additional α-VAChT antibody (Boppana et al., 2017), all of which (supposedly) confirm the cholinergic nature of KCs. A newly developed FRT-STOP-FRT-VAChT::HA line shows strong *VAChT*-driven HA signal in α/β KCs, but not in other KCs (Pankova and Borst, 2017). The novel VAChT-LexA line shows clear labelling in at least α/β and γ KCs (Simpson, 2016), but the presence of α′/β′ KCs is not clear from the published images. A novel rabbit α-VAChT antibody was raised against a unique 15-amino acid sequence in the C terminal region of VAChT. This antibody supposedly labels KCs, but from the micrographs published this is difficult to assess (Boppana et al., 2017).

The KC → DAN synapse is also cholinergic

Another recent study confirmed the cholinergic nature of KCs genetically and physiologically, and uncovered a cholinergic synapse from KCs to DANs (Cervantes-Sandoval et al., 2017). These authors found KC → DAN synapses (that have also been recently identified through EM in larval and adult brains, see Eichler et al., 2017; Takemura et al., 2017) that could be blocked by different concentrations of mecamylamine (Cervantes-Sandoval et al., 2017). For this, the authors used the ATP/$P2X_2$ system to activate KCs, and monitored calcium transients in the MB-V1 PPL1 DAN. 100 µM mecamylamine resulted in a mild but significant loss of connectivity, while 250 and 500 µM mecamylamine produced a more robust block (up to 60 %). Interestingly, the Dα6 nAChR subunit seemed to play no role in V1, but RNAi against Dα1, Dα4, and Dα5 resulted in memory defects when targeted into V1. This suggests that KCs not only release ACh onto MBONs, but also onto V1 DANs, and possibly onto other MB neurons.

Electrophysiological evidence for a nicotinic KC → MBON synapse

Very recently, a dense EM reconstruction of the entire α lobe of an adult *Drosophila melanogaster* MB was published (Takemura et al., 2017). Importantly, the authors confirmed that 250 µM of mecamylamine blocks the KC → MBON synapse. For this, they expressed ChrimsonR in α/β KCs and recorded from MBON-α1 with whole-cell patch-clamp electrophysiology. 100 ms of optogenetic KC activation resulted in fast onset responses that persisted with 1 µM TTX, but that were abolished to the same level of no-ChrimsonR controls in the presence of 250 µM mecamylamine (Takemura et al., 2017, Figure 7 - figure supplement 1). The authors also suggest that previous findings of KC → MBON connectivity (Hige et al., 2015b) may have been confounded by the presence of 100 µM mecamylamine (Takemura et al., 2017).

In the following, I will discuss our findings in more detail, first discussing the evidence for the presence of ChAT/VAChT in KCs (3.6.3), then the evidence for nAChR-mediated responses in MBONs (3.6.4), before discussing the wider implications and outlook of these findings (3.6.5).

3.6.3 ChAT/VAChT expression in KCs

The cholinergic locus and KCs

ChAT and VAChT are not only related by their common function in supporting cholinergic transmission, they also share a common genetic locus. This so-called "cholinergic locus" consists of > 25 kb on the right arm of the third chromosome (18,705,501 – 18,732,344; see Figure 3.31; Kitamoto et al., 1998). This cholinergic locus is unusual in that *VAChT* is completely nested within the first intron of *Cha*, which may be used for the coordinated regulation of both genes (Usdin et al., 1995).

Cha also produces two separate RNA transcripts, A and B, which could be responsible for the finding of ChAT in either a membrane-bound or a soluble form (Pahud et al., 1998).

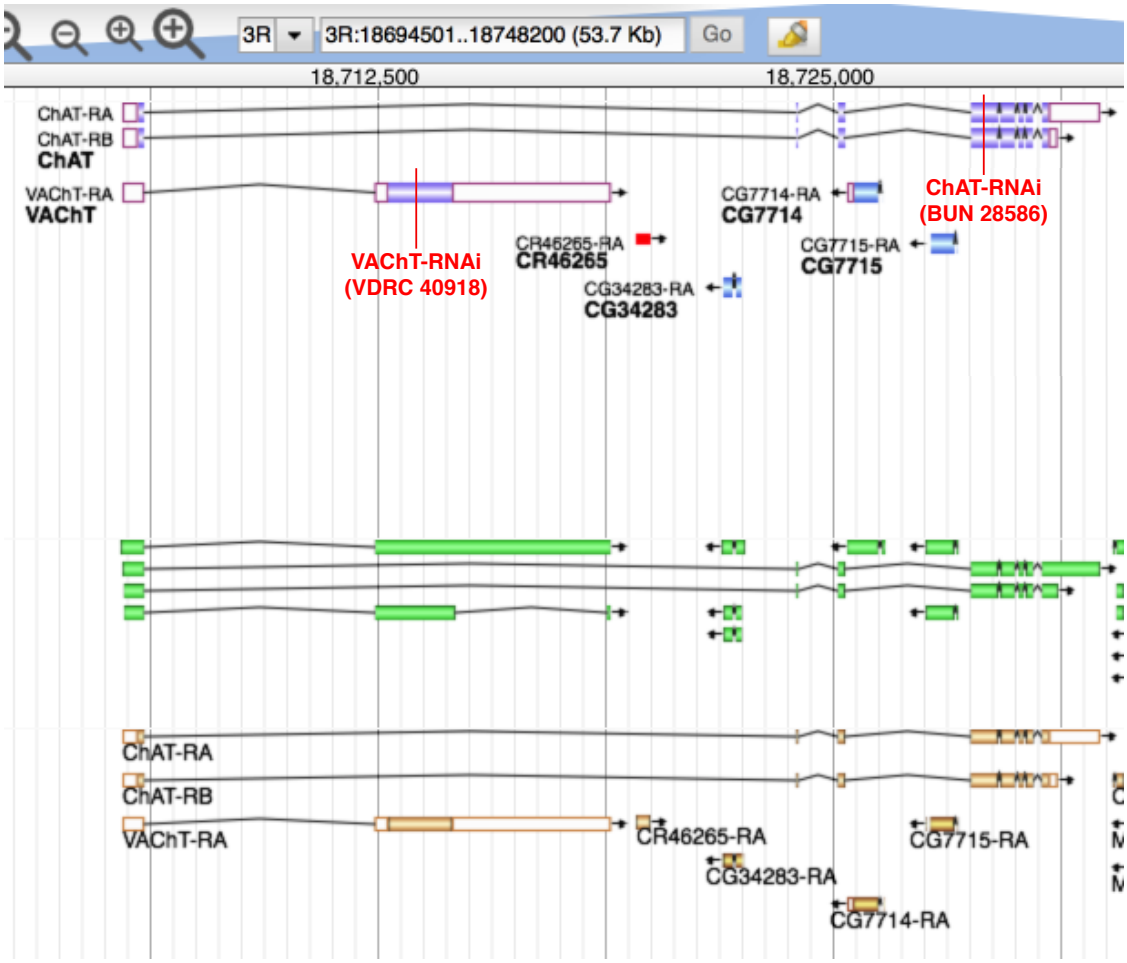


Figure 3.31: The cholinergic locus on 3R and locations of RNAi. *ChAT* and *VAChT* both share a starting exon, followed by introns, but the *VAChT* exon is entirely nested inside the first *ChAT* intron. ChAT produces two transcripts (RA and RB). The two RNAi lines used in this work target either the main *VAChT* exon (VAChT-RNAi), or target the main exon for both *ChAT* isoforms (ChAT-RNAi). Image captured from JBrowse on FlyBase (`jbrowse.flybase.org`; 25.7.17).

Previous ChAT stainings

Previous stainings of adult *Drosophila* brains with α-ChAT antibodies suggested weak to no immunoreactivity, as described before (3.1.6). Upon closer inspection, however, the staining by Buchner et al. (1986) shows some distinctive staining in β and γ lobes, while the peduncle is void, similar to what we found with the α-ChAT4B1 antibody (see Figure 3.11; see also Yasuyama et al., 1995). Although Yasuyama et al. (1995) described all three MB lobes as "unstained", the original image presented (shown in Figure 3.2) clearly shows weak labelling of MBs, similar

to what we found (Figure 3.11). Yasuyama et al. (1995) additionally used Cha7.4kb cDNA transformants with highly enriched α-ChAT immunoreactivity, which suggests that the antibody should be able to detect higher ChAT levels in the MB.

Cell bodies

I found no immunoreactivity in cell bodies with α-ChAT, which could have provided important evidence for the cell identity of the MB lobe staining. The fact that α-ChAT staining is not visible in cell bodies has also been observed previously by others (Barber et al., 1989; Buchner et al., 1986; Gorczyca and Hall, 1987; Yasuyama et al., 1995), and may suggest that the protein only becomes fully translated at the presynapse where it is required. This would also explain why the peduncles have been consistently found to be α-ChAT immunonegative (Buchner et al., 1986; Gorczyca and Hall, 1987).

Why is the α-ChAT staining relatively weak?

One puzzling finding is the surprisingly weak level of α-ChAT immunoreactivity (see Figure 3.16), compared to known cholinergic synapses from AL PNs to calyx or LH (see Figure 3.11). These weak levels have also been previously detected by others (Buchner et al., 1986; Yasuyama et al., 1995), and are likely the main contributor to the notion that KCs would not be cholinergic despite the widely cholinergic nature of excitatory synaptic transmission in the invertebrate brain (see Breer, 1987; Buchner et al., 1986; Gorczyca and Hall, 1987). α-VAChT, on the other hand, shows relatively strong staining in the MB (see Figures 3.14 and 3.16).

Why are α-ChAT levels in the MB so low? There are two main possibilities, given the cholinergic nature of the KC → synapse: 1) The antibody labels ChAT quantities unfaithfully. 2) ChAT quantities are indeed low in the MB, but may be sufficient for cholinergic transmission.

Are ChAT quantities well represented by relative α-ChAT staining? In general, quantitative immunohistochemistry is confounded by the fact that antibody binding in tissue does not linearly reflect antigen quantities. Nonetheless, the α-ChAT staining we have detected in the MB lobes was only between a third and half of that measured in the SMP neuropil (see Figure 3.13). If both areas contain cholinergic synapses, why would the MB staining be much weaker?

First, it should be noted that ChAT4B1 is a monoclonal antibody that will only recognise a single site on the ChAT protein. If this molecular site on the final protein is covered or otherwise inaccessible by diffusion, immunoreactivity will be significantly lower. In the case of MBs, it could be imaginable that the fine KC axons are so densely packed that the antibody might not properly bind, or has difficulty to fully diffuse through this dense tissue. Cha7.4kb cDNA transformants, however, show considerably higher MB immunoreactivity compared to controls (Yasuyama et al., 1995), suggesting that the antibody should be able to also report higher levels of ChAT if they are present.

Another possibility is that KCs (also) use a different ChAT isoform compared to other cholinergic synapses. Both soluble and membrane-bound forms of ChAT have previously been described (Pahud et al., 1998). It is possible that KCs additionally employ a form that may not be readily recognised by previously developed antibodies.

A fan-in architecture might require less ACh release per synapse. Strong α-ChAT immunoreactivity was reliably detected by ChAT4B1 and other previous ChAT antibodies in calyx and LH (Buchner et al., 1986; Yasuyama et al., 1995). AL PN terminals in the calyx form large presynaptic boutons that are each surrounded by several KC dendritic claws. They are among the largest synapses in the *Drosophila* brain (Butcher et al., 2012; Leiss et al., 2009). This fan-out neural architecture, in which only ∼150 cholinergic PNs drive the activity of ∼2,000 KCs through a nicotinic synapse, presumably requires the release of relatively large quantities of ACh, also considering that the calyx additionally receives strong GABAergic

feedback projections from APL (Lin et al., 2014a). It is thus not surprising that very strong α-ChAT immunoreactivity has been found at these synapses.

KC → MBON connections, on the other hand, form a fan-in neural architecture where ∼2,000 KCs provide input to ∼ 33 MBON cells (Aso et al., 2014a; Takemura et al., 2017). This high level of convergence means that either MBONs must only become active at very high concentrations of ACh, or that each KC only releases relatively low concentrations of ACh, if MBONs are to be selective in their response to varying degrees of input. I have previously shown that already 100 µM ACh suffice to drive calcium responses in MBON dendrites (although 1 mM might be required to elicit axonal responses), so that MBONs don't seem to have an exceptionally high threshold to ACh stimulation. In fact, this concentration is at least two magnitudes lower than what is commonly used to stimulate nicotinic synapses in the calyx (see Figure 3.8; Cohn et al., 2015; Inada et al., 2017; Tomchik and Davis, 2009).

KCs, on the other hand, each possess $\sim 20 - 30$ *en passant* synapses per compartment, most of which are to MBONs (Takemura et al., 2017). α lobe compartments are known to have $> 10,000$ KC → MBON synapses (Takemura et al., 2017). Given the observed sensitivity of MBONs to ACh, it would thus seem plausible that each KC releases only relatively low levels of ACh at each presynaptic site. Low quantities of ACh released would also be important to prevent the spread of ACh to other nearby synapses through diffusion (given the high density of synapses in the MB), which could interfere with the specificity of the CS representation (see also Lin et al., 2014a). Furthermore, ChAT seems to synthesise ACh rather efficiently, so that a global reduction of ChAT levels to only 8 % still allowed flies to survive and behave normally (Greenspan, 1980). KCs are also known for their sparse activity to environmental stimuli, so that they might not need to release ACh at a high frequency, thus being content with only relatively little synthesis molecular machinery.

Taken together, these observations would suggest that the low level of α-ChAT staining might truly represent low levels of ChAT protein in the MB. These low

levels of ChAT might be sufficient for synaptic transmission given the sparse activity of KCs and the nature of strong convergence at this fan-in synapse.

Alternatively, we cannot fully rule out the co-expression of another fast excitatory neurotransmitter, although our data (see Figure 3.28) and that of others (see Takemura et al., 2017) strongly suggests that fast excitatory neurotransmission is conveyed solely through nicotinic ACh receptors. It is still possible though that other neurotransmitters could be (co-)released that also act on nAChRs. Such a transmitter could be choline or analogues (see 3.6.3).

Why is α-VAChT staining stronger than α-ChAT?

In this work, I present the first characterisation of MB labelling of a previously developed α-VAChT antibody (see Figures 3.14, 3.15, and 3.16; Kitamoto et al., 1998). Interestingly, this antibody shows labelling comparable to that of other cholinergic neuropils: between 40–200 % of that observed in the SMP (Figure 3.16C). This large variance between lobes probably stems from the fact that antibody penetration was generally very low, with most brains showing very strong staining in the periphery, and markedly lower staining towards the centre of the brain (see Figure 3.14C). The most comparable region to the SMP control region is probably the γ lobe, which shows about 80 % α-VAChT staining intensity compared to the SMP (Figures 3.15 and 3.16). This is much higher than the observed 50 % staining intensity of α-ChAT (Figure 3.16B).

One reason for this difference could be that α-VAChT is a polyclonal antibody (Kitamoto et al., 1998) that has many potential binding sites on the VAChT protein, compared to the monoclonal α-ChAT antibody (Takagawa and Salvaterra, 1996). Similar observations in mammals have previously been suggested to be staining artefacts (Schäfer et al., 1995).

Another possibility could be differential requirements for either protein in KCs. Despite their shared genetic locus, independent transcriptional regulation has been suggested to explain previous findings of differing ChAT and VAChT mRNA levels (Kitamoto et al., 1998). A higher VAChT : ChAT ratio might be useful if only small

ACh quantities were required, but vesicular trafficking would be comparable to that of other cholinergic neurons (see 3.6.3). Another possibility could be the additional use of choline as a co-transmitter that would be trafficked by VAChT (see Bravo et al., 2004), but would not be acetylated by ChAT to ACh (see 3.6.3 for further discussion).

Effects of RNAi on ChAT/VAChT immunoreactivity

While KC-driven ChAT-RNAi reduced α-ChAT immunoreactivity in MB lobes (Figure 3.13), and VAChT-RNAi reduced α-VAChT immunoreactivity (Figure 3.15), as expected from cholinergic KCs, we also surprisingly found that VAChT-RNAi reduced α-ChAT immunoreactivity (Figure 3.16B). This was unexpected since VAChT-RNAi is predicted to have little to no off-target effects (checked with `dscheck.rnai.jp`; Naito et al., 2005). In light of the nested nature of the cholinergic locus, however, it is important to note that this VAChT-RNAi targets not only the *VAChT* exon, but also the *ChAT* intron. Although little is currently known about RNAi targeting intron sequences, it is possible that VAChT-RNAi interferes with ChAT pre-mRNA splicing, thus reducing ChAT protein levels (see also Bosher et al., 1999; Seinen et al., 2011).

Choline as a functional neurotransmitter?

ChAT levels have often been found to be lower in some KCs than VAChT levels. For example, *ChAT* mRNA levels are much lower than *VAChT* mRNA levels in whole fly and fly body extracts (Kitamoto et al., 1998), *ChAT* but not *VAChT* mRNA levels in γ KCs are not significantly elevated compared to other gene transcripts (Crocker et al., 2016), *ChAT* mRNA levels in α/β KCs are somewhat lower in microarray data (Perrat et al., 2013), and α-ChAT immunoreactivity in α/β lobes was only at 20–30 % of that found in the SMP (see Figure 3.16 and 3.13). Similar findings of low ChAT but high VAChT immunoreactivity have been described before in the mammalian brain (Ichikawa et al., 1997; Roghani et al., 1997; Schäfer et al., 1998a,b), and stronger VAChT transcription compared to ChAT transcription was found in the rat PNS (Schütz et al., 2001). While these observations could be due to staining

artefacts (see Schäfer et al., 1995) or differential transcriptional requirements, another interesting idea would be the use of choline as a neurotransmitter.

Choline is the immediate precursor to ACh (see 3.1.6), but its analogue homocholine has also been found to be stored by and released from vesicles in the *Torpedo* electric organ (Luqmani et al., 1980). Choline activates α7 nAChRs in *Xenopus* oocytes (Mandelzys et al., 1995; Papke et al., 1996), and calcium-dependent release of the choline analogue diethylhomocholine was found under conditions of low cytoplasmic ACh concentrations (Welner and Collier, 1985). More recently, it was found that choline can be trafficked into synaptic vesicles by VAChT (Bravo et al., 2004). These findings suggest that choline might indeed be released as a neurotransmitter from presynaptic terminals, and may act on nAChRs.

One advantage of choline as a neurotransmitter compared to ACh would be the fact that a further synthesis step could be 'saved' by KCs, thus possibly allowing for a more efficient transmission/reuptake cycle. This could be advantageous especially in α/βc axons that were recently shown to be very tightly spatially concentrated in the MB lobes, with only few presynaptic boutons (Takemura et al., 2017). Spatial restrictions and energy demands might thus lead to such a 'shortcut' in neurotransmitter cycling.

On the other hand, ChAT does seem to play a role in KCs as KC-driven ChAT-RNAi not only greatly reduces α-ChAT staining in most lobes (see Figure 3.16), but also impairs memory function (see Barnstedt et al., 2016). Furthermore, VAChT has a $\sim 24\times$ higher affinity to transport ACh than choline (Bravo et al., 2004), so that a choline transmission cycle might not be more efficient, after all. It is also not quite clear how the action of choline might be temporally sufficiently restricted, given that rapid ACh hydrolysis through AChE is largely credited for the rapid decay times of cholinergic responses. As my data and that of others show, KC-evoked MBON responses are generally fast and relatively short-lived (see Figure 3.28; Hige et al., 2015b; Takemura et al., 2017). These arguments make choline an unlikely (co-)transmitter.

How could choline (co-)transmission be experimentally tested? Choline is known to act on nAChRs, so choline injections in MB lobes would most likely result in MBON activity, without providing strong evidence for KC-released choline. If choline neurotransmission was restricted to α/β KCs that are important for LTM, then α/β KC-driven ChAT-RNAi might not impair LTM retrieval, while VAChT-RNAi would. Physiologically, I have shown that KC-driven VAChT-RNAi reduces calcium responses in M4β′ axons (see Figure 3.30). If choline were released from α/β KCs, then we might expect ChAT-RNAi in α/β KCs to have no effect on α/β MBON responses, although negative findings with RNAi may also be due to low RNAi efficacy or compensation mechanisms of the system (see Greenspan, 1980). More data on the presence and distribution of AChE in the *Drosophila melanogaster* brain may prove useful, as AChE would be dispensable for choline transmission but required for ACh transmission.

AChE and CHT

Two further proteins involved in cholinergic neurotransmission have so far been studied less in *Drosophila melanogaster*, but may ultimately provide crucial information in understanding the actions of ACh in the synaptic cleft.

AChE is required for hydrolysis of ACh into acetate and choline in the synaptic cleft (see Figure 3.1). The expression pattern of a commercially available α-AChE antibody showed only weak staining of the MB, but surprisingly stained several hundred cell bodies with remarkable similarity to previously described astrocyte-like glia (ALGs; Kremer et al., 2017; see also Figure A.11). Notably, ALGs have been described to innervate calyx and MB lobes, where "the presence of ALG coincides with the presence of synapses" and "they show thin branches with local thickenings at various positions within their network" (Kremer et al., 2017, p. 629). In contrast, the peduncle was shown to contain very few astrocyte-like processes, again supporting the idea that ALGs are enriched near synapses (Kremer et al., 2017), and implying a role in synaptic processes (see also Edenfeld et al., 2005). The fact that the α-AChE staining is very weak outside of these cell bodies could be due to penetration issues.

Previously, AChE activity was found in astrocytes of rats (Koelle, 1954; Souza et al., 2016; Thullbery et al., 2005), roosters, and cats (Brightman and Albers, 1959), suggesting a potential role in the breakdown of ACh at cholinergic synapses. Indeed, considering the AChE staining observed (Figure 3.17), ALG innervations of the MB lobes (Kremer et al., 2017), and previously reported AChE activity of astrocytes (e.g. Souza et al., 2016), it seems plausible that ALGs in the *Drosophila* brain might support cholinergic synapses through AChE activity.

The choline high affinity transporter (CHT) is required for reuptake of deacetylated choline from the synaptic cleft back into the presynaptic terminal (see Figure 3.1). Interestingly, most CHT resides in a subset of VAChT-containing vesicles and not in the plasma membrane – this arrangement is hypothesised to couple ACh release with the availability of functional CHT into the plasma membrane (Ferguson and Blakely, 2004; Ferguson et al., 2003; Ribeiro et al., 2003). In *Drosophila melanogaster*, however, there are so far only two genes predicted to fulfill the role of CHT. These are choline transporter-like Ctl1 (CG1311) and Ctl2 (CG11880) (Martin and Krantz, 2014). The further characterisation of Ctl's function in *Drosophila* should prove helpful in understanding the cholinergic transmission cycle.

How could ACh be measured directly?

Would it be possible to measure ACh directly instead of relying on the presence of ACh-related proteins? So far, no method has been reported that would allow tracking of [ACh] in specific *Drosophila* brain regions.

In mammalian brains, however, recent advances have allowed the real-time *in vivo* monitoring of extracellular choline in freely moving rodents (Baker et al., 2015; Parikh et al., 2007). As has been described previously (see 3.1.6), choline is produced when ACh is degraded by AChE in the synaptic cleft (see Ferguson et al., 2003), so that extracellular [choline] is directly related to ACh release. Choline concentrations can be measured by electrochemical biosensors where electrodes are coated with the enzyme choline oxidase that produces hydrogen peroxide upon reaction with choline and oxygen. The resulting hydrogen peroxide can subsequently be electrochemically

quantified (see Baker et al., 2015). This method has been recently employed successfully to measure ACh transients in the hippocampus and prefrontal cortex of freely moving mice (Howe et al., 2013; Howe et al., 2017; Teles-Grilo Ruivo et al., 2017). The drawback of this method, however, is that these biosensors have a diametre of ∼150 µm to 300 µm (Baker et al., 2015; Teles-Grilo Ruivo et al., 2017), effectively spanning most of the *Drosophila* brain, thus making it impossible to discern specific *Drosophila* brain regions unless its size can be scaled down. This could possibly be achieved by employing individual platinum-based recording sites (15 µm) instead of microelectrode arrays (Howe et al., 2017; Parikh et al., 2007).

A frequently used method to detect dopamine transients in the mammalian brain is fast-scan cyclic voltammetry (Robinson et al., 2003). Intriguingly, this method has also recently been used in adult *Drosophila* brains (Makos et al., 2010; Makos et al., 2009), raising the hope that electrochemical measurements of other neurotransmitters such as ACh may also be performed in the *Drosophila* brain in the near future.

Effects of KC-driven VAChT-RNAi

We observed smaller peak calcium responses from M4/6 neurons when KCs expressed VAChT-RNAi compared to control. On fast rundown trials, initial VAChT-RNAi responses show about half the magnitude of control flies, but within 20 trials, control flies show similar levels of peak calcium response compared to VAChT-RNAi flies (Figure 3.30).

One interpretation for these findings would be that flies carrying VAChT-RNAi have a normal-size pool of vesicles, but many of them would lack ACh due to a lack of VAChT. Upon frequent stimulation, cholinergic vesicles become depleted and both control and VAChT-RNAi groups reach the same response magnitude defined by the rate-limiting step, which is the reuptake of choline with the choline transporter (see Ferguson and Blakely, 2004).

Such a model would be supported by recent findings of VAChT activity at a central cholinergic *Drosophila* synapse (Cash et al., 2016). These authors show that

pharmacological block of VAChT activity results in unchanged quantal size and no decrease in the number of vesicles at the active zone, suggesting that many vesicles indeed lack ACh (Cash et al., 2016; see also Prado et al., 2013).

Driver lines

In line with previous findings, we found Cha7.4kb-GAL4 to express in ∼80 γ and α/β surface KCs (Figure 3.18; Johard et al., 2008; Mehren and Griffith, 2006; Salvaterra and Kitamoto, 2001).

Perhaps surprisingly, the previously uncharacterised Cha3.3kb-LexA::GAD driver showed strong expression in many hundreds of KCs belonging largely to α/β, but also to α′/β′ and some γ (see Figure 3.19).

Cha3.3kb-GAL80 expression is more difficult to interpret as expression estimates can only be drawn from the interaction with other GAL4 drivers, and these interactions may not simply be linear. Previous characterisations of Cha3.3kb-GAL80 found that it removes γ, α′/β′, and α/β surface expression from 30Y-GAL4 (Mehren and Griffith, 2006); it completely removes the γ, and α/β surface expression seen in D52h-GAL4, and completely removes the sparse α/β core expression of c309-GAL4 (Kitamoto, 2002; Yi et al., 2013); it removes γ and α/β surface expression from sNPF-GAL4, but leaves α/β core expression intact (Shang et al., 2013). Our data also show the removal of α/β surface and posterior from c739-GAL4, while leaving α/β core intact (Figure A.9B; Perisse et al., 2013b). In the case of the strongest KC-GAL4 driver, OK107-GAL4, however, neurons in all major lobes remain, albeit drastically sparsened, and with α/β core largely intact (see Figure A.9C). Together, these findings suggest that Cha3.3kb-GAL80 probably drives expression in most γ, α′/β′, and α/βsp KCs, but only in few α/βc KCs.

Overall, our findings and those of others show that, depending on the method used, many KCs seem to express ChAT and VAChT; different methods, however, come to different conclusions on the expression levels of these two proteins in different KC subtypes. For example, Cha7.4kb-GAL4 does not appear to drive expression in any α′/β′ KCs (Figure 3.18), but Cha3.3kb-GAL80 reliably removes

Table 3.4: ChAT/VAChT expression summary. '0' indicates no elevated expression; '–' indicates no data available; '+/ + +/ + ++' indicates relative expression levels.

Method	gamma	a/b prime	a/b	Source
Anti-ChAT	+	+	+/0	this work; Yasuyama et al., 1995
Cha7.4-GAL4	+	0	+	this work; Salvaterra and Kitamoto, 2001
Cha3.3-GAL80	++	++	+++(s)/+(c)	this work; Yi et al., 2013
Cha3.3-LexA	+	+	++	this work; Diegelmann et al., 2008
ChAT mRNA	++	++	+	Perrat et al., 2013
ChAT mRNA	0	-	++	Crocker et al., 2016
Anti-VAChT	++	+	+	this work; Kitamoto et al., 1998
VAChT mRNA	++	+	+	Perrat et al., 2013
VAChT mRNA	+++	-	++	Crocker et al., 2016

α'/β' KCs from GAL4 expression patterns almost completely (see Mehren and Griffith, 2006 and Figure A.9C).

These differences are likely the result of technical limitations inherent to each of these methods, some of which are discussed in 1.5. Overall, however, this shows converging evidence for the expression of ChAT and VAChT in KCs.

3.6.4 ACh receptors in MBONs

Perhaps more tellingly, we found that all types of MBONs, innervating all three major MB lobes, show ACh-evoked calcium responses when injected into their dendrites (see Figure 3.10).

What mediates the ACh-evoked calcium influx in MBONs?

Calcium indicators such as GCaMP can measure relative changes in intracellular [Ca^{2+}], but the source of these calcium changes can be manifold (see Grienberger and Konnerth, 2012 for review). While most activity-dependent calcium increases are likely due to Ca^{2+} influx through VGCCs, nAChRs are also known to conduct Ca^{2+} besides Na^{+}. If MBONs express nAChRs, as my data suggests, these could also possibly be responsible for the GCaMP signals we detect (see also Gu and O'Dowd, 2006). This idea is supported by the fact that, at concentrations of 100 µM ACh, I detected reliable calcium responses in the M4/6 dendrite that closely matched the spread of ACh solution (see Figures A.3 and 3.7), without detecting

axonal responses (data not shown). At ACh concentrations ≥1 mM, however, axonal responses were additionally and simultaneously observed with stimulation onset (data not shown). This could mean that at relatively low concentrations, only few nAChRs are recruited. For higher concentrations of ACh then, the AP threshold would be reached that would lead to the recruitment of VGCCs and the release of APs into the axon.

KCs are not activated by ACh

To test if ACh injections into the MB lobes would also impact KC activity and thus confound our conclusions of a direct action of ACh onto nAChRs in MBONs, I tested the effects of ACh and nicotine injections onto KC calcium activity. My findings clearly show that 1 mM ACh released into the γ5 compartment does not induce calcium responses in KCs (see Figure 3.9). This would suggest that KCs do not have ACh receptors in these lobes. Recent EM data, however, suggests that recurrent KC → KC synapses are widespread in MB lobes and the peduncle in the larval MB and the adult α lobe (Eichler et al., 2017; Takemura et al., 2017). In the larval MB, 60 % of synapses onto KCs were found to come from other KCs (Eichler et al., 2017), and in the adult α lobe most α/βs KC outputs are onto other α/βs KCs (Takemura et al., 2017). The most commonly found KC–KC motif in the adult α lobe are KC ↔ KC ↔ MBON synapses, which are speculated to enable synergistic KC activation of downstream MBONs (Takemura et al., 2017). At this point, however, it is unclear if these are functional synapses, and how CS specificity could be maintained despite such pooling (Takemura et al., 2017).

Indeed, our data shows that ACh or nicotine do not evoke detectable calcium responses in these (Figure 3.9). These experiments, however, were performed on the γ5 lobe, and may not necessarily hold true for other compartments. Another possibility would be that these KC → KC synapses might not serve synergistic functions (as suggested by Takemura et al., 2017) through nAChRs (which would most likely be detected through ACh injections), but instead might use muscarinic ACh receptors (mAChRs; see also 3.6.4). Indeed, mAChRs are often expressed

on presynapses where they are involved in the regulation of ACh release (Hue et al., 1989; Polak, 1971). Thus, instead of a tight temporal synergism, KC → KC synapses could plausibly provide negative feedback to nearby KCs through mAChRs (see Hue et al., 1989; Polak, 1971) that would allow them to regulate ACh release in concordance with the activity of neighbouring KCs. A further possibility would be the release of KC neuropeptides such as sNPF (see chapter 4).

Do different MBONs have different nAChRs?

In this work, I have shown that nAChR subunits Dα1, Dα4, Dα5, Dα6 all might be involved in mediating MBON responses to KC-released ACh, because RNAi against these showed both a decrease in odour-evoked calcium responses (Figure 3.25) as well as a phenocopy of the naïve avoidance behaviour seen with shi^{ts1} block (Barnstedt et al., 2016; cp. Owald et al., 2015b). We chose those four subunits and Dα3 because driver lines from their respective promoter regions would drive expression in MBONs (see Table 3.3), or because a role in MB-related behaviours had previously been uncovered (as is the case for Dα4 which was shown to regulate sleep; Shi et al., 2014).

For odour-evoked calcium responses we observed modest defects that did not hold over all odours tested. It is likely that some proteins are more prone to RNAi effects, while others, that have a longer half-life are more resistant to RNAi. The latter may be the case for receptors (corroborated by personal communication with Vincent Croset). Furthermore, it is possible that compensation mechanisms of nAChR subunit composition might lessen RNAi effects.

Unfortunately, at this point, relatively little is known about nAChR subunit compositions in *Drosophila melanogaster* (see also 3.1.6), and only up to three of the five subunits for a heteropentameric nAChR have been identified to form functioning receptors (see Chamaon et al., 2002; Lansdell et al., 2012). Given our findings with RNAi in M4/6 MBONs, we can speculate that at least two different nAChRs may be present in these neurons. Dα1 is known to form a functional receptor with Dα2 and Dβ2 that is α-BTX-sensitive (Chamaon et al., 2002; Schulz et al., 2002) – two more subunits would currently remain unknown, but could

include Dα4 and Dβ3 (Thany et al., 2007). Furthermore, Dα5, Dα6, and Dα7 can form a high-affinity ACh receptor (Lansdell et al., 2012), and Dα7 expression may also occur in M4/6 neurons (see Figure 3.22). Such a receptor would also require at least one more Dβ subunit to function (see Thany et al., 2007).

Could these different receptor types be expressed in different types of MBONs? It seems likely that different MBONs would make use of different subunit compositions to allow them to respond differently to KC input, given that different compartments have different plasticity rules (see Hige et al., 2015a), and that different KC subtypes play different roles in memory processing (see Keene and Waddell, 2007). In the case of M4/6 neurons, it is plausible that each of these three neurons has a different nAChR subunit composition, although it is likely that M4β′ expresses at least two different nAChRs, because the observed defects in odour responses all stem from imaging in the same compartment, and because with our current limited knowledge on nAChR subunits, it seems unlikely that Dα1, Dα4, Dα5, and Dα6 would together form one receptor.

One way to test subunit compositions further would be to compare MBON response dynamics to stimulation. Unfortunately, my experiments with ACh injections into different MBONs (see Figure 3.10) reveal much trial-to-trial variance, which makes interpretations of different response dynamics between MBONs difficult. Alternatively, MBON responses to odours can be compared as was done recently (Hige et al., 2015b). Their results suggest some variability in odour-evoked calcium responses depending on the odour used and the specific MBON, from strong immediate activation to even inhibition (see Hige et al., 2015b, Extended Data Figure 2). One can speculate that these differences may at least in part be explained by different nAChR subunits. Another way to test subunit compositions further would be the use of specific nAChR antagonists (see 3.6.4).

Mecamylamine block

Mecamylamine mostly acts as a non-selective and non-competitive nAChR antagonist (Bennett et al., 1957). It is non-selective because it acts on most nAChRs

indiscriminately, and it is non-competitive as it does not seem to compete with ACh (Bennett et al., 1957; Varanda et al., 1985).

In previous *Drosophila* explant brain preparations, different concentrations have been used, ranging from 50 µM to 200 µM (Gaudry et al., 2013; Gruntman and Turner, 2013; Hige et al., 2015b; Huang et al., 2010; Liu and Wilson, 2013). I have first used 250 µM (Figures 3.23A, 3.27 and 3.28C-D) to rule out the possibility of false negatives, and then confirmed these results by the use of a more modest concentration of 100 µM (Figures 3.23B and 3.28A-B). Interestingly, 5 min after adding 100 µM mecamylamine to the bath, some calcium responses were still visible with repeated optogenetic KC stimulation (see Figure 3.28A-B), but no more ACh-evoked calcium responses were visible within 100 s of bath addition (see Figure 3.23B). This could have at least two reasons. First, the ITI was 6 s in the former condition, but 20 s in the latter, suggesting a sensitisation of pre- or postsynaptic sites through as yet unknown means (given that mecamylamine is non-competitive, and ACh quickly hydrolysed through AChE). Secondly, ACh injections required a disruption of the perineural sheath, which should make it easier for mecamylamine to penetrate (also, personal communication with P. Jacob), and thus increase the effective concentration at the synapse compared to the optogenetic stimulation in which the perineural sheath was still intact.

Our results of a 100 µM mecamylamine block first seemed to contradict another study that found KC → MBON connectivity with the same concentration of this nAChR antagonist (Hige et al., 2015b). Two recent studies, however, corroborate our findings and suggest that Hige et al.'s findings may be due to residual cholinergic activity (see also 3.6.2). First, KC → DAN connectivity was found to be mecamylamine-sensitive, with a partial block at 100 µM, but stronger blockade with 250 / 500 µM (Cervantes-Sandoval et al., 2017). Secondly, electrophysiological recordings between α/β KCs and MBON-α1 show a clear reduction to baseline with 250 µM mecamylamine (Takemura et al., 2017). It is not quite clear yet why such a relatively high concentration of mecamylamine is required to block this synapse.

High concentrations ($\geq$ 100 µM) of mecamylamine are known to also block NMDARs at the MK-801 site (Fu et al., 2008; O'Dell and Christensen, 1988; Papke et al., 2001; Snell and Johnson, 1989), but our additional results with hexamethonium and MLA (see Figure 3.24) suggest that calcium responses in MBONs are specifically due to nAChR activation.

α-BTX and other specific nAChR antagonists

Mecamylamine, hexamethonium and MLA have the advantage that they are broad nAChR antagonists that minimise the likelihood of false negatives. To investigate characteristics of nAChRs more closely, though, more specific antagonists can be used.

One of the most widely used specific nAChR antagonists is α-bungarotoxin (α-BTX), which divides nAChRs into α-BTX-sensitive and α-BTX-insensitive receptors (see Thany et al., 2007), and has long been detected in the *Drosophila* CNS (Dudai and Amsterdam, 1977; Dudai, 1977a; Schmidt-Nielsen et al., 1977). ACh-evoked neural responses in PNs and KCs of cell cultures and explant brains were shown to be sensitive to α-BTX (Cayre et al., 1999; Gu and O'Dowd, 2006; Huang et al., 2010; Su and O'Dowd, 2003). One problem with the use of α-BTX, however, is its long delay time (∼20 min) until action (see Cayre et al., 1999; Huang et al., 2010; personal observations). This precluded its effective use in the current study as the brain's viability with ACh injections was often compromised at that point in time.

Nonetheless, we could use the fluorescently conjugated α-BTX-TMR to label α-BTX-sensitive nAChRs in the fly brain (see Figure 3.21). These results show labelling in the calyx, as expected (see Cayre et al., 1999; Su and O'Dowd, 2003), but also some labelling of α′/β′ lobes, suggestive of α-BTX-sensitive α′/β′ MBONs. If α′/β′ MBONs thus possess α-BTX-sensitive nAChRs, and other MBONs possess α-BTX-insensitive nAChRs, α-BTX would be predicted to have differential effects on different kinds of learning. Indeed, a similar observation has recently been made in honey bees, where α-BTX was found to selectively impair LTM but not MTM or retrieval processes (Dacher et al., 2005).

Another more specific nAChR antagonist is the insecticide spinosad (Hertlein et al., 2011). Interestingly, spinosad sensitivity seems to be specifically conferred by the Dα6 subunit (Perry et al., 2007, 2015; Somers et al., 2015). Future studies could thus use spinosad application to test for the presence of Dα6 subunits in MBONs.

A role for muscarine?

ACh can also act on muscarinic GPCRs, but we found no effect on calcium transients in M4/6 neurons when I injected muscarine into M4/6 dendrites (see Figure 3.20). As mAChR activity may not be readily detectable through changes in calcium flux, we cannot rule out more subtle effects of mAChR activation in MBONs, if these receptors are present.

Interestingly, a recent study found a role for mAChRs in aversive olfactory learning in larvae (Silva et al., 2015). mAChR-GAL4 (VT021845-GAL4) expresses in larval MB (Silva et al., 2015) and adult α/β KCs (see Figure A.14), and KC-driven mAChR-RNAi impaired aversive olfactory memory (Silva et al., 2015). Also, mAChR-A RNA is strongly expressed in γ and α/β KCs (Crocker et al., 2016). Together with recent findings of KC ↔ KC synapses in the α lobe (Takemura et al., 2017) but no apparent ACh-evoked calcium signals in KCs (see Figure 3.9), this could mean that at least α/β KCs express axonal mAChRs that may help regulate ACh release (see also 3.6.4).

Furthermore, mAChR-B expression was found to be upregulated in MBON-α3 after LTM induction (Crocker et al., 2016), raising the possibility that KC-released ACh may also act on mAChR-B in some MBONs.

Dα7::GFP punctae

We observed dense punctate expression of Dα7::GFP when driven in M4/6 neurons (Figure 3.22). This pattern is similar to the postsynaptic sites previously observed in LPTC dendrites (Leiss et al., 2009), but in contrast to KC postsynaptic claw-like patterns in the calyx (Christiansen et al., 2011; Kremer et al., 2010; Spühler et al., 2016). We estimated the number of punctae to be around 4,000 per hemisphere, which would amount to around 2 postsynaptic sites per KC (see Figure A.12). This

number is in stark contrast to recent EM data from the α lobe, which suggests a synapse density of $\sim 10-14$ KC $\rightarrow$ MBON synapses per KC (Takemura et al., 2017). Given the clear advantage in resolution of dense EM reconstruction over light microscopy, it is well possible that Dα7::GFP was not expressed in every single MBON postsynapse, and that our limited resolution and the process of blind deconvolution followed by automatic object analysis greatly underestimated the number of postsynaptic sites.

3.6.5 Implications and outlook

Why acetylcholine?

Our finding that ACh ist the main KC neurotransmitter is surprising because ACh has long been known to be the main fast excitatory neurotransmitter in the invertebrate brain (Breer, 1987), and the MB has been studied for many decades (Dujardin, 1850; Heisenberg et al., 1985; Kenyon, 1896b). The main reasons for this are probably the weak α-ChAT staining (discussed in 3.6.3), the fact that memory-related plasticity changes occur even without KC transmitter release (Dubnau et al., 2001; McGuire et al., 2001), and the fact that MBONs have remained poorly characterised until recently (Aso et al., 2014a,b; Tanaka et al., 2008).

Nonetheless, ACh as a neurotransmitter for KCs fits into what we know about the structure of sensory systems in the *Drosophila* brain, what we know about MBON responses, and what we know about the MB circuitry.

ACh elicits fast sodium and calcium influx at the postsynapse through ionotropic nAChRs, and is rapidly hydrolysed at the synaptic cleft by AChE, ensuring strong but temporally precise signalling (Dale et al., 2008).

KCs are third-order olfactory neurons. Fast transmission at the two preceding synapses from ORNs to the AL, and AL PNs to KCs is mediated by ACh. Similarly, feedforward projections in the visual system are largely cholinergic (Kolodziejczyk et al., 2008; Raghu et al., 2013). Indeed, "most if not all chemosensory, olfactory, chordotonal and auditory primary sensory neurons may be cholinergic" (Salvaterra and Kitamoto, 2001).

MBONs have previously been shown to produce rapid-onset calcium responses to odour stimulation (Hige et al., 2015b; Owald et al., 2015b; Pai et al., 2013; Plaçais et al., 2013b; Séjourné et al., 2011), suggesting fast excitatory neurotransmission from preceding olfactory neurons, the KCs.

MBONs need to rapidly and faithfully signal the specific valence of a stimulus, and whether to approach, avoid, or ignore it. Especially in the case of aversive stimuli, rapid evaluation of stimulus valence should prove evolutionarily beneficial. ACh would be an ideal neurotransmitter for a fast and reliable readout of previously acquired memories, rapidly evaluating approach- or avoidance-inducing stimuli.

Presynaptic plasticity at a cholinergic synapse in other species

The *Drosophila* MB would not be the only fan-out fan-in neural architecture with a cholinergic fan-in arm. Both octopus as well as cuttlefish possess a structure called the vertical lobe (VL) that also plays a role in learning and memory, similar to the invertebrate MB (Boycott, 1960; Gray, 1970; Shomrat et al., 2008; Young, 1971). Here, relatively few superior frontal lobe (SFL) neurons (about 1.8 million in the octopus) fan out onto a large number of amacrine interneurons (AM; about 25 million) via en-passant glutamatergic synapses, similar to the 150 PNs diverging onto 2,000 KCs in the *Drosophila* MB (see 1.2.1). AM neurons then strongly converge onto relatively few large efferent neurons (LNs; about 65,000) that drive behaviour. This fan-in arm of the VL strongly resembles the convergence of about 2,000 KCs onto only 33 MBONs (see 1.4). Interestingly, this fan-in synapse was recently found to be cholinergic in both cuttlefish and octopus (Shomrat et al., 2011), similar to our findings in *Drosophila melanogaster*. Importantly, this cholinergic synapse has also been shown to undergo presynaptic LTP, at least in cuttlefish, demonstrating presynaptic plasticity at a cholinergic synapse (Shomrat et al., 2011).

Mechanisms of cholinergic presynaptic plasticity

In the mammalian CNS, glutamate is the predominant fast-acting excitatory neurotransmitter, and most studies of synaptic plasticity have focused on glutamatergic NMDA receptors at which LTP was first discovered (Bliss and Lømo,

1973). NMDARs can serve as coincidence detectors as they require an initial depolarisation to remove a Mg^{2+} block, before they can be activated through ligand binding of glutamate. If this mechanism mediates postsynaptic LTP, what about presynaptic depression that is thought to be responsible for learning in *Drosophila* (Cohn et al., 2015; Hige et al., 2015a; Owald et al., 2015a)? The only other system known so far to use presynaptic plasticity at a cholinergic synapse is the cuttlefish (Shomrat et al., 2011), and the mechanisms for the observed LTP there still remain a mystery. Hence, currently we can only speculate about the mechanisms that would generate presynaptic plasticity at a cholinergic synapse.

In the hippocampus, presynaptic long-term synaptic depression (LTD) can be mediated by endocannabinoids (eCB). Here, postsynaptic release of eCBs and binding to a cannabinoid receptor that results in inhibition of VGCCs in the short term, or inhibition of PKA in the long term. There could also be modulation of Rab3-interacting-molecule-α (RIM1α), and an involvement of metabotropic glutamate receptor 1 (reviewed in Lafourcade, 2009). RIM1α is an active zone scaffolding protein that primes docked synaptic vesicles for release (Han et al., 2011).

In *Drosophila melanogaster*, coincident detection is thought to rely on the KC-expressed adenylyl cyclase *rutabaga* (*rut*), which is activated by simultaneous Ca^{2+} stimulation (as from KC activity) and G protein signalling (as from DANs acting on GPCRs). *rut*, in turn triggers a cAMP signalling cascade that activates a *dunce*-encoded phosphodiesterase and PKA that can phosphorylate several targets (see also 1.3.2). Importantly, no synaptic release from KCs seems necessary to form a memory in *Drosophila* (Dubnau et al., 2001; McGuire et al., 2001), making an involvement of muscarinic autoreceptors unlikely, at least for some forms of learning.

cAMP-activated phosphorylation has previously been suggested to be involved in the modulation of ACh release (Sattelle and Breert, 1990, Figure 15). This modulation could possibly be enacted by phosphorylation-dependent decreases of RIM1α-like proteins that would down-regulate synaptic vesicle fusion at the presynaptic membrane (see also Stigloher et al., 2011 for RIM at a cholinergic synapse). Such a mechanism for plasticity would be relatively independent of

transmitter stored in these synaptic vesicles. Given that CHT is the rate-limiting step in ACh synthesis, it is also possible that presynaptic depression at KCs is mediated by a down-regulation of CHT activity (see Sitte and Freissmuth, 2006, pp. 525).

How could this be investigated? A recent RNA-seq study failed to find significant transcriptional differences in KCs after induction of LTM, but found significant transcriptional regulation in MBONs and DAL neurons (Crocker et al., 2016). These findings hint at potential postsynaptic mechanisms involved in LTM formation, but do not rule out changes in presynaptic transcription as plasticity likely would have only occurred in odour-activated KCs, potentially defying the sensitivity of this method that pooled all KCs. As a workaround to this inherent problem, learning could be artificially induced by genetically labelling and activating a subset of KCs (see Vasmer et al., 2014), FACS-sorting these KCs after memory induction (see Perrat et al., 2013), and sequencing only this learning-relevant subset of KCs.

Another way to study presynaptic mechanisms would be to analyse quantal size after learning induction. A reduced quantal size might point to the regulation of CHT or ChAT, whereas a reduced occurrence of spontaneous EPSPs would point towards a regulation of VAChT (see Cash et al., 2016; Song et al., 1997), and a decreased release probability and speed of release would point towards regulation of synaptic vesicle fusion proteins (see Han et al., 2011). These experiments would be similar to what has already been done recently by Hige et al. (2015a).

Comparison with vertebrate neural circuits

Two vertebrate brain structures are often compared to the invertebrate MB: the cerebellum for its similar fan-out fan-in neural architecture, and the hippocampus for its role as the major brain region mediating associative learning.

The cerebellar neural architecture bears semblance with the MB's fan-out fan-in structure. Here, Golgi cells diverge onto KC-like granule cells through mossy fibres. Through the parallel fibre tract, granule cells then converge onto Purkinje cells, similar to KC–MBON convergence (Llinás et al., 2004).

Granule cells show striking similarities with KCs, as they both belong to the smallest cells in their respective brains, are extremely numerous (an estimated 50 billion in the human brain), and show sparse activity. They also extend dendritic claws, but use glutamate as neurotransmitter (Llinás et al., 2004).

The cerebellum is widely considered to play an important role in motor learning, for which predictive input from granule cell parallel fibres is compared with climbing fibre input by Purkinje cells. Presynaptic LTP at granule cell–Purkinje cell synapses was found to also depend on Ca^{2+}-dependent cAMP signalling (Glatt and Snyder, 1993; Linden and Ahn, 1999; Salin et al., 1996; Storm et al., 1998), similar to what has been observed for presynaptic plasticity at the KC–MBON synapse (see Keene and Waddell, 2007).

Finding that the KC transmitter is ACh suggests that cAMP-dependent mechanisms can modulate synaptic connections, regardless of transmitter identity.

The hippocampus receives cholinergic inputs from the medial septum and diagonal band of Broca (MSDB). These cholinergic inputs have been found to play an important role in the generation of gamma rhythms, for synaptic plasticity, and for conveying the aversive US (Fisahn et al., 1998; Gu and Yakel, 2011; Lovett-Barron et al., 2014). So far, no plasticity at these cholinergic terminals is known, but finding presynaptic cholinergic plasticity at a memory-relevant synapse in the invertebrate brain could suggest that such plasticity might also exist in the vertebrate brain.

4

Kenyon cell co-transmitters

Contents

4.1 Background 173
4.1.1 Neuropeptides in *Drosophila* 174
4.1.2 sNPF in the *Drosophila* brain 175
4.1.3 sNPFR1 in the *Drosophila* brain 177
4.1.4 sNPF in the *Drosophila* MB 178
4.2 Results 179
4.2.1 sNPFR1 expression 179
4.2.2 Application of sNPF 180
4.2.3 sNPF- and sNPFR1-RNAi 183
4.2.4 Taurine 187
4.3 Discussion 189
4.3.1 Results summary 189
4.3.2 sNPF and sNPFR1 expression 190
4.3.3 sNPF effects on MBONs 192
4.3.4 sNPF effects on DANs 194
4.3.5 Further sNPF targets? 195
4.3.6 Potential molecular mechanisms 197
4.3.7 State-dependent regulation of sNPF modulation 198

4.1 Background

Besides small-molecule neurotransmitters that can act in a rapid and spatially restricted way, many organisms use neuropeptides to modulate neural signalling.

Neuropeptides are often stored in dense-core vesicles (DCVs) from which fusion with the presynaptic membrane leads to peptide release into the synaptic cleft, often co-released with small-molecule transmitters (Kandel et al., 2013; Nusbaum et al., 2017). Neuropeptides are generally placed into neuropeptide 'families' that share an amino acid sequence, but individual members may differ by as little as one amino acid (Nusbaum et al., 2017).

4.1.1 Neuropeptides in *Drosophila*

In *Drosophila melanogaster*, there are at least 35 neuropeptide precursor genes, some of which can encode multiple neuropeptides (Nässel and Homberg, 2006), and up to 70 more may still be unidentified (Liu, 2005; reviewed in Nässel, 2002; Nusbaum et al., 2017; Taghert and Nitabach, 2012; Taghert and Veenstra, 2003). Common methods of identification include mass spectrometry, immunocytochemistry with antibodies, and *in situ* hybridisation (see Homberg, 2002; Nässel, 2002; Nässel and Homberg, 2006; Winther et al., 2003).

Generally, neuropeptides are thought to act as neuromodulators or co-transmitters on GPCRs (Homberg, 2002; Nässel, 2002; Nusbaum et al., 2001), although there are some cases of ionotropic action (Dürrnagel et al., 2010; Grunder and Assmann, 2015; Lingueglia et al., 1995). About 45 peptide GPCRs have been detected in the *Drosophila* genome (Brody and Cravchik, 2000; Hauser et al., 2006; Hewes and Taghert, 2001; Taghert and Veenstra, 2003).

Neuropeptide co-transmission in *Drosophila* has been implicated in aspects of olfaction (Ignell et al., 2009; Root et al., 2011; Wang, 2012), stress-related responses (Kahsai et al., 2010b; Kapan et al., 2012), and circadian rhythms (Choi et al., 2012). Peptidergic co-transmission is thought to endow even numerically small neural systems with a larger repertoire of flexibility, thus enhancing their computational power (see Nusbaum et al., 2017). Indeed, a recent EM study found DCVs in all neurons innervating the MB, suggesting that all MB-associated neurons release at least one type of neuropeptide (Eichler et al., 2017).

4.1.2 sNPF in the *Drosophila* brain

The *Drosophila snpf* gene encodes two predicted neuropeptides with the C-termini RLRFamide (sNPF-1, 11aa, and -2, 19aa) and two with RLRWamide (sNPF-3 and -4, both 6aa) (Broeck, 2001; Hewes and Taghert, 2001; Lee et al., 2004). Mass spectrometry allowed the identification of some of these predicted peptides in *Drosophila* tissue (Baggerman et al., 2005; Garczynski et al., 2006; Predel et al., 2004; Wegener et al., 2006). In the following, I will refer to sNPF-1 as sNPF. sNPF is structurally related to the NPY homologue dNPF, but contains only 11 amino acids instead of dNPF's 36 (Lee et al., 2004).

Expression in brain

sNPF expression was found in the nervous system of larvae throughout development, as well as that of adults (Lee et al., 2004), but is markedly different from dNPF expression (Johard et al., 2008). An sNPF antibody suggested sNPF expression in the optic lobe medulla and the MB calyx (Lee et al., 2004). This MB staining was later confirmed to be present in KCs (Johard et al., 2008; see 4.1.4).

Besides sNPF staining in the MB and optic lobe, later studies also found sNPF immunoreactivity in the fan-shaped body (FB) of the central complex (CC) (Kahsai et al., 2010b), and in dorsal lateral peptidergic (DLP) neurons (Kahsai et al., 2010a; Kapan et al., 2012). Furthermore, immunoreactivity was found in ORNs (Carlsson et al., 2010; Nässel et al., 2008).

An sNPF-GAL4 driver line confirmed expression in the MB, the OL, FB, and showed expression in pars intercerebralis (PI) neurons (Johard et al., 2008).

Functions

Feeding and energy homeostasis. Due to its structural similarity with dNPF, a role in feeding was first hypothesised for sNPF, and indeed detected: flies with neural overexpression of sNPF consumed more food and gained in body size, while loss-of-function mutant flies had depressed food intake (Lee et al., 2004). This regulation

of body size and glucose levels seems to be mediated by sNPF receptor (sNPFR1)-mediated ERK signalling in insulin producing cells (Dilp2 neurons) (Lee et al., 2008).

On the other hand, sNPF may also act directly on sensory neurons to guide feeding, as was recently demonstrated by Root et al. (2011). Based on previously found sNPF expression in ORNs (Carlsson et al., 2010; Nässel et al., 2008), the authors could show that starvation elevates expression of the sNPF receptor (sNPFR1) in ORNs Or42b. sNPF release and sNPFR1 activation results in presynaptic facilitation that leads to starvation-induced food-search behaviour (Root et al., 2011).

Similarly, sNPFR1 knockdown in neurosecretory cells resulted in increased sensitivity to desiccation and starvation (Kahsai et al., 2010a), presumably because feeding was impaired. Intriguingly, however, knockdown of sNPF in Corazon-GAL4 neurons actually increased resistance to starvation, and sNPF overexpression in these neurons led to decreased starvation resistance (Kapan et al., 2012). These findings suggest that sNPF may take on different – maybe even converse – roles depending on where it is expressed, even though only one common receptor is currently known (see also Nusbaum et al., 2017).

Locomotion and sleep. sNPF also seems to be involved in the regulation of locomotion and sleep. FB-mediated knockdown of sNPF resulted in increased locomotion distance and speed (Kahsai et al., 2010b), although these results may also be explained by an increased food seeking behaviour (see also Shang et al., 2013).

Similarly, thermogenetic activation of sNPF-GAL4 neurons results in increased day sleep, while hyperpolarising these neurons results in decreased day sleep – an effect that is independent of MB expression, but may rely on the FB (Shang et al., 2013). Interestingly, activating sNPF-GAL4 neurons results in a rapid shift toward more sleep, while flies simultaneously showed an increased drive towards a food source, but this food seeking only developed over the course of several days (Shang et al., 2013). These findings suggest that sNPF regulates food seeking and sleep on different timescales.

Mechanisms

How can sNPF mediate this diversity of behavioural functions in the brain? Several mechanisms have been proposed that may be at work conjointly.

Starved flies show enhanced odour-induced calcium responses in the AL – an effect that depends on and can be mimicked by the action of sNPF (Root et al., 2011). The sNPFR1 was found to be upregulated in starved flies, and its overexpression in ORNs was shown to lead to similarly enhanced presynaptic odour responses (Root et al., 2011). This effect depends on the action of insulin, leading to a model where starvation leads to low insulin which releases transcription of sNPFR1 to facilitate PN odour responses (Ko et al., 2015; Root et al., 2011).

In contrast to these facilitatory findings, two other studies actually found hyperpolarising effects: Inducing sNPFR1 expression in third instar larval motor neurons and recording from them in current clamp shows a significant decrease in firing rate compared to vehicle, and a mild hyperpolarisation of the membrane potential could be detected after about one minute (Shang et al., 2013; Vecsey et al., 2014). This change in membrane potential seems to depend on Gαo signalling (Vecsey et al., 2014). cAMP signals were decreased in PDF neurons when sNPF was applied solely or when it was co-applied with DA, but cAMP signals were actually greatly enhanced when co-applied with OA (Shang et al., 2013; Vecsey et al., 2014).

These findings suggest that sNPF and the sNPFR1 may have facilitatory or depressing effects depending on the specific synapse and co-transmitters involved, and potentially pre- and postsynaptic expression.

4.1.3 sNPFR1 in the *Drosophila* brain

A single GPCR (CG7395) has been identified in *Drosophila melanogaster* that is activated by the four originally predicted sNPFs (Feng et al., 2003; Garczynski et al., 2006; Mertens et al., 2002). This receptor shows structural similarities to the mammalian NPYR2 as well as GPCRs for dNPF (De Bono and Bargmann, 1998; Feng et al., 2003; Garczynski et al., 2002; Hewes and Taghert, 2001; Mertens et al., 2002, 2004; Taghert and Veenstra, 2003).

The precise distribution of sNPFR1 in the adult *Drosophila* brain is currently unknown, but a recent study used an sNPFR1 promoter GAL4 (R64H09) (Jenett et al., 2012) and discovered large overlap of identified sNPF-positive structures in the FB with putative sNPFR1 expression (Kahsai et al., 2012). Another study found overlap of α-sNPFR1 immunoreactivity with Dilp2 neurons (Lee et al., 2008), later corroborated by sNPFR1-GAL4 expression in some Dilp2 neurons (Kapan et al., 2012). All three studies, however, only showed small brain regions around the FB and the pars intercerebralis (PI), respectively, leaving the rest of the expression pattern obscure. A recent RNA-seq study suggested that a wide range of MB extrinsic neurons expresses sNPFR1 (Crocker et al., 2016).

It is also unknown which G protein pathway sNPFR1 is coupled to, but in insulin producing cells sNPFR1 was shown to signal via the ERK pathway (Lee et al., 2008).

4.1.4 sNPF in the *Drosophila* MB

Expression in MB

While the first study on *Drosophila* sNPF already found expression in the MB calyx (Lee et al., 2004), it was only later that Kenyon cell bodies were shown to be immunopositive against α-sNPF (Johard et al., 2008). Specifically, *in situ* hybridisation labelled KCs, calyx, peduncle and lobes (Johard et al., 2008). Similarly, a specific antiserum against the *snpf* precursor protein was immunopositive in γ and α/β KCs of adults and larvae, while α′/β′ and α/βc KCs were immunonegative (Johard et al., 2008). Interestingly, certain compartments were observed to be more strongly immunopositive than others, suggesting compartment-specific sNPF release from KC presynapses (Johard et al., 2008). This expression pattern was further corroborated by the use of Trp stimulation and RNAi knockdown, both of which changed the sNPF immunoreactivity in these KCs (Knapek et al., 2013).

These findings were also supported by a recent RNA-seq study that identified very high levels of sNPF mRNA in γ and α/β KCs (Crocker et al., 2016). Furthermore, V2 MBONs were found to express sNPF (Crocker et al., 2016).

Functions

Besides its role in feeding and sleep, sNPF expressed in KCs seems required for 2h appetitive memory formation as KC-restricted knockdown of sNPF yielded memory performance deficits (Knapek et al., 2013). Similarly, sNPFR1 is required for 2h appetitive memory, albeit in yet unidentified neurons other than KCs (Knapek et al., 2013).

Mechanism

How sNPF release from KCs shapes MB learning and which MB neurons express sNPFR1 remains largely unknown at this point. A recent RNA-seq study, however, found that all MB extrinsic neurons studied expressed sNPFR1, and sNPFR1 was upregulated in V2 MBONs following LTM formation (Crocker et al., 2016). Interestingly, sNPF was strongly upregulated in MBON-α3, and mildly upregulated in M4β, but not in KCs, after LTM formation (Crocker et al., 2016). These findings suggest that KCs may co-release sNPF as a slow neuropeptide transmitter together with its fast-acting transmitter ACh (Barnstedt et al., 2016). Such a co-release of fast and slow transmitters was recently discovered in PDF neurons (Frenkel et al., 2017).

As it is thus unclear how KC-released sNPF acts on other MB neurons and where sNPFR1 is expressed, I have performed experiments to tackle these questions, which I will present in the following.

4.2 Results

4.2.1 sNPFR1 expression

sNPF action requires the binding to its only known receptor, sNPFR1 (Mertens et al., 2002). Yet, very little is currently known about the expression of sNPFR1 in the adult brain. To investigate this, I used a GAL4 driver line with an enhancer fragment from the sNPFR1 locus, R64H09-GAL4 (Jenett et al., 2012; see also Kahsai et al., 2012; Kapan et al., 2012), as well as an antibody raised against sNPFR1 (Lee et al., 2008).

sNPFR1-GAL4 expression was revealed by driving UAS-GFP, and co-staining with the general neuropil marker nc82 (see Figure 4.1A-E). GAL4 expression was seen in hundreds of neurons throughout the brain, but particularly in OL neurons, PI neurons, and potential AL interneurons (Figure 4.1A).

GAL4 expression was also seen to a lesser degree in the MB, where individual compartments showed different levels of expression, suggestive of MB extrinsic neurons (Figure 4.1B-E). Quantification of these expression differences suggest relatively strong expression in the α2, the β1, α′1, and γ4 regions, while other regions such as β2, β′2m, and α3 showed relatively low expression (Figure 4.1E). A few α/βc KCs were also weakly expressed (see Figure 4.1D).

An sNPFR1 antibody was generated against the synthetic peptide ASDEDRSG-GIIHN (Lee et al., 2008). Previously, this antibody was shown to label DILP neurons in the PI of *Drosophila* larvae (Lee et al., 2008). When I applied this antibody to adult brains, however, no DILP neurons were labelled (see Figure 4.1F). Some cell bodies seem labelled, but upon closer inspection of the inside of the brain, no neural tracts were visibly stained. Importantly, no staining of the MB was visible (Figure 4.1G-I). To our surprise, however, some immunoreactivity was found in structures surrounding the MB peduncle (see Figure 4.1J). These neurons seem similar to previously described MIP^{+} neurons (Kahsai and Winther, 2011; Kolodziejczyk and Nässel, 2011; Oh et al., 2014) that are known to regulate sleep and circadian rhythms (Kolodziejczyk and Nässel, 2011; Oh et al., 2014), as well as LTM consolidation (L. Scheunemann, personal communication).

4.2.2 Application of sNPF

As I have previously shown, sNPF application alone does not elicit detectable calcium responses in M4/6 neurons (see Figure 3.4). However, sNPF is expressed in KCs and required for memory formation (Johard et al., 2008; Knapek et al., 2013), and was shown to either facilitate odour-evoked responses (Root et al., 2011), or to hyperpolarise neurons and decrease cAMP levels (Shang et al., 2013; Vecsey et al., 2014). This suggests that sNPF has a modulatory effect on its

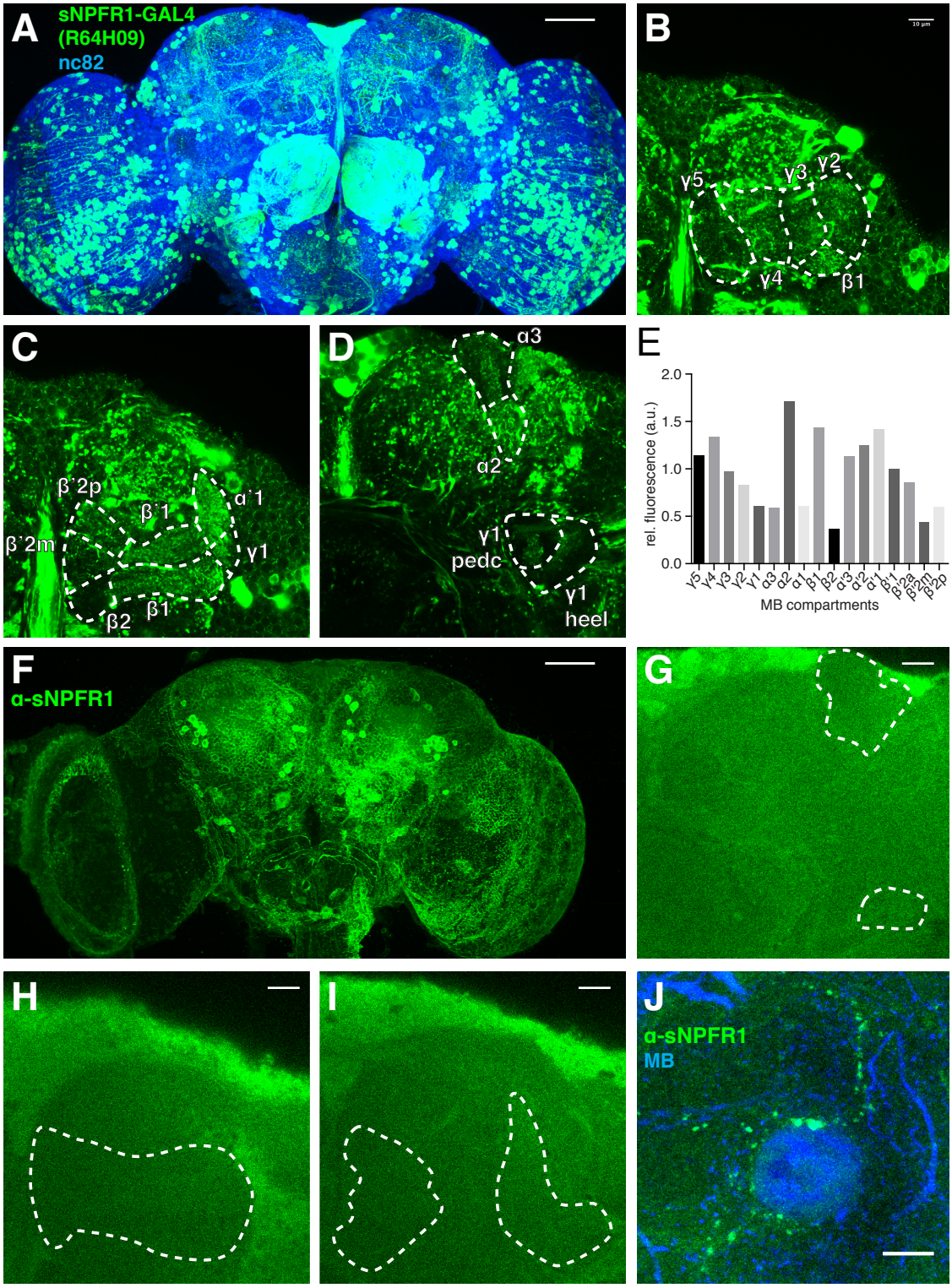


Figure 4.1: sNPFR1 is probably expressed in many neurons, including MB extrinsic neurons. Expression of R64H09-GAL4 with an enhancer fragment from the sNPFR1 locus (A-E) and of an α-sNPFR1 antibody (F-J) are illustrated. A) sNPFR1-GAL4 expresses in a wide range of neurons, particularly in the OL, AL, and PI regions. B-D) GAL4 expression is visible in many MB compartments, but not homogenously between compartments. E) Relative fluorescence (normalised to α-nc82) differs between compartments, with particularly high fluorescence in α2, β1, and γ4. F) α-sNPFR1 antibody stains seems to stain some cell bodies and neurites in the brain. G-I) The MB neuropil seems to show only background staining. J) Immunopositive labelling was found in neurites around the MB peduncle. MB was labelled by 247-LexA ; lexAop-rCD2::mRFP. Scale bars in A and F represent 50 µm, and those in B-D and G-J represent 10 µm.

sNPFR1-expressing target neurons. As the main KC downstream neurons are MBONs to which they are connected via cholinergic synapses (Barnstedt et al., 2016), we sought to address the question of how sNPF modulates MBON responses by co-application of sNPF along with ACh. For this, I first injected ACh while bath-applying sNPF in one set of experiments, and also co-injected ACh along with sNPF in another set of experiments.

sNPF bath application and ACh-evoked calcium responses

As sNPF modulation likely acts on a slower timescale than fast-acting neurotransmitters (see Shang et al., 2013; Vecsey et al., 2014), we reasoned that sNPF bath application while monitoring ACh-evoked calcium responses in MBONs might reveal potential modulatory effects of sNPF. I have previously successfully recorded ACh-evoked calcium responses from M6 neurons innervating the γ5 compartment, and sNPF is probably expressed in γ and α/β KCs (Johard et al., 2008; Knapek et al., 2013).

To test for sNPF modulatory effects, I thus applied 100 µM ACh at 10 second intervals to the γ5 region of M4/6 dendrites while monitoring calcium transients with GCaMP6f, and then applied either 20 µM sNPF or vehicle (see Figure 4.2A). ACh injections resulted in robust and reliable calcium responses that could be evoked for several minutes (see Figure 4.2B). Interestingly, bath application of sNPF seemed to slightly increase calcium responses in the first minute of application, but this trend was not significant (see Figure 4.2C-D).

sNPF co-application with ACh facilitates calcium responses

As neuropeptides are relatively large molecules and may take longer to diffuse into tissue, we sought to directly inject sNPF into the MBON dendrites, together with ACh. While the timescales of action for these two transmitters might be different, co-injection has the advantage that the location of injection is exactly the same, and only a single microinjection pipette is necessary.

Co-injecting 100 µM ACh together with 100 µM sNPF or vehicle resulted in strong and reliable calcium responses in M4/6 dendrites (Figure 4.3). These

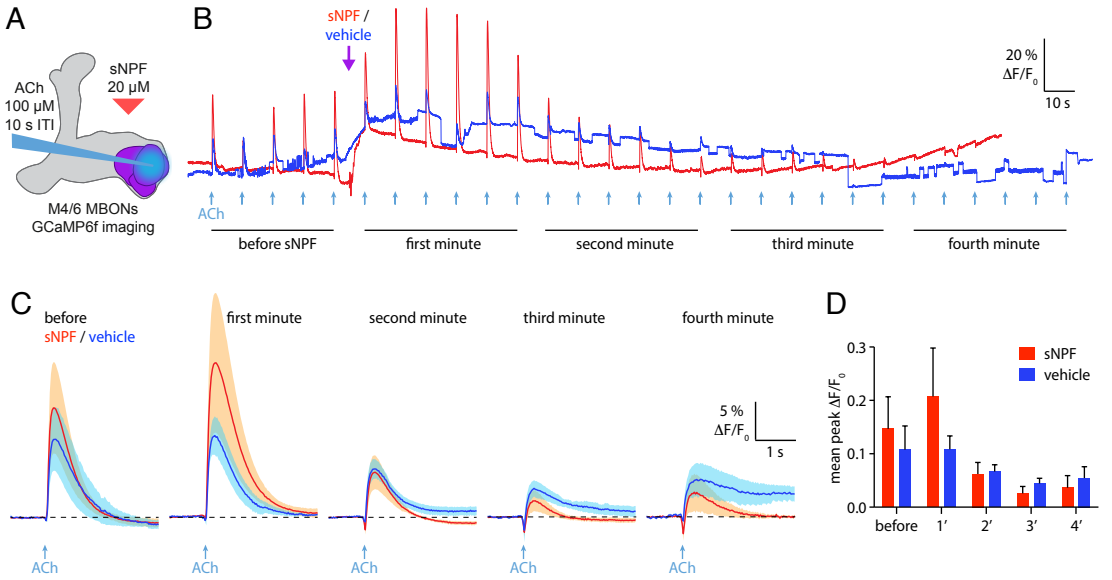


Figure 4.2: Bath application of sNPF does not alter ACh-evoked M4/6 calcium responses. A) 100 µM ACh were injected into the γ5 dendritic compartment of R21D02-GAL4 ; GCaMP6f flies to evoke calcium responses in M4/6 neurons every 10 s. After the first minute, 20 µM sNPF or vehicle were applied, and changes in ACh-evoked calcium responses monitored. B) Sample calcium transients from one brain in which sNPF was bath-applied (red), and one brain in which vehicle was bath-applied (blue). C) Average ACh-evoked calcium responses before the addition of sNPF (red) or vehicle (blue) and in the first four minutes thereafter. For each minute, the mean response from all six ACh-evoked responses was taken for each brain, and compared. D) Mean peak responses for every minute are not significantly different between brains to which sNPF and those to which vehicle was applied (multiple t-tests with Holm-Sidak method, $p > 0.05$, $N = 4 - 5$), although a trend for elevated responses in the first minute of sNPF application is visible. Shade in C and error bars in D represent SEM.

calcium responses were significantly larger when sNPF was co-injected compared to vehicle co-injection (Figure 4.3E). Besides enhanced calcium peaks, sNPF co-injections also significantly decreased rise–decay and decay times (Figure 4.3E), suggesting that sNPF 'sharpens' calcium responses, so that ACh-evoked responses are both larger and narrower.

4.2.3 sNPF- and sNPFR1-RNAi

Directly injecting sNPF at high concentrations is a fairly artificial experimental setting, and may not capture sNPF modulation dynamics as they would normally occur. A more subtle way of probing sNPF response dynamics is the introduction of RNAi to reduce sNPF translation in KCs.

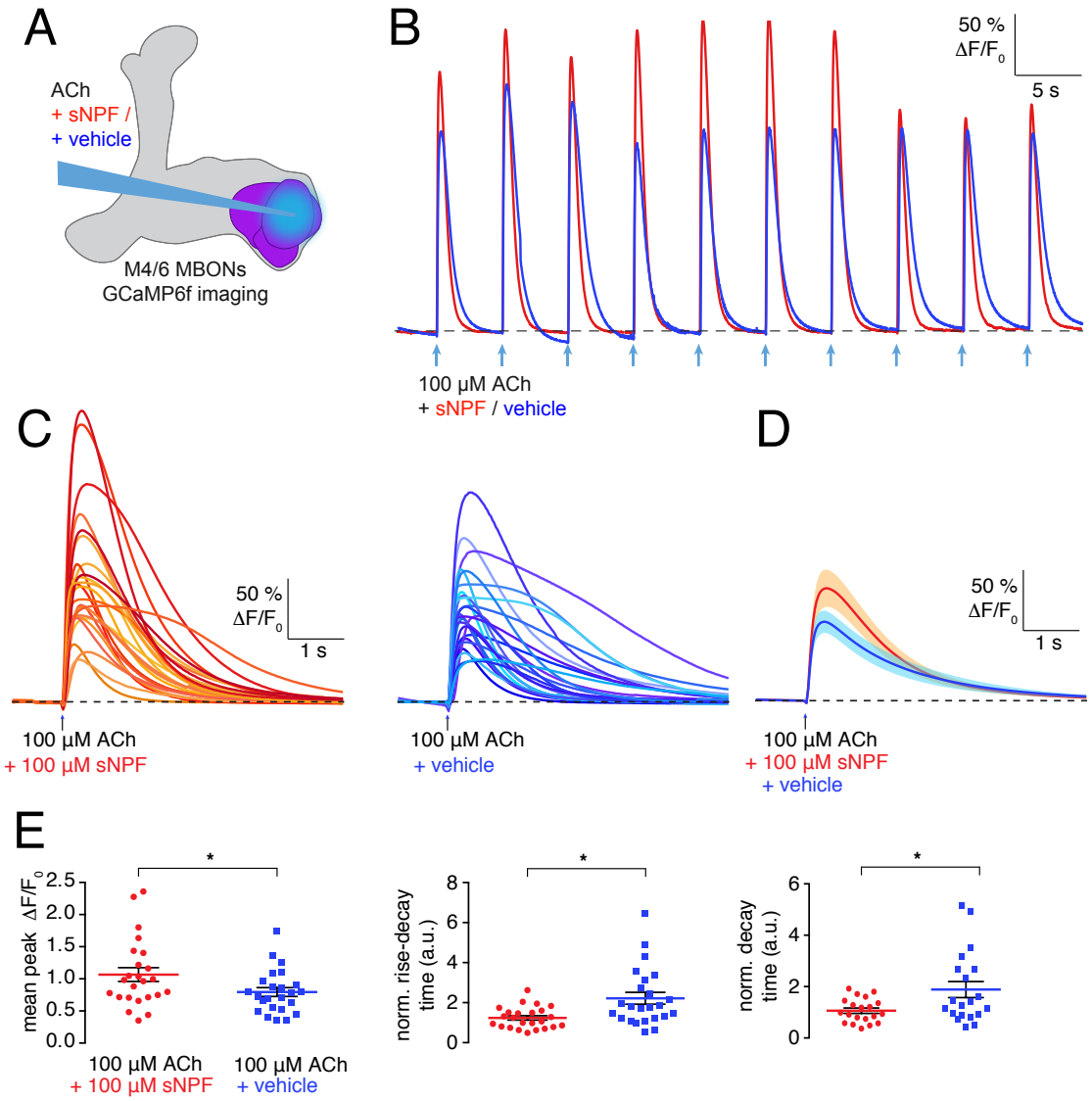


Figure 4.3: sNPF co-application with ACh facilitates calcium responses in M4/6 neurons. A) 100 µM ACh along with either 100 µM sNPF or vehicle was pressure-injected into the γ5 region of M4/6 dendrites in R21D02-GAL4 ; GCaMP6f explant brains, and calcium transients monitored using widefield microscopy. B) Sample calcium transients from two brains into which 100 µM ACh with either 100 µM sNPF (red) or vehicle (blue) were injected at 5 s intervals. C) Mean calcium traces of ten trials from 24 brains per condition. D) Overlaid mean traces from C, ACh plus sNPF (red) and ACh plus vehicle (blue). Shade represents SEM. E) Mean peak calcium responses, normalised rise–decay time, and normalised decay time are significantly higher when ACh is coapplied with 100 µM sNPF than with vehicle (unpaired t-test with Welch's correction, $p < 0.05$, $N = 24$). Rise time was defined as the time from application to 50 % of peak response time, and decay time as the time from peak response to 50 % decay. Rise–decay time and decay time were normalised for each brain by its respective peak response to account for magnitude-dependent response kinetics. Error bars represent SEM. Partly adapted from Barnstedt et al. (2016).

Optogenetic KC activation with sNPF-RNAi

To precisely control KC activity, I used a γ KC GAL4 driver to drive expression of the red light-activated channelrhodopsin CsChrimson as well as sNPF-RNAi. MBON activity was read out by expressing GCaMP6f in different γ MBONs.

200 ms of red light reliably produced strong calcium responses in MBON-γ2α′1, MBON-γ3, and M6 neurons (Figure 4.4). Interestingly, these calcium responses were significantly larger in MBON-γ2α′1 when sNPF-RNAi was co-expressed compared to control (Figure 4.4A). Calcium responses in MBON-γ3 and MBON-γ4>γ1γ2 were not affected by co-expression of sNPF-RNAi in γ KCs (Figure 4.4B-C), while M6 neurons showed a trend toward decreased responses with sNPF-RNAi (Figure 4.4D).

These findings suggest that sNPF may have differential effects on different MBONs: sNPF may suppress activity in MBON-γ2α′1 (see Figure 4.4A), while it may facilitate responses in M6 (see Figure 4.4D and Figure 4.3). Such differential effects have already previously been proposed (Root et al., 2011; Shang et al., 2013; Vecsey et al., 2014).

Odour imaging with sNPFR1-RNAi

Previous observations demonstrated odour-evoked calcium responses in PPL1 neurons that show a positive response at odour onset, but a decrease below baseline during the rest of a 5 s odour presentation (data not shown). This suggests that PPL1 neurons may not only receive excitatory olfactory input, probably through KC-released ACh (see Cervantes-Sandoval et al., 2017), but also through a more slow-acting inhibitory transmitter. The sNPFR1-GAL4 expression also suggests sNPFR1 expression in vertical lobe MB extrinsic neurons that are possibly not MBONs, but in fact PPL1 DANs. These observations suggest that PPL1 neurons may receive inhibition from KC-released sNPF.

To test this hypothesis, I expressed sNPFR1-RNAi broadly in PPL1 DANs, along with GCaMP6f to monitor odour-evoked calcium transients. As has been previously observed, PPL1-α3 and MB-V1 neurons are slightly inhibited by odour presentation (see Figure 4.5). Interestingly, calcium transients in MB-MV1 during the last two

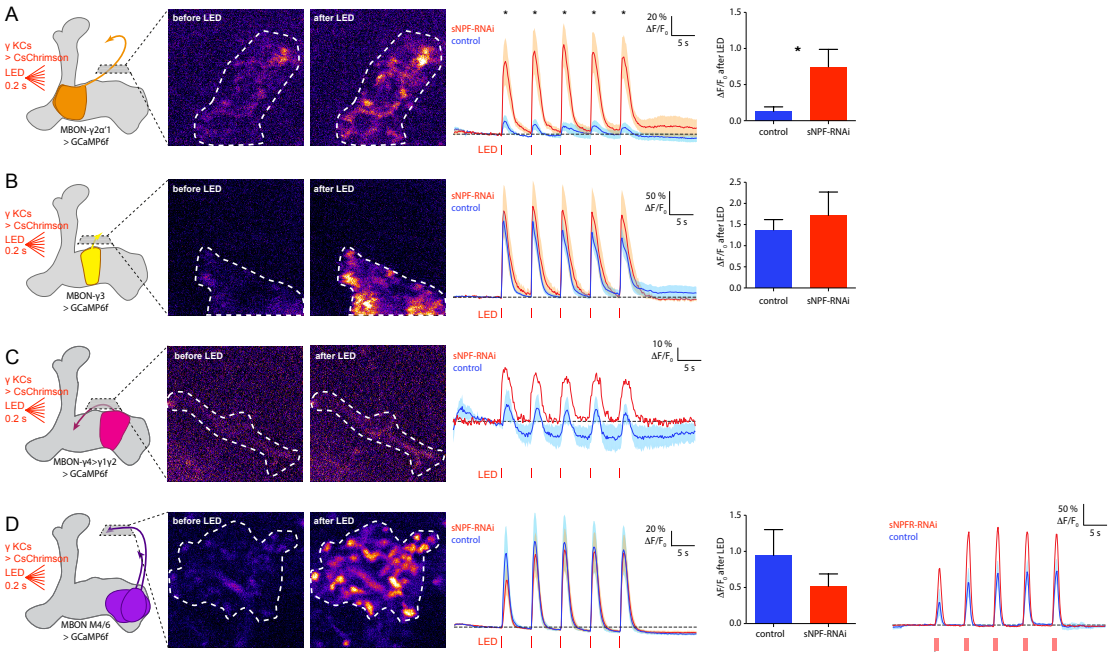


Figure 4.4: Differential effects of γ KC sNPF transmission to different γ MBONs. γ KCs were optogenetically activated using R16A06-GAL4 driven CsChrimson, together with either sNPF(R1)-RNAi (red) or a genetic background control (blue). Calcium transients from γ MBON axons were monitored by GCaMP6f in explant brains, while γ KCs were activated by 200 ms red light (pulsed at 40 Hz, 10 ms). Left panel shows experimental schematics, to the right side of which are sample two-photon images before and after LED stimulation with the ROI encircled as dashed line. To the right side of this are shown average calcium transients during light stimulation. The right side shows $\Delta F/F_0$ after the first LED stimulation. A) Calcium transients from the MBON-γ2α′1 axon (R25D01-LexA) are significantly elevated in flies carrying sNPF-RNAi compared to control for all five stimulation trials (unpaired t-test, $p < 0.05$, $N = 6$). B) No differences were observed in calcium responses between sNPF-RNAi and control in MBON-γ3 (R52G04-LexA) axons (unpaired t-test, $p > 0.05$, $N = 9 - 10$). C) Similar responses were observed in calcium responses between sNPF-RNAi and control in MBON-γ4>γ1γ2 (R53C03-LexA) axons ($N = 1 - 2$, hence no statistical test). D) Left: No differences were observed in calcium responses between sNPF-RNAi and control in M6 axons (VT1211-LexA) axons (unpaired t-test, $p > 0.05$, $N = 6 - 8$), although a trend is visible for slightly smaller initial responses in sNPF-RNAi flies. Right: sNPFR1-RNAi (red) produces similar calcium responses to controls (blue) when R11D09-LexA γ KCs are stimulated for 1 s (40 Hz, 20 ms) and M6 axons recorded in R66C08-GAL4 flies ($N = 1 - 2$, hence no statistical test). Shades and error bars represent SEM.

seconds of odour presentation are significantly increased in one of the three odours tested in flies carrying sNPFR1-RNAi compared to control flies (Figure 4.5C). Calcium responses in MB-MP1 are largely excitatory, and not different between RNAi and control flies (Figure 4.5D). These findings suggest that V1 neurons may indeed receive weak inhibition through sNPFR1, presumably by KC-expressed sNPF.

4.2.4 Taurine

Taurine is a potential neurotransmitter in the CNS of vertebrates and invertebrates (Albrecht and Schousboe, 2005; Martin and Krantz, 2014; Wu and Prentice, 2010), and α-taurine immunoreactivity has been previously observed in KCs (Bicker, 1991; Schäfer et al., 1988; Sinakevitch et al., 2001; Sjöholm et al., 2006; Strausfeld et al., 2003; see also 3.1.2). Focal taurine application, however, showed no effect on M4/6 calcium responses (see Figure 3.4). As taurine is suggested to have hyperpolarising / modulatory effects (McCool and Botting, 2000; Okamoto et al., 1983; Taber et al., 1986), however, it is still possible that taurine may serve as a modulatory KC neurotransmitter. To test this hypothesis, I first tried to confirm taurine synthesis in KCs.

Taurine antibody

To determine the presence of taurine in the adult *Drosophila* brain, I used a previously tested (Sun et al., 2007) commercially available polyclonal antibody against taurine (abcam ab9448) at the prescribed concentration using a standard immunostaining protocol (Wu and Luo, 2006).

Wild-type brains were found to be immunopositive in the SOG ventral of the foramen, in the dFB and associated dorsal paired neuropils, and in a posterior paired cell body ventral of the calyx (Figure 4.6A). Notably, α/βc KCs or indeed any MB neurons were immunonegative (Figure 4.6B). Furthermore, the robust staining of the dFB was not only visible in wild-type flies (Figure 4.6C) but also in taurine synthesis mutants (Figure 4.6D), raising doubts about the specificity of this antibody in the *Drosophila* brain.

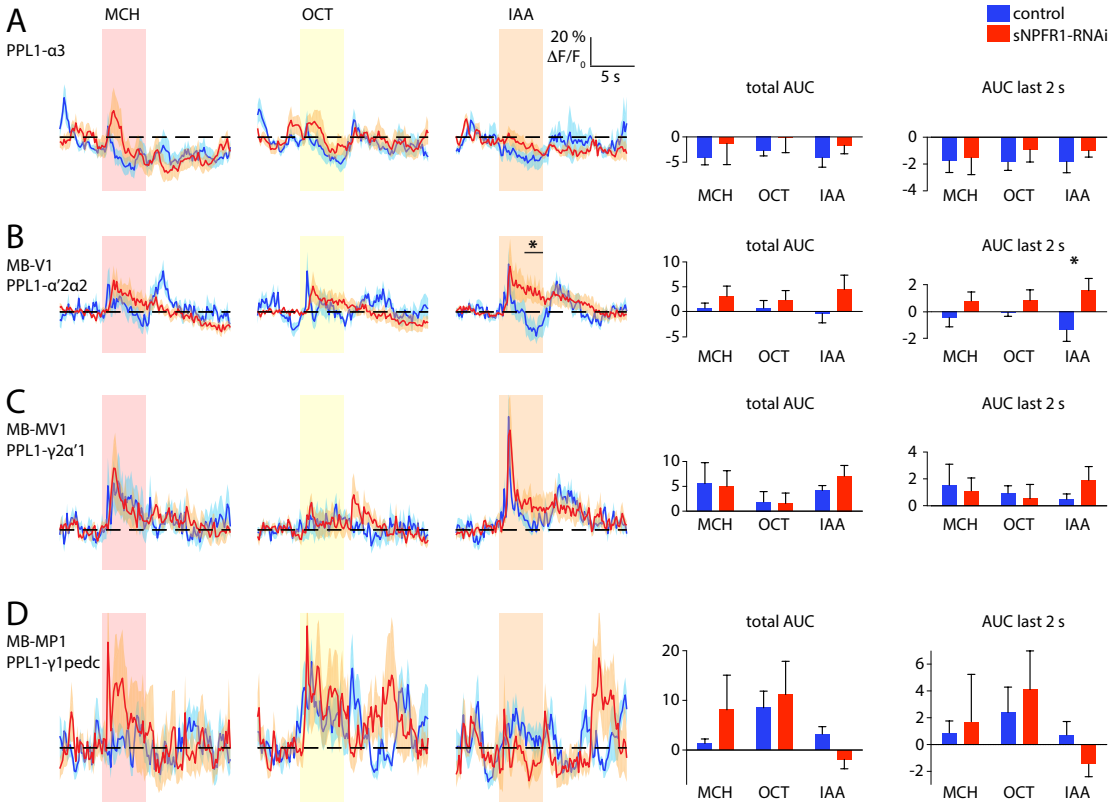


Figure 4.5: sNPFR1-RNAi in PPL1 neurons changes some odour-evoked calcium responses. MB504B ; GCaMP6f flies with sNPFR1-RNAi or control were imaged at different sites along the vertical lobe, covering PPL1-α3 (A), MB-V1 (B), MB-MV1 (C), and MB-MP1 (D) during the presentation of 5s odours MCH, OCT, and IAA. Area under curve (AUC) as sum of $\Delta F/F_0$ during odour presentation (total AUC) and during the last 2 s of odour presentation (AUC last 2 s) was quantified. A) Odour-evoked calcium responses are largely inhibitory in PPL1-α3, but are not significantly different between control and sNPFR1-RNAi flies (multiple t-tests with Holm-Sidak method, $p > 0.05$, $N = 4 - 6$). B) Odour-evoked responses in MB-V1 are first excitatory, but then decrease below baseline during the rest of odour presentation. In flies carrying sNPFR1-RNAi, calcium responses largely stay above baseline. The last 2 s AUC of IAA are significantly higher in sNPFR1-RNAi compared to control (multiple t-tests with Holm-Sidak method, $p < 0.01$, $N = 6 - 7$), but not for the other two odours. C) MB-MV1 neurons show largely excitatory odour responses, and show no significant difference between sNPFR1-RNAi and control flies (multiple t-tests with Holm-Sidak method, $p > 0.05$, $N = 7$). D) MB-MP1 neurons show large variability in calcium signals, but show clear odour-evoked responses that are not significantly different between control and sNPFR1-RNAi flies (multiple t-tests with Holm-Sidak method, $p > 0.05$, $N = 6 - 7$).

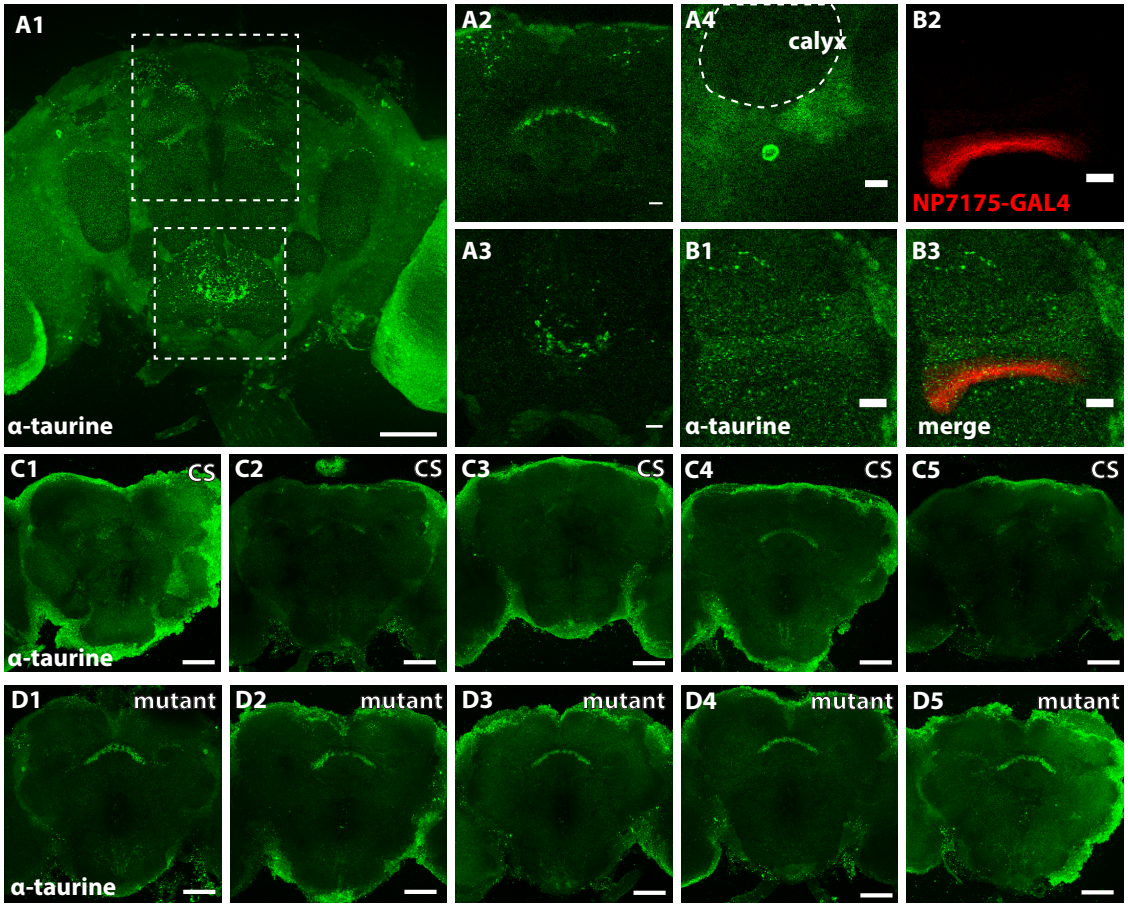


Figure 4.6: Taurine antibody (abcam ab9448) labels SOG and dFB, but no MB neurons. A) Wild-type brains show immunopositive staining in dFB (A2), SOG (A3), and a posterior paired neuron ventral of the calyx (A4). B) Immunopositive staining is not found in MB neurons, as co-staining with NP7175-GAL4 labelled α/βc neurons (red) demonstrates. C) CS flies ($N = 5$) show robust staining in dFB neurons. D) Taurine synthesis mutant flies (DGRC 141-210; $N = 5$) also show robust α-taurine immunoreactivity in dFB neurons. Image in A1 is a maximum projection, while all other images show single planes. Scale bars in A1, C and D represent 50 µm, while those in A2-4 and B represent 10 µm.

4.3 Discussion

4.3.1 Results summary

Using various histochemical and physiological methods, I have presented some evidence for a role of sNPF in modulating cholinergic KC-mediated neural responses in MBONs and DANs through sNPFR1.

sNPFR1-GAL4 expression suggests that some MB-extrinsic neurons express sNPFR1 (Figure 4.1).

Bath application of sNPF shows a trend towards facilitating ACh-evoked calcium

responses in M4/6 neurons (Figure 4.2), and co-injecting sNPF together with ACh resulted in a significant elevation and narrowing of calcium responses (Figure 4.3).

Different MBONs seem to respond differently to sNPF so that sNPF-RNAi in γ KCs actually results in elevated MBON-γ2α′1 responses, no change of MBON-γ3 responses, and a trend towards smaller responses with RNAi is observed in M4/6.

The V1 DAN showed a significant change in its calcium response to the odour IAA with sNPFR1-RNAi, so that the inhibitory response tail normally seen in some DAN responses is missing.

These findings suggest that sNPF may differently modulate neural responses in different KC downstream neurons.

4.3.2 sNPF and sNPFR1 expression

Previous studies showed sNPF immunoreactivity in γ and α/βs KCs with compartment-specific differences (Johard et al., 2008; see also 4.1.4). The authors state that "[s]tronger immunolabelling was seen at the end portions of the α-lobe [...] and the β- and γ-lobes" (Johard et al., 2008, p. 1485), although the micrographs presented mostly point to stronger expression in the α3 compartment (see Johard et al., 2008, Figure 2F1). It will be important in the future to quantify these compartmentalised expression patterns more precisely with our current knowledge of MB compartments (see Aso et al., 2014a; Cohn et al., 2015; Owald and Waddell, 2015), as this information could be key in understanding more precisely potential differences of the effects of sNPF modulation on downstream neurons.

To further investigate potential downstream neurons, we made use of α-sNPFR1 (Figure 4.1F-J), but failed to reproduce earlier findings of α-sNPFR1 immunoreactivity despite using the same antibody (Lee et al., 2008). In their initial and thus far only description of α-sNPFR1 immunoreactivity, the authors describe staining in DILP2 neurons, although the staining pattern seems rather diffuse and weak (see Lee et al., 2008, Figure 1e). It should be noted though that these authors investigated α-sNPFR1 staining in larval *Drosophila* brains, whereas our staining (Figure 4.1F-J) shows immunoreactivity in the adult brain – accordingly, slightly different protocols

were used. Furthermore, Dilp neurons are known to cross-react with antibodies unspecifically, due to their peptide-enriched nature (personal communication with W. Huetteroth, 26.6.2014). This means that the immunostaining observed by Lee et al. (2008) could potentially be due to such cross-reactions.

Instead of DILP2 neurons and instead of expected α-sNPFR1 immunoreactivity in the MB, we only found some weak immunoreactivity around the peduncle (see Figure 4.1J). This staining pattern bears semblance with processes of MIP^+ neurons that have been previously described (Kahsai and Winther, 2011; Kolodziejczyk and Nässel, 2011; Oh et al., 2014). As these neurons are also rich in peptides, we cannot rule out that the observed staining is due to cross-reactivity. The staining pattern observed in Figure 4.1F, including several posterior cell bodies, is most likely due to bleed-through from the channel expressing R64H09-GAL4 (see Figure 4.1A), as revealed by closer inspection and narrowing of detector bandwidths. This leaves open the question of α-sNPFR1 immunoreactivity in the MB, and requires further investigation of sNPFR1 expression.

A recent study using RNA-seq found *sNPFR1* mRNA expression most strongly in V2 MBONs, followed by DAL neurons, and weaker expression in M4β and V3, while no strong expression was found in M6 neurons or γ and α/β KCs (Crocker et al., 2016, Figure 4). These results partly coincide with the observed expression of R64H09-GAL4 that was also strongest in the α2 compartment, and weaker in β2 and α3 (see Figure 4.1E). It should be noted, though, that α3 was previously shown to have strong α-sNPF immunoreactivity (Johard et al., 2008). In Crocker et al. (2016), unfortunately, RNA-seq was performed on only four types of MBONs out of 21, so that sNPFR1 expression levels in the other MBONs currently remain unknown.

In summary, sNPF seems expressed more strongly in the lobe tips, while sNPFR1 expression seems more varied between compartments, with coherently strong expression in V2 MBONs. Further studies, however, are required to assess expression more fully.

4.3.3 sNPF effects on MBONs

sNPF bath application

To investigate modulatory effects of sNPF on cholinergic KC → MBON transmission, I injected ACh into the γ5 region of M4/6 neurons (thus mostly covering the γ KC-sampling M6 neuron), and found a trend towards elevated responses when sNPF was added to the bath saline (see Figure 4.2). This trend was weak and not significant, and only appeared during the first minute. As can be seen from the sample trace (Figure 4.2B), ACh-evoked responses mostly began to decline after the first minute of regular ACh stimulation. Such a decline of responses with repeated stimulation has also been observed before, and is likely due to tissue exhaustion caused by this artificial stimulation and the physical damage associated with the placement of the microinjection pipette and the tissue expansion from stimulation puffs. Importantly, sNPF is a relatively large molecule (molecular weight > 1,300 g/mol) that will require some time to diffuse through a bath solution of > 1 ml, and penetrate into the dense MB tissue that is still largely covered by the perineural sheath. This means that, potentially, the time it would take for sNPF to reach the KC → MBON synapse at sufficient concentrations may be longer than the time reliable ACh-evoked calcium responses could be elicited. This technical problem may hence mask the potential effects of sNPF.

sNPF co-application

In order to overcome this limitation, I therefore changed the experimental approach to include sNPF or vehicle along with ACh in the micropipette solution. This had the advantage that sNPF could be delivered straight to the relevant KC → MBON synapse without having to consider the timing required for diffusion. Co-injecting sNPF along with ACh resulted in M4/6 calcium responses that were significantly increased in magnitude, and slightly narrower than control (see Figure 4.3), confirming the previously observed trend towards response facilitation by sNPF. This effect was relatively small (mean peak $\Delta F/F_0$ 1.05 vs 0.8) but consistent and significant. Interestingly, normalised decay and rise–decay times were significantly

smaller with sNPF co-application, suggesting a narrowing of responses. This timing was normalised to response peaks to compensate for the widening of calcium responses that generally occurs with large responses. A similar trend was visible without normalisation (data not shown). While sNPF might take some time to exert its effects through sNPFR1, we observed no major differences between the first and last ACh-evoked responses, although sampling even more repeated trials per brain resulted in a slightly greater difference (mean peak $\Delta F/F_0$ 0.97 vs 0.67).

sNPF-RNAi

To probe the effects of KC-released sNPF more directly, I tested the effects of sNPF-RNAi in KCs on three different MBONs, and found different effects for different MBONs (Figure 4.4). M6 neurons (sampled from the M6 axon that is clearly separated from the M4β′ axon) showed a trend towards smaller responses with RNAi, again suggesting that sNPF might have a facilitatory effect here. Interestingly, MBON-γ2α′1 showed a significant enhancement of KC-evoked responses with sNPF-RNAi, while there was no difference for MBON-γ3. This suggests that sNPF might actually decrease responses in MBON-γ2α′1, in contrast to its effects on M6.

This differential effect of sNPF on different MBONs may be surprising at first, but is in line with earlier findings that either found facilitating effects at the cholinergic ORN → PN synapse (Root et al., 2011), or hyperpolarising effects when expressing sNPFR1 in larval motor neurons (Shang et al., 2013; Vecsey et al., 2014). Moreover, depending on the neurons in which sNPF pathways were knocked down, differential effects on starvation resistance were previously detected (Kahsai et al., 2010b; Kapan et al., 2012). The mechanisms that could mediate these differential responses will be further discussed in 4.3.6.

Future experiments

At this point, further experiments are clearly required to firmly establish such a differential effect on MBONs, and to extend this knowledge also to other MBONs. This could include ACh-evoked calcium responses in MBON-γ2α′1 with co-application of sNPF to see if sNPF truly diminishes ACh-evoked calcium responses.

To extend optogenetic experiments with sNPF-RNAi in KCs, further MBONs could be sampled. Innervating the γ lobe, for example, are also MBON-γ4>γ1γ2 (Aso et al., 2014a) for which a LexA line (R53C03) has been recently described (Cohn et al., 2015), and MVP2 in the γ1 compartment for which a LexA line (R12G04) has previously been used (Hige et al., 2015a; Perisse et al., 2016), but which failed to drive GCaMP sufficiently for these experiments (data not shown). α/β MBONs could also be sampled. R34B09-GAL4 is a strong but specific α/β KC driver that could be combined with MBON-α1 expressed in R52G04-LexA.

Furthermore, ACh injection experiments could also be repeated with sNPFR1-RNAi to see if this receptor truly mediates any effects of sNPF on the postsynapse. Optogenetic experiments could also be performed with the expression of sNPFR1-RNAi in MBONs targeted through splitGAL4 lines (see Aso et al., 2014a), and CsChrimson expression in γ KCs (e.g. R11D09-LexA) or α/β KCs (e.g. R21D08-LexA).

4.3.4 sNPF effects on DANs

KCs were recently shown not only to act on MBONs but also on DANs through cholinergic synapses (Cervantes-Sandoval et al., 2017; Takemura et al., 2017). Expressing sNPFR1-RNAi in PPL1 DANs, we found a change in calcium response dynamics in V1 neurons during IAA odour presentation (see Figure 4.5). Previous imaging of PPL1 calcium responses showed sustained inhibition during odour stimulation (see Felsenberg et al., 2017, Extended Data Figure 4). We saw similar but weaker inhibition effects in control flies. This may be due to the fact that a similar but different setup was used to the experiments presented in Felsenberg et al., 2017, so that odour concentration and delivery might be slightly different. These inhibitory responses were seen most strongly with IAA in this case (see Figure 4.5B). Interestingly, the expression of sNPFR1-RNAi in PPL1 neurons seemed to abolish this inhibitory response, so that the $\Delta F/F_0$ AUC of the last two seconds of odour presentation was negative in the control, but positive with sNPFR1-RNAi.

This suggests that the inhibitory calcium responses sometimes observed in PPL1 DANs (see Felsenberg et al., 2017) could in fact stem from KC-released sNPF. This might explain why odour-evoked calcium responses evoke a sharp excitatory onset calcium response, but a sustained inhibitory response, given that the action of ACh would be fast and cholinergic, and the action of sNPF might be slow and inhibitory (see Shang et al., 2013; Vecsey et al., 2014).

To establish this, however, further experiments would be necessary. These could include expressing sNPF-RNAi in KCs while observing odour-evoked calcium responses in V1, and co-injections of ACh with sNPF, as done before on MBONs (see Figure 4.3). Furthermore, sNPF action on a potential KC → PAM DAN is also a possibility.

4.3.5 Further sNPF targets?

Besides MBONs and DANs, KCs are known to have several other neurons that they synapse onto, and which could be potential targets of KC-released sNPF.

Another sNPFR1-GAL4 line, R64F07 (Jenett et al., 2012), expresses very specifically in MB-CP1 neurons (see Figure A.16). MB-CP1 neurons (or MBON-calyx; Aso et al., 2014a) have a single cell body per hemisphere, densely innervate the calyx, and project anteriorly into the crepine area (Tanaka et al., 2008). They respond to odours (Hige et al., 2015b), but do not seem to be required for aversive MTM (Bouzaiane et al., 2015). Based on its anatomy and the GAL4 enhancer fragment, it's possible that MB-CP1 activity might be modulated by sNPF.

The α-sNPFR1 immunostaining suggests potential sNPFR1 expression in processes near the peduncle that resemble MIP^+ neurons (see Kahsai and Winther, 2011; Kolodziejczyk and Nässel, 2011; Oh et al., 2014). MIP^+ neurons regulate sleep and circadian rhythms (Kolodziejczyk and Nässel, 2011; Oh et al., 2014), as well as memory (L. Scheunemann, personal communication), similar to what has been found about sNPF (Knapek et al., 2013; Shang et al., 2013). While these findings could point towards a downstream role of MIP^+ neurons, its processes do not innervate the sNPF-positive peduncle, and it is not clear if sNPF release from

the peduncle could reach neurons outside the peduncle. Given the molecular weight of sNPF and the respective speed of diffusion, such signalling would presumably be very slow, but still possible (see Nässel, 2009).

Recently, KC–KC synapses have been described in MB lobes and peduncle (Eichler et al., 2017; Takemura et al., 2017; Zheng et al., 2017). Although no evidence has yet emerged of KCs expressing sNPFR1 (see Crocker et al., 2016; Lee et al., 2008), it is still a possibility that sNPF might mediate KC–KC feedback. Indeed, another sNPFR1-GAL4 line suggests expression in α/βs KCs (Hong et al., 2012). Such a notion would be supported by the similarity of sNPFR1 to the vertebrate NPY Y2 receptor (Feng et al., 2003) that has been found to be predominantly involved in presynaptic inhibition of neurotransmitter release (Michel et al., 1998; Wahlestedt et al., 1986).

APL and DPM neurons are two modulatory neurons innervating most of the MB that play important roles in memory formation (see 1.3.2 and 1.3.3). There is no indication yet that they would express sNPFR1, but their functional roles and anatomical locations would suggest these cannot be ruled out as potential sNPF targets.

Peptidergic neurons expressing SIFamide have been found to send few fine ramifications throughout the MB (Park et al., 2014; Verleyen et al., 2004), where they make postsynaptic contacts with KCs (Takemura et al., 2017). SIFamide has been found to be involved in courtship conditioning (Montague and Baker, 2016), and in the promotion of sleep (Park et al., 2014; Shang et al., 2013; Verleyen et al., 2004). As sNPF was also found to be sleep-promoting (Chen et al., 2013b; Shang et al., 2013), and functional neuropeptide cascades have been previously described (Chen et al., 2016), it is possible that KC-released sNPF could potentially also act on SIFamidergic neurons in the MB, although a recent study has found no significant physiological effects of sNPF release onto SIFamidergic neurons (Martelli et al., 2017).

Given that peptidergic volume transmission can lead to peptide diffusion over tens of micrometres (Jan and Jan, 1982; Nässel, 2009), this list of potential KC-released sNPF targets is not exhaustive.

4.3.6 Potential molecular mechanisms

Given that sNPF might act either as an inhibitory modulator (see Shang et al., 2013; Vecsey et al., 2014; Figures 4.4A and 4.5), or a facilitator of cholinergic responses (see Root et al., 2011; Figure 4.3), how could sNPF act through its only known receptor sNPFR1 to achieve these different results?

sNPFR1 is known to be coupled to several different signalling pathways: sNPFR1 responses in *Xenopus* oocytes required co-expression of the promiscuous G protein $G_{\alpha 16}$, without which neither cAMP, cGMP, or Ca^{2+} responses could be elicited (Feng et al., 2003). Closer analysis revealed that sNPFR1 activates G protein-coupled inwardly rectifying potassium channels (GIRKs) by releasing $G_{\beta\gamma}$ subunits (Reale et al., 2004). Pertussis toxin sensitivity furthermore suggested an involvement of a $G_{\alpha i}$ subunit (Reale et al., 2004; Vecsey et al., 2014). In line with a role for the $G_{\alpha i}$ subunit, cAMP levels were shown to be decreased by sNPF, and co-application with dopamine significantly reduced dopamine-evoked cAMP increase (Shang et al., 2013). sNPF application was also shown to reduce firing rates and hyperpolarise larval motor neurons (Shang et al., 2013).

Another study in *Drosophila* BG2-c6 cells, however, found cAMP elevation upon sNPF stimulation that was dependent on the $G_{\alpha s}$ subunit (Hong et al., 2012). In line with this, co-application of sNPF with octopamine actually resulted in a strong increase of cAMP (Shang et al., 2013).

sNPFR1 was also found to regulate growth by ERK-mediated signalling that involves downstream insulin signalling (Lee et al., 2008).

At this point, it seems possible that different sNPFR1-expressing neurons might involve different G protein-coupled pathways. The dampening of responses seen in MBON-$\gamma 2\alpha' 1$ could be a function of $G_{\beta\gamma}$ and/or $G_{\alpha i}$ coupling, while the facilitation of responses we and others observed could be mediated by $G_{\alpha s}$ signalling. These differences in sNPF response modulation may thus depend on each cell's respective G protein machinery.

4.3.7 State-dependent regulation of sNPF modulation

Would sNPF constitutively act on KC downstream neurons, or would sNPF signalling only occur under certain circumstances?

Previous studies have suggested that high insulin levels generally suppress transcription of sNPFR1, but under starvation conditions, low insulin levels would disinhibit sNPFR1 transcription, leading to facilitatory odour responses in the AL (Hong et al., 2012; Root et al., 2011).

It is thus plausible that a similar enhancement of sNPFR1 transcription also exists in KC downstream neurons. It is interesting to note in this context that sNPF seems to exert differential effects on MBONs of different approach/avoidance arms (see Aso et al., 2014b). Given that MBON-$\gamma 2\alpha'1$ drive approach behaviours and M4/6 neurons drive avoidance behaviours (Aso et al., 2014b; Owald et al., 2015a), however, hunger-dependent upregulation of sNPFR1 would mean hungry flies would have stronger activity of avoidance MBONs, and weaker activity of approach MBONs. Indeed, further data shows that M4/6 odour-evoked responses are in fact reduced in starved flies, presumably by increased inhibition from MVP2 (see Figure 5.5 in the following chapter). This suggests more complex interactions with other state-dependent neuronal regulators that will require further experiments to map out. The molecular and neural pathways involving dNPF pathways of hunger state-dependent memory retrieval will be discussed in chapter 5.

5

MVP2 are inhibitory MBON interneurons

Contents

5.1 Background 199
5.1.1 Hunger as a motivational state 199
5.1.2 Circuits of state-dependent memory expression 202
5.2 Results 203
5.2.1 Voltage imaging of GABA injections into M4/6 204
5.2.2 Optogenetic MVP2 stimulation in explant brain 204
5.2.3 Optogenetic MVP2 stimulation, combined with odours . 207
5.2.4 Optogenetic MVP2 stimulation with odours in starved flies 208
5.3 Discussion 211
5.3.1 Results summary 211
5.3.2 Voltage imaging 211
5.3.3 Shunting inhibition in MBONs 214
5.3.4 Why is no effect of MVP2 activation observed in V2? . 215
5.3.5 Comparison with MV2 217
5.3.6 A model of hunger-dependent retrieval 219

5.1 Background

5.1.1 Hunger as a motivational state

Purposeful behaviour requires animals to be motivated. A particularly strong motivational state that can be well experimentally manipulated is hunger. Hungry animals show an increased motivation to seek and ingest food. Fruit flies, for

example, need to be hungry, in order to learn and express odour–sugar associative memories (Colomb et al., 2009; Krashes et al., 2009; Krashes and Waddell, 2008; Tempel et al., 1983).

Neuropeptide Y (NPY)

In mammals, hunger is largely controlled by neuropeptide Y (NPY) which is a 36 amino acid neuromodulator stimulating food-seeking (Clark et al., 1984; Kalra, 1997; Tatemoto et al., 1982). NPY mRNA was found to be expressed in the arcuate nucleus of the hypothalamus of food-deprived mice (Sahu et al., 1988; Sanacora et al., 1990), and NPY injections into the paraventricular nucleus were shown to increase feeding (Stanley and Leibowitz, 1985). Indeed, the specific ablation of NPY-expressing neurons from adult mice leads these animals to starvation (Bewick et al., 2005; Gropp et al., 2005; Luquet et al., 2005).

NPY is acting through a family of NPY receptors that seem to exert inhibitory effects (Browning and Travagli, 2003; Colmers et al., 1991, 1988; Klapstein and Colmers, 1993; Lin, 2004; Qian et al., 1997; Rhim et al., 1997; Sun et al., 2003).

State-dependence of appetitive memory expression

In *Drosophila*, it was found early on that for appetitive learning and memory to occur, flies needed to be hungry by food-depriving them ideally for about 19–20 hours before training (Tempel et al., 1983).

Neuropeptide F (dNPF)

Invertebrates such as *Drosophila melanogaster* have an orthologue of NPY, which is called neuropeptide F (dNPF), and differs from NPY only by a single amino acid on the C-terminal (Brown et al., 1999; Erickson et al., 1996; Maule et al., 1995; Wahlestedt and Reis, 1993; Zimanyi et al., 1998; see also review in Nässel and Wegener, 2011).

In *Drosophila*, dNPF was found to serve similar functions as the vertebrate NPY (Wu et al., 2003, 2005a,b). Only one receptor for dNPF has been found so

far: the GPCR NPFR1, which is a homologue of the vertebrate NPY receptor (Garczynski et al., 2002).

Hunger is thought to be signalled to dNPF neurons via dS6K in insulin-like producing (DILP) neurons that, in turn, signal to dNPF neurons via the insulin-like receptor dInR (Wu et al., 2005a).

Expression. dNPF mRNA and peptide are expressed in the brain and midgut of *Drosophila* larvae and adults (Brown et al., 1999). Specifically, it is likely expressed in only two pairs of large neurons in the fly brain, located on the posterior side, as demonstrated by immunoreactivity and a dNPF-GAL4 line (Krashes et al., 2009; Wen et al., 2005). These neurons send extensive arborisations throughout the posterior part of the central brain (Krashes et al., 2009; Wen et al., 2005).

Its receptor NPFR1 seems expressed in only two dorsolateral neurons (presumably MB-MP1; see 5.1.2) and three SOG neurons (Wen et al., 2005).

Functions. Like its orthologue NPY, dNPF seems to mainly mediate hunger-induced food-seeking behaviour in flies. Over-expressing dNPF in larvae prolongs feeding behaviour, while ablating dNPF neurons leads to less time spent on food and less feeding responses (Wu et al., 2003, 2005a). Indeed, activating NPFR1 neurons leads sated larvae to ingest even noxious foods tainted with quinine – a behaviour normally only shown when larvae are hungry (Wu et al., 2005b). Similarly, dNPF overexpression leads larvae to delay developmental pupariation in favour of foraging (Wu et al., 2003).

Besides feeding, dNPF and NPFR1 were shown to also mediate ethanol sensitivity in adult flies (Wen et al., 2005), and to impact sleep regulation in male flies (He et al., 2013).

The physiological effects of dNPF binding to NPFR1 currently remain poorly understood, but forskolin-stimulated AC activity was suppressed by successively higher concentrations of dNPF binding to NPFR1 (Garczynski et al., 2002). Similarly, NPY appears to have inhibitory action through its receptor (Browning

and Travagli, 2003; Colmers et al., 1991, 1988; Klapstein and Colmers, 1993; Lin, 2004; Qian et al., 1997; Rhim et al., 1997; Sun et al., 2003).

5.1.2 Circuits of state-dependent memory expression

Flies generally need to be food-deprived in order to express appetitive memories (Krashes and Waddell, 2008; Tempel et al., 1983), but Krashes et al. (2009) could show that artificial activation of dNPF neurons was sufficient for sated flies to still express appetitive memories. This suggests that the hunger state-dependent memory retrieval depends on hunger signals mediated by dNPF, in line with its established role in food-seeking behaviour (Wu et al., 2003, 2005a).

MP1 as dNPF target

A screen for neurons that require NPFR1 expression for appetitive memory retrieval suggested a role for the dopaminergic MB-MP1 neurons of the PPL1 cluster (Krashes et al., 2009; see also 1.3.2). Indeed, activating these dopaminergic neurons in hungry flies during retrieval blocked memory expression, while silencing these neurons in sated flies resulted in state-independent appetitive memory retrieval (Krashes et al., 2009). This shows that both dNPF activation and MP1 inactivation result in appetitive memory retrieval in sated flies (Krashes et al., 2009). Along with previous results suggesting an inhibitory role of NPY (Browning and Travagli, 2003; Colmers et al., 1991, 1988; Klapstein and Colmers, 1993; Lin, 2004; Qian et al., 1997; Rhim et al., 1997; Sun et al., 2003), it was thus suggested that in starved flies dNPF inhibits MP1, which in turn releases hunger-gated MB-dependent memory retrieval (Krashes et al., 2009). Strong starvation was shown to result in a significant decrease of MP1 slow oscillations, providing a possible neural correlate for this hunger state, which can affect downstream neurons (Plaçais et al., 2013a).

MVP2

MP1 neuron terminals occupy the $\gamma 1$ and anterior peduncle region of the MB (Krashes et al., 2009; Tanaka et al., 2008). The same region is innervated by dendrites of the MVP2 MBON (Tanaka et al., 2008), which was identified as

GABAergic and which extends most of its axons largely into the α/β lobes and, to a lesser degree, outside of the MB (Aso et al., 2014a; Perisse et al., 2016).

As MP1 inactivation during retrieval leads to appetitive memory expression even when flies are sated (Krashes et al., 2009) and MP1 activity seems to suppress that of MVP2 (Hige et al., 2015a; Perisse et al., 2016), it is perhaps not surprising that thermogenetic activation of MVP2 neurons during retrieval also leads to appetitive memory expression in sated flies (Perisse et al., 2016). In line with the previously observed reduced activity of MP1 in starved flies and the phenocopy of starved flies when blocking MP1 output (Krashes et al., 2009; Plaçais et al., 2013a), MVP2 odour responses were found to be elevated in starved flies (Perisse et al., 2016).

Where are these hunger state and aversion signals further passed on to? Anatomically, it seems that MVP2 MBONs are mainly projecting into α/β lobes instead of other MBON downstream neuropils (Aso et al., 2014a). More precisely, MVP2 neurons were found to synapse onto the initial axon segments of M4/6 MBONs as well as V2 MBONs (Perisse et al., 2016). These neurons have well-defined roles in state-dependent appetitive memory retrieval (Bouzaiane et al., 2015; Owald et al., 2015a) and aversive memory retrieval (Bouzaiane et al., 2015; Séjourné et al., 2011). This suggests that MVP2 neurons are GABAergic interneurons that may pass on hunger state and aversion signals to other MBONs.

To investigate how MVP2 neurons can influence state-dependent memory expression in the context of findings by Perisse et al. (2016), I have tested the effects of MVP2 activity on downstream MBON partners.

5.2 Results

As previous results demonstrated MVP2 neurons to make GABAergic presynaptic contacts with M4/6 neurons (Aso et al., 2014a; Perisse et al., 2016), I have first investigated the effects of GABA injections into M4/6 neurons, before turning to the optogenetic activation of MVP2 neurons while imaging M4/6 and V2 MBONs.

5.2.1 Voltage imaging of GABA injections into M4/6

1 mM GABA injected into M4/6 dendrites showed no detectable calcium responses in explant brains expressing GCaMP5 in R21D02-GAL4 (Figure 3.4). However, GABA is likely only inhibitory (Bennett and Balcar, 1999), and may thus not be detected by calcium indicators. We have thus decided to make use of the recently developed voltage indicator Ace2::mNeonGreen (Gong et al., 2015), in order to uncover any potential inhibitory effects of GABA on M4/6 neurons.

I expressed Ace2::mNeonGreen in M4/6 neurons with the relatively strong VT1211-GAL4 driver, and used the previously established explant brain preparation to inject 1 mM GABA into M4/6 dendrites. Parts of the dendrite and the ventral part of the axons were imaged at 200 Hz with 64×64 resolution using an Andor Zyla sCMOS camera. When observing voltage transients in M4/6 axons during GABA release, no significant changes were observed (see Figure 5.1). Minor decreases were observed with injections, but these are likely due to small displacements of fluorescent tissue with the injection pressure. Notably, Ace2::mNeonGreen would show fluorescent increases with hyperpolarisations (Gong et al., 2015); these, however, were clearly not observed in this experiment.

5.2.2 Optogenetic MVP2 stimulation in explant brain

Instead of injecting GABA into M4/6 MBONs, we next turned to optogenetic activation of MVP2 neurons, while observing calcium transients in M4/6 neurons.

MVP2 neurons were optogenetically activated using the red-shifted channelrhodopsin CsChrimson (Klapoetke et al., 2014) with the R12G04-LexA driver (Perisse et al., 2016). Calcium transients from the ventral axon segment of M4/6 neurons were recorded with R21D02-GAL4 driven GCaMP6f, using two-photon calcium imaging in explant brains (see Figure 5.2). One second of red LED stimulation resulted in no significant changes in calcium transients, neither at 10 seconds ITI (Figure 5.2C) nor at 3 s ITI (Figure 5.2D). This means that either MVP2 neuron activity shows no discernible effect on M4/6 neurons, or that this could not be captured by this protocol.

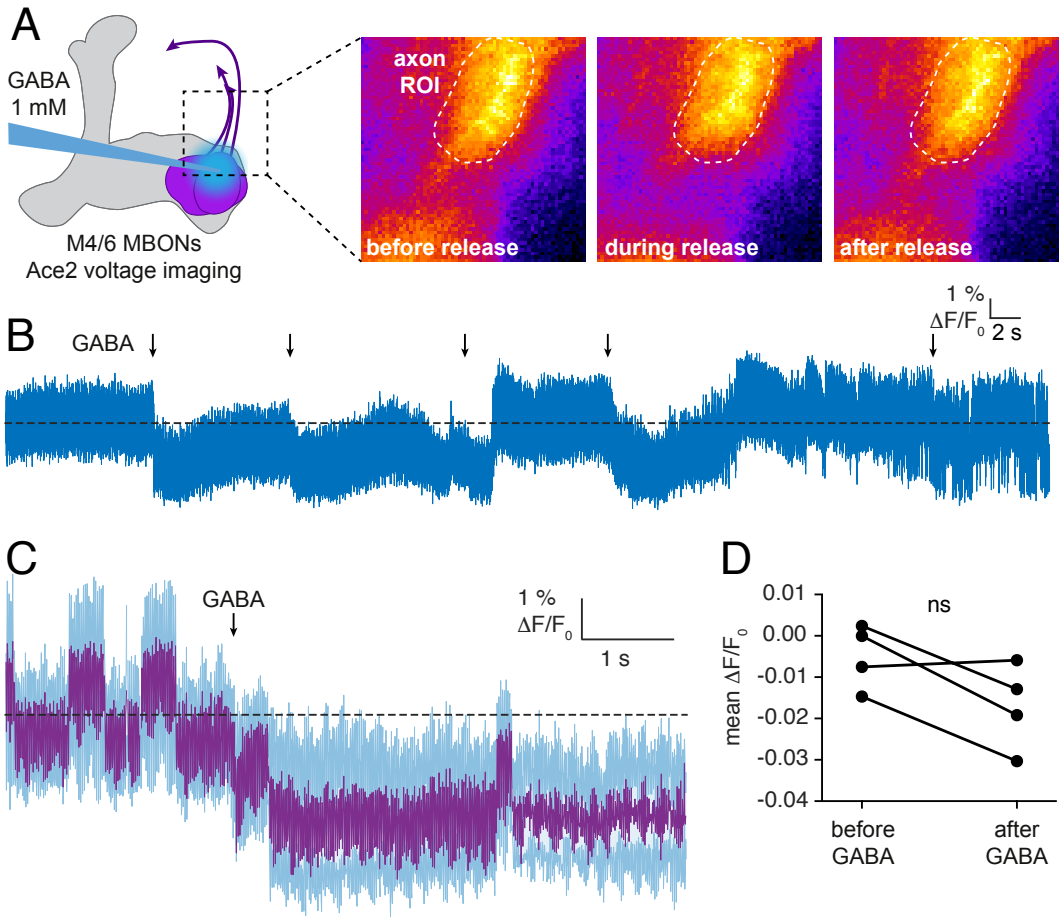


Figure 5.1: Voltage imaging of M4/6 MBONs during GABA injections. A) 1 mM GABA was injected into the γ5 dendritic region of M4/6 MBONs in in explant brains expressing Ace2::mNeonGreen in VT1211-GAL4. Images were acquired at 64×64 pixels resolution at 200 Hz with a sCMOS camera. To the right are shown sample images of dendrites and axons of M4/6 neurons, with the axonal ROI shown in dashes white lines. Note the fluorescent depression at the dendritic level during release, while the axons show no major change. B) Sample voltage transient during several GABA injections. Note the large variance of baseline, and slight decreasing shifts with GABA application. C) Average voltage response to GABA injection from four brains, blue shade represents SEM. D) Voltage signals before and after GABA application are not statistically different (paired t-test, $p > 0.05$, $N = 4$), despite a trend towards a decrease. Mean $\Delta F/F_0$ was taken from average $\Delta F/F_0$ half a second before GABA release and half a second after GABA release.

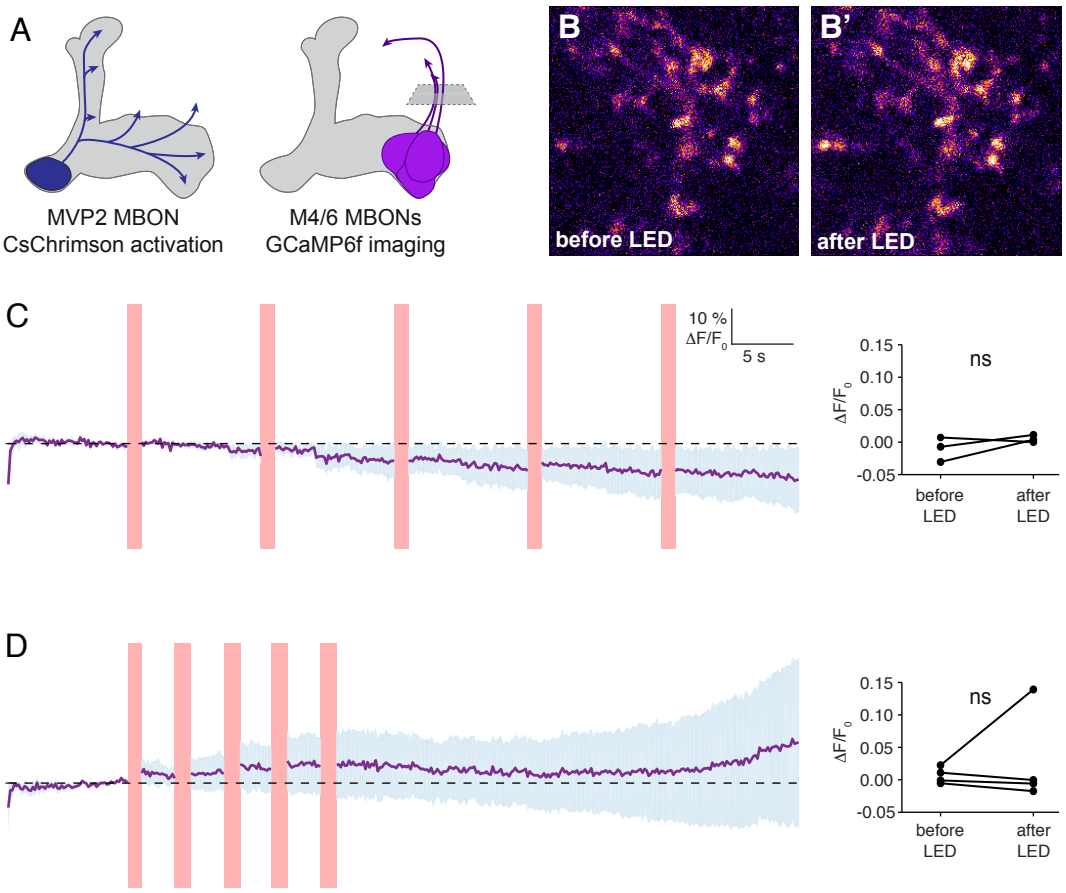


Figure 5.2: Effects of optogenetic activation of MVP2 neurons on M4/6 MBONs in explant brain. A) The optogenetic activator CsChrimson was expressed in R12G04-LexA MVP2 neurons, while GCaMP6f calcium transients were measured in early axon terminals of R21D02-GAL4 M4/6 neurons. B) Sample images from two-photon recordings of imaged M4/6 axonal regions before (B) and after (B') LED activation of MVP2 neurons. C) 1 s light pulses at 10 s intervals (red vertical bars) showed no discernible effect on calcium transients. $\Delta F/F_0$ before and after LED showed no significant difference (paired t-test, $p > 0.05$, $N = 3$). D) 1 s light pulses at 3 s intervals (red vertical bars) showed no discernible effect on calcium transients. $\Delta F/F_0$ before and after LED showed no significant difference (paired t-test, $p > 0.05$, $N = 4$). Purple lines in C and D represent mean calcium transients, and blue shades represent SEM.

5.2.3 Optogenetic MVP2 stimulation, combined with odours

Inhibitory action can either be directly hyperpolarising, or "shunting" so that only excitatory signals already passing through a neural system are diminished (see Knoflach et al., 2016). In order to test indirect hyperpolarisation, we decided to stimulate M4/6 neurons *in vivo* using odour stimulation, while simultaneously activating MVP2 neurons using optogenetic activation, and observing calcium transients in M4/6 axons.

We thus expressed CsChrimson in MVP2 neurons with R12G04-LexA, while expressing GCaMP6f in R21D02-GAL4 M4/6 neurons (see Figure 5.3A). These flies were then tethered, dissected, and presented with odours similar to before (Barnstedt et al., 2016; Owald et al., 2015a). However, I used only a 2 s odour pulse, the last second of which a red LED was turned on to excite MVP2-expressed CsChrimson. This protocol allowed odours to first excite the MBON, and to then study the effect of optogenetic MVP2 stimulation on the already excited MBON. The field of view was again set to the initial axon segment where anatomical overlap between MVP2 and M4/6 was previously observed (Perisse et al., 2016).

M4/6 neurons showed strong odour-evoked calcium responses as observed before (Barnstedt et al., 2016; Owald et al., 2015a). Interestingly, however, MVP2 neuron activation during odour presentation led to a significant decrease of M4/6 $\Delta F/F_0$ following LED stimulation compared to the same point during odour presentation without LED on (see Figure 5.3B-C). This difference disappears one second after LED offset, and could be observed in both odours tested.

We next wondered if such an effect also holds true for another MBON that may receive MVP2 projections: V2 (Aso et al., 2014a; Perisse et al., 2016). I again used R12G04-LexA to drive CsChrimson in MVP2 neurons, but combined it with R71D08-GAL4 (Crocker et al., 2016; Séjourné et al., 2011; Vasmer et al., 2014) to drive GCaMP6f in V2 neurons, and focused on a previously used field of view (Figure 5.3D; see Hige et al., 2015b; Séjourné et al., 2011). Using the same protocol in V2 neurons showed no significant effect of LED stimulation during odour presentation (see Figure 5.2F).

This suggests that MVP2 neurons indeed inhibit stimulus-evoked neural activity in M4/6 neurons, but not in V2 neurons.

I also tested for potential effects of non-experimental parameters when light-activating MVP2 neurons while observing odour-evoked calcium transients in M4/6 neurons.

CsChrimson requires the addition of retinal in fly food in order to fully exhibit its depolarising effects in neurons (Klapoetke et al., 2014). Using flies that were fed no retinal before the optogenetic experiments yielded no significant effects of LED stimulation on the calcium transients (Figure 5.4A). Also, imaging from flies that expressed no CsChrimson in MVP2 or any neuron showed no effects on calcium transients with LED activation (Figure 5.4B). This suggests that red light itself does not alter M4/6 calcium transients, but that it needs to activate CsChrimson-expressing MVP2 neurons for the observed effects (see Figure 5.3).

Furthermore, light stimulation of CsChrimson-expressing MVP2 neurons had no effect on calcium transients *in vivo* when flies were presented with no odours (see Figure 5.4C). This suggests that MVP2 only exhibits discernible inhibition when M4/6 neurons are activated, for example by odours.

5.2.4 Optogenetic MVP2 stimulation with odours in starved flies

MVP2 neurons have a previously established role in mediating starvation-induced hunger signals, in which MP1 dopaminergic input to MVP2 leads to increased odour responses in MVP2 when flies are starved (Perisse et al., 2016). However, it is currently unknown if and how these starvation signals are passed on further in the network. We thus used the previously established protocol of monitoring odour-evoked calcium transients in M4/6 and V2 MBONs during optogenetic MVP2 stimulation on starved and fed flies (see Figure 5.5).

Interestingly, odour-evoked calcium responses were significantly lower in M4/6 neurons when flies were previously starved compared to fed flies (see Figure 5.5A). This finding held true regardless of optogenetic MVP2 stimulation and for both

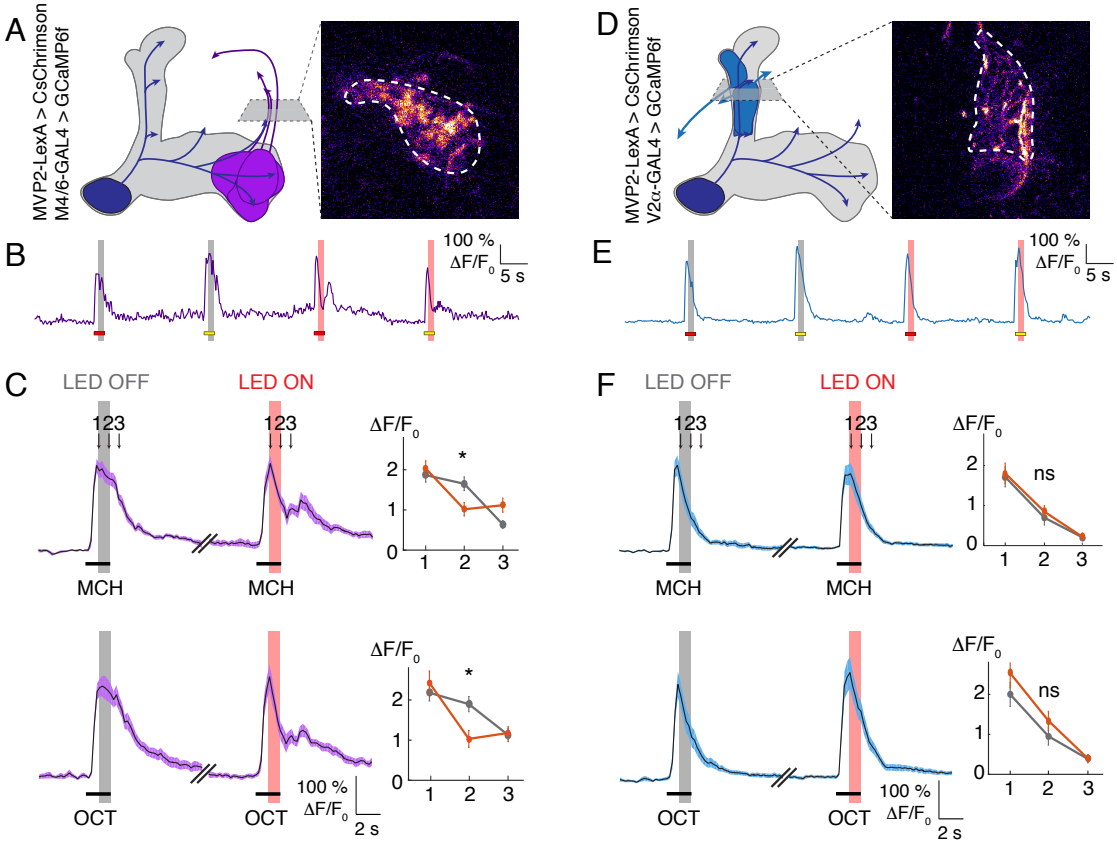


Figure 5.3: Activating MVP2 neurons depresses M4/6 but not V2 odour-evoked calcium responses. The optogenetic activator CsChrimson was expressed in R12G04-LexA MVP2 neurons, while GCaMP6f calcium transients were measured in early axon terminals of MBONs of a tethered fly during odour presentation. MCH and OCT odours were presented for 2 s, the last second of which the red LED was turned on for one second. A) M4/6 axons were imaged from R21D02-GAL4. Right image shows sample image from two-photon recordings of imaged M4/6 axonal regions. B) Sample trace of MCH, OCT, MCH+LED, and OCT+LED. Note the marked depression in calcium transients when is turned on (red vertical bars). C) $\Delta F/F_0$ between LED on and off is not different at time of LED onset (1) or one second after LED offset (3), but significantly depressed by an active LED at time of LED offset (2) for both odours (two-way ANOVA, Sidak's multiple comparisons test, $p < 0.01$, $N = 9$). D) V2 axons were imaged from R71D08-GAL4. Right image shows sample image from two-photon recordings of imaged V2 axonal regions. E) Sample trace of MCH, OCT, MCH+LED, and OCT+LED. F) $\Delta F/F_0$ between LED on and off is not different at time of LED offset (2), or one second after LED offset (3), for both odours, and at time of LED onset (1) for MCH (two-way ANOVA, Sidak's multiple comparisons test, $p > 0.05$, $N = 13$). $\Delta F/F_0$ during LED onset (1) is significantly different between LED on and off for OCT (two-way ANOVA, Sidak's multiple comparisons test, $p < 0.01$, $N = 13$). Dark lines in C and F represent mean calcium transients, and shades and error bars represent SEM. Adapted from Perisse et al. (2016).

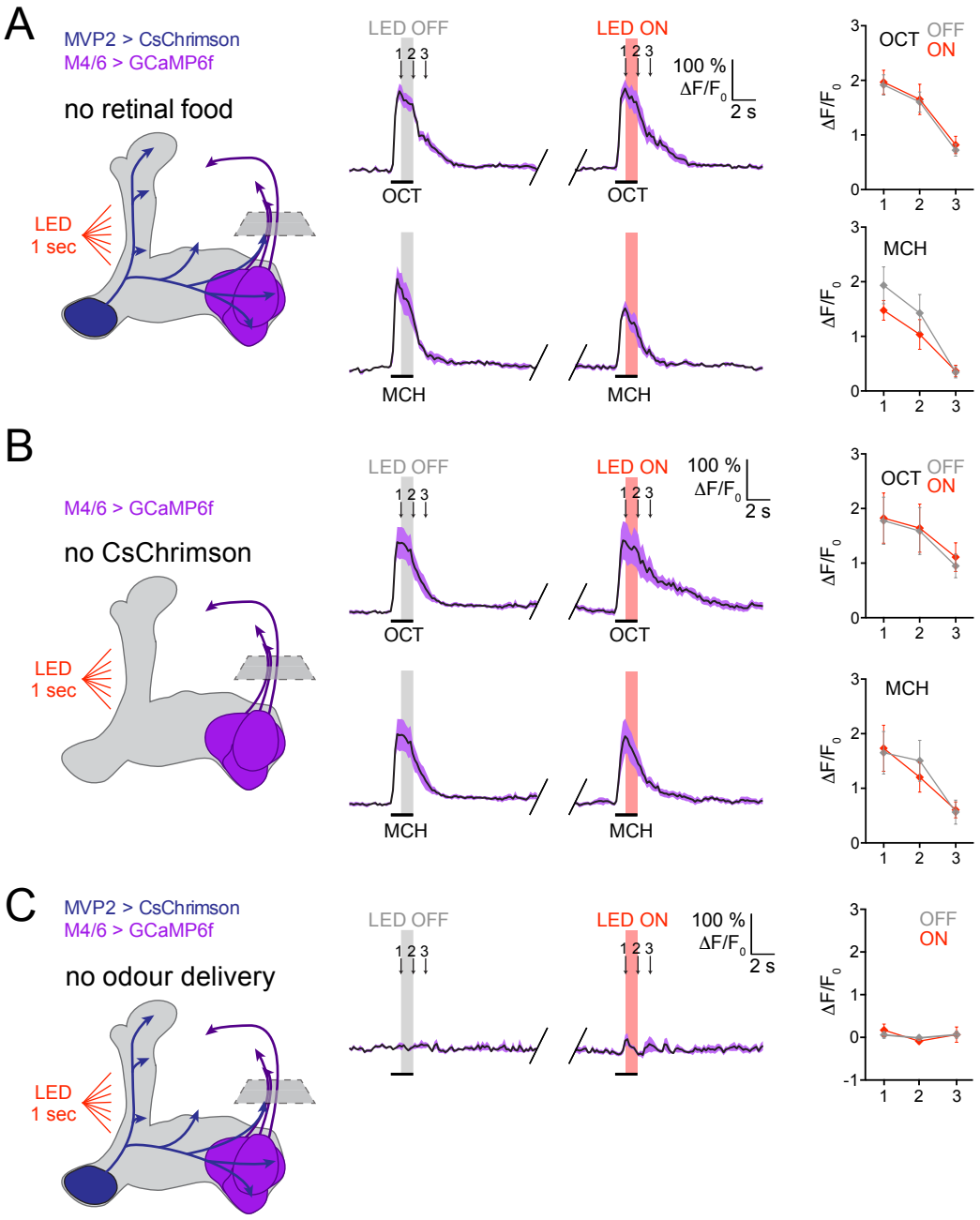


Figure 5.4: Control experiments to Figure 5.3. Effects of MVP2 activation on M4/6 odour responses depend on retinal, CsChrimson, and odour delivery. A) LED activation of MVP2 does not alter M4/6 odour-evoked calcium responses in flies not fed with retinal food (two-way ANOVA, Sidak's multiple comparisons test, $p > 0.05$, $N = 5$). B) LED activity does not alter M4/6 odour-evoked calcium responses in flies not expressing CsChrimson in MVP2 neurons (two-way ANOVA, Sidak's multiple comparisons test, $p > 0.05$, $N = 5$). C) LED activation of MVP2 does not alter M4/6 calcium transients without simultaneous odour stimulation (two-way ANOVA, Sidak's multiple comparisons test, $p > 0.05$, $N = 5$). Dark traces represent mean calcium transients, and shades and error bars represent SEM. Adapted from Perisse et al. (2016).

odours. This suggests that MVP2 neurons may modulate M4/6 signals via two independent mechanisms: one as a slow-acting tonic inhibitor correlated with starvation state, and one as an acute signal that quickly inhibits neural activity.

V2 neurons, on the other hand, showed no starvation state modulation of odour-evoked calcium responses in either condition and for either odour (see Figure 5.5B).

5.3 Discussion

5.3.1 Results summary

How can MVP2 neurons exert their state-dependent influence onto downstream neurons? I show that optogenetic MVP2 activation can inhibit odour-evoked activity in M4/6 neurons but not in V2 neurons (see Figure 5.3). This inhibition critically depends on the light activation of CsChrimson in MVP2 neurons during odours, as light itself or MVP2 activity without simultaneous odour presentation did not yield any effects (see Figure 5.4). In line with previous findings of elevated MVP2 activity in hungry flies (Perisse et al., 2016, Figure 6) and with the inhibitory effects I observed, I found that starvation reduces odour-evoked calcium responses in M4/6 but not V2 MBONs.

These findings suggest that starvation-modulated MVP2 activity exerts inhibition on M4/6 MBONs but not V2 MBONs to promote appropriate learned behaviour.

5.3.2 Voltage imaging

As MVP2 neurons were shown to use the widely inhibitory neurotransmitter GABA (Aso et al., 2014a; Bennett and Balcar, 1999; Perisse et al., 2016, but see also Szabadics et al., 2006), we sought a way to investigate the effects of GABA on M4/6 neurons.

Traditional calcium imaging methods often fail to detect inhibitory responses (see Haynes et al., 2015) as hyperpolarisation may only exert minor effects on internal $[Ca^{2+}]$ ($[Ca^{2+}]_i$). However, inhibitory calcium responses have previously been observed (see Cayre et al., 1999; Cohn et al., 2015; Perisse et al., 2013b, Figures 6.3, 6.5, 6.6, and further personal observations). Key in understanding why

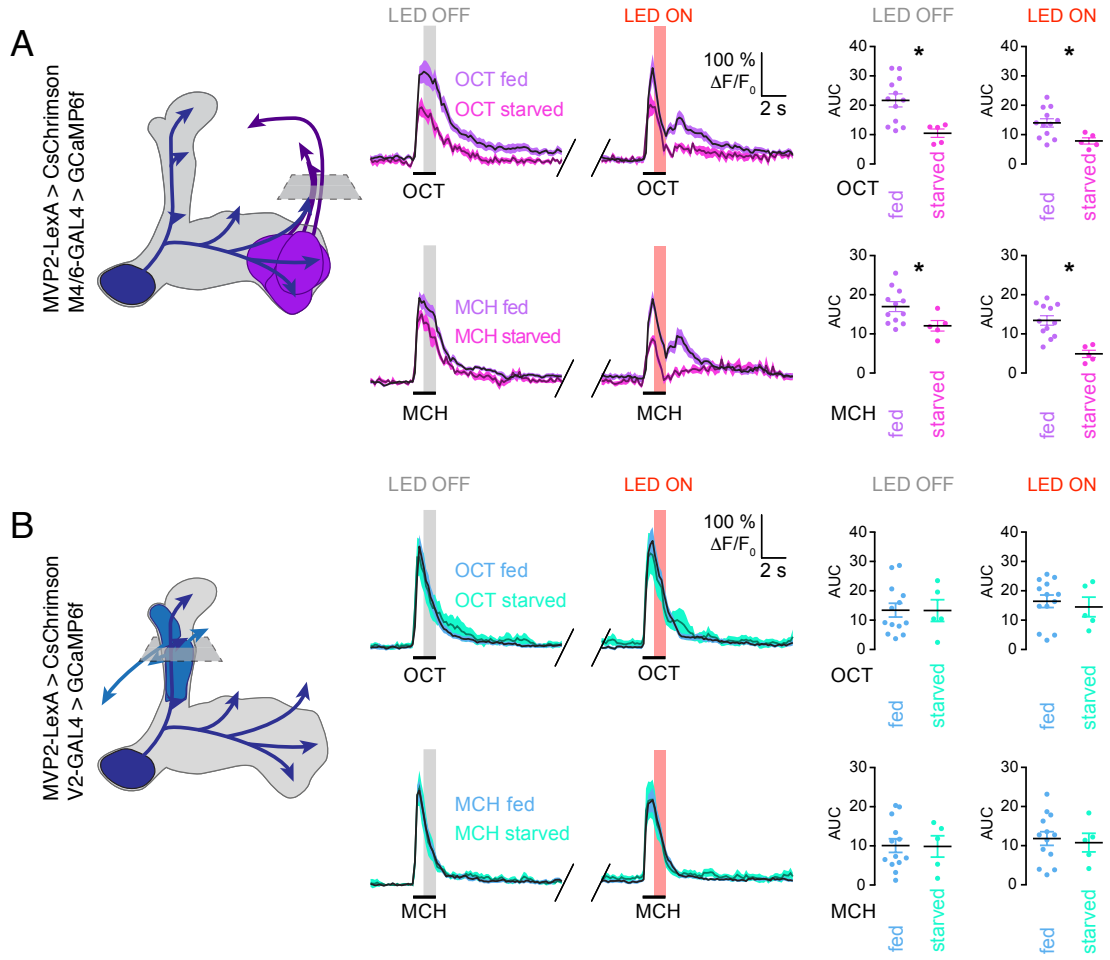


Figure 5.5: Starved flies have smaller odour responses in M4/6 but not V2 neurons. Sated flies and flies that were starved for 20–24 h were imaged as described before, while MVP2 neurons were optogenetically activated using R12G04-LexA driven CsChrimson. Area under curve (AUC) of $\Delta F/F_0$ was measured between LED onset and one second after LED offset. A) M4/6 neurons imaged using R21D02-GAL4 driven GCaMP6f show significantly reduced responses when flies were starved before, irrespective of MVP2 activation (red vertical bar). AUC is significantly different between starved and fed conditions for both odours and both LED conditions (t-test, $p < 0.05$, $N = 5 - 12$). B) V2 neurons imaged using R71D08-GAL4 driven GCaMP6f show no difference in odour responses between starved and fed conditions for both odours and both LED conditions (t-test, $p > 0.05$, $N = 5 - 13$). Adapted from Perisse et al. (2016).

negative responses are sometimes picked up by calcium sensors and sometimes not may be different levels of baseline $[Ca^{2+}]_i$. Cayre et al. (1999) could show that effects of GABA could not be detected if baseline $[Ca^{2+}]_i$ was lower than 100 nM, suggesting that GABA-evoked calcium responses can only be picked up if baseline $[Ca^{2+}]_i$ is high. A further factor to consider is each cell's coupling to various calcium stores and buffers (see Grienberger and Konnerth, 2012), and the specific expression of calcium channels in each cell. Indeed, when injecting 1 mM GABA into M4/6 dendrites, we did not observe changes in calcium levels (see Figure 3.4).

Sensors that can track chloride influx (e.g. SuperClomeleon; Grimley et al., 2013) have been used in the past to monitor inhibitory effects of GABAergic neurons on downstream neurons (see Haynes et al., 2015), but at the time of experiments, our setup would not allow for FRET imaging (see also 1.5.3).

As hyperpolarisations should be clearly visible from direct voltage measurements, we turned to the latest widefield-compatible voltage sensor developed, Ace2::mNeonGreen (Gong et al., 2015). Ace2 had been previously reported to faithfully and rapidly track voltage signals on the millisecond range in *Drosophila in vivo* and in explant brains (Gong et al., 2015). When injecting 1 mM GABA into the M4/6 initial axon segment, we did not observe any significant fluorescent changes in the axon or dendrite (see Figure 5.1). A small trend towards a decrease was visible, but this was most likely due to tissue displacement from the injection pulses, as we had already previously observed (see Figure 3.9).

At this point, it is not clear if this kind of stimulation does simply not induce hyperpolarisations at M4/6 neurons, or if the conditions for Ace2 voltage imaging were not sufficient. Control experiments with cholinergic stimulation of M4/6 neurons, however, suggest the latter (data not shown). Furthermore, additional feeding of ATR did also not improve Ace2 voltage responses (personal communication with K. Jovanoski). It should also be noted that, since the publication of the original article, we are not aware of any published studies that have successfully used Ace2 in *Drosophila*. Future studies could try the use of other voltage indicators, such as ASAP2 (Yang et al., 2016b) or ArcLight (Cao et al., 2013).

5.3.3 Shunting inhibition in MBONs

While we observed no effects of MVP2-released GABA through GABA injections in M4/6 neurons (see Figures 3.4 and 5.1) nor through optogenetic MVP2 activation (see Figures 5.2 and 5.4C), we observed inhibition during odour-evoked calcium transients in M4/6 neurons (Figure 5.3A-C).

In mammals, GABAergic interneurons that target perisomatic regions of their downstream neurons have been found to exert 'shunting' inhibition via $GABA_A$ receptors (Banke and McBain, 2006; Ellender and Paulsen, 2010; Klausberger and Somogyi, 2008; Miles et al., 1996). By targeting perisomatic regions near the initial axon segment, perisomatic inhibition exerts a strong influence over a neuron's spiking pattern, as this is the region where dendritic currents are pooled and the 'decision' to fire action potentials takes place. Through $GABA_A$ receptors with a reversal potential near resting potential, excitatory postsynaptic potentials coming from dendrites can thus be effectively 'shunted' by reducing the local input resistance, and developing action potentials can be stifled. Such inhibition would not be visible as hyperpolarisation because these $GABA_A$ receptors would not hyperpolarise these neurons but merely reduce the local input resistance.

Although shunting inhibition has not previously been directly described in *Drosophila*, the evidence we gathered here supports the idea that the influence of MVP2 neurons on M4/6 is shunting in nature. First, MVP2 terminals target almost exclusively the basal M4/6 axon segment. As invertebrate neurons generally have dendritic arbours that converge into an axon without passing through the soma, this basal axon segment is presumably equivalent to the initial axon segment described in mammals. Functionally, this is the anatomical region where dendritic inputs are pooled, and action potentials are being produced. Thus, MVP2 terminals target an area similar to the perisomatic area described for shunting inhibition in mammals.

Secondly, we have found no hyperpolarising effects of neither GABA injections nor optogenetic MVP2 activation, but instead saw a dampening of excitatory responses when MVP2 neurons were activated during odour presentation. Also, while starved flies showed smaller odour-evoked responses in M4/6 neurons, presumably

through higher activity of MVP2 neurons, no shift in baseline was visible when comparing fed and starved flies (data not shown), suggesting that starvation state only dampened excitatory responses without generally hyperpolarising neurons. These findings, however, may be confounded by the technical limitations of calcium sensors (see also 5.3.2).

Thirdly, the $GABA_A$ subunit Rdl was recently found to be expressed in M4/6 neurons (Crocker et al., 2016, Figure S5), and another $GABA_A$ subunit, Lcch3, was found to be involved in M4/6-guided naive odour avoidance (personal communication with E. Perisse, 3.8.2017). This might mean that shunting inhibition in *Drosophila* could also be mediated by a fast-acting $GABA_A$ receptor, as it is in mammals. In line with this, $GABA_A$ receptors were recently found to be involved in the 'sharpening' of presynaptic voltage responses (Raccuglia et al., 2016), not unlike what we observe in M4/6 neurons of starved flies (see Figure 5.5A). To establish a role for $GABA_A$ receptors in mediating the MVP2 → M4/6 response, however, future studies are needed that could block $GABA_A$ receptors in M4/6 neurons either through RNAi or pharmacologically.

5.3.4 Why is no effect of MVP2 activation observed in V2?

Although MVP2 neurons anatomically also target V2 neurons (see Perisse et al., 2016, Figure 3), we did not observe any effects of optogenetic MVP2 activation on odour-evoked calcium responses in V2 (see Figure 5.3D-F). Perisse et al. (2016) suggest that MVP2 neurons potentially connect to DANs or other neurons instead of V2. This notion, however, does not seem to be the case, according to the very recent publication of EM data of the entire α lobe (Takemura et al., 2017). This data shows that MVP2 in α2 is mostly presynaptic to V2 (117 contacts) and APL (98 contacts over the entire lobe), but only 3 contacts were found from MVP2 to the V1 DAN (Takemura et al., 2017, Table 5). This suggests that anatomical connections to V2 do indeed exist, but unfortunately at this point, we have no data to compare this to the number of MVP2 → M4/6 connections. Light microscopy observations, however, suggest slightly less dense innervation of V2 than M4/6 (Perisse et al., 2016). Also,

the glutamatergic MV2 neuron (MBON-β1>α, which does not innervate M4/6) was found to have 290 presynaptic contacts to V2 (Aso et al., 2014a; Takemura et al., 2017), thus potentially exerting simultaneous glutamatergic excitation that could counter-act GABAergic effects of MVP2 (see also 5.3.5).

Another possibility to consider is that V2 neuronal responses to odours are simply narrower than those of M4/6 (compare Figure 5.3C,F), and are thus less affected by inhibition from MVP2 neurons. Two observations speak against such an interpretation. First, odour-evoked calcium transients in M4/6 show a 'rebound' shape after optogenetic stimulation, in which the transient seems to slightly rise again before falling back to baseline – such a rebound shape is not seen in V2 neurons. Secondly, odour-evoked responses are significantly smaller in M4/6 neurons of starved compared to fed animals (Figure 5.5A), presumably due to the influence of MVP2 neurons. This state-dependent difference is not observed in V2 neurons (Figure 5.5B). Thus, it does not seem like the differences in odour-evoked calcium transient shapes between M4/6 and V2 neurons could explain the observed differences between the two MBONs.

It should also be noted that the GAL4 line used (R71D08; Jenett et al., 2012) also expresses in V2α′ neurons that do not seem to be targeted by MVP2 (Aso et al., 2014a; Pech et al., 2013; Perisse et al., 2016; Séjourné et al., 2011). Axons between V2α and V2α′ are tightly intertwined and could thus not be clearly separated, but whereas V2α′ axons mostly stretch far into the lateral ventral protocerebrum, V2α axons are concentrated in SIP/SLP in immediate vicinity to the α2 lobe (see Aso et al., 2014a; Séjourné et al., 2011), which is where we imaged from (cp. Figure 5.3D). While some V2α′ processes may have thus also been sampled by our odour imaging, the majority of calcium signals was probably taken from V2α.

Another possible explanation for the seemingly silent MVP2 → V2 synapse might be found in the receptor composition. While both M4/6 and V2 neurons seem to express the $GABA_A$ subunit Rdl, V2 neurons also likely express $GABA_BR1$ and $GABA_BR2$ (Crocker et al., 2016, Figure S5). $GABA_B$ receptors are metabotropic GPCRs that can be involved in a wide range of secondary signalling that can

modulate neural activity and behaviour (see Dzitoyeva et al., 2003; Hamasaka et al., 2005; Manev and Dzitoyeva, 2010). They are widely co-expressed together with Rdl in the fly brain, except for the MB lobes where no $GABA_B$ immunoreactivity was found (Enell et al., 2007). MVP2 → V2 synapses, however, would be largely at the edges of the MB where most MBON axons begin (Aso et al., 2014a; Perisse et al., 2016). Although little is still known about the function of $GABA_B$ receptors in the *Drosophila* brain, it is possible that they might mediate differential effects of GABA stimulation through MVP2.

5.3.5 Comparison with MV2

Another MBON interneuron has been recently described (Aso et al., 2014a; see also Ito et al., 1998 and Tanaka et al., 2008 for earlier anatomical descriptions). The glutamatergic MV2 neuron receives input from the β1 compartment, and sends projections onto the α lobe (Aso et al., 2014a). MV2 mostly targets MBONs of the α lobe, but also makes presynaptic contacts with KCs and MVP2 (Takemura et al., 2017). In fact, while MV2 has 21 presynaptic contacts with MVP2, there are only 6 contacts the other way around (Takemura et al., 2017), suggesting a hierarchy in which MV2 seems upstream of MVP2. Compared to MVP2, MV2 has almost thrice as many presynaptic contacts with V2 and almost double as many with V3 (MBON-α3) (Takemura et al., 2017), establishing a stronger input to α lobe MBONs than MVP2. Since MV2 uses glutamate as a neurotransmitter (Aso et al., 2014a), its inputs to V2 could be either excitatory, inhibitory, or modulatory (see Littleton and Ganetzky, 2000; Liu and Wilson, 2013; Parmentier et al., 1996).

Interestingly, MV2 terminals onto MBON-α1 were also found closest to the MBON's axon (Takemura et al., 2017), suggesting a common motif for MBON interneurons to target this region to exert their effects. Functionally, MV2 shows interesting and unique odour response characteristics: it is the only neuron that responds only minimally during early odour trials, but responds very strongly during later repeated odour trials (Hattori et al., 2017, Figure 4B). This suggests a potential role in the sensitisation to stimulation, that would be passed on

to MBONs by successively increasing excitation/inhibition, possibly leading to sensitisation/habituation responses of α MBONs. Future studies should investigate the nature of such a connection to see how other MBON interneurons interact with downstream MBONs.

MP1 and MVP2 for aversive reinforcement

Besides their role in hunger state-dependent LTM consolidation, MP1 neurons also convey direct aversive reinforcement sufficient for aversive STM. Artificial thermogenetic activation of MP1 neurons during odour presentation results in robust aversive STM to that odour, and blocking MP1 during shock pairing resulted in impaired aversive STM and MTM (Aso et al., 2012). Physiologically, optogenetic activation of MP1 neurons during odour presentation results in synaptic long-term depression (LTD), presumably the basis for aversive memory (Hige et al., 2015a). MP1 neurons have also been implicated in active forgetting (Berry et al., 2012).

These neurons also show enhanced slow oscillations at about 0.1 Hz after spaced aversive training, which is required to form LTM (Plaçais et al., 2012). Interestingly, severely starved flies show a significant decrease of these MP1 oscillations, implicating that strong hunger blocks LTM formation via suppression of MP1 oscillations (Plaçais et al., 2013a). Artificially activating MP1 in starved flies between training trials restored LTM formation, but also led to premature death of these flies (Plaçais et al., 2013a). This may be because spaced training and subsequent MP1 signalling to KCs leads to an increased mitochondrial energy flux through DAMB receptors (Plaçais et al., 2017). Such an increase in energy metabolism might be necessary for aversive LTM formation, and leads flies to take up more sucrose (Plaçais et al., 2017).

Similar to the role of its dopaminergic counterpart MP1, MVP2 neurons were found to be required for immediate and 2h aversive olfactory memory, as well as immediate aversive visual memory (Aso et al., 2014b; Ueoka et al., 2017). Indeed, after both artificial odour-pairing with MP1 and training-induced aversive learning, MVP2 activity was found to be depressed (Hige et al., 2015a; Perisse et al., 2016), suggesting MP1-induced synaptic depression of the KC–MBON synapse as the

physiological correlate of an aversive STM (Hige et al., 2015a; Perisse et al., 2016). In line with this, activating MVP2 neurons actually drives approach behaviour (Aso et al., 2014b), so that a decreased drive to MVP2 after aversive learning actually leads to diminished approach behaviour.

Interestingly, blocking MVP2 activity during odour presentation induces an aversive memory of that specific odour (Ueoka et al., 2017). This suggests that MVP2 neurons can act upstream of aversively reinforcing DANs. This might be through contralateral projections into the core of the peduncle that is innervated by MP1 (Aso et al., 2014a), by ipsilateral projections to PPL1 dendritic regions (although these seem sparse; see Takemura et al., 2017), or by secondary effects from MVP2 → MBON → DAN connections (see chapter 6).

5.3.6 A model of hunger-dependent retrieval

Hunger signals were previously shown to be signalled to the MB via dS6K activity in DILP neurons that inhibits dNPF neurons that, in turn, inhibit MP1 DANs (Krashes et al., 2009; Wu et al., 2005a). MP1 inhibits MVP2 activity, leading to increased MVP2 responses in starved flies (Hige et al., 2015a; Perisse et al., 2016). Artificial activation of MVP2 leads to approach behaviour (Aso et al., 2014b).

Our data here shows that MVP2 neuron activity acutely decreases odour-evoked calcium signals in M4/6 axons, either when directly stimulated or in a state of starvation. M4/6 neurons guide avoidance behaviours when activated (Aso et al., 2014b), and 'permit' approach behaviours when blocked (Barnstedt et al., 2016; Owald et al., 2015a) or after learning-induced synaptic depression (Owald et al., 2015a). Retrieval of appetitive memory, and therefore approach of a previously trained odour requires M4/6 neurons and flies to be in a hungry state (Krashes et al., 2009; Owald et al., 2015a). See also Figure 5.6 for a circuit model of hunger-dependent memory retrieval.

Interestingly, M4/6 neurons were also found to be required for the expression of aversive memories, and odour-evoked calcium responses shown to be increased after aversive training (Bouzaiane et al., 2015; Owald et al., 2015a). However, if M4/6

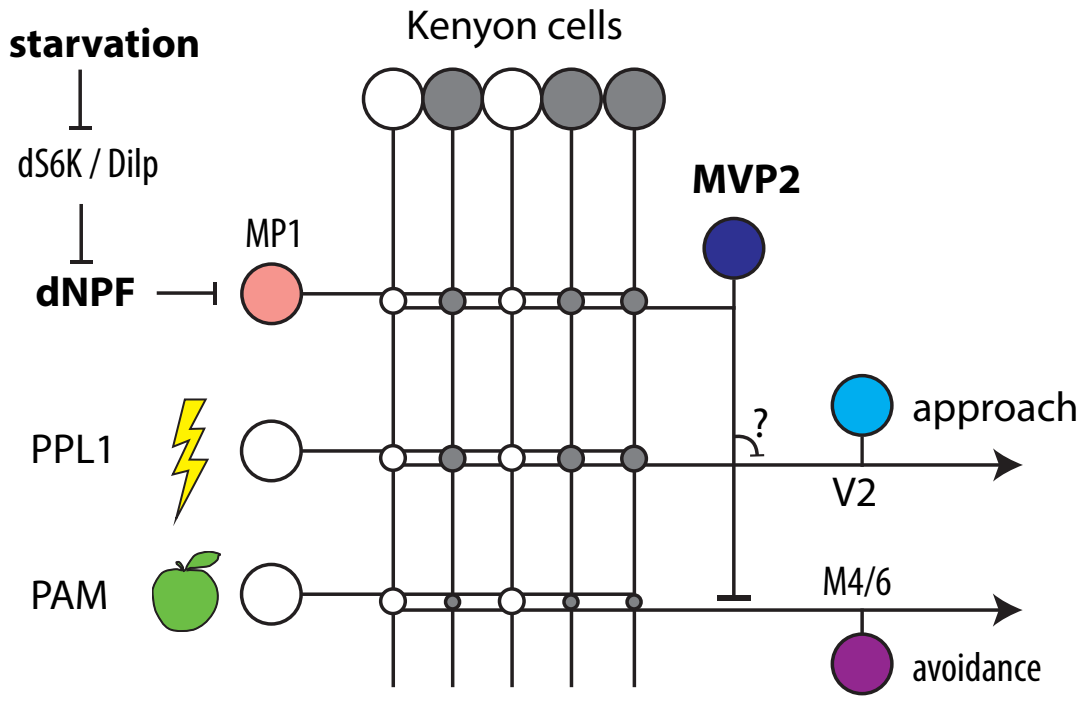


Figure 5.6: Circuit model of hunger-dependent appetitive memory retrieval. Starvation (enhanced activity indicated by bold font) inhibits dS6K activity in Dilp neurons. This disinhibits dNPF neurons that, in turn, inhibit MP1 activity. Decreased MP1 activity releases suppression of MVP2 neurons, so that hungry animals show greater MVP2 activity. MVP2 neurons make synapses onto V2 approach-coding and M4/6 avoidance-coding MBONs, but only those to M4/6 are found to effectively inhibit neuronal activity. After appetitive training, KC → M4/6 synapses are depressed, leading to less CS^+ odour-evoked activity. Starvation-induced MVP2 inhibition on M4/6 neurons thus further depresses the MBON avoidance arm, and favours activity of approach-coding MBONs.

neurons receive dopaminergic input only from reward-coding PAM neurons that drive synaptic depression (Aso et al., 2014a; Owald et al., 2015a), how could aversive learning induce a potentiation of responses? The answer may be that aversive learning triggers synaptic depression at the KC → MVP2 synapse (Hige et al., 2015a), which in turn disinhibits M4/6 neurons, thus leading to elevated responses (see Perisse et al., 2016). A similar mechanism could also explain the training-induced facilitation observed in V3 (Plaçais et al., 2013b), which could possibly be mediated by the glutamatergic MV2 neuron (see connectivity in Takemura et al., 2017).

Similarly, it is conceivable that the induction of strong aversive memories that has been previously observed after artificial MP1 activation (Aso et al., 2012,

2010; Hige et al., 2015a) is partly mediated by a decrease of MVP2 inhibition on M4/6, although other synaptic targets of MVP2 in and outside the MB lobes could also play a role to guide avoidance behaviour. Future connectomics data on the horizontal lobe (cp. Eichler et al., 2017; Takemura et al., 2017; Zheng et al., 2017), and MBON downstream synapses (see Dolan et al., 2017) should soon advance our understanding of these processes further.

Finding that hunger state signals reach MBONs via a GABAergic MBON interneuron ties together the neural circuits that represent state and those that drive learned behaviour, and suggests that neural circuits relying on disinhibition may be a common network motif to guide memory expression (see also Letzkus et al., 2015).

6

Neural circuit mechanisms of extinction and reconsolidation

Contents

6.1 Background 223
6.1.1 Extinction 224
6.1.2 Reconsolidation 229
6.2 Results 232
6.2.1 Driver line access 232
6.2.2 Functional connectivity between V2 and DANs 232
6.2.3 Functional connectivity between M4/6 and PAM neurons 237
6.2.4 MBON-$\gamma 2\alpha'1$ excites several DANs for reconsolidation . 240
6.2.5 MBON-$\gamma 2\alpha'1$ carries a CS^--specific memory trace . . . 245
6.3 Discussion 249
6.3.1 Results summary 249
6.3.2 Functional connectivity between V2 and PPL1 251
6.3.3 Functional connectivity between V2 and PAM 255
6.3.4 M4/6 – PAM interplay 256
6.3.5 MBON-$\gamma 2\alpha'1$ carries a CS^- memory trace 261
6.3.6 Updating memories through MBON–DAN interplay . . 262

6.1 Background

Animals need to constantly re-assess previously learned associations, as changes in their environment may lead memories to become maladaptive over time. Two

updating mechanisms have been frequently studied over the last decades: extinction and reconsolidation.

6.1.1 Extinction

Extinction describes the process of reducing a learned response to a stimulus by repeated presentation of the CS alone, without the US (Pavlov, 1927). Often thought to be related to forgetting, extinction is now widely accepted as a new kind of learning that forms a parallel and competing memory trace to the original memory (see Bouton, 1993; Suzuki et al., 2004). This distinction from forgetting is based on the fact that the original memory can either spontaneously recover, or return after a change in context or presentation of the US (Bouton, 1993; Konorski, 1967; Pavlov, 1927; Rescorla and Heth, 1975).

In mammals, neuronal networks including the amygdala, the medial prefrontal cortex (mPFC), and the hippocampus are involved in fear extinction (see review in Tovote et al., 2015). Extinction learning is thought to largely occur in the basolateral amygdala (BLA) where subpopulations of neurons project to different regions inside the mPFC: those coding for fear memories project to the prelimbic cortex, and those coding for extinction memories project to the infralimbic cortex (IL) (Senn et al., 2014). Extinction training induces NMDAR-dependent plasticity in the IL (Burgos-Robles et al., 2007; Milad and Quirk, 2002), and projections from the IL to the medial central amygdala and its brainstem-targeting output neurons are required for the retrieval of extinction memories (Milad and Quirk, 2002; Quirk et al., 2003).

Extinction in *Drosophila*

Drosophila melanogaster can also undergo extinction learning. Already in the first published study on aversive associative learning in *Drosophila* was it noted that repeated presentation of previously trained flies to the CS alone (in this case the odour octanol) reduced the learned response to near zero within 7–10 presentations (Dudai, 1977b; Quinn et al., 1974). In the aversive conditioning protocol introduced by Tully and Quinn (1985), extinction learning also occurred

but at a much slower rate, so that after 20 extinction cycles about half of the original memory score still persisted.

While the aforementioned studies largely used extinction learning to support their newly established training protocols, Schwaerzel et al. (2002) were the first to explore the mechanisms behind extinction in more detail. In their protocol, they used five CS^+ re-exposures following aversive training, and found a 40 % performance reduction when tested 30 min after training, compared to flies exposed to five CS^- re-exposures (Schwaerzel et al., 2002). Interestingly, both *rut* mutants as well as flies in which KC neurotransmission was temporarily blocked by shi^{ts1} during training and extinction showed extinction learning after CS^+ presentation (Schwaerzel et al., 2002). Synaptic output from AL PNs, however, was still required for extinction to occur (Schwaerzel et al., 2002). These findings suggest that extinction learning happens via a *rut*-independent pathway that involves PN output, but not KC output (Schwaerzel et al., 2002).

Based on the fact that both original learning as well as extinction learning do not require KC synaptic output (Dubnau et al., 2001; McGuire et al., 2001; Schwaerzel et al., 2002), Schwaerzel et al. (2002) argue that this means extinction must be an intracellular process that antagonises synaptic changes that were established during training (Schwaerzel et al., 2002). This would be in contrast to extinction relying on interneuronal circuit processes.

A subsequent study also found that five cycles of CS^+ re-exposure (coined "intense reactivation") resulted in memory extinction of both LTM and ARM (Lagasse et al., 2009). Here, the authors used mechnical shock for the US, reactivation after 24 hours, and tested the flies after another 24 hours (Lagasse et al., 2009). Interestingly, when flies were fed cyclohexamide (CXM) before reactivation to block protein synthesis (see 1.3.2), no memory defects were visible, suggesting that this form of extinction learning relies on *de novo* protein synthesis (Lagasse et al., 2009).

Another study by Qin and Dubnau (2010) used a 24 hour protocol with electric shock as US, in which the CS re-exposure occurred immediately before testing.

Here, 5 cycles of re-exposure did not lead to significant extinction, but 15–30 cycles of re-exposure did (Qin and Dubnau, 2010). As before, both ARM as well as LTM could be extinguished, independent of the memory mutations *rut*, *rugose*, *dNR1*, or *rad* (Qin and Dubnau, 2010).

Appetitively trained flies can also undergo extinction learning: a mere 30 second exposure to the unreinforced CS was sufficient to extinguish the learned response to a CS previously paired with a sucrose reward (Tempel et al., 1983).

A novel protocol to investigate extinction

In order to study the neural circuit mechanisms underlying extinction learning in more detail, Felsenberg et al. (2017) developed a novel robust protocol for the extinction of appetitive memories. Flies were first presented for 2 min with an unpaired CS^- odour, followed by another 2 min with a CS^+ odour paired with sucrose (see Krashes and Waddell, 2008; Tempel et al., 1983; Figure 1.1C). This training protocol is known to induce a long-lasting reward memory (Krashes and Waddell, 2008). After three hours, flies were re-exposed to two cycles of CS^-, CS^+, a novel odour, or air (Felsenberg et al., 2017). After another three hours, flies were then tested in a T-maze to choose between the CS^+ or CS^- odour (see Krashes and Waddell, 2008; Tempel et al., 1983; Tully and Quinn, 1985).

Importantly, only CS^+ re-exposure, but not that of CS^-, novel odour, or air led to a complete loss of memory performance when tested three hours after re-exposure (Felsenberg et al., 2017). This extinction learning occurred irrespective of odour identity, as both OCT/MCH as well as IAA/EB odour pairs could be extinguished by this protocol (Felsenberg et al., 2017). Furthermore, both a single re-exposure cycle as well as three re-exposure cycles resulted in robust memory extinction, and LTM could also be shown to be extinguished by this protocol (Felsenberg et al., 2017). These findings again support the idea that *Drosophila* can undergo extinction learning, and provide a robust protocol that allows for the probing of the neural circuitry underlying extinction learning.

DAN involvement

Reward memories are acquired through coincident activity of CS–coding KCs and US–coding dopaminergic PAM neurons (Burke et al., 2012; Liu et al., 2012; see also 1.3.3). Extinction learning, however, was still intact after synaptic transmission from PAM neurons was thermogenetically blocked during the reactivation phase (Felsenberg et al., 2017). Extinction was impaired, however, when aversive US–coding dopaminergic PPL1 neurons (see 1.3.2) were blocked during reactivation with the CS^+ (Felsenberg et al., 2017). This effect was specific, as neither the blocking of PPL1 neurons without CS reactivation, nor the blocking of PPL1 neurons during novel odour presentation, nor the blocking of PPL1 neurons during preexposure had any effect on memory extinction (Felsenberg et al., 2017).

MBON involvement

PPL1 neurons provide dopaminergic modulation to MB compartments of the vertical lobe that are largely occupied by MBONs of the V2 cluster (Aso et al., 2014a; Tanaka et al., 2008). In line with their shared anatomy, V2 MBONs labelled by the MB052B driver were also found to be required for memory extinction, while other approach-coding MBONs such as MVP2 were not required for extinction (Felsenberg et al., 2017). V2 neurons were also found to be dispensable for appetitive memory retrieval after 3 hours (Felsenberg et al., 2017), suggesting that these MBONs play a distinct role in appetitive memory extinction besides their established role in aversive memory retrieval (Aso et al., 2014b; Séjourné et al., 2011).

Extinction of aversive memories

As has been found earlier (Lagasse et al., 2009; Qin and Dubnau, 2010; Schwaerzel et al., 2002), aversive memories can also be extinguished by repeated exposure to the CS^+. The neural substrates for this, besides a requirement of synaptic transmission from AL PNs (Schwaerzel et al., 2002), remain unknown so far.

Recent studies in our lab, using a previously established extinction protocol (Felsenberg et al., 2017), however, point to a requirement of dopaminergic PAM

neurons and M4/6 MBONs (Felsenberg et al., *in preparation*). This suggests that avoidance-coding MBONs and rewarding DANs are required for the extinction of aversive memories, whereas approach-coding MBONs and punitive DANs are required for the extinction of appetitive memories.

Open questions

Previous experiments in our lab show a specific requirement for dopaminergic PPL1 neurons and cholinergic V2 MBONs for the extinction of appetitive memories (Felsenberg et al., 2017). Reward memories in the MB network are encoded as MBON imbalance that yields relatively stronger drive from approach MBONs of the vertical lobe (Owald et al., 2015b). It is thus hypothesised that relatively stronger drive from V2 MBONs during extinction may drive PPL1 DANs that are known to induce aversive memories (Claridge-Chang et al., 2009; Riemensperger et al., 2005; Schwaerzel et al., 2003). Reward extinction memories might thus be encoded similarly to aversive memories. However, it is currently unknown if V2 MBONs are functionally connected to PPL1 DANs to fulfill this role, despite anatomical evidence that would support this (Aso et al., 2014a). Therefore, I set out to test the functional connectivity from cholinergic V2 MBONs to PPL1 DANs (6.2.2).

Conversely, aversive memories are coded as MBON imbalance that yields relatively stronger drive from horizontal lobe MBONs such as M4/6 (Owald et al., 2015a; Owald and Waddell, 2015). As M4/6 MBONs and PAM DANs are implicated in the extinction of aversive memories, it may thus be hypothesised that relatively stronger drive from M4/6 neurons to PAM neurons during the extinction phase may induce an aversive extinction memory. This, however, would require functional connectivity between M4/6 and PAM. Such a connection would be supported by anatomical evidence (Aso et al., 2014a; Owald et al., 2015a), and previous studies show some evidence for this (Cohn et al., 2015), albeit with pharmacological manipulations. I have thus set out to test the functional connectivity between M4/6 and PAM neurons using optogenetics (6.2.3).

6.1.2 Reconsolidation

Reconsolidation in vertebrates and invertebrates

If the incongruency between an expected outcome and the actual outcome is only small, the initial memory trace may undergo reconsolidation instead of extinction (Díaz-Mataix et al., 2013; Pedreira et al., 2004). Reconsolidation describes the process by which a memory trace, previously labilised from retrieval, is being stabilised again – a process dependent on *de novo* protein synthesis (see Dudai, 2006; Nader et al., 2000).

Reconsolidation has also been previously observed in insects: Honey bees can be trained to associate an odour with a reward by bringing sucrose into contact with the bee's antennae during odour presentation. After successful training, this conditioning protocol leads bees to extend their proboscis to the CS^+ in expectation of a sucrose reward (see Menzel and Müller, 1996).

Recent studies could show that after initial training, reconsolidation processes could only be triggered after the presentation of five consecutive CS trials, but not after a single trial (Stollhoff et al., 2005). Furthermore, it was suggested that this reconsolidation of reward memories occurs independently from the action of ACh, as mecamylamine injection did not seem to interfere (Dacher et al., 2005).

In *Drosophila*, one previous study suggested that three cycles of reactivation were necessary to induce reconsolidation of aversive memories, and that this process requires *de novo* protein synthesis (Lagasse et al., 2009).

Despite these studies, the neural systems mediating reconsolidation have remained obscure thus far.

CS^--triggered reconsolidation

CS^--triggered reconsolidation was recently demonstrated in *Drosophila melanogaster* (Felsenberg et al., 2017): Flies were appetitively trained by first presenting an unpaired CS^- odour for two minutes before pairing a CS^+ odour with a sucrose reward for another two minutes (Krashes and Waddell, 2008; Tempel et al., 1983). After three hours, flies were re-exposed twice to the CS^- before receiving a brief cold

shock (Felsenberg et al., 2017). This cold-shock anaesthesia is known to interfere with labile memory (Krashes and Waddell, 2008). When tested after another three hours, flies that underwent cold shock after CS^- reactivation demonstrated a loss of memory, while flies that only underwent cold shock or CS^- reactivation alone showed normal memory performance (Felsenberg et al., 2017). This effect of cold-shock anaesthesia was not only apparent when induced immediately after CS^- reactivation, but also 30 minutes afterward, but not 90 minutes after reactivation (Felsenberg et al., 2017). Similarly, 24 h LTM was also affected by this procedure (Felsenberg et al., 2017). These findings suggest that the presentation of a CS^- odour can reactivate a previously established associative memory, and brings it into a labile state that lasts for at least 30 minutes after reactivation (Felsenberg et al., 2017).

DAN involvement

What are the neural mechanisms underlying these reconsolidation processes? Using the previously established protocol combined with thermogenetic blockade of synaptic transmission, Felsenberg et al. (2017) could show that blocking dopaminergic PPL1 neurons during the CS^- reactivation phase resulted in a loss of memory when tested three hours later, whereas a block of dopaminergic PAM neurons had no such effect. Simply blocking PPL1 neurons during the reactivation phase without presenting an odour, however, had no impact on later memory performance, suggesting a specific requirement of PPL1 neurons in the reconsolidation of reward memories (Felsenberg et al., 2017). More specifically, the MV1 DAN was found to be required for this process, while other PPL1 DANs (MP1, V1, PPL1-α3, and PPL1-α'3) were found to be dispensable (Felsenberg et al., 2017). Blocking MV1 DANs shortly after reactivation did not impair reconsolidation, and MV1 DANs were not required during the retrieval of 3 h memories (Felsenberg et al., 2017). This suggests that MV1 DANs are specifically required during CS^--triggered reconsolidation.

Does the CS^- reactivation only affect the mnemonic representation of the CS^-, or does CS^- reactivation render both CS^+ and CS^- representations labile? Intriguingly, CS^- reactivation does indeed seem to render the CS^+ representation labile, as MV1

block during CS^- reactivation results in memory loss when flies are later tested to choose between CS^+ and a novel odour (Felsenberg et al., 2017).

MBON involvement

What drives MV1 activity during CS^- reactivation? Anatomy suggests a potential feedback loop between MV1 and its respective MBON-$\gamma2\alpha'1$ that innervates the same compartment (Aso et al., 2014a). Indeed, synaptic output from MBON-$\gamma2\alpha'1$ is required for reconsolidation during CS^- reactivation, but not immediately after, while other related MBONs such as MVP2 have no effect on reconsolidation (Felsenberg et al., 2017). This suggests that both MBON and DAN of the $\gamma2\alpha'1$ compartments play a role in the reconsolidation process, presumably by MBON-$\gamma2\alpha'1$ stimulation of MV1.

Open questions

While MBON-$\gamma2\alpha'1$ has cholinergic terminals that overlap with MV1 dendrites (Aso et al., 2014a), it is not yet clear if and how the two neurons are functionally connected. Furthermore, as PAM neurons are required for later stages of reconsolidation (Felsenberg et al., 2017), it is possible that they might also receive input from MBON-$\gamma2\alpha'1$, as suggested by their anatomy (Aso et al., 2014a). I have thus set out to optogenetically test the functional connectivity from MBON-$\gamma2\alpha'1$ to MV1 and PAM neurons (6.2.4).

If MBON-$\gamma2\alpha'1$ is responsible for CS^--triggered reconsolidation by DANs, it likely possesses a "memory trace" of the CS^- that differs from that of a novel odour, as only CS^- reactivation induces the reconsolidation process (Felsenberg et al., 2017). In order to test this question, I imaged odour responses to CS^+, CS^-, and novel odours in MBON-$\gamma2\alpha'1$ neurons after appetitive training (6.2.5).

6.2 Results

6.2.1 Driver line access

Precise dissection of neural circuits requires genetic tools that allow the manipulation of specific neurons while leaving other neurons undisturbed. Therefore, we have screened and confirmed the expression pattern of various MBON and DAN GAL4 and LexA driver lines (see Figure 6.1 and Table 2.1). Especially LexA lines are generally rarer and harder to find, but vital to study functional connectivity.

6.2.2 Functional connectivity between V2 and DANs

To experimentally test if V2 MBONs are functionally connected to PPL1 DANs, I used different LexA driver lines to express lexAop-CsChrimson-tdt to render them red light-sensitive. I chose the red-shifted channelrhodopsin CsChrimson because it is specifically activated by red light, so as to facilitate simultaneous calcium imaging with minimal light interference of the imaging laser with the channelrhodopsin (see also 1.5.4). Simultaneously, I used GAL4 drivers to drive GCaMP6f in PPL1 neurons in order to obtain an optical readout of calcium activity in PPL1 neurons. After housing flies for several days on retinal food, I would then dissect explant brains that would be imaged under a two-photon microscope and stimulated by a red light LED (for full methods description, see 2.4).

V2 neurons activate PPL1 DANs

I used three different LexA driver lines expressing CsChrimson-tdt in different sets of V2 MBONs to different degrees (see Figure 6.1K,N,O). GCaMP6f was expressed in four PPL1 neurons using the MB504B driver line (see Figure 6.1G). I focused the imaging field of view (FOV) on one prominent cell body located laterally of two large proximal cell bodies. I did not image from dendritic/axonal sites in or around the MB, as both axons and dendrites from V2 and PPL1 are largely overlapping (Aso et al., 2014a; Tanaka et al., 2008), which could have caused inadvertent CsChrimson stimulation from the imaging laser light (personal observations; personal communication with A. Wong, 1.6.2015).

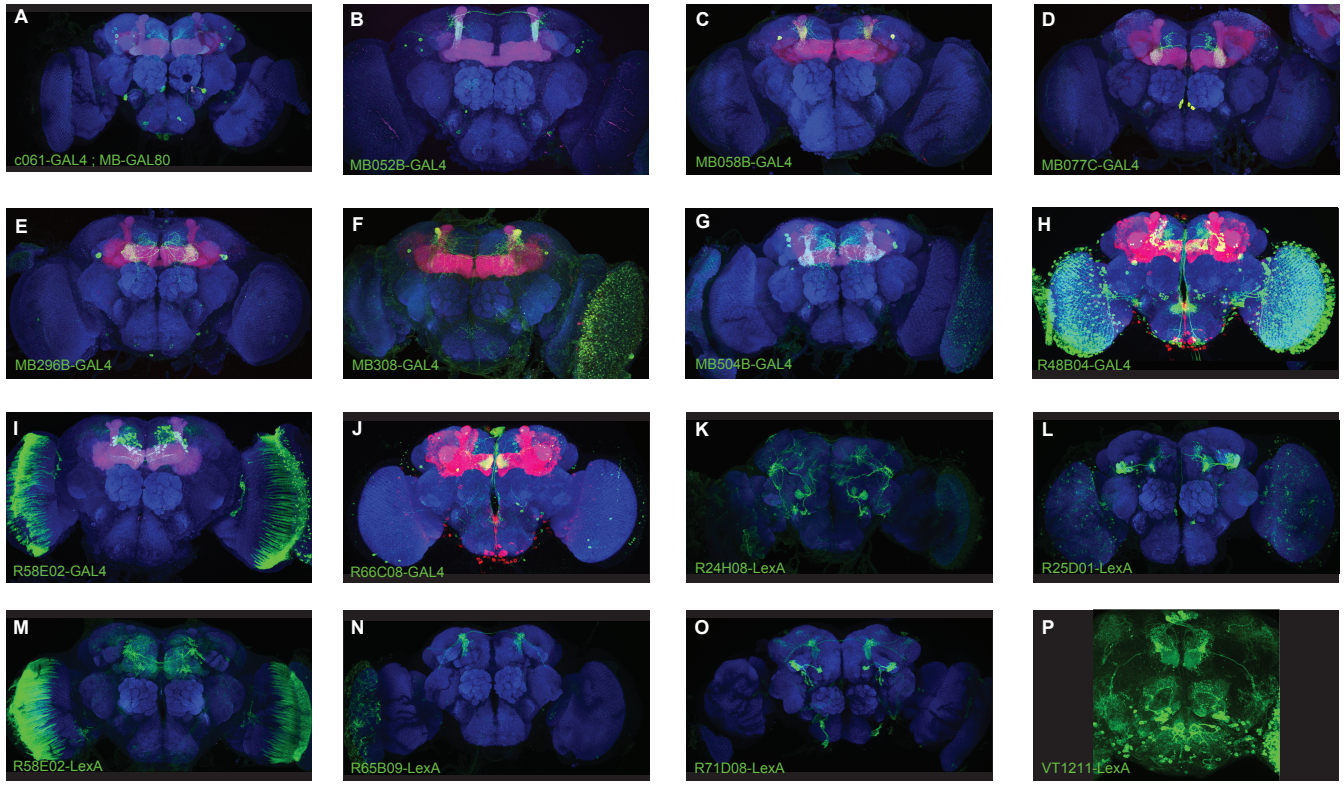


Figure 6.1: Anatomy of driver lines used for extinction and reconsolidation experiments. Panels A-J show GFP expression driven by the relevant GAL4 (green), LexA-driven RFP expression in mushroom body Kenyon cells (red) and general neuropil stained with an antibody to the Bruchpilot presynaptic marker (blue). A) c061-GAL4;MBGAL80 labels MB-MP1 neurons. B) MB052B-GAL4 labels MBON-α′1, V2α, MBON-α2p3p, and V2α′. C) MB058B-GAL4 labels MB-V1 neurons. D) MB077C-GAL4 labels MBON-γ2α′1. E) MB296B-GAL4 labels MB-MV1 neurons. F) MB308B-GAL4 labels PPL1-α′3 and displays weak expression in PPL1-α3. G) MB504B-GAL4 labels MB-MP1, MB-MV1, MB-V1 and PPL1-α3. H) R48B04-GAL4 labels PAM-γ5, PAM-γ4, and PAM-β′2amp. I) R58E02-GAL4 broadly labels rewarding DANs in the PAM cluster. J) R66C08-GAL4 labels M6 MBONs. Panels K-P show GFP expression driven by the relevant LexA (green) and general neuropil stained with an antibody to the Bruchpilot presynaptic marker (blue). K) R24H08-LexA labels MBON-α′1 and V2α′. L) R25D01-LexA labels MBON-γ2α′1. M) R58E02-LexA labels broadly labels rewarding DANs in the PAM cluster. N) R65B09-LexA labels MBON-α′1, V2α, MBON-α2p3p, V4, and V2α′. O) R71D08-LexA labels V2α and V2α′. P) VT1211-LexA labels M6 and M4β′ MBONs. Note that images H and J are derived from stacks made freely available by the FlyLight project (HHMI Janelia Research Campus). Image P was kindly provided by E. Perisse. Partly adapted from Felsenberg et al. (2017).

Optogenetic stimulation with 500 ms pulsed red light resulted in rapid calcium increases in this PPL1 cell body when stimulated with CsChrimson driven by R65B09-LexA (Figure 6.2A), R71D08-LexA (Figure 6.2B), and R24H08-LexA (Figure 6.2C). Spaced stimulations with 6 sec ITI resulted in reliable responses to each light pulse. Comparing $\Delta F/F_0$ one second before the first pulse to one second after onset of the first pulse showed statistically significant increases in $\Delta F/F_0$ for all three LexA driver lines (Figure 6.2).

Heterogeneity in PPL1 responses to V2 activation

Interestingly, I not only observed reliable calcium increases to optogenetic stimulation, but also observed some reliable calcium decreases in response to optogenetic stimulation. As relative cell body locations were very stereotypical between brains, I identified three cell bodies that reliably responded to optogenetic stimulation, and a fourth small one that largely remained silent (data not shown). Using R71D08-LexA driven CsChrimson to stimulate MB504B PPL1 cell bodies, I observed calcium responses also in a second cell body, while a third cell body showed reliably inhibitory calcium responses that decreased after light stimulation (Figure 6.3A-D).

As all four cell bodies tightly fasciculate on their trajectory to the MB lobes and surrounding neuropils, it was unfortunately not possible to unambiguously determine the identity of these cell bodies. Instead, I used different specific GAL4 drivers to drive GCaMP6f expression unambiguously in individual PPL1 neuron cell bodies. Out of these, V1 showed the most reliable excitatory calcium responses, suggestive of this being 'cell 1' (Figure 6.3E). No light-triggered calcium responses were visible when flies were not fed retinal (Figure 6.3F). MP1 neurons, on the other hand, showed less reliable and smaller excitatory calcium responses with two lines tested, indicative of this being 'cell 2' (Figure 6.3G-H). The only cell body that showed inhibitory calcium responses was MV1, suggestive of 'cell 3' – this was, however, only found in few cells, while most remained silent (Figure 6.3I). While PPL1-α3 was also expressed in MB504B, at the time of these experiments, no GAL4 line with unambiguous expression in PPL1-α3 could be found, so that

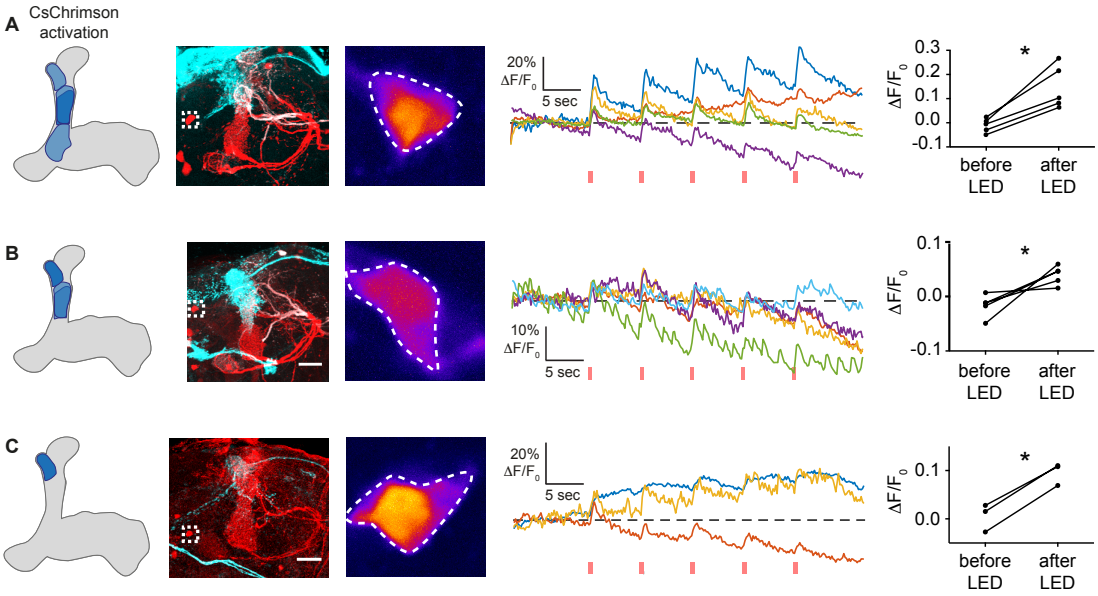


Figure 6.2: Optogenetic activation of V2 MBONs triggers significant calcium responses in a PPL1 neuron cell body. MBONs of the V2 cluster were stimulated with CsChrimson expressed in R65B09-LexA (A), R71D08-LexA (B), or R24H08 (C), and GCaMP6f calcium responses were recorded in MB504B-labelled PPL1 cell bodies. Left two panels show schematics of CsChrimson (blue) and GCaMP6f (red) expression, followed to the right by the respective anatomical confocal maximum projections, scale bar is 20 µm. To the right of this are sample images of the 2P-imaged cell bodies with the ROI used for analysis drawn around as white dashed line. Second from the right are individual calcium transients, each colour representing an individual brain. Horizontal dashed line marks baseline, and light red vertical lines mark the timing of the 500 ms red light, pulsed at 40 Hz and 10 ms. Far right panel shows $\Delta F/F_0$ points from one second before first pulse and one second after pulse onset. All before–after comparisons were significantly elevated (paired t-test, $p < 0.05$, $N = 5$(A), $N = 5$(B), $N = 3$(C)). Adapted from Felsenberg et al. (2017).

these responses could not be determined. A sample trace of PPL1-α′3, however, suggests excitatory calcium responses in PPL1-α′3 (Figure 6.3J).

These findings suggest that V2 MBONs do indeed form a functional connection to PPL1 neurons, activating some PPL1 neurons, and inactivating others. This direct or indirect connection may form the basis for extinction learning as previous behavioural experiments would suggest (Felsenberg et al., 2017).

V2 neurons activate PAM neurons

As PAM neurons represent the opposite arm to PPL1 of the dopaminergic reinforcement system (Burke et al., 2012), I was wondering if V2 MBONs were functionally

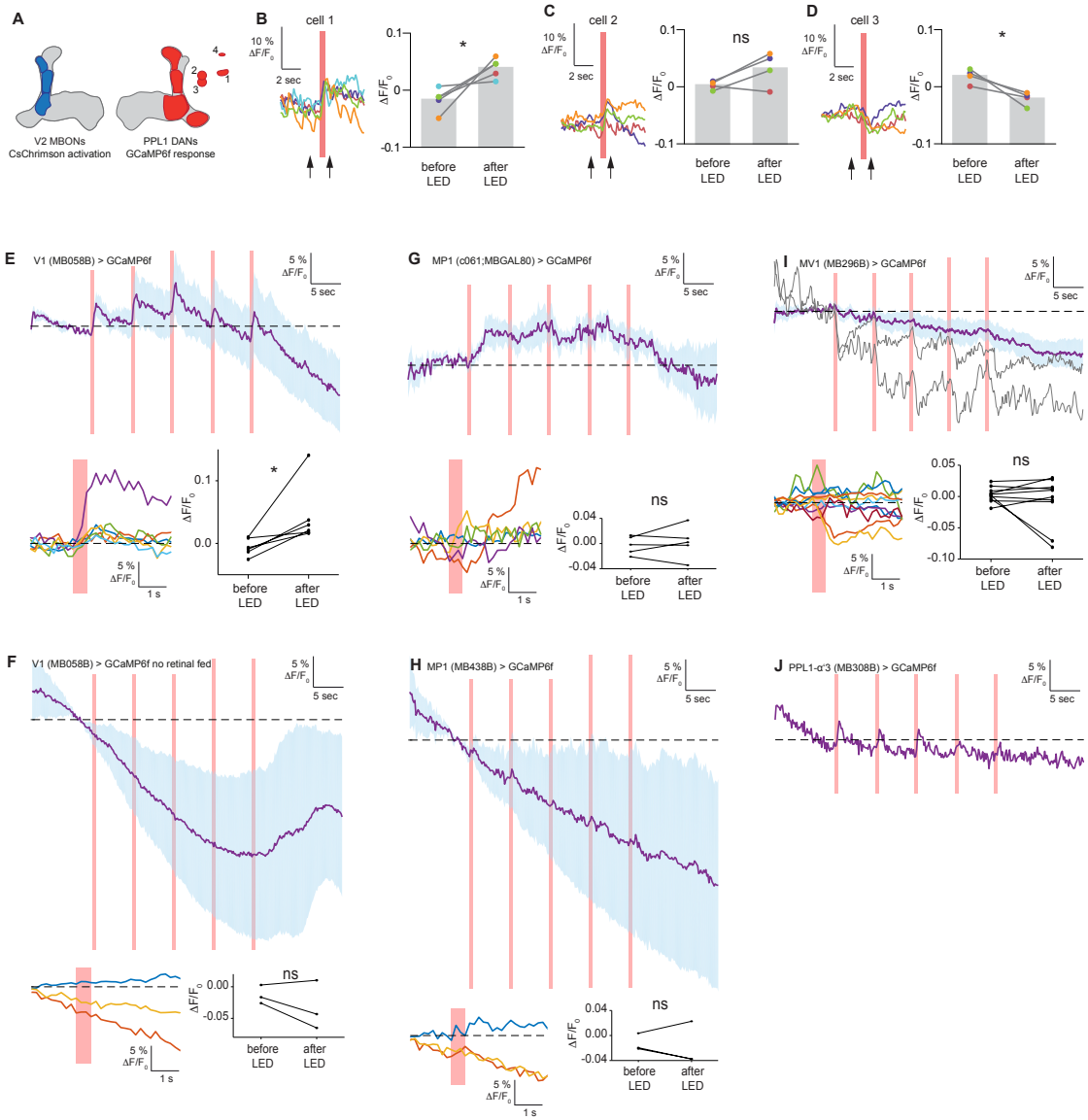


Figure 6.3: Optogenetic activation of V2 MBONs triggers excitatory and inhibitory calcium responses in different PPL1 neurons. A) V2 MBONs were optogenetically stimulated by expressing CsChrimson in R71D08-LexA. PPL1 DAN calcium activity was monitored in explant brains by expressing GCaMP6f in the broad PPL1 line MB504B (B-D) or in more specific single-cell PPL1 driver lines (E-J). MB504B contains four cell bodies with stereotypical anatomical locations, schematically depicted in red; these were numbered 1-4, of which cell 4 was neglected as it showed no calcium responses (data not shown). B) Cell 1 of MB504B PPL1 neurons shows significant calcium responses to light-triggered V2 activation. C) Cell 2 shows a trend towards light-triggered calcium increases that is not statistically significant. D) Cell 3 shows a significant decrease in calcium transients after light-activating V2 neurons. E) Monitoring calcium transients specifically in V1 reveals significant calcium increases after light stimulation. F) Flies without retinal fed show no significant calcium responses in V1 neurons. G-H) MP1 neurons labelled by c061;MBGAL80 (G) or MB438B (H) show no significant calcium responses to light stimulation, although individual traces show some light-triggered calcium increases. I) MV1 neurons show no significant calcium responses, but individual traces (grey lines) show robust calcium decreases upon light stimulation. J) Sample trace of one PPL1-α′3 neuron showing light-triggered calcium responses. Purple traces represent mean; blue shade represents SEM. Asterisks denote significant differences, paired t-test, $p < 0.05$, $N = 3 - 10$. Partly adapted from Felsenberg et al. (2017).

connected also to these DANs. In order to test this, I used R65B09-LexA to drive CsChrimson in V2 MBONs, and R58E02-GAL4 to broadly drive GCaMP6f in PAM neurons. I imaged from different planes of the MB horizontal lobe to capture different compartments with different types of PAM neurons, while avoiding any potential CsChrimson-expressing innervations with the imaging laser.

Interestingly, V2 activation by 500 ms LED light resulted in very strong and large calcium increases in PAM-β1, and smaller less reliable responses in some other compartments (see Figure 6.4). This suggests that V2 can strongly activate both PAM-β1 as well as PPL1 neurons, the function of which can only be speculated on at the moment (see 6.3.3). A role for extinction, however, seems unlikely as blocking PAM neurons during extinction shows no effect on later memory performance (Felsenberg et al., 2017).

6.2.3 Functional connectivity between M4/6 and PAM neurons

M4/6 MBONs feed back to PAM DANs for extinction of aversive memories

M4/6 MBONs and PAM neurons of the horizontal MB lobe are both required for the extinction of aversive memories (Felsenberg et al., *in preparation*), similar to the requirement of V2 MBONs and PPL1 DANs of the vertical lobe for the extinction of appetitive memories (Felsenberg et al., 2017). M4/6 neurons show relatively stronger activity after aversive training (Owald et al., 2015a), while PAM neurons are required and sufficient for reward signalling (Burke et al., 2012; Huetteroth et al., 2015; Liu et al., 2012). Anatomically, M4/6 axon terminals lie in a region innervated by PAM dendrites (Aso et al., 2014a; Owald et al., 2015a). I thus wondered if the extinction of aversive memories relies on M4/6 signalling to PAM neurons. To test such a functional connection, I used VT1211-LexA driven CsChrimson to optogenetically activate M4/6 neurons, and R48B04-GAL4 to drive GCaMP6f in explant brains.

Optogenetic stimulation of M4/6 neurons while monitoring calcium transients in R48B04 PAM neurons shows strong and reliable calcium responses in PAM-γ5 that was statistically significant, while the other compartments showed no clear

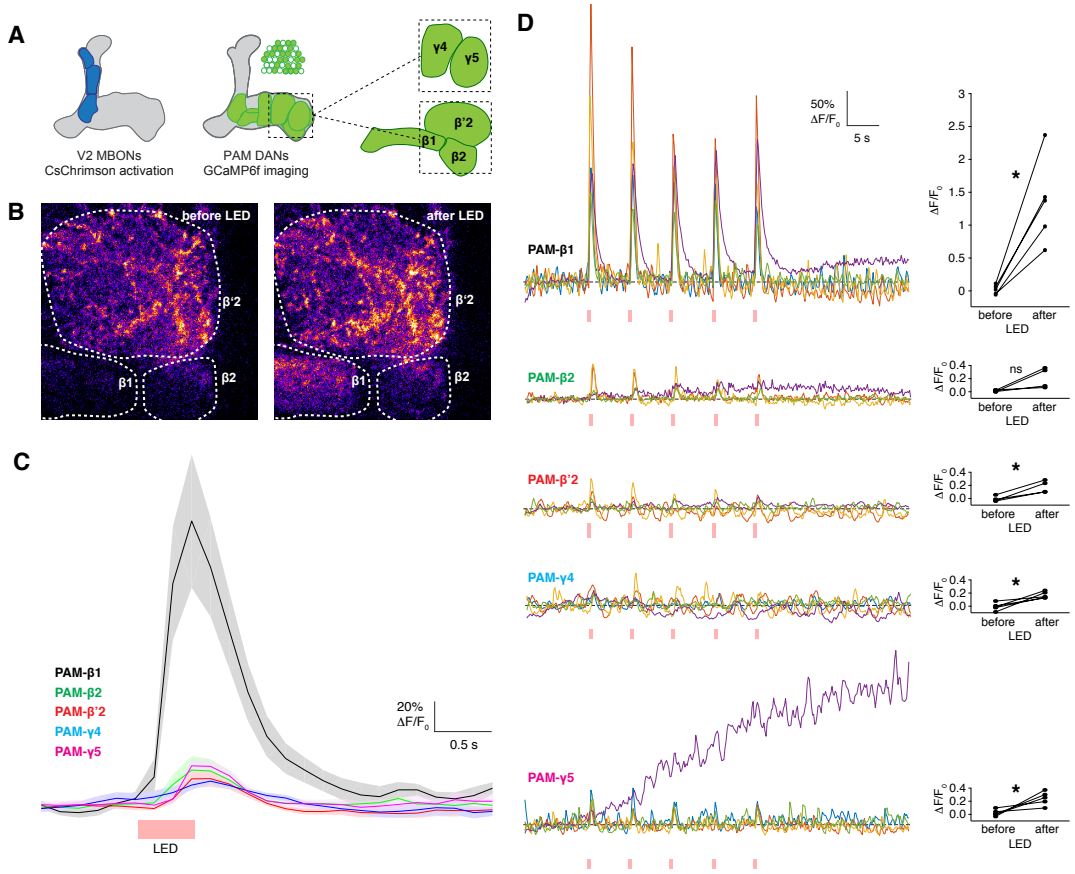


Figure 6.4: Optogenetic activation of V2 MBONs triggers calcium responses in PAM-β1 and other PAM neurons. A) R65B09-LexA driven CsChrimson expression was used to stimulate V2 MBONs, while GCaMP6f was monitored in R58E02-GAL4 driven PAM neurons at different planes to sample several compartments in the same brain. Five explant brains were light-stimulated with 500 ms (40 Hz, 10 ms) LED pulses, and different MB compartments were imaged. B) Sample two-photon images taken on the level of the MB β/β′ tip before and after LED stimulation. Note the strong fluorescence increase in β1. C) Mean calcium responses to V2 light stimulation in different compartments, coded by different colours. PAM-β1 shows very strong responses, while other compartments are also slightly increased. Shade represents SEM. D) Individual calcium transients from 4–5 brains show strong and reliable calcium responses to repeated light-triggered V2 activation in PAM-β1 and also other PAM neurons. Colours of traces represent individual brains. $\Delta F/F_0$ is significantly increased in all PAM neurons except PAM-β2, denoted by an asterisk (paired t-test, $p < 0.05$, $N \geq 4$).

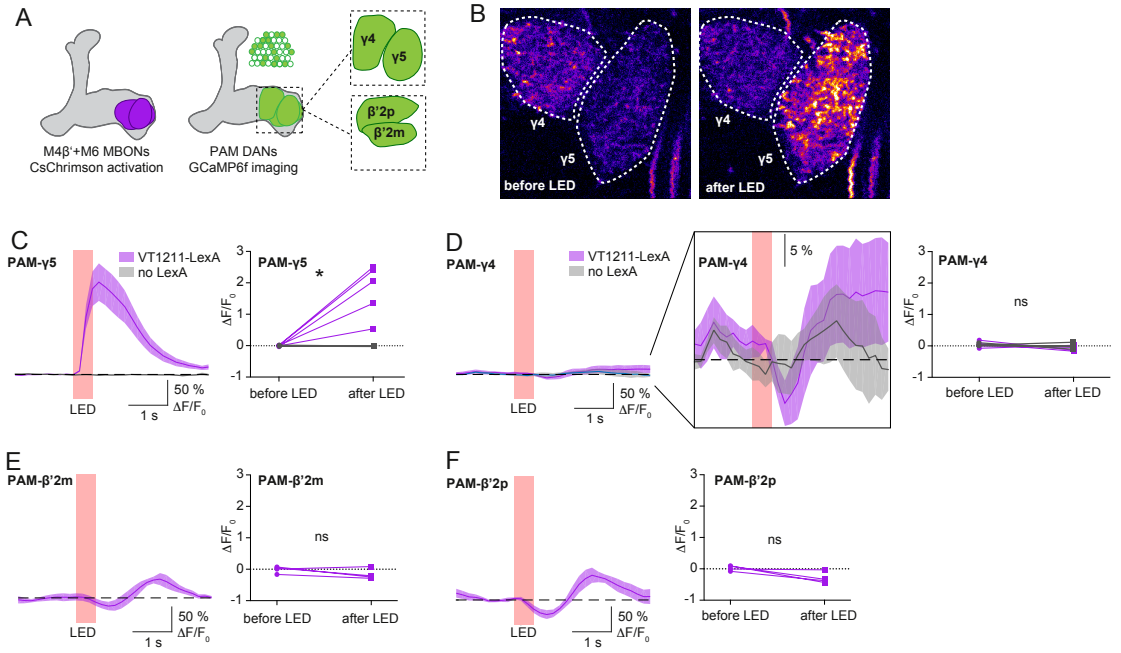


Figure 6.5: Optogenetic activation of M4/6 MBONs triggers calcium responses in PAM-γ5 neurons. Explant brains expressing CsChrimson in VT1211-LexA M4/6 MBONs and GCaMP6f in R48B04-GAL4 PAM neurons were optogenetically stimulated while calcium transients in several MB compartments were monitored. Red LED light triggered elevated calcium responses in PAM-γ5, while PAM-γ4 seems slightly inhibited. PAM-β′2 neurons show biphasic responses. PAM-γ5 responses are significantly increased after LED stimulation (paired t-test, $p < 0.05$, $N = 5$), but not in explant brains lacking the LexA driver (paired t-test, $p < 0.05$, $N = 5$). PAM-γ4 responses are not significantly affected by the LED (paired t-test, $p > 0.05$, $N = 5$).

response (see Figure 6.5). PAM-γ4 showed a mild but insignificant inhibitory response, while PAM-β′2 showed more complex biphasic responses that may be the result of secondary activation. Transients were first mildly decreased towards the end of stimulation, and then showed a mild increase more than one second after the end of stimulation. Flies that lacked the LexA driver, and thus expressed no CsChrimson, showed no calcium responses to the red LED. These findings suggest that M4/6 MBONs do indeed activate some PAM neurons, which may form the neural basis for the extinction of aversive memories.

PAM may exert tonic inhibition on M6 neurons

PAM neurons are known to provide the dopaminergic reinforcement signal required in horizontal lobe compartments to drive reward learning stored as presynaptic

plasticity of KCs (Burke et al., 2012; Owald et al., 2015a). As M4/6 MBONs activate PAM-γ5 neurons (Figure 6.5), we wondered if a positive feedback loop exists that lets PAM neurons also activate M4/6 neurons. To test this question experimentally, I expressed the red-shifted optogenetic activator CsChrimson in R58E02-LexA (see Figure 6.1M) PAM neurons and the calcium indicator GCaMP6f in R66C08-GAL4 (see Figure 6.1J) M6 MBONs, and subjected explant brains to red light stimulation while monitoring calcium transients.

Stimulating PAM neurons optogenetically while monitoring calcium transients in M6 dendrites of the γ5 MB lobe surprisingly yielded no discernible light-triggered calcium responses (see Figure 6.6). Repeated stimulation trials had no effect on the calcium transient at any point. However, it was noted that with the beginning of imaging, the calcium transient baseline rapidly and steadily declined. To test if this might be due to CsChrimson activation, I tested flies that contained no LexA that could drive CsChrimson expression. Interestingly, these control flies showed no light-triggered responses but also no shift in baseline. This suggests that PAM neurons might have no direct effect on M6 MBONs. However, given that R58E02-LexA is a very broad and strong driver line, and CsChrimson is known to be stimulated also by laser light (personal observations; personal communication with Allan Wong, 1.6.2015), it seems reasonable to assume that PAM neurons were activated by the laser light, and are thus responsible for the decline of the baseline. This would suggest that PAM activity actually exerts tonic inhibition on M6 MBONs (see also 6.3.4).

6.2.4 MBON-γ2α′1 excites several DANs for reconsolidation

Both MBON-γ2α′1 as well as its respective DAN, MV1, occupy the γ2α′1 MB compartment, and are required for CS^--triggered reconsolidation of appetitive memories (Aso et al., 2014a; Felsenberg et al., 2017). Besides their overlapping MB zones, MBON-γ2α′1 cholinergic axons also target areas in the SMP where MV1 has

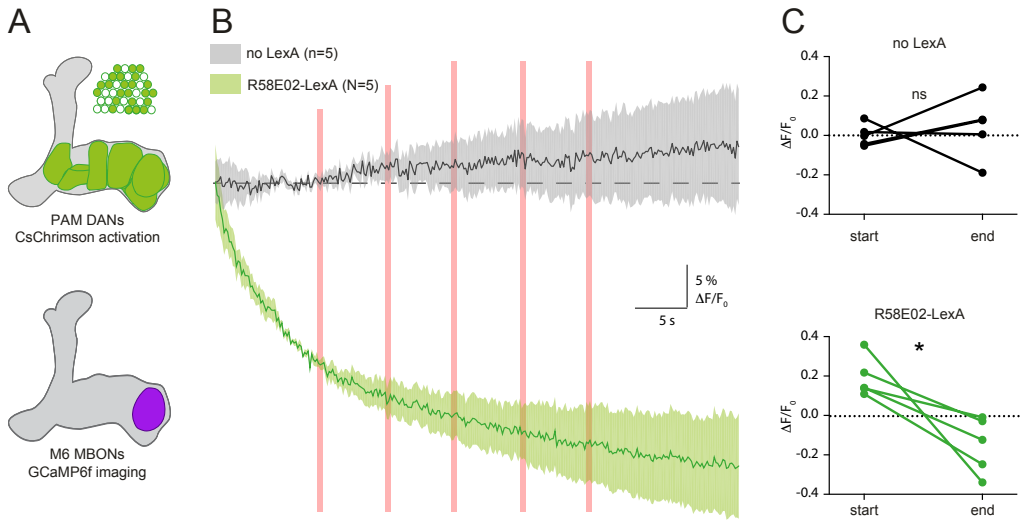


Figure 6.6: Effects of optogenetic activation of PAM neurons on M6 MBONs. A) The optogenetic activator CsChrimson was expressed in R58E02-LexA PAM neurons, while GCaMP6f calcium transients were measured in dendrites of R66C08-GAL4 M6 neurons. B) 500 ms light pulses (red vertical bars) show no discernible effect on calcium transients, but a strong baseline shift is visible from the start of recording in flies carrying R58E02-LexA (green transients), but not in flies lacking the LexA driver (grey transients). Dark lines represent mean calcium transients, and shades represent SEM. C) $\Delta F/F_0$ is not statistically significant between the beginning and end of recording in flies without a PAM LexA driver (paired t-test, $p > 0.05$, $N = 5$), but experimental flies show a significant decrease in $\Delta F/F_0$ (paired t-test, $p < 0.05$, $N = 5$).

dendritic innervation (Aso et al., 2014a). It is thus reasonable to assume that MBON-$\gamma 2\alpha'1$ may activate MV1, and that this functional connectivity forms a necessary part of the neural circuitry underlying reconsolidation. Similarly, PAM neurons are known to have dendritic sites in the SMP, and are required to form reward memories (Burke et al., 2012; Liu et al., 2012). I thus reasoned that MBON-$\gamma 2\alpha'1$ may also activate PAM neurons. To test these potential connections functionally under controlled conditions, I again used CsChrimson optogenetic stimulation in explant brains while reading out downstream activity using the calcium sensor GCaMP6.

MBON-$\gamma 2\alpha'1$ excites its respective DAN MV1

In order to test if MBON-$\gamma 2\alpha'1$ is functionally connected to MV1 I expressed CsChrimson in MBON-$\gamma 2\alpha'1$ using R25D01-LexA (see Figure 6.1L), and GCaMP6f in MV1 using MB296B (see Figure 6.1E). I then monitored calcium transients in

MV1 cell bodies while light-stimulating MBON-γ2α′1. I chose to image from the cell body in order to avoid inadvertent CsChrimson activation from the imaging laser, as dendrites and axons of these two neurons largely overlap (Aso et al., 2014a).

500 ms of optogenetic MBON-γ2α′1 activation resulted in strong reliable calcium responses in MV1 cell bodies (see Figure 6.7). Comparing $\Delta F/F_0$ from before and after stimulation showed significantly enhanced calcium transients with stimulation. As MBON-γ2α′1 are known to be cholinergic, I also tested the dependence of this connection on nicotinic ACh receptors by bath-applying 250 µM of the non-specific nAChR blocker mecamylamine. The addition of mecamylamine greatly reduced light-triggered calcium responses, supporting the idea that MBON-γ2α′1 activates MV1 via its cholinergic projections.

MBON-γ2α′1 activates PAM neurons

As PAM neurons are required for the formation of appetitive memories (Burke et al., 2012), they might also play an important role for the reconsolidation of appetitive memories. Indeed, data from our lab reveals an involvement of PAM neurons half an hour after CS^- reactivation (Felsenberg et al., 2017). As cholinergic MBON-γ2α′1 axons innervate the SMP where PAM neurons have broad dendritic innervation (Aso et al., 2014a; Burke et al., 2012), I reasoned that MBON-γ2α′1 may indeed be functionally connected to PAM neurons.

To test this hypothesis, I used the red-shifted channelrhodopsin CsChrimson::mVenus in MB077C MBON-γ2α′1 (see Figure 6.1D) , while monitoring calcium transients with GCaMP6m in R58E02-LexA (see Figure 6.1M) PAM neurons in explant brains. The use of a broad PAM driver line and the sampling of different planes allowed me to image many horizontal lobe compartments at the same time.

Interestingly, light activation of MBON-γ2α′1 resulted in strong calcium responses in all PAM compartments monitored (see Figure 6.8). This suggests that, indeed, MBON-γ2α′1 activates PAM neurons, and that this connection might play an important role for reconsolidation (Felsenberg et al., 2017).

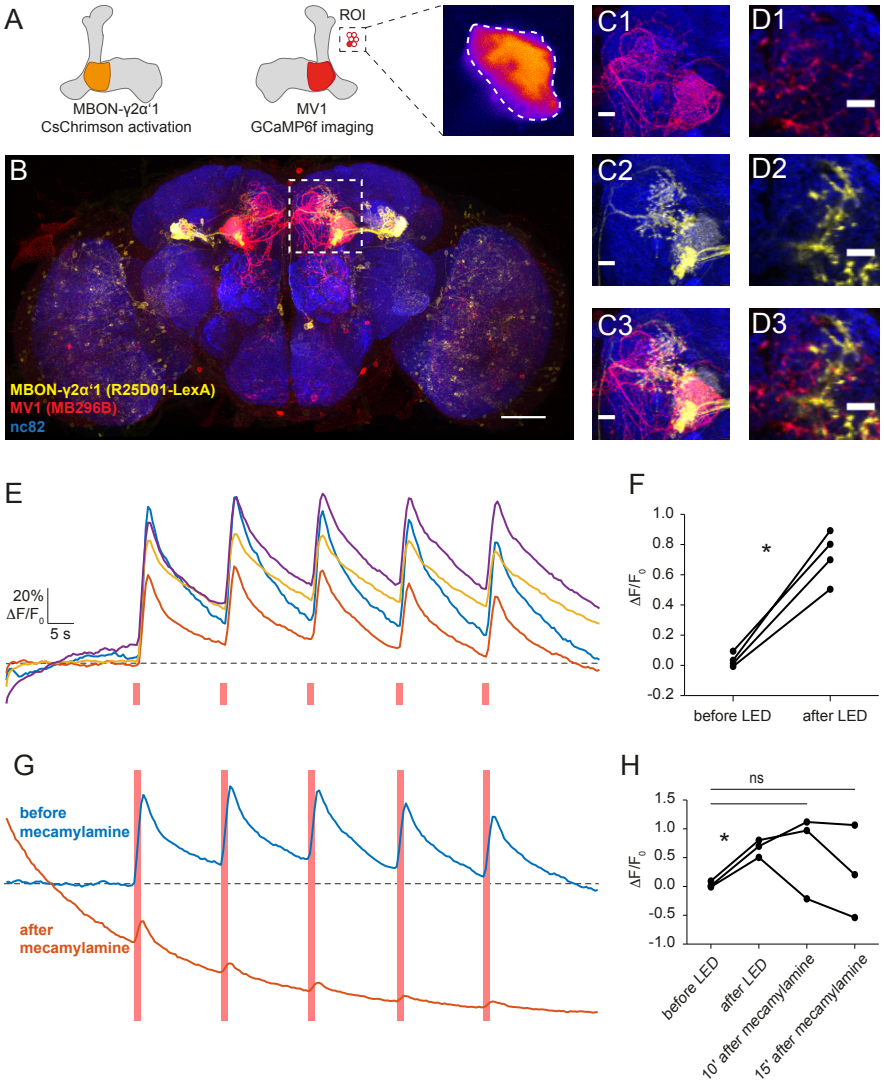


Figure 6.7: Optogenetic activation of MBON-γ2α′1 triggers calcium responses in MV1. A) The red-shifted channelrhodopsin CsChrimson was targeted into R25D01-LexA MBON-γ2α′1, while GCaMP6f was expressed in MB296B MV1 neurons. Explant brains were then optogenetically stimulated while calcium transients from the MV1 cell body were monitored. Right panel shows sample image of the MV1 cell body as imaged via the two-photon microscopy system. B-D) Confocal images of R25D01-LexA (yellow), MB296B (red), and nc82 background staining (blue). Images were taken separately, CMTK registered to a standard brain, and overlaid. B) Maximum projection. Dashed box is shown further in C. Scale bar represents 50 µm. C) Neuronal arbours of MV1 and MBON-γ2α′1 show considerable overlap. D) MBON-γ2α′1 presumptive axons (yellow) are in close proximity to MV1 presumptive dendrites (red). E) All calcium transients from four different brains (each with a different colour). Each 500 ms light pulse, indicated by red bar, induces a strong calcium response in all brains. F) $\Delta F/F_0$ is statistically increased after optogenetic stimulation (paired t-test, $p < 0.05$, $N = 4$). G-H) Bath application of 250 µM of the non-specific nicotinic receptor antagonist mecamylamine reduces calcium responses in MV1. G) Sample calcium transients of one brain before (blue) and after (red) addition of mecamylamine. H) Development of calcium responses at different time points after addition of mecamylamine. Calcium responses after LED presentation are significantly enhanced, but 10 min and 15 min after mecamylamine addition $\Delta F/F_0$ is not statistically different to before LED stimulation (repeated measures ANOVA, Tukey's multiple comparisons test, $p < 0.05$, $N = 3$). Partly adapted from Felsenberg et al. (2017).

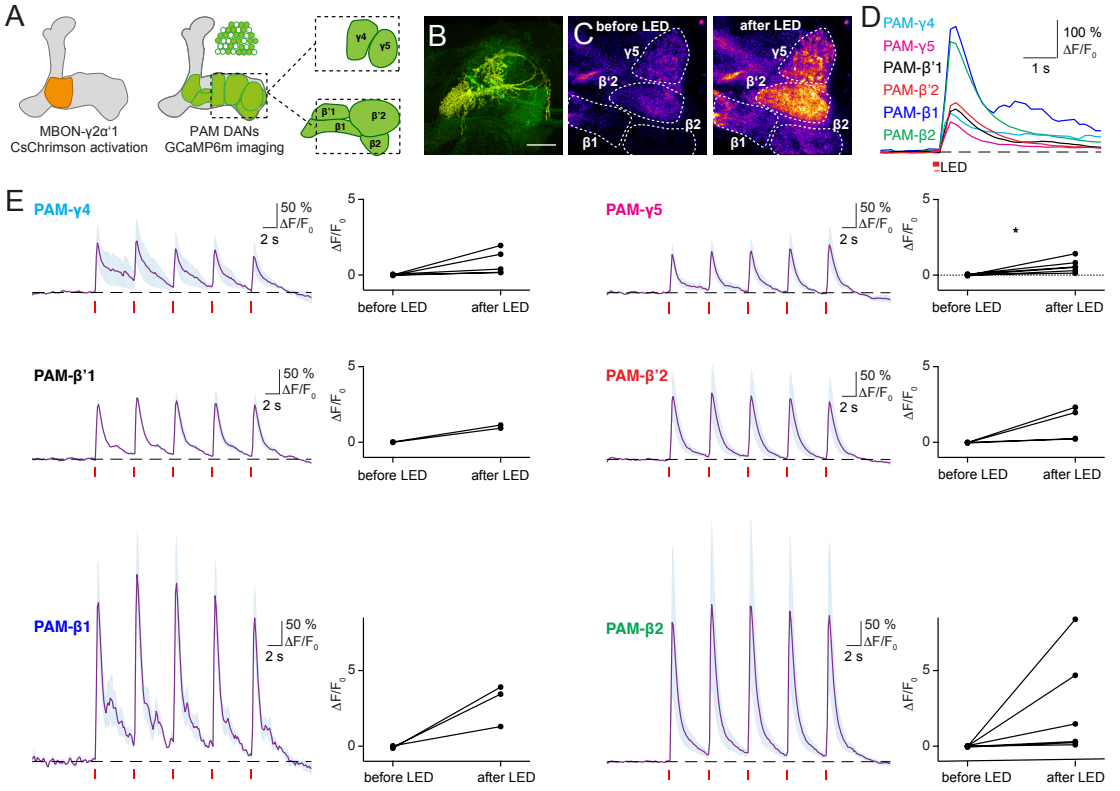


Figure 6.8: Optogenetic activation of MBON-γ2α′1 triggers calcium responses in PAM neurons. A) MBON-γ2α′1 was optogenetically stimulated by MB077C expressing CsChrimson, while PAM DANs were imaged by R58E02-LexA expressing GCaMP6m. Many PAM neurons were monitored in the same brain, focusing on different MB planes. B) Confocal image of brain expressing MB077C (yellow) and R58E02-LexA (green). MBON-γ2α′1 terminals innervate the PAM dendritic area. C) Sample images of one field of view covering several PAM neuron compartments before and after LED stimulation. All compartments show an increase in fluorescence. D) Mean calcium transients of all PAM compartments during first stimulation with 200 ms of red light. Note that all transients are increased, but especially PAM-β1 and PAM-β2. E) Mean transients (purple line) and SEM (blue shade) of all compartments imaged. While all compartments show robust calcium responses, only PAM-γ5 shows a significant increase of $\Delta F/F_0$, as indicated by the asterisk (paired t-test, $p < 0.05$, $N = 3 - 5$). Partly adapted from Felsenberg et al. (2017).

6.2.5 MBON-γ2α′1 carries a CS⁻-specific memory trace

If MBON-γ2α′1 is indeed responsible for CS⁻-triggered reconsolidation of appetitive memories and engages both MV1 (see Figure 6.7) as well as PAM neurons (see Figure 6.8) in the reconsolidation process, then how does MBON-γ2α′1 code for the specific odour identity of the CS⁻? In other words, if novel odours do not trigger reconsolidation, but only the CS⁻ through MBON-γ2α′1 (see Felsenberg et al., 2017), then does MBON-γ2α′1 have a modified representation of the CS⁻ odour? Such a 'memory trace' has been found for the CS⁺ odour in several MBONs (see Bouzaiane et al., 2015; Owald et al., 2015b; Perisse et al., 2016; Plaçais et al., 2013b; Séjourné et al., 2011), but no such memory trace has been uncovered for a CS⁻ odour yet.

I sought to investigate if MBON-γ2α′1 does indeed respond differently to the CS⁻ 3 hours after appetitive training by imaging calcium responses in tethered flies to three odours: the CS⁻, the CS⁺, and a novel odour, repeated three times to observe the time course of these responses. The inclusion of a novel odour can thus be used as an internal control against which odour responses can be normalised. Two groups of flies were tested: appetitively trained flies, and mock-trained flies. Appetitively trained flies were trained normally (Krashes and Waddell, 2008; Tempel et al., 1983), while mock-trained flies were only presented with both CS odours without any sucrose reward (see 2.5; also Owald et al., 2015b; Perisse et al., 2016).

MBON-γ2α′1 carries a CS⁻-specific memory trace

I first imaged flies carrying GCaMP6f in MB077C MBON-γ2α′1 that were either appetitively trained or mock-trained. I focused the field of view on the previously established site of the initial axon segment (Hige et al., 2015a), where I could observe strong and reliable calcium responses to odour onset and during the 5 s of odour presentation for all three odours (see Figure 6.9), as has already been described by others (Hige et al., 2015b). Importantly, when analysing the magnitude of CS responses by taking the area under the curve (AUC; see 2.5) and normalising it to each trial's novel odour AUC, I observed a significant increase in the CS⁻ response compared to mock-trained flies, both for MCH as trained odour as well as OCT

as trained odour. Notably, CS^+ odour responses showed no such difference, and CS^- differences were only observed during the first of three trials. These findings suggest that MBON-$\gamma 2\alpha'1$ might indeed carry a CS^--specific memory trace that could drive reconsolidation in downstream DANs.

V2 MBONs carry no appetitive memory trace

Is this CS^--specific memory trace a unique characteristic of MBON-$\gamma 2\alpha'1$ neurons, or could other MBONs or DANs involved in extinction and reconsolidation also hold a CS^--specific memory trace? In order to test this question, I used the same protocol as before on V2 MBONs and PPL1 DANs.

V2 neurons are known to show decreased odour responses to the CS^+ after aversive training (Séjourné et al., 2011), and to play a crucial role in extinction learning (Felsenberg et al., 2017). To test if V2 neurons might also hold a CS^--specific memory trace, I took MB052B ; GCaMP6f flies, that were either appetitively or mock-trained, before imaging their odour-evoked calcium activity in the initial axon segment (see Hige et al., 2015b; Séjourné et al., 2011) to three odours as before. In contrast to my previous findings with MBON-$\gamma 2\alpha'1$, I did not find any significant changes in odour responses in flies that were appetitively trained compared to mock-trained flies (see Figure 6.10).

Two PPL1 DANs carry no appetitive memory trace

PPL1 neurons are responsible for negative reinforcement during aversive learning (Claridge-Chang et al., 2009; Riemensperger et al., 2005; Schwaerzel et al., 2003), and play an important role in the extinction of appetitive memories (Felsenberg et al., 2017). I thus wondered if PPL1 neurons may also hold a CS^--specific memory trace. In particular, I focused on MP1 and V1 that have been shown to play important roles in aversive reinforcement and hunger signalling (Aso et al., 2012, 2010; Cervantes-Sandoval et al., 2017; Krashes et al., 2009; Plaçais et al., 2013a).

I employed the previous protocol on MB504B ; GCaMP6f flies, and imaged odour-evoked calcium responses in either the MP1 MB region (see Figure 6.11A) or the V1 MB region (see Figure 6.11B). Both regions showed reliable odour-evoked

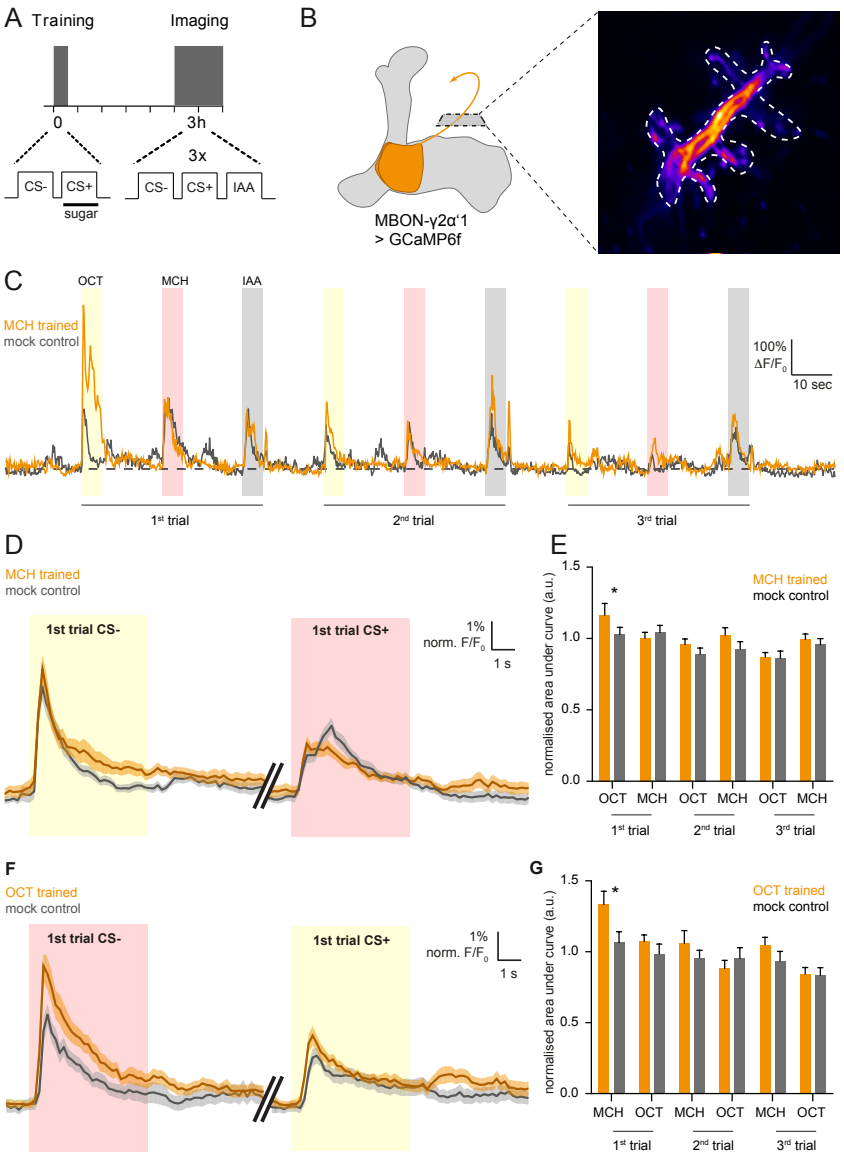


Figure 6.9: Increased calcium responses to CS$^-$ odour 3 h after appetitive training in MBON-γ2α′1. A) MB077C ; GCaMP6f female flies were either appetitively trained or mock-trained, and were then presented with CS$^-$, CS$^+$, and novel odour IAA, for three times while being imaged. B) Schematic of MBON-γ2α′1 in the MB and site of imaging location at initial axon segment. Right panel shows a sample image taken by the two-photon microscope, with the ROI encircled by a dashed line. C) Sample calcium transients from a fly that was trained with MCH as CS$^+$ (orange) and another that was mock-trained (grey). D) Averaged normalised calcium transients in response to OCT as CS$^-$ and MCH as CS$^+$. Note that calcium transients for MCH trained flies (orange) were higher than for mock-trained flies (grey) in the first trial of CS$^-$. E) Statistical analysis of normalised AUC reveals a significantly increased odour response only for the first CS$^-$ presentation (multiple t-tests, $p < 0.05$, $N \geq 14$). F) Averaged normalised calcium transients in response to MCH as CS$^-$ and OCT as CS$^+$. Note that calcium transients for OCT trained flies (orange) were higher than for mock-trained flies (grey) in the first trial of CS$^-$. E) Statistical analysis of normalised AUC reveals a significantly increased odour response only for the first CS$^-$ presentation (multiple t-tests, $p < 0.05$, $N \geq 14$). Shades in D and F, and error bars in E and G represent SEM. Partly adapted from Felsenberg et al. (2017).

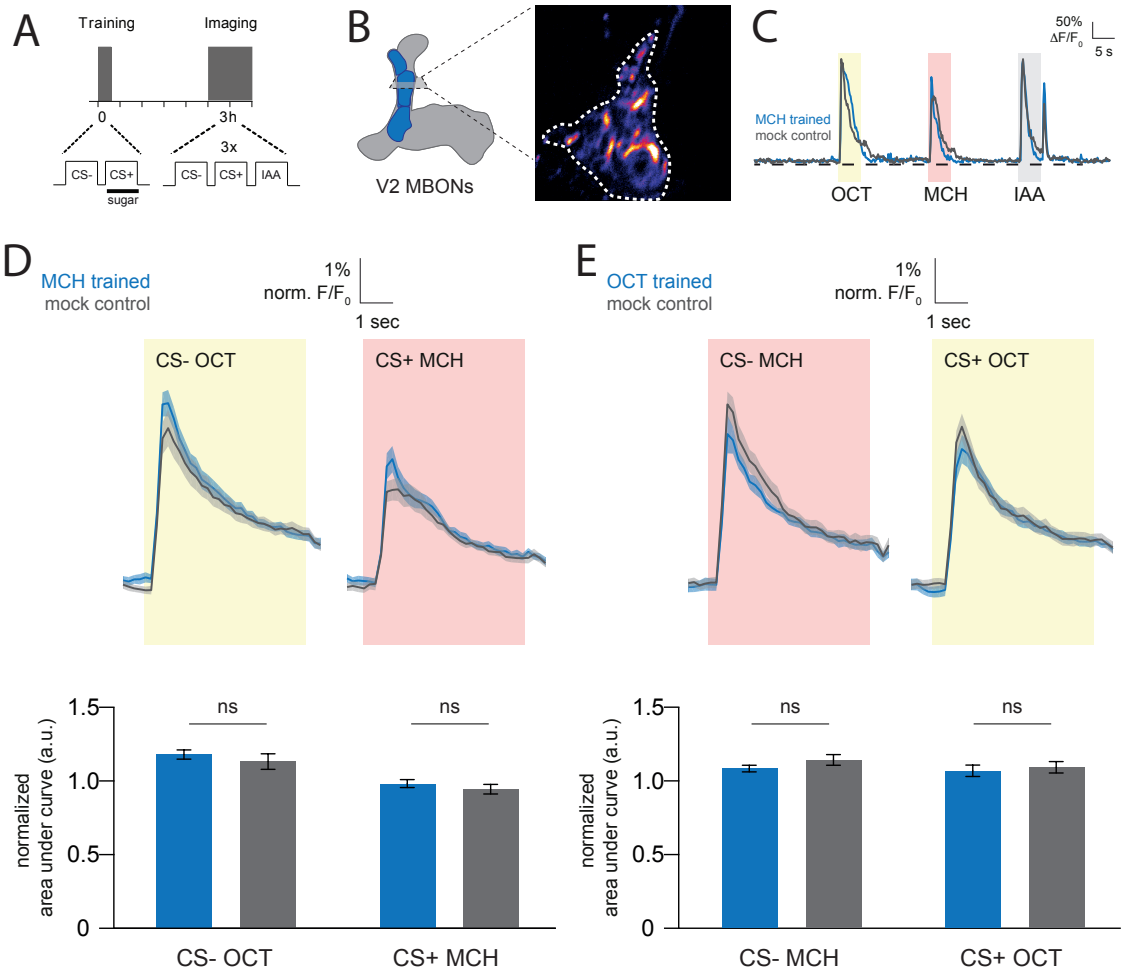


Figure 6.10: Calcium responses to odours after appetitive training in V2 MBONs. A) MB052B ; GCaMP6f female flies were either appetitively trained or mock-trained, and were then presented with CS^-, CS^+, and novel odour IAA, for three times while being imaged. B) Schematic of V2 location in the MB and site of imaging location at initial axon segment. Sample image from live recording was taken by the two-photon microscope, with the ROI encircled by a dashed line. C) Sample calcium transients from a fly that was trained with MCH as CS^+ (blue) and another that was mock-trained (grey). D) Averaged normalised calcium transients in response to OCT as CS^- and MCH as CS^+. Bottom, statistical analysis of normalised AUC reveals no significant difference in normalised AUC (multiple t-tests, $p > 0.05$, $N \geq 14$). E) Averaged normalised calcium transients in response to MCH as CS^- and OCT as CS^+. Bottom, statistical analysis of normalised AUC reveals no significant difference in normalised AUC (multiple t-tests, $p > 0.05$, $N \geq 11$). Shades and error bars in D and E represent SEM. Adapted from Felsenberg et al. (2017).

calcium responses. These were visible as a slow and modest rise of calcium signal in MP1, and a sharp rise to odour onset followed by a sustained decrease below baseline in V1 neurons. Importantly, normalised AUC in neither of these two PPL1 neurons was significantly different between appetitively trained and mock-trained flies for any of the odours tested. This suggests that MBON-γ2α′1 may be rather unique in possessing a CS^--specific memory trace, although of course further neurons not tested herein cannot be ruled out at this stage.

6.3 Discussion

6.3.1 Results summary

Probing the neural mechanisms that underlie extinction and reconsolidation processes in *Drosophila*, I have uncovered widespread connectivity between MBONs and DANs that has rarely been shown on a physiological level before (see Cohn et al., 2015; for anatomical and behavioural evidence, see Aso et al., 2014a; Ichinose et al., 2015). I also demonstrate the first evidence, to the best of my knowledge, for a CS^- memory trace in the *Drosophila* brain.

Specifically, I show that cholinergic V2 MBONs can trigger positive or negative calcium responses in different PPL1 neurons (see Figures 6.2 and 6.3). This activity probably underlies the formation of an appetitive extinction memory (see Felsenberg et al., 2017). Interestingly, V2 neurons also strongly activate PAM-β1 (Figure 6.4), but the functional consequences of this are yet unclear. Extinction of aversive memories, on the other hand, relies on M4/6 MBONs and PAM neurons (Felsenberg et al., *in preparation*). I show here that M4/6 neurons strongly activate PAM-γ5 (Figure 6.5), while PAM activity likely exerts tonic inhibition on M4/6 (Figure 6.6).

Reconsolidation of appetitive memories requires activity of the cholinergic MBON-γ2α′1 and its dopaminergic counterpart MV1, as well as PAM neurons (albeit delayed) (Felsenberg et al., 2017). I show here that MBON-γ2α′1 drives strong cholinergic calcium responses in both MV1 (Figure 6.7) as well as broadly in PAM neurons (Figure 6.8).

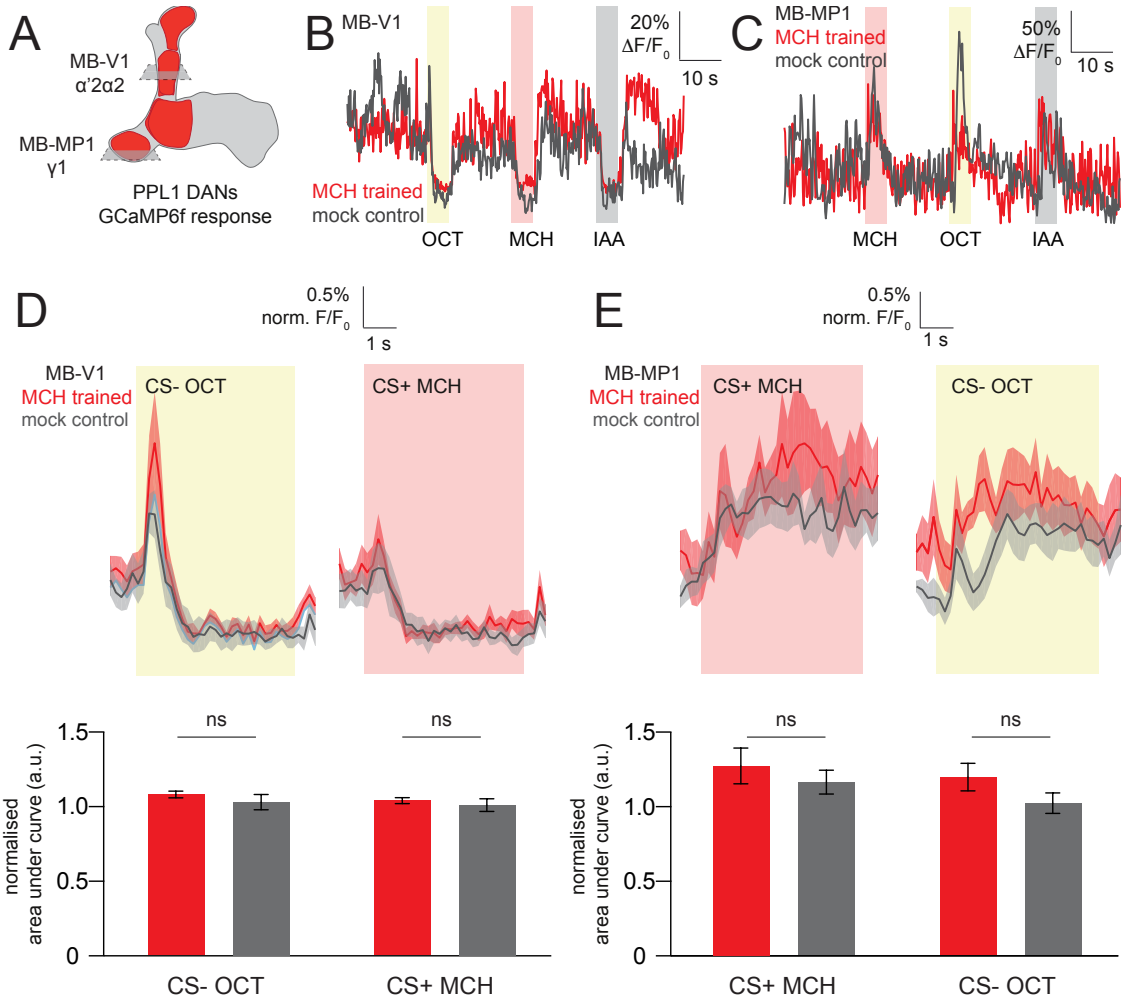


Figure 6.11: Calcium responses to odours after appetitive training in PPL1 neurons. A) MB504B ; GCaMP6f female flies were either appetitively trained or mock-trained, and were then presented with CS^-, CS^+, and novel odour IAA, for three times while being imaged either at the level of the stalk ($\alpha'2\alpha2$) for V1, or at the level of the heel ($\gamma1$) for MP1. B) Sample calcium transients in V1 from a fly that was trained with MCH as CS^+ (red) and another that was mock-trained (grey). Note the pronounced decrease of calcium transients during odour presentation. C) Sample calcium transients in MP1 from a fly that was trained with OCT as CS^+ (red) and another that was mock-trained (grey). D) Averaged normalised calcium transients in response to MCH as CS^+ and OCT as CS^- in V1. Bottom, statistical analysis of normalised AUC reveals no significant difference in normalised AUC (multiple t-tests, $p > 0.05$, $N = 7$). E) Averaged normalised calcium transients in response to OCT as CS^- and MCH as CS^+ in MP1. Bottom, statistical analysis of normalised AUC reveals no significant difference in normalised AUC (multiple t-tests, $p > 0.05$, $N \geq 7$). Shades and error bars represent SEM. Adapted from Felsenberg et al. (2017).

The reconsolidation process is triggered by the presentation of the CS$^-$ odour three hours after initial training (Felsenberg et al., 2017). I found evidence that MBON-$\gamma 2\alpha' 1$ mediates this reconsolidation process by holding an elevated CS$^-$-specific memory trace (Figure 6.9) that I did not observe in V2 MBONs or PPL1 neurons (Figures 6.10 and 6.11).

Overall, these findings show that many MBONs and DANs are functionally connected in many ways, both within arms coding similar valence and across, thus enabling the updating of existing memories.

6.3.2 Functional connectivity between V2 and PPL1

The extinction of appetitive memories requires neurotransmission from both cholinergic V2 MBONs as well as PPL1 DANs (Felsenberg et al., 2017). V2 MBONs are directly driven by cholinergic synapses from KCs to guide behavioural output (Aso et al., 2014b; Barnstedt et al., 2016; Séjourné et al., 2011; Takemura et al., 2017), and PPL1 neurons are known to provide aversive reinforcement (Claridge-Chang et al., 2009; Riemensperger et al., 2005; Schwaerzel et al., 2003). Cholinergic V2 axons lie in close proximity to PPL1 dendrites (Aso et al., 2014a). We thus hypothesised that odour-evoked V2 activity during extinction might activate PPL1 neurons to establish a competing extinction memory trace.

To test such a connection directly, I used the optogenetic activator CsChrimson to drive activity in V2 MBONs while monitoring calcium transients in PPL1 cell bodies, and observed reliable light-triggered calcium responses in PPL1 neurons (Figure 6.2). Interestingly, heterogeneity in responses was observed across different PPL1 neurons (Figure 6.3).

Imaging of cell bodies

I chose to image GCaMP6f from the PPL1 cell bodies to avoid overlapping the field of view with CsChrimson-expressing neurites. CsChrimson is known to also be activated by the two-photon imaging laser (personal observations; see also Figure 3.29; personal communication with Allan Wong, 1.6.2015), and V2 MBONs mostly

overlap with PPL1 neurons inside and outside the MB (see Figures 6.1 and A.17; Aso et al., 2014a; Tanaka et al., 2008). Although the cell bodies of both V2 and PPL1 are also at similar locations near the calyx (see Aso et al., 2014a; Tanaka et al., 2008), a strong focus on the respective cell body of interest greatly reduced the amount of two-photon laser exposure to CsChrimson-expressing V2 cell bodies. Indeed, no shift in baseline was detected at the start of imaging, as was previously seen from laser-induced CsChrimson activation (see Figure 3.29).

Other experiments I have performed suggest that CsChrimson may not always be activated by the two-photon laser (see Figure 6.5). This probably depends on both CsChrimson expression levels in any given field of view (FOV) and the laser intensity required for sufficient GCaMP visualisation. It is thus possible that PPL1 neurons could in the future also be imaged from their MB lobe innervations without interference from inadvertent CsChrimson stimulation. Alternatively, other Chrimson variants could be used in the future that are less sensitive to two-photon light activation, such as the original Chrimson (Klapoetke et al., 2014; personal communication with Allan Wong, 4.6.2015).

Which V2 neurons are responsible?

What I refer to as V2 MBONs in this work are actually a heterogeneous group consisting of MBON-α2sc, MBON-α2p3p, MBON-α′2, MBON-α′3ap, MBON-α′3m, MBON-α2sp, and MBON-α′1 (Aso et al., 2014a; Takemura et al., 2017), most of which are expressed in MB052B that was used previously in behavioural experiments (Felsenberg et al., 2017).

Which of these neurons is likely responsible for the observed activation of PPL1 neurons? I tested three different V2 LexA driver lines to rule out any effects that might stem from LexA expression outside of V2 MBONs; all three lines resulted in elevated calcium responses in PPL1 cell bodies (Figure 6.2). Out of these three, I observed the strongest responses after stimulating the LexA line with the widest expression pattern. I also found positive calcium responses in a LexA line only labelling V2α′. These findings suggest that many individual V2 neurons likely act

together to activate PPL1 neurons synergistically, but that individual V2 MBONs can also already exert effects on PPL1 neurons.

Which PPL1 cell bodies yield which responses?

Similar to V2 MBONs, PPL1 neurons are also a heterogeneous group of DANs. I initially used MB504B to drive GCaMP6f expression in four PPL1 neurons, as this line was also responsible for the behavioural defect when blocked (Felsenberg et al., 2017). MB504B, however, contains four individual PPL1 neurons that innervate different parts of the MB, and may serve different functions (see Figure 6.1G; Aso et al., 2012). Indeed, I found both excitatory as well as inhibitory calcium responses (Figure 6.3). Unfortunately, despite the stereotyped cell body locations, cell identity could not safely be determined.

To determine cell body identity more accurately, I expressed GCaMP6f in splitGAL4 lines containing only one single PPL1 neuron each. Of these, V1 neurons responded most strongly and reliably, similar to the results I saw with 'cell 1'. Two driver lines for MP1 gave non-significant activation results, but these may have been partly confounded by a drift in baseline I observed (Figure 6.3H). Indeed, close inspection of traces suggests some small light-triggered activation, similar to what was observed in 'cell 2'. Lastly, a clean MV1 line showed inhibitory responses in some brains, but this effect was not reliable (Figure 6.3I). It is likely that MV1 thus corresponds to 'cell 3', although the latter showed more reliable inhibitory responses. At this point, clear data from PPL1-α3 would be desirable but at the time of testing no splitGAL4 line with unambiguous expression in PPL1-α3 was available. Thus, I cannot yet safely determine which of these four PPL1 neurons corresponds with the previously monitored cell bodies, but it is clear that V1 reliably shows excitatory responses. It is interesting to note in this regard that, behaviourally, V1 also seems to show the strongest trend of a single neuron for a role in extinction (cp. Felsenberg et al., 2017, Extended Data Figure 3d).

Why are responses comparatively small?

In comparison to other optogenetically triggered calcium responses in downstream neurons, PPL1 responses are relatively small, i.e. mostly on the order of < 10 % $\Delta F/F_0$. In contrast, optogenetic responses of PAM-β1 neurons to V2 stimulation mostly exceeds 100 % $\Delta F/F_0$ (see Figure 6.4). It should be noted, though, that in the latter case, calcium responses were measured from the presynaptic terminals of 4–6 neurons (Aso et al., 2014a). However, cell body calcium responses of MV1 to MBON-γ2α′1 optogenetic stimulation were also largely > 60 % $\Delta F/F_0$ (Figure 6.7).

Another possibility is the fact that, while the three V2 MBON drivers I used are relatively specific in their expression patterns, they may also not be expressing as strongly as other comparable driver lines used to drive CsChrimson. On the other hand, one of these lines reliably elicited strong responses in PAM-β1 (Figure 6.4), making this an unlikely cause.

Another reason for the subtlety of responses in PPL1 neurons could be the idea that the V2 → PPL1 connection is not direct. Anatomically, there is good evidence to support a direct connection as V2 axon terminals in protocerebral areas heavily overlap with PPL1 dendrites (see Aso et al., 2014a; Figures 6.1, and Figure A.17). A direct connection, however, could be experimentally tested by adding the VGSC blocker TTX to the bath.

Evidence from behavioural experiments suggests that all four PPL1 DANs contained in MB504B need to be blocked in order to affect extinction processes, while blocking individual PPL1 DANs had no effect (Felsenberg et al., 2017, Extended Data Figure 3c-f). Indeed, previous studies have shown that most PPL1 DANs require co-activation with other PPL1 DANs to induce aversive memories (Aso et al., 2012; Masek et al., 2015). This suggests that PPL1 DANs need to work synergistically to produce an extinction memory, and could mean that the activity patterns observed per individual cell only represent a fraction of the induced activity in PPL1.

6.3.3 Functional connectivity between V2 and PAM

Besides exciting PPL1 neurons, V2 neurons also excited some PAM neurons (see Figure 6.4). In particular, PAM-β1 showed very strong and reliable light-triggered responses, while those of other PAM neurons were more subtle. It is also important to note that PAM-β1 responses seem to occur within 100–200 ms of LED onset, while the other PAM neurons seem more delayed, responding largely about 400 ms after LED onset (see Figure 6.4C). Both response magnitude and timing suggest that PAM-β1 responses may be due to direct activation from V2 MBONs, whereas that of other PAM neurons could be due to secondary responses. Previously, artificial PAM activation has been found to induce calcium responses in some PAM neurons (Cohn et al., 2015), so that activity of PAM-β1 could reasonably elicit smaller responses in other PAM neurons either directly, or through network activity. PAM-β1, for example, innervates the β1 compartment that is also occupied by MV2 – a glutamatergic MBON that also targets other MBONs of the vertical lobe, such as V2 (see also 5.3.5; Aso et al., 2014a; Takemura et al., 2017). By exciting PAM-β1 and subsequent modulation of MV2, V2 could plausibly receive positive or negative feedback, depending on the acute effects of dopaminergic and glutamatergic signalling in this pathway.

What would be the functional significance of V2 exciting PAM-β1? Previously, dTrpA1 thermogenetic activation of PAM-β1 neurons during odour presentation was shown to be sufficient to implant appetitive LTM that is independent of the hunger state at the time of retrieval (Huetteroth et al., 2015). Similarly, unpublished results from our lab show that optogenetic activation of V2 neurons during odour presentation also results in appetitive memory implantation (P. Cognigni, personal communication). It thus seems likely that these memory implantation effects are mediated by the PAM-β1 excitation that I describe here. As aversive memory formation decreases V2 output (Séjourné et al., 2011), PAM-β1 would be less excited by the CS^+ after training, possibly gating the formation of appetitive LTM formation in the presence of aversive stimuli.

6.3.4 M4/6 – PAM interplay

Unpublished results from our lab show that extinction of aversive memories requires neurotransmission from both M4/6 MBONs as well as PAM neurons (Felsenberg et al., *in preparation*). M4/6 neurons were found to show enhanced responses after aversive training (Bouzaiane et al., 2015; Owald et al., 2015a), and project glutamatergic axons into the SMP/CRE area that is also heavily innervated by PAM dendrites (Burke et al., 2012; Owald et al., 2015a). PAM neurons are required for the formation of appetitive memories (see 1.3.3; Burke et al., 2012; Huetteroth et al., 2015; Liu et al., 2012). I thus wondered if, similar to the appetitive extinction mechanism observed in V2/PPL1 neurons (Felsenberg et al., 2017), M4/6 activity might drive PAM neurons to form competing extinction memories of positive valence after aversive training.

M4/6 → PAM

I could show that M4/6 neurons strongly excite the PAM-γ5 neuron, but have no significant effect on PAM-γ4 and PAM-β′2 (see Figure 6.5). These findings mirror similar results obtained by ATP/$P2X_2$ stimulation of M6 (Cohn et al., 2015). In contrast to the findings by Cohn et al. (2015), however, I saw no significant inhibition of PAM-γ4 (Figure 6.5D). As I still observed a trend towards an inhibited response, this difference in effect size may be due to the fact that Cohn et al. (2015) used the presynaptically targeted sytGCaMP and heavily normalised their responses. As discussed previously, GCaMP is not ideal to pick up inhibitory responses, but may do so under certain circumstances including a high $[Ca^{2+}]_i$ (see 5.3.2).

In addition to effects on γ PAM neurons, I also observed a trend for biphasic responses in PAM-β′2. While no significant differences in calcium transients after stimulation were observed, transients seemed to show a delayed decrease from baseline first, about one second after LED onset, followed by a calcium increase, another second thereafter (see Figure 6.2.3E-F). It is not yet clear what causes these responses, but in light of the observed timing it is likely that the initial decrease in PAM-β′2p stems from a rather direct inhibition, while the delayed

increase from baseline is likely due to secondary responses from the network, or might be caused by an 'overshoot' from recovery.

In contrast to Cohn et al. (2015), I also activated M4β′ along with M6, which might influence the observed calcium responses in PAM. One can speculate that M4β′ activity has only little influence over PAM-γ5 activation, but could possibly act directly on PAM-β′2. In such a case, the observed delayed calcium increase in PAM-β′2 might come from strong PAM-γ5 activity. Interactions between PAM neurons (except PAM-γ1-4; Cohn et al., 2015), have not yet been studied, however. The activation of individual M4/6 neurons while observing calcium transients in a broad PAM line should provide more clarity on this.

Future studies could also investigate the glutamate receptor that mediates the observed calcium responses. Given that PAM-γ5 responds rapidly with a great calcium influx, and without removing a potential magnesium block as would be required for NMDARs, this response might reasonably be mediated by ionotropic glutamate receptors, including DGluR-IA, DGluR-IB, DGluR-IID (Featherstone et al., 2005; Völkner et al., 2000). To test for the requirement of ionotropic glutamate receptors, a broad antagonist such as CNQX (see also Gu and O'Dowd, 2006; Lee and O'Dowd, 1999; Ultsch et al., 1992) could be added to the bath solution, and its effects on optogenetically triggered responses compared. The negative responses in γ4, on the other hand, might be mediated either directly through a glutamate-gated chloride channel (Cully et al., 1996; Liu and Wilson, 2013), or might arise from further network activity such as APL (see 1.3.2). Similarly, the biphasic activity observed in PAM-β′2 might arise from a combination of inhibitory and metabotropic glutamate receptors and network activity. The addition of different specific GluR antagonists and TTX should further resolve these questions in the future.

PAM → M6

If PAM and M4/6 neurons are required for the extinction of aversive memories, and M4/6 neurons activate PAM neurons, it is possible that PAM neurons feed back onto M4/6 to establish a competing extinction memory. Previous studies have shown that

dopaminergic input onto KC–MBON synapses leads to presynaptic depression that results in reduced KC → MBON responses (Cohn et al., 2015; Hige et al., 2015a; Owald et al., 2015a), but it is unclear how DAN activity acutely impacts MBONs.

In my experiments activating PAM neurons with CsChrimson and observing calcium transients in M6 MBONs, I found no direct light-activated calcium responses (see Figure 6.6). I did, however, observe a strong decrease in baseline fluorescence that was only visible when CsChrimson was expressed in PAM neurons. The fact that this shift in baseline relies on CsChrimson suggests that it is not merely a general effect of the imaging laser onto tissue and/or GCaMP activity. Instead, this suggests that the observed decrease in baseline stems from the imaging laser activating CsChrimson in PAM neurons, which in turn, induces a slow reduction in M6 calcium levels. The fact that PAM neurons would be activated by the two-photon imaging laser may not be surprising given the use of a very strong driver line that includes most PAM neurons (R58E02-LexA; see Figure 6.1M), the imaging location of γ5 that is particularly rich with CsChrimson-expressing PAM processes, and the fact that CsChrimson is prone to become activated by two-photon laser light (personal communication with Allan Wong, 1.6.2015).

Previous experiments (see Figure 3.29) suggest that laser activation of CsChrimson follows the same polarity as LED-induced CsChrimson activation. In the case of activating KCs and monitoring KC GCaMP signals, this led to an increase of baseline fluorescence (Figure 3.29), whereas here I observe a clear decrease in baseline fluroescence. This suggests that the acute effect of PAM activity on M6 neurons could actually be inhibitory. This observation mirrors other recent findings on the acute action of dopaminergic input to KC → MBON synapses. Cohn et al. (2015), for example, find that the knockdown of DopR2 in KCs leads to a release of inhibition in γ4/5 compartments. Likewise, Hattori et al. (2017) find that blocking PPL1-α′3 DANs leads to elevated odour responses in the corresponding V2α′ MBON, and coincident PPL1-α′3 activation with odour stimulation leads to strongly reduced odour responses in V2α′. All these findings suggest that the acute action of dopamine in several compartments may result in reduced MBON

calcium levels, similar to its effects leading to synaptic depression after pairing with a CS (see Cohn et al., 2015; Hige et al., 2015a).

A previous study showed a slow rise in calcium levels in M6 upon ATP/$P2X_2$ stimulation of R58E02-LexA PAM neurons (Sitaraman et al., 2015). While it is possible that different modes of stimulation (ATP or CsChrimson) lead to different MBON activation patterns, the very slow calcium dynamics (> 1 min to peak) and large variance might also indicate potential off-target effects. Another recent study showed that optogenetic activation of PAM-α1 also leads to a relatively slow (∼ 5 s to peak) increase in calcium transients of MBON-α1 (Takemura et al., 2017). This could suggest compartment-specific DAN → MBON modulation, possibly depending on the specific dopamine receptors involved, or secondary responses from the network, or, importantly, the role of direct DAN → MBON synapses that have recently been uncovered (Takemura et al., 2017). Indeed, TTX and mecamylamine changed the PAM → MBON responses observed, suggesting a role for DAN → KC → MBON synapses, that cannot be ruled out in my experiments. Clearly, further experiments are needed to resolve the acute influence of DANs on MBONs.

Extinction as an interneuronal MB circuit process

Schwaerzel et al. (2002) previously suggested that extinction learning after aversive training does not require synaptic output from KCs, and that extinction learning is therefore an intracellular process. While I have mainly focused on extinction learning after appetitive training here (see Felsenberg et al., 2017), unpublished results from our lab also suggest an involvement of DANs and MBONs for extinction after aversive training (Felsenberg et al., *in preparation*). Given that MBONs mainly receive input from KCs, and that even DANs receive KC input (Barnstedt et al., 2016; Cervantes-Sandoval et al., 2017; Takemura et al., 2017), how could these seemingly opposing results be explained?

While it is possible that using different extinction protocols (cp. Felsenberg et al., 2017; Schwaerzel et al., 2002) results in differential neuronal requirements, it should be noted that Schwaerzel et al. (2002) only block 700 / 850 KCs (out of ∼ 2,000;

Aso et al., 2009, 2014a) during their experiments, which would presumably still elicit strong responses in MBONs. Our results on extinction processes in the MB network suggest that a skew in the MBON network after conditioning (see Felsenberg and Waddell, 2017; Owald and Waddell, 2015) is responsible for enhanced drive to certain DANs that, in turn, establishes an extinction memory (see Felsenberg et al., 2017). Given that blocking KCs only partially probably still drives the MBON network similarly, albeit slightly more weakly, blocking only a minority of KCs should, in this case, not have major effects on the establishment of an extinction memory.

MBON-γ2α′1 broadly activates DANs

CS^--triggered reconsolidation of appetitive memories requires synaptic output from MBON-γ2α′1 and its associated DAN MV1, and temporally delayed, also PAM DANs (Felsenberg et al., 2017). As odours are known to activate MBON-γ2α′1 (Hige et al., 2015b), and DANs are generally required to induce learning-related plasticity (see Burke et al., 2012; Claridge-Chang et al., 2009; Riemensperger et al., 2005), we wondered if MBON-γ2α′1 activity during the CS^- could activate MV1 to induce reconsolidation. Indeed, optogenetic activation of MBON-γ2α′1 resulted in strong cholinergic calcium responses in MV1 (see Figure 6.7). Furthermore, optogenetic activation of MBON-γ2α′1 also resulted in strong and reliable calcium responses in PAM neurons, even at 200 ms stimulation (see Figure 6.8). These findings establish MBON-γ2α′1 as a major activator for several DANs, and suggests that MBON-γ2α′1 activity could trigger dopamine-dependent reconsolidation processes.

I have not yet studied how MBON-γ2α′1 affects other PPL1 DANs as only the MV1 PPL1 neuron seemed relevant for CS^--triggered reconsolidation (see Felsenberg et al., 2017, Extended Data Figure 3c-f). Given its promiscuous activation pattern of PAM neurons (Figure 6.8), however, it would be interesting to determine if MBON-γ2α′1 actually activates all MB DANs, or only those known to be involved in the reconsolidation process.

6.3.5 MBON-γ2α′1 carries a CS⁻ memory trace

If MBON-γ2α′1 induces DAN-mediated reconsolidation specifically after the CS⁻ odour, but not after novel odours (see Felsenberg et al., 2017), MBON-γ2α′1 must somehow encode the CS⁻ odour differently to other odours. Indeed, I find that MBON-γ2α′1 responds more strongly to the CS⁻ odour than to other odours, compared with a mock-trained control group (see Figure 6.9). I do not find such a CS⁻ memory trace in V2 MBONs or V1/MP1 PPL1 DANs (see Figures 6.10 and 6.11).

However, at this point I cannot rule out that such a CS⁻ memory trace might also be found in MV1 as this PPL1 DAN partners with MBON-γ2α′1 and receives strong activation from it (see Figure 6.7). Indeed, in this light it is also possible that PAM neurons carry a CS⁻ trace as they also receive strong activation from MBON-γ2α′1 (see Figure 6.8).

My experimental design can also not rule out an enhanced calcium response to the first odour presented three hours after training. We chose to not interleave CS⁻ as first or second odour in semblance to the training protocol that generally involves the presentation of the CS⁻ first, followed by the CS⁺ (see Krashes et al., 2009; Tempel et al., 1983). Changes in the order of CS⁻ and CS⁺ presentation (for training / odour exposure under the microscope / interactions) might plausibly elicit a different experience for the fly, and possibly lead to different kinds of memory (personal communication with J. Felsenberg). Nonetheless, future experiments could test combined T-maze and imaging protocols that use the CS⁺ odour first, to see if my results on enhanced CS⁻ calcium responses still hold under these conditions.

How could the CS⁻ become encoded in MBON-γ2α′1, given the absence of direct reinforcement? As the CS⁻ is generally presented 0.5–2.5 min before the CS⁺, the CS⁻ odour identity must still be present at the time of CS⁺ presentation. The continued presence of an odour identity within the MB was previously suggested to be required for memory consolidation in α/β, and performed by a feedback loop of APL/DPM ↔ α′/β′ KCs (see Keene and Waddell, 2007; chapter 1). The resulting observed memory trace is thought to be CS⁺-specific (Cervantes-Sandoval and

Davis, 2012; Keene and Waddell, 2007; Liu and Davis, 2009), but previous studies have not directly investigated if APL or DPM might support compartment-specific CS^- traces: Cervantes-Sandoval et al. (2012) investigated appetitive olfactory memory traces in DPM neurons, but only show CS^- data in which the 'CS^+' did not receive a sucrose reward; Liu et al. (2009) have only investigated APL memory traces after aversive learning that showed a slight but non-significant trend towards a CS^- decrease when signals were pooled across the horizontal lobe.

Future studies could record calcium transients in APL/DPM neurons specifically in the $\gamma 2\alpha' 1$ region, or interfere with network activity after CS^- exposure with a cold shock. If network activity is not responsible for the 'holding' of the CS^- odour identity in MBON-$\gamma 2\alpha' 1$, presynaptic molecular mechanisms could also play a role. It is possible that odour exposure activates certain signalling pathways that will only induce plasticity if dopaminergic signalling occurs after a delay. A similar mechanism has been recently observed by Cohn et al. (2015) where unpaired KC stimulation followed by dopamine stimulation resulted in presynaptic potentiation of KCs to that odour. This could be tested by simply presenting a sucrose reward without the CS^+ odour after CS^- presentation.

MBON-$\gamma 2\alpha' 1$ might play a special role in the MBON ensemble as it is the only MBON that induces approach behaviours when activated, but in contrast to most other approach-coding MBONs, it is also required for the retrieval of appetitive memories (Aso et al., 2014b; Felsenberg et al., 2017). This suggests that a general model of appetitive learning involving rewarding DANs that depress synapses to avoidance-coding MBONs (Owald et al., 2015a; Owald and Waddell, 2015) might be more complex in the case of MBON-$\gamma 2\alpha' 1$.

6.3.6 Updating memories through MBON–DAN interplay

For animals to adaptively navigate their environment, previously established memories need to be regularly re-assessed to account for behaviourally relevant changes. Our data shows that in *Drosophila melanogaster* these updating mechanisms rely on the interplay of widely interconnected MBONs and DANs, and suggests that

MBONs have at least two different roles. On the one hand, they are known to guide behavioural outputs from the MB (see Aso et al., 2014b; Owald et al., 2015a; Perisse et al., 2016; Séjourné et al., 2011), but through previously under-appreciated connectivity to DANs of either the same MB compartment or to DANs of other compartments, MBON activity can guide DANs to induce plasticity when needed.

This suggests that DANs not only become active in the presence of a US, but may constantly modulate the KC → MBON synapse in line with the behavioural state and previous experiences of the fly. Recent observations of state-dependent activity of DANs (Cohn et al., 2015), and the recent findings of a direct cholinergic KC → DAN synapse (Cervantes-Sandoval et al., 2017; Eichler et al., 2017; Takemura et al., 2017) support such an extended role of DAN circuit function.

Importantly, our findings establish a comprehensive neural architecture that can drive extinction and reconsolidation learning in a genetically tractable model organism. It will be interesting to see if mammals might use similar network motifs that enable dopamine-based error prediction and the reassessment of memories (Chang et al., 2016; Merlo et al., 2014; Reichelt et al., 2013; Sevenster et al., 2014; Steinberg et al., 2013).

A
Appendix

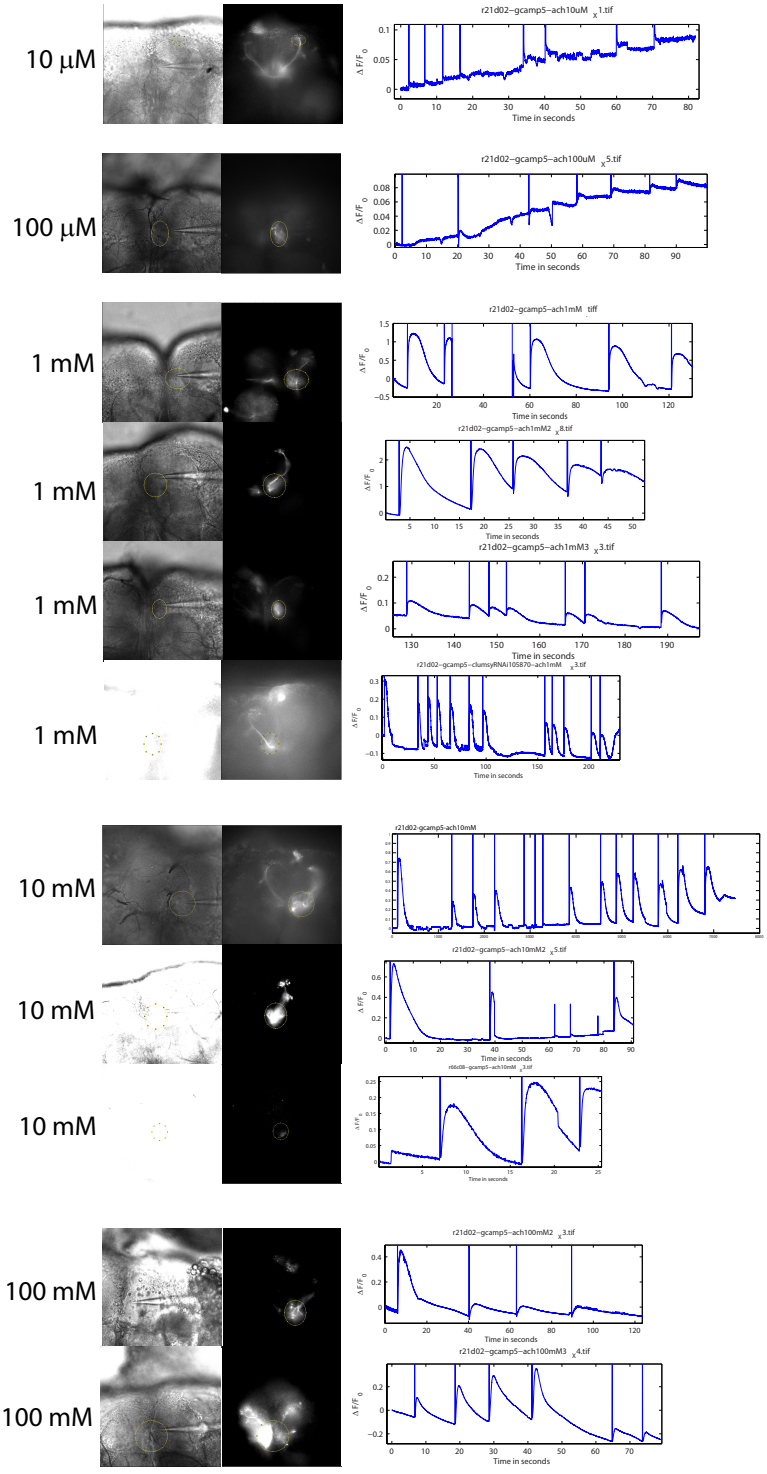


Figure A.1: Sample traces of 11 different brains of R21D02;GCaMP5 flies, injecting 5 different concentrations of ACh into the M4/6 dendritic arbour, starting with 10 µm at the top to 100 mM at the bottom. Each row represents an individual brain. Left micrographs show sample image of infrared channel, right micrographs show the green fluorescence channel. Yellow circles show region of interest (ROI) that was selected to retrieve fluorescent signals over time. Calcium traces (on the right) show reliable increases with stimulation from 100 µM on, and indicate increased responses with higher concentrations. Note that axes are different from brain to brain to visualise also smaller calcium transients, and that straight vertical lines in the signal are white trigger LED artefacts and signal the onset of stimulation.

Table A.1: VAChT immunostaining in KC-driven VAChT-RNAi quantification table, accompanying Figure 3.15.

OK107 > VAChT-RNAi(GD)	gamma	SMP	ratio
1	4.437	15.409	0.2879486
2	2.864	8.819	0.32475337
3	6.804	32.595	0.20874367
4	5.963	27.425	0.21742935
5	5.244	17.244	0.30410578
mean	5.0624	20.2984	0.26859616
OK107 / CS			
1	23.261	27.363	0.85008954
2	49.861	91.623	0.54419742
3	93.993	79.682	1.17960142
4	17.245	28.36	0.60807475
5	18.002	29.513	0.60996849
6	13.06	18.729	0.69731433
mean	35.9036667	45.8783333	0.74820766
CS / VAChT-RNAi(GD)			
1	14.235	21.684	0.65647482
2	21.957	24.021	0.91407518
3	14.253	19.003	0.75003947
4	11.049	17.227	0.64137691
mean	15.3735	20.48375	0.7404916
CS			
1	63.91	129.692	0.4927829
2	24.943	33.078	0.75406615
3	26.286	29.363	0.89520826
4	64.823	61.589	1.05250938
mean	44.9905	63.4305	0.70928812

Table A.2: Absolute quantification of α-ChAT and α-VAChT immunoreactivity in different genotypes and areas of the brain. Note that in three brains α-VAChT penetration was insufficient to extract fluorescence apart from gamma and SMP. These are marked by "VAChT penetration". See Table A.3 for the relative quantification.

CS / ChAT

	SMP ChAT	SMP VAChT	gamma ChAT	gamma VAChT	beta ChAT	beta VAChT	betaprime ChAT	betaprime VAChT	alpha ChAT	alpha VAChT	alphaprime ChAT	alphaprime VAChT
1	75.482	39.689	41.091	34.699	21.137	11.841	25.758	17.57	26.185	62.865	39.754	77.602
2	63.357	54.221	28.849	38.531	14.015	10.785	13.963	15.069	12.296	51.336	20.161	57.183
3	59.083	65.713	25.99	48.32	15.07	17.405	14.643	24.027	18.553	54.381	29.118	73.159

OK107 / ChAT

	SMP ChAT	SMP VAChT	gamma ChAT	gamma VAChT	beta ChAT	beta VAChT	betaprime ChAT	betaprime VAChT	alpha ChAT	alpha VAChT	alphaprime ChAT	alphaprime VAChT
1	17.719	22.554	5.659	32.13	4.124	15.512	3.117	16.084	4.897	44.336	4.32	49.756
2	17.794	20.81	5.25	21.357	4.319	9.544	4.145	10.769	4.282	33.984	4.476	50.171
3	17.564	35.461	3.564	29.508	3.581	10.084	3.815	14.012	4.169	46.762	4.825	51.408
4	33.302	20.294	7.161	13.872	6.506	9.029	5.292	10.969	5.083	54.364	5.471	68.775
5	30.174	61.053	7.921	50.839	5.789	17.479	7.002	26.29	7.667	66.589	7.951	76.559
6	25.126	45.335	5.576	27.468	3.935	11.784	4.356	14.815	5.562	69.861	5.993	80.084
7	23.46	30.695	6.331	27.253	7.055	14.024	4.392	12.687	4.629	43.23	5.035	44.178
8	32.586	38.085	6.807	32.684	6.133	12.569	5.273	17.417	6.967	50.168	6.028	67.645
9	36.567	68.77	11.474	66.68	6.435	16.897	7.077	23.13	6.829	66.076	8.199	67.798

OK107 / VAChT

	SMP ChAT	SMP VAChT	gamma ChAT	gamma VAChT	beta ChAT	beta VAChT	betaprime ChAT	betaprime VAChT	alpha ChAT	alpha VAChT	alphaprime ChAT	alphaprime VAChT
1	53.735	167.296	17.538	61.474	12.784	31.577	13.496	35.872	9.931	56.373	16.112	74.01
2	26.74	99.537	9.607	41.8	6.18	20.694	7.734	26.419	5.369	47.125	9.183	59.562
3	23.688	150.338	7.327	32.267	6.057	17.847	5.355	25.265	1.941	20.124	3.694	33.306
4	36.191	174.529	10.087	37.718	5.709	18.573	7.698	30.868	4.036	29.858	10.151	50.294
5	23.017	182.885	6.043	35.782	4.697	21.468	4.879	23.766	3.201	32.67	6.289	46.306
6	24.528	169.501	4.998	38.025	3.203	27.305	4.456	34.123	3.815	37.862		

CS / VAChT

	SMP ChAT	SMP VAChT	gamma ChAT	gamma VAChT	beta ChAT	beta VAChT	betaprime ChAT	betaprime VAChT	alpha ChAT	alpha VAChT	alphaprime ChAT	alphaprime VAChT
1	78.103	128.763	45.064	85.481	30.133	47.789	34.889	51.997	18.687	84.306	31.724	110.997
2	98.452	140.48	64.085	171.475	37.104	60.38	41.35	81.552	30.943	162.684	51.453	209.16
3	136.925	133.055	74.913	147	48.149	74.471	56.621	86.043	51.996	165.672	84.727	167.335
4	127.6	137.335	83.348	125.65	48.106	45.052	53.271	68.818	41.448	166.014	65.13	220.128
5	92.255	76.596	46.886	46.789	29.114	23.709	27.53	25.072	28.292	37.588	40.811	60.919
6	85.54	130.077	36.644	67.232	25.225	30.591	25.285	34.677	22.328	46.744	42.016	81.929
7	107.632	132.742	48.459	100.587	40.205	55.272	47.007	49.877	25.746	141.15	47.58	175.509
VAChT penetration - 8	89.14	*152.19*	43.509	*52.42*	27.527		29.29		25.776		39.813	
9	55.08	34.283	25.586	25.664	15.345	12.88	14.416	16.986	18.851	42.655	23.702	30.976

OK107 / GD+

	SMP ChAT	SMP VAChT	gamma ChAT	gamma VAChT	beta ChAT	beta VAChT	betaprime ChAT	betaprime VAChT	alpha ChAT	alpha VAChT	alphaprime ChAT	alphaprime VAChT
1	26.172	165.785	13.004	100.518	6.932	33.061	10.162	40.267	6.375	160.699	10.286	155.673
VAChT penetration - 2	25.43	*198.267*	10.069	*85.436*	7.305	47.846	8.75	40.026	4.966	128.831	9.815	124.302
3	36.047	67.783	19.663	49.257	10.837	32.683	14.096	42.041	9.998	198.675	20.829	248.339
VAChT penetration - 4	22.377	*152.262*	9.836	*64.4*	7.218		9.197		4.152		7.514	
5	19.735	106.22	10.982	92.881	7.057	46.44	8.832	49.674	6.56	174.577	11.159	192.315
6	29.367	210.846	12.511	118.134	8.096	34.498	8.897	41.374	7.074	210.085	11.564	196.474

Table A.3: Relative quantification of α-ChAT and α-VAChT immunoreactivity in different genotypes and areas of the brain. Relative values were obtained by dividing all MB areas by each brain's absolute SMP fluorescence. See Figure 3.16 for a graphic display of this quantification. Note that in three brains α-VAChT penetration was insufficient to extract fluorescence, hence the empty values.

CS / ChAT

gamma ChAT	gamma VAChT	beta ChAT	beta VAChT	betaprime ChAT	betaprime VAChT	alpha ChAT	alpha VAChT	alphaprime ChAT	alphaprime VAChT
0.54438144	0.87427247	0.28002703	0.29834463	0.34124692	0.44269193	0.3469039	1.58394013	0.52666861	1.95525208
0.45534037	0.71062872	0.22120681	0.19890817	0.22038607	0.27791815	0.19407485	0.94679183	0.31821267	1.05462828
0.43988965	0.73531873	0.25506491	0.26486388	0.24783779	0.36563541	0.31401588	0.82755315	0.49283212	1.11331091

OK107/ChAT

gamma ChAT	gamma VAChT	beta ChAT	beta VAChT	betaprime ChAT	betaprime VAChT	alpha ChAT	alpha VAChT	alphaprime ChAT	alphaprime VAChT
0.31937468	1.42458101	0.23274451	0.68777157	0.17591286	0.71313293	0.27637	1.96577104	0.24380608	2.20608318
0.29504327	1.02628544	0.24272227	0.45862566	0.23294369	0.51749159	0.24064291	1.63306103	0.25154546	2.41090822
0.20291505	0.83212543	0.20388294	0.28436874	0.21720565	0.39513832	0.23736051	1.31868814	0.27470963	1.44970531
0.21503213	0.68355179	0.19536364	0.44490983	0.15890937	0.54050458	0.15263348	2.67882133	0.16428443	3.38893269
0.26251077	0.83270273	0.19185391	0.28629224	0.23205409	0.43060947	0.25409293	1.09067531	0.263505	1.25397605
0.22192152	0.60588949	0.15661068	0.25993162	0.17336623	0.32678946	0.22136432	1.54099482	0.23851787	1.76649388
0.2698636	0.88786447	0.30072464	0.45688223	0.18721228	0.41332465	0.19731458	1.4083727	0.21462063	1.43925721
0.20889339	0.85818564	0.18820966	0.33002494	0.16181796	0.45731915	0.21380347	1.31726401	0.18498742	1.77615859
0.31378018	0.96960884	0.17597834	0.24570307	0.19353515	0.33633852	0.18675308	0.96082594	0.22421856	0.98586593

OK107 / VAChT

gamma ChAT	gamma VAChT	beta ChAT	beta VAChT	betaprime ChAT	betaprime VAChT	alpha ChAT	alpha VAChT	alphaprime ChAT	alphaprime VAChT
0.32637945	0.36745648	0.23790825	0.18874928	0.25115846	0.21442234	0.18481437	0.33696562	0.29984182	0.44238954
0.3592745	0.41994434	0.23111444	0.20790259	0.28922962	0.26541889	0.20078534	0.47344204	0.3434181	0.59839055
0.30931273	0.2146297	0.25569909	0.1187125	0.22606383	0.16805465	0.08194022	0.13385837	0.15594394	0.22154079
0.2787157	0.21611308	0.1577464	0.17686459	0.21270482	0.17686459	0.11151944	0.17107759	0.2804841	0.28816987
0.26254508	0.19565301	0.20406656	0.11738524	0.21197376	0.12995052	0.13907112	0.17863685	0.27323283	0.25319736
0.20376712	0.22433496	0.13058545	0.1610905	0.18166993	0.20131445	0.15553653	0.22337331		

CS / VAChT

gamma ChAT	gamma VAChT	beta ChAT	beta VAChT	betaprime ChAT	betaprime VAChT	alpha ChAT	alpha VAChT	alphaprime ChAT	alphaprime VAChT
0.57698168	0.66386307	0.38581104	0.37113922	0.44670499	0.40381942	0.23926098	0.65473777	0.40618158	0.86202558
0.65092634	1.22063639	0.37687401	0.42981207	0.42000163	0.58052392	0.31429529	1.15805809	0.52262016	1.48889522
0.54710973	1.10480628	0.35164506	0.55970088	0.41351835	0.64667243	0.37974073	1.24513923	0.61878401	1.25763782
0.65319749	0.91491608	0.37700627	0.32804456	0.41748433	0.50109586	0.32482759	1.20882514	0.5104232	1.60285433
0.50822178	0.61085435	0.31558181	0.30953313	0.29841201	0.3273278	0.30667173	0.49073059	0.44237169	0.79532874
0.42838438	0.51686309	0.29489128	0.23517609	0.29559271	0.26658825	0.26102408	0.35935638	0.49118541	0.62985001
0.45022856	0.75776318	0.37354133	0.41638667	0.43673814	0.37574392	0.23920395	1.06334092	0.44206184	1.06334092
0.48809737		0.30880637		0.32858425		0.28916311		0.44663451	
0.46452433	0.7485926	0.27859477	0.49546422	0.2617284	0.49546422	0.34224764	1.24420267	0.43031954	0.9035382

OK107 / GD+

gamma ChAT	gamma VAChT	beta ChAT	beta VAChT	betaprime ChAT	betaprime VAChT	alpha ChAT	alpha VAChT	alphaprime ChAT	alphaprime VAChT
0.49686688	0.60631541	0.26486321	0.19942094	0.38827755	0.24288687	0.24358093	0.96932171	0.39301544	0.93900534
0.39594967		0.28725914		0.34408179		0.19528116		0.38596146	
0.54548229	0.72668663	0.30063528	0.48217105	0.39104502	0.62022926	0.27736011	2.93104466	0.57782895	3.66373574
0.43955848		0.32256335		0.41100237		0.18554766		0.33579121	
0.55647327	0.87442101	0.35758804	0.4372058	0.44752977	0.46765204	0.33240436	1.64354171	0.56544211	1.81053474
0.42602241	0.56028571	0.27568359	0.16361705	0.3029591	0.19622853	0.24088262	0.99639073	0.39377533	0.93183651

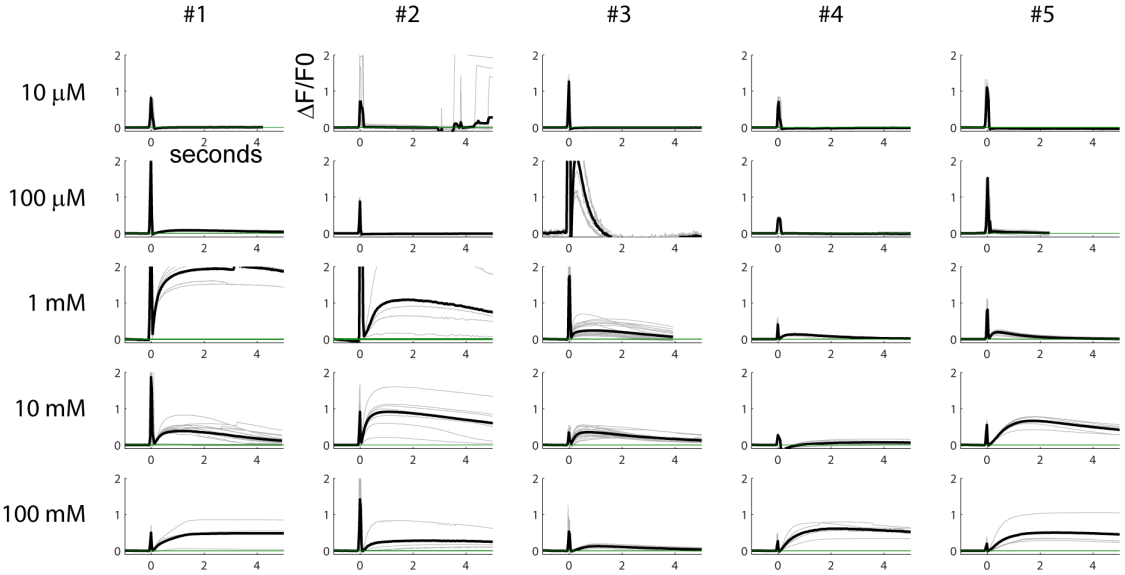


Figure A.2: Overview of calcium transients of 25 R21D02-GAL4 ; GCaMP5 explant brains injected with 5 different concentrations of ACh, from 10 µM to 100 mM. Each horizontal row shows results of five individual brains at a given concentration of ACh. Black line shows the mean calcium transient of all stimulations. Each stimulation calcium transient is shown in grey. See Figure 3.5A for subsequent dose-response curve that shows systematic increase of peak responses with increased concentrations of ACh. Initial peaks at time '0' relate to LED trigger artefact.

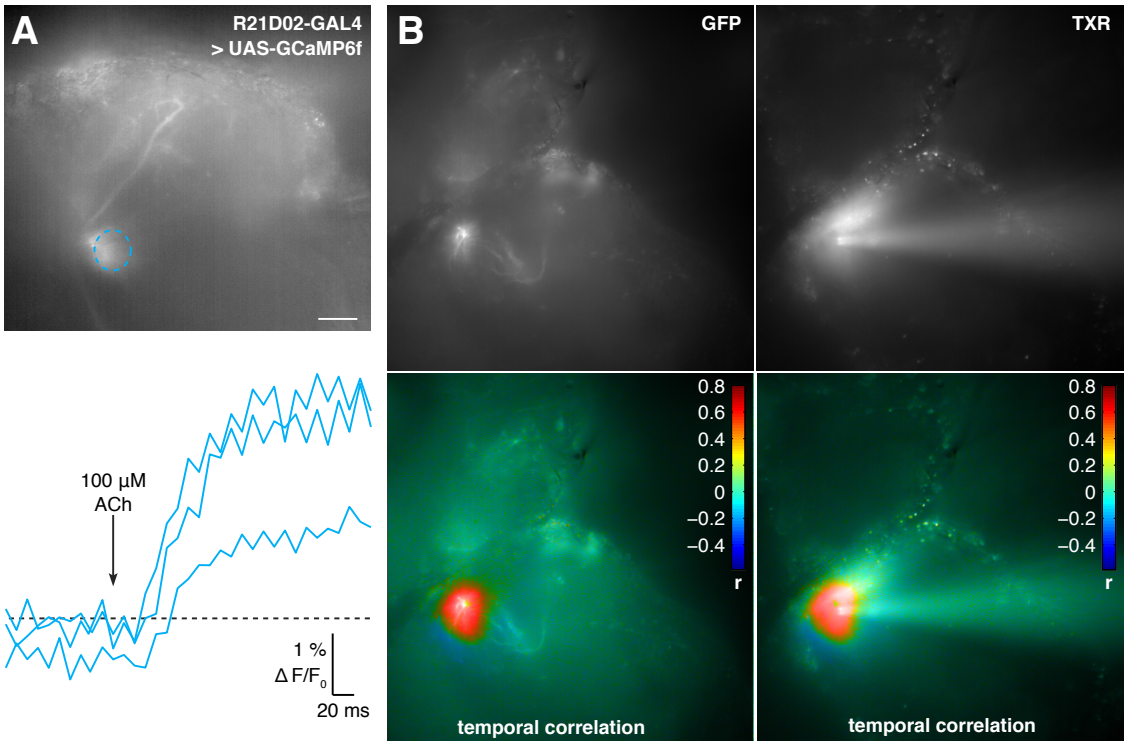


Figure A.3: Calcium responses to ACh are fast and temporally correlate with injected ACh spread. A) Imaging at 100 Hz reveals fast dendritic calcium response onset. I expressed GCaMP6f in R21D02-GAL4 driven M4/6 neurons, and imaged calcium transients at 100 Hz. Top, averaged green fluorescence and the ROI (blue dashed circle) around the M4/6 dendrites from which calcium transients were recorded. Bottom, three trials of calcium transients in response to ACh stimulation. After 3-4 frames, calcium transients start rising, suggesting a GCaMP response after a mere 30-40 ms after stimulation. Data shown is part of Figure 3.6. B) ACh spread correlates temporally with GCaMP6f calcium signal. Calcium transients were first recorded upon stimulation with 100 µM ACh to the dendrite. Subsequently, spread of solution was measured using TXR in the solution, and monitored using the red fluorescent channel. For analysis, each pixel's green/red fluorescent trace was correlated between stimulus onset up to 3 s after. Upper two graphs show a sample image of the recording briefly after stimulation. Lower graphs show the same as above, but with an overlay of the colour-coded temporal correlation of the fluorescent traces between the two. ACh spread and calcium transient strongly correlate in the dendritic region of M4/6. Partly adapted from Barnstedt et al. (2016).

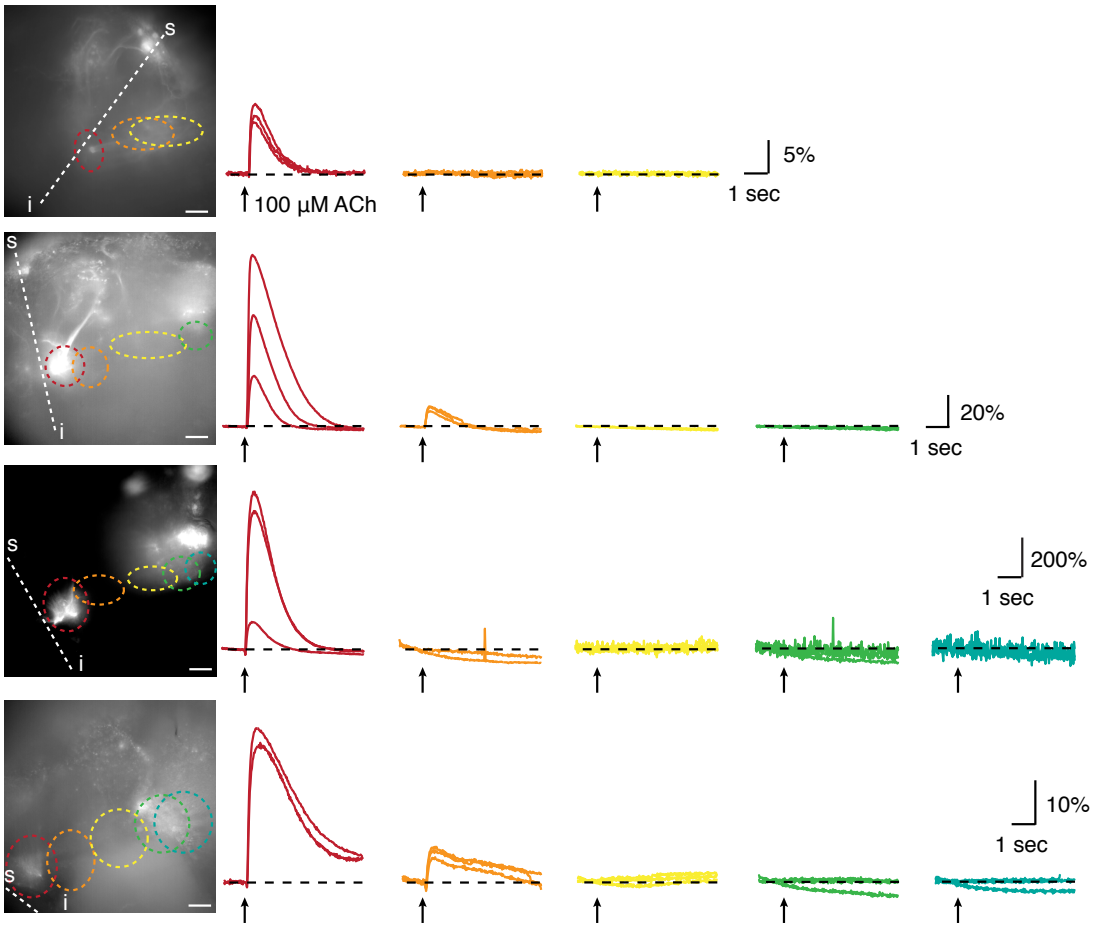


Figure A.4: M4/6 calcium responses are only elicited when ACh is released close to its dendritic arbour. In four different brains 100 µM ACh were released first at the M4/6 dendritic arbour, followed by more distal regions in the SMP. Shown on the left are fluorescent images of the brain, with coloured dashed ellipsoids indicating spread of solution at various regions. Anatomy is indicated by a white dashed line representing the midline, and 's' for superior and 'i' for inferior. Scale bar is 20 µm. Traces on the right are fluorescent traces taken from M4/6 dendritic field upon stimulation in the respective area matched by colour. Calcium responses only appear in close proximity to M4/6 dendritic field (red traces, and orange traces to some degree). Adapted from Barnstedt et al. (2016).

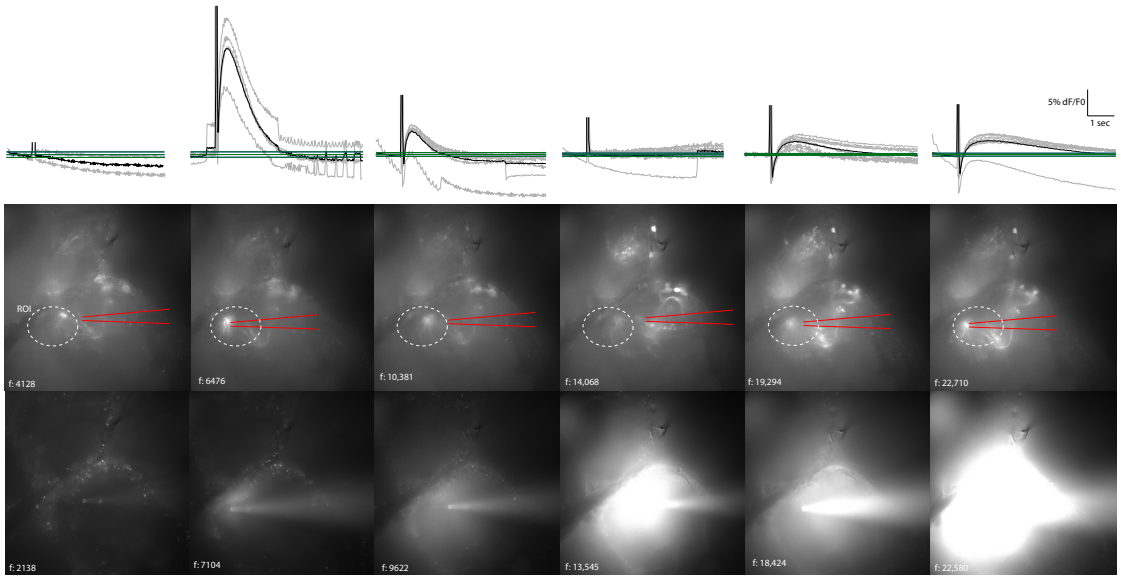


Figure A.5: M4/6 neurons' calcium response depends on distance of injection site to dendritic arbour. In one brain expressing R21D02-GAL4 driven GCaMP5, 1 mM ACh was injected at various distances from the M4/6 dendritic arbour. Upper row shows calcium transients upon pipette release at a location indicated below. Green lines represent baseline fluorescence +/- SD. Red lines represent outline of injection pipette. Upper row of images shows green fluorescent channel at a given time, and lower row shows red fluorescent channel with TXR-marked spread of solution. Fluorescent traces were extracted from ROI marked in white dashed ellipse. Responses are only elicited when the pipette enters the M4/6 dendritic field.

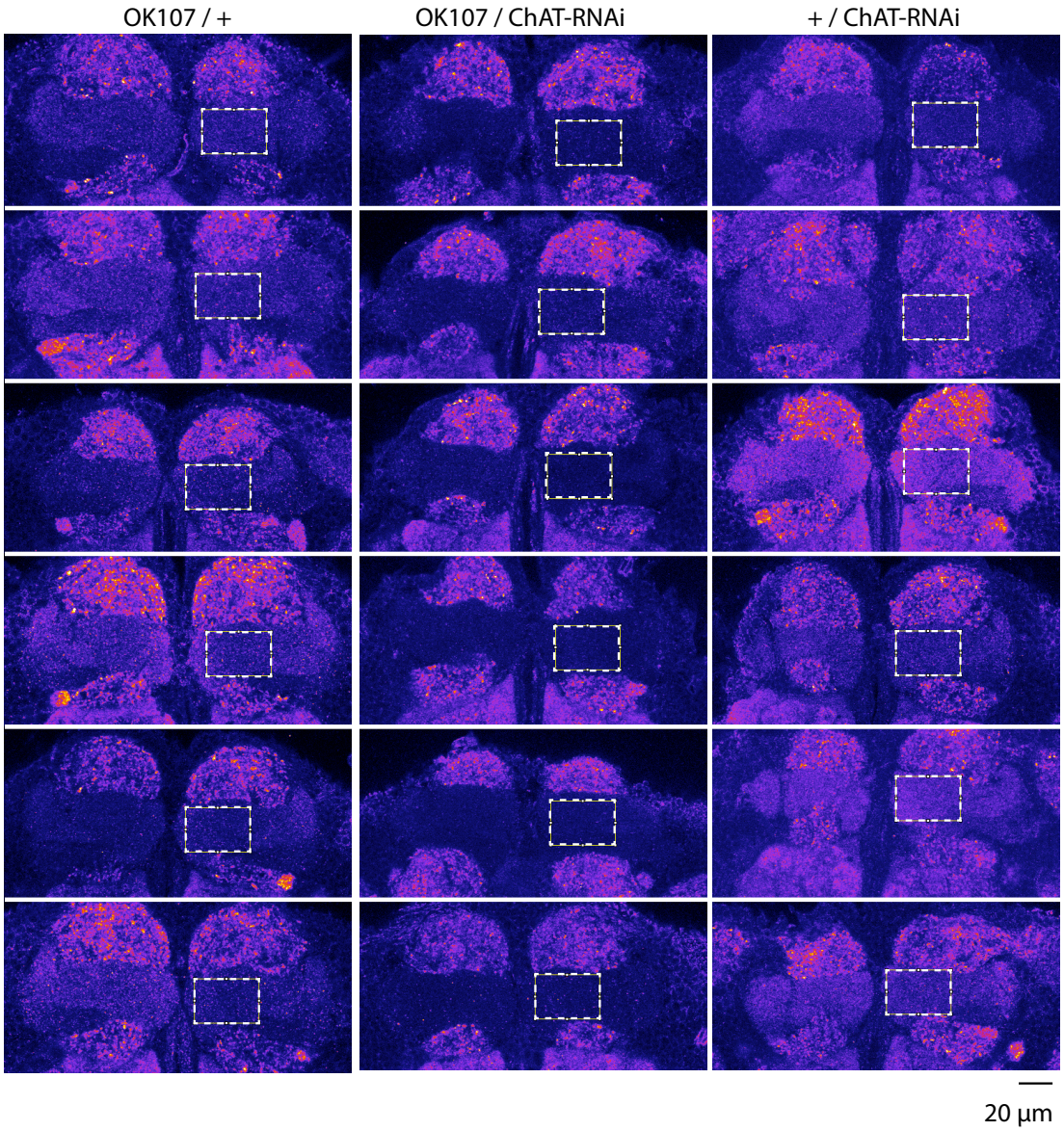


Figure A.6: KC-driven ChAT-RNAi generally reduces ChAT-positive staining. Individual planes at the level of the MB γ lobes of six brains per genotype (OK107/+, left; OK107/ChAT-RNAi, middle; +/ChAT-RNAi, right) are displayed, each brain in a new row. All brains were treated equally at the same time, and scanned and processed with the same parameters. White rectangle (40 × 25 µm) shows area in which fluorescence was sampled for quantification.

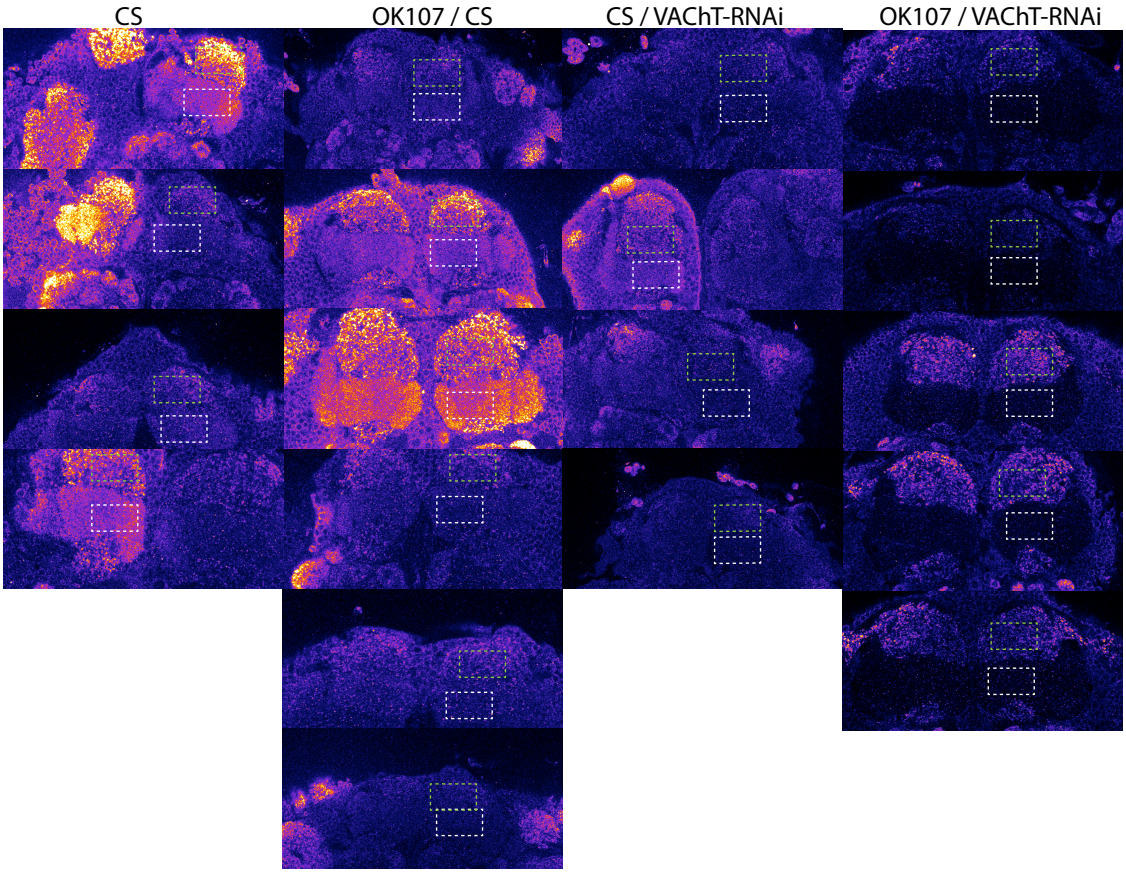


Figure A.7: VAChT immunostaining is significantly decreased in MBs of KC-driven VAChT-RNAi flies. 4-6 brains per genotype are shown at the level the MB gamma lobe. Genotypes are grouped by column (CS, left; OK107-GAL4/CS, second from left; CS/VAChT-RNAi, second from right; OK107-GAL4/VAChT-RNAi, right). Rectangles of 40×25 µm display the areas from which fluorescence was measured. Green rectangles describe the SMP control area, and white rectangles describe the gamma lobe area. Relative fluorescence was calculated as fluorescence in gamma divided by SMP for each brain. This quantification revealed a significant strong decrease in gamma lobe fluorescence in flies expressing VAChT-RNAi in OK107-GAL4 driven KCs (bottom panel). While control flies showed a relative fluorescence of about 80%, experimental flies only had 30% relative fluorescence in gamma lobes. See also Table A.1 for exact numbers.

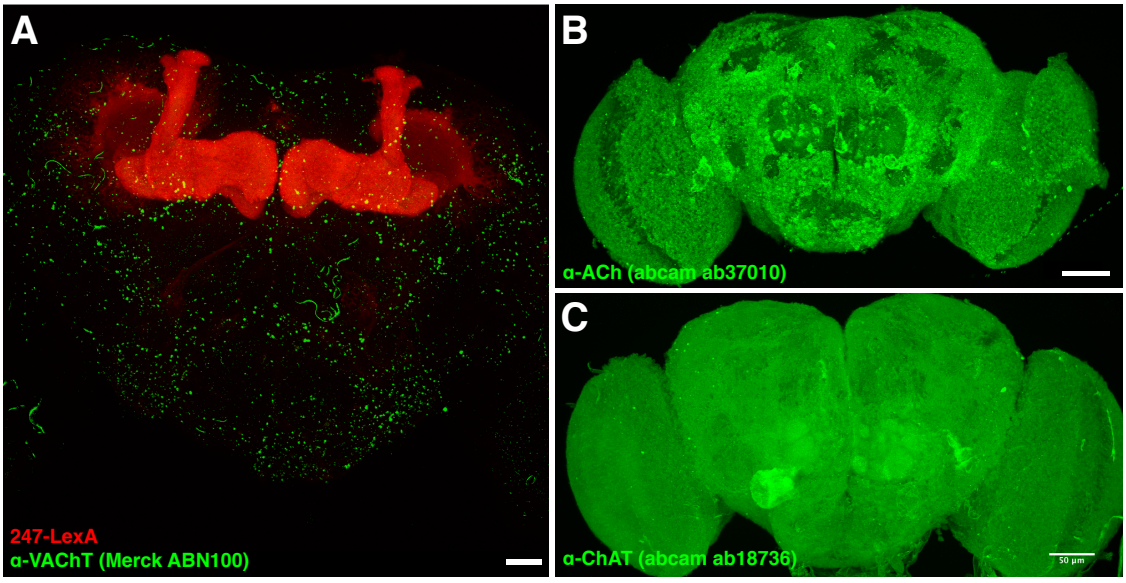


Figure A.8: A) Merck ABN100 goat α-VAChT antibody shows no detectable specific staining in the *Drosophila* brain. The standard staining protocol yielded only unspecific antibody punctae at the surface of the brain (green), and no visible overlap with KCs (red). Scale bars represent 20 µm. antibody used from Merck, tested in Boccaletto, 2013 B) Conjugated ACh antibody (ab37010) shows no specific staining in the *Drosophila* brain. C) Sheep α-ChAT staining shows unspecific staining. After standard staining protocol (see Methods chapter) with ab18736, only superficial unspecific staining is visible. Shown is a maximum Z-projection.

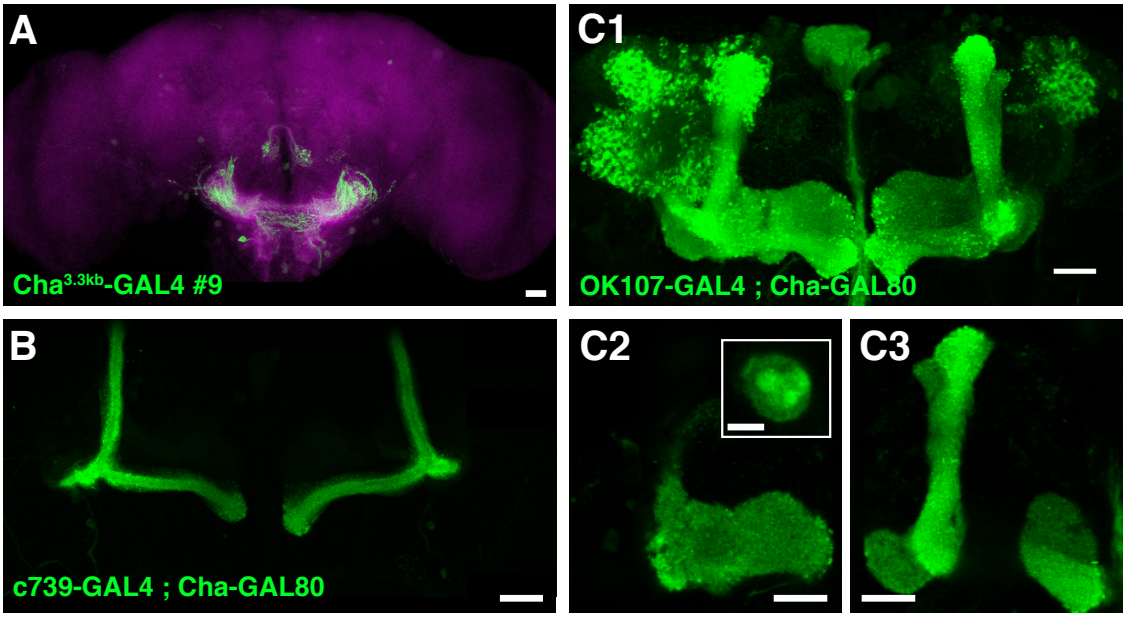


Figure A.9: A) Cha3.3kb-GAL4 only expresses in JO neurons. Cha3.3kb-GAL4 was used to drive UAS-mCD8::GFP (green), and brain was stained against nc82 (magenta). B) c739-GAL4 ; Cha-GAL80 (Kitamoto, 2002; Yang et al., 1995) drivers restrict expression to α/β core neurons. Driver lines were used to drive UAS-mCD8::GFP (green). c739-GAL4 normally drives expression in most α/β neurons Perisse et al., 2013b, raising the possibility that Cha-GAL80 expresses, amongst others, in α/β surface neurons. C) OK107-GAL4 ; Cha-GAL80 reduces expression greatly in γ, α′/β′, and to a lesser degree in α/β. OK107-GAL4 normally drives expression in $> 1,917$ KCs (Aso et al., 2009), but with the addition of Cha-GAL80 this expression is much reduced. All scale bars represent 20 µm.

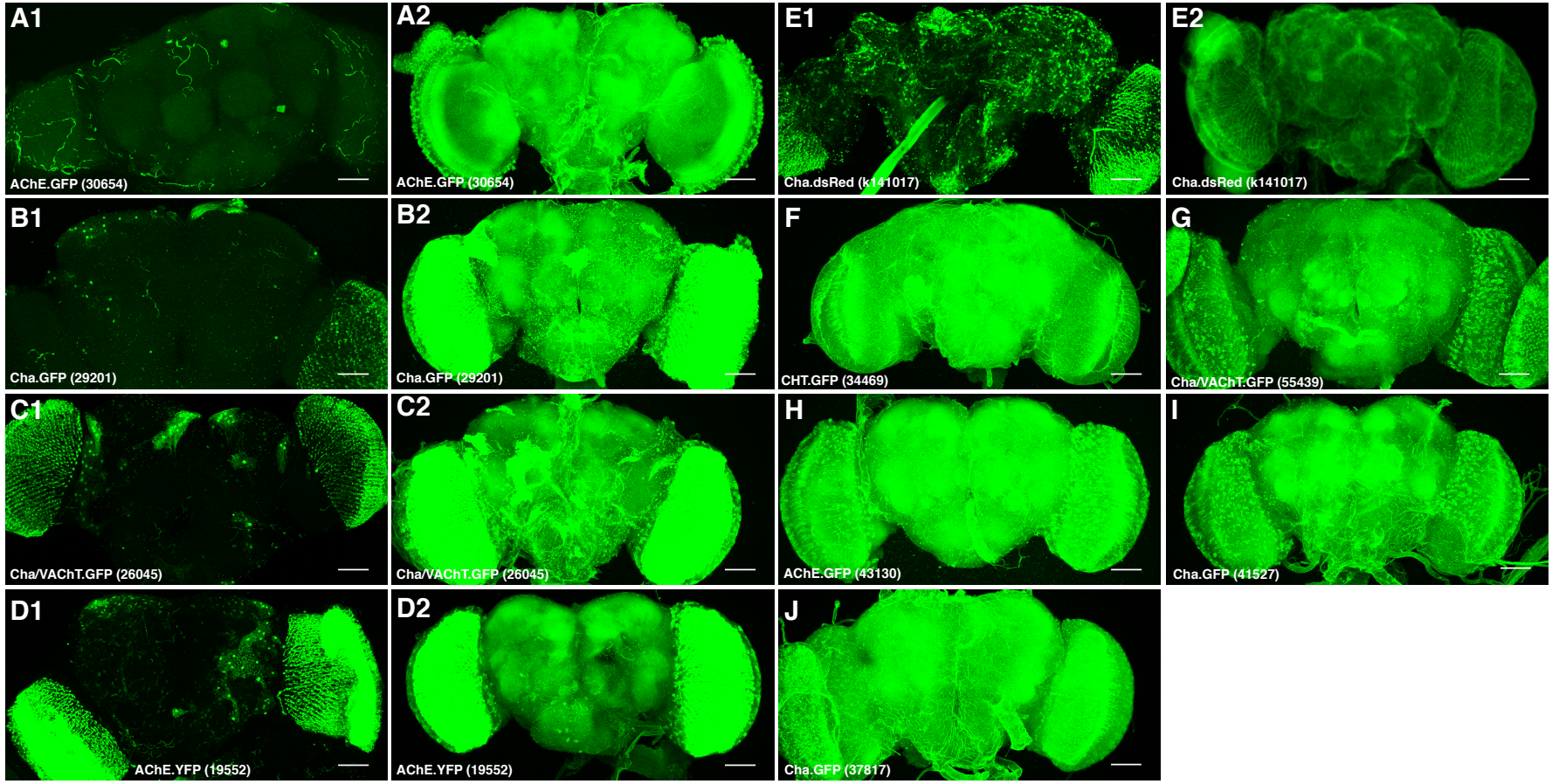


Figure A.10: MiMIC expression of cholinergic genes. The expression patterns of 10 different MiMIC lines with FPs in cholinergic loci were visualised with (A2-E2,F-J) or without (A1-E1) staining against GFP. Expression was generally detected in the optic lobe and some glia. CHT refers to CG7708 which might serve as a choline transporter. Numbers in brackets refer to Bloomington number, except for E which is from Kyoto Stock Center. Scale bars represent 50 µm.

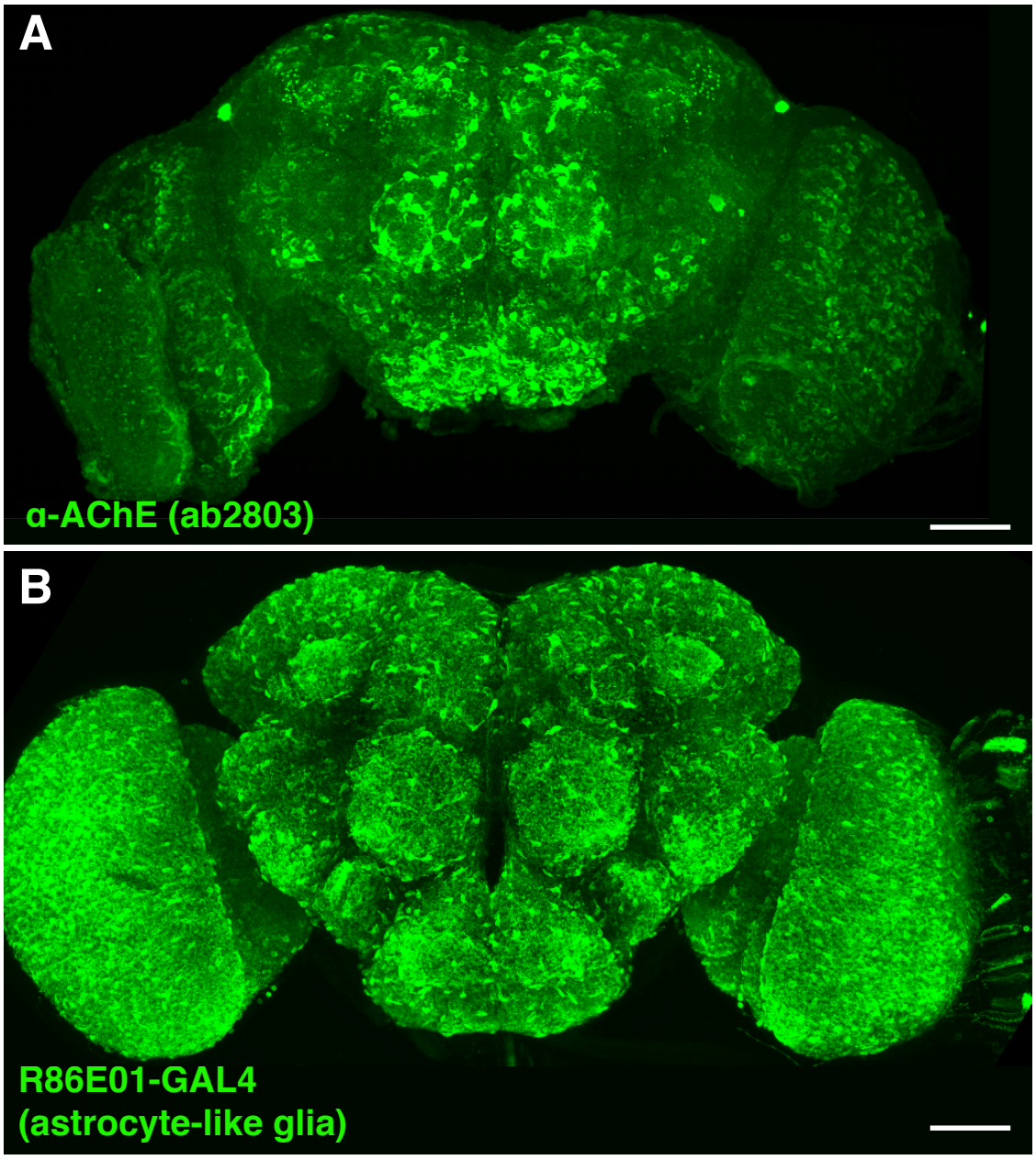


Figure A.11: Comparison of α-AChE staining pattern with astrocyte-like glia expression. A) Maximum projection overview of α-AChE staining, seen in Figure 3.17. Note the labelling of many cell bodies with small neurites, especially in SMP, AL, and SOG. B) Maximum projection overview of R86E01-GAL4 expression pattern, previously shown to represent astrocyte-like glia (ALG) (Kremer et al., 2017). Image was taken from FlyLight (`flweb.janelia.org`; Jenett et al., 2012). Scale bars represent 50 µm.

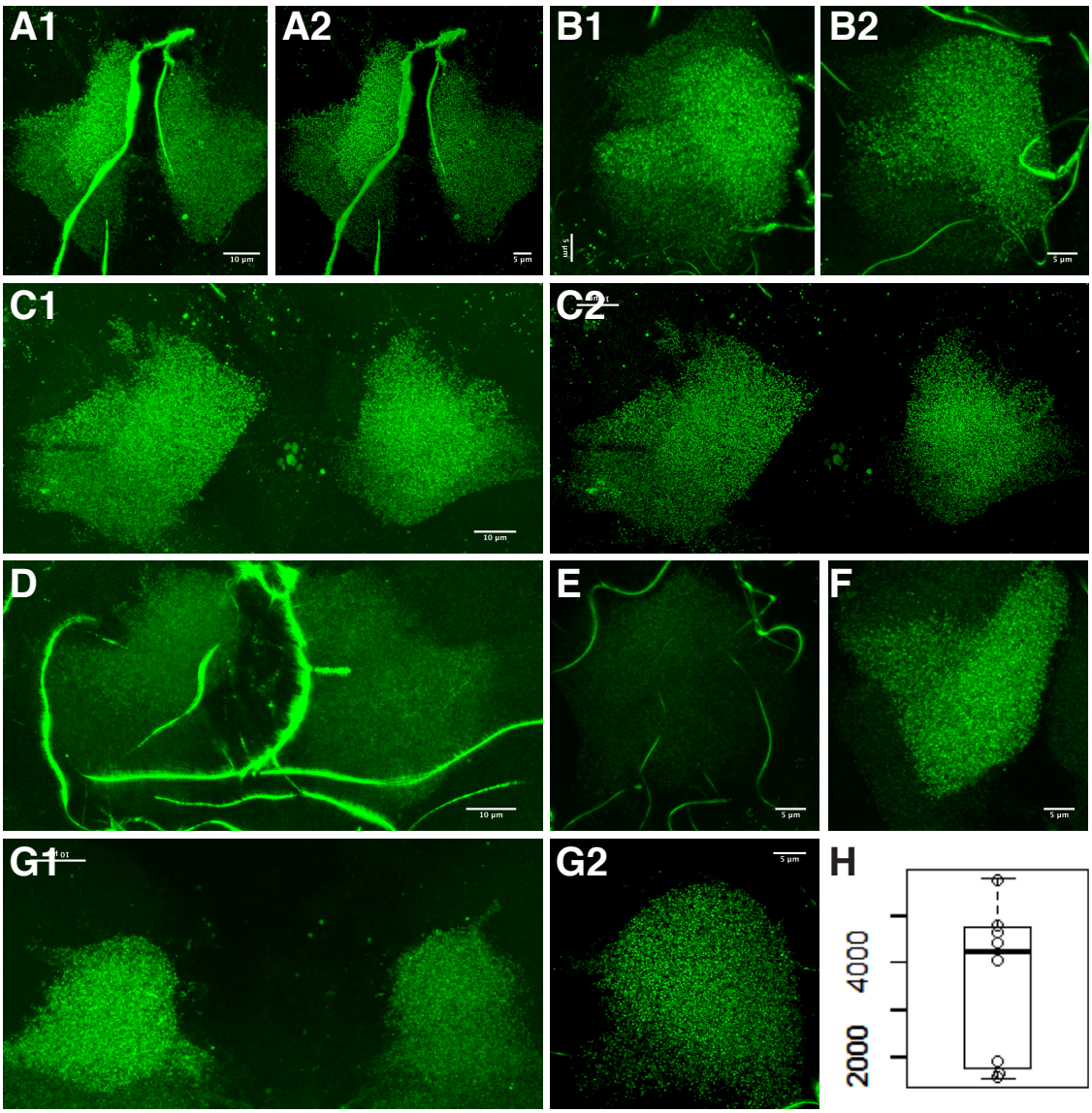


Figure A.12: Dα7::GFP reliably forms punctae in M4/6 dendrites. A-G) 7 brains of flies carrying R21D02-GAL4>UAS-Dα7::GFP were scanned on the level of MB horizontal lobe tips. All brains showed distinct punctae in the dendritic region of M4/6, but none elsewhere. Some images were deconvolved using Huygens software to identify punctae more clearly, these are indicated by the addition of "2". H) Quantification of M4/6 Dα7::GFP punctae reveal about 4,000 per hemisphere in all three compartments together. Punctae were counted using Huygens Object Analyzer.

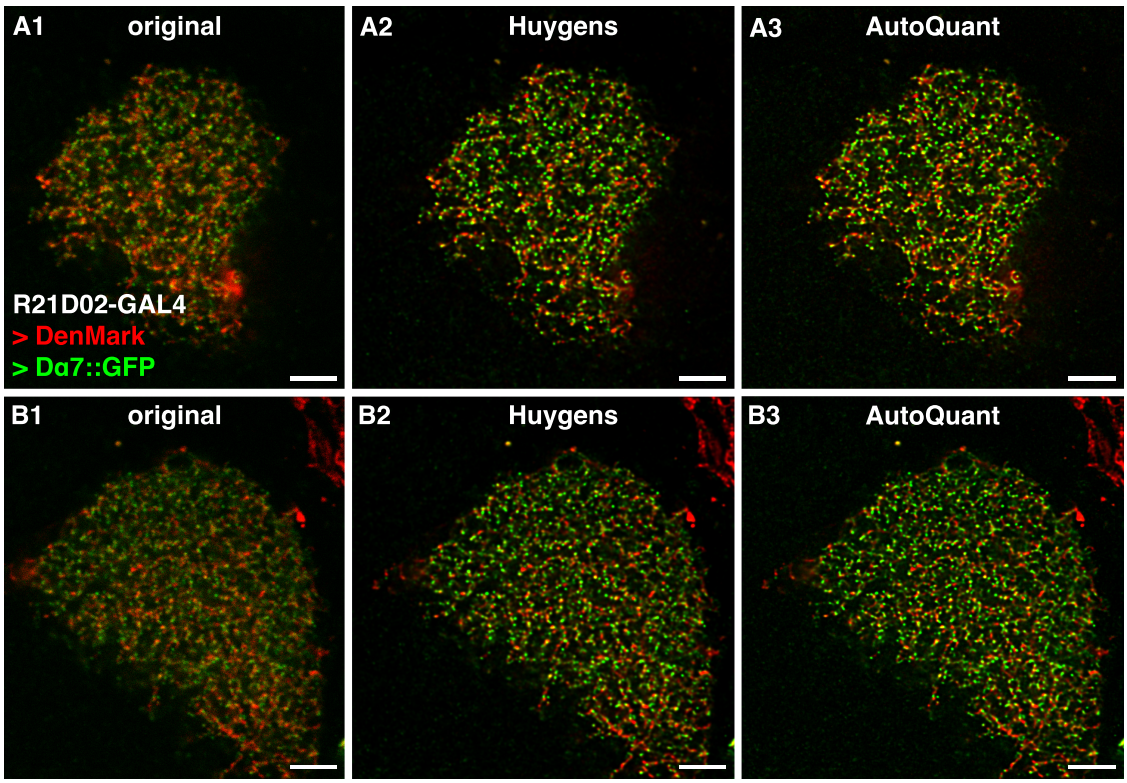


Figure A.13: Dα7::GFP (green) expresses closely to postsynaptic sites marked by DenMark (red) in M4/6 neurons. R21D02-GAL4 was used to express both UAS-Dα7::GFP and the dendritic marker UAS-DenMark. A1/B1) Images shows single planes of the γ5 compartment, with native expression of both fluorophores. A2-3/B2-3) Deconvolved images of Dα7::GFP (green) with DenMark (red) in M4/6 show close proximity of nicotinic receptors with postsynaptic sites. DenMark fluorescence forms thin arbours along which Dα7::GFP punctae are nestled. Blind deconvolution yields comparable results between Huygens Deconvolution (A2/B2) and AutoQuant software (A3/B3)

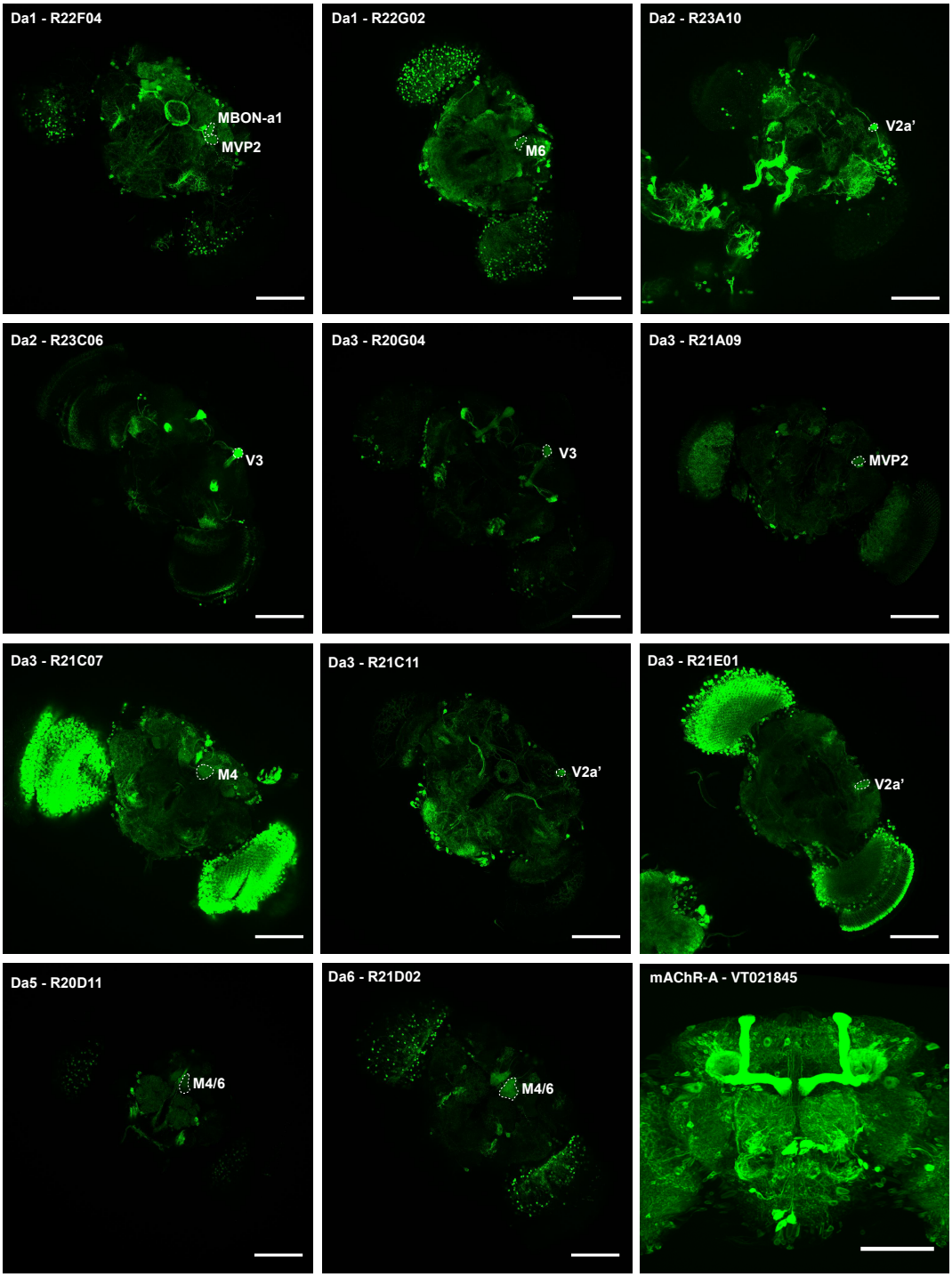


Figure A.14: nAChR promoter fragments drive expression in MBONs; an mAChR promoter fragment drives expression in α/β KCs. From left top to right bottom: Dα1 is expressed in R22G02-GAL4 including M6 neurons, and R22F04-GAL4 including MVP2 neurons. Dα2 is expressed in R23A10-GAL4 including V2α′, and R23C06-GAL4 including V3 neurons. Dα3 is expressed in R20G04-GAL4 including V3 neurons, R21E01-GAL4 including V2α′ neurons, R21C11-GAL4 including V2α′ neurons, R21A09-GAL4 including MVP2 neurons, and R21C07-GAL4 including M4/6 neurons. Dα5 is expressed in R20D11-GAL4 including M4/6 neurons. Dα6 is expressed in R21D02-GAL4 including M4/6 neurons. These images show individual confocal imaging planes obtained from the FlyLight website `flweb.janelia.org` (Jenett et al., 2012). mAChR-A is expressed in VT021845-GAL4 including α/β KCs. Image is a maximum projection of a confocal stack obtained from BrainBase (`brainbase.imp.ac.at`). All scale bars represent 100 µm.

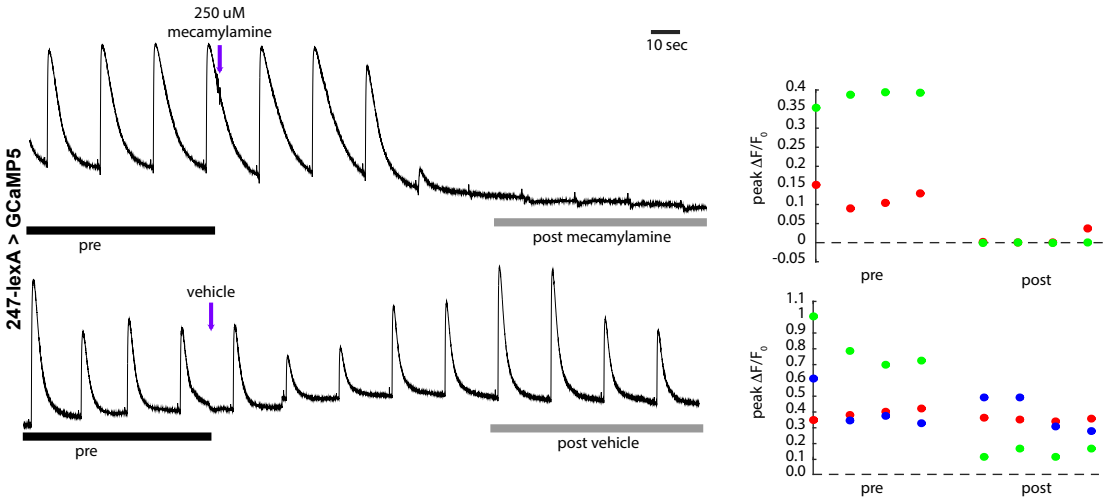


Figure A.15: Mecamylamine blocks ACh-induced calcium responses in KC calyx. 10 mM ACh were injected every 20 seconds into the calyx of 247::GCaMP5 explant brains while calcium transients were recorded from the calyx under widefield microscopy. Left panels show sample calcium transients. The addition of 250 µM mecamylamine rapidly abolishes these ACh-induced responses (upper panel), while the addition of vehicle has no major effect on these (lower panel). Right side shows peak $\Delta F/F_0$ values, each dot representing one peak value after stimulation, each colour representing a different brain. 'Post' values are taken 100 seconds after addition of mecamylamine or vehicle.

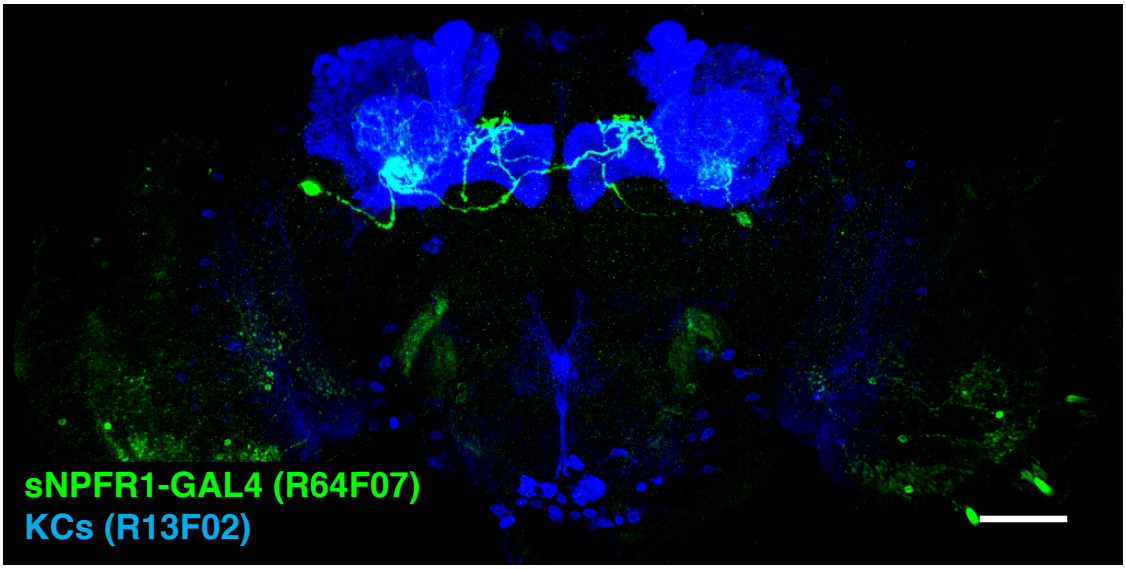


Figure A.16: sNPFR1-GAL4 (R64F07) expresses specifically in MB-CP1 neurons. Maximum projection overview of sNPFR1-GAL4 (R64F07) expression pattern (green) and KCs (R13F02), overlaid. Images are from FlyLight (`flweb.janelia.org`; Jenett et al., 2012), and were registered by the Jefferis lab (Manton et al., 2014a; Milyaev et al., 2012). Scale bar represents 50 µm.

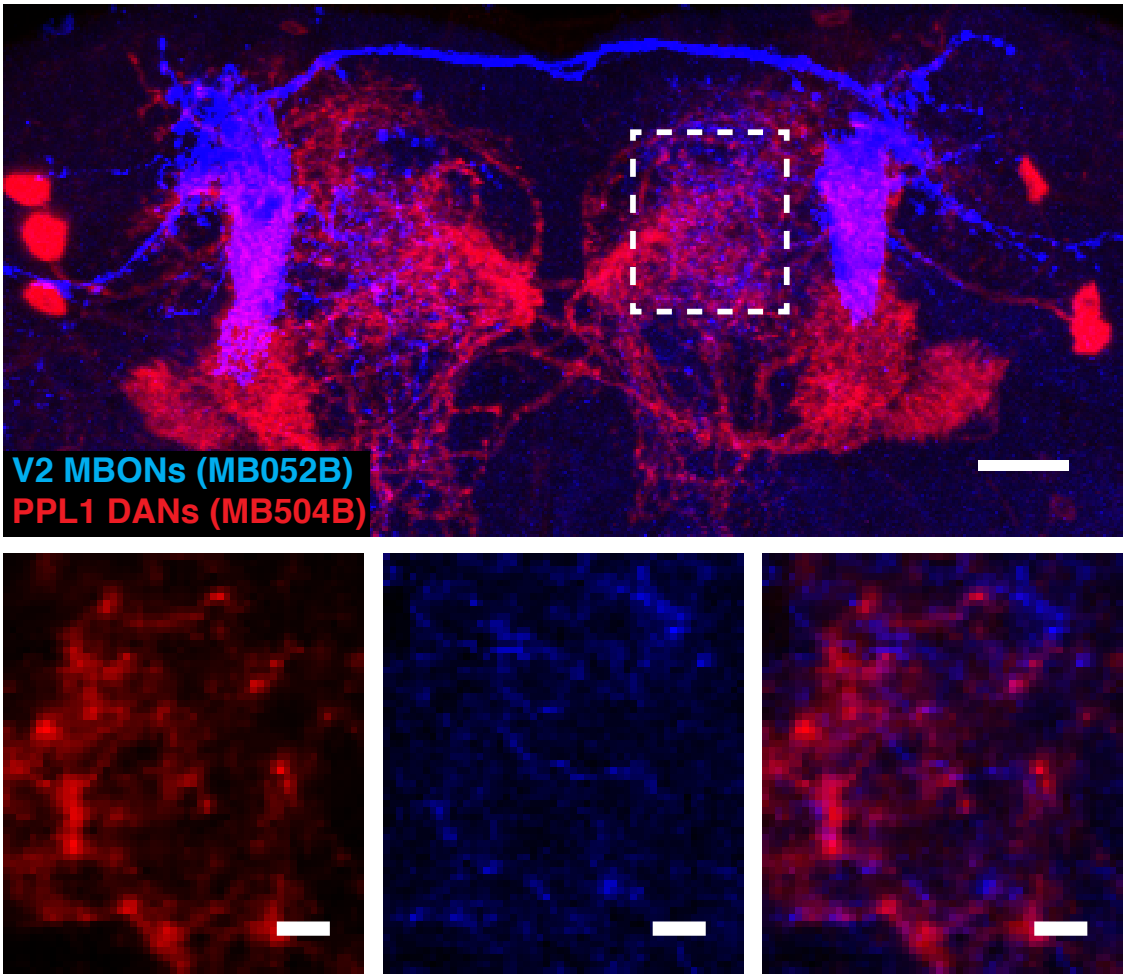


Figure A.17: V2 MBONs and PPL1 DANs have overlapping neurites. Top, maximum projection overview of V2 MBON expression pattern from MB052B (blue) overlaid with PPL1 DAN expression pattern (red) from MB504B. Bottom images show the white dashed area of interest at higher magnification – images shown are from a single plane. Stacks are from Figure 6.1, and were registered to the Janelia standard brain with CMTK registration before being overlaid. Scale bar represents 20 µm in top image, and 5 µm in bottom images.

Article

Neuron

Memory-Relevant Mushroom Body Output Synapses Are Cholinergic

Highlights

- Mushroom body Kenyon cell function requires ChAT and VAChT expression
- Kenyon cell-released acetylcholine drives mushroom body output neurons
- Blocking nicotinic receptors impairs mushroom body output neuron activation
- Acetylcholine interacts with coreleased neuropeptide

Authors

Oliver Barnstedt, David Owald, Johannes Felsenberg, ..., Clifford B. Talbot, Paola N. Perrat, Scott Waddell

Correspondence

david.owald@charite.de (D.O.), scott.waddell@cncb.ox.ac.uk (S.W.)

In Brief

Fruit fly memory involves plasticity of mushroom body synapses. Barnstedt et al. identified acetylcholine as the mushroom body neurotransmitter. Mushroom body output neuron activation requires nicotinic acetylcholine receptors. Impaired receptor function reduces physiological responses and alters odor-driven behavior.

Barnstedt et al., 2016, Neuron *89*, 1237–1247
March 16, 2016 ©2016 The Authors
http://dx.doi.org/10.1016/j.neuron.2016.02.015

CellPress

Neuron
Article

Memory-Relevant Mushroom Body Output Synapses Are Cholinergic

Oliver Barnstedt,[1] David Owald,[1,3,*] Johannes Felsenberg,[1] Ruth Brain,[1] John-Paul Moszynski,[1] Clifford B. Talbot,[1] Paola N. Perrat,[2] and Scott Waddell[1,*]
[1]Centre for Neural Circuits and Behaviour, The University of Oxford, Tinsley Building, Mansfield Road, Oxford OX1 3SR, UK
[2]Department of Neurobiology, UMass Medical School, Worcester, MA 01605, USA
[3]Present address: Institute of Neurophysiology, Charité – Universitätsmedizin Berlin, 10117 Berlin, Germany
*Correspondence: david.owald@charite.de (D.O.), scott.waddell@cncb.ox.ac.uk (S.W.)
http://dx.doi.org/10.1016/j.neuron.2016.02.015
This is an open access article under the CC BY license (http://creativecommons.org/licenses/by/4.0/).

SUMMARY

Memories are stored in the fan-out fan-in neural architectures of the mammalian cerebellum and hippocampus and the insect mushroom bodies. However, whereas key plasticity occurs at glutamatergic synapses in mammals, the neurochemistry of the memory-storing mushroom body Kenyon cell output synapses is unknown. Here we demonstrate a role for acetylcholine (ACh) in *Drosophila*. Kenyon cells express the ACh-processing proteins ChAT and VAChT, and reducing their expression impairs learned olfactory-driven behavior. Local ACh application, or direct Kenyon cell activation, evokes activity in mushroom body output neurons (MBONs). MBON activation depends on VAChT expression in Kenyon cells and is blocked by ACh receptor antagonism. Furthermore, reducing nicotinic ACh receptor subunit expression in MBONs compromises odor-evoked activation and redirects odor-driven behavior. Lastly, peptidergic corelease enhances ACh-evoked responses in MBONs, suggesting an interaction between the fast- and slow-acting transmitters. Therefore, olfactory memories in *Drosophila* are likely stored as plasticity of cholinergic synapses.

INTRODUCTION

Understanding how memories are formed, stored, and retrieved from neural networks is an important pursuit of neuroscience. The insect mushroom bodies (MBs) are prominent bilateral brain structures that have been extensively studied for their universal role in learned behavior (Strausfeld et al., 1998; Heisenberg, 2003; Farris, 2013; Perisse et al., 2013a; Menzel, 2014). In the larger eusocial insects, such as honeybees, the MBs are comprised of a few 100,000 intrinsic neurons or Kenyon cells (KCs), whereas the smaller fruit fly MBs have only around 2,000 neurons per hemisphere. The anatomy of the MB has been compared to the fan-out, fan-in neural architecture of the mammalian cerebellum and hippocampus (Farris, 2011; Stevens, 2015; Menzel, 2014; Owald and Waddell, 2015) and to the cephalopod vertical lobes (Shomrat et al., 2011). Analogies have also been drawn to the vertebrate amygdala, basal ganglia, and pallium (Hige et al., 2015; Waddell 2013; Tomer et al., 2010). It is therefore of interest to understand the logic of how the MB operates and to what level functional principles relate to those of similar neural structures across phyla. Importantly, recent studies suggest that in the *Drosophila* MB cellular mechanisms of neural plasticity can be directly linked to behavioral change (Owald et al., 2015).

In all insects the axons from different subpopulations of KCs are arranged into separate parallel bundles, or lobes (Strausfeld et al., 2009). Some of the anatomical subdivision serves individual sensory modalities such as olfaction, gustation, and vision (Strausfeld et al., 1998; Murthy et al., 2008; Honegger et al., 2011; Campbell et al., 2013; Caron et al., 2013; Vogt et al., 2014; Aso et al., 2014a), while certain KCs may be multimodal (Strausfeld et al., 2009; Kirkhart and Scott, 2015). The primary sensory input to *Drosophila* KCs occurs in the MB calyx where their dendrites receive divergent fan-out input from around 50 classes of cholinergic olfactory projection neurons (Yasuyama et al., 2002; Caron et al., 2013). Odor-specific activity in the projection neuron population is transformed into activation of fairly sparse subpopulations of KCs across the $\alpha\beta$, $\alpha'\beta'$ and γ divisions in the overall MB ensemble (Honegger et al., 2011; Campbell et al., 2013; Lin et al., 2014a). Reinforcing dopaminergic neurons that innervate nonoverlapping zones of the MB lobes are believed to assign positive or negative values to odor-activated KCs during learning (Mao and Davis, 2009; Claridge-Chang et al., 2009; Aso et al., 2012; Liu et al., 2012; Burke et al., 2012; Waddell, 2013). Comprehensive anatomical studies have characterized all of the dopaminergic input and the output pathways of the MB (Tanaka et al., 2008; Aso et al., 2014a). Remarkably, information from the 2,000 KCs converges, or fans-in, onto the dendrites of 21 different types of mushroom body output neurons (MBONs). The MBONs tile the MB lobes into 15 discrete compartments, and each one has a corresponding set of afferent dopaminergic neurons (DANs). This anatomy alone suggests that learning-related plasticity alters odor drive to downstream MBONs whose dendrites occupy the same zones as the reinforcing dopaminergic neurons (Aso et al., 2014b; Owald and Waddell, 2015). Indeed, several studies have shown that reinforcer quality is represented in discrete dopaminergic zones on the MB lobes (Aso et al., 2012; Das et al., 2014; Galili et al., 2014; Lin et al., 2014b; Huetteroth et al., 2015; Yamagata et al., 2015) and have documented altered odor drive to specific MBONs after learning (Séjourné et al., 2011; Plaçais et al.,

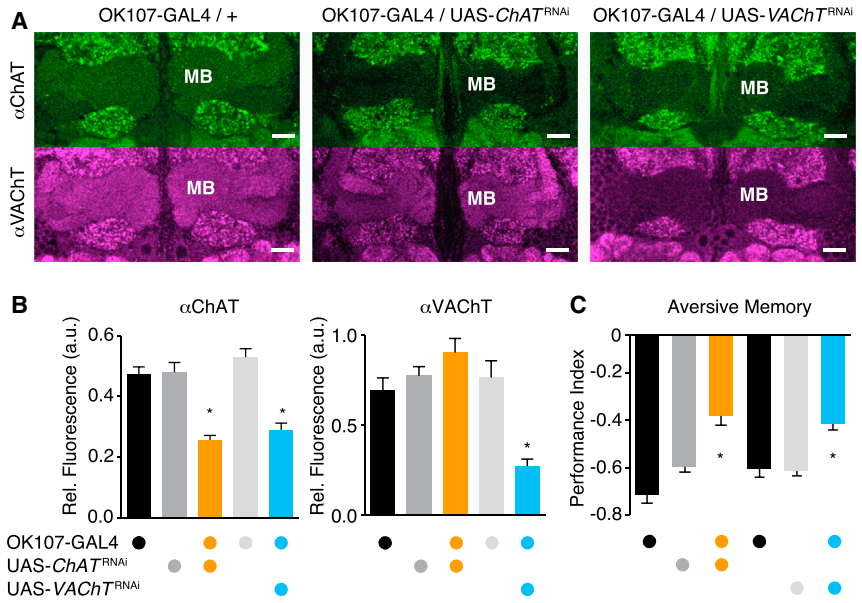


Figure 1. Kenyon Cells Express ChAT and VAChT, and Compromised *ChAT* or *VAChT* Expression Impairs MB Function

(A) MBs label with an antibody to ChAT (upper row) and an antibody to VAChT (bottom row). Pseudocolored images of single confocal sections at the level of the MB γ lobe. OK107-GAL4-driven UAS-*ChAT*^{RNAi} in KCs reduces anti-ChAT label in the MB. UAS-*VAChT*^{RNAi} reduces anti-ChAT and anti-VAChT immunoreactivity in MB. See Figure S1 for additional data. Scale bar, 20 μm.

(B) Quantification of (A). Anti-ChAT label is significantly lower in MBs in UAS-*ChAT*^{RNAi}; OK107-GAL4 and UAS-*VAChT*^{RNAi};OK107-GAL4 flies as compared to all genetic controls. Anti-VAChT signal is significantly lower in MBs in UAS-*VAChT*^{RNAi};OK107-GAL4 flies (n = 3–9, asterisks denote $p < 0.05$; one-way ANOVA, Tukey's HSD post hoc test). Similar results are evident in the α, α′, β, and β′ lobes (data not shown).

(C) Aversive olfactory memory expression requires ACh function in KCs. Performance of UAS-*ChAT*^{RNAi};OK107-GAL4 and UAS-*VAChT*^{RNAi}; OK107-GAL4 flies is significantly different from that of heterozygous controls (n = 6, asterisks denote $p < 0.01$; one-way ANOVA, Tukey's HSD post hoc test). See Figures S2A–S2C for additional experiments. Error bars in (B) and (C) represent the standard error of the mean (SEM).

2013; Pai et al., 2013; Owald et al., 2015; Bouzaiane et al., 2015). Interestingly, reward learning appears to reduce drive to output pathways that direct avoidance behavior, whereas aversive learning increases drive to avoidance pathways while reducing drive to approach pathways (Owald et al., 2015). Learning requires dopamine receptors and cAMP signaling in the KCs (Kim et al., 2007; Qin et al., 2012; Zars et al., 2000; McGuire et al., 2003; Blum et al., 2009; Trannoy et al., 2011), which implies a presynaptic mechanism of plasticity at KC-MBON junctions. In fact, a recent study (Hige et al., 2015) demonstrated that pairing odor presentation with activation of aversive dopaminergic neurons drives odor-specific synaptic depression at KC-MBON junctions. Despite considerable progress in understanding how memory is coded in the MB network, the fast-acting neurotransmitter of the underlying KC-MBON synapses that are modified by learning is not known.

Classic examples of plasticity in *Aplysia* and mammals involve presynaptic and/or postsynaptic effects at glutamatergic synapses (Roberts and Glanzman, 2003; Kandel et al., 2014). Although a small number of *Drosophila* KCs can be labeled with antibodies to glutamate, aspartate, or taurine (Schäfer et al., 1988; Schürmann, 2000; Sinakevitch et al., 2001; Strausfeld et al., 2003), immunostaining cannot differentiate between these molecules being transmitters or simply metabolites. Moreover, expression of the vesicular glutamate transporter is prominent in the fly brain but notably absent from the MB (Daniels et al., 2008). Immunohistochemical studies also suggested that, unlike much of the fly brain, KCs do not express the acetylcholine (ACh) synthesizing enzyme choline acetyltransferase (ChAT) (Gorczyca and Hall, 1987; Buchner et al., 1986; Yasuyama et al., 1995b).

Here we demonstrate using neurochemical, physiological, and behavioral approaches that ACh is a neurotransmitter of the *Drosophila* KCs. A significant part of KC-MBON communication is carried by cholinergic transmission from KCs that activates nicotinic ACh receptors on MBONs. Our data therefore suggest that fly memories are formed by dopamine-directed plasticity at cholinergic KC-MBON synapses.

RESULTS

Drosophila Kenyon Cell Function Requires ChAT Expression

Cholinergic neurons express ChAT to synthesize ACh and the vesicular ACh transporter (VAChT) that loads ACh into synaptic vesicles. Although prior studies concluded that KCs do not express ChAT (Gorczyca and Hall, 1987; Buchner et al., 1986; Yasuyama et al., 1995b), data from a microarray-based characterization of MB-expressed genes (Perrat et al., 2013) revealed levels of ChAT and VAChT that are not lower than elsewhere in the brain (*ChAT*: γ = 8.83, α′β′ = 8.43, αβ = 6.74, rest = 8.86, all p [neurons to rest of brain] > 0.05; *VAChT*: γ = 7.27, α′β′ = 5.94, αβ = 5.89, rest = 7.00, all p [neurons to rest of brain] > 0.05; t test). We therefore reinvestigated *ChAT* and *VAChT* expression in the MB using immunohistochemistry (Figures 1A and 1B; see Figure S1 and Movie S1 available online). We controlled for antibody specificity by staining brains expressing an UAS-*ChAT*^{RNAi} or UAS-*VAChT*^{RNAi} transgene driven in KCs by OK107-GAL4. Levels of ChAT staining appeared lower in the MB than in surrounding areas, consistent with prior studies (Gorczyca and Hall, 1987; Yasuyama et al., 1995b). However, ChAT immunoreactivity in the MB was above that in other areas of the brain, and MB labeling was significantly reduced in flies expressing UAS-*ChAT*^{RNAi} in KCs (Figures 1A and 1B). In comparison, VAChT immunoreactivity in the MB was at a similar level to other brain regions, and was significantly reduced when UAS-*VAChT*^{RNAi} was expressed

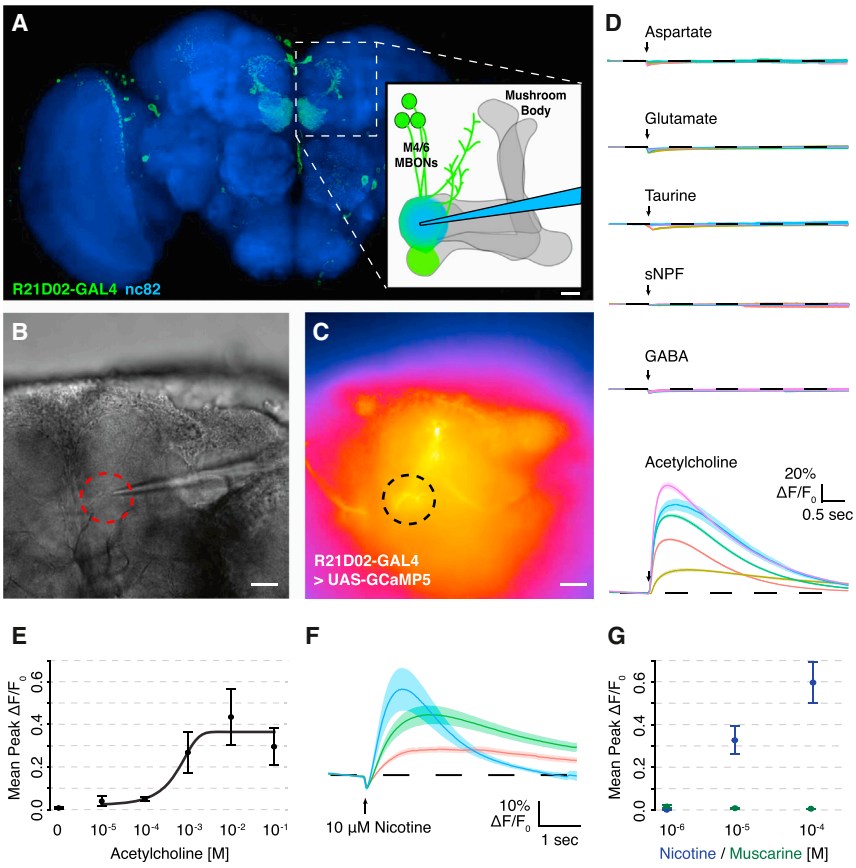


Figure 2. ACh Evokes Calcium Transients in M4/6 Neuron Dendrites

(A) Schematic of experimental setup. A micropipette connected to a pressure ejection system is placed near the dendrites of M4/6 MBONs in the tip of the horizontal MB lobe. M4/6 neural activity is monitored using R21D02-GAL4 (enhancer fragment from the *Dα6* locus)-driven UAS-GCaMP. Brain shown is costained with anti-Bruchpilot, a general neuropil marker (Wagh et al., 2006).

(B) Bright-field image of sample explant brain and micropipette. Region of interest (ROI) from which calcium traces were extracted is marked with a red dashed circle.

(C) Pseudocolor fluorescence image of the same area as in (B).

(D) Direct application of 1 mM of each candidate KC transmitter to M4/6 dendrites reveals activation by ACh only. n = 5 brains for each transmitter with ten trials per brain). Each colored trace represents an individual brain with the solid line representing the mean, and the shade representing the SEM.

(E) Dose-response curve of ACh responses (n = 5 brains per concentration). The line is a sigmoidal fit to the data. Data in (A)–(E) were acquired from R21D02-GAL4; UAS-GCaMP5 brains.

(F) Application of 10 μM nicotine elicits strong calcium responses in M4/6 dendrites. n = 3 brains; each colored line represents an individual brain. Solid line is the mean of five trials and shade the SEM.

(G) Calcium responses to increasing nicotine concentrations. No change is registered after applying muscarine. n = 3 brains each condition, mean of three trials. Data in (F) and (G) were acquired from R21D02-GAL4;UAS-GCaMP6f brains. Scale bar in (A)–(C), 20 μm. See Figure S3 for additional experiments. Error bars in (E) and (G) represent SEM.

in KCs (Figures 1A and 1B). Interestingly, levels of ChAT immunoreactivity were also reduced in the MB in UAS-*VAChT*^{RNAi}; OK107-GAL4 flies, suggesting an interaction between VAChT function and ChAT levels (Figures 1A and 1B). We therefore conclude that KCs express ChAT and VAChT, and that KCs, and not extrinsic neurons, are likely to provide the only cholinergic processes in the MB lobe region.

To test the functional relevance of ChAT and VAChT expression in KCs, we assessed the consequence of *ChAT*^{RNAi} and *VAChT*^{RNAi} disruption in aversive olfactory learning (Tully and Quinn, 1985). Three-minute aversive memory performance of *ChAT*^{RNAi};OK107 and *VAChT*^{RNAi};OK107 flies was statistically different from OK107-GAL4 and the relevant UAS-RNAi flies (Figure 1C). *VAChT*^{RNAi};OK107 flies also exhibited defective appetitive memory (Figure S2A). We expect the partial defect results from residual ChAT and VAChT activity. An early study with conditional *ChAT*^{ts} mutants concluded that normal fly behavior required only 8% of wild-type ChAT activity (Greenspan, 1980). We also tested for a role of GABAergic and glutamatergic transmission from KCs. Flies expressing RNAi against glutamic acid decarboxylase (GAD), the vesicular GABA transporter (vGAT), or the vesicular glutamate transporter (vGlut), driven by OK107-GAL4, had aversive memory performance that was statistically indistinguishable from controls (Figure S2B). We therefore conclude that KC function requires ACh.

ACh Evokes Responses in M4/6 MBONs

Postsynaptic MBONs should respond to ACh if it is a KC neurotransmitter. We therefore used the R21D02-GAL4 driver (Owald et al., 2015) to express the genetically encoded calcium indicator UAS-GCaMP (Akerboom et al., 2012; Chen et al., 2013) and monitored physiological responses to candidate transmitter application (Figure 2A). Brains were removed from R21D02-GAL4;UAS-GCaMP flies and placed on a polylysine-coated glass slide bathed with saline under a wide-field fluorescence microscope. 1 mM of glutamate, aspartate, taurine, sNPF, ACh, or GABA was then locally applied to the dendrites of M4/6 neurons via a glass micropipette using fast pressure ejection (Figures 2B–2D). Only ACh evoked a reproducibly robust increase in intracellular Ca^{2+} in M4/6 dendrites, and a dose response analysis revealed that 10 mM ACh application was sufficient to generate maximal signal (Figure 2E).

Since the KCs are principally driven by cholinergic olfactory projection neurons, we performed experiments to rule out the possibility that the M4/6 responses resulted from indirect activation of KCs. We first included 1 μM tetradotoxin (TTX) in the recording chamber to block voltage-gated sodium channels and thereby inhibit indirect activation through other neurons, and monitored the approximate diffusion of the ejected solution by including Texas red in the micropipette

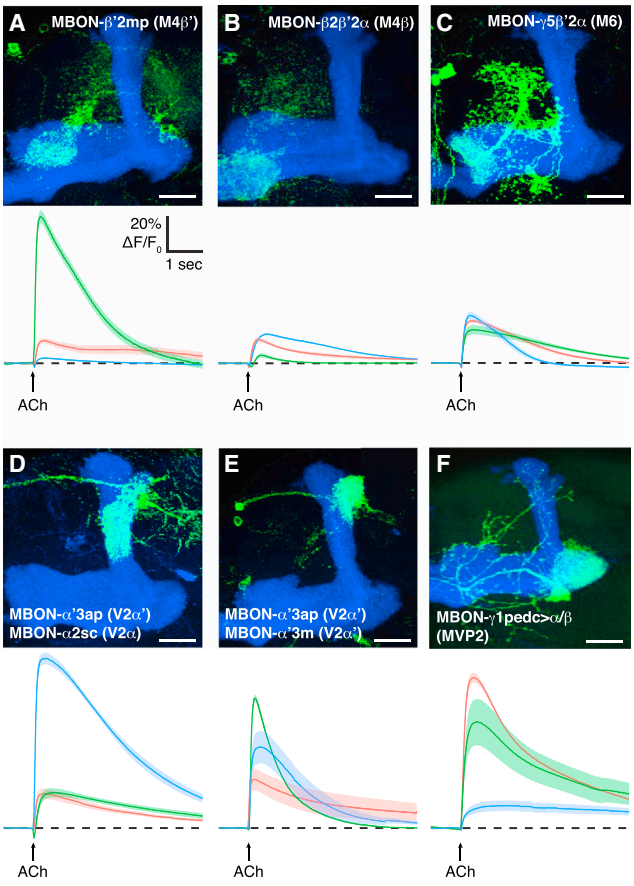


Figure 3. ACh Evokes Responses in Multiple Classes of MBONs

(A–F) Release of ACh onto the dendrites of other MBONs evokes calcium responses. Each panel shows the anatomy of the relevant MBON and below the corresponding GCaMP6f measured physiological responses evoked by 1 mM ACh.

(A–C) Glutamatergic MBONs on the horizontal MB lobe. (A) MBON-β′2mp (M4β′)/R39A05-GAL4, (B) MBON-β2β′2a (M4β)/R56F01-GAL4, and (C) MBON-γ5β′2a (M6)/R66C08-GAL4.

(D and E) Cholinergic MBONs on the vertical MB lobe. (D) MBON-α′3ap (V2α′), MBON-α2sc (V2α)/MB549C, (E) MBON-α′3ap (V2α′), MBON-α′3m (V2α′)/R24H08-GAL4.

(F) GABAergic MBON in the heel region, MBON-γ1pedc>αβ (MVP2)/MB112C. Each colored line represents the mean of ten trials per individual brain, and the shade represents the respective SEM (three brains per genotype). Scale bar, 20 μm. See Figure S4 for additional examples.

(Figure S3A). Visualizing Texas red fluorescence confirmed that activation was local, with the observed activity following the diffusing ACh. We next placed the micropipette tip in different locations with respect to the M4/6 dendrites to test whether more distant application of 100 μM ACh could evoke responses in M4/6 neurons. Maximal responses were only observed when ACh was released local to M4/6 dendrites (Figures S3B–S3D). We also challenged a potentially polysynaptic response by adding high extracellular Mg^{2+} to reduce the efficacy of synaptic transmission. Application of ACh to M4/6 dendrites of brains immersed in saline with high Mg^{2+} (+10 mM) generated responses that were not different to those evoked in low Mg^{2+} (Figure S3E). Importantly, high Mg^{2+} saline impaired the polysynaptic input to M4/6 neurons generated by stimulating KCs with ACh application in the MB calyx (Figure S3E). Finally, local ACh application to the MB lobes did not elicit Ca^{2+} transients in KCs (Figure S3F).

The relatively fast ACh-evoked response suggested that it involved nicotinic ACh receptors (nAChRs). We first tested this model by replacing ACh in the micropipette with 1, 10, or 100 μM of nicotine and applying it to the dendrites of M4/6 neurons (Figures 2F and 2G). Both 10 and 100 μM nicotine evoked robust responses in the M4/6 MBONs that were greater than those evoked by 100 μM ACh. In contrast, muscarine that should activate metabotropic AChRs did not elicit calcium transients at any concentration tested (Figures 2F and 2G). The nonselective nicotinic receptor antagonists mecamylamine (Figures S5A–S5D), hexamethonium (Figures S5G and S5H), and methyllycaconitine (MLA; Figures S5I and S5J) abolished ACh-evoked responses when added to the recording chamber, whereas vehicle had no effect (Figures S5E and S5F). Taken together, these experiments suggest that ACh directly activates M4/6 neurons via nAChRs.

Other MBONs Respond to ACh

We next tested whether other MBONs that are postsynaptic in the horizontal or vertical MB lobes responded to ACh. We restricted expression of GCaMP to a collection of these MBONs using specific GAL4 drivers (Aso et al., 2014b) and locally applied 1 mM ACh to their dendrites in the explant brain preparation (Figures 3A–3F and S4), starting with lines that label single M4/6 neurons. All of the MBONs tested responded to ACh application. This set of MBONs innervates all five of the major MB lobes (α, α′, β, β′, and γ) and represents all three of the characterized glutamatergic, cholinergic, and GABAergic classes of MBONs (Aso et al., 2014b). Although MBONs appeared to respond with distinct kinetics, we cannot currently exclude that differences result from placement of the micropipette. Nevertheless, multiple MBONs respond to ACh, consistent with ACh being released from all KC collaterals.

Optogenetic KC Activation Drives MBONs via nAChRs

To directly demonstrate that KCs are the source of ACh, we optogenetically activated them while recording calcium transients in M4/6 neuron presynaptic boutons using two-photon microscopy. We expressed lexAop-CsChrimson (Klapoetke et al., 2014) in KCs with 247-LexA::VP16 (Pitman et al., 2011) control and evoked activity using a focused red light emitting diode (Figures 4A–4F). Recording with two-photon illumination should minimize nonspecific activation of the Channelrhodopsin in these experiments. As expected (Owald et al., 2015), KC activation evoked intracellular Ca^{2+} transients in M4/6 neurons that were tightly temporally linked to the illumination protocol (Figures 4A–4F). Importantly, these optogenetically evoked M4/6 responses were also blocked by adding 250 μM mecamylamine (Figures 4A–4C), but not vehicle (Figures 4D–4F; Movie S2), to the recording chamber. Comparison of the average peak calcium response from four trials before and after application of mecamylamine or vehicle only revealed a significant difference for the mecamylamine group (Figures 4C and 4F). Importantly,

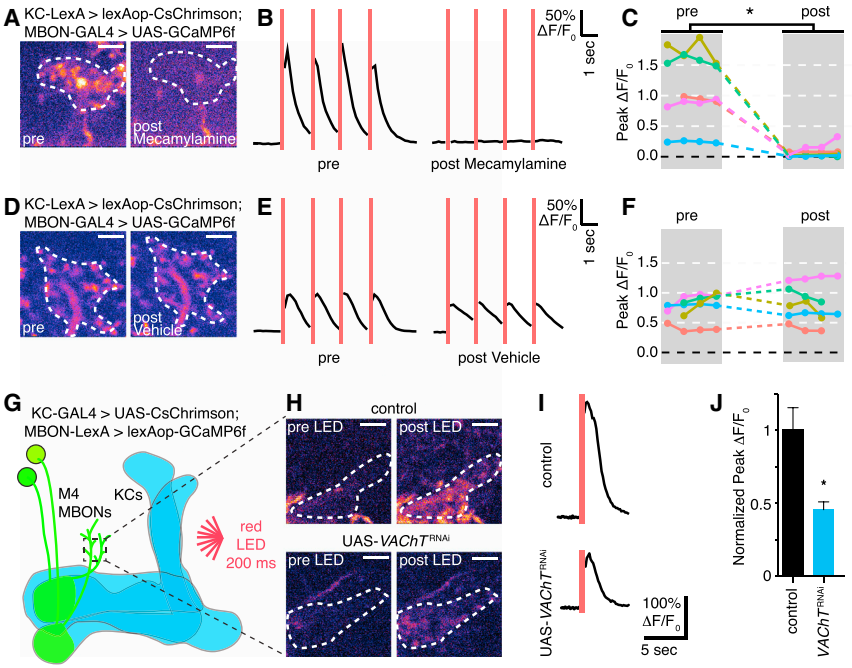


Figure 4. Optogenetic Activation of KCs Evokes ACh-Dependent Calcium Responses in M4/6 Neurons

(A–F) Optogenetic stimulation of KCs triggers M4/6 calcium responses that are blocked by mecamylamine. 247-LexA-driven lexAop-CsChrimson was used to activate KCs, and M4/6 neuron calcium transients were monitored with R21D02-GAL4 driven UAS-GCaMP6f.

(A) Samples of two-photon images of M4/6 presynaptic arbors collected on the first frame after LED stimulation, before and after mecamylamine application. Dotted white circle represents ROI from which $\Delta F/F_0$ is calculated.

(B and C) A total of 200 ms of red LED light (indicated by red vertical lines) triggers strong calcium responses in M4/6 neuron axons that are abolished 5 min after applying 250 μM mecamylamine. (B) Sample trace and (C) quantification, n = 5 brains, asterisk denotes $p < 0.05$, paired samples t test.

(D) KC-evoked M4/6 neuron responses remain stable after application of vehicle.

(E and F) (E) Sample trace and (F) quantification, n = 5 brains, $p > 0.05$, paired samples t test. See Figure S5 for washout experiments and others using 100 μM mecamylamine or additional nicotinic antagonists.

(G–J) KC-expressed UAS-*VAChT*^{RNAi} reduces KC-triggered M4 calcium responses. (G) Illustration of experimental setup. R13F02-GAL4-driven UAS-CsChrimson was used to optogenetically activate KCs while M4 calcium transients were monitored with R15B01-LexA driven lexAop-GCaMP6f. (H) Samples of two-photon images of M4 presynaptic arbors collected before and after LED stimulation in control brains (upper panel) or those coexpressing UAS-*VAChT*^{RNAi} in KCs (lower panel). Dotted white circles represent ROI from which $\Delta F/F_0$ is calculated. (I and J) A total of 200 ms of red light evokes calcium responses in presynaptic arbors of M4 neurons that have a significantly reduced peak when *VAChT*^{RNAi} is coexpressed in KCs. (I) Sample trace and (J) quantification, n = 4–6 brains, asterisk denotes $p < 0.05$, Mann-Whitney U-test. Data are normalized to controls. Scale bars, 5 μM. Error bars represent SEM.

the mecamylamine effect was reversed following washout (Figures S5K–S5N). Consistent with prior studies (Mauss et al., 2014), 100 μM mecamylamine did not abolish responses in this preparation but caused a strong and reversible reduction (Figures S5K and S5L).

We also tested whether reducing VAChT expression in KCs attenuated M4/6 MBON responses. We coexpressed UAS-*VAChT*^{RNAi} and UAS-CsChrimson in KCs with R13F02-GAL4 and lexAop-GCaMP6f in M4 neurons with R15B01-LexA. Strikingly, peak KC-evoked responses were reduced by greater than 50% in flies expressing UAS-*VAChT*^{RNAi} in KCs (Figures 4G–4J). Therefore pharmacological and genetic approaches provide evidence that the KCs release ACh that in turn activates M4/6 MBONs via nAChRs.

Manipulating nAChR Expression in M4/6 MBONs Phenocopies Neural Blockade

We next tested whether downregulating specific nAChR subunits altered odor-evoked responses in M4/6 neurons. We used R21D02-GAL4 to coexpress UAS-GCaMP6f and UAS-RNAi constructs directed toward the Dα1, Dα3, Dα4, Dα5, or Dα6 nAChR subunits. Living flies were mounted under the two-photon microscope, and MCH and OCT odor responses were recorded from M4/6 presynaptic boutons. Expression of *Dα1*, *Dα4*, *Dα5*, and *Dα6* subunit RNAi caused a statistically significant reduction in the peak responses to MCH, as compared to controls (Figures 5A and 5B). *Dα4* and *Dα6* RNAi also significantly reduced the responses to OCT. In comparison, *Dα3* RNAi peak responses were indistinguishable from those of controls for both odors (Figure 5B).

We reasoned that reducing expression of the relevant nicotinic acetylcholine receptor subunits in M4/6 MBONs might also alter odor-driven behavior (Figure 5C). Previous work showed that blocking M4/6 neuron output with VT1211-GAL4-driven UAS-*Shibire*^{ts1} converted naive odor avoidance into odor approach (Owald et al., 2015). We therefore used this assay to assess the role of Dα1, Dα3, Dα4, Dα5, and Dα6 subunits in M4/6 MBONs. Flies were given the choice between a T-maze arm perfused with a 1:1,000 dilution of MCH and an arm with a clean air stream. Whereas control VT1211-GAL4/+ or UAS-RNAi/+ flies displayed MCH avoidance or neutrality, flies expressing UAS-*Dα1*, *Dα4*, *Dα5*, or *Dα6* RNAi in M4/6 MBONs exhibited a significant reversal of odor driven behavior. Flies expressing *Dα3* RNAi were not statistically different from relevant controls. These behavioral phenotypes mirror the defective MCH-evoked physiological responses and resemble the reversal of naive odor behavior observed when M4/6 neurons were blocked (Owald et al., 2015). We therefore conclude that M4/6 neurons are principally driven by KCs via ACh neurotransmission onto nAChRs.

sNPF Potentiates ACh-Evoked Responses in MBONs

The αβ and γ KCs express the sNPF neuropeptide (Johard et al., 2008), and reducing sNPF expression in KCs impairs appetitive memory (Knapek et al., 2013). Finding a role for ACh as a key

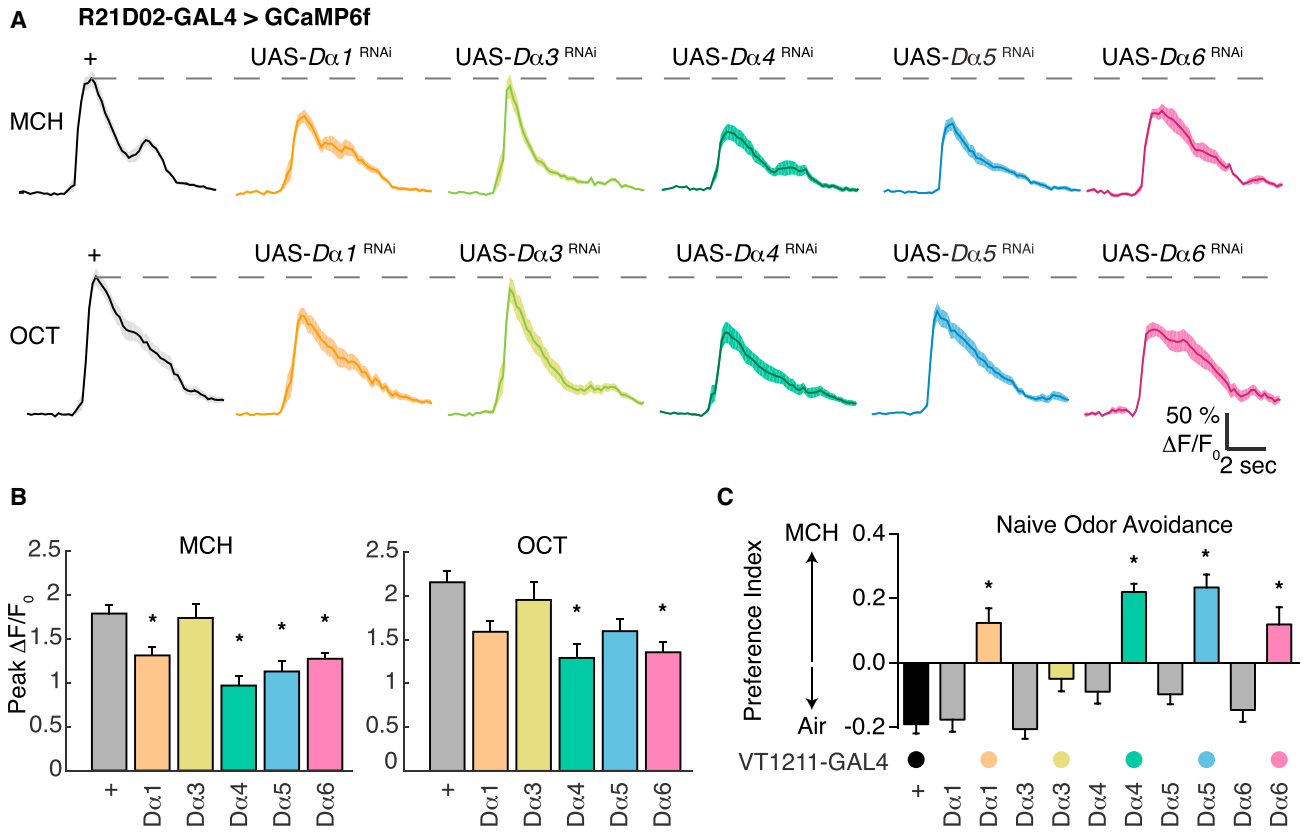


Figure 5. Reducing nAChR Subunit Expression in M4/6 MBONs Impairs Physiological and Behavioral Odor-Evoked Responses

(A) nAChR subunit expression is required for MCH- and OCT-evoked calcium transients in M4/6 neuron axons. Mean traces of activity evoked by 5 s of odor presentation, with SEM as shade (n = 9–16 from 5–10 animals). Head-fixed live flies carrying R21D02-GAL4-driven UAS-GCaMP6f show robust calcium responses to MCH and OCT odors that are impaired by expressing nAChR-directed RNAi.

(B) Quantification of peak calcium responses in (A). MCH-evoked responses are significantly reduced in flies expressing UAS-*Dα1*^{RNAi}, UAS-*Dα4*^{RNAi}, UAS-*Dα5*^{RNAi}, and UAS-*Dα6*^{RNAi} (n = 9–16, asterisk denotes $p < 0.05$, one-way ANOVA with Dunnett's multiple comparisons test). OCT-evoked responses are significantly reduced in flies expressing UAS-*Dα4*^{RNAi} and UAS-*Dα6*^{RNAi} (n = 9–16, asterisk denotes $p < 0.05$, one-way ANOVA with Dunnett's multiple comparisons test).

(C) nAChR RNAi in M4/6 neurons phenocopies the behavioral consequence of neural blockade. Flies were given 2 min in a T maze to choose between a tube perfused with 1:1,000 MCH and another with clean air. VT1211-GAL4;UAS-*Dα1*^{RNAi}, VT1211-GAL4;UAS-*Dα4*^{RNAi}, VT1211-GAL4;UAS-*Dα5*^{RNAi}, and VT1211-GAL4;UAS-*Dα6*^{RNAi} exhibit a significant preference toward MCH when compared to their two respective genetic control groups (n = 18–38, asterisk denotes $p < 0.001$, one-way ANOVA with Tukey's multiple comparisons test). Error bars in (B) and (C) represent SEM.

fast-acting transmitter between KCs and MBONs raises the question of whether coreleased sNPF and ACh interact. We therefore coapplied ACh and sNPF with a micropipette to the M4/6 dendrites in the explant brain preparation, while monitoring calcium transients by wide-field imaging (Figure 6). Calcium transients evoked in M4/6 MBONs by dual ACh and sNPF application were significantly larger than those generated by ACh and vehicle, supporting a likely facilitating interaction between the slow- and fast-acting transmitters.

DISCUSSION

Despite decades of work on learning and memory and other functions of the MB, the identity of the fast-acting neurotransmitter that is released from the KCs has remained elusive. Much of the insect brain was considered to be cholinergic, but the MB was thought to be unique. Histological studies concluded that the MB did not express ChAT (Gorczyca and Hall, 1987; Buchner et al., 1986; Yasuyama et al., 1995b) but that subsets of KCs contained glutamate, aspartate, or taurine (Sinakevitch et al., 2001; Strausfeld et al., 2003). However, conclusive evidence that these molecules are released as neurotransmitters has not materialized.

Here we present multiple lines of evidence that ACh is a KC transmitter. (1) KCs express the ChAT and VAChT proteins that synthesize and package ACh into synaptic vesicles, and the expression of these genes is required for MB-dependent learned behavior. (2) Stimulation of KCs triggers responses in MBONs that are similar to those evoked by direct ACh application. (3) Reducing ACh processing in KCs impairs KC-evoked responses in MBONs. (4) ACh- and KC-evoked responses in MBONs are both sensitive to antagonism of nicotinic ACh

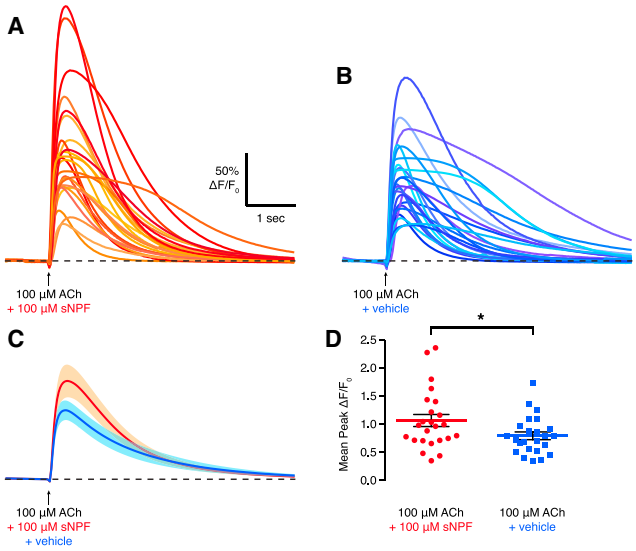


Figure 6. sNPF Increases ACh-Evoked Calcium Transients in M4/6 Neurons

A total of 100 μM of ACh was applied through a micropipette onto the M4/6 dendrites, with either 100 μM sNPF or vehicle. Calcium transients were measured from M4/6 dendrites of R21D02-GAL4; UAS-GCaMP6f explant brains.

(A and B) Mean calcium traces of ten trials from 24 brains per condition.

(C) Overlaid mean traces from (A) ACh plus sNPF and (B) ACh plus vehicle. Shade represents SEM.

(D) Mean peak calcium responses are significantly higher when ACh is coapplied with 100 μM sNPF than with vehicle ($t[39.09] = 2.12$, $p < 0.05$, unpaired t test with Welch's correction). Error bars represent SEM.

receptors. (5) Odor-evoked responses in MBONs are attenuated by reducing the expression of several nicotinic ACh receptor subunits. Taken together, these data provide compelling support that ACh is a major neurotransmitter released from *Drosophila* KCs.

The anatomy of ACh-responsive MBONs suggests that many αβ, α′β′, and γ lobe KCs are likely to be cholinergic. Calcium imaging may miss subtle or inhibitory effects, so it remains possible that subclasses of KC might also release or corelease other small molecule transmitters. It is, for example, notable that the MB neurons express an atypical putative vesicular transporter (Brooks et al., 2011). Furthermore, taurine histology specifically labels the αβ core neurons (Strausfeld et al., 2003). Anatomy suggests that αβ core and αβ surface outputs are pooled by MBONs with dendrites in the α lobe tip and throughout the β lobe, but that the dendrites of MBONs in the α lobe stalk preferentially innervate αβ surface neurons (Perisse et al., 2013b). It will be important to understand how ACh signals from different KCs are integrated by MBONs. The αβ and γ, but not α′β′, KCs can corelease ACh with the sNPF neuropeptide (Johard et al., 2008). Our data raise the possibility that coreleased sNPF may facilitate ACh-evoked responses. sNPF drives autocrine presynaptic facilitation of certain olfactory sensory neurons in the adult fly (Root et al., 2011). Conversely, sNPF decreased the resting membrane potential of larval motor neurons that ectopically express sNPFR (Vecsey et al., 2014). MBONs with dendrites in certain lobes therefore receive different combinations of transmitters and may vary in responding to sNPF.

Finding that ACh is the KC transmitter has important implications for learning-relevant plasticity at KC-MBON synapses. Current models suggest that valence-specific and anatomically restricted reinforcing dopaminergic neurons drive presynaptically expressed plasticity between KCs and particular MBONs (Waddell, 2013; Aso et al., 2014a; Aso et al., 2014b; Owald et al., 2015; Owald and Waddell, 2015). Reward learning skews KC-MBON outputs toward driving approach by depressing the odor drive to MBONs that direct avoidance, whereas aversive learning enhances drive to avoidance by reducing drive to approach MBONs and increasing drive to avoidance pathways (Owald et al., 2015; Owald and Waddell, 2015). The results here indicate that learning is represented as dopaminergic tuning of excitatory cholinergic KC-MBON synapses.

Learning requires dopamine receptor function in the KCs (Kim et al., 2007; Qin et al., 2012), which implies a presynaptic mechanism of plasticity at the KC-MBON junction. Presynaptic plasticity of odor-activated KCs provides a simple means to retain odor specificity of memory in the highly convergent anatomy of the MB—where 2,000 KCs converge onto single or very few MBONs per zone on the MB lobes. The anatomically analogous mammalian cerebellar circuits, to which the insect MBs have been compared (Farris, 2011), exhibit presynaptic glutamatergic plasticity that is cAMP dependent (Salin et al., 1996). Finding that the KC transmitter is ACh suggests that cAMP-dependent mechanisms can modulate synaptic connections, regardless of transmitter identity. The MB KCs appear to be strikingly similar to the large parallel ensemble of cholinergic amacrine cells in the vertical lobe of the cuttlefish (Shomrat et al., 2011). These Cephalopod amacrine cells also share the same fan-out input and fan-in efferent anatomy of the *Drosophila* KCs, and plasticity occurs at the cholinergic connection between amacrine cells and downstream large efferent neurons.

Work in the locust suggested that spike-timing-dependent plasticity (STDP) marks the relevant conditioned odor-activated KC-MBON synapses so that they are susceptible to reinforcing modulation (Cassenaer and Laurent, 2012). STDP relies on coincidence of pre- and postsynaptic activity and influx of postsynaptic Ca^{2+} through NMDA-type glutamate receptors (Feldman, 2012). Recent work in *Drosophila* pairing odor presentation with dopaminergic neuron activation reported odor-specific synaptic depression at a KC-MBON junction that did not require postsynaptic MBON depolarization (Hige et al., 2015). It will be important to determine whether this holds for all DAN-MBON compartments or whether some learning-induced plasticity involves synaptic Ca^{2+} influx through an ACh-triggered nAChR, rather than the more traditional glutamate-gated NMDA receptors.

We identified roles for the Dα1, Dα4, Dα5, and Dα6 nAChR subunits in M4/6 MBONs. Reducing the expression of these subunits lowered odor-evoked signals in MBONs and converted naive odor avoidance into approach behavior. Dα5 and Dα6 subunits can form functional heteromeric channels in vitro (Lansdell et al., 2012). Different MBONs may express unique combinations of AChRs (Le Novère et al., 2002; Chamaon et al., 2002; Thany et al., 2007) and therefore have characteristic physiological

responses to KC-released ACh, as well as perhaps different learning rules and magnitudes of plasticity (Hige et al., 2015). Pre- or postsynaptically localized muscarinic AChRs could provide additional memory-relevant modulation.

Beyond important roles in memory formation, consolidation, and expression, the MB- and DAN-directed modulation of specific MBON pathways has also been implicated in controlling hunger, thirst, temperature, and sleep/wake state-dependent locomotor behaviors (Krashes et al., 2009; Lewis et al., 2015; Lin et al., 2014b; Shih et al., 2015; Sitaraman et al., 2015). It will therefore be important to understand how plasticity of cholinergic KC transmission serves these discrete functions.

EXPERIMENTAL PROCEDURES

Fly Strains

Flies for physiological experiments were reared in vials with standard cornmeal food with additional molasses and active dried yeast. Flies for behavior were raised in bottles with standard cornmeal food. Canton-S flies were the wild-type control. We used Split-GAL4 lines MB002B, MB011B, MB027B, MB112C, MB210B, and MB549C (Aso et al., 2014a) and GAL4 lines R13F02 (Jenett et al., 2012), R21D02 (Jenett et al., 2012; Owald et al., 2015), R24H08, R39A05, R56F01, R66C08, R93F01 (Jenett et al., 2012), OK107 (Connolly et al., 1996), and VT1211 (Owald et al., 2015). We also used LexA lines R15B01 (Jenett et al., 2012; Lewis et al., 2015) and 247-LexA::VP16 (Pitman et al., 2011). UAS-GCaMP5 (Akerboom et al., 2012), UAS-GCaMP6f, and LexAop-GCaMP6f (Chen et al., 2013) were used for calcium imaging. UAS-CsChrimson and lexAop-CsChrimson (Klapoetke et al., 2014) were the optogenetic activators. Prior to optogenetic experiments, all flies were housed on standard cornmeal food with 1 mM retinal for 1–3 days. RNAi lines were UAS-*ChAT*^{RNAi} (Bloomington BUN 25856) (Ni et al., 2009), UAS-*VAChT*^{RNAi} (VDRC ID 27684), UAS-*GAD*^{RNAi} (VDRC ID 32344), UAS-*VGAT*^{RNAi} (VDRC ID 103586), UAS-*VGlut*^{RNAi} (VDRC ID 104324) (Dietzl et al., 2007), and UAS-*nAChR*^{RNAi} (Bloomington BUNs 28688, 27671, 31985, 25943, and 25835) (Ni et al., 2009).

Pharmacology

All candidate neurotransmitters, agonists, and antagonists, except sNPF, were prepared in adult hemolymph-like saline, AHLS (Wang et al., 2003; 2 mM $CaCl_2$, 5 mM KCl, 8.2 mM $MgCl_2$, 108 mM NaCl, 4 mM $NaHCO_3$, 1 mM NaH_2PO_4, 10 mM sucrose, and 5 mM trehalose) to a concentration of 100 mM. Aspartate, glutamate, taurine, GABA, ACh, nicotine, muscarine, mecamylamine, methyllycaconitine, and hexamethonium were all from Sigma Aldrich. Short neuropeptide F (sNPF; Ala-Gln-Arg-Ser-Pro-Ser-Leu-Arg-Leu-Arg-Phe-NH_2) was synthesized by PolyPeptide (Strasbourg, France) to a purity of >95% and was dissolved in DMSO. Each solution delivered in the micropipette also contained 5 μM Texas red dextran (TXR; Life Technologies) to monitor diffusion.

Explant Brain Wide-Field Calcium Imaging

All micropipette ejection experiments were performed on explant brains using wide-field imaging. One- to seven-day-old flies were anesthetized on ice, and brains were dissected in calcium-free AHLS and imaged in AHLS. The pH was adjusted to 7.5 and osmolarity to 265 mOsm. Dissected brains were adhered to a polylysine-coated coverslip and were illuminated with an X-Cite 120PC Q arc lamp. Micropipettes (glass capillaries, Harvard Apparatus, 300092) with an opening diameter of approximately 3 μm were connected to a picospritzer III (Intracell). The tip of the pipette was positioned near the M4/6 dendrites in the tip of the MB horizontal lobes (Figure 2B), unless stated otherwise. A custom white LED provided a stimulus trigger signal 1 s before stimulation. Air pressure to the picospritzer was set to the minimum required to eject solution from the pipette. Release of solution was verified by applying small test pulses while observing TXR in the red fluorescence channel.

Image series were acquired using a Scientifica Slicescope with a 40×, 0.8 NA water-immersion objective and Andor Zyla sCMOS camera with Andor Solis software (v4.27). Time series were acquired at 33.3 Hz with 512 × 512 pixels and 16 bit (or 100 Hz for traces shown in Figure S3E). Experiments in Figures S3E and S3F were acquired with a Guppy Pro CCD camera (Allied) with AVT SmartView software (v1.14). These time series were acquired at 12 Hz with 640 × 480 pixels and 8 bit. Image stacks were subsequently analyzed in Matlab (Mathworks Inc.) using custom-written scripts. In brief, elliptical ROIs (e.g., Figure 2B) were manually drawn around M4/6 dendrites (unless stated otherwise), and the mean fluorescence F of this ROI was calculated for each image. The resulting trace was scanned for LED trigger signals, and individual $\Delta F/F_0$ response traces were extracted from 1 s before and 3–10 s after the stimulation trigger. F_0 was defined for each trial as the mean F from 1 s before stimulation up to the point of stimulation. The peak $\Delta F/F_0$ was obtained by taking the maximum $\Delta F/F_0$ value acquired between the time of the trigger signal and 3 s afterward. Neural responsiveness was verified by applying 500 mM KCl at the end of each experiment.

Explant Brain Two-Photon Calcium Imaging

Combined optogenetic and calcium imaging experiments were conducted using a two-photon microscope (Scientifica) to minimize inadvertent optogenetic stimulation through imaging light. Explant brains were bathed in carbogenated (95% O_2, 5% CO_2) buffer solution (103 mM NaCl, 3 mM KCl, 5 mM N-Tris, 10 mM trehalose, 10 mM glucose, 7 mM sucrose, 26 mM $NaHCO_3$, 1 mM NaH_2PO_4, 1.5 mM $CaCl_2$, 4 mM $MgCl_2$, osmolarity 275 mOsm [pH 7.3]) following dissection in calcium-free buffer. For light stimulation, we used a high-power LED (Multicomp OSW-6338, 630 nm) relayed onto the specimen via a 50 mm diameter lens with focal length 60 mm. The power at the specimen was measured to be 0.85 mW/mm^2. The LED was triggered using a microcontroller (Arduino MEGA). Light pulses were delivered at 40 Hz, with 10 ms duration for a total of 200 ms per stimulation.

Fluorescence was excited using 140 fs pulses, 80 MHz repetition rate, centered on 910 nm generated by a Ti-Sapphire laser (Chameleon Ultra II, Coherent). Images of 256 × 256 pixels were acquired at 5.92 Hz, controlled by ScanImage 3.8 software (Pologruto et al., 2003). Two-photon fluorescence images were manually segmented using ImageJ and further analyzed using the custom-written MATLAB scripts described above.

For washout experiments, explant brains were continuously perfused with carbogenated buffer at about 2 ml/min using a Watson-Marlow 120S/DV WM Sci Q400-1H1D perfusion system. Antagonist action was measured 5 min after addition to the bath, followed by washout. The result of washout was measured 30 min later.

In Vivo Two-Photon Calcium Imaging

Two-photon imaging of odor-evoked calcium responses was performed according to Owald et al. (2015). Three- to eight-day-old flies were briefly anesthetized on ice and mounted in a custom chamber. The head capsule was opened under room temperature carbogenated buffer (see above). The legs and proboscis were immobilized with wax. Odors were delivered on a clean air carrier stream using a custom-designed system (Shang et al., 2007), which also synchronizes the timing of odor delivery and the two-photon image acquisition. Two-photon fluorescence images were manually segmented using ImageJ. Movement of the animal was small enough such that images did not require registration. Where possible, each hemisphere was separately evaluated and treated as an independent "n." All subsequent analyses utilized custom-written Matlab routines. After applying test pulses, flies were exposed to 5 s MCH (air stream passing over 10^{-2} odor dilution in mineral oil, and then further blended 1:9 with a clean air stream), then 15 s clean air, followed by a 5 s OCT pulse. Peaks were taken as maximum $\Delta F/F_0$ between 1 and 2 s after the beginning of odor stimulation. F_0 was defined as the mean F from 2 s before odor stimulation to the beginning of stimulation.

Immunohistochemistry

Brains were dissected on ice, fixed in 4% paraformaldehyde, and stained according to Wu and Luo (2006). For ChAT and VAChT staining, brains were incubated in PBT (0.3% Triton) supplemented with anti-ChAT primary mouse antibody (Yasuyama et al., 1995a) (diluted 1:100) and anti-VAChT primary rabbit antibody (Kitamoto et al., 1998) (diluted 1:1,000) for 2 days, followed by

2 days' incubation with secondary antibodies (anti-mouse Alexa 488/anti-rabbit Alexa 546, Sigma). For GAL4 visualization, anti-GFP (rabbit, Invitrogen, dilution 1:100) and anti-nc82 (DSHB, dilution 1:50) were used as primary antibodies. All confocal images were acquired on a Leica SP5 at manually adjusted laser intensity and gain. The same settings were used for all brains when comparing ChAT/VAChT antibody label.

For antibody quantification, a defined rectangular ROI of approximately 40 × 25 μm was placed over a single frame of the gamma lobe as well as the superior medial protocerebrum (SMP), the mean fluorescence was assessed using ImageJ, and each brain's gamma lobe intensity was normalized to the respective SMP intensity, individually for each channel.

Behavior

Mixed-sex populations of 4- to 9-day-old flies were tested together in all memory experiments. Aversive training was performed as in Perisse et al. (2013b). Briefly, flies were exposed to CS+ for 1 min with 12 90 V electric shocks at 5 s intervals followed by 45 s of air and the CS− for 1 min. For testing, flies were given 2 min to choose between the CS+ and CS− in a T maze. Performance index (PI) was calculated as the number of flies in the conditioned odor, minus the number of flies going the other direction, divided by the total number of flies in the experiment. A single PI value is the average score from flies of the identical genotype tested with the reciprocal reinforced/nonreinforced odor combination (Tully and Quinn, 1985; Perisse et al., 2013b). Odor dilutions were adjusted between experiments and odor batches to minimize bias (MCH 5–8 μl in 8 ml mineral oil and OCT 7–8 μl in 8 ml mineral oil). Appetitive conditioning was performed as in Perisse et al. (2013b). Naive odor avoidance experiments were performed as in Owald et al. (2015). Briefly, 5-day-old flies starved for 21–24 hr were given 2 min to choose between MCH (diluted 1:1,000 in mineral oil) and mineral oil-suffused air streams. Preference index was calculated as the number of flies approaching the odor minus the number approaching mineral oil, divided by the total number of flies in the experiment. One "n" corresponds to a single test trial.

Statistics

Statistical analyses were performed in either Matlab, GraphPad Prism 6, or R. The sigmoid dose-response curve fit for ACh application was performed in GraphPad Prism, based on the average of three trials per brain, with five brains per condition. Effects of pharmacological treatments were investigated using a paired t test to compare the average response peak before and after application. Groups in antibody quantification and behavioral experiments were compared using one-way ANOVA followed by Tukey's multiple comparisons test. Dunnett's multiple comparisons test was used for $nAChR^{RNAi}$ odor-evoked calcium responses. The effects of $VAChT^{RNAi}$ on calcium response peaks were measured using the Mann-Whitney U-test for nonparametric data. Calcium responses in Figure 6 were compared using an unpaired t test with Welch's correction.

SUPPLEMENTAL INFORMATION

Supplemental Information includes five figures and two movies and can be found with this article at http://dx.doi.org/10.1016/j.neuron.2016.02.015.

AUTHOR CONTRIBUTIONS

O.B., D.O., and S.W. conceived the project and designed all experiments. O.B. performed and with D.O. analyzed all experiments, except behavior, which was performed by J.F. Imaging data were acquired using custom hardware and software designed by J.-P.M. and C.B.T. Microarray data were generated by P.N.P. Essential fly lines were constructed by R.B. The manuscript was written by S.W., D.O., and O.B.

ACKNOWLEDGMENTS

We thank G. Miesenböck, members of the Waddell and Miesenböck labs, and M. Dolan for support, technical help, and discussion. O.B. also thanks A. Petzold and Q. Geissmann. We are grateful to M. Landgraf, G. Rubin, and the Janelia FlyLight Project; B. Dickson and the VDRC; and the Bloomington stock center for fly lines. We also thank T. Kitamoto and the Iowa Developmental Studies Hybridoma Bank for antibodies. O.B. is funded by the Medical Research Council and a University College War Memorial Studentship. D.O. was supported by an EMBO Long-Term Fellowship and a Sir Henry Wellcome Postdoctoral Fellowship. J.F. is funded by the Deutsche Forschungsgemeinschaft (GZ:FE 1563/1-1). S.W. is funded by a Wellcome Trust Senior Research Fellowship in the Basic Biomedical Sciences and by funds from the Gatsby Charitable Foundation, the Oxford Martin School, and the Bettencourt-Schueller Foundation.

Received: July 22, 2015
Revised: January 4, 2016
Accepted: January 27, 2016
Published: March 3, 2016

REFERENCES

Akerboom, J., Chen, T.W., Wardill, T.J., Tian, L., Marvin, J.S., Mutlu, S., Calderón, N.C., Esposti, F., Borghuis, B.G., Sun, X.R., et al. (2012). Optimization of a GCaMP calcium indicator for neural activity imaging. J. Neurosci. *32*, 13819–13840.

Aso, Y., Herb, A., Ogueta, M., Siwanowicz, I., Templier, T., Friedrich, A.B., Ito, K., Scholz, H., and Tanimoto, H. (2012). Three dopamine pathways induce aversive odor memories with different stability. PLoS Genet. *8*, e1002768.

Aso, Y., Hattori, D., Yu, Y., Johnston, R.M., Iyer, N.A., Ngo, T.T., Dionne, H., Abbott, L.F., Axel, R., Tanimoto, H., and Rubin, G.M. (2014a). The neuronal architecture of the mushroom body provides a logic for associative learning. eLife *3*, e04577.

Aso, Y., Sitaraman, D., Ichinose, T., Kaun, K.R., Vogt, K., Belliart-Guérin, G., Plaçais, P.Y., Robie, A.A., Yamagata, N., Schnaitmann, C., et al. (2014b). Mushroom body output neurons encode valence and guide memory-based action selection in Drosophila. eLife *3*, e04580.

Blum, A.L., Li, W., Cressy, M., and Dubnau, J. (2009). Short- and long-term memory in Drosophila require cAMP signaling in distinct neuron types. Curr. Biol. *19*, 1341–1350.

Bouzaiane, E., Trannoy, S., Scheunemann, L., Plaçais, P.Y., and Preat, T. (2015). Two independent mushroom body output circuits retrieve the six discrete components of Drosophila aversive memory. Cell Rep. *11*, 1280–1292.

Brooks, E.S., Greer, C.L., Romero-Calderón, R., Serway, C.N., Grygoruk, A., Haimovitz, J.M., Nguyen, B.T., Najibi, R., Tabone, C.J., de Belle, J.S., and Krantz, D.E. (2011). A putative vesicular transporter expressed in Drosophila mushroom bodies that mediates sexual behavior may define a neurotransmitter system. Neuron *72*, 316–329.

Buchner, E., Buchner, S., Crawford, G., Mason, W.T., and Salvaterra, P.M. (1986). Choline acetyltransferase-like immunoreactivity in the brain of Drosophila melanogaster. Cell Tissue Res. *246*, 57–62.

Burke, C.J., Huetteroth, W., Owald, D., Perisse, E., Krashes, M.J., Das, G., Gohl, D., Silies, M., Certel, S., and Waddell, S. (2012). Layered reward signalling through octopamine and dopamine in Drosophila. Nature *492*, 433–437.

Campbell, R.A., Honegger, K.S., Qin, H., Li, W., Demir, E., and Turner, G.C. (2013). Imaging a population code for odor identity in the Drosophila mushroom body. J. Neurosci. *33*, 10568–10581.

Caron, S.J., Ruta, V., Abbott, L.F., and Axel, R. (2013). Random convergence of olfactory inputs in the Drosophila mushroom body. Nature *497*, 113–117.

Cassenaer, S., and Laurent, G. (2012). Conditional modulation of spike-timing-dependent plasticity for olfactory learning. Nature *482*, 47–52.

Chamaon, K., Smalla, K.H., Thomas, U., and Gundelfinger, E.D. (2002). Nicotinic acetylcholine receptors of Drosophila: three subunits encoded by genomically linked genes can co-assemble into the same receptor complex. J. Neurochem. *80*, 149–157.

Chen, T.W., Wardill, T.J., Sun, Y., Pulver, S.R., Renninger, S.L., Baohan, A., Schreiter, E.R., Kerr, R.A., Orger, M.B., Jayaraman, V., et al. (2013).

Ultrasensitive fluorescent proteins for imaging neuronal activity. Nature *499*, 295–300.

Claridge-Chang, A., Roorda, R.D., Vrontou, E., Sjulson, L., Li, H., Hirsh, J., and Miesenböck, G. (2009). Writing memories with light-addressable reinforcement circuitry. Cell *139*, 405–415.

Connolly, J.B., Roberts, I.J., Armstrong, J.D., Kaiser, K., Forte, M., Tully, T., and O'Kane, C.J. (1996). Associative learning disrupted by impaired Gs signaling in Drosophila mushroom bodies. Science *274*, 2104–2107.

Daniels, R.W., Gelfand, M.V., Collins, C.A., and DiAntonio, A. (2008). Visualizing glutamatergic cell bodies and synapses in Drosophila larval and adult CNS. J. Comp. Neurol. *508*, 131–152.

Das, G., Klappenbach, M., Vrontou, E., Perisse, E., Clark, C.M., Burke, C.J., and Waddell, S. (2014). Drosophila learn opposing components of a compound food stimulus. Curr. Biol. *24*, 1723–1730.

Dietzl, G., Chen, D., Schnorrer, F., Su, K.C., Barinova, Y., Fellner, M., Gasser, B., Kinsey, K., Oppel, S., Scheiblauer, S., et al. (2007). A genome-wide transgenic RNAi library for conditional gene inactivation in Drosophila. Nature *448*, 151–156.

Farris, S.M. (2011). Are mushroom bodies cerebellum-like structures? Arthropod Struct. Dev. *40*, 368–379.

Farris, S.M. (2013). Evolution of complex higher brain centers and behaviors: behavioral correlates of mushroom body elaboration in insects. Brain Behav. Evol. *82*, 9–18.

Feldman, D.E. (2012). The spike-timing dependence of plasticity. Neuron *75*, 556–571.

Galili, D.S., Dylla, K.V., Lüdke, A., Friedrich, A.B., Yamagata, N., Wong, J.Y., Ho, C.H., Szyszka, P., and Tanimoto, H. (2014). Converging circuits mediate temperature and shock aversive olfactory conditioning in Drosophila. Curr. Biol. *24*, 1712–1722.

Gorczyca, M.G., and Hall, J.C. (1987). Immunohistochemical localization of choline acetyltransferase during development and in Chats mutants of Drosophila melanogaster. J. Neurosci. *7*, 1361–1369.

Greenspan, R. (1980). Mutations of Choline Acetyltransferase and associated neural defects in *Drosophila melanogaster*. J. Comp. Physiol. *137*, 83–92.

Heisenberg, M. (2003). Mushroom body memoir: from maps to models. Nat. Rev. Neurosci. *4*, 266–275.

Hige, T., Aso, Y., Modi, M.N., Rubin, G.M., and Turner, G.C. (2015). Heterosynaptic Plasticity Underlies Aversive Olfactory Learning in Drosophila. Neuron *88*, 985–998.

Honegger, K.S., Campbell, R.A., and Turner, G.C. (2011). Cellular-resolution population imaging reveals robust sparse coding in the Drosophila mushroom body. J. Neurosci. *31*, 11772–11785.

Huetteroth, W., Perisse, E., Lin, S., Klappenbach, M., Burke, C., and Waddell, S. (2015). Sweet taste and nutrient value subdivide rewarding dopaminergic neurons in Drosophila. Curr. Biol. *25*, 751–758.

Jenett, A., Rubin, G.M., Ngo, T.T., Shepherd, D., Murphy, C., Dionne, H., Pfeiffer, B.D., Cavallaro, A., Hall, D., Jeter, J., et al. (2012). A GAL4-driver line resource for Drosophila neurobiology. Cell Rep. *2*, 991–1001.

Johard, H.A., Enell, L.E., Gustafsson, E., Trifilieff, P., Veenstra, J.A., and Nässel, D.R. (2008). Intrinsic neurons of Drosophila mushroom bodies express short neuropeptide F: relations to extrinsic neurons expressing different neurotransmitters. J. Comp. Neurol. *507*, 1479–1496.

Kandel, E.R., Dudai, Y., and Mayford, M.R. (2014). The molecular and systems biology of memory. Cell *157*, 163–186.

Kim, Y.C., Lee, H.G., and Han, K.A. (2007). D1 dopamine receptor dDA1 is required in the mushroom body neurons for aversive and appetitive learning in Drosophila. J. Neurosci. *27*, 7640–7647.

Kirkhart, C., and Scott, K. (2015). Gustatory learning and processing in the Drosophila mushroom bodies. J. Neurosci. *35*, 5950–5958.

Kitamoto, T., Wang, W., and Salvaterra, P.M. (1998). Structure and organization of the Drosophila cholinergic locus. J. Biol. Chem. *273*, 2706–2713.

Klapoetke, N.C., Murata, Y., Kim, S.S., Pulver, S.R., Birdsey-Benson, A., Cho, Y.K., Morimoto, T.K., Chuong, A.S., Carpenter, E.J., Tian, Z., et al. (2014). Independent optical excitation of distinct neural populations. Nat. Methods *11*, 338–346.

Knapek, S., Kahsai, L., Winther, A.M., Tanimoto, H., and Nässel, D.R. (2013). Short neuropeptide F acts as a functional neuromodulator for olfactory memory in Kenyon cells of Drosophila mushroom bodies. J. Neurosci. *33*, 5340–5345.

Krashes, M.J., DasGupta, S., Vreede, A., White, B., Armstrong, J.D., and Waddell, S. (2009). A neural circuit mechanism integrating motivational state with memory expression in Drosophila. Cell *139*, 416–427.

Lansdell, S.J., Collins, T., Goodchild, J., and Millar, N.S. (2012). The Drosophila nicotinic acetylcholine receptor subunits Dα5 and Dα7 form functional homomeric and heteromeric ion channels. BMC Neurosci. *13*, 73.

Le Novère, N., Corringer, P.J., and Changeux, J.P. (2002). The diversity of subunit composition in nAChRs: evolutionary origins, physiologic and pharmacologic consequences. J. Neurobiol. *53*, 447–456.

Lewis, L.P., Siju, K.P., Aso, Y., Friedrich, A.B., Bulteel, A.J., Rubin, G.M., and Grunwald Kadow, I.C. (2015). A Higher Brain Circuit for Immediate Integration of Conflicting Sensory Information in Drosophila. Curr. Biol. *25*, 2203–2214.

Lin, A.C., Bygrave, A.M., de Calignon, A., Lee, T., and Miesenböck, G. (2014a). Sparse, decorrelated odor coding in the mushroom body enhances learned odor discrimination. Nat. Neurosci. *17*, 559–568.

Lin, S., Owald, D., Chandra, V., Talbot, C., Huetteroth, W., and Waddell, S. (2014b). Neural correlates of water reward in thirsty Drosophila. Nat. Neurosci. *17*, 1536–1542.

Liu, C., Plaçais, P.Y., Yamagata, N., Pfeiffer, B.D., Aso, Y., Friedrich, A.B., Siwanowicz, I., Rubin, G.M., Preat, T., and Tanimoto, H. (2012). A subset of dopamine neurons signals reward for odour memory in Drosophila. Nature *488*, 512–516.

Mao, Z., and Davis, R.L. (2009). Eight different types of dopaminergic neurons innervate the Drosophila mushroom body neuropil: anatomical and physiological heterogeneity. Front. Neural Circuits *3*, 5.

Mauss, A.S., Meier, M., Serbe, E., and Borst, A. (2014). Optogenetic and pharmacologic dissection of feedforward inhibition in Drosophila motion vision. J. Neurosci. *34*, 2254–2263.

McGuire, S.E., Le, P.T., Osborn, A.J., Matsumoto, K., and Davis, R.L. (2003). Spatiotemporal rescue of memory dysfunction in Drosophila. Science *302*, 1765–1768.

Menzel, R. (2014). The insect mushroom body, an experience-dependent recoding device. J. Physiol. Paris *108*, 84–95.

Murthy, M., Fiete, I., and Laurent, G. (2008). Testing odor response stereotypy in the Drosophila mushroom body. Neuron *59*, 1009–1023.

Ni, J.Q., Liu, L.P., Binari, R., Hardy, R., Shim, H.S., Cavallaro, A., Booker, M., Pfeiffer, B.D., Markstein, M., Wang, H., et al. (2009). A Drosophila resource of transgenic RNAi lines for neurogenetics. Genetics *182*, 1089–1100.

Owald, D., and Waddell, S. (2015). Olfactory learning skews mushroom body output pathways to steer behavioral choice in Drosophila. Curr. Opin. Neurobiol. *35*, 178–184.

Owald, D., Felsenberg, J., Talbot, C.B., Das, G., Perisse, E., Huetteroth, W., and Waddell, S. (2015). Activity of defined mushroom body output neurons underlies learned olfactory behavior in Drosophila. Neuron *86*, 417–427.

Pai, T.P., Chen, C.C., Lin, H.H., Chin, A.L., Lai, J.S., Lee, P.T., Tully, T., and Chiang, A.S. (2013). Drosophila ORB protein in two mushroom body output neurons is necessary for long-term memory formation. Proc. Natl. Acad. Sci. USA *110*, 7898–7903.

Perisse, E., Burke, C., Huetteroth, W., and Waddell, S. (2013a). Shocking revelations and saccharin sweetness in the study of Drosophila olfactory memory. Curr. Biol. *23*, R752–R763.

Perisse, E., Yin, Y., Lin, A.C., Lin, S., Huetteroth, W., and Waddell, S. (2013b). Different kenyon cell populations drive learned approach and avoidance in Drosophila. Neuron *79*, 945–956.

Perrat, P.N., DasGupta, S., Wang, J., Theurkauf, W., Weng, Z., Rosbash, M., and Waddell, S. (2013). Transposition-driven genomic heterogeneity in the Drosophila brain. Science *340*, 91–95.

Pitman, J.L., Huetteroth, W., Burke, C.J., Krashes, M.J., Lai, S.L., Lee, T., and Waddell, S. (2011). A pair of inhibitory neurons are required to sustain labile memory in the Drosophila mushroom body. Curr. Biol. *21*, 855–861.

Plaçais, P.Y., Trannoy, S., Friedrich, A.B., Tanimoto, H., and Preat, T. (2013). Two pairs of mushroom body efferent neurons are required for appetitive long-term memory retrieval in Drosophila. Cell Rep. *5*, 769–780.

Pologruto, T.A., Sabatini, B.L., and Svoboda, K. (2003). ScanImage: flexible software for operating laser scanning microscopes. Biomed. Eng. Online *2*, 13.

Qin, H., Cressy, M., Li, W., Coravos, J.S., Izzi, S.A., and Dubnau, J. (2012). Gamma neurons mediate dopaminergic input during aversive olfactory memory formation in Drosophila. Curr. Biol. *22*, 608–614.

Roberts, A.C., and Glanzman, D.L. (2003). Learning in Aplysia: looking at synaptic plasticity from both sides. Trends Neurosci. *26*, 662–670.

Root, C.M., Ko, K.I., Jafari, A., and Wang, J.W. (2011). Presynaptic facilitation by neuropeptide signaling mediates odor-driven food search. Cell *145*, 133–144.

Salin, P.A., Malenka, R.C., and Nicoll, R.A. (1996). Cyclic AMP mediates a presynaptic form of LTP at cerebellar parallel fiber synapses. Neuron *16*, 797–803.

Schäfer, S., Bicker, G., Ottersen, O.P., and Storm-Mathisen, J. (1988). Taurine-like immunoreactivity in the brain of the honeybee. J. Comp. Neurol. *268*, 60–70.

Schürmann, F.W. (2000). Acetylcholine, GABA, glutamate and NO as putative transmitters indicated by immunocytochemistry in the olfactory mushroom body system of the insect brain. Acta Biol. Hung. *51*, 355–362.

Séjourné, J., Plaçais, P.Y., Aso, Y., Siwanowicz, I., Trannoy, S., Thoma, V., Tedjakumala, S.R., Rubin, G.M., Tchénio, P., Ito, K., et al. (2011). Mushroom body efferent neurons responsible for aversive olfactory memory retrieval in Drosophila. Nat. Neurosci. *14*, 903–910.

Shang, Y., Claridge-Chang, A., Sjulson, L., Pypaert, M., and Miesenböck, G. (2007). Excitatory local circuits and their implications for olfactory processing in the fly antennal lobe. Cell *128*, 601–612.

Shih, H.W., Wu, C.L., Chang, S.W., Liu, T.H., Lai, J.S., Fu, T.F., Fu, C.C., and Chiang, A.S. (2015). Parallel circuits control temperature preference in Drosophila during ageing. Nat. Commun. *6*, 7775.

Shomrat, T., Graindorge, N., Bellanger, C., Fiorito, G., Loewenstein, Y., and Hochner, B. (2011). Alternative sites of synaptic plasticity in two homologous "fan-out fan-in" learning and memory networks. Curr. Biol. *21*, 1773–1782.

Sinakevitch, I., Farris, S.M., and Strausfeld, N.J. (2001). Taurine-, aspartate- and glutamate-like immunoreactivity identifies chemically distinct subdivisions of Kenyon cells in the cockroach mushroom body. J. Comp. Neurol. *439*, 352–367.

Sitaraman, D., Aso, Y., Jin, X., Chen, N., Felix, M., Rubin, G.M., and Nitabach, M.N. (2015). Propagation of Homeostatic Sleep Signals by Segregated Synaptic Microcircuits of the Drosophila Mushroom Body. Curr. Biol. *25*, 2915–2927.

Stevens, C.F. (2015). What the fly's nose tells the fly's brain. Proc. Natl. Acad. Sci. USA *112*, 9460–9465.

Strausfeld, N.J., Hansen, L., Li, Y., Gomez, R.S., and Ito, K. (1998). Evolution, discovery, and interpretations of arthropod mushroom bodies. Learn. Mem. *5*, 11–37.

Strausfeld, N.J., Sinakevitch, I., and Vilinsky, I. (2003). The mushroom bodies of Drosophila melanogaster: an immunocytological and golgi study of Kenyon cell organization in the calyces and lobes. Microsc. Res. Tech. *62*, 151–169.

Strausfeld, N.J., Sinakevitch, I., Brown, S.M., and Farris, S.M. (2009). Ground plan of the insect mushroom body: functional and evolutionary implications. J. Comp. Neurol. *513*, 265–291.

Tanaka, N.K., Tanimoto, H., and Ito, K. (2008). Neuronal assemblies of the Drosophila mushroom body. J. Comp. Neurol. *508*, 711–755.

Thany, S.H., Lenaers, G., Raymond-Delpech, V., Sattelle, D.B., and Lapied, B. (2007). Exploring the pharmacological properties of insect nicotinic acetylcholine receptors. Trends Pharmacol. Sci. *28*, 14–22.

Tomer, R., Denes, A.S., Tessmar-Raible, K., and Arendt, D. (2010). Profiling by image registration reveals common origin of annelid mushroom bodies and vertebrate pallium. Cell *142*, 800–809.

Trannoy, S., Redt-Clouet, C., Dura, J.M., and Preat, T. (2011). Parallel processing of appetitive short- and long-term memories in Drosophila. Curr. Biol. *21*, 1647–1653.

Tully, T., and Quinn, W.G. (1985). Classical conditioning and retention in normal and mutant Drosophila melanogaster. J. Comp. Physiol. A Neuroethol. Sens. Neural Behav. Physiol. *157*, 263–277.

Vecsey, C.G., Pírez, N., and Griffith, L.C. (2014). The Drosophila neuropeptides PDF and sNPF have opposing electrophysiological and molecular effects on central neurons. J. Neurophysiol. *111*, 1033–1045.

Vogt, K., Schnaitmann, C., Dylla, K.V., Knapek, S., Aso, Y., Rubin, G.M., and Tanimoto, H. (2014). Shared mushroom body circuits underlie visual and olfactory memories in Drosophila. eLife *3*, e02395.

Waddell, S. (2013). Reinforcement signalling in Drosophila; dopamine does it all after all. Curr. Opin. Neurobiol. *23*, 324–329.

Wagh, D.A., Rasse, T.M., Asan, E., Hofbauer, A., Schwenkert, I., Dürrbeck, H., Buchner, S., Dabauvalle, M.C., Schmidt, M., Qin, G., et al. (2006). Bruchpilot, a protein with homology to ELKS/CAST, is required for structural integrity and function of synaptic active zones in Drosophila. Neuron *49*, 833–844.

Wang, J.W., Wong, A.M., Flores, J., Vosshall, L.B., and Axel, R. (2003). Two-photon calcium imaging reveals an odor-evoked map of activity in the fly brain. Cell *112*, 271–282.

Wu, J.S., and Luo, L. (2006). A protocol for dissecting Drosophila melanogaster brains for live imaging or immunostaining. Nat. Protoc. *1*, 2110–2115.

Yamagata, N., Ichinose, T., Aso, Y., Plaçais, P.Y., Friedrich, A.B., Sima, R.J., Preat, T., Rubin, G.M., and Tanimoto, H. (2015). Distinct dopamine neurons mediate reward signals for short- and long-term memories. Proc. Natl. Acad. Sci. USA *112*, 578–583.

Yasuyama, K., Kitamoto, T., and Salvaterra, P.M. (1995a). Localization of choline acetyltransferase-expressing neurons in the larval visual system of Drosophila melanogaster. Cell Tissue Res. *282*, 193–202.

Yasuyama, K., Kitamoto, T., and Salvaterra, P.M. (1995b). Immunocytochemical study of choline acetyltransferase in Drosophila melanogaster: an analysis of cis-regulatory regions controlling expression in the brain of cDNA-transformed flies. J. Comp. Neurol. *361*, 25–37.

Yasuyama, K., Meinertzhagen, I.A., and Schürmann, F.W. (2002). Synaptic organization of the mushroom body calyx in Drosophila melanogaster. J. Comp. Neurol. *445*, 211–226.

Zars, T., Fischer, M., Schulz, R., and Heisenberg, M. (2000). Localization of a short-term memory in Drosophila. Science *288*, 672–675.

Neuron, Volume *89*

Supplemental Information

Memory-Relevant Mushroom Body Output Synapses Are Cholinergic

Oliver Barnstedt, David Owald, Johannes Felsenberg, Ruth Brain, John-Paul Moszynski, Clifford B. Talbot, Paola N. Perrat, and Scott Waddell

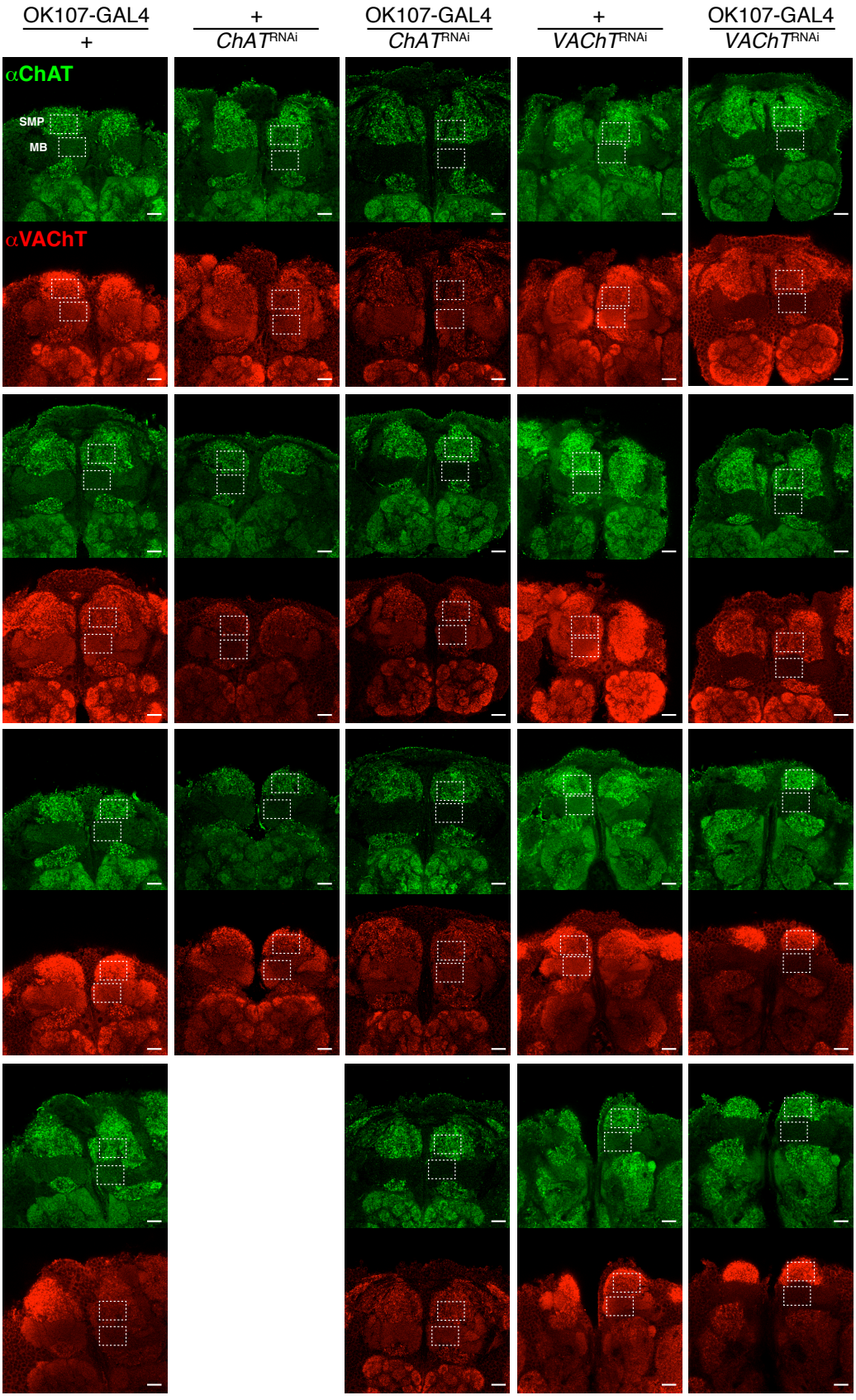
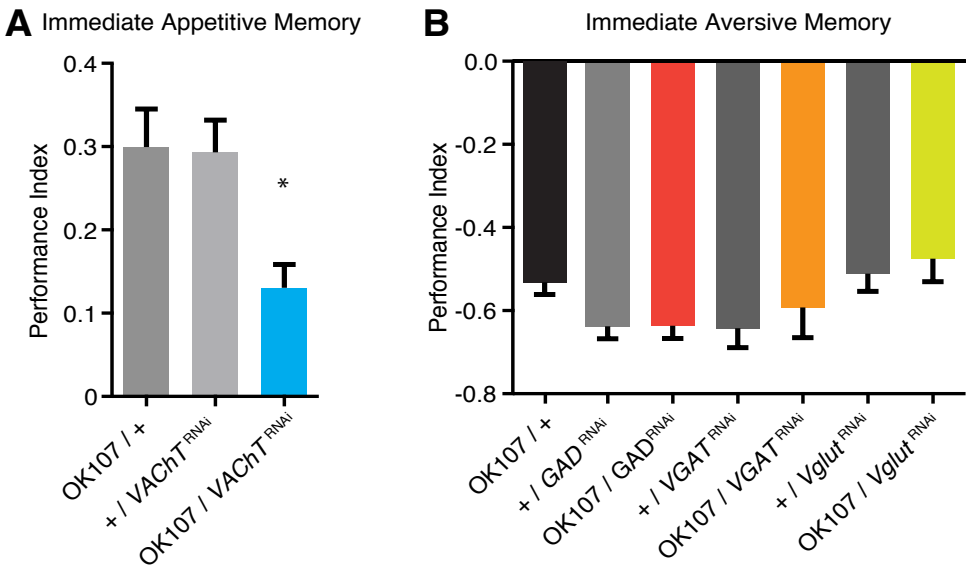

OK107-GAL4 / +
+ / ChATRNAi
OK107-GAL4 / ChATRNAi
+ / VAChTRNAi
OK107-GAL4 / VAChTRNAi
αChAT
SMP
MB
αVAChT

Figure S1, related to Figure 1A and B. ChAT and VAChT immunostaining labels Kenyon cells. Single confocal sections through representative sample of brains of UAS-*ChAT*^{RNAi}; OK107-GAL4 and UAS-*VAChT*^{RNAi}; OK107-GAL4 flies and their genetic controls, shown at the level of the MB γ lobe neurons. αChAT labeling is visibly lower in comparable images from brains of UAS-*ChAT*^{RNAi}; OK107-GAL4 flies demonstrating that the signal in control flies represents intrinsic labeling of KCs. Each lane presents both channels of single confocal sections at the level of the γ lobe from three to four representative brains per genotype. All flies were raised and processed for immunostaining in parallel before being imaged using the same confocal settings. Scale bars 20 μm. White dashed rectangles denote areas taken for quantification. See Movie S1 for comparison of a whole stack. Similar levels of staining and RNAi-reduction were observed for the other MB lobes (not shown).



C

	naïve preference MCH	naïve preference OCT
OK107-Gal4	n = 7 -0.67 ± 0.04	n = 8 -0.19 ± 0.05
UAS-*ChAT*^{RNAi}	n = 7 -0.16 ± 0.05	n = 10 -0.12 ± 0.03
UAS-*VAChT*^{RNAi}	n = 8 -0.49 ± 0.08	n = 10 -0.13 ± 0.05
OK107 > *ChAT*^{RNAi}	n = 7 -0.24 ± 0.08	n = 10 -0.22 ± 0.03
OK107 > *VAChT*^{RNAi}	n = 8 -0.42 ± 0.08	n = 10 -0.19 ± 0.03

Figure S2, related to Figure 1C. RNAi directed towards ACh but not GABAergic and glutamatergic transmission compromises olfactory memory. (A) KC-driven UAS-*VAChT*^{RNAi} impairs immediate appetitive memory (n = 10-12, asterisk denotes $p < 0.05$; one-way ANOVA, Tukey's HSD post-hoc test). (B) KC-driven UAS-*GAD*^{RNAi}, UAS-*VGAT*^{RNAi} (both required for GABAergic signaling), and UAS-*VGlut*^{RNAi} (required for glutamatergic signaling) did not significantly impact immediate aversive memory performance, as compared to the relevant genetic control flies (n = 4-7, $p > 0.05$; one-way ANOVA, Tukey's HSD post-hoc test). Error bars in (A) and (B) represent SEM. (C) Naïve OCT and MCH avoidance performance of all fly strains tested for aversive behavioral memory in Figure 1C. Displayed are mean performance index values +/- SEM. No statistical differences were evident between the groups (n = 7-10, all $p > 0.05$, one-way ANOVA, Tukey's HSD post-hoc test) other than OK107; UAS-*ChAT*^{RNAi} and +; UAS-*ChAT*^{RNAi} flies which exhibit defective MCH avoidance compared to OK107; + (n = 7, $p < 0.05$, one-way ANOVA, Tukey's HSD post-hoc test). MCH concentration was 1:500.

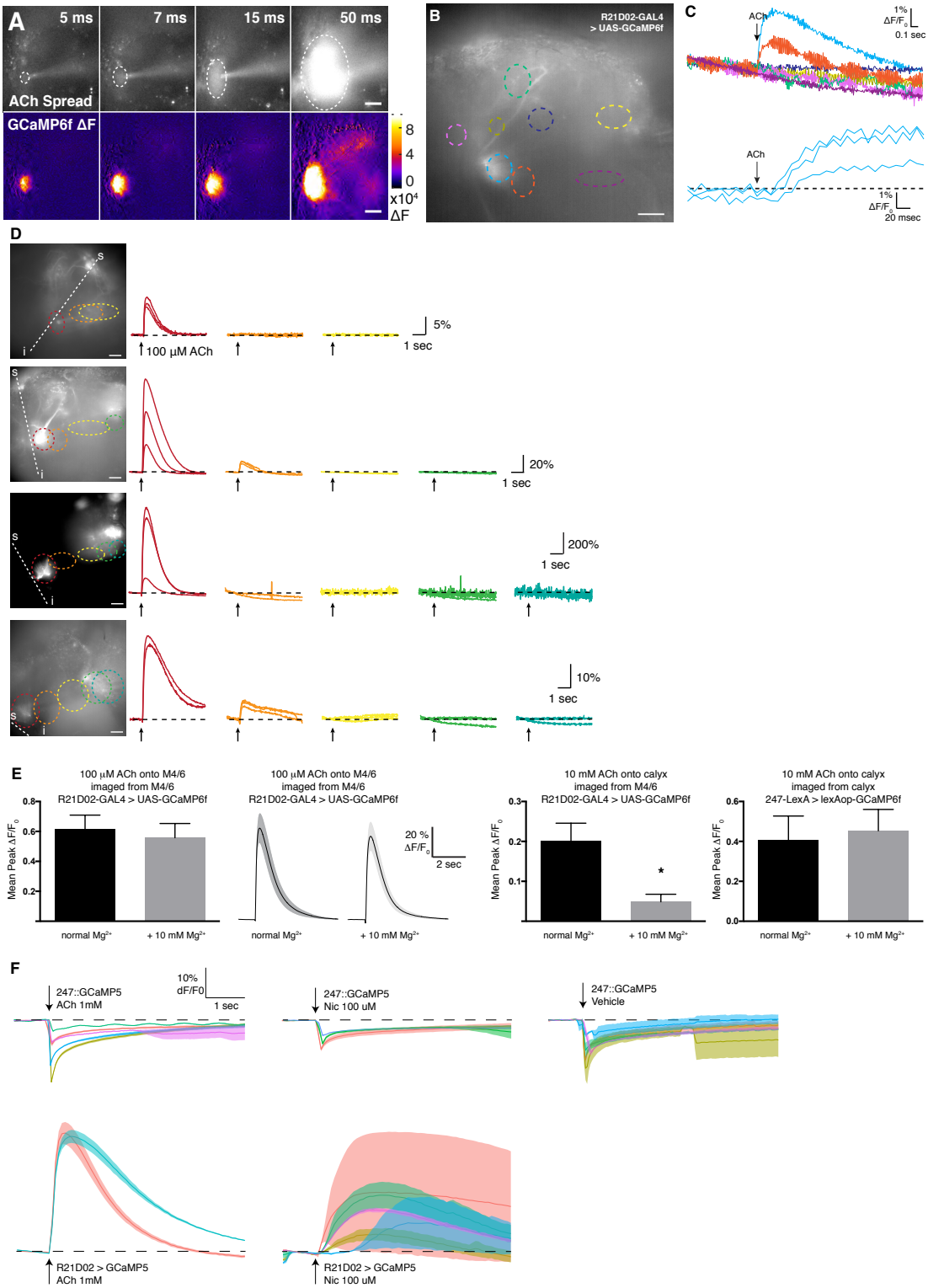

A
5 ms
7 ms
15 ms
50 ms
ACh Spread
GCaMP6f ΔF
8
4
0
x10⁴
ΔF
B
R21D02-GAL4
> UAS-GCaMP6f
C
ACh
1%
ΔF/F₀
0.1 sec
ACh
1%
ΔF/F₀
20 msec
D
100 μM ACh
5%
1 sec
20%
1 sec
200%
1 sec
10%
1 sec
E
100 μM ACh onto M4/6
imaged from M4/6
R21D02-GAL4 > UAS-GCaMP6f
Mean Peak ΔF/F₀
normal Mg²⁺
+ 10 mM Mg²⁺
100 μM ACh onto M4/6
imaged from M4/6
R21D02-GAL4 > UAS-GCaMP6f
20 %
ΔF/F₀
2 sec
normal Mg²⁺
+ 10 mM Mg²⁺
10 mM ACh onto calyx
imaged from M4/6
R21D02-GAL4 > UAS-GCaMP6f
Mean Peak ΔF/F₀
*
normal Mg²⁺
+ 10 mM Mg²⁺
10 mM ACh onto calyx
imaged from calyx
247-LexA > lexAop-GCaMP6f
Mean Peak ΔF/F₀
normal Mg²⁺
+ 10 mM Mg²⁺
F
247::GCaMP5
ACh 1mM
10%
dF/F0
1 sec
247::GCaMP5
Nic 100 uM
247::GCaMP5
Vehicle
R21D02 > GCaMP5
ACh 1mM
R21D02 > GCaMP5
Nic 100 uM

Figure S3, related to Figure 2. Only local dendritic application of ACh evokes calcium transients in M4/6 neurons. 100 μM ACh was applied to the M4/6 dendritic region in R21D02-GAL4; UAS-GCaMP6f brains. (A) The breadth of the evoked calcium response in M4/6 dendrites depends on the spread of the applied ACh. Upper panels follow the spread of Texas Red that was co-applied with 100 μM ACh. The ejection dose was successively increased from a 5 ms to 50 ms application. Lower panels depict ΔF (mean of responses 1.5 s after ACh application – mean 1 s before application). Each pixel is color-coded. (B and C) ACh elicits calcium responses in M4/6 neurons only when locally applied to the dendritic region. (B) 100 μM ACh was ejected at different positions within the protocerebrum, while the spread of the solution was monitored with Texas Red. Spread outlines are marked with colored dashed ellipses. (C) Mean trace of three application trials, each trace relates to the corresponding application outline shown in (B). Only ACh delivery close to M4/6 dendrites (the orange and bright blue traces) evoked calcium responses. A magnified view of the individual traces underlying the 'bright blue' response reveals a 30-40 ms response onset. The experiments in A-C contained 1 μM tetradotoxin (TTX). (D) The injection pipette was moved to successively more distant locations away from the dendrite, while calcium responses were recorded using widefield imaging. Each row depicts a different brain. Dashed white line represents the midline of the brain for orientation purposes; s - superior, i - inferior. Colored dashed ellipses represent spread of ACh, monitored by Texas Red; colors of calcium traces correspond to the matching dashed colored ellipses. Scale bars in A, B and D 20 μm. (E) 100 μM ACh still evokes M4/6 responses under conditions of high magnesium in AHLS. Addition of 10 mM Mg^{2+} did not affect responses evoked in M4/6 neurons when 100 μM ACh was applied to the M4/6 neuron dendrites (first panel; $n = 6$, $p > 0.05$, independent samples t-test). Calcium responses in M4/6 also show similar kinetics with and without additional 10 mM Mg^{2+} (second panel). Mean traces are shown with SEM in shade. Calcium responses in M4/6 neurons were significantly decreased at 10 mM Mg^{2+} when they were stimulated via 10 mM ACh applied in the calyx (third panel; $n = 3$-4, $p < 0.05$, independent samples t-test). Additional 10 mM Mg^{2+} did not decrease KC responses evoked by applying 10 mM ACh to the MB calyx (fourth panel; $n = 2$, $p > 0.05$, independent samples t-test). Error bars represent SEM. (F) KCs do not respond to cholinergic stimulation in the MB lobes. Application of 1 mM ACh or 100 μM nicotine to the MB lobes does not elicit calcium responses in KCs (upper row), while both agonists evoke strong calcium responses in M4/6 neurons when applied in the same location (bottom panels). Displayed are mean traces with the respective SEM as shade, each color representing an individual brain. Note that the reduced $\Delta F/F_0$ signal observed in the upper panels likely results from tissue displacement caused by pressure-evoked release of ACh or vehicle.

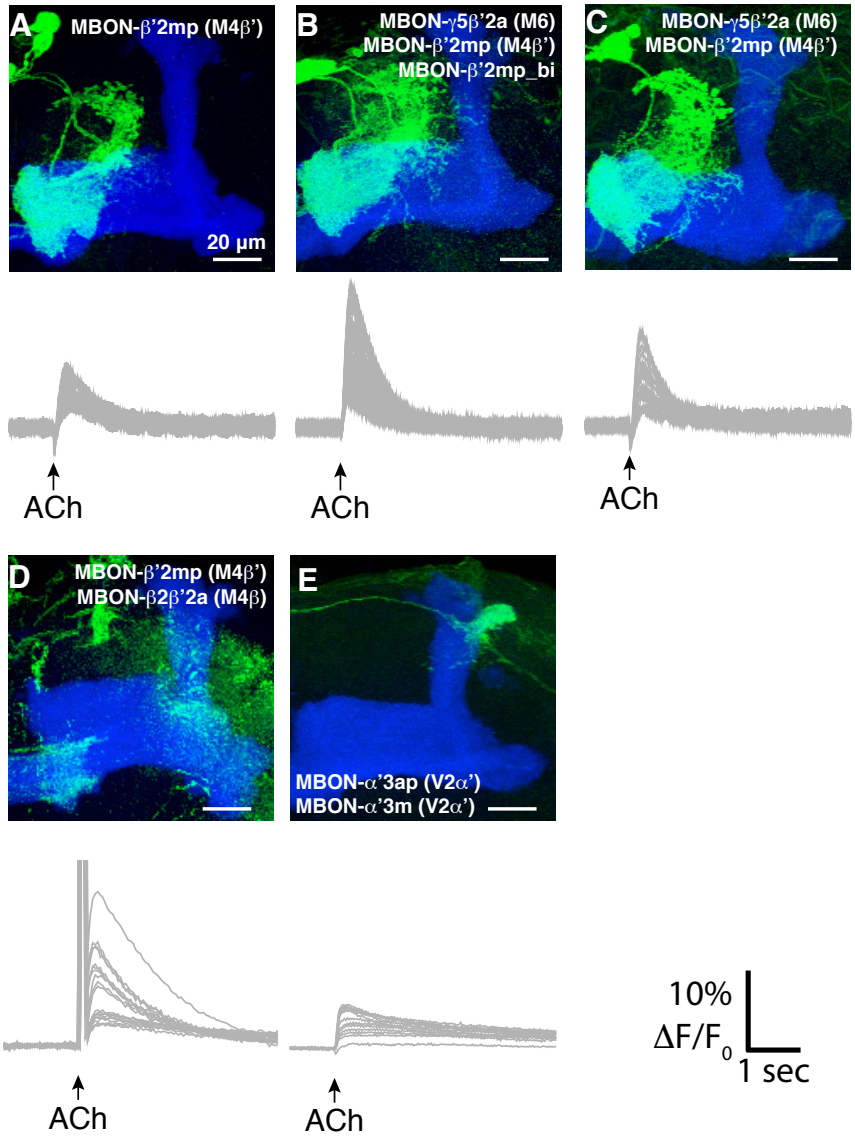


Figure S4, related to Figure 3. ACh evokes responses in multiple classes of MBONs. Each panel shows the anatomy of the relevant MBON and below the corresponding GCaMP6f measured physiological responses elicited by 1 mM acetylcholine application. Data represent individual ACh-evoked traces from one brain per genotype. (A) MB002B labels MBON-β′2mp (M4β'). (B), MB011B labels MBON-γ5β′2a (M6), MBON-β′2mp (M4β') and MBON-β′2mp_bi.(C), MB210B labels MBON-γ5β′2a (M6) and MBON-β′2mp (M4β'). (D) R93F01-GAL4 labels MBON-β′2mp (M4β') and MBON-γ5β′2a (M6). (E) MB027B labels MBON-α′3ap (V2α') and MBON-α′3m (V2α'). Initial increase in traces of (D) is an artifact of the LED trigger.

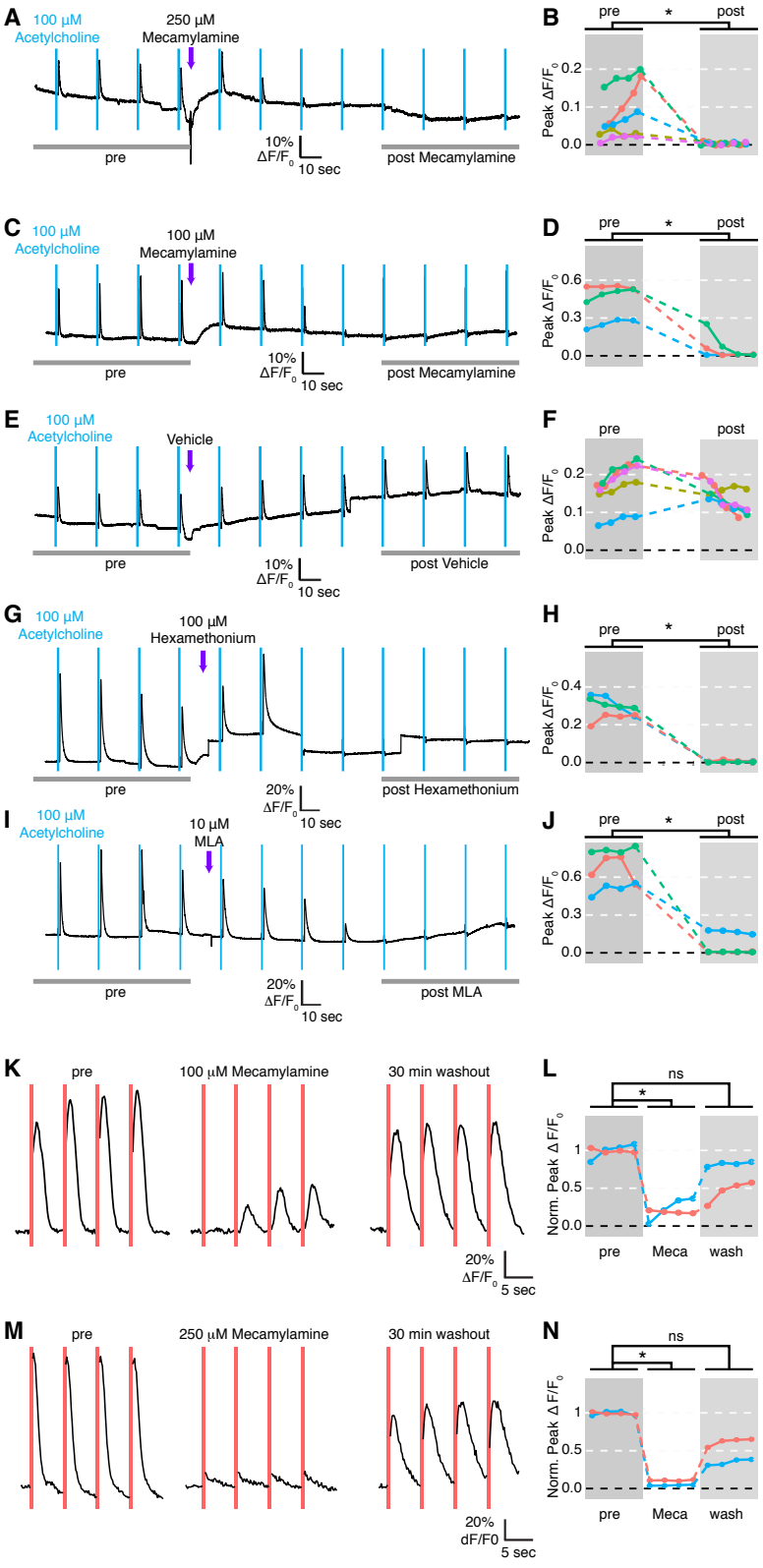

A
100 µM Acetylcholine
250 µM Mecamylamine
pre
post Mecamylamine
10% ΔF/F0
10 sec
B
pre
*
post
Peak ΔF/F0
0.2
0.1
0.0
C
100 µM Acetylcholine
100 µM Mecamylamine
pre
post Mecamylamine
10% ΔF/F0
10 sec
D
pre
*
post
Peak ΔF/F0
0.6
0.3
0.0
E
100 µM Acetylcholine
Vehicle
pre
post Vehicle
10% ΔF/F0
10 sec
F
pre
post
Peak ΔF/F0
0.2
0.1
0.0
G
100 µM Acetylcholine
100 µM Hexamethonium
pre
post Hexamethonium
20% ΔF/F0
10 sec
H
pre
*
post
Peak ΔF/F0
0.4
0.2
0.0
I
100 µM Acetylcholine
10 µM MLA
pre
post MLA
20% ΔF/F0
10 sec
J
pre
*
post
Peak ΔF/F0
0.6
0.3
0.0
K
pre
100 µM Mecamylamine
30 min washout
20% ΔF/F0
5 sec
L
ns
*
Norm. Peak Δ F/F0
1
0.5
0.0
pre
Meca
wash
M
pre
250 µM Mecamylamine
30 min washout
20% dF/F0
5 sec
N
ns
*
Norm. Peak Δ F/F0
1
0.5
0.0
pre
Meca
wash

Figure S5, related to Figure 4. M4/6 neuron calcium responses can be reversibly blocked by nicotinic receptor antagonists. (A-J) Local ACh evoked calcium responses in M4/6 dendrites are blocked by the non-selective nicotinic receptor antagonists mecamylamine, hexamethonium, and MLA. (A-B) ACh responses vanish within 100 s of applying 250 μM mecamylamine to the recording chamber. (A) Sample trace and (B) quantification, n = 5 brains, average of four trials, asterisk denotes $p < 0.05$, paired samples t-test. (C-D) ACh responses also decrease within 100 s of applying 100 μM mecamylamine to the recording chamber. (C) Sample trace and (D) quantification, n = 3 brains, average of four trials, asterisk denotes $p < 0.05$, paired samples t-test. (E-F) Application of a vehicle control has no effect on the ACh-evoked responses. (E) Sample trace and (F) quantification, n = 5 brains, average of four trials, $p > 0.05$, paired samples t-test. (G-H) ACh responses vanish within 100 s of applying 100 μM hexamethonium to the recording chamber. (G) Sample trace and (H) quantification, n = 3 brains, average of four trials, asterisk denotes $p < 0.05$, paired samples t-test. (I-J) ACh responses vanish within 100 s of applying 10 μM MLA to the recording chamber. (I) Sample trace and (J) quantification, n = 3 brains, average of four trials, asterisk denotes $p < 0.05$, paired samples t-test. (K-N) Optogenetic stimulation of KCs triggers M4/6 neuron calcium responses that are significantly reduced by application of mecamylamine, and partially recovered after washout. (K) Sample trace and (L) quantification of applying 100 μM mecamylamine, n = 2 brains, average of four trials, asterisk denotes $p < 0.05$, paired samples t-test. Genotype: lexAop-CsChrimson / UAS-GCaMP6f; R21D02-GAL4 / 247-LexA::VP16. (M) Sample trace and (N) quantification of applying 250 μM mecamylamine, n = 2 brains, average of four trials, asterisk denotes $p < 0.05$, paired samples t-test. Genotype: R15B01-LexA, lexAop-GCaMP6f / UAS-CsChrimson; R13F02-GAL4 / +. $\Delta F/F_0$ was normalized to each experiment's average initial four responses.

Movie S1, related to Figure 1A. Kenyon cells are ChAT- and VAChT-immunopositive. ChAT and VAChT immunofluorescence in the mushroom body lobes are greatly reduced by OK107-GAL4 directed expression of UAS-*ChAT*^{RNAi} or UAS-*VAChT*^{RNAi} respectively (middle panels). Movie shows a representative sample stack at 0.5 μm/frame. All flies were raised and processed for immunostaining in parallel before being imaged using the same confocal settings. Scale bar 50 μm.

Movie S2, related to Figure 4A and D. Mecamylamine abolishes Kenyon cell-driven M4/6 responses. Optogenetic KC activation via 247-LexA expressed lexAop-CsChrimson and red light illumination leads to robust calcium responses in M4/6 axons. R21D02-GAL4; UAS-GCaMP6f explant brains monitored with two-photon imaging. Frame rate: 5.92 Hz. Two representative samples before and after addition of the nicotinic receptor antagonist mecamylamine (250 μM) or vehicle, are shown. The data in these movies is also presented as static views in Figures 4 G-L. White horizontal stripes that appear at regular intervals are artifacts from LED stimulation.

Article

Neuron

Aversive Learning and Appetitive Motivation Toggle Feed-Forward Inhibition in the *Drosophila* Mushroom Body

Highlights

- Aversive learning reduces odor-specific feed-forward inhibition in mushroom body
- Feed-forward inhibition selectively inhibits avoidance-directing neural pathways
- Appetitive motivation increases feed-forward inhibition in the mushroom body
- Imposing feed-forward inhibition favors appetitive memory expression

Authors

Emmanuel Perisse, David Owald, Oliver Barnstedt, Clifford B. Talbot, Wolf Huetteroth, Scott Waddell

Correspondence

scott.waddell@cncb.ox.ac.uk

In Brief

Fruit fly memory and its state-dependent behavioral expression involve modulation of mushroom body output synapses. Perisse et al. demonstrate aversive learning and appetitive motivation toggle alternate modes of feed-forward inhibition in mushroom body, favoring either conditioned avoidance or approach behavior.

Perisse et al., 2016, Neuron *90*, 1086–1099
June 1, 2016 © 2016 The Author(s). Published by Elsevier Inc.
http://dx.doi.org/10.1016/j.neuron.2016.04.034

CellPress

CellPress

Neuron
Article

Aversive Learning and Appetitive Motivation Toggle Feed-Forward Inhibition in the *Drosophila* Mushroom Body

Emmanuel Perisse,[1,2] David Owald,[1,2,3] Oliver Barnstedt,[1] Clifford B. Talbot,[1] Wolf Huetteroth,[1,4] and Scott Waddell[1,*]
[1]Centre for Neural Circuits and Behaviour, The University of Oxford, Tinsley Building, Mansfield Road, Oxford, OX1 3SR, UK
[2]Co-first author
[3]Present address: Institute of Neurophysiology, Charité – Universitätsmedizin Berlin, 10117 Berlin, Germany
[4]Present address: Zukunftskolleg, University of Konstanz, Box 624, 78457 Konstanz, Germany
*Correspondence: scott.waddell@cncb.ox.ac.uk
http://dx.doi.org/10.1016/j.neuron.2016.04.034

SUMMARY

In *Drosophila*, negatively reinforcing dopaminergic neurons also provide the inhibitory control of satiety over appetitive memory expression. Here we show that aversive learning causes a persistent depression of the conditioned odor drive to two downstream feed-forward inhibitory GABAergic interneurons of the mushroom body, called MVP2, or mushroom body output neuron (MBON)-γ1pedc>α/β. However, MVP2 neuron output is only essential for expression of short-term aversive memory. Stimulating MVP2 neurons preferentially inhibits the odor-evoked activity of avoidance-directing MBONs and odor-driven avoidance behavior, whereas their inhibition enhances odor avoidance. In contrast, odor-evoked activity of MVP2 neurons is elevated in hungry flies, and their feed-forward inhibition is required for expression of appetitive memory at all times. Moreover, imposing MVP2 activity promotes inappropriate appetitive memory expression in food-satiated flies. Aversive learning and appetitive motivation therefore toggle alternate modes of a common feed-forward inhibitory MVP2 pathway to promote conditioned odor avoidance or approach.

INTRODUCTION

Learning and internal states guide appropriate behavior by altering the properties of neural circuits. A great number of studies across phyla have elucidated brain structures and cellular mechanisms that underlie these changes, but we still know relatively little about how experience and states are implemented in the functional connectivity of a neural network. Inhibition across a range of timescales from milliseconds to days, mediated by neurotransmitters, neuromodulators, and a variety of neuropeptides, is emerging as a critical and general operating principle of neural circuit function and behavioral control (Klausberger and Somogyi, 2008; Fishell and Rudy, 2011; Letzkus et al., 2015).

Fast inhibition can spatially and temporally refine neural representations of sensory stimuli so that specificity is maintained and windows of time in which neural integration can take place are established (Gabernet et al., 2005). In addition, fast and persistent inhibition can alter neural excitability and the efficacy of synaptic transmission and thereby re-route the flow of information through circuits (Vogels and Abbott, 2005; Schwab and Houk, 2015). It is therefore important to understand the mechanisms that control, and the circumstances in which, the level of inhibition is altered in the nervous system.

The reduced numerical complexity of the *Drosophila* brain permits an understanding of these mechanisms at cellular resolution. Studies in flies, mice, and primates have established that dopaminergic neurons (DANs) play a critical role in reinforcement and motivation (Schultz et al., 1997; Wise, 2004; Bromberg-Martin et al., 2010; Berridge, 2012; Waddell, 2013). Across phyla DANs appear to be heterogeneous (Matsumoto and Hikosaka, 2009; Lammel et al., 2011, 2012; Menegas et al., 2015; Beier et al., 2015; Lerner et al., 2015; Mao and Davis, 2009; Claridge-Chang et al., 2009; Krashes et al., 2009; Aso et al., 2010, 2012; Liu et al., 2012; Burke et al., 2012; Riemensperger et al., 2013), and recordings suggest that some DANs respond to reward-related events and others react to aversive, salient, or surprising cues (Schultz, 2015; Matsumoto and Hikosaka, 2009; Cohen et al., 2012; Horvitz, 2000; Matsumoto and Takada, 2013). Genetic approaches in *Drosophila* and mice revealed that DANs that can provide teaching signals to reinforce either appetitive or aversive memories, project to different locations in the brain (Claridge-Chang et al., 2009; Aso et al., 2010, 2012; Liu et al., 2012; Burke et al., 2012; Zweifel et al., 2011; Darvas et al., 2011; Lammel et al., 2011, 2012). However, it is currently unclear how the processes of reinforcement relate to those of motivational salience.

Olfactory learning in *Drosophila* could provide an inroad. Flies assign negative and positive values to odors in aversive and reward based paradigms (Tully and Quinn, 1985; Tempel et al., 1983). When subsequently tested for odor preference, they either avoid or approach the conditioned odor. Individual odors are uniquely represented as activity in relatively sparse subpopulations of the ~2,000 intrinsic Kenyon cells (KCs) per hemisphere of the mushroom body (MB), providing cellular specificity to odor memories (Honegger et al., 2011). During learning, odor-activated KCs receive coincident reinforcing input from

This is an open access article under the CC BY license (http://creativecommons.org/licenses/by/4.0/).

combinations of positively or negatively reinforcing DANs (Waddell, 2013). Stimuli such as sweet taste, nutrient value, and water activate distinct populations of rewarding DANs in the protocerebral anterior medial (PAM) cluster, which innervate different zones on the horizontal lobes of the MB (Burke et al., 2012; Liu et al., 2012; Lin et al., 2014; Huetteroth et al., 2015; Yamagata et al., 2015). Reward quality therefore seems to be represented in different DANs, and memories of these rewarding stimuli are presumably formed within the relevant orthogonal zones along the odor-activated KC arbor (Owald and Waddell, 2015). In contrast, aversive DANs innervate the heel, peduncle, and vertical lobes of the MB (Riemensperger et al., 2005; Mao and Davis, 2009; Claridge-Chang et al., 2009; Aso et al., 2010), but electric shock, heat, and bitter taste appear to bottle-neck onto the same MP1, also called PPL1-γ1pedc DANs (Aso et al., 2012; Das et al., 2014; Galili et al., 2014), suggesting that aversive memory lacks quality information and might simply represent the magnitude of aversion. Interestingly, studies suggest that negatively reinforcing MP1 DANs also mediate hunger-dependent motivational control over appetitive memory expression (Krashes et al., 2009; Waddell, 2013). In this context, MP1 DANs appear to be inhibitory since blocking them releases inappropriate memory expression in food-satiated flies (Krashes et al., 2009). Moreover, MP1 DANs are themselves controlled by peptidergic inhibition—dNPF, the fly equivalent of NPY—demonstrating that behavior can be controlled through a hierarchical layering of inhibitory pathways.

Each of the 15 discrete MB zones that is defined by the innervation of a particular type of DAN has a corresponding set of MB output neurons (MBONs) (Aso et al., 2014a), suggesting that DANs specifically modulate the efficacy of the KC-MBON connection within a zone (Owald and Waddell, 2015). Indeed, recent work has revealed a clear model for how DAN reinforcement during learning can shape odor-driven behavior (Owald et al., 2015; Owald and Waddell, 2015). Reward learning engages DANs that modulate and suppress the conditioned odor-drive from KCs to glutamatergic MBONs that intrinsically direct avoidance behavior (Owald et al., 2015). In contrast, aversive learning enhances conditioned odor-drive to these avoidance MBONs (Owald et al., 2015; Bouzaiane et al., 2015) while also inhibiting odor-drive to cholinergic (Séjourné et al., 2011), and perhaps GABAergic, MBONs driving approach. Learning and internal states are therefore likely to tune collections of MBON pathways to skew the overall MBON network toward either directing approach or aversion (Owald and Waddell, 2015).

The presynaptic terminals of MP1/PPL1-γ1pedc DANs are intermingled with the dendrites of MVP2 neurons (also called MBON-γ1pedc>α/β; Aso et al., 2014b), consistent with these DANs modifying the KC-MVP2 junction (Owald and Waddell, 2015). Artificial activation of MP1 paired with odor presentation was recently reported to induce an odor-specific depression at this site (Hige et al., 2015). Here we show that aversive learning causes a persistent and specific reduction in the relative conditioned odor drive to MVP2, yet MVP2 output is only required for the expression of short-term aversive memory. Anatomical and functional connectivity suggests that MVP2 exert asymmetric feed-forward inhibition over MBONs on the horizontal and vertical MB lobes, preferentially promoting approach by inhibiting avoidance directing pathways. Consistent with this model, hunger generally increases MVP2 odor-driven responses, and MVP2-dependent inhibition is required for the expression of appetitive memory at all times in hungry flies. Moreover, activation of MVP2 neurons promotes the expression of appetitive memory in food-satiated flies. Aversive learning and appetitive motivation therefore differentially modulate the odor-drive of the MVP2 neurons, which alters feed-forward inhibition onto other MBON pathways within the neural network of the MB. Reduced feed-forward inhibition is required for conditioned avoidance, whereas increased feed-forward inhibition promotes expression of conditioned approach.

RESULTS

GAL4 Control of GABA-ergic MVP2 Neurons

We used the R83A12-GAL4 (Jenett et al., 2012) and the MB112C split-GAL4 combination (Aso et al., 2014b; Aso et al., 2014a) drivers to investigate the role of MVP2 (MBON-γ1pedc>αβ) neurons. Expression of a UAS-CD8::GFP transgene revealed that R83A12 labels the MVP2 neurons in addition to six large cells with processes confined to the sub-esophageal ganglion (Figure 1A). Neural expression in MB112C is restricted to MVP2 neurons (Aso et al., 2014a) (Figure 1B). Double labeling the MB with rCD2::RFP revealed that most MVP2 processes lie within or in close proximity to the structure of the MB lobes, with a few processes projecting outside in the crepine and superior intermediate protocerebrum (Ito et al., 2014; Aso et al., 2014a) (Figures 1A–1C and S1; Movie S1). Expressing the dendritic UAS-DenMark (Nicolaï et al., 2010) and presynaptic UAS-GFP-Syd-1 (Owald et al., 2010) markers in MVP2 neurons with R83A12 control suggests that dendrites of MVP2 occupy the γ1 and base of the peduncle regions of the MB (Figure 1C), where they are interspersed with the processes of the MP1 DANs (Figure 1D), whereas the presynaptic regions are mostly within, or in close proximity to, the MB lobes (Figure 1C). UAS-GFP-Syd-1 also labels a ring of presynaptic active zones at the level of the αβ surface ($\alpha\beta_s$) neurons, suggesting plausible feedback in this area (inset Figure 1C). GABA immunostaining revealed that MVP2 neurons are likely to be inhibitory (Figure 1E). A prior study concluded that MVP2 neurons predominantly innervate the α1, α2, α3, and β1 and β2 regions of the MB lobes, where they could potentially provide feed-forward inhibition to other MBON compartments (Aso et al., 2014a) (Figure S1).

Aversive Learning Depresses Conditioned Odor Drive to MVP2 Neurons

Several reports suggest that learning alters odor-drive to collections of MBONs (Séjourné et al., 2011; Plaçais et al., 2013; Pai et al., 2013; Owald et al., 2015; Bouzaiane et al., 2015) to either skew the overall MB output toward favoring approach or avoidance (Owald et al., 2015; Owald and Waddell, 2015). Since the presynaptic terminals of aversively reinforcing MP1/PPL1-γ1pedc DANs are confined to the same MB zones as the dendrites of MVP2 neurons (Krashes et al., 2009; Aso et al., 2014b) (Figure 1D), we reasoned that aversive learning might alter the KC-MVP2 connection. We therefore measured odor-evoked activity of MVP2 neurons in trained and control flies. We expressed GCaMP6f (Chen et al., 2013) under MB112C

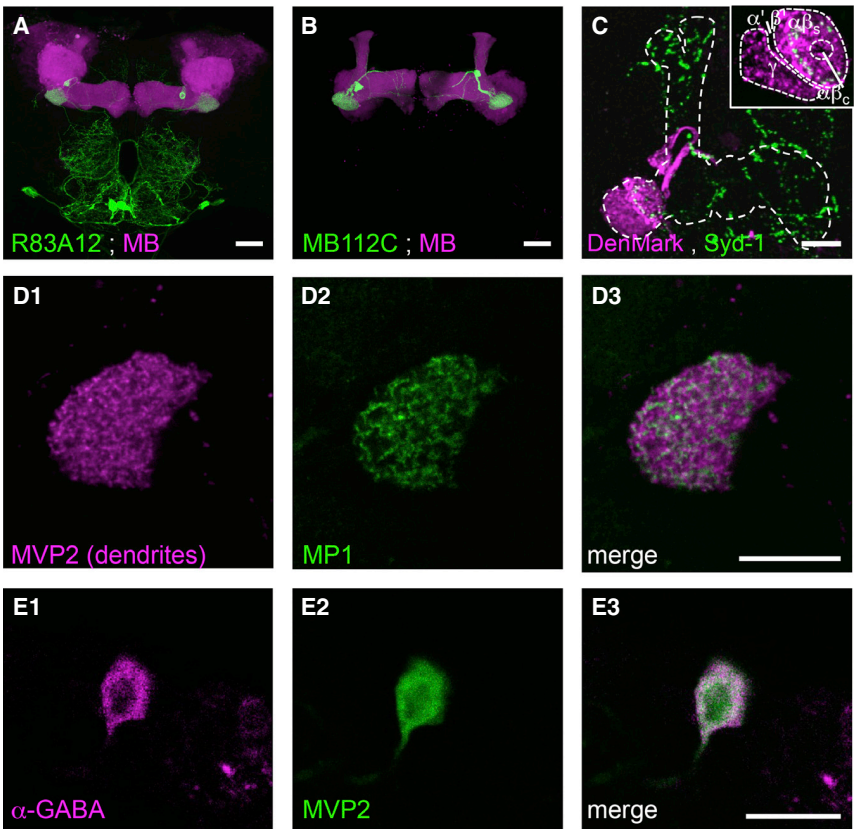


Figure 1. MVP2 MBONs Are Local GABAergic Interneurons of the MB

(A and B) (A) R83A12-GAL4- and (B) MB112C-GAL4-driven UAS-mCD8::GFP labels a single MVP2 neuron per hemisphere. The most prominent MVP2 neuron process innervates the heel (γ1) regions of the MB. MB co-labeled (magenta) with 247-LexA::VP16-driven lexAop-rCD2::mRFP. (C) DenMark labels MVP2 dendrites in γ1 and $\alpha\beta$ surface at the base of the MB peduncle. The presynaptic active zone marker Syd-1 labels large puncta throughout the α and β lobes and around and outside the MB in the crepine and superior intermediate protocerebrum (see also Figure S1; Movie S1). Inset shows single confocal section through MVP2 dendrites detailing innervation of the γ and $\alpha\beta_s$, but not $\alpha\beta_c$ or $\alpha'\beta'$ regions. A ring of Syd-1 labeling within the dendritic field suggests MVP2 also feed back within the $\alpha\beta_s$. Scale bars 20 μm.

(D1–D3) (D1) MVP2 dendrites labeled by R12G04-LexA;lexAop-rCD2::mRFP are interspersed with (D2) processes of MP1 DANs labeled by R22B12-GAL4;UAS-mCD8::GFP. (D3) merge of (D1) and (D2); scale bar 10 μm.

(E1–E3) (E1) GABA immunostaining overlaps with (E2) MVP2 labeled with MB112C;UAS-mCD8::GFP. (E3) Merge of (E1) and (E2); scale bar 10 μm.

control and performed two-photon functional calcium imaging of odor-evoked responses at the level of the MVP2 dendrites in living flies (Figure 2A). We first determined that MVP2 neurons responded to odors, including 4-methylcyclohexanol (MCH) and 3-octanol (OCT) that are typically used for olfactory learning (Figure 2B; also Figure 6A). To test the effect of aversive training, flies were loaded into the training arm of a T-maze and subjected to either of two protocols: the "trained" group received 1 min OCT (or MCH) presentation paired with 12 electric shocks (CS+) followed by 1 min of MCH (or OCT) without reinforcement (CS−); the control "mock" group experienced the same odor regimen but without shock presentation. Flies were subsequently captured and individually mounted under the microscope within 30–60 min after training. Aversive conditioning decreased the response to the CS+ relative to the CS− for the trained groups (Figures 2C and 2D). Importantly, no change was apparent in the responses of mock-trained flies (Figure 2C). As in a previous study (Owald et al., 2015), we also analyzed the difference between the OCT to MCH (or MCH to OCT) responses per individual fly and then compared the averaged difference curves between the trained and the mock-trained groups. Again, a robust depression of the CS+ relative to the CS− was observed for the peak responses of the trained groups (Figure 2D). The observed depression persisted for at least 3 to 4 hr after training (Figures 2E and 2F). These data are consistent with a model that learning drives synaptic weight changes of KC-MBON connections (Okada et al., 2007; Cassenaer and Laurent, 2012; Séjourné et al., 2011; Owald et al., 2015) and with a recent study that reported odor-specific depression following the pairing of odor exposure with artificial stimulation of MP1 DANs (Hige et al., 2015).

MVP2 Neurons Are Required for Expression of Short-Term Aversive Memory

MP1 DANs mostly reinforce short-term aversive memory (Aso et al., 2012). We therefore tested the requirement of MVP2 neurons in aversive memory by blocking their output during memory testing using R83A12 and MB112C to express the dominant temperature-sensitive UAS-*shibire*^{ts1} (*shi*^{ts1}) (Kitamoto, 2001). In each experiment we compared the performance of flies with MVP2 neural blockade to controls carrying only the GAL4 or UAS-*shi*^{ts1} transgene. We first tested 30 min aversive memory performance by training flies at permissive 23°C and raising them to restrictive 33°C before and during memory testing (Figure 2G). Performance of R83A12;*shi*^{ts1} and MB112C;*shi*^{ts1} flies with impaired MVP2 neurons was statistically different to that of their respective controls. Importantly, experiments performed at permissive 23°C throughout did not reveal significant differences between the relevant groups (Figure S2A). We next tested the requirement of MVP2 neurons for 3 hr aversive memory. Flies were trained at permissive 23°C and raised to restrictive 33°C 30 min before and during testing. Strikingly, performance of R83A12;*shi*^{ts1} flies with blocked MVP2 neurons was statistically indistinguishable from that of control flies at this time (Figure 2H). Therefore, although the decrease in conditioned odor-drive to MVP2 neurons persists, MVP2 output is only essential for the

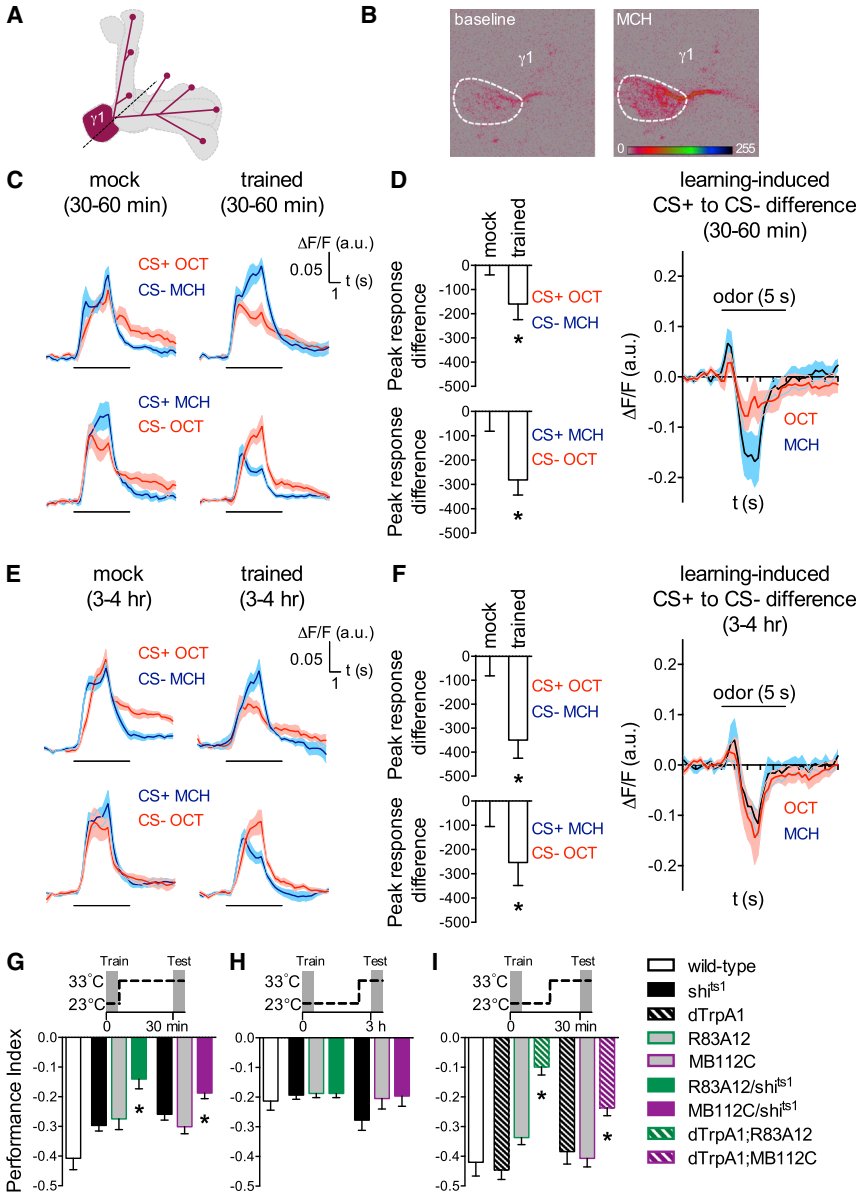


Figure 2. Aversive Learning Drives Persistent Depression of Conditioned Odor Drive to MVP2 Neurons yet Output Is Only Required to Express Short-Term Aversive Memory

(A) Schematic of MVP2 neuron showing imaging plane (dotted line).

(B) Example pseudocolor images of baseline and MCH-evoked GCaMP fluorescence recorded from MVP2 dendrites in a living fly. ROI indicated by white ellipse.

(C) Aversive conditioning depresses the relative CS+ to CS− odor-drive to MVP2 neurons. CS+ and CS− odor-evoked calcium transients were imaged 30–60 min after mock or regular shock conditioning (red curves: OCT, blue curves: MCH). Data are mean [solid line] ± SEM [shaded area] normalized curves (see Experimental Procedures).

(D) Bar graphs represent percent difference to the mean mock integrated peak response (4.5 ± 1.5 s after odor delivery, see methods) (Mann-Whitney U-test; OCT is CS+ (top): n(mock) = 7, n(trained) = 11, $p < 0.05$. MCH is CS+ (bottom): n(mock) = 8, n(trained) = 11, $p < 0.05$).

Difference of responses evoked by CS+ and CS− after aversive conditioning relative to the mean responses after mock training (red curve: OCT is CS+, blue curve: MCH is CS+). Data are mean [solid line] ± SEM [shaded area] normalized curves (see Experimental Procedures).

(E and F) Same as in (C) and (D), but odor-responses were imaged 3 to 4 hr after training. Bar graphs represent percent difference to the mean mock integrated peak response (4.5 ± 1.5 s after odor delivery) (Mann-Whitney U-test; OCT is CS+ (top): n(mock) = 5, n(trained) = 5, $p < 0.05$. MCH is CS+ (bottom): n(mock) = 11, n(trained) = 8, $p < 0.05$).

(G) Blocking output from R83A12 or MB112C neurons during testing impaired 30 min aversive memory performance compared to the relevant controls (Kruskal-Wallis, n = 18–22, $p < 0.001$ and ANOVA, n = 10–13, $p < 0.01$, respectively).

(H) Blocking output from R83A12 or MB112C neurons during testing did not impair 3 hr aversive memory (Kruskal-Wallis, n = 25, $p > 0.9$ and ANOVA, n = 9 to 10, $p > 0.2$, respectively).

(I) Activating R83A12 or MB112C neurons during testing impaired 30 min aversive memory (ANOVA, n = 9 to 10, $p < 0.001$ and ANOVA, n = 13 to 14, $p < 0.01$, respectively).

(G–I) Schematics depict temperature protocols. All flies were trained at 23°C and tested at 33°C. Data are mean ± SEM. See Figure S2 for permissive control. Asterisks indicate statistical significance.

expression of short-term aversive memory. These data are consistent with MP1 DANs principally reinforcing short-term memory by modifying the KC-MVP2 junction, whereas expression of later phases of aversive memory relies on other pathways such as V2α MBONs on the vertical MB lobes (Séjourné et al., 2011; Bouzaiane et al., 2015).

We also tested whether MVP2 neuron stimulation with UAS-*dTrpA1* (Hamada et al., 2008) altered expression of aversive memory. Flies in which MVP2 neurons were activated 15 min prior to and during testing aversive memory showed a significant decrease in performance compared to controls (Figure 2I). Importantly, no significant differences were apparent if the experiment was performed at 23°C throughout (Figure S2B). We note that stimulating MVP2 neurons during memory testing produced a similar defect to that obtained when MVP2 neurons were blocked. A plausible explanation is that, when blocked, the flies cannot transmit the learned relative odor-specific drive from KCs to MVP2 neurons to the relevant downstream neurons. Similarly, when the MVP2 neurons are continuously stimulated the relative odor-specificity of MVP2 activity is lost.

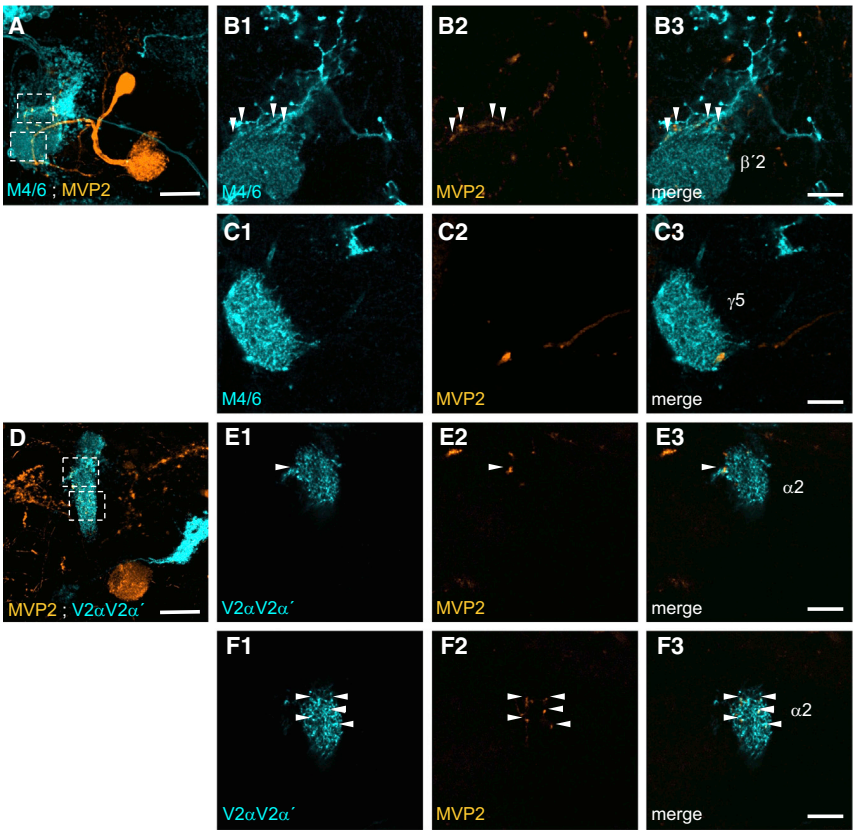


Figure 3. Anatomy of MVP2 Processes in Relation to M4/6 and V2αV2α′ MBONs

(A) Confocal projection of single MVP2 neuron with the M4/6 neurons labeled with R83A12-GAL4; UAS-GCaMP6f (orange) and R21D02-LexA; lexAop-rCD2::mRFP (cyan), respectively. Scale bar 20 μm.

(B1–B3) Separate and merged channels of single confocal section at the level of the M4/6 dendrites in the β′2 zone showing MVP2 processes intermingled with the M4/6 axonal segment (white arrows). Scale bar 10 μm.

(C1–C3) Separate and merged channels of single confocal section at the level of the M6 dendrites in the γ5 zone show no overlap with MVP2 processes except for a large diameter neurite passing through. Scale bar 10 μm. Also see Movie S2.

(D) Confocal projection of single MVP2 neuron with the V2αV2α′ neurons labeled with R12G04-LexA; lexAop-rCD2::mRFP (orange) and R71D08-GAL4; UAS-mCD8::GFP (cyan), respectively. Scale bar 20 μm.

(E1–E3) Separate and merged channels of single confocal section at the level of the V2αV2α′ dendrites in the α2α′2 zone of the vertical MB lobe showing a single MVP2 process close to the axonal segment of V2αV2α′ (white arrow).

(F1–F3) Separate and merged channels of another single confocal section showing several MVP2 processes (white arrows) within the mass of the V2αV2α′ dendrites. Scale bar 10 μm. Also see Movie S3.

MVP2 Neurons Asymmetrically Inhibit the MBON Network

Optogenetic activation of MVP2 drives approach behavior (Aso et al., 2014b), and most MVP2 processes lie within, or in close proximity to the MB. We therefore hypothesized that MVP2 neurons might skew the MBON network toward approach by preferentially inhibiting avoidance-directing MBONs. We first investigated this model by looking at the anatomy of MVP2 presynaptic neurites and MBON processes in the vertical and horizontal MB lobes. We used compatible GAL4 and LexA drivers to co-label MVP2 neurons with either the M4/6 MBONs on the horizontal lobes or the V2α and V2α′ MBONs on the vertical lobes (Figure 3). These confocal analyses suggest that MVP2 presynaptic terminals lie mostly outside the main dendritic fields of the M4/6 neurons in the horizontal lobe tips and instead appear clustered on the M4/6 neurites as they exit the MB lobe region (Figures 3A–3C; Movie S2). In contrast, many MVP2 terminals lie within the MB neuropil occupied by dendrites of V2α and V2α′ MBONs (Figures 3D–3F; Movie S3).

Since the detail of light microscope level anatomy is limited, we next used odor-evoked activity and optogenetic control of MVP2 neurons to test for functional connectivity between MVP2 and M4/6 or V2αV2α′ MBONs (Figure 4). Flies were constructed that expressed GCaMP6f in M4/6 or V2αV2α′ MBONs using either R21D02-GAL4 or R71D08-GAL4, respectively, and CsChrimson (Klapoetke et al., 2014; Hoopfer et al., 2015) in MVP2 neurons under R12G04-LexA. We then monitored MCH- or OCT-evoked responses in the presynaptic processes of M4/6 or V2αV2α′ MBONs before, during and following red-light-triggered MVP2 activation. Strikingly, whereas MVP2 activation induced a rapid and robust inhibition of OCT- and MCH-evoked responses in M4/6 MBONs (Figure 4A) that recovered after the activation ended, no effect was evident in V2αV2α′ responses (Figure 4B). Importantly, flies lacking retinal or the CsChrimson transgene did not exhibit a measurable difference on OCT- or MCH-evoked responses in M4/6 MBONs (Figures S3A and S3B). Moreover, stimulating MVP2 neurons without concurrent odor delivery did not induce a measurable M4/6 calcium response (Figure S3C). These data are consistent with MVP2 neurons preferentially inhibiting horizontal lobe MBONs. In addition, since aversive learning reduces conditioned odor-drive to MVP2 neurons, disinhibition might explain why aversive learning caused a relative increase in conditioned odor-evoked responses in M4/6 neurons (Owald et al., 2015).

Naive odor-driven behavior can be steered by skewing the balance of the outputs in the overall MBON network (Owald and Waddell, 2015). Blocking either input or synaptic output from the M4/6 MBONs converts naive odor avoidance into approach (Barnstedt et al., 2016; Owald et al., 2015). We therefore also used naive odor-avoidance behavior to test whether MVP2 neurons exert asymmetric influence on the MBON network. We expressed UAS-*shi*^{ts1} with R83A12 or MB112C and determined the effect on naive odor avoidance of blocking MVP2 neurons (Figure 5). Flies chose between T-maze arms

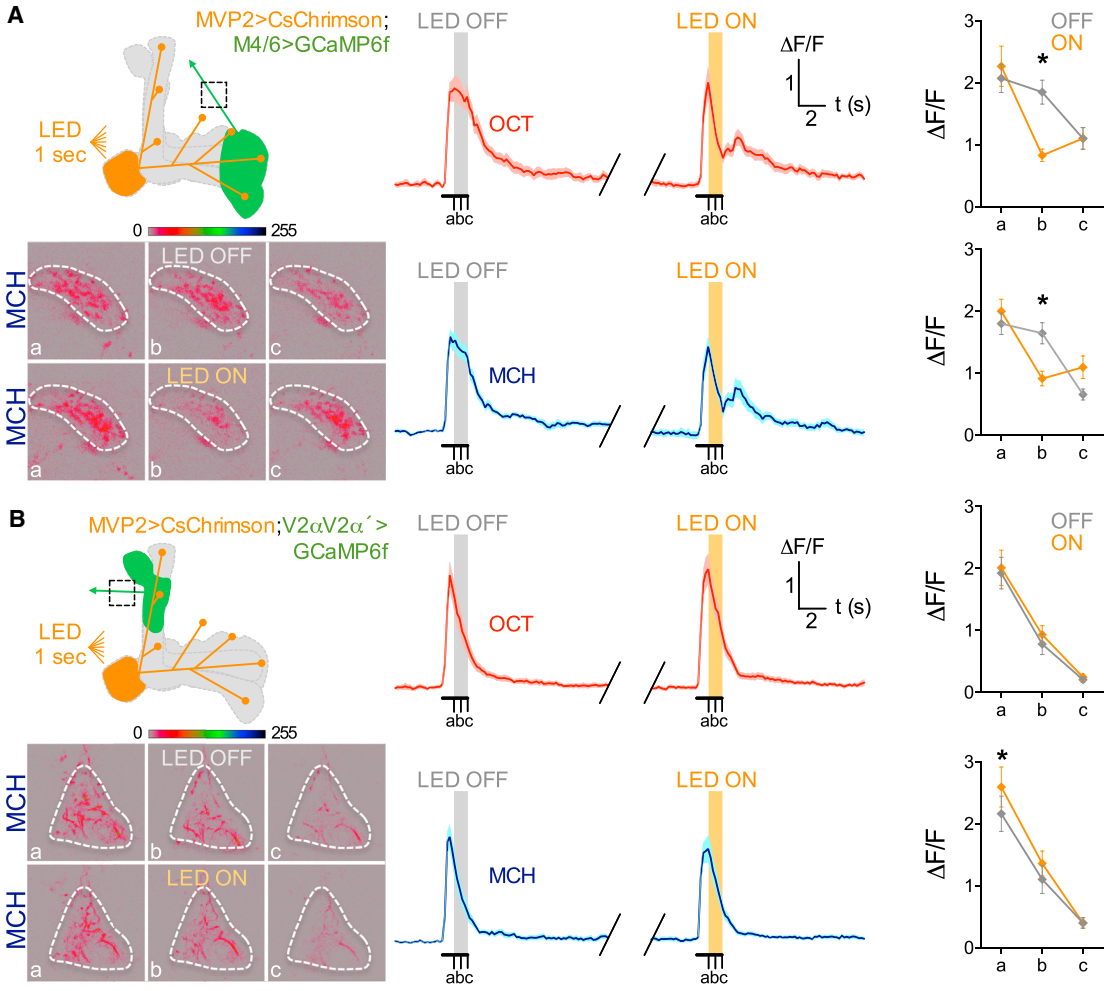


Figure 4. MVP2 Neurons Inhibit Odor-Evoked Responses in M4/6, but Not V2αV2α′ MBONs

Odor-evoked GCaMP6f responses measured in (A) M4/6 or (B) V2αV2α′ MBON axons (green) while CsChrimson-expressing MVP2 MBONs (orange) were light-triggered.

(A) Schematic of experiment (top left). Data acquired from the most ventral part of M4β′ axons (dashed square). Lower left panels; representative images taken at time points a, b, and c, after MCH presentation without and with stimulation of MVP2 neurons. Calcium traces during OCT (middle top panels, red) or MCH (middle bottom panels, blue) presentation show robust odor-evoked responses in M4β′ axons in absence of LED stimulation. Triggering MVP2 neurons for 1 s with LED ON produced a clear and reversible depression of the odor-evoked calcium transient. Data are mean curves [solid line] ± SEM [shaded area]. Quantification of the ΔF/F at the a–c time points reveals a significant difference in the odor-evoked responses with LED ON (orange) compared to the same time point with LED OFF (gray), for both OCT (top right) and MCH (bottom right) (two-way repeated-measures ANOVA, both interaction effect $p < 0.001$, $n = 9$).

(B) Schematic of experiment (top left). Data were acquired from the V2αV2α′ proximal axon segment (dashed square). Bottom left panels; representative images taken at time points a, b, and c, after MCH presentation without and with stimulation of MVP2 neurons. Calcium traces during OCT (middle top panels, red) or MCH (middle bottom panels, blue) presentation show robust odor-evoked responses in V2αV2α′ axons without and with LED-triggered stimulation of MVP2 neurons. Data are mean curves [solid line] ± SEM [shaded area]. Quantification of the ΔF/F at the a–c time points reveals no significant difference in the odor-evoked responses with LED ON (orange) compared to the same time point with LED OFF (gray), for both OCT (top right) and MCH (bottom right) (OCT: two-way repeated-measures ANOVA, no interaction effect $p > 0.6$, $n = 13$; MCH: Two-way repeated-measures ANOVA, interaction effect $p < 0.05$, "a" LED OFF versus LED ON, $p = 0.001$, $n = 13$).

containing clean air or with MCH or OCT. Both R83A12;*shi*^{ts1} and MB112C;*shi*^{ts1} flies exhibited significantly enhanced MCH (Figure 5A) and OCT (Figure 5B) avoidance behavior at restrictive 33°C but not permissive 23°C (Figures S4A and S4B). We also expressed *dTrpA1* in MVP2 neurons and tested whether stimulating MVP2 neurons suppressed naive odor avoidance behavior. Whereas all flies robustly avoided MCH or OCT at 23°C (Figures S4C and S4D), at restrictive 33°C, R83A12;*dTrpA1* and MB112C;*dTrpA1* flies displayed significantly weaker avoidance of MCH (Figure 5C) and OCT (Figure 5D). Taken with the aversive memory defect seen when MVP2 neurons are blocked (Figure 2G) and the structural and functional anatomy (Figures 3 and 4), these naive fly data are consistent with GABA-ergic MVP2 neurons skewing the MBON network by

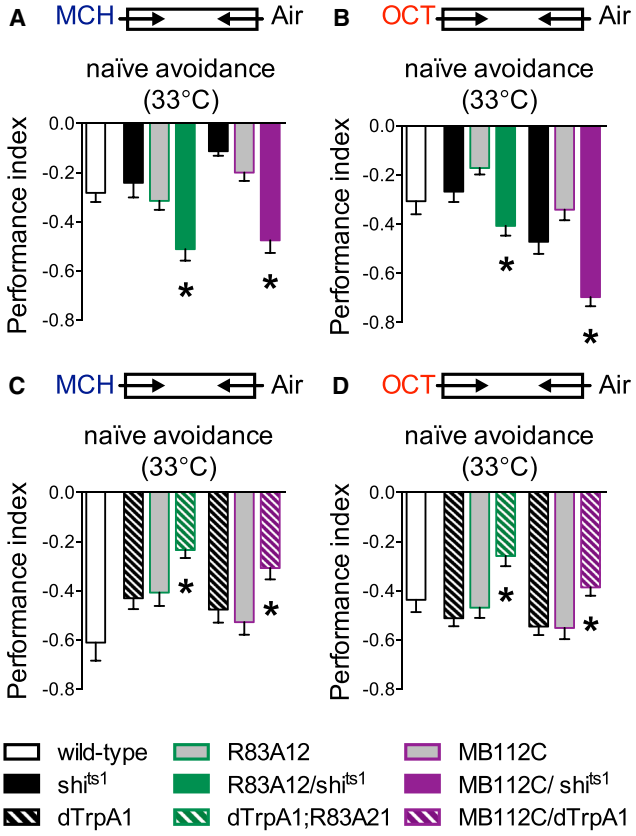


Figure 5. MVP2 Neurons Inhibit Naive Odor Avoidance Behavior

(A and B) Blocking MVP2 neuron output in naive flies increases odor avoidance for (A) MCH (R83A12: ANOVA, n = 10–12, $p < 0.01$; MB112C: ANOVA, n = 8–12, $p < 0.01$) and for (B) OCT (R83A12: ANOVA, $n \geq 16$–20, $p < 0.01$; MB112C: ANOVA, n = 15 to 16, $p < 0.01$).

(C and D) Stimulating MVP2 neurons in naive flies inhibits odor avoidance for (C) MCH (R83A12: Kruskal-Wallis, n = 10–12, $p = 0.01$; MB112C: ANOVA, n = 8–12, $p < 0.01$) and for (D) OCT (R83A12: ANOVA, n = 14–16, $p < 0.01$; MB112C: Kruskal-Wallis, n = 16–20, $p < 0.01$). Flies chose between T-maze arms containing MCH or OCT or a clean air stream at 33°C. See Figure S4 for permissive controls.

preferentially inhibiting MBON pathways that generate avoidance behavior.

Hunger Potentiates Odor-Evoked Activity of MVP2 Neurons

In addition to conveying negative reinforcement, the MP1 DANs inhibit expression of sugar-reinforced appetitive memory in food-satiated flies (Krashes et al., 2009). Furthermore, MP1 DANs are more active in food-satiated than in hungry flies (Plaçais and Preat, 2013). We therefore tested whether hunger modulated MVP2 activity by monitoring odor-evoked responses in hungry and food-satiated flies (Figure 6A). We again expressed GCaMP6f in MVP2 neurons using MB112C. Flies were either housed in food vials and allowed to feed ad libitum (fed) or were stored in vials with 1% agar as a water source and deprived of food for 22–26 hr (starved) before being prepared for live imaging. These experiments revealed a clear elevation of odor-evoked activity in starved compared to satiated flies. Peak responses to MCH, OCT, ethyl acetate (EA), and pentyl acetate (PA) were all significantly greater in starved versus satiated flies. 6-methyl-5-heptan-2-one and geranylacetate showed a trend toward increased responses in starved flies but did not reach statistical significance (data not shown). The shape of the responses, an odor-specific signature, appeared to be preserved in fed and starved flies. These data suggest that hunger increases general odor-drive from KCs to MVP2 neurons—an expectation of a release of MP1-directed modulation of the KC-MVP2 junction—and thereby increases feed-forward inhibition in the MBON network.

We also tested whether appetitive conditioning altered relative odor-drive to MVP2 neurons (Figures S5A and S5B). Flies were again subjected to either of two protocols: the "trained" group received 2 min OCT (or MCH) without reinforcement (CS−) followed by 2 min of MCH (or OCT) paired with sucrose (CS+); the "mock" group experienced the same odor regimen but without reinforcer. Flies were individually mounted under the microscope 30–60 min after training. The averaged difference curves between the trained and the mock-trained groups revealed a potentiation of the CS+ relative to the CS− for the peak responses of the OCT but not the MCH-trained groups (Figures S5A and S5B). We conclude that appetitive conditioning may potentiate the relative conditioned odor-drive to MVP2 neurons.

MVP2 Neurons Are Generally Required for the Expression of Appetitive Memory

Since MVP2 neurons are more excitable in hungry flies, we reasoned that their output might be required to promote state-dependent appetitive memory expression by inhibiting avoidance-directing MBONs. We therefore used R83A12-and MB112C-driven UAS-*shi*^{ts1} to assess the role of MVP2 neurons in appetitive memory. All flies were food-deprived and trained with odor and sugar at permissive 23°C, after which they were raised to restrictive 33°C 30 min before and during testing 30 min, 3 hr, or 24 hr appetitive memory. Performance of flies with blocked MVP2 neurons was statistically different to that of their respective controls at every time point (Figures 6B–6D). Experiments performed at 23°C throughout did not reveal significant differences between the relevant groups (Figures S5C–S5E). Therefore, whereas MVP2 neurons only contribute to the expression of short-term aversive memory, they are required for flies to express all phases of sugar-reinforced appetitive memory.

MVP2 Activation Promotes Appetitive Memory Expression in Food-Satiated Flies

We hypothesized that blocking MVP2 output might impair appetitive memory performance because the flies are effectively stuck in a food-satiated condition. To test this idea, we used R83A12- and MB112C-driven expression of *dTrpA1* to activate MVP2 in food-satiated flies before and during assaying memory performance. These flies and all controls were food-deprived and trained with odor and sugar at 23°C. After training, flies were transferred to 23°C food vials and were either kept at this condition before testing 3 hr memory

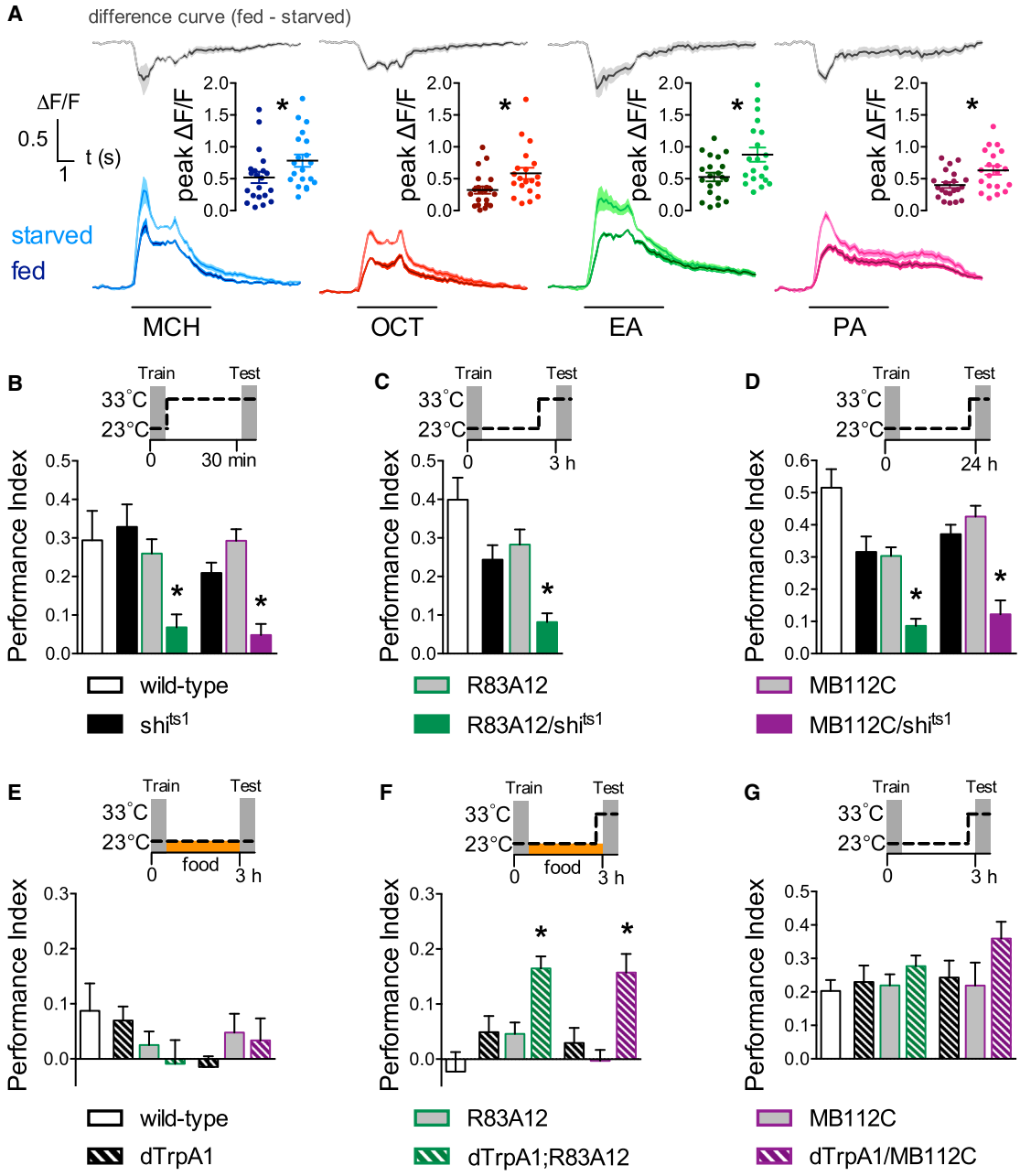


Figure 6. Elevated MVP2 Activity Promotes Appetitive Memory Expression in Hungry Flies

(A) Hunger increases odor-evoked responses in MVP2 neurons. Peak responses in starved flies (light curves; mean [solid line] ± SEM [shaded area]) are statistically different to those in fed flies (dark curves; mean [solid line] ± SEM [shaded area]). Flies were exposed to 4-methylcyclohexanol (MCH), 3-octanol (OCT), ethylacetate (EA), or pentylacetate (PA) for 5 s. Top: difference curves (gray) between the mean responses from fed and starved flies. Insets show quantification of peak responses (4.5 ± 1.5 s after odor delivery, see Experimental Procedures; asterisks denote statistical significance; Mann-Whitney U-tests; all n(starved) = 20, n(fed) = 21, $p < 0.05$).

(B–D) Blocking MVP2 output during memory testing impairs appetitive memory performance at all times. Flies were trained at 23°C and raised to 33°C before and during testing (B) 30 min, (C) 3 hr, or (D) 24 hr memory. Performance of MVP2;UAS-*shi*^{ts1} flies was statistically different from controls for (B) (R83A12: Kruskal-Wallis, n = 9, $p < 0.01$. MB112C: Kruskal-Wallis, n = 8 to 9, $p < 0.01$), (C) (R83A12: ANOVA, $n \geq 11$, $p < 0.01$), and (D) (R83A12: ANOVA, n = 10–12, $p < 0.01$. MB112C: ANOVA, n = 10–12, $p < 0.01$).

(E) Feeding flies after training suppresses appetitive memory performance. Hungry flies were trained at 23°C, then stored in food vials before testing 3 hr memory at 23°C. No statistical differences were apparent between flies expressing UAS-*dTrpA1* in MVP2 neurons and relevant controls (R83A12: ANOVA, n = 10, $p > 0.2$; MB112C: ANOVA, n = 9 to 10, $p > 0.3$).

(legend continued on next page)

(Figure 6E) or were raised to 33°C 15 min before and during testing 3 hr memory (Figure 6F). Feeding after training suppressed performance in all groups except the R83A12;*dTrpA1* and MB112C;*dTrpA1* flies that were exposed to elevated temperature prior to and during testing (Figures 6E and 6F). Therefore, MVP2 neuron activation promotes inappropriate appetitive memory expression in food-satiated flies. We also used R83A12;*dTrpA1* and MB112C;*dTrpA1* to stimulate MVP2 neurons prior to 3 hr memory testing in food-deprived flies (Figure 6G). No significant improvement in memory performance was apparent when MVP2 neurons were stimulated in this condition.

In parallel, we reproduced the finding that MP1 DAN block promotes appetitive memory performance in satiated flies (Krashes et al., 2009). We used the same food deprivation and training conditions as for the above MVP2 experiments, but expressed UAS-*shi*^{ts1} in MP1 DANs using c061-GAL4;MBGAL80 (Figures S5F–S5H). In these experiments, only satiated c061;MBGAL80; *shi*^{ts1} flies that were exposed to elevated temperature 30 min prior to and during testing displayed robust appetitive memory performance (Figures S5F and S5G). As for MVP2 neuron activation, blocking MP1 neurons in hungry flies did not further enhance appetitive memory performance (Figure S5H). Therefore, MP1 inhibition and MVP2 activation promote appetitive memory performance, consistent with the MP1:KC:MVP2 pathway representing a key part of the state of hunger in the neural circuitry of the MB.

DISCUSSION

Prior work in *Drosophila* indicated that negative reinforcement and hunger-state-dependent motivational control of appetitive memory performance might be controlled by the same DANs (Krashes et al., 2009; Claridge-Chang et al., 2009; Aso et al., 2010, 2012). The presynaptic field of the MP1/PPL1-γ1pedc DANs occupies a defined region of the MB that also contains the MVP2/MBON-γ1pedc>αβ dendrites (Krashes et al., 2009; Aso et al., 2010, 2014b), suggesting that these DANs modulate the efficacy of this specific KC-MBON connection. Our results here demonstrate that the MVP2 MBONs also play a critical role in the expression of short-term aversive memory and the state-dependence of appetitive memory expression. Since these findings directly mirror the described roles for the MP1 DANs (Krashes et al., 2009), we conclude that DAN modulation of the KC-MVP2 junction is critical for both negative reinforcement during olfactory learning and the motivational salience of appetitive odor cues.

The GABA-ergic MVP2 neurons have postsynaptic and presynaptic processes in the MB, suggesting that they are interneurons of the MB and feed-forward inhibit other MBON compartments. Dendrites of MVP2 neurons (and the presynaptic terminals of the MP1 DANs) innervate the γ1 region and more densely innervate the $\alpha\beta_s$ than the αβ core ($\alpha\beta_c$) region of the αβ ensemble (Krashes et al., 2009). MVP2 are therefore likely to be primarily driven by $\alpha\beta_s$ KCs. Since $\alpha\beta_s$ neurons contribute to conditioned approach and avoidance, whereas $\alpha\beta_c$ are particularly important for conditioned approach (Perisse et al., 2013), there is an imbalance in the drive to approach and avoidance behaviors at this level of the MBON network.

Artificial activation of MVP2 neurons in naive flies drives approach behavior (Aso et al., 2014b), consistent with them preferentially inhibiting MBON compartments that direct avoidance—as opposed to those that drive approach. Our anatomical and functional connectivity and odor-directed behavioral data are consistent with such a model. MVP2 stimulation inhibits odor-evoked activity in M4/6 but not in V2αV2α′ MBONs. MVP2 stimulation also promotes expression of approach memory in food-satiated flies, yet it inhibits naive odor avoidance behavior. We conclude that MVP2 directly inhibit the M4/6 class of horizontal lobe MBONs through synapses made on the primary axonal segment as it exits the MB lobes. Inhibition exerted in this area might be expected to control the gain of the MBON responses following integration of KC inputs in the MBON dendrite in a manner similar to perisomatic inhibition in mammals (Miles et al., 1996; Klausberger and Somogyi, 2008; Ellender and Paulsen, 2010). Consistent with this anatomy and idea, we and others (Lewis et al., 2015) did not find obvious changes in the odor drive to the dendritic region of M4/6 neurons between hungry and satiated flies (data not shown), but a hunger-dependent decrease was apparent when odor-evoked responses were measured in the efferent neurites (Figure S6A). In contrast, MVP2 neurons do not functionally inhibit or densely innervate the neurites of V2αV2α′ MBONs, nor does hunger reduce odor-evoked responses in V2αV2α′ MBONs (Figure S6B). It therefore seems likely that MVP2 neurons contact DANs or other neurons that occupy the α2 compartment of the MB lobe (Aso et al., 2014a).

Our data also demonstrate that aversive learning reduces the relative conditioned odor drive to MVP2 neurons, which would presumably decrease feed-forward inhibition onto the relevant MBON compartments and thereby render them more responsive to odors. Output from the glutamatergic M4/6 neurons, which are postsynaptic to the KCs in the horizontal tip regions, is required for expression of aversive and appetitive memory. Furthermore, the relative odor-drive to M4/6 neurons was shown to be depressed by reward learning (Owald et al., 2015) and potentiated by aversive learning (Owald et al., 2015; Bouzaiane et al., 2015). Since aversive learning reduces the conditioned odor drive of the MVP2 neuron, we propose that the observed increase in odor-drive to M4/6 after aversive learning results from reduced feed-forward inhibition from MVP2. This would mean that bi-directional output plasticity could emerge via a direct junctional plasticity following reward conditioning, but a network property of reduced MVP2 feed-forward inhibition after aversive

(F) Appetitive memory expression is promoted in fed flies by activation of MVP2 neurons 15 min prior to and during testing 3 hr memory (R83A12: ANOVA, n = 11–19, $p < 0.01$; MB112C: ANOVA, n = 14–17, $p < 0.01$). Hungry flies were trained, then stored in food vials before testing 3 hr memory at 33°C.
(G) Activating MVP2 neurons does not further enhance appetitive memory performance in hungry flies (R83A12: ANOVA, n = 9 to 10, $p > 0.5$; MB112C: Kruskal-Wallis, n = 8–10, $p > 0.1$). Hungry flies were trained, stored in empty vials and tested for 3 hr memory at 33°C. All data are mean ± SEM. Schematics illustrate the temperature protocols. See Figure S5 for permissive temperature controls.

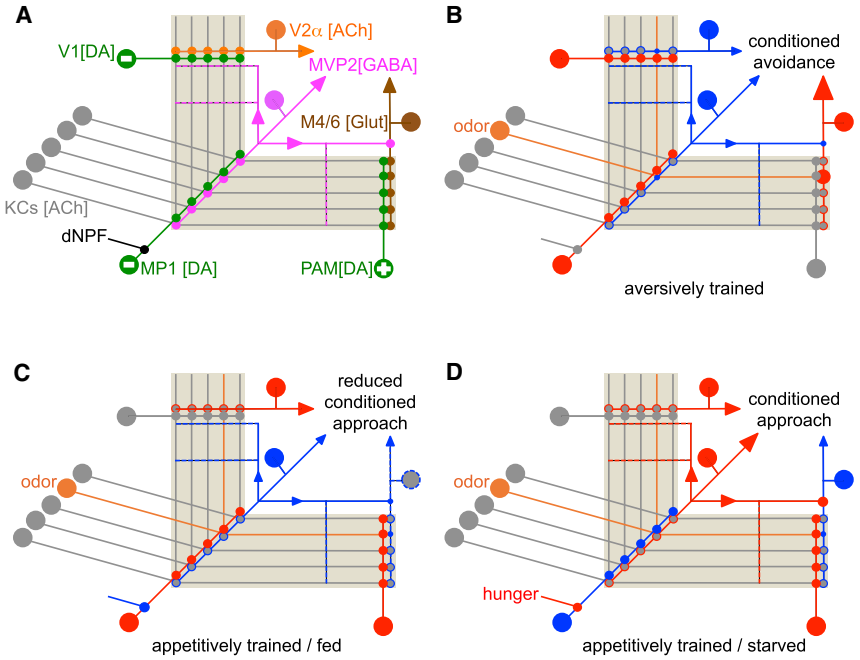


Figure 7. Model Accommodating Role for MVP2 in Aversive Learning and Appetitive Motivation

(A) Wiring diagram of the relevant neurons in the MB network. The MP1/PPL1-γ1pedc DANs (green) have a dual role in aversive reinforcement and appetitive motivation and are modulated by the hunger-sensitive dNPF-releasing neurons (black). MP1 and V1 DANs convey negative reinforcing properties of aversive stimuli (minus symbol) to specific zones in the MB ensemble where they modulate the connection between odor-activated KCs (gray, inactive) and the GABAergic MVP2/MBON-γ1pedc>α/β inter-neuron (magenta) or the V2α (orange) MBONs, respectively. Active MVP2 neurons feed-forward inhibit other parts of the MB network where they modulate the odor-drive to some MBONs including the glutamatergic (Glut) M4/6 MBONs (brown) that promote avoidance behavior. It is currently unclear what other MVP2 projections in the horizontal and vertical lobes connect to (dashed lines). Rewarding stimuli activate positively reinforcing DANs of the PAM cluster (green with plus symbol), which modulate connections between KCs and the M4/6 MBONs. We propose that MVP2 neurons exert their function by bridging between MBON compartments that each have their own DAN input.

(B) Mode of the network evoked by aversive training. Red symbolizes high and blue low neural activity. Size of arrowhead indicates relative drive. Sites of plasticity denoted by a change in the size of synaptic connections (circles), with smaller representing depression and larger representing potentiation. For simplicity, only an effect on the neurons carrying the conditioned odor is illustrated. During aversive conditioning, coincidence between odor-driven activity in KCs (now orange) with phasic MP1 and MV1-released dopamine leads to odor-specific synaptic depression (smaller blue circles) between odor-activated KC and the MVP2 and V2α MBONs. After training, the reduced conditioned-odor drive to MVP2 (now blue) selectively weakens feed-forward inhibition onto the conditioned-odor drive to M4/6 MBONs (red) that favor avoidance behavior. Via this feed-forward inhibitory mechanism, MP1-induced synaptic depression at the KC-MVP2 junction is sign-inverted to an apparent potentiation of the KC-M4/6 junction (larger red circle)—importantly, while odor-specificity is maintained.

(C) Mode of the network following appetitive training and feeding. During appetitive conditioning coincidence between odor-driven activity in KCs with phasic PAM-released dopamine leads to odor-specific synaptic depression (smaller blue circle) between odor-activated KC and the M4/6 MBONs. Satiation imposes tonic activity of MP1 (red), which reduces general odor-drive to the KC-MVP2 junction, thereby switching MVP2 into a low mode (now blue). Learning-triggered synaptic depression is effectively neutralized by reduced MVP2-mediated inhibition so that the drive to avoidance MBONs is maintained (now dashed blue arrow) and approach behavior cannot be efficiently expressed.

(D) Mode of the network following appetitive training and food deprivation. Hunger triggers dNPF neuron activity (now red) that suppresses MP1 activity (now blue). This leads to general elevation of odor-evoked MVP2 activity (now red), which feeds forward to inhibit the avoidance MBON pathways. Increased feed-forward inhibition, combined with odor-specific synaptic depression at the KC M4/6 junction (small blue circle) further reduces drive of avoidance MBONs and skews the MBON network toward promoting conditioned approach behavior.

conditioning (Figure 7). Such a layered feed-forward network architecture linking one site of DAN-driven KC-MBON plasticity to another KC-MBON connection would provide a means to achieve odor-specific bi-directional plasticity at a particular synaptic junction using dopamine-driven synaptic depression in two different places. We propose that this circuit design principle in which plasticity at one site of a neuron can, via feed-forward inhibition, indirectly alter the efficacy of output elsewhere in the same neuron, could be a general feature in the brain of the fly and other animals. It is possible that the KC-MVP2 junction also exhibits bi-directional plasticity, notably with inverted polarity relative to M4/6 plasticity traces.

The layered network architecture places the aversive memory relevant MVP2 plasticity on top of the M4/6 plasticity that is relevant for appetitive memory (Owald et al., 2015). This organization could accommodate the co-existence of aversive and appetitive olfactory memories following conditioning reinforced by sugar laced with bitter taste (Das et al., 2014). Immediately after such training flies avoid the conditioned odor because the aversive taste memory relieves feed-forward inhibition onto the sites that are depressed by appetitive sugar plasticity and therefore over-rides the expression of approach memory. However, as the aversive memory decays, feed-forward inhibition returns and appetitive memory is then expressed. A similar mechanism might account for the time-dependent switch from conditioned aversion to approach following odor conditioning reinforced by alcohol (Kaun et al., 2011). It is notable that learning-induced plasticity of relative odor-drive to MVP2 persists for at least 3 hr after training whereas output from MVP2 is dispensable for the expression of aversive memory at that time. Since expression of different phases of aversive memory requires distinct combinations of MBON pathways (Bouzaiane et al., 2015), we propose that more persistent MVP2 plasticity might provide a permissive gate for both the formation of aversive memory in,

and the expression from, other parts of the MBON network. This would be reminiscent of fear conditioning in the neural circuitry of the mouse amygdala, where dopamine suppresses feed-forward GABA-ergic inhibition from local interneurons to facilitate the induction of long-term potentiation (Bissière et al., 2003).

MVP2 neuron output is required for the expression of sugar-reinforced approach memory at all times. Moreover, odors evoked larger MVP2 responses in hungry than in food-satiated flies, and elevating MVP2 activity in satiated flies promoted inappropriate expression of appetitive memory. These results are consistent with the model that hunger generally increases feed-forward inhibition through MVP2 to support appetitive memory expression (Figure 7). This result is also the mirror-image of that with MP1 DANs whose activity increases when the flies are satiated (Plaçais and Preat, 2013) and whose inhibition leads to the expression of appetitive memory in satiated flies (Krashes et al., 2009). Taken with prior work (Shen and Cai, 2001; Wu et al., 2003; Krashes et al., 2009), we therefore propose that hunger increases dNPF, which releases MP1 inhibition over the KC-MVP2 connection. This results in an increase of odor-evoked MVP2 feed-forward inhibition onto the MBON compartments such as M4/6 that contain the KC-MBON synapses that are directly modified by appetitive conditioning (Figure S6A) (Owald et al., 2015). The increase of MVP2 inhibition into these, and other, compartments allows more efficient expression of the appetitive memory-directed approach behavior by effectively raising the motivational salience of learned food-related odors. Appetitive conditioning may also increase odor-specific recruitment of MVP2 feed-forward inhibition.

Our findings therefore suggest that the MVP2 neuron pathway functions in at least three modes that are presumably selected by the aversively reinforcing MP1 DANs. If the flies are aversively conditioned, phasic MP1 specifically depresses conditioned-odor drive to MVP2 neurons (Figure 7B). In a food-satiated fly, tonic MP1 limits general odor-driven MVP2 activity (Figure 7C). Lastly, in the hungry fly, lower MP1 activity generally enhances odor-drive to MVP2 (Figure 7D). In the OFF modes, low-level MVP2 feed-forward inhibition skews the MBON network toward behavioral avoidance, whereas in the ON mode the increased feed-forward inhibition from MVP2 skews the MBON network toward favoring conditioned approach. The MP1 DANs signal the aversive reinforcing properties of electric shock (Aso et al., 2010; Aso et al., 2012), heat (Galili et al., 2014), and bitter taste (Das et al., 2014), suggesting they provide general aversive influence. The satiated state presumably uses a tonic version of this aversive signal (Plaçais and Preat, 2013) to limit the fly approaching an appetitive odor cue.

The parallels between the fly and mammalian dopaminergic systems appear striking. DANs in the basal ganglia of the mammalian brain also support reinforcement learning and the prediction of stimuli that potentially lead to rewarding outcomes (Bromberg-Martin et al., 2010; Smith et al., 2011; Berridge, 2012; Pignatelli and Bonci, 2015). Furthermore, like the fly DANs, mammalian DANs can be anatomically divided into those that generate aversion and different types of reward (Lammel et al., 2011, 2012; Cohen et al., 2012; Lerner et al., 2015; Beier et al., 2015; Tellez et al., 2016). GABA-ergic neurons in the mouse ventral tegmental area, whose cell bodies are interspersed with the DANs, have been proposed to signal the value of expected reward and provide a source of subtraction to DANs that calculate a reward prediction error (Eshel et al., 2015). Negatively reinforcing MP1 DANs in the fly modulate odor-drive to the MVP2 neurons to provide the motivational control over actions to gain reward. Therefore, MVP2 neurons may provide an inhibitory bridge between MBON domains that are controlled by aversive and rewarding DANs.

EXPERIMENTAL PROCEDURES

Fly Strains

Fly stocks were raised on standard cornmeal food at 25°C and 40%–50% relative humidity. All strain details are provided in the Supplemental Information.

Behavioral Analysis

Mixed sex populations flies were tested together in all behavior experiments. For the UAS-*Shi*^{ts1} experiments, flies were 4- to 8-day-old and raised at 25°C and 60% relative humidity (activation was 30 min prior to and during the test). For the UAS-*dTrpA1* experiments, the flies were 8 to 11 days old and raised at 20°C and 50% relative humidity (activation was 15 min prior to and during the test). Aversive and appetitive memory were assayed using a T-maze as described previously (Tully and Quinn, 1985; Krashes and Waddell, 2008; Perisse et al., 2013) and as described in more detail in the Supplemental Information.

Imaging

To visualize native GFP or mRFP, we collected adult flies 4–6 days after eclosion, and brains were dissected in ice-cold 4% paraformaldehyde solution in PBS (1.86 mM NaH_2PO_4, 8.41 mM Na_2HPO_4, and 175 mM NaCl) and fixed for an additional 60 min at room temperature. Samples were then washed 3 × 10 min with PBS containing 0.1% Triton X-100 (PBT) and 2 × 10 min in PBS before mounting in Vectashield (Vector Labs). Imaging was performed on Leica TCS SP5 X. The resolution of the image stack was 1,024 × 1,024 with 1 μm step size and a frame average of 4. Images were processed in AMIRA 5.3 (Mercury Systems). The immunostaining against GFP, RFP, and GABA was performed as described previously (Burke et al., 2012). We used anti-GFP (chicken, abcam13970, 1:2,000), primary anti-DsRed (Rabbit, Clontech 632496, 1:2,000) and anti-GABA (Rabbit, Sigma A2052, 1:2,000).

Two Photon Calcium Imaging

3- to 8-day-old UAS-GCaMP6f; MB112C female flies were imaged 30–60 min or 3 to 4 hr after aversive or mock conditioning (Figures 2A–2F) and 30–60 min after appetitive or mock conditioning in a T-maze (Figures S5A and S5B) or following 22–26 hr of starvation or ad libitum feeding (Figure 6A). Flies were trained as described. Imaging experiments were performed essentially as described previously (Owald et al., 2015) and are described in more detail in the Supplemental Information. In brief, flies were anesthetized <10 s on ice and mounted in a custom-made chamber. The head capsule was opened under room temperature sugar-free HL3-like saline (Yoshihara, 2012), and legs and proboscis were immobilized with wax. Fluorescence was excited using ~140 fs pulses, 80 MHz repetition rate, centered on 910 nm generated by a Ti-Sapphire laser (Chameleon Ultra II, Coherent). Images were acquired using two-photon microscopy (Scientifica) with a 40×, 0.8 NA water-immersion objective, controlled by ScanImage 3.8 software (Pologruto et al., 2003). Odors were delivered on a clean air carrier stream using a custom-designed system (Shang et al., 2007).

In Vivo Optogenetic Stimulation

Female flies used for optogenetic stimulation were treated as for two photon calcium imaging. Prior to optogenetic experiments all flies were housed on standard cornmeal food with 1 mM retinal for 1–3 days. Saline used was carbogenated (95% O_2, 5% CO_2) buffer solution (103 mM NaCl, 3 mM KCl, 5 mM N-Tris, 10 mM trehalose, 10 mM glucose, 7 mM sucrose, 26 mM $NaHCO_3$, 1 mM NaH_2PO_4, 1.5 mM $CaCl_2$, 4 mM $MgCl_2$, osmolarity 275 mOsm,

pH 7.3). MCH and OCT were presented twice for 2 s, with 20 s inter-trial interval. For light stimulation, a custom-made Labview-triggered LED (Multicomp OSW-6338, 630 nm, 0.85 mW/mm^2 at specimen) was used at a distance to the brain of 10–15 cm. Light pulses were delivered at 40 Hz, with 10 ms duration, for a total of 1 s per stimulation. The LED was turned on after 1 s of odor onset, during the second round of MCH and OCT presentation. Two-photon fluorescence images were taken from the initial axon segments. A 500/10 filter was used to minimize LED artifacts during imaging. F_0 was defined as the mean F of the first second of imaging. Time points chosen for comparison were (a) onset of LED, (b) end of LED stimulation, and (c) 1 s after end of LED stimulation.

Statistical Analysis

Data were analyzed using Matlab and Prism 6 (GraphPad Software). All behavioral data was tested for normality using the D'Agostino and Pearson omnibus test. Normally distributed data were analyzed with one-way ANOVA followed by Tukey's honest significant difference (HSD) post hoc test. For non-Gaussian distributed data, Kruskall-Wallis test was performed followed by Dunn's multiple comparison test. Behavioral data from wild-type flies was not included in the statistical analysis. Imaging data were analyzed using Mann-Whitney U-test or two-way repeated-measures ANOVA followed by Sidak's multiple comparisons test. Definition of statistical significance was set at $p < 0.05$. Graphs were created in Prism 6.

SUPPLEMENTAL INFORMATION

Supplemental Information includes six figures, three movies, and Supplemental Experimental Procedures and can be found with this article online at http://dx.doi.org/10.1016/j.neuron.2016.04.034.

AUTHOR CONTRIBUTIONS

E.P., D.O., and S.W. conceived the project and designed all experiments. E.P. performed and analyzed all behavioral experiments. D.O. and O.B performed imaging experiments with some help from E.P. Imaging data were analyzed by D.O., O.B., and C.B.T. Anatomical data were collected by E.P., D.O., and W.H. The manuscript was written by S.W., E.P., and D.O.

ACKNOWLEDGMENTS

We thank G. Rubin, the Janelia Project, B. Dickson, the VDRC, the Bloomington stock center, and D.J. Anderson for flies. E.P. thanks the Philippe and Bettencourt-Schueller Foundations. D.O. was supported by an EMBO Long-Term and a Sir Henry Wellcome Postdoctoral Fellowship. O.B is funded by the Medical Research Council and University College War Memorial Studentship. S.W. is funded by a Wellcome Trust Senior Research Fellowship in the Basic Biomedical Sciences, Gatsby Charitable Foundation, Oxford Martin School and Bettencourt-Schueller Foundation.

Received: October 16, 2015
Revised: March 27, 2016
Accepted: April 19, 2016
Published: May 19, 2016

REFERENCES

Aso, Y., Siwanowicz, I., Bräcker, L., Ito, K., Kitamoto, T., and Tanimoto, H. (2010). Specific dopaminergic neurons for the formation of labile aversive memory. Curr. Biol. *20*, 1445–1451.

Aso, Y., Herb, A., Ogueta, M., Siwanowicz, I., Templier, T., Friedrich, A.B., Ito, K., Scholz, H., and Tanimoto, H. (2012). Three dopamine pathways induce aversive odor memories with different stability. PLoS Genet. *8*, e1002768.

Aso, Y., Hattori, D., Yu, Y., Johnston, R.M., Iyer, N.A., Ngo, T.T., Dionne, H., Abbott, L.F., Axel, R., Tanimoto, H., and Rubin, G.M. (2014a). The neuronal architecture of the mushroom body provides a logic for associative learning. eLife *3*, e04577.

Aso, Y., Sitaraman, D., Ichinose, T., Kaun, K.R., Vogt, K., Belliart-Guérin, G., Plaçais, P.Y., Robie, A.A., Yamagata, N., Schnaitmann, C., et al. (2014b). Mushroom body output neurons encode valence and guide memory-based action selection in Drosophila. eLife *3*, e04580.

Barnstedt, O., Owald, D., Felsenberg, J., Brain, R., Moszynski, J.-P., Talbot, C.B., Perrat, P.N., and Waddell, S. (2016). Memory-relevant mushroom body output synapses are cholinergic. Neuron *89*, 1237–1247.

Beier, K.T., Steinberg, E.E., DeLoach, K.E., Xie, S., Miyamichi, K., Schwarz, L., Gao, X.J., Kremer, E.J., Malenka, R.C., and Luo, L. (2015). Circuit Architecture of VTA Dopamine Neurons Revealed by Systematic Input-Output Mapping. Cell *162*, 622–634.

Berridge, K.C. (2012). From prediction error to incentive salience: mesolimbic computation of reward motivation. Eur. J. Neurosci. *35*, 1124–1143.

Bissière, S., Humeau, Y., and Lüthi, A. (2003). Dopamine gates LTP induction in lateral amygdala by suppressing feedforward inhibition. Nat. Neurosci. *6*, 587–592.

Bouzaiane, E., Trannoy, S., Scheunemann, L., Plaçais, P.Y., and Preat, T. (2015). Two independent mushroom body output circuits retrieve the six discrete components of Drosophila aversive memory. Cell Rep. *11*, 1280–1292.

Bromberg-Martin, E.S., Matsumoto, M., and Hikosaka, O. (2010). Dopamine in motivational control: rewarding, aversive, and alerting. Neuron *68*, 815–834.

Burke, C.J., Huetteroth, W., Owald, D., Perisse, E., Krashes, M.J., Das, G., Gohl, D., Silies, M., Certel, S., and Waddell, S. (2012). Layered reward signalling through octopamine and dopamine in Drosophila. Nature *492*, 433–437.

Cassenaer, S., and Laurent, G. (2012). Conditional modulation of spike-timing-dependent plasticity for olfactory learning. Nature *482*, 47–52.

Chen, T.W., Wardill, T.J., Sun, Y., Pulver, S.R., Renninger, S.L., Baohan, A., Schreiter, E.R., Kerr, R.A., Orger, M.B., Jayaraman, V., et al. (2013). Ultrasensitive fluorescent proteins for imaging neuronal activity. Nature *499*, 295–300.

Claridge-Chang, A., Roorda, R.D., Vrontou, E., Sjulson, L., Li, H., Hirsh, J., and Miesenböck, G. (2009). Writing memories with light-addressable reinforcement circuitry. Cell *139*, 405–415.

Cohen, J.Y., Haesler, S., Vong, L., Lowell, B.B., and Uchida, N. (2012). Neuron-type-specific signals for reward and punishment in the ventral tegmental area. Nature *482*, 85–88.

Darvas, M., Fadok, J.P., and Palmiter, R.D. (2011). Requirement of dopamine signaling in the amygdala and striatum for learning and maintenance of a conditioned avoidance response. Learn. Mem. *18*, 136–143.

Das, G., Klappenbach, M., Vrontou, E., Perisse, E., Clark, C.M., Burke, C.J., and Waddell, S. (2014). Drosophila learn opposing components of a compound food stimulus. Curr. Biol. *24*, 1723–1730.

Ellender, T.J., and Paulsen, O. (2010). The many tunes of perisomatic targeting interneurons in the hippocampal network. Front. Cell Neurosci. http://dx.doi.org/10.3389/fncel.2010.00026.

Eshel, N., Bukwich, M., Rao, V., Hemmelder, V., Tian, J., and Uchida, N. (2015). Arithmetic and local circuitry underlying dopamine prediction errors. Nature *525*, 243–246.

Fishell, G., and Rudy, B. (2011). Mechanisms of inhibition within the telencephalon: "where the wild things are". Annu. Rev. Neurosci. *34*, 535–567.

Gabernet, L., Jadhav, S.P., Feldman, D.E., Carandini, M., and Scanziani, M. (2005). Somatosensory integration controlled by dynamic thalamocortical feed-forward inhibition. Neuron *48*, 315–327.

Galili, D.S., Dylla, K.V., Lüdke, A., Friedrich, A.B., Yamagata, N., Wong, J.Y., Ho, C.H., Szyszka, P., and Tanimoto, H. (2014). Converging circuits mediate temperature and shock aversive olfactory conditioning in Drosophila. Curr. Biol. *24*, 1712–1722.

Hamada, F.N., Rosenzweig, M., Kang, K., Pulver, S.R., Ghezzi, A., Jegla, T.J., and Garrity, P.A. (2008). An internal thermal sensor controlling temperature preference in Drosophila. Nature *454*, 217–220.

Hige, T., Aso, Y., Modi, M.N., Rubin, G.M., and Turner, G.C. (2015). Heterosynaptic Plasticity Underlies Aversive Olfactory Learning in Drosophila. Neuron *88*, 985–998.

Honegger, K.S., Campbell, R.A., and Turner, G.C. (2011). Cellular-resolution population imaging reveals robust sparse coding in the Drosophila mushroom body. J. Neurosci. *31*, 11772–11785.

Hoopfer, E.D., Jung, Y., Inagaki, H.K., Rubin, G.M., and Anderson, D.J. (2015). P1 interneurons promote a persistent internal state that enhances inter-male aggression in Drosophila. eLife *4*, e11346.

Horvitz, J.C. (2000). Mesolimbocortical and nigrostriatal dopamine responses to salient non-reward events. Neuroscience *96*, 651–656.

Huetteroth, W., Perisse, E., Lin, S., Klappenbach, M., Burke, C., and Waddell, S. (2015). Sweet taste and nutrient value subdivide rewarding dopaminergic neurons in Drosophila. Curr. Biol. *25*, 751–758.

Ito, K., Shinomiya, K., Ito, M., Armstrong, J.D., Boyan, G., Hartenstein, V., Harzsch, S., Heisenberg, M., Homberg, U., Jenett, A., et al.; Insect Brain Name Working Group (2014). A systematic nomenclature for the insect brain. Neuron *81*, 755–765.

Jenett, A., Rubin, G.M., Ngo, T.T., Shepherd, D., Murphy, C., Dionne, H., Pfeiffer, B.D., Cavallaro, A., Hall, D., Jeter, J., et al. (2012). A GAL4-driver line resource for Drosophila neurobiology. Cell Rep. *2*, 991–1001.

Kaun, K.R., Azanchi, R., Maung, Z., Hirsh, J., and Heberlein, U. (2011). A Drosophila model for alcohol reward. Nat. Neurosci. *14*, 612–619.

Kitamoto, T. (2001). Conditional modification of behavior in Drosophila by targeted expression of a temperature-sensitive shibire allele in defined neurons. J. Neurobiol. *47*, 81–92.

Klapoetke, N.C., Murata, Y., Kim, S.S., Pulver, S.R., Birdsey-Benson, A., Cho, Y.K., Morimoto, T.K., Chuong, A.S., Carpenter, E.J., Tian, Z., et al. (2014). Independent optical excitation of distinct neural populations. Nat. Methods *11*, 338–346.

Klausberger, T., and Somogyi, P. (2008). Neuronal diversity and temporal dynamics: the unity of hippocampal circuit operations. Science *321*, 53–57.

Krashes, M.J., and Waddell, S. (2008). Rapid consolidation to a radish and protein synthesis-dependent long-term memory after single-session appetitive olfactory conditioning in Drosophila. J. Neurosci. *28*, 3103–3113.

Krashes, M.J., DasGupta, S., Vreede, A., White, B., Armstrong, J.D., and Waddell, S. (2009). A neural circuit mechanism integrating motivational state with memory expression in Drosophila. Cell *139*, 416–427.

Lammel, S., Ion, D.I., Roeper, J., and Malenka, R.C. (2011). Projection-specific modulation of dopamine neuron synapses by aversive and rewarding stimuli. Neuron *70*, 855–862.

Lammel, S., Lim, B.K., Ran, C., Huang, K.W., Betley, M.J., Tye, K.M., Deisseroth, K., and Malenka, R.C. (2012). Input-specific control of reward and aversion in the ventral tegmental area. Nature *491*, 212–217.

Lerner, T.N., Shilyansky, C., Davidson, T.J., Evans, K.E., Beier, K.T., Zalocusky, K.A., Crow, A.K., Malenka, R.C., Luo, L., Tomer, R., and Deisseroth, K. (2015). Intact-Brain Analyses Reveal Distinct Information Carried by SNc Dopamine Subcircuits. Cell *162*, 635–647.

Letzkus, J.J., Wolff, S.B., and Lüthi, A. (2015). Disinhibition, a Circuit Mechanism for Associative Learning and Memory. Neuron *88*, 264–276.

Lewis, L.P., Siju, K.P., Aso, Y., Friedrich, A.B., Bulteel, A.J., Rubin, G.M., and Grunwald Kadow, I.C. (2015). A Higher Brain Circuit for Immediate Integration of Conflicting Sensory Information in Drosophila. Curr. Biol. *25*, 2203–2214.

Lin, S., Owald, D., Chandra, V., Talbot, C., Huetteroth, W., and Waddell, S. (2014). Neural correlates of water reward in thirsty Drosophila. Nat. Neurosci. *17*, 1536–1542.

Liu, C., Plaçais, P.Y., Yamagata, N., Pfeiffer, B.D., Aso, Y., Friedrich, A.B., Siwanowicz, I., Rubin, G.M., Preat, T., and Tanimoto, H. (2012). A subset of dopamine neurons signals reward for odour memory in Drosophila. Nature *488*, 512–516.

Mao, Z., and Davis, R.L. (2009). Eight different types of dopaminergic neurons innervate the Drosophila mushroom body neuropil: anatomical and physiological heterogeneity. Front. Neural Circuits *3*, 5.

Matsumoto, M., and Hikosaka, O. (2009). Two types of dopamine neuron distinctly convey positive and negative motivational signals. Nature *459*, 837–841.

Matsumoto, M., and Takada, M. (2013). Distinct representations of cognitive and motivational signals in midbrain dopamine neurons. Neuron *79*, 1011–1024.

Menegas, W., Bergan, J.F., Ogawa, S.K., Isogai, Y., Umadevi Venkataraju, K., Osten, P., Uchida, N., and Watabe-Uchida, M. (2015). Dopamine neurons projecting to the posterior striatum form an anatomically distinct subclass. Elife. http://dx.doi.org/10.7554/eLife.10032.

Miles, R., Toth, K., Gulyas, A.I., Hajos, N., and Freund, T.F. (1996). Differences between somatic and dendritic inhibition in the hippocampus. Neuron *16*, 815–823.

Nicolaï, L.J., Ramaekers, A., Raemaekers, T., Drozdzecki, A., Mauss, A.S., Yan, J., Landgraf, M., Annaert, W., and Hassan, B.A. (2010). Genetically encoded dendritic marker sheds light on neuronal connectivity in Drosophila. Proc. Natl. Acad. Sci. USA *107*, 20553–20558.

Okada, R., Rybak, J., Manz, G., and Menzel, R. (2007). Learning-related plasticity in PE1 and other mushroom body-extrinsic neurons in the honeybee brain. J. Neurosci. *27*, 11736–11747.

Owald, D., and Waddell, S. (2015). Olfactory learning skews mushroom body output pathways to steer behavioral choice in Drosophila. Curr. Opin. Neurobiol. *35*, 178–184.

Owald, D., Fouquet, W., Schmidt, M., Wichmann, C., Mertel, S., Depner, H., Christiansen, F., Zube, C., Quentin, C., Körner, J., et al. (2010). A Syd-1 homologue regulates pre- and postsynaptic maturation in Drosophila. J. Cell Biol. *188*, 565–579.

Owald, D., Felsenberg, J., Talbot, C.B., Das, G., Perisse, E., Huetteroth, W., and Waddell, S. (2015). Activity of defined mushroom body output neurons underlies learned olfactory behavior in Drosophila. Neuron *86*, 417–427.

Pai, T.P., Chen, C.C., Lin, H.H., Chin, A.L., Lai, J.S., Lee, P.T., Tully, T., and Chiang, A.S. (2013). Drosophila ORB protein in two mushroom body output neurons is necessary for long-term memory formation. Proc. Natl. Acad. Sci. USA *110*, 7898–7903.

Perisse, E., Yin, Y., Lin, A.C., Lin, S., Huetteroth, W., and Waddell, S. (2013). Different kenyon cell populations drive learned approach and avoidance in Drosophila. Neuron *79*, 945–956.

Pignatelli, M., and Bonci, A. (2015). Role of Dopamine Neurons in Reward and Aversion: A Synaptic Plasticity Perspective. Neuron *86*, 1145–1157.

Plaçais, P.Y., and Preat, T. (2013). To favor survival under food shortage, the brain disables costly memory. Science *339*, 440–442.

Plaçais, P.Y., Trannoy, S., Friedrich, A.B., Tanimoto, H., and Preat, T. (2013). Two pairs of mushroom body efferent neurons are required for appetitive long-term memory retrieval in Drosophila. Cell Rep. *5*, 769–780.

Pologruto, T.A., Sabatini, B.L., and Svoboda, K. (2003). ScanImage: flexible software for operating laser scanning microscopes. Biomed. Eng. Online *2*, 13.

Riemensperger, T., Völler, T., Stock, P., Buchner, E., and Fiala, A. (2005). Punishment prediction by dopaminergic neurons in Drosophila. Curr. Biol. *15*, 1953–1960.

Riemensperger, T., Issa, A.R., Pech, U., Coulom, H., Nguyen, M.V., Cassar, M., Jacquet, M., Fiala, A., and Birman, S. (2013). A single dopamine pathway underlies progressive locomotor deficits in a Drosophila model of Parkinson disease. Cell Rep. *5*, 952–960.

Schultz, W. (2015). Neuronal Reward and Decision Signals: From Theories to Data. Physiol. Rev. *95*, 853–951.

Schultz, W., Dayan, P., and Montague, P.R. (1997). A neural substrate of prediction and reward. Science *275*, 1593–1599.

Schwab, D.J., and Houk, J.C. (2015). Presynaptic Inhibition in the Striatum of the Basal Ganglia Improves Pattern Classification and Thus Promotes Superior Goal Selection. Front. Syst. Neurosci. *9*, 152.

Séjourné, J., Plaçais, P.Y., Aso, Y., Siwanowicz, I., Trannoy, S., Thoma, V., Tedjakumala, S.R., Rubin, G.M., Tchénio, P., Ito, K., et al. (2011). Mushroom body efferent neurons responsible for aversive olfactory memory retrieval in Drosophila. Nat. Neurosci. *14*, 903–910.

Shang, Y., Claridge-Chang, A., Sjulson, L., Pypaert, M., and Miesenböck, G. (2007). Excitatory local circuits and their implications for olfactory processing in the fly antennal lobe. Cell *128*, 601–612.

Shen, P., and Cai, H.N. (2001). Drosophila neuropeptide F mediates integration of chemosensory stimulation and conditioning of the nervous system by food. J. Neurobiol. *47*, 16–25.

Smith, K.S., Berridge, K.C., and Aldridge, J.W. (2011). Disentangling pleasure from incentive salience and learning signals in brain reward circuitry. Proc. Natl. Acad. Sci. USA *108*, E255–E264.

Tellez, L.A., Han, W., Zhang, X., Ferreira, T.L., Perez, I.O., Shammah-Lagnado, S.J., van den Pol, A.N., and de Araujo, I.E. (2016). Separate circuitries encode the hedonic and nutritional values of sugar. Nat. Neurosci. *19*, 465–470.

Tempel, B.L., Bonini, N., Dawson, D.R., and Quinn, W.G. (1983). Reward learning in normal and mutant Drosophila. Proc. Natl. Acad. Sci. USA *80*, 1482–1486.

Tully, T., and Quinn, W.G. (1985). Classical conditioning and retention in normal and mutant Drosophila melanogaster. J. Comp. Physiol. A Neuroethol. Sens. Neural Behav. Physiol. *157*, 263–277.

Vogels, T.P., and Abbott, L.F. (2005). Signal propagation and logic gating in networks of integrate-and-fire neurons. J. Neurosci. *25*, 10786–10795.

Waddell, S. (2013). Reinforcement signalling in Drosophila; dopamine does it all after all. Curr. Opin. Neurobiol. *23*, 324–329.

Wise, R.A. (2004). Dopamine, learning and motivation. Nat. Rev. Neurosci. *5*, 483–494.

Wu, Q., Wen, T., Lee, G., Park, J.H., Cai, H.N., and Shen, P. (2003). Developmental control of foraging and social behavior by the Drosophila neuropeptide Y-like system. Neuron *39*, 147–161.

Yamagata, N., Ichinose, T., Aso, Y., Plaçais, P.Y., Friedrich, A.B., Sima, R.J., Preat, T., Rubin, G.M., and Tanimoto, H. (2015). Distinct dopamine neurons mediate reward signals for short- and long-term memories. Proc. Natl. Acad. Sci. USA *112*, 578–583.

Yoshihara, M. (2012). Simultaneous recording of calcium signals from identified neurons and feeding behavior of Drosophila melanogaster. J. Vis. Exp. http://dx.doi.org/10.3791/3625.

Zweifel, L.S., Fadok, J.P., Argilli, E., Garelick, M.G., Jones, G.L., Dickerson, T.M., Allen, J.M., Mizumori, S.J., Bonci, A., and Palmiter, R.D. (2011). Activation of dopamine neurons is critical for aversive conditioning and prevention of generalized anxiety. Nat. Neurosci. *14*, 620–626.

Neuron, Volume *90*

Supplemental Information

Aversive Learning and Appetitive Motivation Toggle Feed-Forward Inhibition in the *Drosophila* Mushroom Body

Emmanuel Perisse, David Owald, Oliver Barnstedt, Clifford B. Talbot, Wolf Huetteroth, and Scott Waddell

Fly Strains

The wild-type *Drosophila* strain used in this study is Canton-S. UAS-mCD8::GFP (Lee and Luo, 1999), 247-LexA::VP16 (Pitman et al., 2011), lexAop-rCD2::RFP (Lai and Lee, 2006), UAS-DenMark (Nicolai et al., 2010) and UAS-GFP-Syd-1 (Owald et al., 2010) flies are described. The MVP2 neuron (MBON-γ1pedc>$\alpha\beta$) expressing lines, R83A12-GAL4, MB112C-GAL4 and R12G04-LexA , as well as the M4/6 expressing line R21D02-GAL4 (described in Owald et al., 2015) and the V2αV2α´expressing line R71D08-GAL4 are from the FlyLight collection (Jenett et al., 2012; Aso et al., 2014b). UAS-GCaMP6f is that in Chen et al. (2013); these strains were obtained from the Bloomington Stock Center. The lexAop-CsChrimson-tdtomato,UAS-GCaMP6f flies are described (Hoopfer et al., 2015). The MP1 (PPL1-γ1pedc) DAN expressing c061:MBGAL80 combination is that in Krashes et al. (2009). We used flies carrying UAS-*shi*^{ts1} (Kitamoto, 2001) on the third chromosome. UAS-*dTrpA1* flies are described (Hamada et al., 2008). We generated flies expressing *shi*^{ts1} or *dTrpA1* in MVP2 drivers by crossing UAS-*shi*^{ts1} or UAS-*dTrpA1* females to R83A12 and MB112C males. For imaging MB112C and UAS-GCaMP6f were combined. We generated flies expressing *shi*^{ts1} or *dTrpA1* in MP1 neurons by crossing c061:MBGAL80 females to UAS-*shi*^{ts1} or UAS-*dTrpA1* males. For the optogenetic experiments we used the appropriate female progeny from crosses between lexAop-CsChrimson-tdtomato,uas-GCaMP6f males and R12G04-LexA/CyO;R21D02-GAL4 or R12G04-LexA/CyO;R71D08-GAL4/TM3 females.

Behavioral analysis

For appetitive memory groups of ~100 flies were food-deprived in a 25 ml vial, containing 1% agar and a 20 x 60 mm piece of filter paper for 19–23 h before training. Flies were conditioned as follows: 2 min with odor A without reinforcement, 30 s of air, 2 min with odor B with saturated ~5.8M sucrose, dried on a filter paper. To test 30 min, 3 h or 24 h memory flies were trained and stored in food vials, or food-deprivation vials, until testing.

For aversive memory, groups of ~100 flies were housed for 18–24 h before training in a 25 ml vial containing standard cornmeal/agar food and a 20 x 60 mm piece of filter paper. Flies were conditioned as follows: 1 min odor A with 12 120 V shocks at 5 s interstimulus interval, 45 s air, and 1 min odor B without reinforcement.

Memory performance was tested in the dark by allowing the flies 2 min to choose between the odors presented during training. Performance index (PI) was calculated as the number of flies approaching (appetitive memory) or avoiding (aversive memory) the conditioned odor minus the number of flies going the other direction, divided by the total number of flies in the experiment. A single PI value is the average score from flies of the identical genotype tested with the reciprocal reinforced/ non-reinforced odor combination. The odors used for conditioning were 3-octanol (7 µl in 8 ml mineral oil) and 4-methylcyclohexanol (7 µl in 8 ml mineral oil).

Naïve avoidance was performed as described (Owald et al., 2015). Fed flies were transferred to 33 °C 30 min (for the *shi*^{ts1} experiments) or 15 min (for the *dTrpA1* experiments) before a 2 min test in the dark between MCH or OCT diluted in mineral oil (1:10^{-6}) versus mineral oil.

Two photon calcium imaging

One hemisphere per fly was randomly chosen and imaged. Two-photon fluorescence images were manually segmented using ImageJ. Animal movement was small enough that images did not require registration. Fluorescence over the defined region of interest (ROI) was summed at each frame to yield one fluorescence trace, F(t). The protocol to test responses after training was that in Owald et al. (2015). Flies were exposed to 5 s MCH (air stream passing over 10^{-2} odor dilution in mineral oil, and then further blended 1:9 with a clean air stream), 30 s clean air, followed by 5 s OCT. This odor regimen was delivered twice. Baseline fluorescence (F) corresponds to the average fluorescence signal across an 8 s window starting 9 s after scan onset and terminating 3 s before the first air or odor exposure. Baseline was then used to compute the relative change in fluorescence (ΔF(t)/F = (F(t) – F)/F). Responses were determined to start approximately 2.25 s after the instrumentation odor delivery command and to end within 12.5 s. This delayed onset accounts for the computational, electronic, mechanical and fluid flow lag. We corrected for small changes in the background fluorescence between odor presentations by subtracting the mean fluorescence between 0 and 2.25 s from each curve. The response curves were normalized and averaged over the two paired odor presentations:

$$\mathrm{CS}_n^{+/-}(t) = \frac{1}{2}\sum_{i=1}^{2} \frac{\mathrm{CS}_{n,i}^{+/-}(t)}{\int_0^{12.5}\left(\frac{\mathrm{CS}_{n,i}^{+}(t) + \mathrm{CS}_{n,i}^{-}(t)}{2}\right)dt}$$

Equation (i)

$CS_{n,i}^{+/-}(t)$ are the background subtracted ΔF(*t*)/F response curves of the n'th experiment to the i'th odor stimulation protocol. The normalization factor was chosen to be the average of the total CS+ and CS- response to avoid bias towards one or the other and was calculated as the sum over the acquisition time points of the ΔF(*t*)/F curves multiplied by the sampling interval. We (1) computed the mean responses for all normalized CS+ and CS- responses and (2) computed the odor response difference for each n, $D_n(t) = CS_n^+ - CS_n^-$. To quantify the difference between the trained and mock groups, the area under the peak of each D_n curve (defined as 4.5± 1.5 s after odor delivery for experiments following training) was computed following Owald et al. (2015).

The peak values obtained from each trained group were compared with those of the corresponding mock group using the Mann-Whitney U-test. The learning-induced difference curve, L(t), is the difference between the mean ± SEM of the $D_n(t)$ curves of the trained and corresponding mock groups. The errors were combined in the usual way – i.e. error in $L(t) = \sqrt{SEM(t)_{trained}^2 + SEM(t)_{mock}^2}$. For naïve odor response experiments (Fig. 6A) only one round of odors was applied per fly; the intervals between odor presentation onset was 30 s. Odor response traces were averaged across flies per group and thus no normalization was applied. Peaks of naïve traces were also estimated at 4.5± 1.5 s across odors.

Supplementary References

Lai, S. L., and Lee, T. (2006). Genetic mosaic with dual binary transcriptional systems in Drosophila. Nat. Neurosci. *9*, 703-709.

Lee, T., and Luo, L. (1999). Mosaic analysis with a repressible cell marker for studies of gene function in neuronal morphogenesis. Neuron *22*, 451-461.

Pitman, J. L., Huetteroth, W., Burke, C. J., Krashes, M. J., Lai, S. L., Lee, T., and Waddell, S. (2011). A pair of inhibitory neurons are required to sustain labile memory in the Drosophila mushroom body. Curr. Biol. *21*, 855-861.

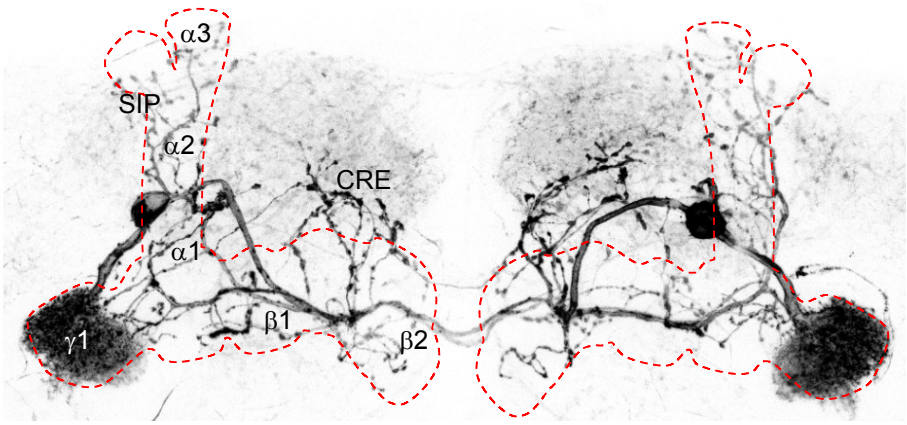


Figure S1. Anatomy of MVP2 neuron projections within and outside the MB (related to Figure 1).

Black and white confocal projection of MB112C driven UAS-mCitrine reveals the detailed morphology of MVP2 processes. The dendritic field lies in the $\alpha\beta_s$ a□□ γ1 zone whereas presynaptic processes innervate the α1, α2, α3, β1 and β2 compartments of the MB lobes as well as outside the MB in the crepine (CRE) and superior intermediate protocerebrum (SIP).

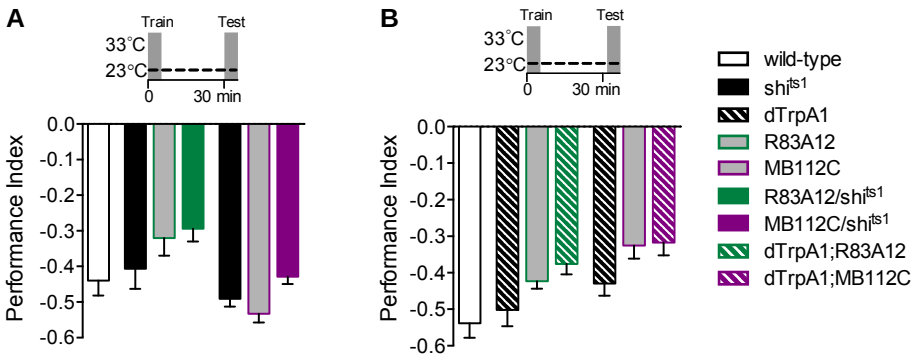


Figure S2. Expressing UAS-*shi*^{ts1} or UAS-*dTrpA1* in MVP2 neurons does not disrupt 30 min aversive memory performance at the permissive temperature (related to Figure 2).

(A) No statistical differences were apparent between MVP2 expressing UAS-*shi*^{ts1} flies and their relevant GAL4 or UAS-*shi*^{ts1} controls (R83A12: ANOVA, n = 8, P > 0.2. MB112C: ANOVA, n = 10-12, P < 0.01. (B) No statistical differences in 30 min aversive memory performance were apparent between MVP2 expressing UAS-*dTrpA1* flies and their relevant GAL4 or UAS-*dTrpA1* controls (R83A12: ANOVA, n = 8-10, P = 0.03. MB112C: ANOVA, n = 8-10, P > 0.05). All flies were trained, stored and tested at 23 °C. All data are mean ± SEM.

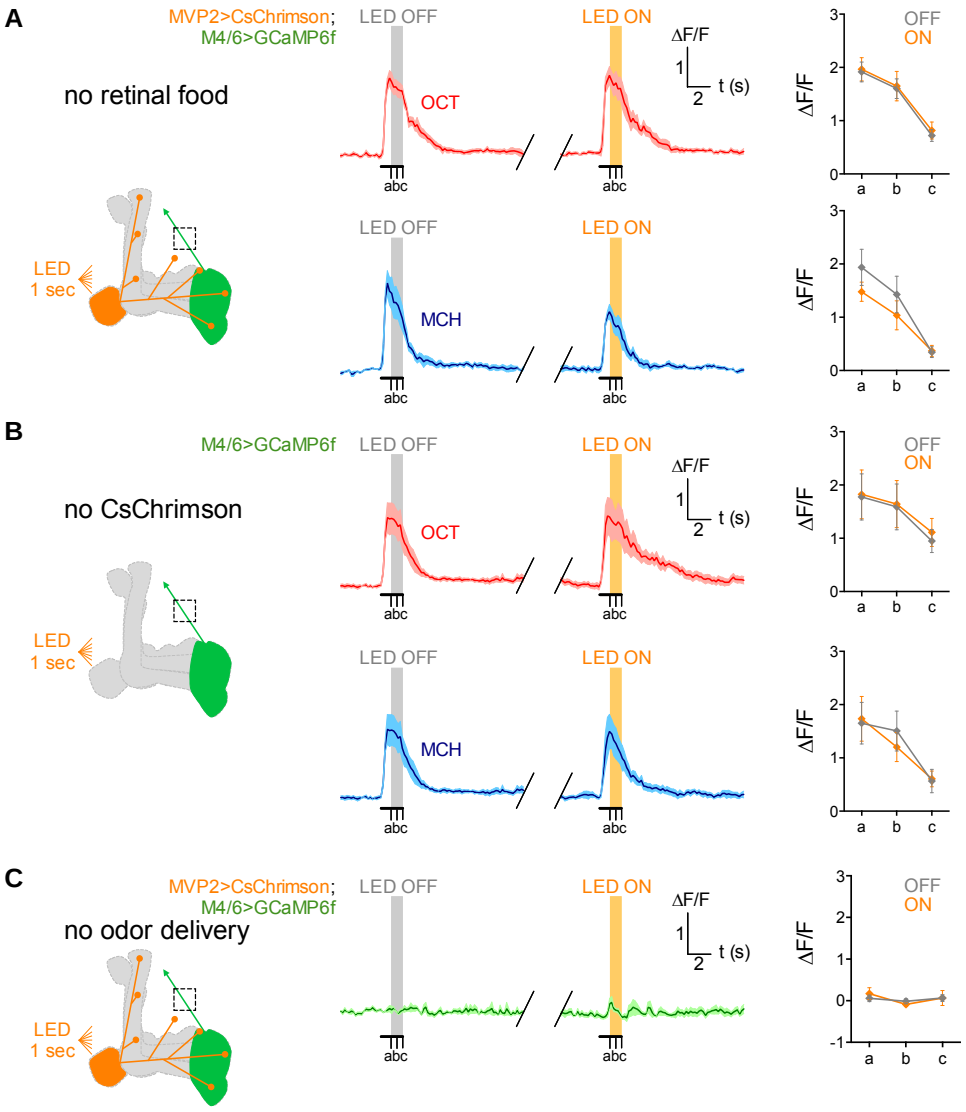


Figure S3. Control experiments related to Figure 4

Odor evoked GCaMP6f responses were measured in M4/6 MBON axons (green). Left panels, schematics of experiment. (A) Flies not fed with retinal before the experiment. Calcium traces during OCT (top middle panel, red) or MCH (bottom middle panel, blue) presentation show robust odor-evoked responses in M4β′ axons. Data are mean [solid line] ± SEM [shaded area]. LED ON illumination for one second did not change the odor-evoked responses compared to the LED OFF condition. Quantification of the ΔF/F at the a-c time points did not reveal a significant difference in the odor-evoked responses with LED ON (orange) compared to the same time point with LED OFF (grey), for either OCT (top right) or MCH (bottom right) (Both two-way repeated measures ANOVA, no interaction effect P > 0.2, n =

5). (B) Flies lacked the UAS-CsChrimson transgene. Calcium traces during OCT (middle top panel, red) or MCH (middle bottom panel, blue) presentation show robust odor-evoked responses in M4β´ axons. Data are mean [solid line] ± SEM [shaded area]. LED ON did not impair odor-evoked calcium responses compared to the LED OFF condition. Quantification of the ΔF/F at the a-c time points did not reveal a significant difference between the conditions; LED ON (orange), LED OFF (grey), for either OCT (top right) or MCH (bottom right) (Both two-way repeated measures ANOVA, no interaction effect $P > 0.05$, $n = 5$). (C) Flies were not exposed to odors. Data are mean [solid line] ± SEM [shaded area]. Triggering MVP2 activity with LED ON for one second did not reveal an obvious change in calcium signal in M4β´ axons compared to the LED OFF condition. Quantification of the ΔF/F at the a-c time points did not reveal a significant difference between the conditions; LED ON (orange), LED OFF (grey) (Two-way repeated measures ANOVA, no interaction effect $P > 0.4$, $n = 5$).

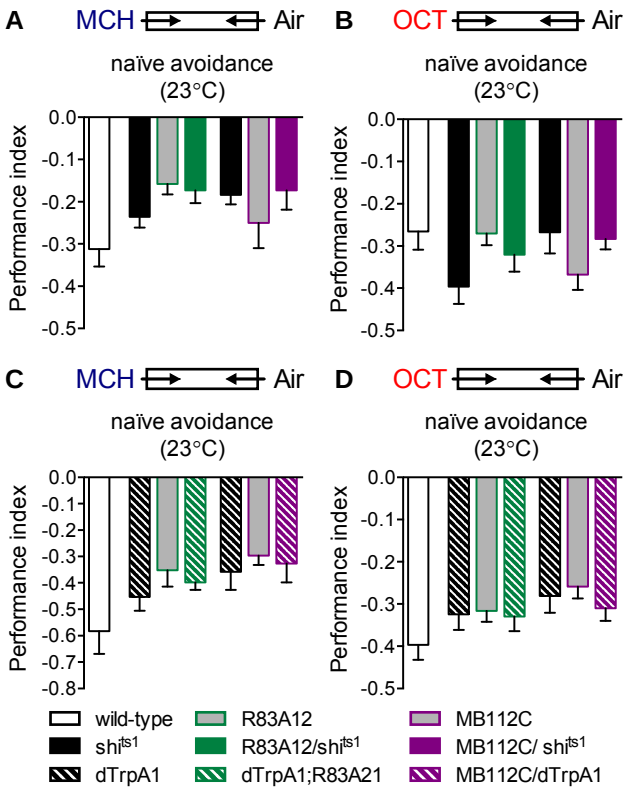


Figure S4. UAS-*shi*^{ts1} or UAS-*dTrpA1* expression in MVP2 neurons does not alter odor avoidance behavior at permissive temperature (related to Figure 5)

Flies chose between T-maze arms perfused with MCH or OCT versus a clean air stream at 23°C. (A-B) No significant differences in naïve odor avoidance were apparent between MVP2;UAS-*shi*^{ts1} flies and their relevant GAL4 or UAS-*shi*^{ts1} controls for (A) MCH (R83A12: ANOVA, n = 10-15, P > 0.1. MB112C: ANOVA, n = 8-13, P > 0.4) or for (B) OCT (R83A12: ANOVA, n ≥ 16-20, P < 0.05. MB112C: ANOVA, n = 10-17, P > 0.01). (C-D) No statistical differences in naïve odor avoidance were apparent between MVP2; UAS-*dTrpA1* flies and their relevant GAL4 or UAS-*dTrpA1* controls for (C) MCH (R83A12: ANOVA, n = 10-15, P > 0.3. MB112C: ANOVA, n = 10-12, P > 0.7) or for (D) OCT (R83A12: ANOVA, n = 11-17, P > 0.9. MB112C: ANOVA, n = 12, P > 0.5).

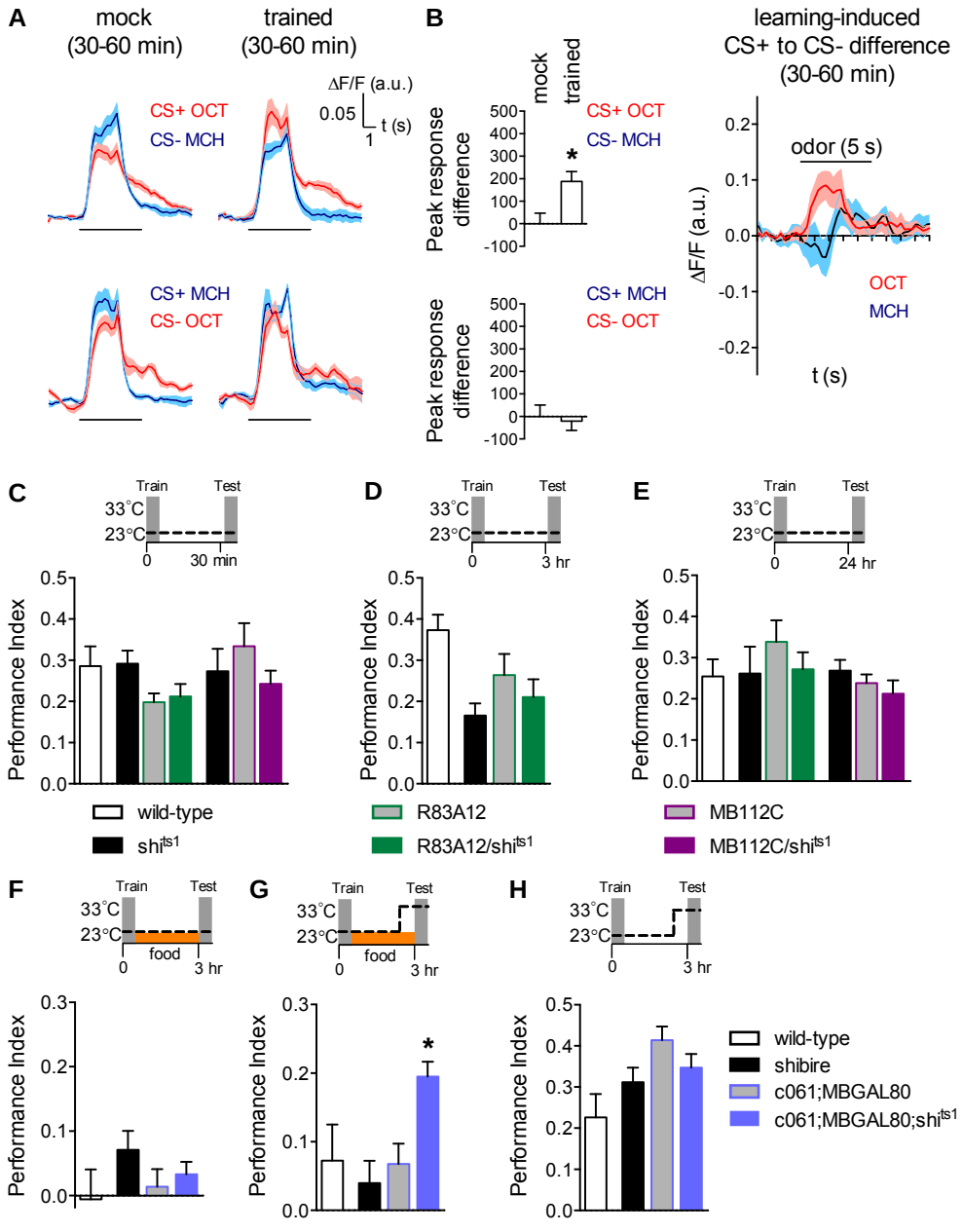


Figure S5. Control experiments related to Figure 6

(A) Flies were trained by pairing one odor with sugar (CS+) and another odor without (CS-), or they were mock trained with only odor exposure. Odor-evoked calcium transients were measured 30-60 min after conditioning. Appetitive conditioning; CS+ (normalized mean ± SEM) to CS- (normalized mean ± SEM). (B) Bar graphs represent percent difference to the mean mock integrated peak response (4.5 ± 1.5s after odor delivery, see methods). Asterisk indicates statistical significance. (Mann-Whitney U-test; OCT is CS+: n(mock) = 9, n(trained) = 11, $P < 0.05$. MCH is CS+:

n(mock) = 7, n(trained) = 7, P > 0.05; curves are normalized, see methods). Difference of responses evoked by CS+ and CS- after appetitive conditioning relative to the mean responses after mock training (red curve: OCT is CS+, blue curve: MCH is CS+). Data are mean [solid line] ± SEM [shaded area]. (C-E) All flies were trained with odors and sugar reward and tested for memory performance at 23°C. No statistical differences were apparent between any groups and their relevant controls. (C) 30 min (R83A12: ANOVA, n = 8-10, P > 0.05. MB112C: ANOVA, n = 8, P > 0.4). (D) 3 h (R83A12: ANOVA, n = 10-11, P > 0.2). (E) 24 h (R83A12: ANOVA, n = 8-10, P > 0.5. MB112C: ANOVA, n = 12-14, P >0.3). (F) Feeding flies after training suppresses appetitive memory performance. Flies were trained at 23 °C, stored in food vials and tested for 3 h memory performance at 23 °C. No statistical differences were apparent between flies expressing UAS-*shi*^{ts1} in MP1 neurons (c061;MBGAL80) and their relevant controls (ANOVA, n = 10, P > 0.2). (G) Blocking MP1 DANs 30 min prior to and during testing promotes the expression of appetitive memory (ANOVA, n = 10-12, P < 0.001). Flies were trained, stored in food vials and tested for 3 h memory at 33°C. (H) Blocking MP1 DANs in hungry flies did not further elevate 3 h appetitive memory performance (ANOVA, n = 8, P > 0.1). Data are mean ± SEM.

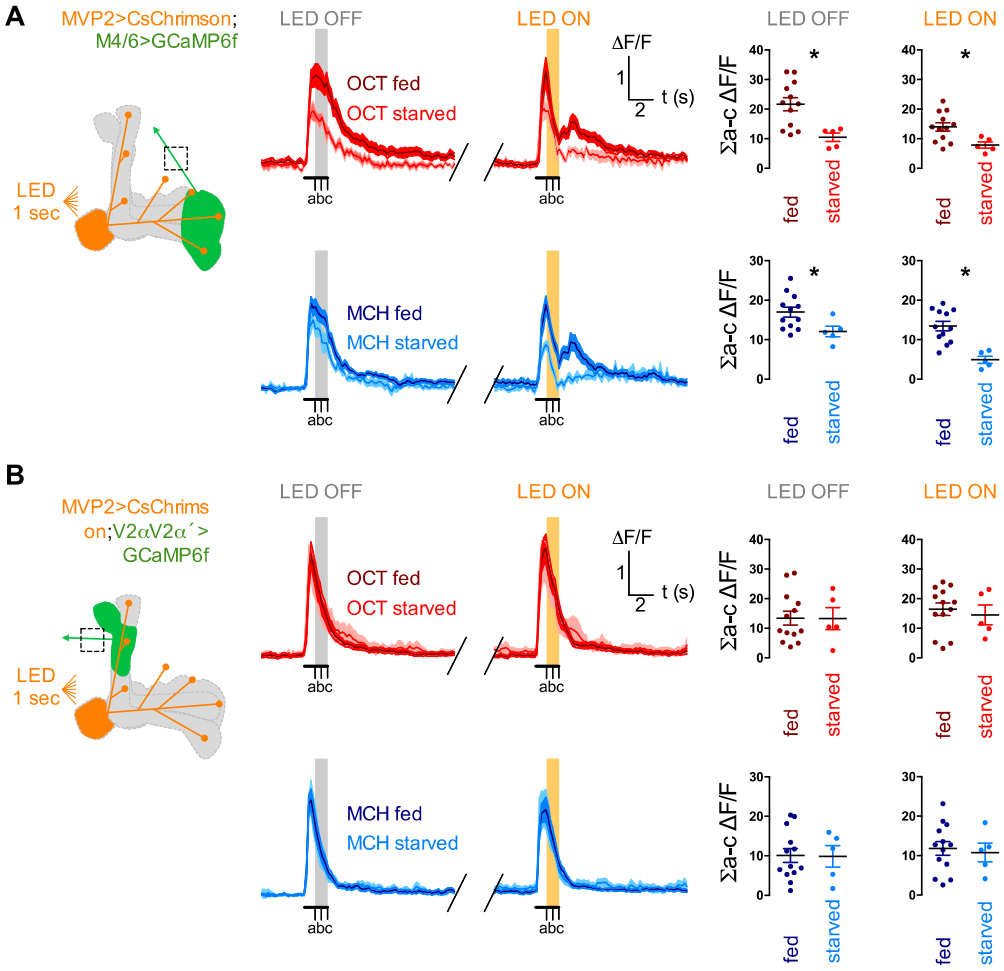


Figure S6. Odor-evoked activity in M4/6 but not V2αV2α´ MBONs is reduced in hungry flies (related to Figure 4 and 6).

Left panels, schematics of experiment. Odor evoked GCaMP6f responses were measured in (A) M4/6 or (B) V2αV2α´ MBON axons (black dashed box on green arrow) while CsChrimson-expressing MVP2 MBONs (orange) were light-triggered. Responses compared between fed (data from Figure 4) and starved flies. (A) OCT (middle top panel, red) and MCH (middle bottom panel, blue) evoked calcium transients in M4β´ axons are markedly smaller in starved versus fed flies. Activating MVP2 neurons with LED ON for one second caused a clear depression in the calcium transient in both conditions. Data are mean curves [solid line] ± SEM [shaded area]. Quantifying the area under the curve of the ΔF/F during the odor presentation (∑a-c) shows a significant difference in the starved responses compared to fed for both OCT (top right panels) and MCH (bottom right panels) and between LED OFF and LED ON. (All Mann-Whitney, $P < 0.05$, $n = 5$-12). (B) OCT

(middle top panel, red) and MCH (middle bottom panel, blue) evoke similar calcium responses in V2αV2α´ axons in starved and fed flies. Triggering MVP2 neurons with LED ON (orange) for one second did not alter the calcium responses in either condition. Data are mean curves [solid line] ± SEM [shaded area]. Quantifying the area under the curve of the ΔF/F during the odor presentation (∑a-c) did not reveal any statistical differences in V2αV2α´ OCT (right top panels) or MCH (right bottom panels) odor responses between fed or starved flies, or for LED OFF versus LED ON. (All Mann-Whitney, P > 0.7, n = 5-13).

Movie S1, related to Figure 1 and S1. Projection view of the MVP2 neurons. Projection of MB112C driven UAS-mCitrine reveals the detailed three-dimensional morphology of MVP2 processes.

Movie S2, related to Figure 3 and 4. Projection view of the innervation of the MVP2 and M4/6 neurons in the horizontal lobe tip of the MB. R83A12-GAL4; UAS-GCaMP6f (MVP2, orange) and R21D02-LexA; lexAop-rCD2::mRFP (M4/6 cyan).

Movie S3, related to Figure 3 and 4. Projection view of the innervation of the MVP2 and V2αV2α´ neurons in the vertical lobe of the MB. R12G04-LexA; lexAop-rCD2::mRFP (MVP2, orange) and R71D08-GAL4; UAS-mCD8::GFP (V2αV2α´, cyan).

References

Aceves-Piña, E. O. and W. G. Quinn (1979). "Learning in normal and mutant Drosophila larvae." In: *Science (New York, N.Y.)* 206.4414, pp. 93–6.

Aceves-Pina, E., R. Booker, J. Duerr, M. Livingstone, W. Quinn, R. Smith, P. Sziber, B. Tempel, and T. Tully (1983). "Learning and Memory in Drosophila, Studied with Mutants". In: *Cold Spring Harbor Symposia on Quantitative Biology* 48, pp. 831–840.

Adamantidis, A. R., F. Zhang, A. M. Aravanis, K. Deisseroth, and L. de Lecea (2007). "Neural substrates of awakening probed with optogenetic control of hypocretin neurons." In: *Nature* 450.7168, pp. 420–4.

Aidley, D. J. and D. J. Ashley (1998). *The physiology of excitable cells*. Vol. 4. Cambridge University Press Cambridge.

Airan, R. D., K. R. Thompson, L. E. Fenno, H. Bernstein, and K. Deisseroth (2009). "Temporally precise in vivo control of intracellular signalling." In: *Nature* 458.7241, pp. 1025–9.

Akalal, D.-B. G., D. Yu, and R. L. Davis (2010). "A late-phase, long-term memory trace forms in the γ neurons of Drosophila mushroom bodies after olfactory classical conditioning." In: *The Journal of Neuroscience* 30.49, pp. 16699–16708.

Akemann, W., H. Mutoh, A. Perron, J. Rossier, and T. Knöpfel (2010). "Imaging brain electric signals with genetically targeted voltage-sensitive fluorescent proteins." In: *Nature methods* 7.8, pp. 643–649.

Akerboom, J., N. Carreras Calderón, L. Tian, S. Wabnig, M. Prigge, J. Tolö, A. Gordus, M. B. Orger, K. E. Severi, J. J. Macklin, R. Patel, S. R. Pulver, T. J. Wardill, E. Fischer, C. Schüler, T.-W. Chen, K. S. Sarkisyan, J. S. Marvin, C. I. Bargmann, D. S. Kim, S. Kügler, L. Lagnado, P. Hegemann, A. Gottschalk, E. R. Schreiter, and L. L. Looger (2013). "Genetically encoded calcium indicators for multi-color neural activity imaging and combination with optogenetics." In: *Frontiers in molecular neuroscience* 6.March, p. 2.

Akerboom, J., J. D. V. Rivera, M. M. Rodríguez Guilbe, E. C. A. Malavé, H. H. Hernandez, L. Tian, S. A. Hires, J. S. Marvin, L. L. Looger, and E. R. Schreiter (2009). "Crystal structures of the GCaMP calcium sensor reveal the mechanism of fluorescence signal change and aid rational design". In: *Journal of Biological Chemistry* 284.10, pp. 6455–6464.

Akerboom, J. et al. (2012). "Optimization of a GCaMP calcium indicator for neural activity imaging." In: *The Journal of neuroscience : the official journal of the Society for Neuroscience* 32.40, pp. 13819–40.

Alberts, B., A. Johnson, J. Lewis, D. Morgan, M. Raff, K. Roberts, and P. Walter (2014). *Molecular Biology of the Cell 6e*. 6th ed. Vol. 6. 6, p. 1465.

Alberts, B., A. Johnson, J. Lewis, M. Raff, K. Roberts, and P. Walter (2008). *Molecular Biology of the Cell*. 5th ed., p. 1728.

Albin, S. D., K. R. Kaun, J.-m. Knapp, P. Chung, U. Heberlein, and J. H. Simpson (2015). "A Subset of Serotonergic Neurons Evokes Hunger in Adult Drosophila". In: *Current Biology* 25.18, pp. 2435–2440.

Albrecht, J. and A. Schousboe (2005). "Taurine interaction with neurotransmitter receptors in the CNS: an update." In: *Neurochemical research* 30.12, pp. 1615–21.

Alekseyenko, O. V., Y.-B. Chan, M. d. l. P. Fernandez, T. Bülow, M. J. Pankratz, and E. A. Kravitz (2014). "Single Serotonergic Neurons that Modulate Aggression in Drosophila". In: *Current Biology*, pp. 1–8.

Alekseyenko, O. V., C. Lee, and E. A. Kravitz (2010). "Targeted manipulation of serotonergic neurotransmission affects the escalation of aggression in adult male drosophila melanogaster". In: *PLoS ONE* 5.5.

Allen, B. D., A. C. Singer, and E. S. Boyden (2015). "Principles of designing interpretable optogenetic behavior experiments". In: *Learning & Memory* 22.4, pp. 232–238.

Andor (2017). *Comparing sCMOS*. URL: `http://www.andor.com/learning-academy/comparing-scmos-compare-scmos-with-other-detectors` (visited on 04/16/2017).

Arakawa, S., J. D. Gocayne, W. R. McCombie, D. A. Urquhart, L. M. Hall, C. M. Fraser, and J. C. Venter (1990). "Cloning, localization, and permanent expression of a Drosophila octopamine receptor". In: *Neuron* 4.3, pp. 343–354.

Aronstein, K., V. Auld, and R. Ffrench-Constant (1996). "Distribution of two GABA receptor-like subunits in the Drosophila CNS." In: *Invertebrate neuroscience : IN* 2.2, pp. 115–120.

Aronstein, K. and R. Ffrench-Constant (1995). "Immunocytochemistry of a novel GABA receptor subunit Rdl in Drosophila melanogaster". In: *Invertebrate Neuroscience* 1.1, pp. 25–31.

Aso, Y., K. Grübel, S. Busch, A. B. Friedrich, I. Siwanowicz, and H. Tanimoto (2009). "The mushroom body of adult Drosophila characterized by GAL4 drivers." In: *Journal of Neurogenetics* 23.1-2, pp. 156–72.

Aso, Y., D. Hattori, Y. Yu, R. M. Johnston, N. A. Iyer, T.-T. T. B. Ngo, H. Dionne, L. F. Abbott, R. Axel, H. Tanimoto, and G. M. Rubin (2014a). "The neuronal architecture of the mushroom body provides a logic for associative learning". In: *eLife* 3, pp. 1–47.

Aso, Y., A. Herb, M. Ogueta, I. Siwanowicz, T. Templier, A. B. Friedrich, K. Ito, H. Scholz, and H. Tanimoto (2012). "Three Dopamine pathways induce aversive odor memories with different stability". In: *PLoS Genetics* 8.7.

Aso, Y. and G. M. Rubin (2016). "Dopaminergic neurons write and update memories with cell-type-specific rules". In: *eLife* 5.

Aso, Y., D. Sitaraman, T. Ichinose, K. R. Kaun, K. Vogt, G. Belliart-Guérin, P.-Y. Plaçais, A. a. Robie, N. Yamagata, C. Schnaitmann, W. J. Rowell, R. M. Johnston, T.-T. B. Ngo, N. Chen, W. Korff, M. N. Nitabach, U. Heberlein, T. Preat, K. M. Branson, H. Tanimoto, and G. M. Rubin (2014b). "Mushroom body output neurons encode valence and guide memory-based action selection in Drosophila". In: *eLife* 3.3, pp. 1–42.

Aso, Y., I. Siwanowicz, L. Bräcker, K. Ito, T. Kitamoto, and H. Tanimoto (2010). "Specific dopaminergic neurons for the formation of labile aversive memory." In: *Current Biology* 20.16, pp. 1445–51.

Aswani, K., T. Jinadasa, and C. M. Brown (2012). "Fluorescence Microscopy Light Sources". In: *Microscopy Today* 20.04, pp. 22–28.

Baggerman, G., K. Boonen, P. Verleyen, A. De Loof, and L. Schoofs (2005). "Peptidomic analysis of the larval Drosophila melanogaster central nervous system by two-dimensional capillary liquid chromatography quadrupole time-of-flight mass spectrometry". In: *Journal of Mass Spectrometry* 40.2, pp. 250–260.

Baker, K. L., F. B. Bolger, and J. P. Lowry (2015). "A microelectrochemical biosensor for real-time in vivo monitoring of brain extracellular choline". In: *The Analyst* 140.11, pp. 3738–3745.

Balu, D. T. and J. T. Coyle (2015). "The NMDA receptor 'glycine modulatory site' in schizophrenia: D-serine, glycine, and beyond". In: *Current Opinion in Pharmacology* 20, pp. 109–115.

Banke, T. G. and C. J. McBain (2006). "GABAergic input onto CA3 hippocampal interneurons remains shunting throughout development." In: *The Journal of Neuroscience* 26.45, pp. 11720–11725.

Bao, X., B. Wang, J. Zhang, T. Yan, W. Yang, F. Jiao, J. Liu, and S. Wang (2010). "Localization of serotonin/tryptophan-hydroxylase-immunoreactive cells in the brain and suboesophageal ganglion of Drosophila melanogaster". In: *Cell and Tissue Research* 340.1, pp. 51–59.

Barber, R. P., H. Sugihara, M. Lee, J. E. Vaughn, and P. M. Salvaterra (1989). "Localization of Drosophila neurons that contain choline acetyltransferase messenger RNA: an in situ hybridization study." In: *The Journal of comparative neurology* 280, pp. 533–543.

Barnstedt, O., D. Owald, J. Felsenberg, R. Brain, J.-P. Moszynski, C. B. Talbot, P. N. Perrat, and S. Waddell (2016). "Memory-Relevant Mushroom Body Output Synapses Are Cholinergic." In: *Neuron* 89.6, pp. 1237–1247.

Barolo, S., B. Castro, and J. W. Posakony (2004). "New Drosophila transgenic reporters: insulated P-element vectors expressing fast-maturing RFP." In: *BioTechniques* 36.3, pp. 436–40, 442.

Bayliss, A., G. Roselli, and P. D. Evans (2013). "A comparison of the signalling properties of two tyramine receptors from Drosophila". In: *Journal of Neurochemistry* 125.1, pp. 37–48.

Belle, J. S. de and M. Heisenberg (1994). "Associative Odor Learning in Drosophila Abolished by Chemical Ablation of Mushroom Bodies J . Steven de Belle * and Martin Heisenberg". In: *Science* 263.5147, pp. 692–695.

Bellmann, D., A. Richardt, R. Freyberger, N. Nuwal, M. Schwärzel, A. Fiala, and K. F. Störtkuhl (2010). "Optogenetically Induced Olfactory Stimulation in Drosophila Larvae Reveals the Neuronal Basis of Odor-Aversion behavior." In: *Frontiers in behavioral neuroscience* 4.June, p. 27.

Bennett, G., C. Tyler, and E. Zaimis (1957). "Mecamylamine and its mode of action". In: *The Lancet* 270.6988, pp. 218–222.

Bennett, M. R. and V. J. Balcar (1999). "Forty years of amino acid transmission in the brain". In: *Neurochemistry International* 35.4, pp. 269–280.

Benzer, S. (1967). "Behavioral mutants of Drosophila isolated by countercurrent distribution". In: *Proceedings of the National Academy of Sciences* 58.3, pp. 1112–1119.

Benzer, S. (1971). "From the Gene to Behavior". In: *JAMA: The Journal of the American Medical Association* 218.7, p. 1015.

Berndt, A., O. Yizhar, L. a. Gunaydin, P. Hegemann, and K. Deisseroth (2009). "Bi-stable neural state switches." In: *Nature neuroscience* 12.2, pp. 229–34.

Bernstein, J. G., P. a. Garrity, and E. S. Boyden (2012). "Optogenetics and thermogenetics: technologies for controlling the activity of targeted cells within intact neural circuits." In: *Current opinion in neurobiology* 22.1, pp. 61–71.

Berridge, M. J. M. J., P. Lipp, and M. D. M. D. Bootman (2000). "The versatility and universality of calcium signalling." In: *Nature reviews. Molecular cell biology* 1.1, pp. 11–21.

Berry, J. A., I. Cervantes-Sandoval, E. P. Nicholas, and R. L. Davis (2012). "Dopamine Is Required for Learning and Forgetting in Drosophila". In: *Neuron* 74.3, pp. 530–542.

Bertrand, D., M. Ballivet, M. Gomez, S. Bertrand, B. Phannavong, and E. D. Gundelfinger (1994). "Physiological properties of neuronal nicotinic receptors reconstituted from the vertebrate beta 2 subunit and Drosophila alpha subunits." In: *The European journal of neuroscience* 6, pp. 869–875.

Besson, M. T., I. Sinakevitch, C. Melon, M. Iché-Torres, and S. Birman (2011). "Involvement of the Drosophila taurine/aspartate transporter dEAAT2 in selective olfactory and gustatory perceptions". In: *Journal of Comparative Neurology* 519.14, pp. 2734–2757.

Besson, M. T., D. B. Ré, M. Moulin, and S. Birman (2005). "High affinity transport of taurine by the Drosophila aspartate transporter dEAAT2". In: *Journal of Biological Chemistry* 280.8, pp. 6621–6626.

Besson, M. T., L. Soustelle, and S. Birman (2000). "Selective high-affinity transport of aspartate by a Drosophila homologue of the excitatory amino-acid transporters". In: *Current Biology* 10.4, pp. 207–210.

Bewick, G. A., W. S. Dhillo, S. J. Darch, K. G. Murphy, J. V. Gardiner, P. H. Jethwa, M. K. Wing, M. A. Ghatei, and S. R. Bloom (2005). "Hypothalamic cocaine- and amphetamine-regulated transcript (CART) and agouti-related protein (AgRP) neurons coexpress the NOP1 receptor and nociceptin alters CART and AgRP release". In: *Endocrinology* 146.8, pp. 3526–3534.

Bicker, G., S. Schäfer, O. P. Ottersen, and J. Storm-Mathisen (1988). "Glutamate-like immunoreactivity in identified neuronal populations of insect nervous systems." In: *The Journal of neuroscience : the official journal of the Society for Neuroscience* 8.6, pp. 2108–2122.

Bicker, G. (1991). "Taurine-like immunoreactivity in photoreceptor cells and mushroom bodies: a comparison of the chemical architecture of insect nervous systems". In: *Brain Research* 560.1-2, pp. 201–206.

— (1999). "Histochemistry of classical neurotransmitters in antennal lobes and mushroom bodies of the honeybee". In: *Microscopy Research and Technique* 45.3, pp. 174–183.

Blake, A. D., N. M. Anthony, H. H. Chen, J. B. Harrison, N. M. Nathanson, and D. B. Sattelle (1993). "Drosophila nervous system muscarinic acetylcholine receptor: transient functional expression and localization by immunocytochemistry." In: *Molecular pharmacology* 44.4, pp. 716–724.

Blenau, W., S. Daniel, S. Balfanz, M. Thamm, and A. Baumann (2017). "Dm5-HT2B: Pharmacological Characterization of the Fifth Serotonin Receptor Subtype of Drosophila melanogaster". In: *Frontiers in Systems Neuroscience* 11.May, p. 28.

Blenau, W. and M. Thamm (2011). "Distribution of serotonin (5-HT) and its receptors in the insect brain with focus on the mushroom bodies. Lessons from Drosophila melanogaster and Apis mellifera". In: *Arthropod Structure and Development* 40.5, pp. 381–394.

Bliek, A. M. van der and E. M. Meyerowitz (1991). "Dynamin-like protein encoded by the Drosophila shibire gene associated with vesicular traffic." In: *Nature* 351.6325, pp. 411–414.

Bliss, T. V. P. and T. Lømo (1973). "Long-lasting potentiation of synaptic transmission in the dentate area of the anaesthetized rabbit following stimulation of the perforant path". In: *The Journal of Physiology* 232.2, pp. 331–356.

Boccaletto, P. (2013). "The marine flatworm Macrostomum lignano as model for nervous system regeneration: role of pro neural genes in the CNS". PhD thesis.

Boppana, S., N. Kendall, O. Akinrinsola, D. White, K. Patel, and H. Lawal (2017). "Immunolocalization of the vesicular acetylcholine transporter in larval and adult Drosophila neurons". In: *Neuroscience Letters* 643, pp. 76–83.

Bosher, J. M., P. Dufourcq, S. Sookhareea, and M. Labouesse (1999). "RNA interference can target pre-mRNA: Consequences for gene expression in a Caenorhabditis elegans operon". In: *Genetics* 153.3, pp. 1245–1256.

Boto, T., T. Louis, K. Jindachomthong, K. Jalink, and S. M. Tomchik (2014). "Dopaminergic Modulation of cAMP Drives Nonlinear Plasticity across the Drosophila Mushroom Body Lobes". In: *Current Biology* 24.8, pp. 822–831.

Bouton, M. E. (1993). "Context, time, and memory retrieval in the interference paradigms of Pavlovian learning." In: *Psychological bulletin* 114.1, p. 80.

Boutros, M. and J. Ahringer (2008). "The art and design of genetic screens: RNA interference." In: *Nature Reviews Genetics* 9.7, pp. 554–566.

Bouzaiane, E., S. Trannoy, L. Scheunemann, P.-Y. Plaçais, and T. Preat (2015). "Two Independent Mushroom Body Output Circuits Retrieve the Six Discrete Components of Drosophila Aversive Memory". In: *Cell Reports* 11.8, pp. 1280–1292.

Boycott, B. B. (1960). "The functional organization of the brain of the cuttlefish Sepia officinalis". In: *Proceedings of the Royal Society B: Biological Sciences* 153.20, pp. 503–534.

Boyden, E. S. (2015). "Optogenetics and the future of neuroscience." In: *Nature neuroscience* 18.9, pp. 1200–1.

Boyden, E. S., F. Zhang, E. Bamberg, G. Nagel, and K. Deisseroth (2005). "Millisecond-timescale, genetically targeted optical control of neural activity." In: *Nature neuroscience* 8.9, pp. 1263–8.

Boynton, S. and T. Tully (1992). "latheo, a new gene involved in associative learning and memory in Drosophila melanogaster, identified from P element mutagenesis". In: *Genetics* 131.3, pp. 655–672.

Bradford, S. E. and J. V. Nadler (2004). "Aspartate release from rat hippocampal synaptosomes". In: *Neuroscience* 128.4, pp. 751–765.

Brake, A. J., M. J. Wagenbach, and D. Julius (1994). *New structural motif for ligand-gated ion channels defined by an ionotropic ATP receptor.*

Brand, A. H. and N. Perrimon (1993). "Targeted gene expression as a means of altering cell fates and generating dominant phenotypes." In: *Development (Cambridge, England)* 118.2, pp. 401–15.

Bravo, D. T., N. G. Kolmakova, and S. M. Parsons (2004). "Choline is transported by vesicular acetylcholine transporter". In: *Journal of Neurochemistry* 91.3, pp. 766–768.

Breer, H. (1987). "Neurochemical aspects of cholinergic synapses in the insect brain". In: *Arthropod brain: its evolution, development, structure and functions.* New York: Wiley, pp. 415–437.

Brembs, B., F. Christiansen, H. J. Pfluger, and C. Duch (2007). "Flight Initiation and Maintenance Deficits in Flies with Genetically Altered Biogenic Amine Levels". In: *Journal of Neuroscience* 27.41, pp. 11122–11131.

Brightman, M. W. and R. W. Albers (1959). "Species differences in the distribution of extraneuronal cholinesterases within the vertebrate central nervous system." In: *Journal of neurochemistry* 4.3, pp. 244–50.

Brody, T. and A. Cravchik (2000). "Drosophila melanogaster G protein-coupled receptors." In: *The Journal of Cell Biology* 150.2, F83–F88.

Broeck, J. V. (2001). "Insect G protein-coupled receptors and signal transduction". In: *Archives of Insect Biochemistry and Physiology* 48.1, pp. 1–12.

Brooks, E. S., C. L. Greer, R. Romero-Calderón, C. N. Serway, A. Grygoruk, J. M. Haimovitz, B. T. Nguyen, R. Najibi, C. J. Tabone, J. S. de Belle, and D. E. Krantz (2011). "A putative vesicular transporter expressed in Drosophila mushroom bodies that mediates sexual behavior may define a neurotransmitter system." In: *Neuron* 72.2, pp. 316–29.

Brotz, T. M., B. Bochenek, K. Aronstein, R. H. Ffrench-Constant, and A. Borst (1997). "gamma-Aminobutyric acid receptor distribution in the mushroom bodies of a fly (Calliphora erythrocephala): a functional subdivision of Kenyon cells?" In: *The Journal of comparative neurology* 383.1, pp. 42–8.

Brown, J. E., L. B. Cohen, P. De Weer, L. H. Pinto, W. N. Ross, and B. M. Salzberg (1975). "Rapid changes in intracellular free calcium concentration. Detection by metallochromic indicator dyes in squid giant axon." In: *Biophysical journal* 15.11, pp. 1155–60.

Brown, M. R., J. W. Crim, R. C. Arata, H. N. Cai, C. Chun, and P. Shen (1999). "Identification of a Drosophila brain-gut peptide related to the neuropeptide Y family". In: *Peptides* 20.9, pp. 1035–1042.

Browning, K. N. and R. A. Travagli (2003). "Neuropeptide Y and Peptide YY Inhibit Excitatory Synaptic Transmission in the Rat Dorsal Motor Nucleus of the Vagus". In: *The Journal of Physiology* 549.3, pp. 775–785.

Brunelli, M., V. Castellucci, and E. Kandel (1976). "Synaptic facilitation and behavioral sensitization in Aplysia: possible role of serotonin and cyclic AMP". In: *Science* 194.4270, pp. 1178–1181.

Buchner, E., S. Buchner, M. G. Burg, A. Hofbauer, W. L. Pak, and I. Pollack (1993). "Histamine is a major mechanosensory neurotransmitter candidate in Drosophila melanogaster". In: *Cell and Tissue Research* 273.1, pp. 119–125.

Buchner, E., S. Buchner, G. Crawford, W. Mason, P. Salvaterra, and D. Sattelle (1986). "Choline acetyltransferase-like immunoreactivity in the brain of Drosophila melanogaster". In: *Cell and Tissue Research* 246.1, pp. 57–62.

Burg, M. G., P. V. Sarthy, G. Koliantz, and W. L. Pak (1993). "Genetic and molecular identification of a Drosophila histidine decarboxylase gene required in photoreceptor transmitter synthesis." In: *The EMBO journal* 12.3, pp. 911–9.

Burgos-Robles, A., I. Vidal-Gonzalez, E. Santini, and G. J. Quirk (2007). "Consolidation of Fear Extinction Requires NMDA Receptor-Dependent Bursting in the Ventromedial Prefrontal Cortex". In: *Neuron* 53.6, pp. 871–880.

Burke, C. J., W. Huetteroth, D. Owald, E. Perisse, M. J. Krashes, G. Das, D. Gohl, M. Silies, S. Certel, S. Waddell, J. Michael, G. Das, D. Gohl, M. Silies, and S. Certel (2012). "Layered reward signalling through octopamine and dopamine in Drosophila". In: *Nature* 492.7429, pp. 433–7.

Burke, C. J. and S. Waddell (2011). "Remembering nutrient quality of sugar in Drosophila." In: *Current Biology* 21.9, pp. 746–50.

Busch, S., M. Selcho, K. Ito, and H. Tanimoto (2009). "A map of octopaminergic neurons in the Drosophila brain". In: *The Journal of Comparative Neurology* 513.6, pp. 643–667.

Butcher, N. J., A. B. Friedrich, Z. Lu, H. Tanimoto, and I. A. Meinertzhagen (2012). "Different classes of input and output neurons reveal new features in microglomeruli of the adult Drosophila mushroom body calyx". In: *Journal of Comparative Neurology* 520.10, pp. 2185–2201.

Byers, D., R. L. Davis, and J. a. Kiger (1981). "Defect in cyclic AMP phosphodiesterase due to the dunce mutation of learning in Drosophila melanogaster". In: *Nature* 289.5793, pp. 79–81.

Byrne, J. H. and E. R. Kandel (1996). "Presynaptic facilitation revisited: state and time dependence." In: *The Journal of neuroscience* 16.2, pp. 425–435.

Campbell, R. A. A., K. S. Honegger, H. Qin, W. Li, E. Demir, and G. C. Turner (2013). "Imaging a population code for odor identity in the Drosophila mushroom body." In: *The Journal of neuroscience : the official journal of the Society for Neuroscience* 33.25, pp. 10568–81.

Campistron, G., R. M. Buijs, and M. Geffard (1986). "Specific antibodies against aspartate and their immunocytochemical application in the rat brain". In: *Brain Research* 365.1, pp. 179–184.

Cao, G., J. Platisa, V. a. Pieribone, D. Raccuglia, M. Kunst, and M. N. Nitabach (2013). "Genetically targeted optical electrophysiology in intact neural circuits." In: *Cell* 154.4, pp. 904–13.

Carlsson, M. A., M. Diesner, J. Schachtner, and D. R. Nässel (2010). "Multiple neuropeptides in the drosophila antennal lobe suggest complex modulatory circuits". In: *Journal of Comparative Neurology* 518.16, pp. 3359–3380.

Caron, S. J. C., V. Ruta, L. F. Abbott, and R. Axel (2013). "Random convergence of olfactory inputs in the Drosophila mushroom body." In: *Nature* 497.7447, pp. 113–7.

Cash, F., S. W. Vernon, P. Phelan, J. Goodchild, and R. A. Baines (2016). "Central cholinergic synaptic vesicle loading obeys the set-point model in Drosophila". In: *Journal of Neurophysiology* 115.2, pp. 843–850.

Cassenaer, S. and G. Laurent (2007). "Hebbian STDP in mushroom bodies facilitates the synchronous flow of olfactory information in locusts." In: *Nature* 448.7154, pp. 709–13.

Castellucci, V. F. and E. R. Kandel (1974). "A quantal analysis of the synaptic depression underlying habituation of the gill-withdrawal reflex in Aplysia." In: *Proceedings of the National Academy of Sciences of the United States of America* 71.12, pp. 5004–8.

Cayre, M., S. D. Buckingham, S. Yagodin, and D. B. Sattelle (1999). "Cultured insect mushroom body neurons express functional receptors for acetylcholine, GABA, glutamate, octopamine, and dopamine." In: *Journal of neurophysiology* 81.1, pp. 1–14.

Cazzamali, G., D. A. Klaerke, and C. J. P. Grimmelikhuijzen (2005). "A new family of insect tyramine receptors". In: *Biochemical and Biophysical Research Communications* 338.2, pp. 1189–1196.

Cervantes-Sandoval, I. and R. L. Davis (2012). "Distinct traces for appetitive versus aversive olfactory memories in DPM neurons of Drosophila." In: *Current Biology* 22.13, pp. 1247–52.

Cervantes-Sandoval, I., A. Martin-Pena, J. A. Berry, and R. L. Davis (2013). "System-Like Consolidation of Olfactory Memories in Drosophila". In: *Journal of Neuroscience* 33.23, pp. 9846–9854.

Cervantes-Sandoval, I., A. Phan, M. Chakraborty, and R. L. Davis (2017). "Reciprocal synapses between mushroom body and dopamine neurons form a positive feedback loop required for learning". In: *eLife* 6, pp. 1–16.

Chalfie, M., Y. Tu, G. Euskirchen, W. Ward, and D. Prasher (1994). "Green fluorescent protein as a marker for gene expression". In: *Science* 263.5148, pp. 802–805.

Chamaon, K., R. Schulz, S. Bertrand, K. H. Smalla, E. D. Gundelfinger, and D. Bertrand (2000). "Neuronal nicotinic acetylcholine receptors from Drosophila: two different types of alpha subunits coassemble within the same receptor complex." In: *Journal of neurochemistry* 74.6, pp. 2537–46.

Chamaon, K., K. H. Smalla, U. Thomas, and E. D. Gundelfinger (2002). "Nicotinic acetylcholine receptors of Drosophila: Three subunits encoded by genomically linked genes can co-assemble into the same receptor complex". In: *Journal of Neurochemistry* 80, pp. 149–157.

Chang, C. Y., G. R. Esber, Y. Marrero-Garcia, H.-J. Yau, A. Bonci, and G. Schoenbaum (2016). "Brief optogenetic inhibition of dopamine neurons mimics endogenous negative reward prediction errors." In: *Nature neuroscience* 19.1, pp. 111–6.

Chen, C.-C., J.-K. Wu, H.-W. Lin, T.-P. Pai, T.-F. Fu, C.-L. Wu, T. Tully, and A.-S. Chiang (2012). "Visualizing long-term memory formation in two neurons of the Drosophila brain." In: *Science* 335.6069, pp. 678–85.

Chen, J., W. Reiher, C. Hermann-Luibl, A. Sellami, P. Cognigni, S. Kondo, C. Helfrich-Förster, J. A. Veenstra, and C. Wegener (2016). "Allatostatin A Signalling in Drosophila Regulates Feeding and Sleep and Is Modulated by PDF". In: *PLoS Genetics* 12.9, pp. 1–33.

Chen, M. S., R. a. Obar, C. C. Schroeder, T. W. Austin, C. a. Poodry, S. C. Wadsworth, and R. B. Vallee (1991). "Multiple forms of dynamin are encoded by shibire, a Drosophila gene involved in endocytosis." In: *Nature* 351.6327, pp. 583–586.

Chen, T.-W., T. J. Wardill, Y. Sun, S. R. Pulver, S. L. Renninger, A. Baohan, E. R. Schreiter, R. a. Kerr, M. B. Orger, V. Jayaraman, L. L. Looger, K. Svoboda, and D. S. Kim (2013a). "Ultrasensitive fluorescent proteins for imaging neuronal activity." In: *Nature* 499.7458, pp. 295–300.

Chen, W., W. Shi, L. Li, Z. Zheng, T. Li, W. Bai, and Z. Zhao (2013b). "Regulation of sleep by the short neuropeptide F (sNPF) in Drosophila melanogaster". In: *Insect Biochemistry and Molecular Biology* 43.9, pp. 809–819.

Cheng, Y., K. Endo, K. Wu, A. R. Rodan, U. Heberlein, and R. L. Davis (2001). "Drosophila fasciclin II is required for the formation of odor memories and for normal sensistivity to ethanol". In: *Cell* 105, pp. 757–768.

Choi, C., G. Cao, A. K. Tanenhaus, E. v. McCarthy, M. Jung, W. Schleyer, Y. Shang, M. Rosbash, J. C. P. Yin, and M. N. Nitabach (2012). "Autoreceptor Control of Peptide/Neurotransmitter Corelease from PDF Neurons Determines Allocation of Circadian Activity in Drosophila". In: *Cell Reports* 2.2, pp. 332–344.

Christiansen, F., C. Zube, T. F. M. Andlauer, C. Wichmann, W. Fouquet, D. Owald, S. Mertel, F. Leiss, G. Tavosanis, A. J. F. Luna, A. Fiala, and S. J. Sigrist (2011). "Presynapses in Kenyon cell dendrites in the mushroom body calyx of Drosophila." In: *The Journal of neuroscience : the official journal of the Society for Neuroscience* 31.26, pp. 9696–707.

Claridge-Chang, A., R. D. Roorda, E. Vrontou, L. Sjulson, H. Li, J. Hirsh, and G. Miesenböck (2009). "Writing memories with light-addressable reinforcement circuitry." In: *Cell* 139.2, pp. 405–15.

Clark, J. T., P. S. Kalra, W. R. Crowley, and S. P. Kalra (1984). "Neuropeptide Y and human Pancreatic polypeptide stimulate feeding behavior in rats". In: *Endocrinology* 115.1, pp. 427–429.

Coates, K. E., A. T. Majot, X. Zhang, C. T. Michael, S. L. Spitzer, Q. Gaudry, and A. M. Dacks (2017). "Identified Serotonergic Modulatory Neurons Have Heterogeneous Synaptic Connectivity within the Olfactory System of Drosophila". In: *The Journal of Neuroscience* 37.31, pp. 7318–7331.

Cohn, R., I. Morantte, and V. Ruta (2015). "Coordinated and Compartmentalized Neuromodulation Shapes Sensory Processing in Drosophila". In: *Cell* 163.7, pp. 1742–1755.

Cole, S. H., G. E. Carney, C. A. McClung, S. S. Willard, B. J. Taylor, and J. Hirsh (2005). "Two functional but noncomplementing Drosophila tyrosine decarboxylase genes: Distinct roles for neural tyramine and octopamine in female fertility". In: *Journal of Biological Chemistry* 280.15, pp. 14948–14955.

Collin, C., F. Hauser, E. G. De Valdivia, S. Li, J. Reisenberger, E. M. M. Carlsen, Z. Khan, N. O. Hansen, F. Puhm, L. Søndergaard, J. Niemiec, M. Heninger, G. R. Ren, and C. J. P. Grimmelikhuijzen (2013). "Two types of muscarinic acetylcholine receptors in Drosophila and other arthropods". In: *Cellular and Molecular Life Sciences* 70, pp. 3231–3242.

Colmers, W. F., G. J. Klapstein, a. Fournier, S. St-Pierre, and K. a. Treherne (1991). "Presynaptic inhibition by neuropeptide Y in rat hippocampal slice in vitro is mediated by a Y2 receptor." In: *British journal of pharmacology* 102.1, pp. 41–44.

Colmers, W. F., K. Lukowiak, and Q. J. Pittman (1988). "Neuropeptide Y action in the rat hippocampal slice: site and mechanism of presynaptic inhibition." In: *The Journal of neuroscience : the official journal of the Society for Neuroscience* 8.10, pp. 3827–3837.

Colomb, J., L. Kaiser, M. A. Chabaud, and T. Preat (2009). "Parametric and genetic analysis of Drosophila appetitive long-term memory and sugar motivation". In: *Genes, Brain and Behavior* 8.4, pp. 407–415.

Connolly, J. B., I. J. Roberts, J. D. Armstrong, K. Kaiser, M. Forte, T. Tully, and C. J. O'Kane (1996). "Associative learning disrupted by impaired Gs signaling in Drosophila mushroom bodies." In: *Science (New York, N.Y.)* 274.5295, pp. 2104–7.

Coons, A. H., H. J. Creech, and N. R. Jones (1941). "Immunological properties of an antibody containing a fluorescent group." In: *Proceedings of the Society ...* 47, pp. 200–202.

Cormack, B. P., R. H. Valdivia, and S. Falkow (1996). "FACS-optimized mutants of the green fluorescent protein (GFP)". In: *Gene* 173.1, pp. 33–38.

Couto, A., M. Alenius, and B. J. Dickson (2005). "Molecular, Anatomical, and Functional Organization of the Drosophila Olfactory System". In: *Current Biology* 15.17, pp. 1535–1547.

Crawford, G., J. R. Slemmon, and P. M. Salvaterra (1982). "Monoclonal antibodies selective for Drosophila melanogaster choline acetyltransferase." In: *Journal of Biological Chemistry* 257.7, pp. 3853–3856.

Crittenden, J. and E. M. Skoulakis (1998). "Tripartite mushroom body architecture revealed by antigenic markers". In: *Learning & Memory* 5, pp. 38–51.

Crocker, A., X.-J. Guan, C. T. Murphy, and M. Murthy (2016). "Cell-Type-Specific Transcriptome Analysis in the Drosophila Mushroom Body Reveals Memory-Related Changes in Gene Expression". In: *Cell Reports* 15.7, pp. 1580–1596.

Crocker, A. and A. Sehgal (2008). "Octopamine Regulates Sleep in Drosophila through Protein Kinase A-Dependent Mechanisms". In: *Journal of Neuroscience* 28.38, pp. 9377–9385.

Cully, D. F., P. S. Paress, K. K. Liu, J. M. Schaeffer, and J. P. Arena (1996). "Identification of a Drosophila melanogaster glutamate-gated chloride channel sensitive to the antiparasitic agent avermectin". In: *Journal of Biological Chemistry* 271.33, pp. 20187–20191.

Curtis, D. R. and J. C. Watkins (1960). "The Excitation and Depression of Spinal Neurones by Structurally Related Amino Acids". In: *Journal of Neurochemistry* 6.2, pp. 117–141.

— (1965). "The pharmacology of amino acids related to gamma-aminobutyric acid". In: *Pharmacological Reviews* 17.4, pp. 347–391.

Dacher, M., A. Lagarrigue, and M. Gauthier (2005). "Antennal tactile learning in the honeybee: Effect of nicotinic antagonists on memory dynamics". In: *Neuroscience* 130.1, pp. 37–50.

Dale, M., J. Ritter, R. Fowler, and H. Rang (2008). *Rang and Dale's Pharmacology.* 6th ed. Churchill Livingstone.

Daly, J. W. (2005). "Nicotinic agonists, antagonists, and modulators from natural sources". In: *Cellular and Molecular Neurobiology* 25.June, pp. 513–552.

Dana, H., B. Mohar, Y. Sun, S. Narayan, A. Gordus, J. P. Hasseman, G. Tsegaye, G. T. Holt, A. Hu, D. Walpita, R. Patel, J. J. Macklin, C. I. Bargmann, M. B. Ahrens, E. R. Schreiter, V. Jayaraman, L. L. Looger, K. Svoboda, and D. S. Kim (2016). "Sensitive red protein calcium indicators for imaging neural activity". In: *eLife* 5.

Daniels, R. W., C. A. Collins, K. Chen, M. V. Gelfand, D. E. Featherstone, and A. DiAntonio (2006). "A single vesicular glutamate transporter is sufficient to fill a synaptic vesicle". In: *Neuron* 49.1, pp. 11–16.

Daniels, R. W., C. A. Collins, M. V. Gelfand, J. Dant, E. S. Brooks, D. E. Krantz, and A. DiAntonio (2004). "Increased expression of the Drosophila vesicular glutamate transporter leads to excess glutamate release and a compensatory decrease in quantal content." In: *The Journal of neuroscience : the official journal of the Society for Neuroscience* 24.46, pp. 10466–74.

Daniels, R. W., M. V. Gelfand, C. a. Collins, and A. DiAntonio (2008). "Visualizing glutamatergic cell bodies and synapses in Drosophila larval and adult CNS." In: *The Journal of comparative neurology* 508.1, pp. 131–52.

Davison, A. and L. Kaczmarek (1971). "Taurine - a Possible Neurotransmitter?" In: *Nature* 234, pp. 107–108.

Dawydow, A., R. Gueta, D. Ljaschenko, S. Ullrich, M. Hermann, N. Ehmann, S. Gao, A. Fiala, T. Langenhan, G. Nagel, and R. J. Kittel (2014). "Channelrhodopsin-2-XXL, a powerful optogenetic tool for low-light applications." In: *Proceedings of the National Academy of Sciences of the United States of America* 111.38, pp. 13972–7.

De Biasi, M. and J. A. Dani (2011). "Reward, addiction, withdrawal to nicotine." In: *Annual review of neuroscience* 34, pp. 105–30.

De Bono, M. and C. I. Bargmann (1998). "Natural variation in a neuropeptide Y receptor homolog modifies social behavior and food response in C. elegans". In: *Cell* 94.5, pp. 679–689.

Deisseroth, K. (2011). "Optogenetics." In: *Nature methods* 8.1, pp. 26–29.
Demmer, H. and P. Kloppenburg (2009). "Intrinsic Membrane Properties and Inhibitory Synaptic Input of Kenyon Cells as Mechanisms for Sparse Coding?" In: *Journal of Neurophysiology* 102.3, pp. 1538–1550.
Denk, W., J. H. Strickler, and W. W. Webb (1990). "Two-photon laser scanning fluorescence microscopy." In: *Science (New York, N.Y.)* 248.4951, pp. 73–6.
DeZazzo, J., D. Sandstrom, S. de Belle, K. Velinzon, P. Smith, L. Grady, M. DelVecchio, M. Ramaswami, and T. Tully (2000). "nalyot, a mutation of the Drosophila myb-related Adf1 transcription factor, disrupts synapse formation and olfactory memory." In: *Neuron* 27.1, pp. 145–58.
DeZazzo, J. and T. Tully (1995). "Dissection of memory formation: from behavioral pharmacology to molecular genetics". In: *Trends in Neurosciences* 18.5, pp. 212–218.
Díaz-Mataix, L., R. C. Ruiz Martinez, G. E. Schafe, J. E. Ledoux, and V. Doyère (2013). "Detection of a temporal error triggers reconsolidation of amygdala-dependent memories". In: *Current Biology* 23.6, pp. 467–472.
Diegelmann, S., M. Bate, and M. Landgraf (2008). "Gateway cloning vectors for the LexA-based binary expression system in drosophila". In: *Fly* 2.4, pp. 236–239.
Dietzl, G., D. Chen, F. Schnorrer, K.-C. Su, Y. Barinova, M. Fellner, B. Gasser, K. Kinsey, S. Oppel, S. Scheiblauer, A. Couto, V. Marra, K. Keleman, and B. J. Dickson (2007). "A genome-wide transgenic RNAi library for conditional gene inactivation in Drosophila." In: *Nature* 448.7150, pp. 151–6.
Dolan, M.-J., G. Belliart-Guerin, Y. Aso, A. S. Bates, S. Frechter, A. Wong, A. Hammad, G. M. Rubin, T. Preat, P.-Y. Placais, and G. S. X. E. Jefferis (2017). "Memory retrieval recruits both innate and learned olfactory processing centres in Drosophila". In: *bioRxiv*.
Drasdo, A., M. Caulfield, D. Bertrand, S. Bertrand, and S. Wonnacott (1992). "Methyl lycaconitine: A novel nicotinic antagonist". In: *Molecular and Cellular Neuroscience* 3.3, pp. 237–243.
DRSC/TRiP Functional Genomics Resources (2017). *Using TRiP lines*. URL: `https://fgr.hms.harvard.edu/using-trip-lines-0` (visited on 05/09/2017).
Dubnau, J., L. Grady, T. Kitamoto, and T. Tully (2001). "Disruption of neurotransmission in Drosophila mushroom body blocks retrieval but not acquisition of memory." In: *Nature* 411.May, pp. 476–480.
Dubnau, J., A.-S. Chiang, L. Grady, J. Barditch, S. Gossweiler, J. McNeil, P. Smith, F. Buldoc, R. Scott, U. Certa, C. Broger, and T. Tully (2003). "The staufen/pumilio pathway is involved in Drosophila long-term memory." In: *Current Biology* 13.4, pp. 286–296.
Dudai, Y. and A. Amsterdam (1977). "Nicotinic receptors in the brain of Drosophila melanogaster demonstrated by autoradiography with [125I]alpha-bungarotoxin". In: *Brain Res* 130.3, pp. 551–555.
Dudai, Y. (1977a). "Demonstration of an alpha-bungarotoxin-binding nicotinic receptor in flies." In: *FEBS letters* 76.2, pp. 211–213.
— (1977b). "Properties of learning and memory in Drosophila melanogaster". In: *Journal of Comparative Physiology A* 114.1, pp. 69–89.
— (2006). "Reconsolidation: the advantage of being refocused". In: *Current Opinion in Neurobiology* 16.2, pp. 174–178.

Dudai, Y., Y. N. Jan, D. Byers, W. G. Quinn, and S. Benzer (1976). "dunce, a mutant of Drosophila deficient in learning". In: *Proceedings of the National Academy of Sciences of the United States of America* 73.5, pp. 1684–1688.

Dujardin, F. (1850). "Mémoire sur le système nerveux des insectes". In: *Ann Sci Nat Zool* 14, pp. 195–206.

Dura, J. M., T. Preat, and T. Tully (1993). "Identification of linotte, a new gene affecting learning and memory in Drosophila melanogaster." In: *Journal of neurogenetics* 9.1, pp. 1–14.

Dürrnagel, S., A. Kuhn, C. D. Tsiairis, M. Williamson, H. Kalbacher, C. J. P. Grimmelikhuijzen, T. W. Holstein, and S. Gründer (2010). "Three homologous subunits form a high affinity peptide-gated ion channel in Hydra". In: *Journal of Biological Chemistry* 285.16, pp. 11958–11965.

Dzitoyeva, S., N. Dimitrijevic, and H. Manev (2003). "Gamma-aminobutyric acid B receptor 1 mediates behavior-impairing actions of alcohol Drosophila: adult RNA interference and pharmacological evidence." In: *Proceedings of the National Academy of Sciences of the United States of America* 100.9, pp. 5485–5490.

Edenfeld, G., T. Stork, and C. Klämbt (2005). "Neuron-glia interaction in the insect nervous system". In: *Current Opinion in Neurobiology* 15.1, pp. 34–39.

Eichler, K., F. Li, A. Litwin-Kumar, Y. Park, I. Andrade, C. M. Schneider-Mizell, T. Saumweber, A. Huser, C. Eschbach, B. Gerber, R. D. Fetter, J. W. Truman, C. E. Priebe, L. F. Abbott, A. S. Thum, M. Zlatic, and A. Cardona (2017). "The complete connectome of a learning and memory centre in an insect brain". In: *Nature* 548.7666, pp. 175–182.

Ellender, T. J. and O. Paulsen (2010). "The many tunes of perisomatic targeting interneurons in the hippocampal network". In: *Frontiers in Cellular Neuroscience* 4.July, p. 26.

Enell, L., Y. Hamasaka, A. Kolodziejczyk, and D. R. Nässel (2007). "γ-Aminobutyric acid (GABA) signaling components in Drosophila : Immunocytochemical localization of GABA B receptors in relation to the GABA A receptor subunit RDL and a vesicular GABA transporter". In: *The Journal of Comparative Neurology* 505.1, pp. 18–31.

Erber, J., T. H. Masuhr, and R. Menzel (1980). "Localization of short-term memory in the brain of the bee, Apis mellifera". In: *Physiological Entomology* 5.4, pp. 343–358.

Erickson, J. C., G. Hollopeter, and R. D. Palmiter (1996). "Attenuation of the obesity syndrome of ob/ob mice by the loss of neuropeptide Y." In: *Science (New York, N.Y.)* 274.5293, pp. 1704–1707.

Estes, W. K. and B. F. Skinner (1941). "Some quantitative properties of anxiety." In: *Journal of Experimental Psychology* 29.5, pp. 390–400.

Evans, R. J., V. Derkach, and A. Surprenant (1992). "ATP mediates fast synaptic transmission in mammalian neurons." In: *Nature* 357.6378, pp. 503–505.

Farris, S. M. and N. J. Strausfeld (2001). "Development of laminar organization in the mushroom bodies of the cockroach: Kenyon cell proliferation, outgrowth, and maturation". In: *Journal of Comparative Neurology* 439.3, pp. 331–351.

Fayyazuddin, A., M. a. Zaheer, P. R. Hiesinger, and H. J. Bellen (2006). "The nicotinic acetylcholine receptor Da7 is required for an escape behavior in Drosophila". In: *PLoS Biology* 4.3, pp. 0420–0431.

Featherstone, D. E., E. Rushton, J. Rohrbough, F. Liebl, J. Karr, Q. Sheng, C. K. Rodesch, and K. Broadie (2005). "An essential Drosophila glutamate receptor subunit that functions in both central neuropil and neuromuscular junction." In: *The*

Journal of neuroscience : the official journal of the Society for Neuroscience 25.12, pp. 3199–208.

Felsenberg, J., O. Barnstedt, P. Cognigni, S. Lin, and S. Waddell (2017). "Re-evaluation of learned information in Drosophila". In: *Nature* 544.7649, pp. 240–244.

Felsenberg, J. and S. Waddell (2017). "Neural Networks for a Reward System in Drosophila". In: *Learning and Memory: A Comprehensive Reference*. Third Edit. Elsevier, pp. 505–522.

Feng, G., V. Reale, H. Chatwin, K. Kennedy, R. Venard, C. Ericsson, K. Yu, P. D. Evans, and L. M. Hall (2003). "Functional characterization of a neuropeptide F-like receptor from Drosophila melanogaster". In: *European Journal of Neuroscience* 18.2, pp. 227–238.

Ferguson, S. M. and R. D. Blakely (2004). "The choline transporter resurfaces: new roles for synaptic vesicles?" In: *Molecular interventions* 4.1, pp. 22–37.

Ferguson, S. M., V. Savchenko, S. Apparsundaram, M. Zwick, J. Wright, C. J. Heilman, H. Yi, A. I. Levey, and R. D. Blakely (2003). "Vesicular localization and activity-dependent trafficking of presynaptic choline transporters." In: *The Journal of neuroscience : the official journal of the Society for Neuroscience* 23.30, pp. 9697–9709.

Ferris, J., H. Ge, L. Liu, and G. Roman (2006). "G(o) signaling is required for Drosophila associative learning". In: *Nature Neuroscience* 9.8, pp. 1036–1040.

Ffrench-Constant, R. H., T. A. Rocheleau, J. C. Steichen, and A. E. Chalmers (1993). "A point mutation in a Drosophila GABA receptor confers insecticide resistance." In: *Nature* 363.6428, pp. 449–51.

Fire, A., S. Xu, M. K. Montgomery, S. A. Kostas, S. E. Driver, and C. C. Mello (1998). "Potent and specific genetic interference by double-stranded RNA in Caenorhabditis elegans". In: *Nature* 391.6669, pp. 806–811.

Fisahn, A., F. G. Pike, E. H. Buhl, and O. Paulsen (1998). "Cholinergic induction of network oscillations at 40 Hz in the hippocampus in vitro". In: *Nature* 394.6689, pp. 186–189.

Fischer, J., E. Giniger, T. Maniatis, and M. Ptashne (1988). "GAL4 activates transcription in Drosophila". In: *Nature* 332.April, pp. 853–856.

Fleck, M. W., D. a. Henze, G. Barrionuevo, and a. M. Palmer (1993). "Aspartate and glutamate mediate excitatory synaptic transmission in area CA1 of the hippocampus." In: *The Journal of neuroscience : the official journal of the Society for Neuroscience* 13.September, pp. 3944–3955.

FlyBase (1992). *FlyBase curation.* URL: `http://flybase.org/reports/FBgn0036975.html`.

Folkers, E., P. Drain, and W. G. Quinn (1993). "Radish, a Drosophila mutant deficient in consolidated memory." In: *Proceedings of the National Academy of Sciences of the United States of America* 90.17, pp. 8123–7.

Freeman, E. G., Z. Wisotsky, and A. Dahanukar (2014). "Detection of sweet tastants by a conserved group of insect gustatory receptors". In: *Proceedings of the National Academy of Sciences* 111.4, pp. 1598–1603.

Freeman, M. R., J. Delrow, J. Kim, E. Johnson, and C. Q. Doe (2003). "Unwrapping glial biology: Gcm target genes regulating glial development, diversification, and function". In: *Neuron* 38.4, pp. 567–580.

Frenkel, L., N. I. Muraro, A. N. Beltrán González, M. S. Marcora, G. Bernabó, C. Hermann-Luibl, J. I. Romero, C. Helfrich-Förster, E. M. Castaño,

C. Marino-Busjle, D. J. Calvo, and M. F. Ceriani (2017). "Organization of Circadian Behavior Relies on Glycinergic Transmission". In: *Cell Reports* 19.1, pp. 72–85.

Friggi-Grelin, F., H. Coulom, M. Meller, D. Gomez, J. Hirsh, and S. Birman (2003). "Targeted gene expression in Drosophila dopaminergic cells using regulatory sequences from tyrosine hydroxylase". In: *Journal of Neurobiology* 54.4, pp. 618–627.

Frontali, N. (1964). "Brain glutamic acid decarboxylase and synthesis of amino-butyric acid in vertebrate and invertebrate species". In: *Comparative Neurochemistry*. Ed. by D. Richter, pp. 185–192.

Fu, H., J. Dou, W. Li, J. Luo, K. C. Li, C. S. C. Lam, N. T. K. Lee, M. Li, and Y. Han (2008). "Mecamylamine prevents neuronal apoptosis induced by glutamate and low potassium via differential anticholinergic-independent mechanisms". In: *Neuropharmacology* 54.4, pp. 755–765.

Fujii, S., A. Yavuz, J. Slone, C. Jagge, X. Song, and H. Amrein (2015). "Drosophila sugar receptors in sweet taste perception, olfaction, and internal nutrient sensing". In: *Current Biology* 25.5, pp. 621–627.

Galili, D. S., K. V. Dylla, A. Lüdke, A. B. Friedrich, N. Yamagata, J. Y. H. Wong, C. H. Ho, P. Szyszka, and H. Tanimoto (2014). "Converging Circuits Mediate Temperature and Shock Aversive Olfactory Conditioning in Drosophila". In: *Current Biology* 24.15, pp. 1712–1722.

Ganeshina, O. and R. Menzel (2001). "GABA immunoreactive neurons in the mushroom bodies of the honey bee: An electron microscopic study". In: *Journal of Comparative Neurology* 437.3, pp. 335–349.

Garczynski, S. F., M. R. Brown, and J. W. Crim (2006). "Structural studies of Drosophila short neuropeptide F: Occurrence and receptor binding activity". In: *Peptides* 27.3, pp. 575–582.

Garczynski, S. F., M. R. Brown, P. Shen, T. F. Murray, and J. W. Crim (2002). "Characterization of a functional neuropeptide F receptor from Drosophila melanogaster". In: *Peptides* 23.4, pp. 773–780.

Gaudry, Q., E. J. Hong, J. Kain, B. L. de Bivort, and R. I. Wilson (2013). "Asymmetric neurotransmitter release enables rapid odour lateralization in Drosophila." In: *Nature* 493.7432, pp. 424–8.

Gerber, B., H. Tanimoto, and M. Heisenberg (2004). "An engram found? Evaluating the evidence from fruit flies". In: *Current Opinion in Neurobiology* 14.6, pp. 737–744.

Gervasi, N., P. Tchénio, and T. Preat (2010). "PKA dynamics in a Drosophila learning center: coincidence detection by rutabaga adenylyl cyclase and spatial regulation by dunce phosphodiesterase." In: *Neuron* 65.4, pp. 516–29.

Giles, D. and P. N. R. Usherwood (1985). "The effects of putative amino acid neurotransmitters on somata isolated from neurons of the locust central nervous system". In: *Comparative Biochemistry and Physiology. Part C, Comparative* 80.2, pp. 231–236.

Giurfa, M. (2003). "Cognitive neuroethology : dissecting non-elemental learning in a honeybee brain". In: *Current opinion in neurobiology*, pp. 726–735.

Glatt, C. E. and S. H. Snyder (1993). "Cloning and expression of an adenylyl cyclase localized to the corpus striatum." In: *Nature* 361.6412, pp. 536–538.

Gluck, M. A., E. Mercado, and C. E. Myers (2016). *Learning and Memory*. Macmillan Learning.

Göhler, A. (2015). *Detectors for microscopy - CCDs, sCMOS, APDs and PMTs*. URL: `http://downloads.micron.ox.ac.uk/lectures/micron%7B%5C_%7Dcourse%7B%`

5C_%7D2015/Lecture%7B%5C_%7D10%7B%5C_%7Dcameras.pdf (visited on 04/16/2017).

Golic, K. G. and S. Lindquist (1989). "The FLP recombinase of yeast catalyzes site-specific recombination in the Drosophila genome." In: *Cell* 59.3, pp. 499–509.

Gong, Y., C. Huang, J. Z. Li, B. F. Grewe, Y. Zhang, S. Eismann, and M. J. Schnitzer (2015). "High-speed recording of neural spikes in awake mice and flies with a fluorescent voltage sensor". In: *Science* 350.6266, pp. 1361–1366.

Gorczyca, M. G. and J. C. Hall (1987). "Immunohistochemical localization of choline acetyltransferase during development and in Chats mutants of Drosophila melanogaster." In: *The Journal of neuroscience : the official journal of the Society for Neuroscience* 7.5, pp. 1361–9.

Gotzes, F., S. Balfanz, and A. Baumann (1993). "Primary structure and functional characterization of a Drosophila dopamine receptor with high homology to human D1/5 receptors." In: *Receptors & channels* 2.2, pp. 131–141.

Govorunova, E. G., O. A. Sineshchekov, R. Janz, X. Liu, and J. L. Spudich (2015). "Natural light-gated anion channels: A family of microbial rhodopsins for advanced optogenetics". In: *Science* 349.6248, pp. 647–650.

Gras, C., E. Herzog, G. C. Bellenchi, P. Ravassard, M. Pohl, B. Gasnier, B. Giros, and S. E. Mestikawy (2002). "A Third Vesicular Glutamate Transporter Expressed by Cholinergic and Serotoninergic Neurons". In: *Journal of Neuroscience* 22.13, pp. 5442–5451.

Grauso, M., R. A. Reenan, E. Culetto, and D. B. Sattelle (2002). "Novel putative nicotinic acetylcholine receptor subunit genes, Dalpha5, Dalpha6 and Dalpha7, in Drosophila melanogaster identify a new and highly conserved target of adenosine deaminase acting on RNA-mediated A-to-I pre-mRNA editing." In: *Genetics* 160.4, pp. 1519–33.

Gray, E. G. (1970). "The fine structure of the vertical lobe of octopus brain." In: *Philosophical transactions of the Royal Society of London. Series B, Biological sciences* 258.827, pp. 379–94.

Green, E. W., G. Fedele, F. Giorgini, and C. P. Kyriacou (2014). "A Drosophila RNAi collection is subject to dominant phenotypic effects". In: *Nature Methods* 11.3, pp. 222–223.

Green, J., A. Adachi, K. K. Shah, J. D. Hirokawa, P. S. Magani, and G. Maimon (2017). "A neural circuit architecture for angular integration in Drosophila." In: *Nature* 546.7656, pp. 101–106.

Greenspan, R. J. (1980). "Mutations of choline acetyltransferase and associated neural defects". In: *Journal of Comparative Physiology A* 137.1, pp. 83–92.

Greenspan, R. J. (1997). "Fly pushing: The theory and practice of Drosophila genetics". In: *Cold Spring Harbor Laboratory Press*.

Grienberger, C. and A. Konnerth (2012). "Imaging calcium in neurons." In: *Neuron* 73.5, pp. 862–85.

Grimley, J. S., L. Li, W. Wang, L. Wen, L. S. Beese, H. W. Hellinga, and G. J. Augustine (2013). "Visualization of synaptic inhibition with an optogenetic sensor developed by cell-free protein engineering automation." In: *The Journal of neuroscience : the official journal of the Society for Neuroscience* 33.41, pp. 16297–309.

Gropp, E., M. Shanabrough, E. Borok, A. W. Xu, R. Janoschek, T. Buch, L. Plum, N. Balthasar, B. Hampel, A. Waisman, G. S. Barsh, T. L. Horvath, and

J. C. Brüning (2005). “Agouti-related peptide–expressing neurons are mandatory for feeding”. In: *Nature Neuroscience* 8.10, pp. 1289–1291.

Grotewiel, M. S., C. D. O. Beck, K. H. Wu, X.-R. Zhu, and R. L. Davis (1998). “Integrin-mediated short-term memory in Drosophila”. In: *Nature* 391.6666, pp. 455–460.

Grunder, S. and M. Assmann (2015). “Peptide-gated ion channels and the simple nervous system of Hydra”. In: *Journal of Experimental Biology* 218.4, pp. 551–561.

Gruntman, E. and G. C. Turner (2013). “Integration of the olfactory code across dendritic claws of single mushroom body neurons”. In: *Nature Neuroscience* 16.October, pp. 1–11.

Grynkiewicz, G., M. Poenie, and R. Y. Tsien (1985). “A new generation of Ca2+ indicators with greatly improved fluorescence properties”. In: *Journal of Biological Chemistry* 260.6, pp. 3440–3450.

Gu, H. and D. K. O’Dowd (2006). “Cholinergic synaptic transmission in adult Drosophila Kenyon cells in situ.” In: *The Journal of neuroscience : the official journal of the Society for Neuroscience* 26.1, pp. 265–272.

Gu, Z. and J. L. Yakel (2011). “Timing-Dependent Septal Cholinergic Induction of Dynamic Hippocampal Synaptic Plasticity”. In: *Neuron* 71.1, pp. 155–165.

Gundersen, V., F. a. Chaudhry, J. G. Bjaalie, F. Fonnum, O. P. Ottersen, and J. Storm-Mathisen (1998). “Synaptic vesicular localization and exocytosis of L-aspartate in excitatory nerve terminals: a quantitative immunogold analysis in rat hippocampus.” In: *The Journal of neuroscience : the official journal of the Society for Neuroscience* 18.16, pp. 6059–6070.

Haan, R. de, Y.-J. Lee, and K. Nordström (2012). “Octopaminergic modulation of contrast sensitivity”. In: *Frontiers in Integrative Neuroscience* 6.August, p. 55.

Hall, J. C., S. N. Alahiotis, D. A. Strumpf, and K. White (1980). “Behavioral and biochemical defects in temperature-sensitive acetylcholinesterase mutants of Drosophila melanogaster.” In: *Genetics* 96.4, pp. 939–965.

Hamada, F. N., M. Rosenzweig, K. Kang, S. R. Pulver, A. Ghezzi, T. J. Jegla, and P. a. Garrity (2008). “An internal thermal sensor controlling temperature preference in Drosophila”. In: *Nature* 454.7201, pp. 217–220.

Hamasaka, Y., C. Wegener, and D. R. Nässel (2005). “GABA modulates Drosophila circadian clock neurons via GABAB receptors and decreases in calcium”. In: *Journal of Neurobiology* 65.3, pp. 225–240.

Hammer, M. (1993). “An identified neuron mediates the unconditioned stimulus in associative olfactory learning in honeybees”. In: *Nature* 366.6450, pp. 59–63.

Han, K. A., N. S. Millar, and R. L. Davis (1998). “A novel octopamine receptor with preferential expression in Drosophila mushroom bodies.” In: *The Journal of neuroscience : the official journal of the Society for Neuroscience* 18.10, pp. 3650–3658.

Han, K. A., N. S. Millar, M. S. Grotewiel, and R. L. Davis (1996). “DAMB, a novel dopamine receptor expressed specifically in Drosophila mushroom bodies”. In: *Neuron* 16.6, pp. 1127–1135.

Han, P. L., L. R. Levin, R. R. Reed, and R. L. Davis (1992). “Preferential expression of the drosophila rutabaga gene in mushroom bodies, neural centers for learning in insects”. In: *Neuron* 9.4, pp. 619–627.

Han, Y., P. S. Kaeser, T. C. Südhof, and R. Schneggenburger (2011). "RIM determines Ca2+ channel density and vesicle docking at the presynaptic active zone". In: *Neuron* 69.2, pp. 304–316.

Hannan, F. and L. M. Hall (1996). "Temporal and spatial expression patterns of two G-protein coupled receptors in Drosophila melanogaster." In: *Invertebrate neuroscience : IN* 2.1, pp. 71–83.

Hardie, R. C. (1987). "Is histamine a neurotransmitter in insect photoreceptors?" In: *Journal of Comparative Physiology A* 161.2, pp. 201–213.

Harris, D. T., B. R. Kallman, B. C. Mullaney, and K. Scott (2015). "Representations of Taste Modality in the Drosophila Brain". In: *Neuron* 86.6, pp. 1449–1460.

Harrison, J. B., H. H. Chen, E. Sattelle, P. J. Barker, N. S. Huskisson, J. J. Rauh, D. Bai, and D. B. Sattelle (1996). "Immunocytochemical mapping of a C-terminus anti-peptide antibody to the GABA receptor subunit, RDL in the nervous system of Drosophila melanogaster". In: *Cell and Tissue Research* 284.2, pp. 269–278.

Harvey, R. J. (2008). "A critical role for glycine transporters in hyperexcitability disorders". In: *Frontiers in Molecular Neuroscience* 1.March, pp. 1–6.

Harz, H. and P. Hegemann (1991). "Rhodopsin-regulated calcium currents in Chlamydomonas". In: *Nature* 351.6326, pp. 489–491.

Hattori, D., Y. Aso, K. J. Swartz, G. M. Rubin, L. Abbott, and R. Axel (2017). "Representations of Novelty and Familiarity in a Mushroom Body Compartment". In: *Cell* 169.5, 956–969.e17.

Hauser, F., G. Cazzamali, M. Williamson, W. Blenau, and C. J. P. Grimmelikhuijzen (2006). "A review of neurohormone GPCRs present in the fruitfly Drosophila melanogaster and the honey bee Apis mellifera". In: *Progress in Neurobiology* 80.1, pp. 1–19.

Haynes, P. R., B. L. Christmann, and L. C. Griffith (2015). "A single pair of neurons links sleep to memory consolidation in Drosophila melanogaster". In: *eLife* 4.January, pp. 1–24.

He, C., Y. Yang, M. Zhang, J. L. Price, and Z. Zhao (2013). "Regulation of Sleep by Neuropeptide Y-Like System in Drosophila melanogaster". In: *PLoS ONE* 8.9, e74237.

Heimbeck, G., V. Bugnon, N. Gendre, a. Keller, and R. F. Stocker (2001). "A central neural circuit for experience-independent olfactory and courtship behavior in Drosophila melanogaster." In: *Proceedings of the National Academy of Sciences of the United States of America* 98.26, pp. 15336–41.

Heisenberg, M. (1980). "Mutants of Brain Structure and Function: What is the Significance of the Mushroom Bodies for Behavior?" In: *Development and Neurobiology of Drosophila*. Ed. by O. Siddiqi, P. Babu, L. M. Hall, and J. C. Hall. Boston, MA: Springer US, pp. 373–390.

— (2003). "Mushroom body memoir: from maps to models". In: *Nature Reviews Neuroscience* 4.April, pp. 266–275.

Heisenberg, M. and K. Böhl (1979). "Isolation of Anatomical Brain Mutants of Drosophila by Histological Means". In: *Zeitschrift für Naturforschung - Section C Journal of Biosciences* 34.1-2, pp. 143–147.

Heisenberg, M., A. Borst, S. Wagner, and D. Byers (1985). "Drosophila mushroom body mutants are deficient in olfactory learning." In: *Journal of neurogenetics* 2.1, pp. 1–30.

Herring, B. E., K. Silm, R. H. Edwards, and R. A. Nicoll (2015). "Is Aspartate an Excitatory Neurotransmitter?" In: *Journal of Neuroscience* 35.28, pp. 10168–10171.

Hertlein, M. B., G. D. Thompson, B. Subramanyam, and C. G. Athanassiou (2011). "Spinosad: A new natural product for stored grain protection". In: *Journal of Stored Products Research* 47.3, pp. 131–146.

Hewes, R. S. and P. H. Taghert (2001). "Neuropeptides and neuropeptide receptors in the Drosophila melanogaster genome." In: *Genome research* 11.6, pp. 1126–42.

Hige, T., Y. Aso, M. N. Modi, G. M. Rubin, and G. C. Turner (2015a). "Heterosynaptic Plasticity Underlies Aversive Olfactory Learning in Drosophila." In: *Neuron* 88.5, pp. 985–98.

Hige, T., Y. Aso, G. M. Rubin, and G. C. Turner (2015b). "Plasticity-driven individualization of olfactory coding in mushroom body output neurons". In: *Nature* 526.7572, pp. 258–262.

Hirano, Y., T. Masuda, S. Naganos, M. Matsuno, K. Ueno, T. Miyashita, J. Horiuchi, and M. Saitoe (2013). "Fasting launches CRTC to facilitate long-term memory formation in Drosophila." In: *Science* 339.6118, pp. 443–6.

Homberg, U. (2002). "Neurotransmitters and neuropeptides in the brain of the locust". In: *Microscopy Research and Technique* 56.3, pp. 189–209.

Homberg, U., J. Seyfarth, U. Binkle, M. Monastirioti, and M. J. Alkema (2013). "Identification of distinct tyraminergic and octopaminergic neurons innervating the central complex of the desert locust, Schistocerca gregaria". In: *Journal of Comparative Neurology* 521.9, pp. 2025–2041.

Honegger, K. S., R. A. A. Campbell, and G. C. Turner (2011). "Cellular-Resolution Population Imaging Reveals Robust Sparse Coding in the Drosophila Mushroom Body". In: *Journal of Neuroscience* 31.33, pp. 11772–11785.

Hong, S. H., K. S. Lee, S. J. Kwak, A. K. Kim, H. Bai, M. S. Jung, O. Y. Kwon, W. J. Song, M. Tatar, and K. Yu (2012). "Minibrain/Dyrk1a Regulates Food Intake through the Sir2-FOXO-sNPF/NPY Pathway in Drosophila and Mammals". In: *PLoS Genetics* 8.8, pp. 1–15.

Hoopfer, E. D., Y. Jung, H. K. Inagaki, G. M. Rubin, and D. J. Anderson (2015). "P1 interneurons promote a persistent internal state that enhances inter-male aggression in Drosophila". In: *eLife* 4.December.

Howe, W. M., A. S. Berry, J. Francois, G. Gilmour, J. M. Carp, M. Tricklebank, C. Lustig, and M. Sarter (2013). "Prefrontal Cholinergic Mechanisms Instigating Shifts from Monitoring for Cues to Cue-Guided Performance: Converging Electrochemical and fMRI Evidence from Rats and Humans". In: *Journal of Neuroscience* 33.20, pp. 8742–8752.

Howe, W. M., H. J. Gritton, N. A. Lusk, E. A. Roberts, V. L. Hetrick, J. D. Berke, and M. Sarter (2017). "Acetylcholine Release in Prefrontal Cortex Promotes Gamma Oscillations and Theta–Gamma Coupling during Cue Detection". In: *The Journal of Neuroscience* 37.12, pp. 3215–3230.

Hoyer, S. C., A. Eckart, A. Herrel, T. Zars, S. A. Fischer, S. L. Hardie, and M. Heisenberg (2008). "Octopamine in Male Aggression of Drosophila". In: *Current Biology* 18.3, pp. 159–167.

Huang, J., W. Zhang, W. Qiao, A. Hu, and Z. Wang (2010). "Functional connectivity and selective odor responses of excitatory local interneurons in drosophila antennal lobe". In: *Neuron* 67.6, pp. 1021–1033.

Hue, B., B. Lapied, and O. Malecot (1989). "Do Presynaptic muscarinic receptors regulate acetylcholine release in the central nervous system of the cockroach periplaneta americana?" In: *J.Exp.Biol.* 142, pp. 447–451.

Huetteroth, W., E. Perisse, S. Lin, M. Klappenbach, C. Burke, and S. Waddell (2015). "Sweet taste and nutrient value subdivide rewarding dopaminergic neurons in Drosophila." In: *Current biology : CB* 25.6, pp. 751–8.

Hwang, R. Y., L. Zhong, Y. Xu, T. Johnson, F. Zhang, K. Deisseroth, and W. D. Tracey (2007). "Nociceptive Neurons Protect Drosophila Larvae from Parasitoid Wasps". In: *Current Biology* 17.24, pp. 2105–2116.

Ichikawa, T., K. Ajiki, J. Matsuura, and H. Misawa (1997). "Localization of two cholinergic markers, choline acetyltransferase and vesicular acetylcholine transporter in the central nervous system of the rat: In situ hybridization histochemistry and immunohistochemistry". In: *Journal of Chemical Neuroanatomy* 13.1, pp. 23–39.

Ichinose, T., Y. Aso, N. Yamagata, A. Abe, G. M. Rubin, and H. Tanimoto (2015). "Reward signal in a recurrent circuit drives appetitive long-term memory formation." In: *eLife* 4, e10719.

Ignell, R., C. M. Root, R. T. Birse, J. W. Wang, D. R. Nässel, and Å. M. E. Winther (2009). "Presynaptic peptidergic modulation of olfactory receptor neurons in Drosophila". In: *Proceedings of the National Academy of Sciences* 106.31, pp. 13070–13075.

Inada, K., Y. Tsuchimoto, and H. Kazama (2017). "Origins of Cell-Type-Specific Olfactory Processing in the Drosophila Mushroom Body Circuit". In: *Neuron* 95.2, 357–367.e4.

Inagaki, H. K., Y. Jung, E. D. Hoopfer, A. M. Wong, N. Mishra, J. Y. Lin, R. Y. Tsien, and D. J. Anderson (2014). "Optogenetic control of Drosophila using a red-shifted channelrhodopsin reveals experience-dependent influences on courtship." In: *Nature methods* 11.3, pp. 325–32.

Inoue, M., A. Takeuchi, S.-I. Horigane, M. Ohkura, K. Gengyo-Ando, H. Fujii, S. Kamijo, S. Takemoto-Kimura, M. Kano, J. Nakai, K. Kitamura, and H. Bito (2015). "Rational design of a high-affinity, fast, red calcium indicator R-CaMP2." In: *Nature methods* 12.1, pp. 64–70.

Isabel, G., A. Pascual, and T. Preat (2004). "Exclusive consolidated memory phases in Drosophila." In: *Science (New York, N.Y.)* 304.5673, pp. 1024–7.

Ito, I., R. C.-Y. Ong, B. Raman, and M. Stopfer (2008). "Sparse odor representation and olfactory learning." In: *Nature neuroscience* 11.10, pp. 1177–1184.

Ito, K., K. Suzuki, P. Estes, M. Ramaswami, D. Yamamoto, and N. J. Strausfeld (1998). "The organization of extrinsic neurons and their implications in the functional roles of the mushroom bodies in Drosophila melanogaster Meigen." In: *Learning & memory (Cold Spring Harbor, N.Y.)* 5.1-2, pp. 52–77.

Ito, K., W. Awano, K. Suzuki, Y. Hiromi, and D. Yamamoto (1997). "The Drosophila mushroom body is a quadruple structure of clonal units each of which contains a virtually identical set of neurones and glial cells". In: *Development* 771, pp. 761–771.

Iwai, Y., T. Usui, S. Hirano, R. Steward, M. Takeichi, and T. Uemura (1997). "Axon patterning requires DN-cadherin, a novel neuronal adhesion receptor, in the drosophila embryonic CNS". In: *Neuron* 19.1, pp. 77–89.

Jackson, F. R., L. M. Newby, and S. J. Kulkarni (1990). "Drosophila GABAergic Systems: Sequence and Expression of Glutamic Acid Decarboxylase". In: *Journal of Neurochemistry* 54.3, pp. 1068–1078.

Jan, L. Y. and Y. N. Jan (1976). "L-glutamate as an excitatory transmitter at the Drosophila larval neuromuscular junction." In: *The Journal of physiology* 262.1, pp. 215–36.

Jan, L. Y. and Y. N. Jan (1982). "Peptidergic transmission in sympathetic ganglia of the frog." In: *The Journal of Physiology* 327.1, pp. 219–246.

Jenett, A. et al. (2012). "A GAL4-Driver Line Resource for Drosophila Neurobiology." In: *Cell Reports* 2.4, pp. 991–1001.

Johard, H. A. D., L. E. Enell, E. Gustafsson, P. Trifilieff, J. A. Veenstra, and D. R. Nässel (2008). "Intrinsic neurons of Drosophila mushroom bodies express short neuropeptide F: relations to extrinsic neurons expressing different neurotransmitters". In: *Journal of Comparative Neurology* 1496.October 2007, pp. 1479–1496.

Johnston, D. S. (2002). "The art and design of genetic screens: Drosophila melanogaster." In: *Nature Reviews Genetics* 3.3, pp. 176–88.

Jonas, P. E., B. Phannavong, R. Schuster, C. Schröder, and E. D. Gundelfinger (1994). "Expression of the ligand-binding nicotinic acetylcholine receptor subunit D alpha 2 in the Drosophila central nervous system." In: *Journal of neurobiology* 25.12, pp. 1494–508.

Jones, A. K. and D. B. Sattelle (2010). "Diversity of insect nicotinic acetylcholine receptor subunits". In: *Advances in experimental medicine and biology* 683. Ed. by S. H. Thany, pp. 25–43.

Jortner, R. A., S. S. Farivar, and G. Laurent (2007). "A Simple Connectivity Scheme for Sparse Coding in an Olfactory System". In: *Journal of Neuroscience* 27.7, pp. 1659–1669.

Kahsai, L., M. A. Carlsson, Å. M. E. Winther, and D. R. Nässel (2012). "Distribution of metabotropic receptors of serotonin, dopamine, GABA, glutamate, and short neuropeptide F in the central complex of Drosophila". In: *Neuroscience* 208, pp. 11–26.

Kahsai, L., N. Kapan, H. Dircksen, Å. M. E. Winther, and D. R. Nässel (2010a). "Metabolic stress responses in Drosophila are modulated by brain neurosecretory cells that produce multiple neuropeptides". In: *PLoS ONE* 5.7.

Kahsai, L., J.-R. Martin, and Å. M. E. Winther (2010b). "Neuropeptides in the Drosophila central complex in modulation of locomotor behavior". In: *Journal of Experimental Biology* 213.13, pp. 2256–2265.

Kahsai, L. and Å. M. E. Winther (2011). "Chemical neuroanatomy of the Drosophila central complex: Distribution of multiple neuropeptides in relation to neurotransmitters". In: *Journal of Comparative Neurology* 519.2, pp. 290–315.

Kalra, S. P. (1997). "Appetite and body weight regulation: Is it all in the brain?" In: *Neuron* 19.2, pp. 227–230.

Kandel, E. R., J. H. Schwartz, T. M. Jessell, S. Mack, J. Dodd, J. Butler, H. Lebowitz, S. Dahlgren, P. Supervisor, E. Siegel, A. Manager, J. Ackerman, J. Cuddihy, P. Graphics, and R. R. Donnelley (2013). *Principles of Neural Science*. Ed. by E. Kandel, J. Schwartz, T. Jessell, S. A. Siegelbaum, and A. J. Hudspeth. 5th ed. 1. McGraw-Hill, Inc., p. 1760.

Kapan, N., O. V. Lushchak, J. Luo, and D. R. Nässel (2012). "Identified peptidergic neurons in the Drosophila brain regulate insulin-producing cells, stress responses and metabolism by coexpressed short neuropeptide F and corazonin." In: *Cellular and molecular life sciences : CMLS* 69.23, pp. 4051–66.

Kappel, C. (2011). *Step by Step Guide to Hybrid Detection and Photon Counting*. URL: `http://www.leica-microsystems.com/products/confocal-microscopes/details/product/leica-hyd/` (visited on 04/16/2017).

Kaun, K. R., R. Azanchi, Z. Maung, J. Hirsh, and U. Heberlein (2011). “A Drosophila model for alcohol reward”. In: *Nature Neuroscience* 14.5, pp. 612–619.

Keene, A. C., M. J. Krashes, B. Leung, J. A. Bernard, and S. Waddell (2006). “Drosophila dorsal paired medial neurons provide a general mechanism for memory consolidation.” In: *Current Biology* 16.15, pp. 1524–30.

Keene, A. C. and P. Masek (2012). “Optogenetic induction of aversive taste memory.” In: *Neuroscience* 222, pp. 173–80.

Keene, A. C., M. Stratmann, A. Keller, P. N. Perrat, L. B. Vosshall, and S. Waddell (2004). “Diverse odor-conditioned memories require uniquely timed dorsal paired medial neuron output.” In: *Neuron* 44.3, pp. 521–533.

Keene, A. C. and S. Waddell (2007). “Drosophila olfactory memory: single genes to complex neural circuits.” In: *Nature Reviews Neuroscience* 8.5, pp. 341–54.

Kenyon, F. C. (1896a). “The brain of the bee. A preliminary contribution to the morphology of the nervous system of the arthropoda”. In: *Journal of Comparative Neurology* 6.3, pp. 133–210.

— (1896b). “The Meaning and Structure of the So-Called "Mushroom Bodies" of the Hexapod Brain”. In: *The American Naturalist* 30.356, pp. 643–650.

El-Kholy, S., F. Stephano, Y. Li, A. Bhandari, C. Fink, and T. Roeder (2015). “Expression analysis of octopamine and tyramine receptors in Drosophila”. In: *Cell and Tissue Research* 361.3, pp. 669–684.

Kim, H., C. Kirkhart, and K. Scott (2017). “Long-range projection neurons in the taste circuit of Drosophila”. In: *eLife* 6.16.

Kim, S. S., R. Franconville, D. Turner-Evans, and V. Jayaraman (2015). “New Techniques in Systems Neuroscience”. In: *New Techniques in Systems Neuroscience*. Chap. 6, pp. 97–127.

Kim, Y.-C., H.-G. Lee, and K.-A. Han (2007). “D1 Dopamine Receptor dDA1 Is Required in the Mushroom Body Neurons for Aversive and Appetitive Learning in Drosophila”. In: *Journal of Neuroscience* 27.29, pp. 7640–7647.

Kim, Y. T., V. K. Haftel, S. Kumar, and R. V. Bellamkonda (2008). “The role of aligned polymer fiber-based constructs in the bridging of long peripheral nerve gaps”. In: *Biomaterials* 29, pp. 3117–3127.

Kirkhart, C. and K. Scott (2015). “Gustatory Learning and Processing in the Drosophila Mushroom Bodies”. In: *Journal of Neuroscience* 35.15, pp. 5950–5958.

Kitamoto, T. (2001). “Conditional modification of behavior inDrosophila by targeted expression of a temperature-sensitiveshibire allele in defined neurons”. In: *Journal of Neurobiology* 47.2, pp. 81–92.

— (2002). “Conditional disruption of synaptic transmission induces male-male courtship behavior in Drosophila.” In: *Proceedings of the National Academy of Sciences of the United States of America* 99.20, pp. 13232–13237.

Kitamoto, T., K. Ikeda, and P. M. Salvaterra (1995). “Regulation of Choline Acetyltransferase/Lacz Fusion Gene-Expression in Putative Cholinergic Neurons of Drosophila-Melanogaster”. In: *Journal of Neurobiology* 28.1, pp. 70–81.

Kitamoto, T., K. Ikeda, and P. M. Salvaterra (1992). “Analysis of cis-regulatory elements in the 5’ flanking region of the Drosophila melanogaster choline acetyltransferase gene.” In: *The Journal of neuroscience* 12.5, pp. 1628–39.

Kitamoto, T., W. Wang, P. M. Salvaterra, T. Kitamoto, W. Wang, W. Wang, P. M. Salvaterra, and P. M. Salvaterra (1998). “Structure and Organization of the

Drosophila Cholinergic Locus". In: *Journal of Biological Chemistry* 273.5, pp. 2706–2713.

Kitamoto, T., X. J. Xie, C. F. Wu, and P. M. Salvaterra (2000). "Isolation and characterization of mutants for the vesicular acetylcholine transporter gene in Drosophila melanogaster". In: *Journal of Neurobiology* 42.2, pp. 161–171.

Klapoetke, N. C., Y. Murata, S. S. Kim, S. R. Pulver, A. Birdsey-Benson, Y. K. Cho, T. K. Morimoto, A. S. Chuong, E. J. Carpenter, Z. Tian, J. Wang, Y. Xie, Z. Yan, Y. Zhang, B. Y. Chow, B. Surek, M. Melkonian, V. Jayaraman, M. Constantine-Paton, G. K.-S. Wong, and E. S. Boyden (2014). "Independent optical excitation of distinct neural populations." In: *Nature methods* 11.3, pp. 338–46.

Klapstein, G. J. and W. F. Colmers (1993). "On the sites of presynaptic inhibition by neuropeptide Y in rat hippocampus in vitro". In: *Hippocampus* 3.1050-9631 SB - M, pp. 103–111.

Klausberger, T. and P. Somogyi (2008). "Neuronal diversity and temporal dynamics: the unity of hippocampal circuit operations." In: *Science (New York, N.Y.)* 321.5885, pp. 53–7.

Klemm, N. (1976). "Histochemistry of putative transmitter substances in the insect brain". In: *Progress in Neurobiology* 7.PART 2, pp. 99–169.

Knapek, S., L. Kahsai, Å. M. E. Winther, H. Tanimoto, and D. R. Nässel (2013). "Short neuropeptide F acts as a functional neuromodulator for olfactory memory in Kenyon cells of Drosophila mushroom bodies." In: *The Journal of neuroscience : the official journal of the Society for Neuroscience* 33.12, pp. 5340–5.

Knoflach, F., M. C. Hernandez, and D. Bertrand (2016). "GABAA receptor-mediated neurotransmission: Not so simple after all". In: *Biochemical Pharmacology* 115, pp. 10–17.

Ko, K. I., C. M. Root, S. A. Lindsay, O. A. Zaninovich, A. K. Shepherd, S. A. Wasserman, S. M. Kim, and J. W. Wang (2015). "Starvation promotes concerted modulation of appetitive olfactory behavior via parallel neuromodulatory circuits." In: *eLife* 4, pp. 1–17.

Koelle, G. B. (1954). "The histochemical localization of cholinesterases in the central nervous system of the rat." In: *The Journal of comparative neurology* 100.1, pp. 211–35.

Koenig, J. H., K. Saito, and K. Ikeda (1983). "Reversible control of synaptic transmission in a single gene mutant of Drosophila melanogaster". In: *Journal of Cell Biology* 96.6, pp. 1517–1522.

Koenig, S., R. Wolf, and M. Heisenberg (2016). "Visual Attention in Flies—Dopamine in the Mushroom Bodies Mediates the After-Effect of Cueing". In: *Plos One*, pp. 1–21.

Kohl, J., J. Ng, S. Cachero, E. Ciabatti, M.-J. Dolan, B. Sutcliffe, A. Tozer, S. Ruehle, D. Krueger, S. Frechter, T. Branco, M. Tripodi, and G. S. X. E. Jefferis (2014). "Ultrafast tissue staining with chemical tags. SI". In: *Proceedings of the National Academy of Sciences of the United States of America* 2014.36, pp. 1–11.

Kolodziejczyk, A. and D. R. Nässel (2011). "A novel wide-field neuron with branches in the lamina of the Drosophila visual system expresses myoinhibitory peptide and may be associated with the clock". In: *Cell and Tissue Research* 343.2, pp. 357–369.

Kolodziejczyk, A., X. Sun, I. a. Meinertzhagen, and D. R. Nässel (2008). "Glutamate, GABA and acetylcholine signaling components in the lamina of the Drosophila visual system". In: *PLoS ONE* 3.5.

Kononenko, N. L., H. Wolfenberg, and H. J. Pflüger (2009). "Tyramine as an independent transmitter and a precursor of octopamine in the locust central nervous system: An immunocytochemical study". In: *Journal of Comparative Neurology* 512.4, pp. 433–452.

Konopka, R. J. and S. Benzer (1971). "Clock mutants of Drosophila melanogaster." In: *Proceedings of the National Academy of Sciences of the United States of America* 68.9, pp. 2112–6.

Konorski, J. (1948). *Conditioned reflexes and neuron organization.* Cambridge: Cambridge University Press.

— (1967). *Integrative activity of the brain : an interdisciplinary approach.* Chicago: University of Chicago Press.

Konrad, K. D. and J. Marsh (1987). "Developmental expression and spatial distribution of dopa decarboxylase in Drosophila". In: *Developmental Biology* 122.1, pp. 172–185.

Kosaka, T. and K. Ikeda (1983). "Reversible blockage of membrane retrieval and endocytosis in the garland cell of the temperature-sensitive mutant of Drosophila melanogaster, shibirets1." In: *The Journal of cell biology* 97.2, pp. 499–507.

Krashes, M. J., S. DasGupta, A. Vreede, B. White, J. D. Armstrong, and S. Waddell (2009). "A neural circuit mechanism integrating motivational state with memory expression in Drosophila." In: *Cell* 139.2, pp. 416–27.

Krashes, M. J., A. C. Keene, B. Leung, J. D. Armstrong, and S. Waddell (2007). "Sequential use of mushroom body neuron subsets during drosophila odor memory processing." In: *Neuron* 53.1, pp. 103–115.

Krashes, M. J. and S. Waddell (2008). "Rapid consolidation to a radish and protein synthesis-dependent long-term memory after single-session appetitive olfactory conditioning in Drosophila." In: *The Journal of Neuroscience* 28.12, pp. 3103–13.

Kravitz, A. V., B. S. Freeze, P. R. L. Parker, K. Kay, M. T. Thwin, K. Deisseroth, and A. C. Kreitzer (2010). "Regulation of parkinsonian motor behaviours by optogenetic control of basal ganglia circuitry". In: *Nature* 466.7306, pp. 622–626.

Kremer, M. C., F. Christiansen, F. Leiss, M. Paehler, S. Knapek, T. F. M. Andlauer, F. Förstner, P. Kloppenburg, S. J. Sigrist, and G. Tavosanis (2010). "Structural long-term changes at mushroom body input synapses". In: *Current Biology* 20.21, pp. 1938–1944.

Kremer, M. C., C. Jung, S. Batelli, G. M. Rubin, and U. Gaul (2017). "The glia of the adult Drosophila nervous system". In: *GLIA* 65.4, pp. 606–638.

Kubitscheck, U. (2017). *Fluorescence Microscopy: From Principles to Biological Applications.* Ed. by U. Kubitscheck. 2nd ed. Wiley-Blackwell.

Kucharski, R., E. Ball, D. Hayward, and R. Maleszka (2000). "Molecular cloning and expression analysis of a cDNA encoding a glutamate transporter in the honeybee brain". In: *Gene* 242.1-2, pp. 399–405.

Kuhar, M. J. and L. C. Murrin (1978). "Sodium-dependent, high-affinity choline uptake". In: *Journal of neurochemistry* 30.1, pp. 15–21.

Kvon, E. Z., T. Kazmar, G. Stampfel, J. O. Yáñez-Cuna, M. Pagani, K. Schernhuber, B. J. Dickson, and A. Stark (2014). "Genome-scale functional characterization of Drosophila developmental enhancers in vivo." In: *Nature* 512.7512, pp. 91–5.

Lafourcade, C. A. (2009). "Presynaptic Mechanisms of Endocannabinoid-Mediated Long-Term Depression in the Hippocampus". In: *Journal of Neurophysiology* 102, pp. 2009–2012.

Lagasse, F., J.-M. Devaud, and F. Mery (2009). "A switch from cycloheximide-resistant consolidated memory to cycloheximide-sensitive reconsolidation and extinction in Drosophila." In: *The Journal of Neuroscience* 29.7, pp. 2225–2230.

Lai, S.-L. and T. Lee (2006). "Genetic mosaic with dual binary transcriptional systems in Drosophila." In: *Nature neuroscience* 9.5, pp. 703–9.

Laissue, P. P. and L. B. Vosshall (2008). "The Olfactory Sensory Map in Drosophila". In: *Brain Development in Drosophila melanogaster*. New York, NY: Springer New York, pp. 102–114.

Lakowicz, J. R. (2006). *Principles of Fluorescence Spectroscopy*. 3rd ed. Boston, MA: Springer.

Lange, A. B. (2009). "Tyramine: From octopamine precursor to neuroactive chemical in insects". In: *General and Comparative Endocrinology* 162.1, pp. 18–26.

Lansdell, S. J., T. Collins, J. Goodchild, and N. S. Millar (2012). "The Drosophila nicotinic acetylcholine receptor subunits Dα5 and Dα7 form functional homomeric and heteromeric ion channels". In: *BMC Neuroscience* 13.1, p. 73.

Lansdell, S. J. and N. S. Millar (2004). "Molecular characterization of Dalpha6 and Dalpha7 nicotinic acetylcholine receptor subunits from Drosophila: formation of a high-affinity alpha-bungarotoxin binding site revealed by expression of subunit chimeras". In: *Journal of Neurochemistry* 90.2, pp. 479–489.

Larsson, M. C., A. I. Domingos, W. D. Jones, M. E. Chiappe, H. Amrein, and L. B. Vosshall (2004). "Or83b encodes a broadly expressed odorant receptor essential for Drosophila olfaction". In: *Neuron* 43.5, pp. 703–714.

Laurent, G. (2002). "Olfactory network dynamics and the coding of multidimensional signals". In: *Nature Reviews Neuroscience* 3.11, pp. 884–895.

Lee, D. and D. K. O'Dowd (1999). "Fast excitatory synaptic transmission mediated by nicotinic acetylcholine receptors in Drosophila neurons." In: *The Journal of neuroscience : the official journal of the Society for Neuroscience* 19.13, pp. 5311–5321.

Lee, K.-S., O.-Y. Kwon, J. H. Lee, K. Kwon, K.-J. Min, S.-A. Jung, A.-K. Kim, K.-H. You, M. Tatar, and K. Yu (2008). "Drosophila short neuropeptide F signalling regulates growth by ERK-mediated insulin signalling." In: *Nature cell biology* 10.4, pp. 468–75.

Lee, K.-S., K.-H. You, J.-K. Choo, Y.-M. Han, and K. Yu (2004). "Drosophila short neuropeptide F regulates food intake and body size". In: *Journal of Biological Chemistry* 279.49, pp. 50781–50789.

Lee, P.-T., H.-W. Lin, Y.-H. Chang, T.-F. Fu, J. Dubnau, J. Hirsh, T. Lee, and A.-S. Chiang (2011). "Serotonin-mushroom body circuit modulating the formation of anesthesia-resistant memory in Drosophila". In: *Proceedings of the National Academy of Sciences* 108.33, pp. 13794–13799.

Lee, T. and L. Luo (1999). "Mosaic analysis with a repressible cell marker for studies of gene function in neuronal morphogenesis." In: *Neuron* 22.3, pp. 451–61.

Leiss, F., E. Koper, I. Hein, W. Fouquet, J. Lindner, S. Sigrist, and G. Tavosanis (2009). "Characterization of dendritic spines in the Drosophila central nervous system". In: *Developmental Neurobiology* 69.4, pp. 221–234.

Leitch, B., B. Leitch, G. Laurent, and G. Laurent (1996). "GABAergic Synapses in the Antennal Lobe and Mushroom Body of the Locust Olfactory System". In: *the Journal of Comparative Neurology* 514.372, pp. 487–514.

Letzkus, J. J., S. B. E. Wolff, and A. Lüthi (2015). "Disinhibition, a Circuit Mechanism for Associative Learning and Memory". In: *Neuron* 88.2, pp. 264–276.

Leurs, R., R. A. Bakker, H. Timmerman, and I. J. P. de Esch (2005). "The histamine H3 receptor: from gene cloning to H3 receptor drugs." In: *Nature reviews. Drug discovery* 4.2, pp. 107–20.

Levin, L. R., P. L. Han, P. M. Hwang, P. G. Feinstein, R. L. Davis, and R. R. Reed (1992). "The Drosophila learning and memory gene rutabaga encodes a Ca2+ calmodulin-responsive adenylyl cyclase". In: *Cell* 68.3, pp. 479–489.

Lewis, L., K. Siju, Y. Aso, A. Friedrich, A. Bulteel, G. Rubin, and I. C. Grunwald Kadow (2015). "A Higher Brain Circuit for Immediate Integration of Conflicting Sensory Information in Drosophila". In: *Current Biology* 25.17, pp. 2203–2214.

Li, L., X. Tian, M. Zhu, D. Bulgari, M. a. Böhme, F. Goettfert, C. Wichmann, S. J. Sigrist, E. S. Levitan, and C. Wu (2014). "Drosophila Syd-1, Liprin-α, and protein phosphatase 2A B' subunit Wrd function in a linear pathway to prevent ectopic accumulation of synaptic materials in distal axons." In: *The Journal of neuroscience : the official journal of the Society for Neuroscience* 34.25, pp. 8474–87.

Lima, S. Q. and G. Miesenböck (2005). "Remote Control of Behavior through Genetically Targeted Photostimulation of Neurons". In: *Cell* 121.1, pp. 141–152.

Lin, A. C., A. M. Bygrave, A. de Calignon, T. Lee, and G. Miesenböck (2014a). "Sparse, decorrelated odor coding in the mushroom body enhances learned odor discrimination". In: *Nature Neuroscience* 17.4, pp. 559–568.

Lin, H.-H., J. S.-Y. Lai, A.-L. Chin, Y.-C. Chen, and A.-S. Chiang (2007). "A map of olfactory representation in the Drosophila mushroom body." In: *Cell* 128.6, pp. 1205–1217.

Lin, J. Y., P. M. Knutsen, A. Muller, D. Kleinfeld, and R. Y. Tsien (2013). "ReaChR: a red-shifted variant of channelrhodopsin enables deep transcranial optogenetic excitation." In: *Nature neuroscience* 16.10, pp. 1499–508.

Lin, K., W. Sadée, and J. M. Quillan (1999). "Rapid measurements of intracellular calcium using a fluorescence plate reader." In: *BioTechniques* 26.2, pp. 318–22, 324–6.

Lin, S., D. Owald, V. Chandra, C. Talbot, W. Huetteroth, and S. Waddell (2014b). "Neural correlates of water reward in thirsty Drosophila". In: *Nature Neuroscience* September, pp. 1–9.

Lin, Y. (2004). "The Neuropeptide Pigment-Dispersing Factor Coordinates Pacemaker Interactions in the Drosophila Circadian System". In: *Journal of Neuroscience* 24.36, pp. 7951–7957.

Linden, D. J. and S. Ahn (1999). "Activation of presynaptic cAMP-dependent protein kinase is required for induction of cerebellar long-term potentiation." In: *The Journal of neuroscience : the official journal of the Society for Neuroscience* 19.23, pp. 10221–7.

Lindenburg, L. H., J. L. Vinkenborg, J. Oortwijn, S. J. A. Aper, and M. Merkx (2013). "MagFRET: The first genetically encoded fluorescent Mg2+ sensor". In: *PLoS ONE* 8.12.

Lingueglia, E., G. Champigny, M. Lazdunski, and P. Barbry (1995). "Cloning of the amiloride-sensitive FMRFamide peptide-gated sodium channel". In: *Nature* 378.6558, pp. 730–733.

Littleton, J. and B. Ganetzky (2000). "Ion Channels and Synaptic Organization". In: *Neuron* 26.1, pp. 35–43.

Liu, C., P.-Y. Plaçais, N. Yamagata, B. D. Pfeiffer, Y. Aso, A. B. Friedrich, I. Siwanowicz, G. M. Rubin, T. Preat, and H. Tanimoto (2012). "A subset of dopamine neurons signals reward for odour memory in Drosophila". In: *Nature* 488.7412, pp. 512–516.

Liu, F. (2005). "In Silico Identification of New Secretory Peptide Genes in Drosophila melanogaster". In: *Molecular & Cellular Proteomics* 5.3, pp. 510–522.

Liu, Q., X. Yang, J. Tian, Z. Gao, M. Wang, Y. Li, and A. Guo (2016). "Gap junction networks in mushroom bodies participate in visual learning and memory in Drosophila". In: *eLife* 5, pp. 1–18.

Liu, W. W., O. Mazor, and R. I. Wilson (2015). "Thermosensory processing in the Drosophila brain". In: *Nature* 519.7543, pp. 353–357.

Liu, W. W. and R. I. Wilson (2013). "Glutamate is an inhibitory neurotransmitter in the Drosophila olfactory system." In: *Proceedings of the National Academy of Sciences of the United States of America* 110.25, pp. 10294–9.

Liu, X. and R. L. Davis (2009). "The GABAergic anterior paired lateral neuron suppresses and is suppressed by olfactory learning." In: *Nature Neuroscience* 12.1, pp. 53–59.

Liu, X., W. C. Krause, and R. L. Davis (2007). "GABAA Receptor RDL Inhibits Drosophila Olfactory Associative Learning". In: *Neuron* 56.6, pp. 1090–1102.

Ljaschenko, D., N. Ehmann, and R. J. Kittel (2013). "Hebbian Plasticity Guides Maturation of Glutamate Receptor Fields InVivo". In: *Cell Reports* 3.5, pp. 1407–1413.

Llinás, R. R., K. D. Walton, and E. J. Lang (2004). "Cerebellum". In: *The Synaptic Organization of the Brain*. Oxford University Press, pp. 271–310.

Logan, W. J. and S. H. Snyder (1972). "High affinity uptake systems for glycine, glutamic and aspartic acids in synaptosomes of rat central nervous tissues". In: *Brain Research* 42.2, pp. 413–431.

Lovett-Barron, M., P. Kaifosh, M. A. Kheirbek, N. Danielson, J. D. Zaremba, T. R. Reardon, G. F. Turi, R. Hen, B. V. Zemelman, and A. Losonczy (2014). "Dendritic Inhibition in the Hippocampus Supports Fear Learning". In: *Science* 343.6173, pp. 857–863.

Lozano, V., C. Armengaud, and M. Gauthier (2001). "Memory impairment induced by cholinergic antagonists injected into the mushroom bodies of the honeybee". In: *Journal of Comparative Physiology - A Sensory, Neural, and Behavioral Physiology* 187, pp. 249–254.

Luan, H., N. C. Peabody, C. R. Vinson, and B. H. White (2006). "Refined Spatial Manipulation of Neuronal Function by Combinatorial Restriction of Transgene Expression". In: *Neuron* 52.3, pp. 425–436.

Luqmani, Y. A., G. Sudlow, and V. P. Whittaker (1980). "Homocholine and acetylhomocholine: False transmitters in the cholinergic electromotor system of Torpedo". In: *Neuroscience* 5.1, pp. 153–160.

Luquet, S., F. A. Perez, T. S. Hnasko, and R. D. Palmiter (2005). "NPY/AgRP neurons are essential for feeding in adult mice but can be ablated in neonates." In: *Science (New York, N.Y.)* 310.5748, pp. 683–5.

Machado, D. R., D. J. Afonso, A. R. Kenny, A. Öztürk-Çolak, E. H. Moscato, B. Mainwaring, M. Kayser, and K. Koh (2017). "Identification of octopaminergic neurons that modulate sleep suppression by male sex drive". In: *eLife* 6, pp. 1–21.

Madalan, A., X. Yang, J. Ferris, S. Zhang, and G. Roman (2011). "G(o) activation is required for both appetitive and aversive memory acquisition in Drosophila". In: *Learning & Memory* 19.1, pp. 26–34.

Mahr, A. and H. Aberle (2006). "The expression pattern of the Drosophila vesicular glutamate transporter: A marker protein for motoneurons and glutamatergic centers in the brain". In: *Gene Expression Patterns* 6.3, pp. 299–309.

Maia, T. V. (2009). "Reinforcement learning, conditioning, and the brain: Successes and challenges." In: *Cognitive, affective & behavioral neuroscience* 9.4, pp. 343–364.

Makos, M. a., K.-A. Han, M. L. Heien, and A. G. Ewing (2010). "Using In Vivo Electrochemistry to Study the Physiological Effects of Cocaine and Other Stimulants on the Drosophila melanogaster Dopamine Transporter." In: *ACS chemical neuroscience* 1.1, pp. 74–83.

Makos, M. A., Y. C. Kim, K. A. Han, M. L. Heien, and A. G. Ewing (2009). "In vivo electrochemical measurements of exogenously applied dopamine in Drosophila melanogaster". In: *Analytical Chemistry* 81.5, pp. 1848–1854.

Maleszka, R., P. Helliwell, and R. Kucharski (2000). "Pharmacological interference with glutamate re-uptake impairs long-term memory in the honeybee, Apis mellifera". In: *Behavioural Brain Research* 115.1, pp. 49–53.

Malun, D. (1991). "Synaptic relationships between GABA-immunoreactive neurons and an identified uniglomerular projection neuron in the antennal lobe of Periplaneta americana: a double-labeling electron microscopic study". In: *Histochemistry* 96.3, pp. 197–207.

Mandelzys, A., P. De Koninck, and E. Cooper (1995). "Agonist and toxin sensitivities of ACh-evoked currents on neurons expressing multiple nicotinic ACh receptor subunits." In: *Journal of neurophysiology* 74.3, pp. 1212–21.

Manev, H. and S. Dzitoyeva (2010). "GABA-B receptors in drosophila". In: *Advances in Pharmacology* 58.C, pp. 453–464.

Manning, S. A., A. Kulkarni, J. H. A. Vissers, and K. F. Harvey (2016). "A Drosophila RNAi library modulates Hippo pathway-dependent tissue growth". In: *Nature Communications* 7, pp. 1–6.

Manton, J. D., A. D. Ostrovsky, L. Goetz, M. Costa, and T. Rohlfing (2014a). "Combining genome-scale Drosophila 3D neuroanatomical data by bridging template brains". In: *bioRxiv*, p. 6353.

Manton, J. D., A. D. Ostrovsky, L. Goetz, M. Costa, T. Rohlfing, and G. S. X. E. Jefferis (2014b). "Combining genome-scale Drosophila 3D neuroanatomical data by bridging template brains". In: *bioRxiv*, p. 6353.

Mao, T., D. H. O'Connor, V. Scheuss, J. Nakai, and K. Svoboda (2008). "Characterization and subcellular targeting of GCaMP-type genetically-encoded calcium indicators". In: *PLoS ONE* 3.3, pp. 1–10.

Mao, Z. and R. L. Davis (2009). "Eight different types of dopaminergic neurons innervate the Drosophila mushroom body neuropil: anatomical and physiological heterogeneity." In: *Frontiers in neural circuits* 3.July, p. 5.

Martelli, C., U. Pech, S. Kobbenbring, D. Pauls, B. Bahl, M. V. Sommer, A. Pooryasin, J. Barth, C. W. P. Arias, C. Vassiliou, A. J. F. Luna, H. Poppinga, F. G. Richter, C. Wegener, A. Fiala, and T. Riemensperger (2017). "SIFamide Translates Hunger Signals into Appetitive and Feeding Behavior in Drosophila". In: *Cell Reports* 20.2, pp. 464–478.

Martin, C. A. and D. E. Krantz (2014). "Drosophila melanogaster as a genetic model system to study neurotransmitter transporters". In: *Neurochemistry International* 73.1, pp. 71–88.

Martín-Peña, A., A. Acebes, J.-R. Rodríguez, V. Chevalier, S. Casas-Tinto, T. Triphan, R. Strauss, and A. Ferrús (2014). "Cell types and coincident synapses in the ellipsoid body of Drosophila." In: *The European journal of neuroscience* 39.10, pp. 1586–601.

Masek, P., K. Worden, Y. Aso, G. M. Rubin, and A. C. Keene (2015). "A dopamine-modulated neural circuit regulating aversive taste memory in drosophila". In: *Current Biology* 25.11, pp. 1535–1541.

Masse, N. Y., G. C. Turner, and G. S. X. E. Jefferis (2009). "Olfactory information processing in Drosophila." In: *Current biology : CB* 19.16, R700–13.

Maule, A. G., D. W. Halton, and C. Shaw (1995). "Neuropeptide F: a ubiquitous invertebrate neuromediator?" In: *Hydrobiologia: The International Journal of Aquatic Sciences* 305.1, pp. 297–303.

McCool, B. a. and S. K. Botting (2000). "Characterization of strychnine-sensitive glycine receptors in acutely isolated adult rat basolateral amygdala neurons." In: *Brain research* 859.2, pp. 341–51.

McGaugh, J. L. (2000). "Memory–a Century of Consolidation". In: *Science* 287.5451, pp. 248–251.

McGuire, S. E., M. Deshazer, and R. L. Davis (2005). "Thirty years of olfactory learning and memory research in Drosophila melanogaster." In: *Progress in Neurobiology* 76.5, pp. 328–347.

McGuire, S. E., P. T. Le, and R. L. Davis (2001). "The role of Drosophila mushroom body signaling in olfactory memory." In: *Science* 293.5533, pp. 1330–3.

McGuire, S. E., P. T. Le, A. J. Osborn, K. Matsumoto, and R. L. Davis (2003). "Spatiotemporal Rescue of Memory Dysfunction in Drosophila". In: *Science* 302.5651, pp. 1765–1768.

McGuire, T. R. (1984). "Learning in three species of diptera: The blow fly Phormia regina, the fruit fly Drosophila melanogaster, and the house fly Musca domestica". In: *Behavior Genetics* 14.5, pp. 479–526.

Mehren, J. E. and L. C. Griffith (2006). "Cholinergic neurons mediate CaMKII-dependent enhancement of courtship suppression". In: *Learning & Memory* 13.6, pp. 686–689.

Melzig, J., S. Buchner, F. Wiebel, R. Wolf, M. Burg, W. L. Pak, and E. Buchner (1996). "Genetic depletion of histamine from the nervous system of Drosophila eliminates specific visual and mechanosensory behavior." In: *Journal of comparative physiology. A, Sensory, neural, and behavioral physiology* 179.6, pp. 763–773.

Menzel, R. and U. Müller (1996). "Learning and memory in honeybees: from behavior to neural substrates." In: *Annual review of neuroscience* 19.1, pp. 379–404.

Merlo, E., A. L. Milton, Z. Y. Goozee, D. E. Theobald, and B. J. Everitt (2014). "Reconsolidation and Extinction Are Dissociable and Mutually Exclusive Processes: Behavioral and Molecular Evidence". In: *Journal of Neuroscience* 34.7, pp. 2422–2431.

Mertens, I., T. Meeusen, R. Huybrechts, A. De Loof, L. Schoofs, S. F. Garczynski, M. R. Brown, P. Shen, T. F. Murray, and J. W. Crim (2002). "Characterization of the short neuropeptide F receptor from Drosophila melanogaster". In: *Biochemical and biophysical research communications* 297.5, pp. 1140–1148.

Mertens, I., A. Vandingenen, T. Meeusen, T. Janssen, W. Luyten, R. J. Nachman, A. De Loof, and L. Schoofs (2004). "Functional characterization of the putative orphan

neuropeptide G-protein coupled receptor C26F1.6 in Caenorhabditis elegans". In: *FEBS Letters* 573.1-3, pp. 55–60.

Mezler, M., T. Müller, and K. Raming (2001). "Cloning and functional expression of GABAB receptors from Drosophila". In: *European Journal of Neuroscience* 13.3, pp. 477–486.

Michel, M. C., A. Beck-Sickinger, H. Cox, H. N. Doods, H. Herzog, D. Larhammar, R. Quirion, T. Schwartz, and T. Westfall (1998). "XVI. International Union of Pharmacology Recommendations for the Nomenclature of Neuropeptide Y, Peptide YY, and Pancreatic Polypeptide Receptors." In: *Pharmacological Reviews* 50.1, pp. 143–50.

Miesenböck, G., D. A. De Angelis, and J. E. Rothman (1998). "Visualizing secretion and synaptic transmission with pH-sensitive green fluorescent proteins." In: *Nature* 394.6689, pp. 192–5.

Milad, M. R. and G. J. Quirk (2002). "Neurons in medial prefrontal cortex signal memory for fear extinction". In: *Nature* 420.6911, pp. 70–74.

Miles, R., K. Tóth, A. I. Gulyás, N. Hájos, and T. F. Freund (1996). "Differences between somatic and dendritic inhibition in the hippocampus". In: *Neuron* 16.4, pp. 815–823.

Millar, N. S. and I. Denholm (2007). "Nicotinic acetylcholine receptors: Targets for commercially important insecticides". In: *Invertebrate Neuroscience* 7, pp. 53–66.

Milyaev, N., D. Osumi-sutherland, S. Reeve, N. Burton, R. A. Baldock, and J. D. Armstrong (2012). "The virtual fly brain browser and query interface". In: *Bioinformatics* 28.3, pp. 411–415.

Miyaji, T., N. Echigo, M. Hiasa, S. Senoh, H. Omote, and Y. Moriyama (2008). "Identification of a vesicular aspartate transporter". In: *Proceedings of the National Academy of Sciences* 105.33, pp. 11720–11724.

Miyamoto, T., J. Slone, X. Song, and H. Amrein (2012). "A fructose receptor functions as a nutrient sensor in the drosophila brain". In: *Cell* 151.5, pp. 1113–1125.

Miyawaki, a., J. Llopis, R. Heim, J. M. McCaffery, J. a. Adams, M. Ikura, and R. Y. Tsien (1997). "Fluorescent indicators for Ca2+ based on green fluorescent proteins and calmodulin." In: *Nature* 388.6645, pp. 882–887.

Mohammad, F., J. C. Stewart, S. Ott, K. Chlebikova, J. Y. Chua, T.-W. Koh, J. Ho, and A. Claridge-Chang (2017). "Optogenetic inhibition of behavior with anion channelrhodopsins". In: *Nature Methods* 14.3, pp. 271–274.

Monastirioti, M., C. E. Linn, and K. White (1996). "Characterization of Drosophila tyramine beta-hydroxylase gene and isolation of mutant flies lacking octopamine." In: *The Journal of neuroscience : the official journal of the Society for Neuroscience* 16.12, pp. 3900–3911.

Monastirioti, M. (2003). "Distinct octopamine cell population residing in the CNS abdominal ganglion controls ovulation in Drosophila melanogaster". In: *Developmental Biology* 264.1, pp. 38–49.

Montague, S. A. and B. S. Baker (2016). "Memory Elicited by Courtship Conditioning Requires Mushroom Body Neuronal Subsets Similar to Those Utilized in Appetitive Memory". In: *Plos One* 11.10, e0164516.

Morgan, T. H. (1910). "Sex limited inheritance in Drosophila". In: *Science* 32.812, pp. 120–122.

— (1915). *The Mechanism of Mendelian Heredity*. H. Holt.

Morland, C., K. Nordengen, M. Larsson, L. M. Prolo, Z. Farzampour, R. J. Reimer, and V. Gundersen (2013). "Vesicular uptake and exocytosis of L-aspartate is independent of sialin". In: *FASEB Journal* 27.3, pp. 1264–1274.

Moss, R. L., M. R. Sollins, and F. J. Julian (1976). "Aspartate and glutamate as possible transmitters of excitatory hippocampal afferents". In: *Nature* 260, pp. 538–540.

Musso, P.-Y., P. Tchenio, and T. Preat (2015). "Delayed Dopamine Signaling of Energy Level Builds Appetitive Long-Term Memory in Drosophila". In: *Cell Reports* 10.7, pp. 1023–1031.

Nader, K., G. E. Schafe, and J. E. Le Doux (2000). "Fear memories require protein synthesis in the amygdala for reconsolidation after retrieval." In: *Nature* 406.6797, pp. 722–726.

Nadler, J. V. (2011). "Aspartate release and signalling in the hippocampus". In: *Neurochemical Research* 36.4, pp. 668–676.

Nagaya, Y., M. Kutsukake, S. I. Chigusa, and A. Komatsu (2002). *A trace amine, tyramine, functions as a neuromodulator in Drosophila melanogaster.*

Nagel, G., T. Szellas, W. Huhn, S. Kateriya, N. Adeishvili, P. Berthold, D. Ollig, P. Hegemann, and E. Bamberg (2003). "Channelrhodopsin-2, a directly light-gated cation-selective membrane channel." In: *Proceedings of the National Academy of Sciences of the United States of America* 100.24, pp. 13940–5.

Naito, Y., T. Yamada, T. Matsumiya, K. Ui-Tei, K. Saigo, and S. Morishita (2005). "dsCheck: Highly sensitive off-target search software for double-stranded RNA-mediated RNA interference". In: *Nucleic Acids Research* 33.SUPPL. 2, pp. 589–591.

Nakai, J., M. Ohkura, and K. Imoto (2001). "A high signal-to-noise Ca(2+) probe composed of a single green fluorescent protein." In: *Nature biotechnology* 19.2, pp. 137–41.

Narahashi, T., J. W. Moore, and W. R. Scott (1964). "Tetrodotoxin Blockage of Sodium Conductance Increase in Lobster Giant Axons". In: *The Journal of General Physiology* 47.5, pp. 965–974.

Nässel, D. R. (1999). "Histamine in the brain of insects: A review". In: *Microscopy Research and Technique* 44.2-3, pp. 121–136.

— (2002). "Neuropeptides in the nervous system of Drosophila and other insects: multiple roles as neuromodulators and neurohormones." In: *Progress in neurobiology* 68.1, pp. 1–84.

— (2009). "Neuropeptide signaling near and far: How localized and timed is the action of neuropeptides in brain circuits?" In: *Invertebrate Neuroscience* 9.2, pp. 57–75.

Nässel, D. R. and K. Elekes (1992). "Aminergic neurons in the brain of blowflies and Drosophila: dopamine- and tyrosine hydroxylase-immunoreactive neurons and their relationship with putative histaminergic neurons". In: *Cell & Tissue Research* 267.1, pp. 147–167.

Nässel, D. R., L. E. Enell, J. G. Santos, C. Wegener, and H. a. D. Johard (2008). "A large population of diverse neurons in the Drosophila central nervous system expresses short neuropeptide F, suggesting multiple distributed peptide functions." In: *BMC neuroscience* 9, p. 90.

Nässel, D. R., M. H. Holmqvist, R. C. Hardie, R. Håkanson, and F. Sundler (1988). "Histamine-like immunoreactivity in photoreceptors of the compound eyes and ocelli of the flies Calliphora erythrocephala and Musca domestica". In: *Cell and Tissue Research* 253.3, pp. 639–646.

Nässel, D. R. and U. Homberg (2006). "Neuropeptides in interneurons of the insect brain". In: *Cell and Tissue Research* 326.1, pp. 1–24.

Nässel, D. R. and C. Wegener (2011). "A comparative review of short and long neuropeptide F signaling in invertebrates: Any similarities to vertebrate neuropeptide Y signaling?" In: *Peptides* 32.6, pp. 1335–55.

Neckameyer, W. S. and K. White (1993). "Drosophila Tyrosine Hydroxylase is Encoded by the Pale Locus". In: *Journal of Neurogenetics* 8.4, pp. 189–199.

Nelson, D. L. and M. M. Cox (2013). *Lehninger Principles of Biochemistry*. 6th ed., pp. 1–1198.

Ng, M., R. D. Roorda, S. Q. Lima, B. V. Zemelman, P. Morcillo, and G. Miesenbock (2002). "Transmission of olfactory information between three populations in the antennal lobe of the of neurons fly". In: *Neuron* 36.3, pp. 463–474.

Ni, J.-Q., L.-P. Liu, R. Binari, R. Hardy, H.-S. Shim, A. Cavallaro, M. Booker, B. D. Pfeiffer, M. Markstein, H. Wang, C. Villalta, T. R. Laverty, L. a. Perkins, and N. Perrimon (2009). "A Drosophila resource of transgenic RNAi lines for neurogenetics." In: *Genetics* 182.4, pp. 1089–100.

Ni, J.-Q., M. Markstein, R. Binari, B. Pfeiffer, L.-P. Liu, C. Villalta, M. Booker, L. Perkins, and N. Perrimon (2008). "Vector and parameters for targeted transgenic RNA interference in Drosophila melanogaster." In: *Nature Methods* 5.1, pp. 49–51.

Nickell, J. R., V. P. Grinevich, K. B. Siripurapu, A. M. Smith, and L. P. Dwoskin (2013). "Potential therapeutic uses of mecamylamine and its stereoisomers". In: *Pharmacology Biochemistry and Behavior* 108, pp. 28–43.

Nicolaï, L. J. J., A. Ramaekers, T. Raemaekers, A. Drozdzecki, A. S. Mauss, J. Yan, M. Landgraf, W. Annaert, and B. a. Hassan (2010). "Genetically encoded dendritic marker sheds light on neuronal connectivity in Drosophila." In: *Proceedings of the National Academy of Sciences of the United States of America* 107.47, pp. 20553–8.

Niewalda, T., N. Singhal, A. Fiala, T. Saumweber, S. Wegener, and B. Gerber (2008). "Salt processing in larval drosophila: Choice, feeding, and learning shift from appetitive to aversive in a concentration-dependent way". In: *Chemical Senses* 33.8, pp. 685–692.

Nighorn, A., M. J. Healy, and R. L. Davis (1991). "The cyclic AMP phosphodiesterase encoded by the Drosophila dunce gene is concentrated in the mushroom body neuropil." In: *Neuron* 6.3, pp. 455–467.

Nusbaum, M. P., D. M. Blitz, and E. Marder (2017). "Functional consequences of neuropeptide and small-molecule co-transmission". In: *Nat Rev Neurosci* advance on.

Nusbaum, M. P., D. M. Blitz, A. M. Swensen, D. Wood, and E. Marder (2001). "The roles of co-transmission in neural network modulation". In: *Trends in Neurosciences* 24.3, pp. 146–154.

O'Dell, T. J. and B. N. Christensen (1988). "Mecamylamine is a selective non-competitive antagonist of N-methyl-d-aspartate- and aspartate-induced currents in horizontal cells dissociated from the catfish retina". In: *Neuroscience Letters* 94.1-2, pp. 93–98.

Oh, Y., S. E. Yoon, Q. Zhang, H. S. Chae, I. Daubnerová, O. T. Shafer, J. Choe, and Y. J. Kim (2014). "A Homeostatic Sleep-Stabilizing Pathway in Drosophila Composed of the Sex Peptide Receptor and Its Ligand, the Myoinhibitory Peptide". In: *PLoS Biology* 12.10.

Okada, R., T. Awasaki, and K. Ito (2009). "Gamma-aminobutyric acid (GABA)-mediated neural connections in the Drosophila antennal lobe". In: *Journal of Comparative Neurology* 514.1, pp. 74–91.

Okamoto, K., H. Kimura, and Y. Sakai (1983). "Evidence for taurine as an inhibitory neurotransmitter in cerebellar stellate interneurons: selective antagonism by TAG (6-aminomethyl-3-methyl-4H,1,2,4-benzothiadiazine-1,1-dioxide)". In: *Brain Research* 265.1, pp. 163–168.

Owald, D., J. Felsenberg, C. B. Talbot, G. Das, E. Perisse, W. Huetteroth, and S. Waddell (2015a). "Activity of Defined Mushroom Body Output Neurons Underlies Learned Olfactory Behavior in Drosophila". In: *Neuron* 86.2, pp. 417–427.

Owald, D., S. Lin, and S. Waddell (2015b). "Light, heat, action: neural control of fruit fly behaviour." In: *Philosophical transactions of the Royal Society of London. Series B, Biological sciences* 370.1677, pp. 20140211–.

Owald, D. and S. Waddell (2015). "Olfactory learning skews mushroom body output pathways to steer behavioral choice in Drosophila". In: *Current Opinion in Neurobiology* 35.Figure 1, pp. 178–184.

Pahud, G., N. Salem, J. Van De Goor, J. Medilanski, N. Pellegrinelli, and L. Eder-Colli (1998). "Study of subcellular localization of membrane-bound choline acetyltransferase in Drosophila central nervous system and its association with membranes". In: *European Journal of Neuroscience* 10.5, pp. 1644–1653.

Pai, T.-P., C.-C. Chen, H.-H. Lin, A.-L. Chin, J. S.-Y. Lai, P.-T. Lee, T. Tully, and A.-S. Chiang (2013). "Drosophila ORB protein in two mushroom body output neurons is necessary for long-term memory formation". In: *Proceedings of the National Academy of Sciences* 110.19, pp. 7898–7903.

Pankova, K. and A. Borst (2017). "Transgenic line for the identification of cholinergic release sites in Drosophila melanogaster". In: *The Journal of Experimental Biology* February, jeb.149369.

Papke, R. L., P. R. Sanberg, and R. D. Shytle (2001). "Analysis of mecamylamine stereoisomers on human nicotinic receptor subtypes." In: *The Journal of pharmacology and experimental therapeutics* 297.2, pp. 646–656.

Papke, R. L., M. Bencherif, and P. Lippiello (1996). "An evaluation of neuronal nicotinic acetylcholine receptor activation by quaternary nitrogen compounds indicates that choline is selective for the $\alpha 7$ subtype". In: *Neuroscience Letters* 213.3, pp. 201–204.

Parikh, V., R. Kozak, V. Martinez, and M. Sarter (2007). "Prefrontal Acetylcholine Release Controls Cue Detection on Multiple Timescales". In: *Neuron* 56.1, pp. 141–154.

Park, S., J. Y. Sonn, Y. Oh, C. Lim, and J. Choe (2014). "SIFamide and SIFamide Receptor Defines a Novel Neuropeptide Signaling to Promote Sleep in Drosophila." In: *Molecules and cells* 37.4, pp. 295–301.

Parmentier, M. L., J. P. Pin, J. Bockaert, and Y. Grau (1996). "Cloning and functional expression of a Drosophila metabotropic glutamate receptor expressed in the embryonic CNS." In: *The Journal of neuroscience : the official journal of the Society for Neuroscience* 16.21, pp. 6687–94.

Pascual, A. and T. Préat (2001). "Localization of long-term memory within the Drosophila mushroom body." In: *Science* 294.5544, pp. 1115–1117.

Patneau, D. K. and M. L. Mayer (1990). "Structure-activity relationships for amino acid transmitter candidates acting at N-methyl-D-aspartate and quisqualate receptors." In: *The Journal of neuroscience : the official journal of the Society for Neuroscience* 10.7, pp. 2385–99.

Pavlov, I. (1927). *Conditioned reflexes: an investigation of the physiological activity of the cerebral cortex*. London: Oxford University Press.

Pech, U., A. Pooryasin, S. Birman, and A. Fiala (2013). "Localization of the Contacts Between Kenyon Cells and Aminergic Neurons in the Drosophila melanogaster Brain Using SplitGFP Reconstitution". In: *Journal of Comparative Neurology* 521.17, pp. 3992–4026.

Pech, U., N. H. Revelo, K. J. Seitz, S. O. Rizzoli, and A. Fiala (2015). "Optical Dissection of Experience-Dependent Pre- and Postsynaptic Plasticity in the Drosophila Brain". In: *Cell Reports* 10.12, pp. 2083–2095.

Pedreira, M. E., L. M. Pérez-Cuesta, and H. Maldonado (2004). "Mismatch between what is expected and what actually occurs triggers memory reconsolidation or extinction." In: *Learning & Memory* 11.5, pp. 579–85.

Perazzona, B., G. Isabel, T. Preat, and R. L. Davis (2004). "The Role of cAMP Response Element-Binding Protein in Drosophila Long-Term Memory". In: *J. Neurosci.* 24.40, pp. 8823–8828.

Perez-Orive, J., O. Mazor, G. C. Turner, S. Cassenaer, R. I. Wilson, and G. Laurent (2002). "Oscillations and sparsening of odor representations in the mushroom body." In: *Science (New York, N.Y.)* 297.5580, pp. 359–365.

Perisse, E., C. Burke, W. Huetteroth, and S. Waddell (2013a). "Shocking Revelations and Saccharin Sweetness in the Study of Drosophila Olfactory Memory". In: *Current Biology* 23.17, R752–R763.

Perisse, E., D. Owald, O. Barnstedt, C. B. Talbot, W. Huetteroth, and S. Waddell (2016). "Aversive Learning and Appetitive Motivation Toggle Feed-Forward Inhibition in the Drosophila Mushroom Body". In: *Neuron* 90.5, pp. 1086–1099.

Perisse, E., Y. Yin, A. C. Lin, S. Lin, W. Huetteroth, and S. Waddell (2013b). "Different Kenyon Cell Populations Drive Learned Approach and Avoidance in Drosophila". In: *Neuron* 79.5, pp. 945–956.

Perrat, P. N., S. DasGupta, J. Wang, W. Theurkauf, Z. Weng, M. Rosbash, and S. Waddell (2013). "Transposition-Driven Genomic Heterogeneity in the Drosophila Brain". In: *Science* 340.6128, pp. 91–95.

Perron, A., H. Mutoh, W. Akemann, S. G. Gautam, D. Dimitrov, Y. Iwamoto, and T. Knöpfel (2009). "Second and third generation voltage-sensitive fluorescent proteins for monitoring membrane potential." In: *Frontiers in molecular neuroscience* 2, p. 5.

Perry, T., J. a. McKenzie, and P. Batterham (2007). "A Dalpha6 knockout strain of Drosophila melanogaster confers a high level of resistance to spinosad." In: *Insect biochemistry and molecular biology* 37.2, pp. 184–8.

Perry, T., J. Somers, Y. T. Yang, and P. Batterham (2015). "Expression of insect α6-like nicotinic acetylcholine receptors in Drosophila melanogaster highlights a high level of conservation of the receptor:spinosyn interaction". In: *Insect Biochemistry and Molecular Biology*, pp. 1–10.

Pfeiffer, B. D., A. Jenett, A. S. Hammonds, T.-T. B. Ngo, S. Misra, C. Murphy, A. Scully, J. W. Carlson, K. H. Wan, T. R. Laverty, C. Mungall, R. Svirskas, J. T. Kadonaga, C. Q. Doe, M. B. Eisen, S. E. Celniker, and G. M. Rubin (2008). "Tools for neuroanatomy and neurogenetics in Drosophila." In: *Proceedings of the National Academy of Sciences of the United States of America* 105.28, pp. 9715–9720.

Pfeiffer, B. D., T. T. B. Ngo, K. L. Hibbard, C. Murphy, A. Jenett, J. W. Truman, and G. M. Rubin (2010). "Refinement of tools for targeted gene expression in Drosophila". In: *Genetics* 186.2, pp. 735–755.

Pitman, J. L., W. Huetteroth, C. J. Burke, M. J. Krashes, S.-L. Lai, T. Lee, and S. Waddell (2011). "A pair of inhibitory neurons are required to sustain labile memory in the Drosophila mushroom body." In: *Current Biology* 21.10, pp. 855–61.

Plaçais, P.-Y., T. Preat, P.-Y. Placais, and T. Preat (2013a). "To Favor Survival Under Food Shortage, the Brain Disables Costly Memory". In: *Science* 339.6118, pp. 440–442.

Plaçais, P.-Y., S. Trannoy, A. B. Friedrich, H. Tanimoto, and T. Preat (2013b). "Two pairs of mushroom body efferent neurons are required for appetitive long-term memory retrieval in Drosophila." In: *Cell reports* 5.3, pp. 769–80.

Plaçais, P.-Y., S. Trannoy, G. Isabel, Y. Aso, I. Siwanowicz, G. Belliart-Guérin, P. Vernier, S. Birman, H. Tanimoto, and T. Preat (2012). "Slow oscillations in two pairs of dopaminergic neurons gate long-term memory formation in Drosophila." In: *Nature Neuroscience* 15.4, pp. 592–599.

Plaçais, P.-Y., É. de Tredern, L. Scheunemann, S. Trannoy, V. Goguel, K.-A. Han, G. Isabel, and T. Preat (2017). "Upregulated energy metabolism in the Drosophila mushroom body is the trigger for long-term memory." In: *Nature communications* 8, p. 15510.

Polak, R. L. (1971). "Stimulating action of atropine on the release of acetylcholine by rat cerebral cortex in vitro". In: *British Journal of Pharmacology* 41.4, pp. 600–606.

Pollack, I. and A. Hofbauer (1991). "Histamine-like immunoreactivity in the visual system and brain of an orthopteran and a hymenopteran insect". In: *Cell and Tissue Research* 266.1, pp. 391–398.

Pologruto, T. A., B. L. Sabatini, and K. Svoboda (2003). "ScanImage: Flexible software for operating laser scanning microscopes". In: *BioMedical Engineering OnLine* 2.1, p. 13.

Pooryasin, A. and A. Fiala (2015). "Identified Serotonin-Releasing Neurons Induce Behavioral Quiescence and Suppress Mating in Drosophila". In: *Journal of Neuroscience* 35.37, pp. 12792–12812.

Potter, C. J., B. Tasic, E. V. Russler, L. Liang, and L. Luo (2010). "The Q system: A repressible binary system for transgene expression, lineage tracing, and mosaic analysis". In: *Cell* 141.3, pp. 536–548.

Prado, V. F., A. Roy, B. Kolisnyk, R. Gros, and M. a. M. Prado (2013). "Regulation of cholinergic activity by the vesicular acetylcholine transporter." In: *The Biochemical journal* 450, pp. 265–74.

Pramod, A. B., J. Foster, L. Carvelli, and L. K. Henry (2013). "SLC6 transporters: Structure, function, regulation, disease association and therapeutics". In: *Molecular Aspects of Medicine* 34.2-3, pp. 197–219.

Prasher, D. C., V. K. Eckenrode, W. W. Ward, F. G. Prendergast, and M. J. Cormier (1992). "Primary structure of the Aequorea victoria green-fluorescent protein". In: *Gene* 111.2, pp. 229–233.

Predel, R., C. Wegener, W. K. Russell, S. E. Tichy, D. H. Russell, and R. J. Nachman (2004). "Peptidomics of CNS-associated neurohemal systems of adult Drosophila melanogaster: A mass spectrometric survey of peptides from individual flies". In: *Journal of Comparative Neurology* 474.3, pp. 379–392.

Pulver, S. R., S. L. Pashkovski, N. J. Hornstein, P. a. Garrity, and L. C. Griffith (2009). "Temporal dynamics of neuronal activation by Channelrhodopsin-2 and TRPA1 determine behavioral output in Drosophila larvae." In: *Journal of neurophysiology* 101.6, pp. 3075–88.

Qian, J., W. F. Colmers, and P. Saggau (1997). "Inhibition of synaptic transmission by neuropeptide Y in rat hippocampal area CA1: modulation of presynaptic Ca2+ entry". In: *The Journal of neuroscience : the official journal of the Society for Neuroscience* 17.21, pp. 8169–8177.

Qin, H. and J. Dubnau (2010). "Genetic disruptions of Drosophila Pavlovian learning leave extinction learning intact". In: *Genes, Brain and Behavior* 9.2, pp. 203–212.

Qin, H., M. Cressy, W. Li, J. S. Coravos, S. a. Izzi, and J. Dubnau (2012). "Gamma neurons mediate dopaminergic input during aversive olfactory memory formation in Drosophila." In: *Current Biology* 22.7, pp. 608–14.

Quinn, W. G. and Y. Dudai (1976). "Memory phases in Drosophila". In: *Nature* 262, pp. 576–577.

Quinn, W. G., W. A. Harris, and S. Benzer (1974). "Conditioned behavior in Drosophila melanogaster." In: *Proceedings of the National Academy of Sciences of the United States of America* 71.3, pp. 708–12.

Quinn, W. G., P. P. Sziber, and R. Booker (1979). "The Drosophila memory mutant amnesiac". In: *Nature* 277.5693, pp. 212–214.

Quirk, G. J., E. Likhtik, J. G. Pelletier, and D. Pare (2003). "Stimulation of medial prefrontal cortex decreases the responsiveness of central amygdala output neurons". In: *J Neurosci* 23.25, pp. 8800–8807.

Raccuglia, D., L. Yan McCurdy, M. Demir, S. Gorur-Shandilya, M. Kunst, T. Emonet, and M. N. Nitabach (2016). "Presynaptic GABA Receptors Mediate Temporal Contrast Enhancement in Drosophila Olfactory Sensory Neurons and Modulate Odor-Driven Behavioral Kinetics". In: *eNeuro* 3.4, pp. 0080–16.

Raghu, S. V. and A. Borst (2011). "Candidate glutamatergic neurons in the visual system of drosophila". In: *PLoS ONE* 6.5, pp. 1–11.

Raghu, S. V., J. Claussen, and A. Borst (2013). "Neurons with GABAergic phenotype in the visual system of Drosophila". In: *Journal of Comparative Neurology* 521.1, pp. 252–265.

Rakhilin, S., R. C. Drisdel, D. Sagher, D. S. McGehee, Y. Vallejo, and W. N. Green (1999). "alpha-bungarotoxin receptors contain alpha7 subunits in two different disulfide-bonded conformations." In: *The Journal of cell biology* 146.1, pp. 203–18.

Reale, V., H. M. Chatwin, and P. D. Evans (2004). "The activation of G-protein gated inwardly rectifying K+ channels by a cloned Drosophila melanogaster neuropeptide F-like receptor". In: *European Journal of Neuroscience* 19.3, pp. 570–576.

Reale, V., F. Hannan, J. M. Midgley, and P. D. Evans (1997). "The expression of a cloned Drosophila octopamine/tyramine receptor in Xenopus oocytes". In: *Brain Research* 769.2, pp. 309–320.

Reichelt, A. C., M. T. Exton-McGuinness, and J. L. C. Lee (2013). "Ventral Tegmental Dopamine Dysregulation Prevents Appetitive Memory Destabilization". In: *Journal of Neuroscience* 33.35, pp. 14205–14210.

Rescorla, R. A. and C. D. Heth (1975). "Reinstatement of fear to an extinguished conditioned stimulus." In: *Journal of Experimental Psychology: Animal Behavior Processes* 1.1, p. 88.

Resh, M. D. (1999). "Fatty acylation of proteins: new insights into membrane targeting of myristylated and palmitoylated proteins". In: *Biochimica et Biophysica Acta - Molecular Cell Research* 1451.1, pp. 1–16.

Rhim, H., G. a. Kinney, P. J. Emmerson, and R. J. Miller (1997). "Regulation of neurotransmission in the arcuate nucleus of the rat by different neuropeptide Y

receptors." In: *The Journal of neuroscience : the official journal of the Society for Neuroscience* 17.8, pp. 2980–2989.

Ribeiro, F. M., J. Alves-Silva, W. Volknandt, C. Martins-Silva, H. Mahmud, A. Wilhelm, M. V. Gomez, R. J. Rylett, S. S. G. Ferguson, V. F. Prado, and M. A. M. Prado (2003). "The hemicholinium-3 sensitive high affinity choline transporter is internalized by clathrin-mediated endocytosis and is present in endosomes and synaptic vesicles". In: *Journal of Neurochemistry* 87.1, pp. 136–146.

Riemensperger, T., F. Bilz, and A. Fiala (2017). "Visualization of Synapses and Synaptic Plasticity in the Drosophila Brain". In: *Decoding Neural Circuit Structure and Function*. Cham: Springer International Publishing, pp. 309–319.

Riemensperger, T., R. J. Kittel, and A. Fiala (2016). "Optogenetics in Drosophila Neuroscience". In: *Optogenetics: Methods and Protocols*. Ed. by A. Kianianmomeni. Vol. 1408. Springer. Chap. 11, pp. 167–175.

Riemensperger, T., T. Völler, P. Stock, E. Buchner, and A. Fiala (2005). "Punishment prediction by dopaminergic neurons in Drosophila". In: *Current Biology* 15.21, pp. 1953–1960.

Robb, S., T. R. Cheek, F. L. Hannan, L. M. Hall, J. M. Midgley, and P. D. Evans (1994). "Agonist-specific coupling of a cloned Drosophila octopamine/tyramine receptor to multiple second messenger systems." In: *The EMBO journal* 13.6, pp. 1325–30.

Robinson, D. L., B. J. Venton, M. L. A. V. Heien, and R. M. Wightman (2003). "Detecting subsecond dopamine release with fast-scan cyclic voltammetry in vivo". In: *Clinical Chemistry* 49.10, pp. 1763–1773.

Robinson, I. M., R. Ranjan, and T. L. Schwarz (2002). "Synaptotagmins I and IV promote transmitter release independently of Ca(2+) binding in the C(2)A domain." In: *Nature* 418.6895, pp. 336–340.

Rodriguez, E. A., R. E. Campbell, J. Y. Lin, M. Z. Lin, A. Miyawaki, A. E. Palmer, X. Shu, J. Zhang, and R. Y. Tsien (2017). "The Growing and Glowing Toolbox of Fluorescent and Photoactive Proteins". In: *Trends in Biochemical Sciences* 42.2, pp. 111–129.

Roeder, T. (2003). "Metabotropic histamine receptors - Nothing for invertebrates?" In: *European Journal of Pharmacology* 466.1-2, pp. 85–90.

— (2005). "Tyramine and octopamine: ruling behavior and metabolism." In: *Annual review of entomology* 50.1, pp. 447–77.

Roghani, A., A. Shirzadi, L. L. Butcher, and R. H. Edwards (1997). "Distribution of the vesicular transporter for acetylcholine in the rat central nervous system". In: *Neuroscience* 82.4, pp. 1195–1212.

Root, C. M., K. I. Ko, A. Jafari, and J. W. Wang (2011). "Presynaptic facilitation by neuropeptide signaling mediates odor-driven food search". In: *Cell* 145.1, pp. 133–144.

Root, C. M., K. Masuyama, D. S. Green, L. E. Enell, D. R. Nässel, C. H. Lee, and J. W. Wang (2008). "A Presynaptic Gain Control Mechanism Fine-Tunes Olfactory Behavior". In: *Neuron* 59.2, pp. 311–321.

Root, C. M., A. M. Wong, J. Flores, and J. W. Wang (2013). "Calcium imaging in the Drosophila olfactory system with a genetic indicator." In: *Cold Spring Harbor protocols* 2013.11, pp. 1064–1070.

Rudloff, E. (1978). "Acetylcholine receptors in the central nervous system of Drosophila melanogaster". In: *Experimental Cell Research* 111.1, pp. 185–190.

Sahu, A., P. S. Kalra, and S. P. Kalra (1988). "Food deprivation and ingestion induce reciprocal changes in neuropeptide Y concentrations in the paraventricular nucleus". In: *Peptides* 9.1, pp. 83–86.

Salcedo, E., a. Huber, S. Henrich, L. V. Chadwell, W. H. Chou, R. Paulsen, and S. G. Britt (1999). "Blue- and green-absorbing visual pigments of Drosophila: ectopic expression and physiological characterization of the R8 photoreceptor cell-specific Rh5 and Rh6 rhodopsins." In: *The Journal of neuroscience : the official journal of the Society for Neuroscience* 19.24, pp. 10716–10726.

Salin, P. A., R. C. Malenka, and R. A. Nicoll (1996). "Cyclic AMP Mediates a Presynaptic Form of LTP at Cerebellar Parallel Fiber Synapses". In: *Neuron* 16, pp. 797–803.

Salvaterra, P. M. and T. Kitamoto (2001). "Drosophila cholinergic neurons and processes visualized with Gal4/UAS-GFP". In: *Gene Expression Patterns* 1.1, pp. 73–82.

Sanacora, G., M. Kershaw, J. A. Finkelstein, and J. D. White (1990). "Increased Hypothalamic Content of Preproneuropeptide-Y Messenger-Ribonucleic-Acid in Genetically-Obese Zucker Rats and Its Regulation By Food-Deprivation". In: *Endocrinology* 127.2, pp. 730–737.

Saraswati, S., L. E. Fox, D. R. Soll, and C. F. Wu (2004). "Tyramine and Octopamine Have Opposite Effects on the Locomotion of Drosophila Larvae". In: *Journal of Neurobiology* 58.4, pp. 425–441.

Sattelle, D. B. (1980). "Acetylcholine receptors of insects". In: *Advances in insect physiology* 15, pp. 215–315.

Sattelle, D. B. and H. Breert (1990). "Cholinergic Nerve Terminals in the Central Nervous System of insects". In: *Journal of neuroendocrinology* 2.3, pp. 241–256.

Saudou, F., N. Amlaiky, J. L. Plassat, E. Borrelli, and R. Hen (1990). "Cloning and characterization of a Drosophila tyramine receptor." In: *The EMBO journal* 9.11, pp. 3611–7.

Saudou, F., U. Boschert, N. Amlaiky, J. L. Plassat, and R. Hen (1992). "A family of Drosophila serotonin receptors with distinct intracellular signalling properties and expression patterns." In: *The EMBO journal* 11.1, pp. 7–17.

Schäfer, M. K. H., L. E. Eiden, and E. Weihe (1998a). "Cholinergic neurons and terminal fields revealed by immunohistochemistry for the vesicular acetylcholine transporter. I. Central nervous system". In: *Neuroscience* 84.2, pp. 331–359.

— (1998b). "Colinergic neurons and terminal fields revealed by immunohistochemistry for the vesicular acetylcholine transporter in the peripheral nervous system". In: *Neuroscience* 84.2, pp. 361–376.

Schäfer, M. K. H., E. Weihe, J. D. Erickson, and L. E. Eiden (1995). "Human and monkey cholinergic neurons visualized in paraffin-embedded tissues by immunoreactivity for VAChT, the vesicular acetylcholine transporter". In: *Journal of Molecular Neuroscience* 6.4, pp. 225–235.

Schäfer, S., G. Bicker, O. P. Ottersen, and J. Storm-Mathisen (1988). "Taurine-like immunoreactivity in the brain of the honeybee." In: *The Journal of comparative neurology* 268.1, pp. 60–70.

Schindelin, J., I. Arganda-Carreras, E. Frise, V. Kaynig, M. Longair, T. Pietzsch, S. Preibisch, C. Rueden, S. Saalfeld, B. Schmid, J.-Y. Tinevez, D. J. White, V. Hartenstein, K. Eliceiri, P. Tomancak, and A. Cardona (2012). "Fiji: an open-source platform for biological-image analysis." In: *Nature methods* 9.7, pp. 676–82.

Schleyer, M., D. Miura, T. Tanimura, and B. Gerber (2015). "Learning the specific quality of taste reinforcement in larval Drosophila". In: *eLife* 4, pp. 1–10.

Schloss, P., H. Betz, C. Schröder, and E. D. Gundelfinger (1991). "Neuronal nicotinic acetylcholine receptors in Drosophila: antibodies against an alpha-like and a non-alpha-subunit recognize the same high-affinity alpha-bungarotoxin binding complex." In: *Journal of neurochemistry* 57, pp. 1556–1562.

Schmidt-Nielsen, B. K., J. I. Gepner, N. N. H. Teng, and L. M. Hall (1977). "Characterization of an alpha-Bungarotoxin binding component from Drosophila melanogaster". In: *Journal of neurochemistry* 29.5, pp. 1013–1029.

Schneiderman, N., I. Fuentes, and I. Gormezano (1962). "Acquisition and Extinction of the Classically Conditioned Eyelid Response in the Albino Rabbit". In: *Science* 136.3516, pp. 650–652.

Schoepfer, R., W. G. Conroy, P. Whiting, M. Gore, and J. Lindstrom (1990). "Brain alpha-bungarotoxin binding protein cDNAs and MAbs reveal subtypes of this branch of the ligand-gated ion channel gene superfamily." In: *Neuron* 5.1, pp. 35–48.

Scholz, H., J. Ramond, C. M. Singh, and U. Heberlein (2000). "Functional Ethanol Tolerance in Drosophila". In: *Neuron* 28.1, pp. 261–271.

Schroll, C., T. Riemensperger, D. Bucher, J. Ehmer, T. Völler, K. Erbguth, B. Gerber, T. Hendel, G. Nagel, E. Buchner, and A. Fiala (2006). "Light-Induced Activation of Distinct Modulatory Neurons Triggers Appetitive or Aversive Learning in Drosophila Larvae". In: *Current Biology* 16.17, pp. 1741–1747.

Schuldiner, O., D. Berdnik, J. M. Levy, J. S. Wu, D. Luginbuhl, A. C. Gontang, and L. Luo (2008). "piggyBac-Based Mosaic Screen Identifies a Postmitotic Function for Cohesin in Regulating Developmental Axon Pruning". In: *Developmental Cell* 14.2, pp. 227–238.

Schultz, W., P. Dayan, and P. R. Montague (1997). "A neural substrate of prediction and reward." In: *Science* 275.June 1994, pp. 1593–1599.

Schulz, R., S. Bertrand, K. Chamaon, K.-H. Smalla, E. D. Gundelfinger, and D. Bertrand (2002). "Neuronal Nicotinic Acetylcholine Receptors from Drosophila: Two Different Types of α Subunits Coassemble Within the Same Receptor Complex". In: *Journal of Neurochemistry* 74.6, pp. 2537–2546.

Schulz, R., E. Sawruk, C. Mülhardt, S. Bertrand, A. Baumann, B. Phannavong, H. Betz, D. Bertrand, E. D. Gundelfinger, and B. Schmitt (1998). "D alpha3, a new functional alpha subunit of nicotinic acetylcholine receptors from Drosophila." In: *Journal of neurochemistry* 71, pp. 853–862.

Schürmann, F. W., O. P. Ottersen, and H. W. Honegger (2000). "Glutamate-like immunoreactivity marks compartments of the mushroom bodies in the brain of the cricket". In: *Journal of Comparative Neurology* 418.2, pp. 227–239.

Schürmann, F.-W. (2016). "Fine structure of synaptic sites and circuits in mushroom bodies of insect brains". In: *Arthropod Structure & Development* 45.5, pp. 399–421.

Schuster, R., B. Phannavong, C. Schröder, and E. D. Gundelfinger (1993). "Immunohistochemical localization of a ligand-binding and a structural subunit of nicotinic acetylcholine receptors in the central nervous system of Drosophila melanogaster." In: *The Journal of comparative neurology* 335.2, pp. 149–62.

Schütz, B., E. Weihe, and L. E. Eiden (2001). "Independent patterns of transcription for the products of the rat cholinergic gene locus". In: *Neuroscience* 104.3, pp. 633–642.

Schwaerzel, M., M. Heisenberg, and T. Zars (2002). "Extinction antagonizes olfactory memory at the subcellular level". In: *Neuron* 35.5, pp. 951–960.

Schwaerzel, M., M. Monastirioti, H. Scholz, F. Friggi-Grelin, S. Birman, and M. Heisenberg (2003). "Dopamine and octopamine differentiate between aversive and appetitive olfactory memories in Drosophila." In: *The Journal of Neuroscience* 23.33, pp. 10495–502.

Scientifica (2015). *Photon Collection*. URL: `http://www.scientifica.uk.com/research-news/photon-collection` (visited on 06/14/2017).

Seal, R., G. Daniels, W. Wolfgang, M. Forte, and S. Amara (1998). "Identification and characterization of a cDNA encoding a neuronal glutamate transporter from Drosophila melanogaster". In: *Receptors and Channels* 6.1.

Seinen, E., J. G. M. Burgerhof, R. C. Jansen, and O. C. M. Sibon (2011). "RNAi-induced off-target effects in Drosophila melanogaster: Frequencies and solutions". In: *Briefings in Functional Genomics* 10.4, pp. 206–214.

Séjourné, J., P.-Y. Plaçais, Y. Aso, I. Siwanowicz, S. Trannoy, V. Thoma, S. R. Tedjakumala, G. M. Rubin, P. Tchénio, K. Ito, G. Isabel, H. Tanimoto, and T. Preat (2011). "Mushroom body efferent neurons responsible for aversive olfactory memory retrieval in Drosophila." In: *Nature neuroscience* 14.7, pp. 903–10.

Seki, Y., H. K. M. Dweck, J. Rybak, D. Wicher, S. Sachse, and B. S. Hansson (2017). "Olfactory coding from the periphery to higher brain centers in the Drosophila brain". In: *BMC Biology*, pp. 18–22.

Senn, V., S. B. Wolff, C. Herry, F. Grenier, I. Ehrlich, J. Gründemann, J. P. Fadok, C. Müller, J. J. Letzkus, and A. Lüthi (2014). "Long-Range Connectivity Defines Behavioral Specificity of Amygdala Neurons". In: *Neuron* 81.2, pp. 428–437.

Sevenster, D., T. Beckers, and M. Kindt (2014). "Prediction error demarcates the transition from retrieval, to reconsolidation, to new learning". In: *Learning & Memory* 21.11, pp. 580–584.

Shafer, O. T., D. J. Kim, R. Dunbar-Yaffe, V. O. Nikolaev, M. J. Lohse, and P. H. Taghert (2008). "Widespread Receptivity to Neuropeptide PDF throughout the Neuronal Circadian Clock Network of Drosophila Revealed by Real-Time Cyclic AMP Imaging". In: *Neuron* 58.2, pp. 223–237.

Shaner, N. C., G. G. Lambert, A. Chammas, Y. Ni, P. J. Cranfill, M. a. Baird, B. R. Sell, J. R. Allen, R. N. Day, M. Israelsson, M. W. Davidson, and J. Wang (2013). "A bright monomeric green fluorescent protein derived from Branchiostoma lanceolatum." In: *Nature methods* 10.5, pp. 407–409.

Shaner, N. C., P. A. Steinbach, and R. Y. Tsien (2005). "A guide to choosing fluorescent proteins". In: *Nature Methods* 2.12, pp. 905–909.

Shang, Y., A. Claridge-Chang, L. Sjulson, M. Pypaert, and G. Miesenböck (2007). "Excitatory Local Circuits and Their Implications for Olfactory Processing in the Fly Antennal Lobe". In: *Cell* 128.3, pp. 601–612.

Shang, Y., N. C. Donelson, C. G. Vecsey, F. Guo, M. Rosbash, and L. C. Griffith (2013). "Short neuropeptide F is a sleep-promoting inhibitory modulator." In: *Neuron* 80.1, pp. 171–83.

Shapiro, R. a., B. T. Wakimoto, E. M. Subers, and N. M. Nathanson (1989). "Characterization and functional expression in mammalian cells of genomic and cDNA clones encoding a Drosophila muscarinic acetylcholine receptor." In: *Proceedings of the National Academy of Sciences of the United States of America* 86.22, pp. 9039–43.

Shearin, H. K., I. S. MacDonald, L. P. Spector, and R. Steven Stowers (2014). "Hexameric GFP and mCherry reporters for the Drosophila GAL4, Q, and LexA transcription systems". In: *Genetics* 196.4, pp. 951–960.

Shi, M., Z. Yue, A. Kuryatov, J. M. Lindstrom, and A. Sehgal (2014). "Identification of Redeye, a new sleep-regulating protein whose expression is modulated by sleep amount". In: *eLife* 2014.3, pp. 1–17.

Shimizu, K. and M. Stopfer (2017). "A population of projection neurons that inhibits the lateral horn but excites the antennal lobe through chemical synapses in Drosophila". In: *Frontiers in Neural Circuits* 11.May, p. 30.

Shimomura, O., F. H. Johnson, and Y. Saiga (1962). "Extraction, purification and properties of aequorin, a bioluminescent protein from the luminous hydromedusan, Aequorea." eng. In: *Journal of cellular and comparative physiology* 59, pp. 223–239.

Shindo, A., Y. Hara, T. S. Yamamoto, M. Ohkura, J. Nakai, and N. Ueno (2010). "Tissue-tissue interaction-triggered calcium elevation is required for cell polarization during Xenopus gastrulation". In: *PLoS ONE* 5.2.

Shomrat, T., N. Graindorge, C. Bellanger, G. Fiorito, Y. Loewenstein, and B. Hochner (2011). "Alternative sites of synaptic plasticity in two homologous "fan-out fan-in" learning and memory networks". In: *Current Biology* 21.21, pp. 1773–1782.

Shomrat, T., I. Zarrella, G. Fiorito, and B. Hochner (2008). "The Octopus Vertical Lobe Modulates Short-Term Learning Rate and Uses LTP to Acquire Long-Term Memory". In: *Current Biology* 18.5, pp. 337–342.

Shyu, W.-h., T.-h. Chiu, M.-h. Chiang, Y.-c. Cheng, Y.-L. Tsai, T.-F. Fu, T. Wu, and C.-L. Wu (2017). "Neural circuits for long-term water-reward memory processing in thirsty Drosophila". In: *Nature Communications* 8.May, p. 15230.

Silva, B., C. Molina-Fernández, M. B. Ugalde, E. I. Tognarelli, C. Angel, and J. M. Campusano (2015). "Muscarinic ACh Receptors Contribute to Aversive Olfactory Learning in Drosophila". In: *Neural Plasticity* 2015, pp. 1–10.

Simpson, J. H. (2016). "Rationally subdividing the fly nervous system with versatile expression reagents". In: *Journal of Neurogenetics* 30.3-4, pp. 185–194.

Sinakevitch, I., S. M. Farris, and N. J. Strausfeld (2001). "Taurine-, aspartate- and glutamate-like immunoreactivity identifies chemically distinct subdivisions of Kenyon cells in the cockroach mushroom body." In: *The Journal of comparative neurology* 439.3, pp. 352–67.

Sinakevitch, I., Y. Grau, N. J. Strausfeld, and S. Birman (2010). "Dynamics of glutamatergic signaling in the mushroom body of young adult Drosophila." In: *Neural development* 5, p. 10.

Sinakevitch, I., M. Sjöholm, B. S. Hansson, and N. J. Strausfeld (2008). "Global and local modulatory supply to the mushroom bodies of the moth Spodoptera littoralis." In: *Arthropod structure & development* 37.4, pp. 260–72.

Sinakevitch, I. and N. J. Strausfeld (2006). "Comparison of octopamine-like immunoreactivity in the brains of the fruit fly and blow fly". In: *Journal of Comparative Neurology* 494.3, pp. 460–475.

Sinakevitch-Pean, I., M. Geffard, and S. I. Plotnikova (2001). "Localization of glutamate in the nervous system of Drosophila melanogaster: immunocytochemical study". In: *Zhurnal evoliutsionnoĭ biokhimii i fiziologii* 37.1, pp. 83–88.

Sitaraman, D., Y. Aso, G. M. Rubin, and M. N. Nitabach (2015). "Control of Sleep by Dopaminergic Inputs to the Drosophila Mushroom Body". In: *Frontiers in Neural Circuits* 9.November, pp. 1–8.

Sitaraman, D., M. Zars, H. Laferriere, Y.-C. Chen, A. Sable-Smith, T. Kitamoto, G. E. Rottinghaus, and T. Zars (2008). "Serotonin is necessary for place memory in Drosophila." In: *Proceedings of the National Academy of Sciences of the United States of America* 105.14, pp. 5579–84.

Sitte, H. and M. Freissmuth (2006). *Neurotransmitter Transporters*. Handbook of Experimental Pharmacology. Springer Berlin Heidelberg.

Siuda, E. R., J. G. McCall, R. Al-Hasani, G. Shin, S. Il Park, M. J. Schmidt, S. L. Anderson, W. J. Planer, J. A. Rogers, and M. R. Bruchas (2015). "Optodynamic simulation of β-adrenergic receptor signalling". In: *Nature Communications* 6, p. 8480.

Sivanantharajah, L. and B. Zhang (2015). "Current techniques for high-resolution mapping of behavioral circuits in Drosophila". In: *Journal of Comparative Physiology A: Neuroethology, Sensory, Neural, and Behavioral Physiology* 201.9, pp. 895–909.

Sjöholm, M., I. Sinakevitch, N. J. Strausfeld, R. Ignell, and B. S. Hansson (2006). "Functional division of intrinsic neurons in the mushroom bodies of male Spodoptera littoralis revealed by antibodies against aspartate, taurine, FMRF-amide, Mas-allatotropin and DC0." In: *Arthropod structure & development* 35.3, pp. 153–68.

Skinner, B. F. (1953). *Science and human behavior*. Macmillan.

Skoulakis, E. M. and R. L. Davis (1996). "Olfactory Learning Deficits in Mutants for leonardo, a Drosophila Gene Encoding a 14-3-3 Protein". In: *Neuron* 17, pp. 931–944.

Skoulakis, E. M., D. Kalderon, and R. L. Davis (1993). "Preferential expression in mushroom bodies of the catalytic subunit of protein kinase A and its role in learning and memory". In: *Neuron* 11.2, pp. 197–208.

Snell, L. D. and K. M. Johnson (1989). "Effects of nicotinic agonists and antagonists on N-methyl-D-aspartate-induced3H-norepinephrine release and3H-(1-[1-(2-thienyl)cyclohexyl]-piperidine) binding in rat hippocampus". In: *Synapse* 3.2, pp. 129–135.

Sohal, V. S., F. Zhang, O. Yizhar, and K. Deisseroth (2009). "Parvalbumin neurons and gamma rhythms enhance cortical circuit performance." In: *Nature* 459.7247, pp. 698–702.

Somers, J., J. Nguyen, C. Lumb, P. Batterham, and T. Perry (2015). "In vivo functional analysis of the Drosophila melanogaster nicotinic acetylcholine receptor Dα6 using the insecticide Spinosad". In: *Insect Biochemistry and Molecular Biology*, pp. 1–12.

Song, H. J., G. L. Ming, E. Fon, E. Bellocchio, R. H. Edwards, and M. M. Poo (1997). "Expression of a putative vesicular acetylcholine transporter facilitates quantal transmitter packaging". In: *Neuron* 18.5, pp. 815–826.

Soustelle, L., M.-T. Besson, T. Rival, and S. Birman (2002). "Terminal Glial Differentiation Involves Regulated Expression of the Excitatory Amino Acid Transporters in the Drosophila Embryonic CNS". In: *Developmental Biology* 248.2, pp. 294–306.

Souza, D. G., B. Bellaver, G. Hansel, B. A. Arús, G. Bellaver, A. Longoni, J. Kolling, A. T. S. Wyse, D. O. Souza, and A. Quincozes-Santos (2016). "Characterization of Amino Acid Profile and Enzymatic Activity in Adult Rat Astrocyte Cultures." In: *Neurochemical research* 41.7, pp. 1578–86.

Spatz, H., A. Emanns, and H. Reichert (1974). "Associative learning of Drosophila melanogaster." In: *Nature* 248.March, pp. 359–361.

Spring, K. R. and M. W. Davidson (2016). *Introduction to Fluorescence Microscopy*. URL: `https://www.microscopyu.com/techniques/fluorescence/introduction-to-fluorescence-microscopy` (visited on 04/16/2017).

Spühler, I. A., G. M. Conley, F. Scheffold, and S. G. Sprecher (2016). "Super Resolution Imaging of Genetically Labeled Synapses in Drosophila Brain Tissue". In: *Frontiers in Cellular Neuroscience* 10.

Stanley, B. G. and S. F. Leibowitz (1985). "Neuropeptide Y injected in the paraventricular hypothalamus: a powerful stimulant of feeding behavior." In: *Proceedings of the National Academy of Sciences of the United States of America* 82.11, pp. 3940–3943.

Steinberg, E. E., R. Keiflin, J. R. Boivin, I. B. Witten, K. Deisseroth, and P. H. Janak (2013). "A causal link between prediction errors, dopamine neurons and learning". In: *Nature Neuroscience* 16.7, pp. 966–973.

Stigloher, C., H. Zhan, M. Zhen, J. Richmond, and J.-l. Bessereau (2011). "The presynaptic dense projection of the Caenorhabditis elegans cholinergic neuromuscular junction localizes synaptic vesicles at the active zone through SYD-2/liprin and UNC-10/RIM-dependent interactions." In: *The Journal of neuroscience : the official journal of the Society for Neuroscience* 31.12, pp. 4388–96.

Stocker, R. F., M. C. Lienhard, A. Borst, and K. F. Fischbach (1990). "Neuronal architecture of the antennal lobe in Drosophila melanogaster". In: *Cell and Tissue Research* 262.1, pp. 9–34.

Stollhoff, N., R. Menzel, and D. Eisenhardt (2005). "Spontaneous recovery from extinction depends on the reconsolidation of the acquisition memory in an appetitive learning paradigm in the honeybee (Apis mellifera)." In: *The Journal of neuroscience : the official journal of the Society for Neuroscience* 25.18, pp. 4485–4492.

Stopfer, M. (2014). "Central processing in the mushroom bodies". In: *Current Opinion in Insect Science* 6, pp. 99–103.

Storm, D. R., C. Hansel, B. Hacker, A. Parent, and D. J. Linden (1998). "Impaired cerebellar long-term potentiation in type I adenylyl cyclase mutant mice". In: *Neuron* 20.6, pp. 1199–1210.

Strausfeld, N. J., I. Sinakevitch, and I. Vilinsky (2003). "The mushroom bodies of Drosophila melanogaster: an immunocytological and golgi study of Kenyon cell organization in the calyces and lobes." In: *Microscopy research and technique* 62.2, pp. 151–69.

Su, H. and D. K. O'Dowd (2003). "Fast synaptic currents in Drosophila mushroom body Kenyon cells are mediated by alpha-bungarotoxin-sensitive nicotinic acetylcholine receptors and picrotoxin-sensitive GABA receptors." In: *The Journal of neuroscience : the official journal of the Society for Neuroscience* 23.27, pp. 9246–9253.

Suh, G. S., S. Ben-Tabou de Leon, H. Tanimoto, A. Fiala, S. Benzer, and D. J. Anderson (2007). "Light Activation of an Innate Olfactory Avoidance Response in Drosophila". In: *Current Biology* 17.10, pp. 905–908.

Sun, D., A. J. Vingrys, and M. Kalloniatis (2007). "Metabolic and functional profiling of the normal rat retina". In: *Journal of Comparative Neurology* 505.1, pp. 92–113.

Sun, Q.-Q., S. C. Baraban, D. a. Prince, and J. R. Huguenard (2003). "Target-specific neuropeptide Y-ergic synaptic inhibition and its network consequences within the mammalian thalamus." In: *The Journal of neuroscience : the official journal of the Society for Neuroscience* 23.29, pp. 9639–49.

Suzuki, A., S. A. Josselyn, P. W. Frankland, S. Masushige, A. J. Silva, and S. Kida (2004). "Memory Reconsolidation and Extinction Have Distinct Temporal and Biochemical Signatures". In: *The Journal of Neuroscience* 24.20, pp. 4787–4795.

Svoboda, K. and R. Yasuda (2006). "Principles of two-photon excitation microscopy and its applications to neuroscience." In: *Neuron* 50.6, pp. 823–39.

Szabadics, J., C. Varga, G. Molnár, S. Oláh, P. Barzó, and G. Tamás (2006). "Excitatory effect of GABAergic axo-axonic cells in cortical microcircuits." In: *Science (New York, N.Y.)* 311.5758, pp. 233–5.

Taber, K. H., C. T. Lin, J. W. Liu, R. H. Thalmann, and J. Y. Wu (1986). "Taurine in hippocampus: Localization and postsynaptic action". In: *Brain Research* 386.1-2, pp. 113–121.

Taghert, P. H. and M. N. Nitabach (2012). "Peptide neuromodulation in invertebrate model systems." In: *Neuron* 76.1, pp. 82–97.

Taghert, P. H. and J. A. Veenstra (2003). "Drosophila Neuropeptide Signaling". In: *Advances in Genetics* 49, pp. 1–65.

Takagawa, K. and P. M. Salvaterra (1996). "Analysis of choline acetyltransferase protein in temperature sensitive mutant flies using newly generated monoclonal antibody". In: *Neuroscience Research* 24, pp. 237–243.

Takamori, S. (2006). "VGLUTs: 'Exciting' times for glutamatergic research?" In: *Neuroscience Research* 55.4, pp. 343–351.

Takemura, S.-y., Y. Aso, T. Hige, A. Wong, Z. Lu, C. S. Xu, P. K. Rivlin, H. F. Hess, T. Zhao, T. Parag, S. Berg, G. Huang, W. Katz, D. J. Olbris, S. Plaza, L. Umayam, R. Aniceto, L.-A. Chang, S. Lauchie, O. Ogundeyi, C. Ordish, A. Shinomiya, C. Sigmund, S. Takemura, J. Tran, G. C. Turner, G. M. Rubin, and L. K. Scheffer (2017). "A connectome of a learning and memory center in the adult Drosophila brain". In: *eLife* 6.

Takemura, S.-y., Z. Lu, and I. A. Meinertzhagen (2008). "Synaptic circuits of the Drosophila optic lobe: The input terminals to the medulla". In: *Journal of Comparative Neurology* 509.5, pp. 493–513.

Tallini, Y. N., M. Ohkura, B.-R. R. Choi, G. Ji, K. Imoto, R. Doran, J. Lee, P. Plan, J. Wilson, H.-B. B. Xin, A. Sanbe, J. Gulick, J. Mathai, J. Robbins, G. Salama, J. Nakai, and M. I. Kotlikoff (2006). "Imaging cellular signals in the heart in vivo: Cardiac expression of the high-signal Ca2+ indicator GCaMP2." In: *Proceedings of the National Academy of Sciences of the United States of America* 103.12, pp. 4753–4758.

Tanaka, N. K., K. Endo, and K. Ito (2012). "Organization of antennal lobe-associated neurons in adult Drosophila melanogaster brain". In: *Journal of Comparative Neurology* 520.18, pp. 4067–4130.

Tanaka, N. K., K. Ito, and M. A. Stopfer (2009). "Odor-Evoked Neural Oscillations in Drosophila Are Mediated by Widely Branching Interneurons". In: *Journal of Neuroscience* 29.26, pp. 8595–8603.

Tanaka, N. K., H. Tanimoto, and K. Ito (2008). "Neuronal assemblies of the Drosophila mushroom body." In: *The Journal of comparative neurology* 508.5, pp. 711–55.

Tanimoto, H., M. Heisenberg, and B. Gerber (2004). "Experimental psychology: Event timing turns punishment to reward". In: *Nature* 430.7003, pp. 983–983.

Tatemoto, K., M. Carlquist, and V. Mutt (1982). *Neuropeptide Y–a novel brain peptide with structural similarities to peptide YY and pancreatic polypeptide.*

Teles-Grilo Ruivo, L. M., K. L. Baker, M. W. Conway, P. J. Kinsley, G. Gilmour, K. G. Phillips, J. T. Isaac, J. P. Lowry, and J. R. Mellor (2017). "Coordinated Acetylcholine Release in Prefrontal Cortex and Hippocampus Is Associated with Arousal and Reward on Distinct Timescales". In: *Cell Reports* 18.4, pp. 905–917.

Tempel, B. L., N. Bonini, D. R. Dawson, and W. G. Quinn (1983). "Reward learning in normal and mutant Drosophila." In: *Proceedings of the National Academy of Sciences of the United States of America* 80.5, pp. 1482–6.

Thamm, M., C. Scholl, T. Reim, K. Grübel, K. Möller, W. Rössler, and R. Scheiner (2017). "Neuronal distribution of tyramine and the tyramine receptor AmTAR1 in the honeybee brain." In: *The Journal of comparative neurology* 520.Sfb 655, pp. 633–655.

Thany, S. H. (2010). "Insect Nicotinic Acetylcholine Receptors". In: *Advances in Experimental Medicince and Biology* 683.

Thany, S. H., G. Lenaers, V. Raymond-Delpech, D. B. Sattelle, and B. Lapied (2007). "Exploring the pharmacological properties of insect nicotinic acetylcholine receptors". In: *Trends in Pharmacological Sciences* 28.1, pp. 14–22.

Thimgan, M. S., J. S. Berg, and A. E. Stuart (2006). "Comparative sequence analysis and tissue localization of members of the SLC6 family of transporters in adult Drosophila melanogaster." In: *The Journal of experimental biology* 209.Pt 17, pp. 3383–404.

Thompson, R. F. (1990). "Neural mechanisms of classical conditioning in mammals." In: *Philosophical transactions of the Royal Society of London. Series B, Biological sciences* 329.1253, pp. 161–170.

Thullbery, M. D., H. D. Cox, T. Schule, C. M. Thompson, and K. M. George (2005). "Differential localization of acetylcholinesterase in neuronal and non-neuronal cells". In: *Journal of Cellular Biochemistry* 96.3, pp. 599–610.

Tian, L., S. A. Hires, T. Mao, D. Huber, M. E. Chiappe, S. H. Chalasani, L. Petreanu, J. Akerboom, S. a. McKinney, E. R. Schreiter, C. I. Bargmann, V. Jayaraman, K. Svoboda, and L. L. Looger (2009). "Imaging neural activity in worms, flies and mice with improved GCaMP calcium indicators." In: *Nature methods* 6.12, pp. 875–81.

Tomchik, S. M. and R. L. Davis (2009). "Dynamics of Learning-Related cAMP Signaling and Stimulus Integration in the Drosophila Olfactory Pathway". In: *Neuron* 64.4, pp. 510–521.

Toshima, N. and T. Tanimura (2012). "Taste preference for amino acids is dependent on internal nutritional state in Drosophila melanogaster". In: *Journal of Experimental Biology* 215.16, pp. 2827–2832.

Tovote, P., J. P. Fadok, and A. Lüthi (2015). "Neuronal circuits for fear and anxiety". In: *Nature Publishing Group* 16.6, pp. 317–331.

Trannoy, S., C. Redt-Clouet, J.-M. Dura, and T. Preat (2011). "Parallel Processing of Appetitive Short- and Long-Term Memories In Drosophila". In: *Current Biology* 21.19, pp. 1647–1653.

Tsai, H.-C., F. Zhang, A. Adamantidis, G. D. Stuber, A. Bonci, L. de Lecea, and K. Deisseroth (2009). "Phasic Firing in Dopaminergic Neurons Is Sufficient for Behavioral Conditioning". In: *Science* 324.5930, pp. 1080–1084.

Tsien, R. Y. (1998). "The Green Fluorescent Protein". In: *Annual Review of Biochemistry* 67.1, pp. 509–544.

Tully, T. (1984). "Drosophila learning: Behavior and biochemistry." In: *Behavior Genetics* 14.5, pp. 527–557.

Tully, T., S. Boynton, C. Brandes, J. Dura, R. Mihalek, T. Preat, and A. Villella (1990). "Genetic Dissection of Memory Formation in Drosophila melanogaster". In: *Cold Spring Harbor Symposia on Quantitative Biology* 55, pp. 203–211.

Tully, T., T. Preat, S. C. Boynton, M. D. Vecchio, and C. S. Harbor (1994). "Genetic dissection of consolidated memory in Drosophila". In: *Cell* 79, pp. 35–47.

Tully, T. and W. G. Quinn (1985). "Classical conditioning and retention in normal and mutant Drosophila melanogaster". In: *Journal of Comparative Physiology A* 157.2, pp. 263–277.

Turner, G. C., M. Bazhenov, and G. Laurent (2008). "Olfactory Representations by". In: *Journal of Neurophysiology*, pp. 734–746.

Tye, K. M. and K. Deisseroth (2012). "Optogenetic investigation of neural circuits underlying brain disease in animal models." In: *Nature reviews. Neuroscience* 13.4, pp. 251–66.

Ueoka, Y., M. Hiroi, T. Abe, and T. Tabata (2017). "Suppression of a single pair of mushroom body output neurons in Drosophila triggers aversive associations". In: *FEBS Open Bio* 7.4, pp. 562–576.

Ultsch, A., C. M. Schuster, B. Laube, P. Schloss, B. Schmitt, and H. Betz (1992). "Glutamate receptors of Drosophila melanogaster: cloning of a kainate-selective subunit expressed in the central nervous system." In: *Proceedings of the National Academy of Sciences of the United States of America* 89.21, pp. 10484–8.

Usdin, T. B., L. E. Eiden, T. I. Bonner, and J. D. Erickson (1995). "Molecular biology of the vesicular ACh transporter". In: *Science* 1992.

Vaccari, A. (1993). "The tyramine binding site in the central nervous system: an overview." In: *Neurochemical Research* 18.8, pp. 861–868.

Valera, S., N. Hussy, R. J. Evans, N. Adami, R. A. North, A. Surprenant, and G. Buell (1994). *A new class of ligand-gated ion channel defined by P2x receptor for extracellular ATP.*

Varanda, W. a., Y. Aracava, S. M. Sherby, W. G. VanMeter, M. E. Eldefrawi, and E. X. Albuquerque (1985). "The acetylcholine receptor of the neuromuscular junction recognizes mecamylamine as a noncompetitive antagonist." In: *Molecular pharmacology* 28.2, pp. 128–37.

Vasmer, D., A. Pooryasin, T. Riemensperger, and A. Fiala (2014). "Induction of aversive learning through thermogenetic activation of Kenyon cell ensembles in Drosophila." In: *Frontiers in behavioral neuroscience* 8.May, p. 174.

VDRC (2017). *RNAi Libraries*. URL: `http://stockcenter.vdrc.at/control/library%7B%5C_%7Drnai` (visited on 05/08/2017).

Vecsey, C. G., N. Pirez, and L. C. Griffith (2014). "The Drosophila neuropeptides PDF and sNPF have opposing electrophysiological and molecular effects on central neurons". In: *Journal of Neurophysiology* 111.5, pp. 1033–1045.

Venken, K. J. T., K. L. Schulze, N. a. Haelterman, H. Pan, Y. He, M. Evans-Holm, J. W. Carlson, R. W. Levis, A. C. Spradling, R. a. Hoskins, and H. J. Bellen (2011). "MiMIC: a highly versatile transposon insertion resource for engineering Drosophila melanogaster genes." In: *Nature methods* 8.9, pp. 737–43.

Verleyen, P., J. Huybrechts, G. Baggerman, A. Van Lommel, A. De Loof, and L. Schoofs (2004). "SIFamide is a highly conserved neuropeptide: A comparative study in different insect species". In: *Biochemical and Biophysical Research Communications* 320.2, pp. 334–341.

Vilmont, V., B. Cadot, G. Ouanounou, and E. R. Gomes (2016). "A system for studying mechanisms of neuromuscular junction development and maintenance". In: *Development* 143.13, pp. 2464–2477.

Völkner, M., B. Lenz-Böhme, H. Betz, and B. Schmitt (2000). "Novel CNS glutamate receptor subunit genes of Drosophila melanogaster." In: *Journal of neurochemistry* 75.5, pp. 1791–1799.

Vosshall, L. B., A. M. Wong, and R. Axel (2000). "An olfactory sensory map in the fly brain." In: *Cell* 102.2, pp. 147–59.

Waddell, S. (2013). "Reinforcement signalling in Drosophila; dopamine does it all after all". In: *Current Opinion in Neurobiology* 23.3, pp. 324–329.

Waddell, S., J. D. Armstrong, T. Kitamoto, K. Kaiser, and W. G. Quinn (2000). "The amnesiac gene product is expressed in two neurons in the Drosophila brain that are critical for memory." In: *Cell* 103.5, pp. 805–13.

Wagh, D., T. M. Rasse, E. Asan, A. Hofbauer, I. Schwenkert, H. Dürrbeck, S. Buchner, M.-C. Dabauvalle, M. Schmidt, G. Qin, C. Wichmann, R. Kittel, S. J. Sigrist, and E. Buchner (2006). "Bruchpilot, a protein with homology to ELKS/CAST, is required for structural integrity and function of synaptic active zones in Drosophila." In: *Neuron* 49.6, pp. 833–44.

Wahlestedt, C. and D. Reis (1993). "Receptors-Are the Receptors Potential Therapeutic Drug Targets ?" In: *New York*.

Wahlestedt, C., N. Yanaihara, and R. Håkanson (1986). "Evidence for different pre- and post-junctional receptors for neuropeptide Y and related peptides". In: *Regulatory Peptides* 13.3-4, pp. 307–318.

Walker, R. J. and G. Kerkut (1978). "The first family (adrenaline, noradrenaline, dopamine, octopamine, tyramine, phenylethanolamine and phenylethylamine)". In: *Comparative Biochemistry and Physiology Part C: Comparative Pharmacology* 61.2, pp. 261–266.

Wang, J. W. (2012). "Presynaptic modulation of early olfactory processing in Drosophila". In: *Developmental Neurobiology* 72.1, pp. 87–99.

Wang, J. W., A. M. Wong, J. Flores, L. B. Vosshall, and R. Axel (2003). "Two-photon calcium imaging reveals an odor-evoked map of activity in the fly brain". In: *Cell* 112, pp. 271–282.

Wang, Y., N. J. Wright, H. Guo, Z. Xie, K. Svoboda, R. Malinow, D. P. Smith, and Y. Zhong (2001). "Genetic manipulation of the odor-evoked distributed neural activity in the Drosophila mushroom body." In: *Neuron* 29.1, pp. 267–76.

Wang, Y., H.-F. Guo, T. A. Pologruto, F. Hannan, I. Hakker, K. Svoboda, and Y. Zhong (2004). "Stereotyped odor-evoked activity in the mushroom body of Drosophila revealed by green fluorescent protein-based Ca2+ imaging." In: *The Journal of neuroscience : the official journal of the Society for Neuroscience* 24.29, pp. 6507–14.

Wegener, C., T. Reinl, L. Jänsch, and R. Predel (2006). "Direct mass spectrometric peptide profiling and fragmentation of larval peptide hormone release sites in Drosophila melanogaster reveals tagma-specific peptide expression and differential processing". In: *Journal of Neurochemistry* 96.5, pp. 1362–1374.

Welner, S. A. and B. Collier (1985). "Accumulation, Acetylation, and Releasability of Diethylhomocholine from a Sympathetic Ganglion". In: *Journal of Neurochemistry* 45.1, pp. 210–218.

Wen, T., C. A. Parrish, D. Xu, Q. Wu, and P. Shen (2005). "Drosophila neuropeptide F and its receptor, NPFR1, define a signaling pathway that acutely modulates alcohol

sensitivity". In: *Proceedings of the National Academy of Sciences* 102.6, pp. 2141–2146.

Whitton, P. S., R. A. Nicholson, and R. H. C. Strang (1988a). "Effect of Taurine on Calcium Accumulation in Resting and Depolarised Insect Synaptosomes". In: *Journal of Neurochemistry* 50.6, pp. 1743–1746.

— (1988b). "Effect of Taurine on Neurotransmitter Release from Insect Synaptosomes". In: *Journal of Neurochemistry* 51.5, pp. 1356–1360.

Wilson, R. I. (2013). "Early olfactory processing in Drosophila: mechanisms and principles." In: *Annual review of neuroscience* 36, pp. 217–41.

Wilson, R. I. and G. Laurent (2005). "Role of GABAergic inhibition in shaping odor-evoked spatiotemporal patterns in the Drosophila antennal lobe." In: *The Journal of neuroscience : the official journal of the Society for Neuroscience* 25.40, pp. 9069–79.

Wilson, R. I., G. C. Turner, and G. Laurent (2004). "Transformation of Olfactory Representations in the Drosophila Antennal Lobe". In: *Science* 303.5656, pp. 366–370.

Winther, Å. M. E., R. J. Siviter, R. E. Isaac, R. Predel, and D. R. Nässel (2003). "Neuronal expression of tachykinin-related peptides and gene transcript during postembryonic development of Drosophila". In: *Journal of Comparative Neurology* 464.2, pp. 180–196.

Witz, P., N. Amlaiky, J. L. Plassat, L. Maroteaux, E. Borrelli, and R. Hen (1990). "Cloning and characterization of a Drosophila serotonin receptor that activates adenylate cyclase." In: *Proceedings of the National Academy of Sciences of the United States of America* 87.22, pp. 8940–8944.

Wolfgang, W. J. and M. a. Forte (1989). "Expression of acetylcholinesterase during visual system development in Drosophila." In: *Developmental biology* 131.2, pp. 321–330.

Wu, C.-L., M.-f. M. Shih, J. S.-y. Lai, H.-t. Yang, G. C. Turner, L. Chen, and A.-S. Chiang (2011). "Heterotypic gap junctions between two neurons in the drosophila brain are critical for memory." In: *Current Biology* 21.10, pp. 848–54.

Wu, C.-L., S. Xia, T.-F. Fu, H. Wang, Y.-H. Chen, D. Leong, A.-S. Chiang, and T. Tully (2007). "Specific requirement of NMDA receptors for long-term memory consolidation in Drosophila ellipsoid body." In: *Nature Neuroscience* 10.12, pp. 1578–1586.

Wu, J.-Y. and H. Prentice (2010). "Role of taurine in the central nervous system." In: *Journal of biomedical science* 17 Suppl 1.Suppl 1, S1.

Wu, J. S. and L. Luo (2006). "A protocol for dissecting Drosophila melanogaster brains for live imaging or immunostaining." In: *Nature protocols* 1.4, pp. 2110–2115.

Wu, M., J. E. Robinson, and W. J. Joiner (2014). "SLEEPLESS is a bifunctional regulator of excitability and cholinergic synaptic transmission". In: *Current Biology* 24.6, pp. 621–629.

Wu, Q., T. Wen, G. Lee, J. H. Park, H. N. Cai, and P. Shen (2003). "Developmental control of foraging and social behavior by the Drosophila neuropeptide Y-like system". In: *Neuron* 39.1, pp. 147–161.

Wu, Q., Y. Zhang, J. Xu, and P. Shen (2005a). "Regulation of hunger-driven behaviors by neural ribosomal S6 kinase in Drosophila". In: *Proceedings of the National Academy of Sciences* 102.37, pp. 13289–13294.

Wu, Q., Z. Zhao, and P. Shen (2005b). "Regulation of aversion to noxious food by Drosophila neuropeptide Y– and insulin-like systems". In: *Nature Neuroscience* 8.10, pp. 1350–1355.

Wut, P., D. Ma, M. Pierzchala, J. Wu, L. C. Yang, X. Mai, X. Chang, and T. Schmidt-Glenewinkel (2005). "The Drosophila acetylcholine receptor subunit Dα5 is part of an α-bungarotoxin binding acetylcholine receptor". In: *Journal of Biological Chemistry* 280.22, pp. 20987–20994.

Xie, Z., C. Huang, B. Ci, L. Wang, and Y. Zhong (2013). "Requirement of the combination of mushroom body lobe and / lobes for the retrieval of both aversive and appetitive early memories in Drosophila". In: *Learning & Memory* 20.9, pp. 474–481.

Yagi, R., Y. Mabuchi, M. Mizunami, and N. K. Tanaka (2016). "Convergence of multimodal sensory pathways to the mushroom body calyx in Drosophila melanogaster". In: *Scientific Reports* 6.April, p. 29481.

Yamagata, N., M. Hiroi, S. Kondo, A. Abe, and H. Tanimoto (2016). "Suppression of Dopamine Neurons Mediates Reward". In: *PLOS Biology* 14.12, e1002586.

Yamagata, N., T. Ichinose, Y. Aso, P.-Y. Plaçais, A. B. Friedrich, R. J. Sima, T. Preat, G. M. Rubin, and H. Tanimoto (2015). "Distinct dopamine neurons mediate reward signals for short- and long-term memories". In: *Proceedings of the National Academy of Sciences* 112.2, pp. 578–583.

Yamashita, A., S. K. Singh, T. Kawate, Y. Jin, and E. Gouaux (2005). "Crystal structure of a bacterial homologue of Na+/Cl–dependent neurotransmitter transporters". In: *Nature* 437.7056, pp. 215–223.

Yamazaki, Y., M. Nishikawa, and M. Mizunami (1998). "Three classes of GABA-like immunoreactive neurons in the mushroom body of the cockroach". In: *Brain Research* 788.1-2, pp. 80–86.

Yang, C.-H., M.-F. M. Shih, C.-C. Chang, M.-H. Chiang, H.-W. Shih, Y.-L. Tsai, A.-S. Chiang, T.-F. Fu, and C.-L. Wu (2016a). "Additive Expression of Consolidated Memory through Drosophila Mushroom Body Subsets". In: *PLOS Genetics* 12.5, e1006061.

Yang, H. H., F. St-Pierre, X. Sun, X. Ding, M. Z. Lin, and T. R. Clandinin (2016b). "Subcellular Imaging of Voltage and Calcium Signals Reveals Neural Processing In Vivo". In: *Cell* 166.1, pp. 245–257.

Yang, M. Y., J. D. Armstrong, I. Vilinsky, N. J. Strausfeld, and K. Kaiser (1995). "Subdivision of the Drosophila mushroom bodies by enhancer-trap expression patterns." In: *Neuron* 15.1, pp. 45–54.

Yarali, A., T. Niewalda, Y. chun Chen, H. Tanimoto, S. Duerrnagel, and B. Gerber (2008). "'Pain relief' learning in fruit flies". In: *Animal Behaviour* 76.4, pp. 1173–1185.

Yasuyama, K., T. Kitamoto, and P. M. Salvaterra (1995). "Immunocytochemical study of choline acetyltransferase in Drosophila melanogaster: An analysis of cis-regulatory regions controlling expression in the brain of cDNA-transformed flies". In: *Journal of Comparative Neurology* 361, pp. 25–37.

— (1996). "Differential Regulation Of Choline Acetyltransferase Expression In Adult Drosophila Melanogaster Brain". In: *Journal of Neurobiology* 30.2, pp. 205–218.

Yasuyama, K., I. A. Meinertzhagen, and F.-W. Schürmann (2002). "Synaptic organization of the mushroom body calyx in Drosophila melanogaster". In: *Journal of Comparative Neurology* 445.3, pp. 211–226.

Yasuyama, K. and P. M. Salvaterra (1999). "Localization of choline acetyltransferase-expressing neurons in Drosophila nervous system". In: *Microscopy Research and Technique* 45.July 1998, pp. 65–79.

Yi, W., Y. Zhang, Y. Tian, J. Guo, Y. Li, and A. Guo (2013). "A subset of cholinergic mushroom body neurons requires Go signaling to regulate sleep in Drosophila." In: *Sleep* 36.12, pp. 1809–21.

Yin, J. C., J. S. Wallach, M. Del Vecchio, E. L. Wilder, H. Zhou, W. G. Quinn, and T. Tully (1994). "Induction of a dominant negative CREB transgene specifically blocks long-term memory in Drosophila." In: *Cell* 79.1, pp. 49–58.

Yizhar, O., L. E. Fenno, M. Prigge, F. Schneider, T. J. Davidson, D. J. O'Shea, V. S. Sohal, I. Goshen, J. Finkelstein, J. T. Paz, K. Stehfest, R. Fudim, C. Ramakrishnan, J. R. Huguenard, P. Hegemann, and K. Deisseroth (2011). "Neocortical excitation/inhibition balance in information processing and social dysfunction." In: *Nature* 477.7363, pp. 171–178.

Young, J. Z. (1971). "Anatomy of the Nervous System of Octopus vulgaris". In:

Yu, D., D.-B. G. Akalal, and R. L. Davis (2006). "Drosophila alpha/beta mushroom body neurons form a branch-specific, long-term cellular memory trace after spaced olfactory conditioning." In: *Neuron* 52.5, pp. 845–55.

Yu, D., A. C. Keene, A. Srivatsan, S. Waddell, and R. L. Davis (2005). "Drosophila DPM neurons form a delayed and branch-specific memory trace after olfactory classical conditioning." In: *Cell* 123.5, pp. 945–57.

Yuan, Q., W. J. Joiner, and A. Sehgal (2006). "A Sleep-Promoting Role for the Drosophila Serotonin Receptor 1A". In: *Current Biology* 16.11, pp. 1051–1062.

Yuan, Q., F. Lin, X. Zheng, and A. Sehgal (2005). "Serotonin modulates circadian entrainment in Drosophila". In: *Neuron* 47.1, pp. 115–127.

Yuzaki, M., D. Forrest, T. Curran, and J. A. Connor (1996). "Selective activation of calcium permeability by aspartate in Purkinje cells." In: *Science (New York, N.Y.)* 273.August, pp. 1112–1114.

Zeilhofer, H. U., H. Wildner, and G. E. Yevenes (2012). "Fast Synaptic Inhibition in Spinal Sensory Processing and Pain Control". In: *Physiological Reviews* 92.1, pp. 193–235.

Zemelman, B. V., G. A. Lee, M. Ng, and G. Miesenböck (2002). "Selective photostimulation of genetically chARGed neurons". In: *Neuron* 33.1, pp. 15–22.

Zerangue, N. and M. P. Kavanaugh (1996). "Flux coupling in a neuronal glutamate transporter". In: *Nature* 383.6601, pp. 634–637.

Zhang, S. and G. Roman (2013). "Presynaptic inhibition of gamma lobe neurons is required for olfactory learning in Drosophila". In: *Current Biology* 23.24, pp. 2519–2527.

Zheng, Z., J. S. Lauritzen, E. Perlman, C. G. Robinson, D. Milkie, O. Torrens, J. Price, C. B. Fisher, N. Sharifi, L. Kmecova, I. J. Ali, B. Karsh, E. T. Trautman, J. Bogovic, P. Hanslovsky, G. S. X. E. Jefferis, M. Kazhdan, K. Khairy, R. D. Fetter, D. D. Bock, and N. Square (2017). "A Complete Electron Microscopy Volume Of The Brain Of Adult Drosophila melanogaster". In: *bioRxiv*.

Zhou, C., Y. Rao, and Y. Rao (2008). "A subset of octopaminergic neurons are important for Drosophila aggression". In: *Nature Neuroscience* 11.9, pp. 1059–1067.

Zimanyi, I. A., Z. Fathi, and G. S. Poindexter (1998). "Central control of feeding behavior by neuropeptide Y." In: *Current pharmaceutical design* 4.4, pp. 349–66.

Zimmermann, G., L. P. Wang, A. G. Vaughan, D. S. Manoli, F. Zhang, K. Deisseroth, B. S. Baker, and M. P. Scott (2009). "Manipulation of an innate escape response in Drosophila: Photoexcitation of acj6 neurons induces the escape response". In: *PLoS ONE* 4.4.

Zipfel, W. R., R. M. Williams, and W. W. Webb (2003). "Nonlinear magic: multiphoton microscopy in the biosciences." In: *Nature biotechnology* 21.11, pp. 1369–77.

Žurauskas, M., O. Barnstedt, M. Frade-Rodriguez, S. Waddell, and M. J. Booth (2017). "Rapid adaptive remote focusing microscope for sensing of volumetric neural activity". In: *Biomedical Optics Express* 8.10, p. 4369.